

POLYMER-IMMOBILISED IONIC LIQUID PHASE (PIILP) CATALYSIS: SUPPORTS FOR MOLECULAR AND NANOPARTICLES CATALYSTS

A Thesis Submitted to

The School of Natural and Environmental Sciences: Chemistry

of

Newcastle University

By

Einas Abdulaziz Abood

In Partial Fulfillment of the
Requirements for the Degree

of

Doctor of Philosophy in Chemistry



June 2018

Newcastle University

Newcastle upon Tyne, UK

PREFACE

DECLARATION

This thesis is submitted to Newcastle University for the degree requirements of Doctor of Philosophy in Chemistry. The research detailed within was performed during the period of 2014-2018 and was conducted in Newcastle University laboratories under the supervision of Dr. Simon Doherty and Dr. Julian Knight. I certify that all material is original except where acknowledged by reference and that none of the material offered in this thesis has been previously submitted by me for a degree or any other qualification at this or any other university.

“Life is not easy for any of us. But what of that?

We must have perseverance and above all confidence in ourselves.

We must believe that we are gifted for something

and that this thing must be attained.”

Marie Curie, 1867 to 1934

“Chemistry, unlike other sciences,

sprang originally from delusions and superstitions

and was at its commencement exactly

on a par with magic and astrology.”

Thomas Thomson, 1773 to 1852

“Experimental science hardly ever affords us

more than approximations to the truth,

and whenever many agents are concerned

we are in great danger of being mistaken.”

Humphry Davy, 1778 to 1829

“You may encounter many defeats, but you must not be defeated

In fact, it may be necessary to encounter the defeats,

so, you can know who you are, what you can rise from,

how you can still come out of it.”

Maya Angelou, 1928 to 2014

To my loving parents,

My beloved sister and brothers,

My loyal friends,

For all their love, support, and encouragement throughout my doctoral journey

ACKNOWLEDGMENTS

Finishing up the research and writing up a thesis was not a smooth journey and it has not been possible without the supporting and encouraging of many an amazing people around me.

First and foremost, I would like to thank my research supervisor's Dr Simon Doherty and Dr Julian Knight for their kindness, invaluable guidance, patience, and encouragement toward the completion of my degree throughout the past four years.

I would like to acknowledge the various individuals and organizations that have made this research possible Ministry of Higher Education and Scientific Research-Iraq and Iraqi Cultural Attaché – UK for the financial and the valuable support.

Many thanks to our collaborator Prof. Ian Fairlamb-York University. My sincere appreciations also go to the technical support staff at Newcastle University including Nanolab team (XPS), Dr. Corinne Wills (NMR), Dr. Kathryn White (SEM/ EDX), Dr. Maggie White (XRD) Jane Davis (ICP), Kripasindhu Sardar (TGA). I wish to thank all the technical support staff who work at other universities, Meg Stark from the University of York for (TEM), Stuart Micklethwaite from the University of Leeds for (SEM), David Apperley from Durham University for (solid-state NMR), and Stephen Boyer from London Metropolitan University for (CHN).

My special thanks should go to Khalil Hassan for (BET analysis) and his supporting in the interpretation of most of the characterisation methods.

I also thank current and past Simon and Julian's group members, especially Jack Ellison for his help whilst starting out, Tom Backhouse and Hind Alshaikh who were also working on PIILP, my colleagues: Phillip, Tina, Nuha and Matokah for their commitment, support, and encouragement during my research projects.

I owe special thanks from the very bottom of my heart, all my friends and family, in particular my parents and lovely sister, my little brother, my ever-patient Shaima'a for always being there for me no matter what tolerating me during the writing up, my friend Zeenah and Fatimah for believing in me, even when I did not believe in myself.

Finally, I would like to thank anyone gives the chance to be who I am today, either good people who bring me happiness and make me shine or the bad people who they have taught me a life Lesson.

LIST OF SYMBOLS AND ABBREVIATIONS

^1H	Proton
^{13}C	Carbon-13
AIBN	Azobis(isobutyronitrile)
BET	Brunauer-Emmett-Teller
BJH	Barrett-Joyner-Halenda
Bistriflimide ([NTf₂]⁻)	Bis(trifluoromethane)sulfonimide
[BMIm]Cl	1-butyl-3-methylimidazolium chloride
DBT	Dibenzothiophene
BOX	bis(oxazoline)
[Bpy]BF₄	N-n-butylpyridinium tetrafluoroborate
Conv.	Conversion
DCM	Dichloromethane
DCPD	Dicyclopentadiene
DMF	<i>N,N</i> -Dimethyl formamide
DMSO	Dimethyl sulfoxide
[Dopy]BF₄)	N-n-dodecylpyridinium tetrafluoroborate
DSC	Differential scanning calorimetry
DLVO	Derjaguin-Landau-Verwey-Overbeek
EDX	Energy-Dispersive X-ray Spectroscopy
eq.	Equivalents
Et₂O	Diethyl ether (ether)
[EtPy]⁺[BF₄]⁻	1-ethyl-pyridinium tetrafluoroborate
[EtPy]⁺[CF₃COO]⁻	1-ethyl-pyridinium trifluoroacetate
fcc	Face-centered cubic
FT-IR	Fourier transform infrared spectroscopy
FWHM	Full width half maximum
GC	Gas chromatography
GC-MS	Gas Chromatography Mass Spectrometry
h	Hour
HOMO	Highest occupied molecular orbital

ICP-OES	Inductively Coupled Plasma Optical Emission Spectrometry
IL	Ionic liquid
ILMs	Ionic liquids monomers
LUMO	Lowest unoccupied molecular orbital
MA	Metal-based anion
MeCN	Acetonitrile
MeOH	Methanol
MHz	Megahertz
MimAm	3-Aminoethyl-1-methylimidazolium
Min	Minutes
NHC	<i>N</i> -heterocyclic carbene
NMR	Nuclear magnetic resonance
NOESY NMR	Nuclear overhauser effect spectroscopy
NP	Nanoparticle
³¹P	Phosphorus-31
PDI	Polydispersity index
PdNP	Palladium nanoparticle
PIL	Poly-ionic liquid
PIILP	Polymer immobilised ionic liquid phase
POM	Polyoxometalates
ppm	parts per million
Psi	Pounds per square inch
PVP	polyvinylpyrrolidone
RAFT	Reversible addition–fragmentation chain-transfer
ROMP	Ring-Opening Metathesis Polymerisation
SCIL	Solid catalyst in/with ionic liquids
SEC	Size Exclusion Chromatography
Selec.	Selectivity
SEM	Size Exclusion Chromatography
SEM	Scanning Electron Microscopy
SILCs	Supported ionic liquid catalysts
SILP	Supported Ionic Liquid Phase
TEM	Transmission Electron Microscopy

TGA-DSC	Thermal Gravimetric Analysis – Differential Scanning Calorimetry
TOF	Turnover frequency
TON	Turnover number
tppti	Tri(m-sulfonyl) triphenyl phosphine tris(1-butyl-3-methylimidazolium)
Triflate ([OTf]⁻)	Trifluoromethanesulfonate
TSIL	Task Specific Ionic Liquid
XPS	X-ray Photoelectron Spectroscopy

ABSTRACT OF THE THESIS

Polymer-Immobilised Ionic Liquid Phase (PIILP) Catalysis: Supports for Molecular and Nanoparticles Catalysts

by

Einas Abdulaziz Abood

The Polymer Immobilised Ionic Liquids (PIILs) has been an area of interest recently, particularly, Doherty-Knight group has recently explored and developed this concept, with the aim of designing novel functionalised PIILPs and utilising them as supports to immobilise transition metals catalysts and nanoparticles and then exploring their applications.

The second chapter describes the synthesis of tungstate and polyoxotungstate based catalysts for the selective oxidation of sulfides. The polymer immobilised ionic liquids were based on linear pyrrolidinium-modified norbornene-cyclooctene co-polymers prepared by ring opening metathesis polymerisation and the corresponding catalysts were prepared by exchange of the polymer anions with either tungstate or polyoxotungstate. High selectivity for sulfoxide was obtained across a range of aryl-alkyl sulfides using either ($\text{WO}_4@\text{ROMP}_x$ or $\text{PW}_{12}\text{O}_{40}@\text{ROMP}_1$) in either acetonitrile or methanol with 2.5 equivalents of hydrogen peroxide for 15 minutes at room temperature. Different catalytic activity was observed based on the nature of the cross-linker whether it is linear (ROMP_1) or cyclic (ROMP_2).

The third chapter describes the synthesis and characterisation of a range heteroatom donor modified polymer immobilised palladium nanoparticles. Three types of polystyrene-based PIILP (amino-, phosphino-, and pyrrolidino-) were prepared via free radical polymerisation and used to support platinum group metal nanoparticles ($\text{MNP}@\text{R-PIILP}$; $\text{R} = \text{CH}_2\text{NH}_2$, PPh_2 , CH_2Pyrr). All the prepared catalysts have been characterised by a range of techniques including solid-state NMR spectroscopy, SEM, TEM, XRD, XPS, EDX, ICP, TGA and BET analysis.

Chapter 4 presents the results of our systematic evaluation of the efficacy of the newly prepared $\text{MNP}@\text{PIILP}$ ($\text{M} = \text{Pd}$, Pt) systems as catalysts for the selective hydrogenation of α , β -unsaturated aldehydes. Our studies have shown that $\text{PdNP}@\text{PPh}_2\text{-PIILP}$ catalyses

the hydrogenation of trans-cinnamaldehyde in water with high selectivity for reduction of the C=C double bond to afford dihydrocinnamaldehyde in 76 % selectivity at 96 % conversion under mild conditions and in short reaction times. Notably, the addition of base (K_2CO_3) to the reaction allows higher selectivities to be obtained (up to 95 % for C=C reduction), however, this results in a decrease in reaction rate (96 to 67.5 %).

Chapter 5 explores the use of PdNP@R-PIILP ($R = NH_2, PPh_2$) as catalysts for the Suzuki-Miyaura cross-coupling. Interestingly, palladium NPs stabilised by amino-decorated polymer immobilised ionic liquids (PdNP@NH₂-PIILP) were shown to be inactive for the Suzuki-Miyaura cross-coupling of aryl bromides with phenyl boronic acid. However, the corresponding PdNP@NH₂-PIILP generated by *in-situ* by reduction of PdCl₄@NH₂-PIILP was highly active for the Suzuki-Miyaura cross-coupling. Kinetic studies, reaction dilution experiments, mercury poisoning and catalyst loading studies have been employed to investigate the difference between the performance of *pre-reduced* PdNPs and those generated *in-situ*.

CONTENTS

Chapter 1. POLYMER-IMMOBILISED IONIC LIQUIDS	1
1.1 Ionic Liquids.....	1
1.2 Supported Ionic Liquid Phase.....	10
1.3 Polymer-Immobilised Ionic Liquid Phase Catalysis.....	15
1.4 Polymerisation Methods.....	21
1.4.1 Radical Polymerisation.....	21
1.4.2 Ring-Opening Polymerisation.....	22
1.5 PIILP – Stabilized Metal Nanoparticles for Catalysis.....	25
 Chapter 2. TUNGSTATE AND POLYOXOTUNGSTATE BASED-ROMP FOR CATALYSED THE OXIDATION OF SULFIDES	 29
2.1 Introduction.....	29
2.2 Synthesis of Styrene Based Monomer.....	31
2.3 Ring-Opening Polymerisation.....	34
2.4 Immobilisation of Tungstate and Polyoxotungstate Species.....	37
2.5 Experimental Studies on Optimization of Sulfide Oxidation System Process Parameters.....	40
2.5.1 Temperature Optimization Studies.....	43
2.5.2 Time Optimization Studies.....	49
2.5.3 Hydrogen Peroxide Concentration Optimization Studies.....	52
2.5.4 Sulfide Substrate Screening Studies.....	59
2.5.5 Recycle Studies	60
2.6 Characterisations Methods.....	64
2.6.1 Elemental Analysis (CHN).....	64
2.6.2 BET Surface Area Analysis	64
2.6.3 Solid-State Nuclear Magnetic Resonance (SSNMR).....	66
2.6.4 Infrared Radiation (FT-IR).....	68
2.6.5 Scanning Electron Microscope (SEM).....	69
2.6.6 Scanning Electron Microscopy with Energy-Dispersive X-ray Spectroscopy (SEM/EDX).....	72
2.6.7 Thermogravimetric Analysis (TGA).....	74
2.7 Conclusions.....	76
2.8 Laboratory Preparation Procedures.....	77
• General Comments	77
2.8.1 Synthesis of 2-methylbicyclo [2.2.1] hept-5-ene-2-carbonitrile (2.1).....	78
2.8.2 Synthesis of (2-methylbicyclo[2.2.1]hept-5-en-2-yl)methylamine (2.2).....	79
2.8.3 Synthesis of 1-(2-methylbicyclo[2.2.1]hept-5-en-2-yl)methylpyrrolidine (2.3).....	80
2.8.4 Synthesis of 1-benzyl-1-((2-methylbicyclo[2.2.1]hept-5-en-2-yl)methyl)pyrrolidin-1-ium bromide (2.4).....	81
2.8.5 Ring Opening Metathesis Polymerisation of 1-benzyl-1-((2-methylbicyclo[2.2.1]hept-5-en-2-yl)methyl)pyrrolidin-1-ium bromide with Cis-cyclooctene (2.5).....	82

2.8.6 Ring Opening Metathesis Polymerisation of 1-benzyl-1-((2-methylbicyclo[2.2.1] hept-5-en-2-yl)methyl)pyrrolidin-1-ium bromide with Dicyclopentadiene (2.6).....	83
2.8.7 Synthesis of Polymer Supported Tungstate (2.7).....	84
2.8.8 Synthesis of Polymer Supported Tungstate (2.8).....	85
2.8.9 Synthesis of Polymer Supported Polyoxotungstate (2.9).....	86
2.8.10 Catalysts Applications and Optimization Studies.....	87
• Typical Procedure for Catalytic Sulfoxidation Reaction	87
• Reaction Temperature Optimization Studies	87
• Reaction Time Optimization Studies	88
• Hydrogen Peroxide Concentration Optimization Studies	88
• General Procedure for Catalytic Sulfoxidation Recycle Studies with Catalyst (2.7)	89
• General Procedure for Catalytic Sulfoxidation Recycle Studies with Catalyst (2.8 and 2.9)	90

Chapter 3. PALLADIUM AND PLATINUM NANOPARTICLES LOADED ON POLYMER-IMMOBILISED IONIC LIQUIDS	91
3.1 Introduction.....	91
3.2 Synthesis of Monomers and Cross – linker.....	93
3.3 Radical Polymerisation of Cross-linked Poly Ionic Liquid.....	96
3.4 Synthesis of Polymer Decorated with Palladium and Platinum Nanoparticles.....	97
3.5 Characterisations Methods.....	98
3.5.1 BET Surface Area Analysis	98
3.5.2 Solid-State Nuclear Magnetic Resonance (SSNMR).....	101
3.5.3 Transmission Electron Microscopy (TEM).....	103
3.5.4 Scanning Electron Microscopy with Energy-Dispersive X-ray Spectroscopy (SEM/EDX).....	106
3.5.5 X-Ray Powder Diffraction (XRD).....	107
3.5.6 ICP Optical Emission Spectrometry (ICP-OES).....	112
3.5.7 Thermogravimetric Analysis (TGA).....	112
3.5.8 X-Ray Photoelectron Spectroscopy (XPS).....	114
3.6 Conclusions.....	117
3.7 Laboratory Preparation Procedures.....	118
• General Comments	118
3.7.1 Synthesis of 1, 2-Dimethyl-3-(4-vinylbenzyl) imidazolium Chloride [DMVBIM][Cl] (3.2).....	120
3.7.2 Synthesis of N-[(4-vinylphenyl) alkyl] phthalimide (3.3).....	121
3.7.3 Hydrazinolysis of Phthalimides to Afford (3.4).....	122
3.7.4 Synthesis of Cross-linker (3.6).....	123
• Synthesis of 2-methyl-1-(4-vinylbenzyl)-1H-imidazole (3.5)	123
• Synthesis of 2-methyl-1,3-bis(4-vinylbenzyl)-1H-imidazol-3-ium chloride (3.6).....	124
3.7.5 Synthesis of 1-[(4-ethenylphenyl) methyl]-pyrrolidine (3.7).....	125
3.7.6 Synthesis of Diphenyl (4-vinylphenyl) phosphine (3.9).....	126
3.7.7 Procedure for the Polymerization (3.10, 3.11, 3.12).....	127

3.7.8 Procedure for Synthesis of Palladium Chloride Loaded on Polymer (3.13, 3.14, 3.15).....	128
3.7.9 Procedure for Synthesis of Palladium Nanoparticles Amino- And Phosphino-Decorated Polymer Immobilized Ionic Liquids (3.16, 3.17).....	129
3.7.10 Palladium Nanoparticles Loaded on Pyrrolidino- Decorated Polymer Immobilized Ionic Liquids (3.18).....	130
3.7.11 Synthesis of Platinum Chloride Loaded on Polymer (3.19).....	131
3.7.12 Platinum Nanoparticles Loaded on Amino- and Phosphino-Decorated Polymer Immobilized Ionic Liquids (3.20).....	132

Chapter 4. CATALYTIC HYDROGENATION OF α,β -UNSATURATED ALDEHYDES WITH POLYMER-IMMOBILISED IONIC LIQUIDS STABILISED PALLADIUM NANOPARTICLES

133

4.1 Introduction.....	133
4.2 Optimization Studies.....	134
4.2.1 Solvent Screening Studies.....	136
4.2.2 Temperature Optimisation Studies.....	140
4.2.3 Pressure experiment Optimisation Studies.....	142
4.2.4 Effect of Additives Studies (Base Addition).....	144
1.Sodium hydroxide (NaOH)	144
2.Potassium carbonate (K_2CO_3)	146
3.Potassium phosphate (K_3PO_4)	147
4.Triethylamine (NEt_3)	148
4.2.5 α,β -Unsaturated Compounds Screening Studies.....	149
4.2.6 Recycling Studies.....	151
4.2.7 Transmission Electron Microscopy (TEM).....	154
4.2.8 Further Comparison Investigation Using Platinum Nanoparticles Loaded PIILP.....	157
4.3 Conclusion.....	158
4.4 Laboratory Preparation Procedures.....	159
• General Comments	159
• General Procedure for Catalytic Hydrogenation of α,β -Unsaturated Aldehydes in Batch	160

Chapter 5. PIILP PALLADIUM NANOPARTICLES-CATALYSED SUZUKI-MIYAUURA CROSS-COUPPLING REACTION

161

5.1 Introduction.....	161
5.2 Experimental Studies on Optimization of Suzuki-Miyaura Cross-Coupling System Process Parameters.....	163
5.2.1 Aryl Bromide Substrate Screening Studies.....	165
5.3 Further Studies on the Suzuki-Miyaura Cross-Coupling Catalyzed by PdNP@R-PIILP.....	170

5.3.1 Kinetic Studies	170
➤ Kinetic Studies with 4-bromotoluene	170
➤ Kinetic Studies of 4-bromobenzonitrile	171
➤ Kinetic Studies of 1-bromo-3-nitrobenzene	172
5.3.2 Catalyst Loading Studies.....	174
5.3.3 Reaction Dilution Studies.....	174
5.3.4 Comparison with Commercially Available Pd/C.....	175
5.3.5 Mercury Poisoning Experiments.....	176
5.4 Mechanism of the Palladium Nanoparticle Catalysed Suzuki-Miyaura Cross-Coupling.....	178
5.5 Conclusion.....	180
4.4 Laboratory Preparation Procedures.....	181
• General Comments	181
• General Procedure for Catalytic Suzuki-Miyaura Couplings in Batch	182

Chapter 6. Summary **183**

REFERENCES **185**

APPENDICES **193**

Appendix A. Nuclear magnetic resonance spectra (NMR).....	193
Appendix B. Solid-State Nuclear Magnetic Resonance (SSNMR).....	208
Appendix C. Scanning Electron Microscope (SEM).....	226
Appendix D. Energy-Dispersive X-Ray Spectroscopy (EDX).....	259
Appendix E. X-Ray Photoelectron Spectroscopy (XPS).....	265
Appendix F. Infrared Radiation (FT-IR).....	276
Appendix G. BET Surface Area Analysis.....	280

VITA **298**



Chapter 1

POLYMER-IMMOBILISED IONIC LIQUIDS

Chapter 1. POLYMER-IMMOBILISED IONIC LIQUIDS

1.1 Ionic Liquids

It has been about two decades since Michael Freemantle published an article in Chemical & Engineering News Entitled “Designer Solvents - Ionic Liquids May Boost Clean Technology Development” engage with an effective renaissance in scientific and engineering interest in both “salts” and “liquids”.^{1,2} Ionic liquids (ILs) are an inorganic or organic salt, comprised of anion and cation pairs, with a melting point below 100 °C.³ In 1914, Walden synthesized the first ionic liquid ethylammonium nitrate [C₂H₅NH₃][NO₃] (melting point 13-14°C) by neutralisation of ethylamine with concentrated nitric acid.⁴ ⁵ Since the mid 1980’s, ionic liquids have attracted considerable attention due to their fundamental scientific curiosity as well as their potentially useful and quite remarkable properties, such as negligible vapour pressure, non-flammable, tunable polarity, high thermal stability, high ionic conductivity, broad electrochemical potential window, versatile synthetic flexibility, ease of recyclability and suitable choices of cations and anions, they are classified as green solvents for chemical synthesis.⁵⁻⁸ Properties such as hydrophilicity/hydrophobicity, viscosity, density and Lewis acidity can be modified as required by fine-tuning parameters through a judicious choice of cation and anion and the length of the chain attached to cation.⁷ This structural diversity which gives desirable aspects of ILs applications allow fine tuning of their properties to fit specific needs. In general, the physical properties of ionic liquids such as melting point, density and viscosity are controlled by the cation whilst the chemical properties and reactivity are controlled by the anion.⁹

While a great number of cation and anion permutations (Figure 1) are possible only limited number are in common use. Those containing imidazolium cations are among the most widely used, because of their low viscosity, stability within oxidative and reductive conditions, and the ease of synthesis. Many reports have been published concerning the application of imidazolium-based ILs as solvents for catalysis due to their improvement in reaction rate, yield and chemoselectivity.^{3, 5, 8}

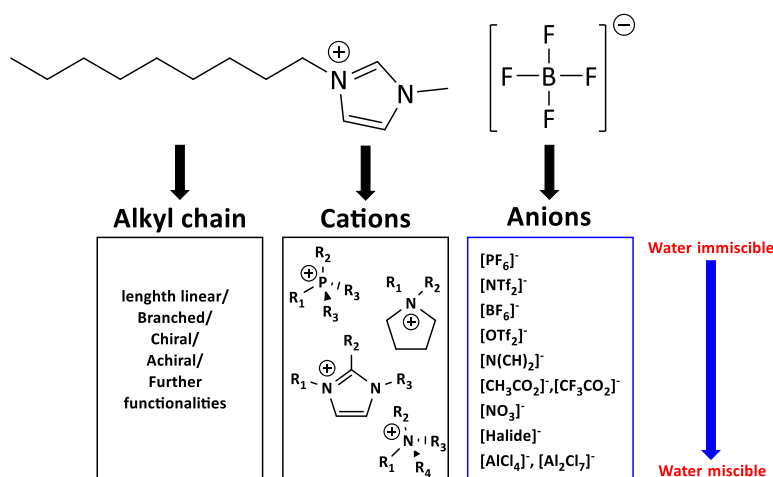


Figure 1 A selection of cations and anions to composition ionic liquids.

There are numerous advantages associated with the use of ionic liquids as solvents in catalysis but there are also several drawbacks, which includes their sensitivity to air and moisture, leaching, and high viscosity. The long-term toxicity and biodegradability of ionic liquids has yet to be determined and they are also prohibitively expensive which has prevented their commercial implementation on a wide scale.^{5-7, 10}

Since the ionic liquids consist entirely of ions (cations/anions), they were considered as an ideal medium to stabilise reactive charged intermediates which have resulted in an improvement in the selectivity and reaction rate. As a result of their green potential in enhancements of selectivity and reaction rates, they find increasing applications in the synthesis of organic compounds. Furthermore, ionic liquids act as an effective media in dehydration reaction for imine formation.¹¹

As stated previously, ionic liquids have incredibly broad and varied properties due to functionalisation of the cation/anion combination. The most important property of ILs is polarity, and how this will affect the interaction between the Ionic liquids and the solutes. It could be expected that the ILs behave as super polar solvents due to their ionic nature, however, there is no accurate measurement of an ionic liquid's polarity, but they show moderate polarities similar in magnitude to acetonitrile and methanol.^{12,}

13

The inter- and intramolecular force of ILs and the ion pair Coulombic interactions play an important role in determining the properties of ionic liquids. The common type of IL

used is the dialkylimidazolium type (Figure 2) shows the possible multiple intermolecular interactions, including:

- 1) Hydrogen-bond donation between the cation protons as the donor and the anion as acceptor.
- 2) The possible Van der Waals interactions between the alkyl side chains and the π -stacking from the imidazolium aromatic ring.

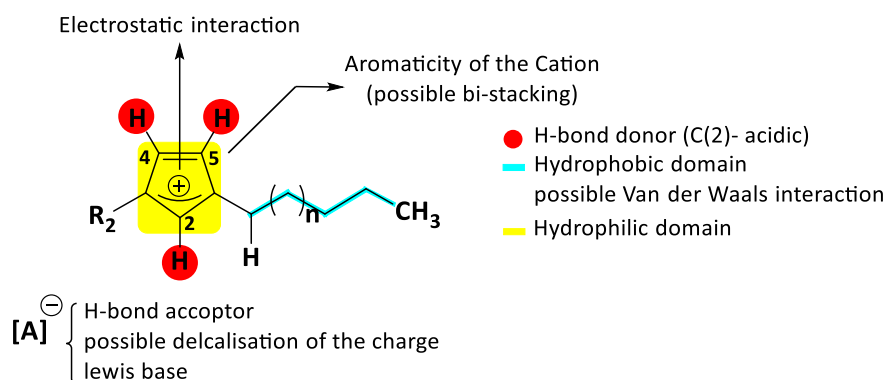
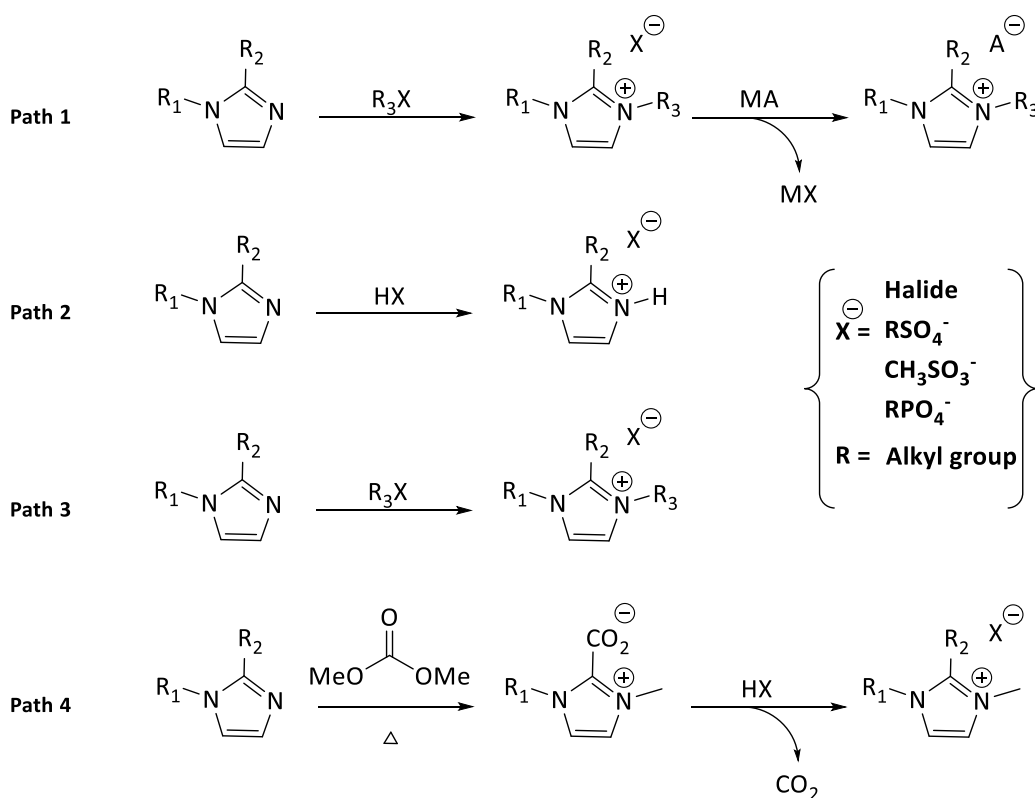


Figure 2 The different possible interactions in an imidazolium-based ionic liquid.¹³

As a result of what it is described above about the combination of the interactions, ILs have a unique solubility which enables them to dissolve both polar and nonpolar substrates. There are several aspects about the imidazolium-based ILs and their anions that need to be considered, including the strength of the interaction between the anion and the imidazolium, the hydrogen bonding between the ionic species, the type of anions and its symmetry and delocalisation of the positive charge of the imidazolium.¹³ Furthermore, the ionic liquid bulk structural organisations, for instance, its three-dimensional structure can play a considerable role in understanding their reactions role. The H-bonding interactions with dialkylimidazolium chlorides formed polymeric networks that could be observed by a host of different techniques such as NMR, X-ray diffraction², NOESY NMR spectroscopy.¹⁴ The choice of anion for a specific cation has been shown to have a profound effect on the melting point. The melting points will be higher if the cations coordinate with hydrophilic anions such as halides while it will be lower when it is weakly coordinate with hydrophobic anions such as triflates ([OTf]⁻) and triflamides ([NTf₂]⁻). Furthermore, the melting point can also be altered by fine-tuning the length of the alkyl side chain with longer chains lowering the melting point.¹⁵ In

addition to the positive charge delocalisation and the molecular symmetry disruption which make the crystallisation process more difficult. Another concern of ILs is their viscosity, in general, ILs exhibit high viscosities in comparison with conventional organic solvent. This, in turn, can have a detrimental effect on the dynamics and kinetics of a reaction as the mass transfer may be inherently limited. In catalysis, this concept is important as the reactant must have access to the active site. However, it is possible to lower the viscosity by tuning the ILs where the choice of anion has the greater effect, or by addition of a small amount of water.¹⁶ (Figure 1) illustrates a selection of the different kinds of IL architectures, however, the most frequent ILs used are those based on the dialkylimidazolium cation. (Scheme 1) below shown possible pathways that are used to prepare ILs and each route has it is own advantages and disadvantages.



Scheme 1 The typical Pathways used to synthesise imidazolium based ILs.

The first pathway (anion exchange quartenisation metathesis) is the most popular where the synthesis could be achieved via metathesis of a halide salt with a suitable group (1) metal-based anion (MA), while the second path is a Brønsted-Lowry neutralization using a Brønsted acid. (Path 3) involves alkylation of an alkylimidazole,

while (Path 4) is carbonation reaction. In case of using (Path 2), it would be difficult to generate a highly pure ILs using pathway 2 as there is likely to be a trace amount of acids or alkylimidazole, while (Path 3) has been used to synthesis phosphate, sulfonate or sulfate based ILs. (Path 4) is a new pathway that uses dimethyl carbonate as a methylating agent instead of an alkyl halide.^{13, 17, 18}

In 1986 Wilkes *et al.* developed binary catalysts consisting of mixtures dialkylimidazolium chloride and aluminium chloride and explored their use in Friedel-Crafts acylations and alkylations. The imidazolium chloroaluminate was used as a solvent and catalyst.¹⁹ Friedel-Crafts is an important and widely used reaction in the industry and synthetic chemistry, Malhotra and Xiao published an investigation of using pyridinium based ILs as media for acylation reactions. Two ionic liquid catalysts were employed, 1-ethyl-pyridinium trifluoroacetate and 1-ethyl-pyridinium tetrafluoroborate (Figure 3). High yields were obtained when $[\text{EtPy}]^+[\text{CF}_3\text{COO}]^-$ - FeCl_3 was used at a lower temperature in comparison with the literature studies which reported similar results but at high temperatures.²⁰

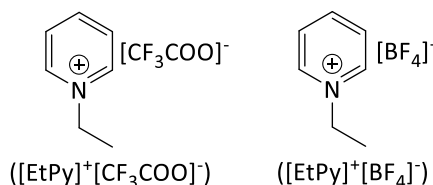


Figure 3 Pyridinium-based ILs Catalysts.

They also applied the same solvent-catalyst system to another study on benzene alkylation, and a good improvement was achieved in the form of the green credentials of the reaction by the successful catalyst-ILs recycling and reuse.²¹

The use of a solid catalyst with ionic liquids (SCIL) is a relatively new concept that has been rarely used. Essentially, synergistic effects could be gained by the combination of the benefits of using an IL as a solvent with the fundamental properties of a solid catalyst in a single system. Several studies have been published on the advantages of IL for solid catalyst-based. For example, Schüth *et al.* demonstrated the advantages of using a combination of 1-butyl-3-methylimidazolium chloride [BMIm]Cl with dry Amberlyst-15 as a solvent-catalyst system for the depolymerisation of cellulose. In this case of using

[BMIm]Cl which has the ability to disperse the cellulose by solvation, and the catalyst proved to be highly effective in the depolymerisation reaction where it cannot be hydrolysed by the conventional acids used.²² There is currently great interest in the use of ionic liquids in catalysis as more than half of the publication involving ionic liquids are based in this area. In this sense, ionic liquids have unique solvation properties allowing them to simplify the product isolation either by distillation or extraction. In addition, the physiochemical properties of ILs can be fine-tuned to tailor the hydrophilicity, hydrophobicity, and miscibility for use in biphasic or triphasic systems (Figure 4). In the biphasic system, the catalyst is dissolved in the ionic liquid layer while the reactant(s) and products are retained in the organic phase. Moreover, the limited solubility of the reaction product in the ionic phase allows a simple decantation of both layers. Even though this kind of reaction systems require a several subsequent extractions steps for enhancing the obtained yields, in which this may lead to a leaching problem which is a major limitation of using ionic liquids. In addition to that, the resulting product could be contaminated if one or both of the catalyst or IL leaches into the organic phase which means an additional purification step may be required in addition to the problem of losing the expensive designer solvents, catalyst and ligand.^{23, 24}

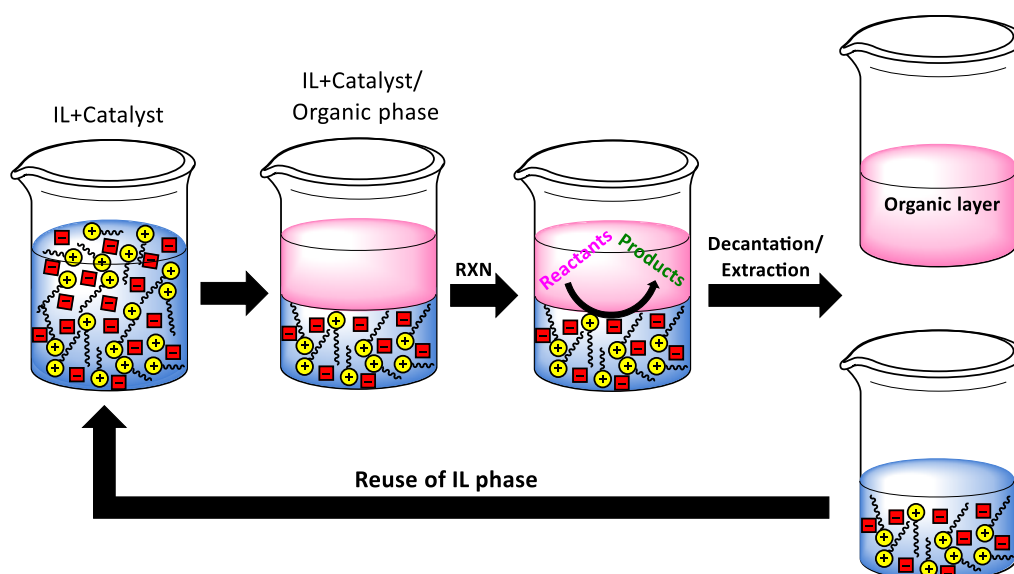


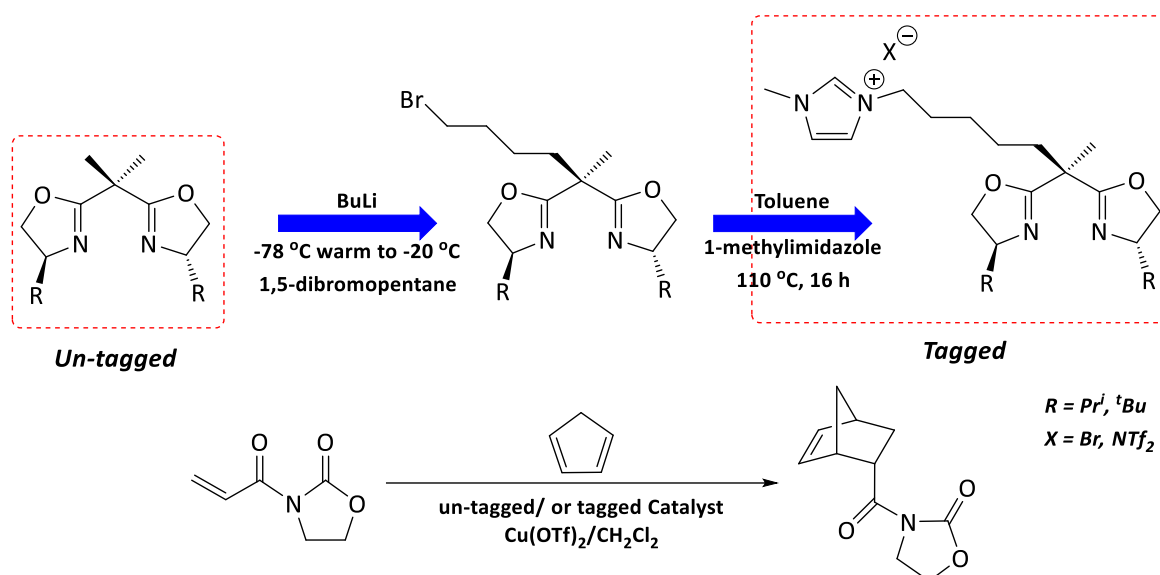
Figure 4 An ionic liquid-based aqueous biphasic catalytic system.

Furthermore, the Liquid-liquid biphasic systems shown an altering in the selectivity and the product distribution, and this may attribute to the differences in the products

solubility in such reaction system. Again, in this regard, the ILs performance can be optimised by fine-tuning of catalysts, in order to demonstrate the reaction selectivity, activity, retention, and stability in a rational manner. The neutral catalytic species are less soluble in the reaction system therefore they are more likely to leach during extraction, while when the catalyst is charged the probability of the metal leaching or the ligand leaching or even both will be likely occurred, and it depends on existence of the catalyst active species in equilibrium between the metal bound and unbound.^{25, 26}

The use of a biphasic system also enables the catalyst to be recycled and reused after removal of the product, the ionic liquid phase could be directly reused or after drying and purification. Reuse of catalyst or ionic liquid is one of the most important benefits due to their high cost, however, there is often a decrease in activity and/or selectivity on successive recycles. This problem is connected to leaching as it is stated previously, so, from this sense, the need for developing ionic liquid systems has become urgent to improve catalyst retention. In this regard, tagged-ionic liquids or task-specific ionic liquids (TSILs) have been developed. In a TSIL the ionic liquid is functionalised by a ligand which coordinates to a metal to form the active catalyst. The resulting ionic liquid tagged catalyst should have improved retention in the ionic liquid phase and thereby recycle more efficiently. However, this success of this approach will depend on the rate and equilibrium of metal-ligand dissociation.

Both chiral and achiral tagged ligands have a wide variety application on transition metal-catalysed reactions such as transfer hydrogenation, hydroformylation, metathesis and Suzuki-Miyaura cross-coupling.²⁷ In 2006, the Doherty research group published details of an imidazolium-tagged bis(oxazoline) ligand for use in Cu(II)-catalysed Mukaiyama-Aldol additions (Scheme 2). The functionalised catalyst showed an improvement in stability as it recycled 10 times without any marked decrease in either activity or enantioselectivity, in contrast with the uncharged ligand which suffering from considerable leaching problem then the activity had significantly dropped.²⁸

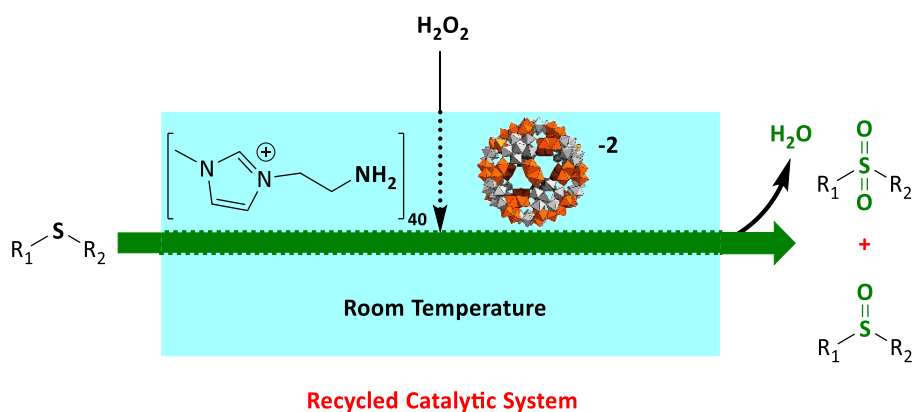


Scheme 2 Tagged and untagged imidazolium bis(oxazolines) ligands used in Cu(II)-catalysed Diels-Alder reactions.

The practical advantage of using the TSIL catalysts and its wide applications is associated with improved retention in the IL phase, and this benefit is not limited to retention of tagged-catalyst but also about the IL fragments functionalisation which is working on facilitating mechanisms of the reactions and improving the catalyst activity.²⁹ For example: using fluorous-tagged IL-toluene in hydrosilylation reaction³⁰, in addition to using IL- water catalytic systems in hydrogenation reactions^{31, 32}. In this sense, the formation of favourable reaction transition state could be stabilised depending on a suitable functional group presence, in addition to that, this functional group could provide a kind of interactions between ligands and the transition metal centres.

Despite all the facts about the benefits of using TSILs catalysts, there is a major limitation that must be taken into account which is the expense and the difficulty of synthesis to prepare a special tagged-ligand for specific needs.

The oxidation of sulfides has received an increasing amount of interest, particularly, in industrial organic synthesis because of the importance of sulfoxides and sulfones as manufacturing intermediates and valuable products.³³ Recently, Farsani and co-workers reported a new catalyst consisting of Keplerate POM-anions based on IL-cations $[(\text{NH}_4)_2(\text{MimAm})_{40}[\text{Mo}_{132}\text{O}_{372}(\text{CH}_3\text{COO})_{30}(\text{H}_2\text{O})_{72}]$. They have been proven it as an efficient, green catalyst in the oxidation of sulfides which is carried out under mild conditions where H_2O_2 is used as green oxidant and water as green solvent (Scheme 3).³³



Scheme 3 Catalytic sulfide oxidation to corresponding sulfoxides and sulfones.

Since the catalyst helped to provide the reaction an easy and practical protocol, such as shorten the reaction time, increasing the chemical recyclability and selectivity, this method become more suitable for large scale industrial production chemistry.²⁸

To conclude, ILs have unique and important properties which enables them to enhance catalyst performance especially in terms of recycling and reuse by providing an excellent reaction media with a sufficient stability to hold an ionic or polar catalytically active species, in addition, their variety and tuneability allows their properties to be optimised for a specific need. Although their role and impact on the reaction system is quite complex and cannot be easily predicted. ILs simply considered sources of an ionic environment for the reaction system with their special physicochemical properties that play an important role in the mechanism of the reactions. Despite their clear advantages, the high viscosity and cost and the problem of leaching may limit their use, this has led researchers to develop various methodologies that reduce their drawbacks such as immobilised the ionic liquids on supporting materials or incorporating them as fragments within a polymer matrix.

1.2 Supported Ionic Liquid Phase

The concept of Supported Ionic Liquid Phase (SILP) catalysis was developed by Mehnert *et al.*^{34, 35} to overcome some of the limitations associated with using ionic liquids as the bulk solvent for catalysis. In SILP catalysis a thin film of IL is confined to the surface of a porous solid such as silica, alumina, activated carbon and clay and used to support a homogeneous catalyst (Figure 5).^{6, 36, 37}

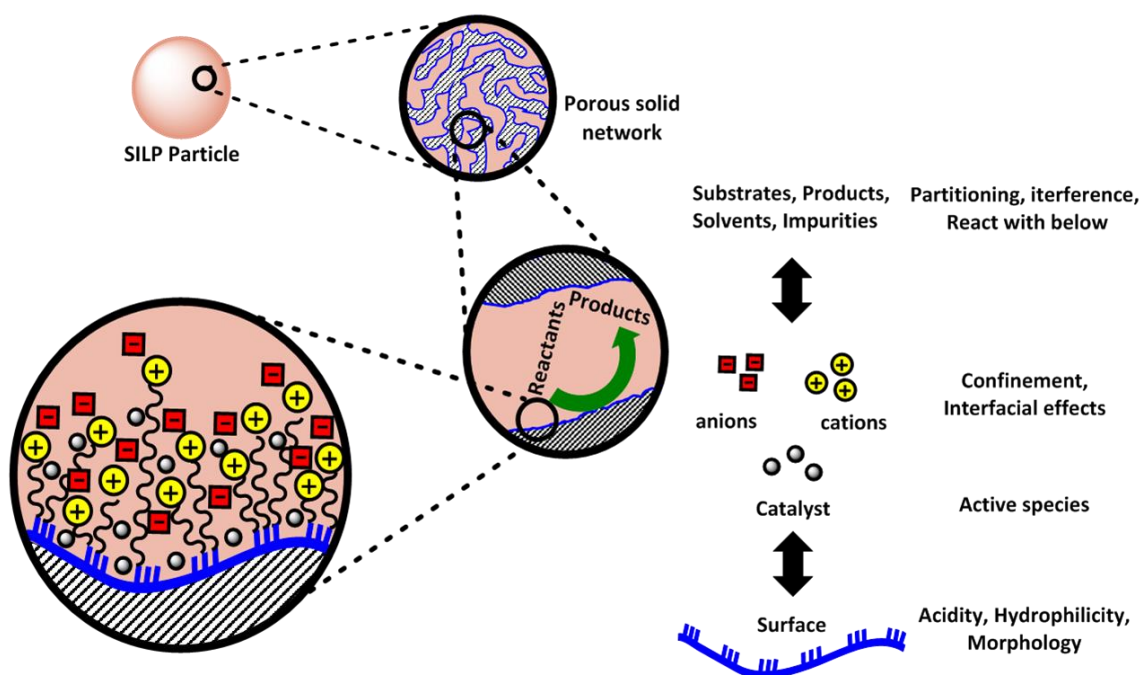


Figure 5 A schematic diagram of Supported Ionic Liquid Phase Catalyst (SILP).

The use of only a thin film of IL to coat a solid support increases the available interphase area and thereby decreases the diffusion pathway and reduces the likelihood of reactions being limited by mass transfer. From a thermodynamic point of view, the IL film still acts like a bulk liquid. The SILP catalysis is a heterogenisation of homogeneous catalyst and therefore combines the favourable properties of both systems to thereby enhance the performance of the catalytic processes. The homogeneous catalyst is dissolved in the ionic liquid film with the advantage that the surface area of the ionic liquid is greatly enhanced relative to its volume and the substrate can therefore readily diffuse to the catalyst. SILP catalysis is ideally suited for gas phase reactions and has the potential for continuous-flow operation. However, for use with liquid phase reactions,

careful tuning of the polarities of all reaction constituents is required in order to prevent or limit leaching of the catalyst and/or the ionic liquid.³⁸ SILP catalysis also overcomes the mass transport limitations from the gas to the liquid phase due to this high interfacial area, while the non-volatile nature of the IL also prevents loss of the solvent into the liquid or gas phase. Despite the clear advantages of SILP catalysis, several limitations such as pore blocking of the catalyst support, low activities, and selectivities, irreproducibility and leaching of the catalyst can be affected by the nature of the support surface.³⁷ In this regard, understanding the effect of the support material has on the nature of the catalyst is still lacking.³⁹

The polarity of an ionic liquid is one of the basic standards that determine the ILs final properties, therefore the SILPs properties will be also affected. In addition to, the advanced SILP catalytic properties which could be tuned by using different functional groups have a different polarity.⁶ One of the most significant problems facing recovery and recycling of a SILP system is the frequent purification after each reuse, typically by distillation purification which will stand like an obstacle stone preventing their application to the industrial field. In addition to the above, the cost of the ILs compared to the conventional organic solvents remains high, therefore, finding another way to reduce the amount of ILs used and hence the cost has become a necessity.⁴⁰

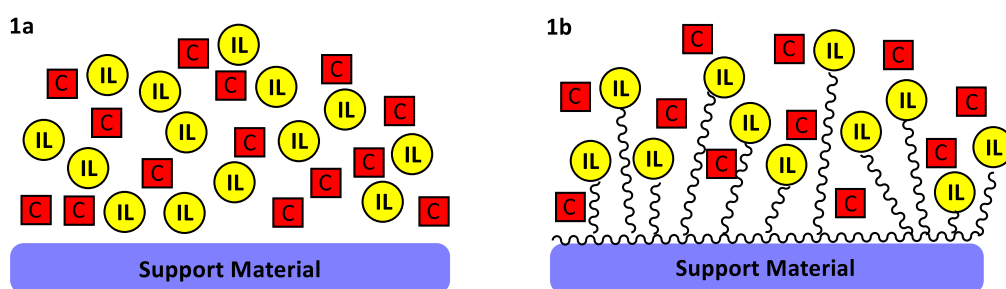


Figure 6 Type 1/a (catalyst/IL/support) and type 1/b (catalyst/IL/IL-support).

There are three kinds of SILP material divided into four subclasses depending on their preparation methods: Firstly, (Figure 6, type 1/a) the immersion is one of the most important methods that have received great attention and the easiest way to prepare SILP which involves immobilising the IL as a thin film on a porous support. Practically, the preparation of SILP by wet impregnation is straightforward as an IL solution is simply

prepared by dissolving a small amount of IL in a conventional organic solvent with the catalyst complex. The support material is then added to this solution and the solvent is then removed under reduced pressure to afford a thin layer of the ionic liquid-catalyst mixture adhering to the support. In another approach (Figure 6, type 1/b) the surface of the support is first modified by a monolayer of IL which is covalently anchored to the surface.⁴¹

Next, additional IL and the catalyst are impregnated onto the modified support. Advantages associated with SILP-based catalysts include the ease of isolation, recyclability and enhancement in rates due to the ILs thickness which make the ILs much closer the reaction interface, however, there is some an unexpected effects as consequence of the confinement effects of the support material should be taken into account.⁴²

Mehnert and co-workers reported a SILP-based catalyst for hydroformylation of hexene to produce heptanal (Figure 7). The modified silica gel which was prepared by covalently anchoring a monolayer of the ionic liquid [bmim]-[PF₆] in the presence of tri(*m*-sulfonyl) triphenyl phosphine tris(1-butyl-3-methyl-imidazolium) salt (tppti) ligand. The support material was then loaded with HRh(CO)(tppti)₃ to afford the target multi-layer SILP catalyst. This catalyst improves the reaction rate due to the high concentration of active rhodium species at the supporting material interface. However, unfortunately, because of there is no solvent in the system which was removed under reduced pressure in the catalyst preparation step so there is no ability for catalyst regeneration.^{34, 35}

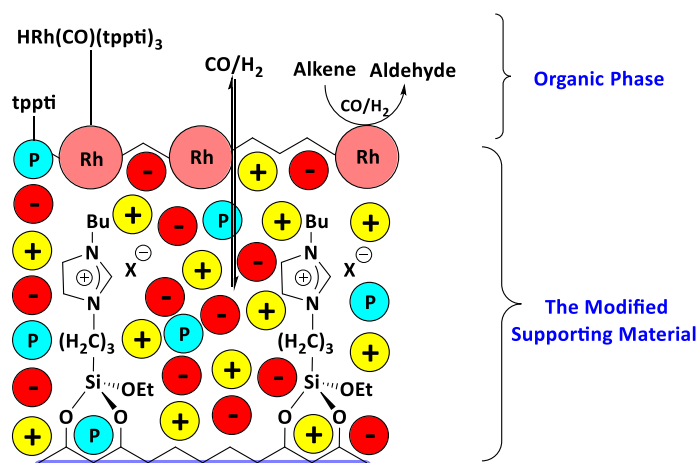


Figure 7 Hydroformylation reaction catalysed by supporting material Type 1/b.

The leaching issue associated with SILP materials was one of the drivers behind developing type 2 supported catalysts (Figure 8). This type of catalyst, also known as prepared by modifying the support material with a monolayer of ionic liquid; this can be achieved either by covalently anchored the functionalised ionic liquid or via sol-gel synthesis. In this regard, the IL is covalently bonded to the surface of support material via the cation; ion exchange occurs between the IL anion and an anionic catalyst such as: $[\text{WO}_4]^{2-}$, $[\text{CuCl}_4]^{2-}$, $[\text{PdCl}_4]^{2-}$, $[\text{SnCl}_5]^-$, $[\text{NiCl}_4]^{2-}$ or binding via the anion, in this case, the ligand or the (catalyst - IL fragments) will covalently anchor binding with surface instead of the IL fragments in (type 1/b).⁴¹

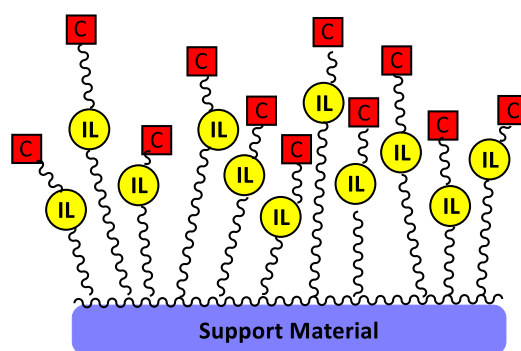


Figure 8 Type 2 (catalyst-IL-support + IL-support).

The main difference between this type and the type one system is that there is no excess free ligand immobilised on the supporting material.⁴³ Moreover, this procedure will reduce the amount of expensive ionic liquid required and this is a desirable benefit. The investigation about immobilising the L-proline on modified silica to catalyse the aldol reaction is a good example of this type (Figure 9).⁴⁴

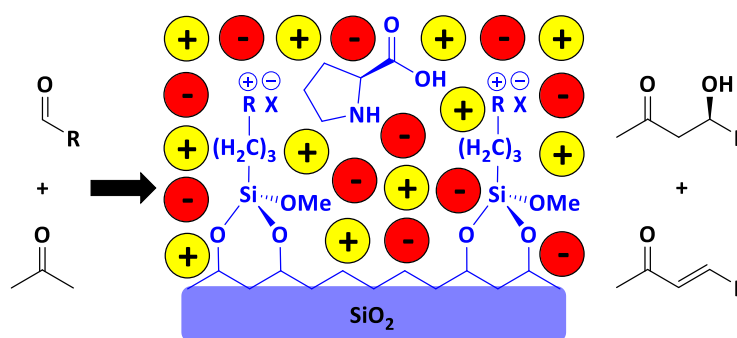


Figure 9 Aldol reaction catalysed by supporting material Type 2.

Type 3 systems (Figure 10) are “solid catalysts with ionic liquid layer” (SCIL), in which the SCIL is prepared by impregnating IL on the surface of a support material; these supports are typically conventional heterogeneous catalysts or supported transition-metal nanoparticles.⁴¹ For example, SCIL catalysts have recently been applied to the oxidative S-S coupling of aliphatic and aromatic thiols, where the nature of the IL was shown to have a significant impact on the activity of the catalyst, as well as provide extra stabilisation by providing a protective layer against sulfation.⁴⁵

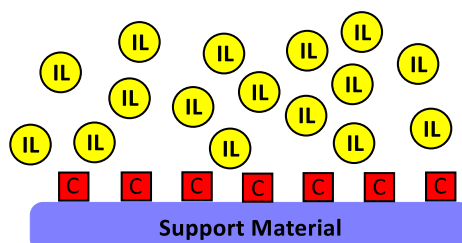


Figure 10 Type 3 (IL/catalyst-support).

A significant difference between SILP and SCIL strategies is that in the former the IL is immobilised on inert material while in the latter, the IL is bound through intermolecular interactions to a *pre-formed* heterogeneous catalyst. Furthermore, the activity and selectivity of SCIL would be changed and affected depending on nature of IL on the internal surface of the solid catalyst. There are two possible reasons for this; firstly, the IL coating may alter the chemical properties of the solid catalyst by interacting with it at the interface, or secondly, the nature of the IL (polarity/hydrophobicity, etc.) may increase the concentration of the reactants through favourable intermolecular interactions.⁴⁶

1.3 Polymer-Immobilised Ionic Liquid Phase Catalysis

The Doherty group has recently been exploring the concept of Polymer Immobilised Ionic Liquid Phase (PIILP) catalysis, which could be considered to be a polymer-based version of SILP in which the ionic liquid is immobilised in the form of a cation decorated polymer (Figure 11). This is in principle a potentially powerful concept as it should be possible to tune polymer properties such as charge density and distribution, functionality, porosity, hydrophobicity/hydrophilicity as well as microstructure in a rational manner and thereby optimise support-catalyst interactions and performance.

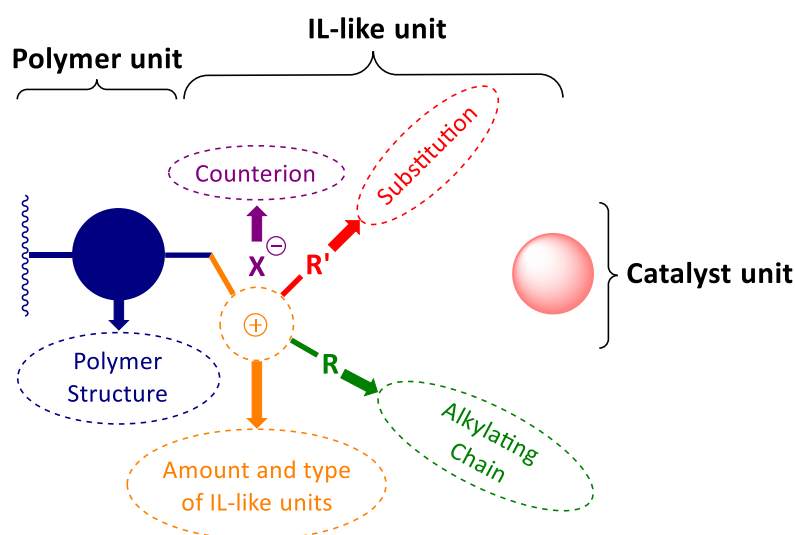
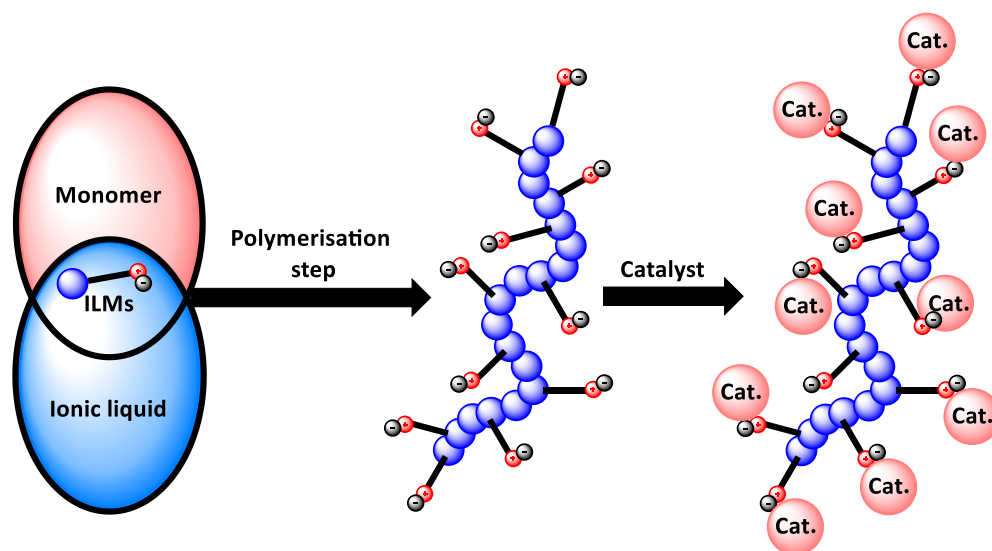


Figure 11 The structure of Polymer Immobilised Ionic Liquid Phase (PIILP).

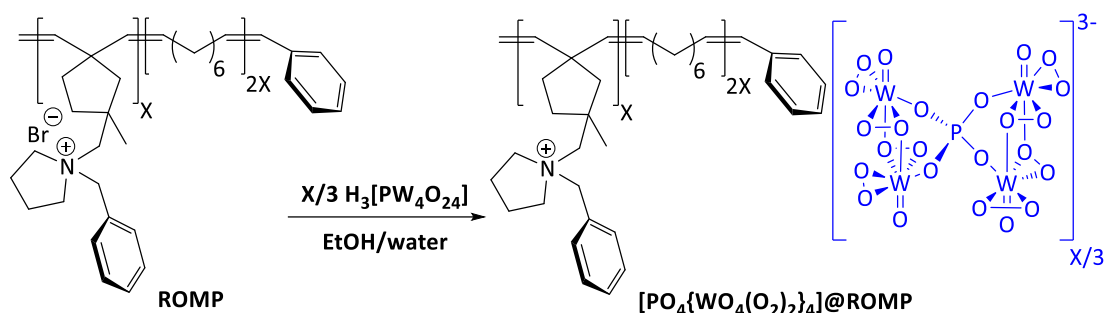
In this regard, there are two general pathways to generate poly-ionic liquids; the first type is the post polymerisation modification of polymer by covalently anchoring or tagging a suitable IL fragment. The other one (Scheme 4) is the most common, where a suitable monomer is functionalised with specific IL moieties (ILMs) and then polymerised with a co-monomer to generate the target poly-ionic liquid (PIL).



Scheme 4 Preparation steps of poly-ionic liquids (PILs) from ionic liquids monomers (ILMs).

Polymer immobilised ionic liquids are synthesized by the free radical polymerisation of suitable ionic liquid monomers. The first PIL was reported in the 70's by Salamone and co-worker⁴⁷, however, this development did not attract much attention until the 90's when Ohno and co-workers used several kinds of IL monomer to prepare PILs for use as solid conductor materials.⁴⁸

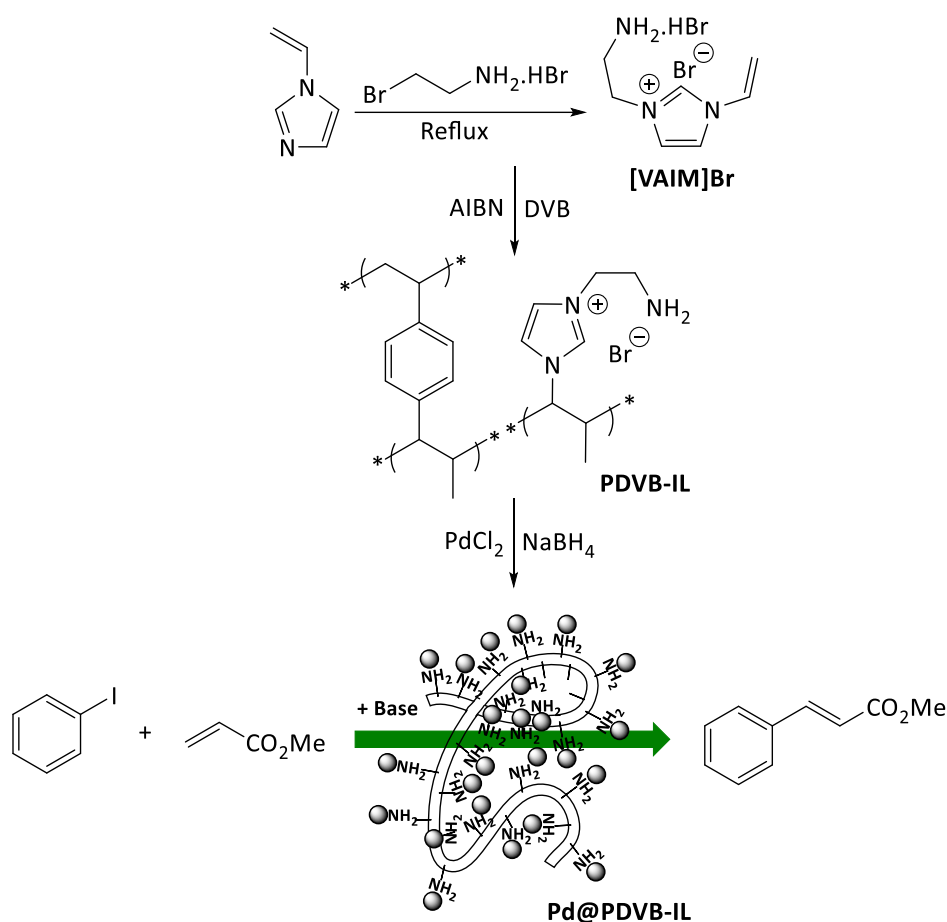
The use of polymer immobilised ionic liquids as supports for catalysis has started to receive increasing attention in recent years.^{49,50} For example, the Doherty/Knight group have shown that the peroxometalate-based PIILP system, $[\text{PO}_4\{\text{WO}(\text{O}_2)_2\}_4]@\text{PIILP}$, (Scheme 5) is an efficient, selective and recyclable catalyst for the hydrogen peroxide-mediated epoxidation of alkenes and allylic alcohols. In this case, the PIILP was prepared via Ring-Opening Metathesis Polymerisation (ROMP) between cis-cyclooctene and the functionalised monomer (a pyrrolidinium-functionalised norbornene), using the first generation Grubbs' catalyst.⁵¹ Since this initial foray, there have been several additional seminal papers describing the efficiency of Polymer Immobilised Ionic Liquid Phase catalyst in organic reactions.⁵¹⁻⁵⁴



Scheme 5 Preparation of peroxometalate-based PIILP from a pyrrolidinium-based ROMP-derived polymer.

While the overwhelming majority of studies on the use of poly-ionic liquids as supports have been conducted with polystyrene-based systems the Doherty group initially targeted ROMP-derived PIILs as it is a well-behaved living process and the catalyst is highly active, stable and functional group tolerant.

Palladium nanoparticles chemistry has received a great attention especially in the field of catalysis due to their high catalytic activity in addition to their importance in carbon-carbon bond formation such as Stille, Heck and Suzuki coupling reactions.⁵⁵ The active Pd(0) species could generate quite easily via the reduction of Pd(II)-precursor using NaBH_4 , for instance, Han *et.al* published a paper entitled "Immobilisation of Pd nanoparticles with functional ionic liquid grafted onto cross-linked polymer for solvent-free Heck reaction" where they synthesized (Scheme 6) a 1-aminoethyl-3-vinylimidazolium bromide [VAIM]Br cross-linked co-polymer from 1-vinyl-imidazole, 2-bromoethylamine hydrobromide and the cross-linker divinylbenzene (DVB) using AIBN to producing PDVB-IL, which was shown to be an effective support material for the stabilisation of PdNPs. The synthesised PdNP@PDVB-IL was a highly active and stable catalyst for the Heck coupling reaction for a range of substrates. The system also recycled efficiently due to its ease separation from the reaction products; this was attributed to the insolubility nature of Pd@PDVB-IL and the strong coordination between the PdNPs and NH_2 groups. The authors claimed that the supported metal nanoparticles could be used to prepare active and stable catalysts for various reactions.⁵⁶



Scheme 6 Synthesis of the PDVB-IL co-polymer and its catalytic performance in the Heck reaction.

Towards developing novel PILs all the efforts were concentrated on vinyl-imidazolium-based PILs with different functional substituents. Cinzia *et.al* described a new type (Figure 12) of highly cross-linked vinyl imidazolium-based polymer grafted to the surface of silica gel which was used to immobilise palladium catalysts. The influence of the linker and its length on catalyst performance and reusability was studied.⁵⁷

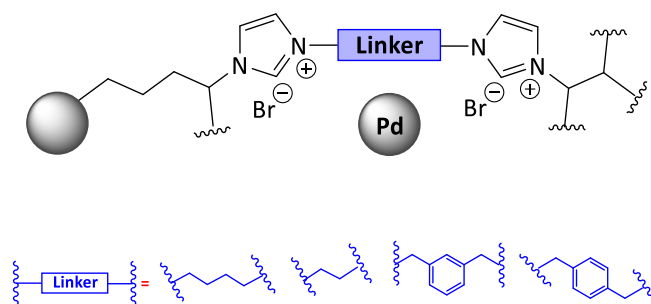
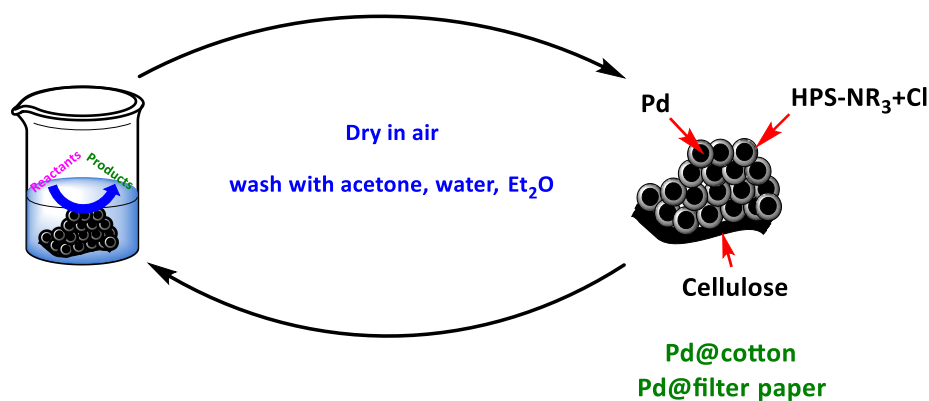


Figure 12 Synthesis of new series of PdNPs supported on poly cross-linked imidazolium catalysts.

Again, in this sense, there is an increasing interest in developing a system that is environmentally friendly and solving the problems associated with homogeneous catalysts. To this end, immobilisation of an active catalyst on to a solid support is one way to avoid the problems of using homogeneous catalysts. Particularly, when the supporting material is a polymer, this technique has recently become a very hot topic in synthetic organic chemistry. Furthermore, the active catalytic species could be either an organometallic (transition-metal) fragment or a metal nanoparticle.⁵⁸ In this regard, two directly relevant examples have been reported by Barbaro *et.al*, the first of these investigated the efficiency and reusability of a hydrogenation catalyst, in which PdNPs were generated *in-situ* in the flask used for the catalytic reaction.⁵⁹ The second reported the generation of PdNPs on gel type ion-exchange resin under catalytic conditions which were highly active, selective and durable in the partial hydrogenation of substrates containing C=C and C=O bonds under mild conditions, where the reduction was selective for C=C multiple bonds.⁶⁰ Nagashima *et.al* have recently reported that Pd@cotton and Pd@filter paper are reusable catalysts in cross-coupling and hydrogenation reactions, especially the filter paper (Scheme 7) catalyst was highly active for hydrogenation and cross-coupling.⁵⁸



Scheme 7 The catalyst recycle reaction using Pd@cotton and Pd@filter paper, HPS (Hyperbranched polystyrenes).

Although, there is no clear and precise definition for PILs it is possible to explain the concept through their preparation method i.e. conventional polymerisation. Mostly, PILs and ILs have similar physical properties but not necessarily to be linked to each other. The ILs structural diversity could be affected by ion metathesis i.e. the replacement/exchange of the anions or cations, while the PIILs structure could vary by using a different diversity of both components (anions or cations), and/or the backbone of the polymer.

A PIIL could be designed to have an entirely different structural architecture, even if the PIIL has the same number of ILs monomer units, for the instant: linear, hyperbranched or star shaped polymers. In addition to the types which mentioned previously, there is another type of polymer called PIIL block copolymer and can be formed by covalent binding between polymers and PIILs.⁶¹ The disadvantages of using PIILs is limited in comparing with ILs disadvantages which include the catalyst reactivity under specific reaction conditions, while the only consideration about using PIILs is the side reactions of the planned reactions. However, the PIILs may well find industrial applications specifically in the industry of energy due to their tuneable physicochemical properties.⁸

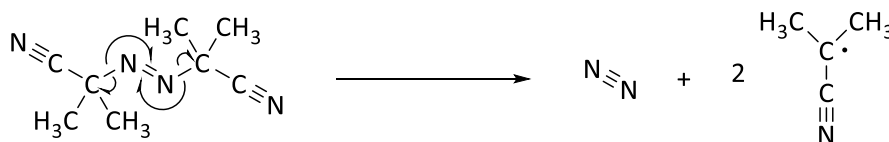
1.4 Polymerisation Methods

To synthesise polymers decorated with ionic liquids, particularly PIILP materials, there is a range of different polymerisation methods that should be considered. Moreover, the chosen polymerisation method should also provide a high degree of functionalisation to enable the microstructure, surface properties, ionic microenvironment, stability and porosity to be modified in a rational manner. Moreover, which could affect the optimisation of the substrate efficiency accessibility, enabled the catalyst-surface interactions to be tailored to establish an activity/selectivity relationships.⁶¹⁻⁶⁵

1.4.1 Radical Polymerisation

Radical polymerisation is a widely used polymerisation by which variety of polymers could be formed, through thermal or photolytic free-radical initiation. Free radicals could be formed by several mechanisms including separate initiator molecules, followed by propagation to generate a growing chain, by the addition of the initiating free radical to a monomer unit.⁶⁶

The radical polymerisation chemistry is the most common and versatile polymerisation method used in industry. Radical polymerisation proceeds via the addition of an unsaturated monomer to the active centre of the polymer growing chain, the use of this polymerisation consist of three steps, initiation followed by propagation then termination. This active site of the grown chain can be attacked the π -bond of the peroxides and azo-compounds such as 2,2'-azobisisobutyronitrile (AIBN) which undergo homolytic bond breaking through either photolysis or thermal decomposition to produce an active radical (Scheme 8).^{66, 67}



Scheme 8 Initiation and propagation of radical polymerisation of styrene initiated by AIBN.

However, there are few limitations via using the free radical polymerisation technique, such as the poorly control on molecular weights of the polymers and their distribution. And the lack of control of architectural of polymers formations, also it could prevent of the desirable formations of block copolymers.

1.4.2 Ring-Opening Polymerisation

Ring-Opening Metathesis Polymerisation (ROMP) is a type of olefin metathesis chain-growth polymerisation that produces important products and has industrial applications.⁶⁸⁻⁷¹ The driving force for the reaction is relief of ring strain in cyclic olefins (e.g. norbornene or cyclopentene) and a wide variety of catalysts have been discovered/developed.

ROMP is now a well-developed and highly versatile methodology that has a wide range of application in synthesis and polymer chemistry.^{72, 73} The main advantages of ROMP polymerisation are the ease of synthesis of the ionic liquid-like monomers and functional co-monomers, the functional group tolerance and stability of the catalyst, which combined will enable a range of PIILs to be prepared directly. Moreover, it avoids the need for post polymerisation modification, which is often required to prepare polystyrene based PIILs.

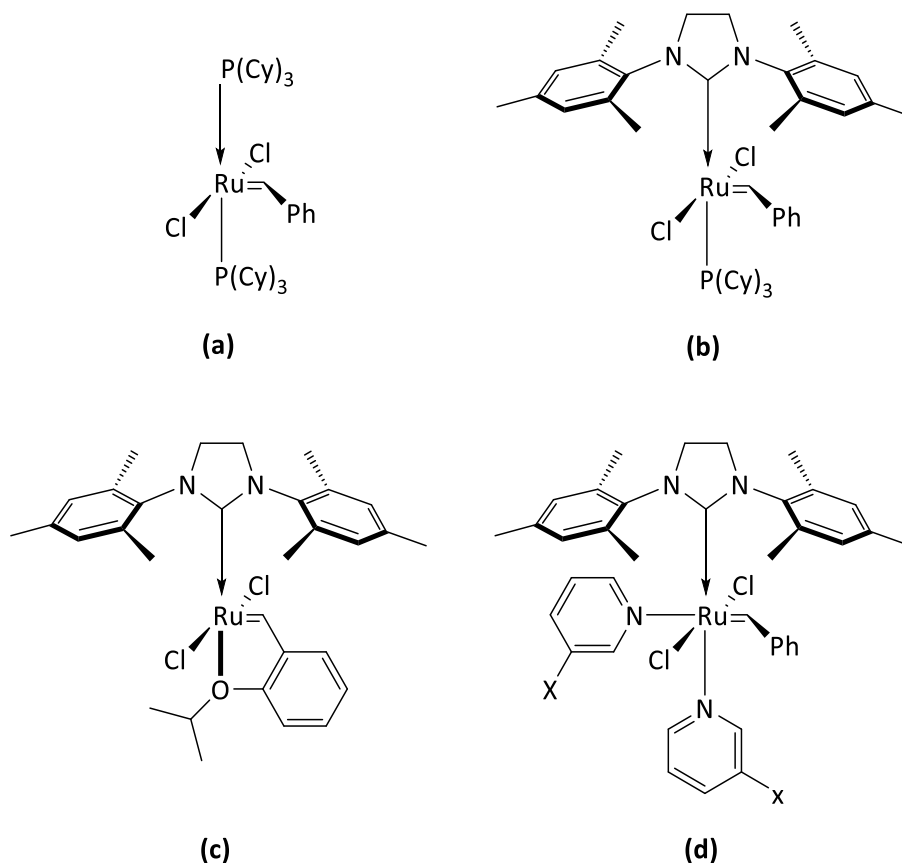
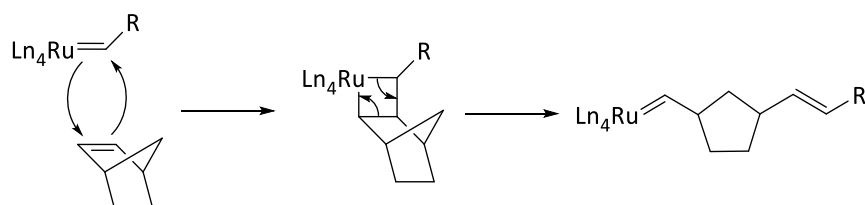


Figure 13 (a), (b) The first and second generation of Grubbs' ruthenium metathesis catalysts; (c), (d) The first and second generation of Hoveyda– Grubbs' third-generation catalysts, respectively.

ROMP based polymerisation with 1st generation Grubbs' catalyst (Figure 13 a) occurs via cycloaddition between the ruthenium carbene and the double bond of the strained bicyclic monomer to afford a metallocyclobutane intermediate (Scheme 9) which subsequently ring opens to generate a new carbene that can react with another equivalent of monomer; the reaction is driven by relief of steric strain.



Scheme 9 Cycloaddition reaction using 1st generation of Grubbs' catalyst.

Typically, in ROMP, the rate of initiation will be larger than the rate of propagation which ensures that the polymer chain grows at a constant rate to afford a polymer with a very narrow molecular weight distribution, i.e. all the polymer chains are of comparable length. A measure of this is the polydispersity index (PDI), the proportion of the weight average molecular weight to the number average molecular weight of a sample. The ideal value for PDI will be 1 when the two averages are equal; PDIs < 1.1 are typical in ROMP reactions when the Grubbs' catalyst is used. Thus, the use of Grubbs' catalyst for ROMP will enable the length of polymer chains, microstructure, and ionic microenvironment to be controlled simply by altering the concentration of catalyst and the ratio of monomer to co-monomer. A further advantage of the use of ROMP to prepare PIILs is that the monomers required can be prepared in a straightforward manner using Lewis acid catalysed Diels-Alder cycloaddition between cyclopentadiene and an appropriate enophile; the resulting adduct can then be further modified/functionalised to afford a wide-range of IL-based monomers and functional co-monomers. For example, the Doherty group have prepared PIILs via ROMP of pyrrolidinium-based monomer (Figure 14) using cyclooctene as a neutral co-monomer.^{51, 54}

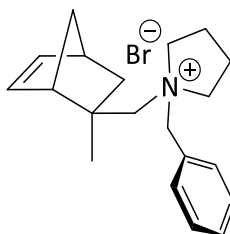
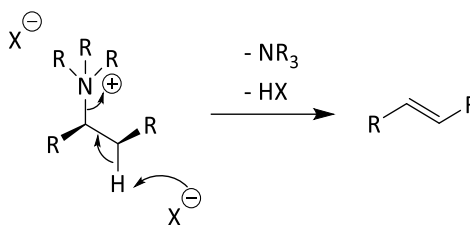


Figure 14 The chemical structure of (pyrrolidinium- functionalised norbornene) monomer unit.

Pyrrolidinium monomer was designed to ensure high stability with the 2-methyl substituent and N-benzyl group being chosen to avoid decomposition by a β -elimination Hofmann pathway (Scheme 10).



Scheme 10 Possible beta elimination pathway.

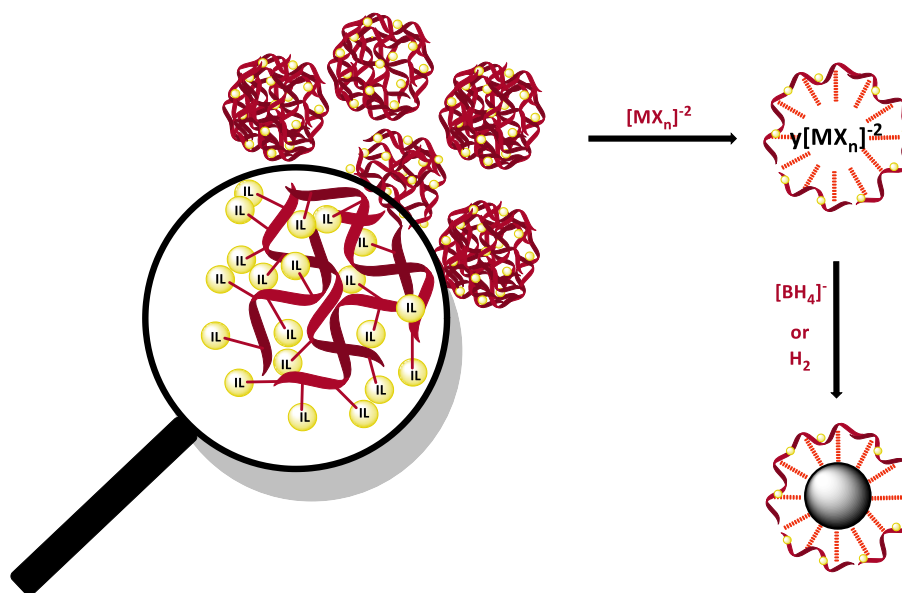
1.5 PIILP – Stabilized Metal Nanoparticles for Catalysis

The use of noble metal nanoparticles (NPs) for catalysis is a rapidly evolving and potentially powerful and enabling technology with applications across a range of areas including reduction and oxidation chemistry, carbon-carbon and carbon-heteroatom bond formation and more recently biomass conversion. The activity and selectivity of a NP catalyst is influenced by a number of factors including the size, the type of exposed crystal faces, the interactions between the surface and the stabilising agent, as well as the presence of modifiers.⁷⁴⁻⁷⁷ One of main problems facing the use of NPs for catalysis is aggregation⁷⁸ which in turn reduces the surface area and activity. This is because smaller nanoparticles are less stable and more disposed to aggregation (Ostwald ripening) by attractive Van der Waals forces. Early studies showed that ionic liquids provided stabilisation of NPs, however, the large quantities required for catalysis, their excessively high cost and losses that arise as a result of leaching are major issues that limit their use in catalysis.⁷⁹⁻⁸¹ More recently styrene-based IL-like polymers have been shown to stabilise transition metal NPs with respect to aggregation with the advantage that they are not as expensive and do not leach.^{46, 82} Recently, alkyl ammonium ions have been used to control the morphological growth of nanoparticles. In this regard, the ability to control the shape and the size of the metal particles is an important factor in optimising catalyst activity and selectivity, efficiently utilising the metal/maximising the surface area.⁸³ Furthermore, mixtures of ionic polymer (IP) and IL have been shown to stabilise palladium nanoparticles with respects to aggregation and interestingly the palladium-NP-IP-IL combination was markedly more active than the corresponding NP-IL system.^{82, 84} Again this discovery has been limited to polystyrene-based systems and there appear to be no studies aimed at understanding how the microenvironment of the polymer influences surface properties and interactions. If noble metal NP catalysts

supported by ionic liquid-based polymers are to be utilised properly it will be necessary to establish whether or not it is possible to stabilise the NPs with respect to aggregation as well as control nanoparticle size, morphological growth, and size distribution through the ionic microenvironment and/or the microstructure and porosity of the support material and how these factors influence catalyst performance. These effects will need to be investigated in a methodical and systematic manner in order to achieve understandable and rational trends; this is unlikely to be achievable using polystyrene-based systems due to the random nature of conventional radical-based polymerisation. More controlled means of generating polystyrene systems such as RAFT polymerisation are also not ideal due to the harsh reaction conditions that limit the polymer functionality. In contrast, the mild conditions and well-behaved living nature of ROMP will allow the polymer architecture to be systematically modified which may enable property-function relationships to be developed. Interestingly, the addition of heteroatom donors to ionic liquid stabilised NPs either in the form of an additive or as a functional group attached to the ionic liquid has been shown to improve their lifetime and modify their selectivity.⁸⁵⁻⁸⁷ The latter approach should improve retention of the catalyst in the ionic liquid and thereby reduce leaching and facilitate recycling.⁷⁹⁻⁸¹ However, there only a limited number of reports of the use of heteroatom-modified ionic liquids for the stabilisation of NPs and as far as we are aware there have not been any reports of the use of heteroatom donor modified PIILs for the stabilisation of NPs for use in catalysis. To this end, the innovation and timeliness of this project lie in the use of heteroatom decorated polymer immobilised ionic liquids to stabilise noble metal NPs and developing an understanding of how the macromolecular architecture and functionality control their size and morphology and thereby performance as catalysts across a range of reactions. In addition to improving the lifetime and/or activity of NP catalysts, heteroatom donors have also been shown to modify catalyst selectivity or been crucial to achieving the desired reactivity and to this end, a recent perspective discusses the influence of N- and O-heteroatom donors on the chemoselectivity of hydrogenation.⁸⁸ For example, PdNPs immobilised on an amine-decorated polymer catalyse the hydrogenation of alkynes with high selectivity for the Z-alkene⁸⁹ while resins bearing amino groups cooperated with PdNPs to affect the highly selective decomposition of formic acid to CO₂ and hydrogen, amine capped PtCoNPs selectively catalyse the hydrogenation of the C=O bond in α,β -unsaturated aldehydes⁹⁰ and alkyl

amine stabilised RuNPs are efficient highly stable recyclable catalysts for the hydrogenation of arenes.⁹¹ Part of this project (Scheme 11) is about preparing functionalised polymer immobilised ionic liquids by ROMP as well as free radical polymerisation methods with the aim of exploring how the performance of the resulting MNP@PIILP catalyst depends on the ionic microenvironment, functionality, porosity and microstructure of the support.

MNP catalysts based on the PIILP are usually prepared in a similar method to conventional heterogeneous metal catalysts by loading the supporting material with a soluble metal salt followed by the metal reduction process either by hydrogenation using hydrogen gas or by a reducing agent such as NaBH₄. One of the best advantages of using PIILP is that stabilisation of NPs occurs via the IL charge which is part of the synthetic polymer supporting material.⁵



Scheme 11 Preparation of PIILP–Stabilized Metal Nanoparticles.

In addition, the use of nanomaterial catalysts based on a supporting material has gained widespread attention due to its unique dual properties which are the high efficiency and the ease of catalyst separation in addition to the possibility of recycling the catalyst or developing a continuous flow process.

Although, the preparation of this type of catalyst can suffer from some negative effects including difficulty reproducing the NPs size and shape of controlling. In addition to all the previous, the preparation process is difficult and not environmentally friendly. Mostly, the majority of the research in this area is to improve the MNP synthesis i.e. to be more acceptable, more sustainable, as well as to identify industrial applications by using minimal amounts of reagents at mild conditions, for instance: the using of *in-situ* version of PdNPs supported on resin as a green catalyst in the hydrogenation reactions.⁹² Using PIILP to stabilise the MNPs has significant advantages such as it could be commercially available with low cost or easy to moderate preparation pathway, the PIILP also has steric and electrostatic effects to immobilise the NPs, the high resistance to the thermal, chemical and mechanical factors.

Chapter 2

TUNGSTATE AND POLYOXOTUNGSTATE
BASED-ROMP FOR CATALYSED
THE OXIDATION OF SULFIDES

Chapter 2. TUNGSTATE AND POLYOXOTUNGSTATE BASED-ROMP FOR CATALYSED THE OXIDATION OF SULFIDES

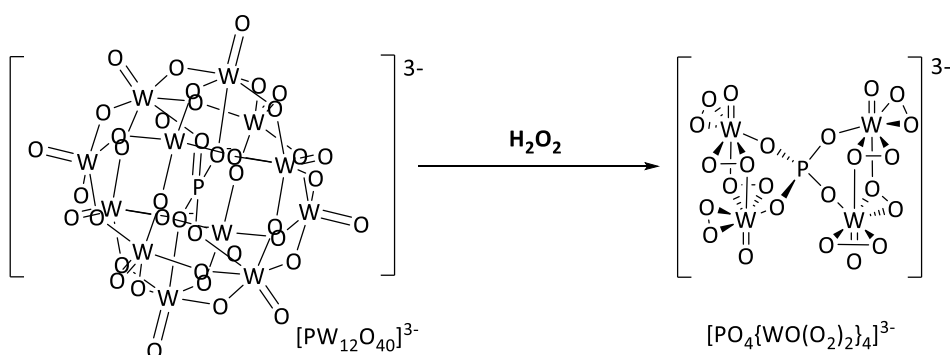
2.1 Introduction

Catalytic oxidation reactions are important chemical reactions due to their wide applications in industry for the synthesis of key intermediates and value-added products.^{93, 94} For instance, sulfoxidations have attracted much attention recently due to their valuable products (sulfoxide and sulfone) in the chemical industry and pharmaceutical industry.⁹⁵ Many studies showed the application of various types of catalysts and reaction conditions to achieve sulfoxidation reactions, however, there are a number of limitations associated with catalytic oxidations such as the harsh reaction conditions, high cost, and the generation of undesirable products. From this point of view, there is an urgent need to identify a selective catalyst which could lead the reaction under mild conditions, for example using the ionic liquids as a solvent or to stabilise the catalyst by immobilising to provide an ideal environment for improving the sulfoxidation reaction production.^{93, 94, 96}

On the other hand, using hydrogen peroxide as the oxidant in the presence of catalyst has attracted considerable attention since it is both economically and environmentally friendly. In addition, a variety of organometallic catalytic system has been developed⁴ as well as, catalytic systems based on transition metal such as tungsten⁹⁷ molybdenum^{97, 98}, ruthenium⁹⁹, vanadium¹⁰⁰, and titanium have been explored in the sulfoxidation reaction.¹⁰¹ Despite the fact of numerous advantages of using such catalysts, for instance, the high stability and selectivity and the ease preparation process, unlikely there are some disadvantages such as the isolation of the catalyst and its recovery, recyclability properties.

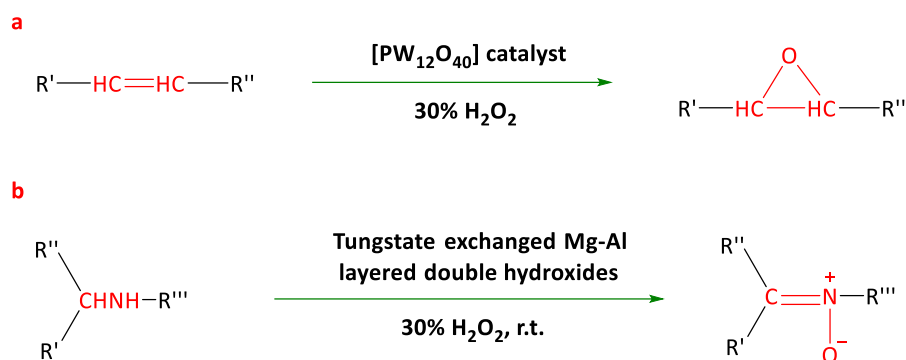
The use of polyoxometalates (POMs) as a catalyst in oxidation reactions has received considerable attention and it is the most investigated areas due to their special framework, the α -Keggin structure which has metal-oxo cages.¹⁰² Other considerable advantages have been noticed in using this kind of catalyst which is the high oxidative stability, in addition to the possibility of accessing to different simple structural types by changing either the stoichiometry or the pH of the reaction during their synthesis.¹⁰³ In this regard, phosphotungstic acid ($\text{H}_3\text{PW}_{12}\text{O}_{40}$) is considered as one of the most common

POMs and it is usually used as a catalyst, especially in hydrogen peroxide-based oxidations. A group of various structures formed from the degradation of the phosphotungstic acid during its interaction with the hydrogen peroxide and were detected by phosphorus NMR. One of the most important structure is the Venturello peroxoxometalate $[\text{PO}_4\{\text{WO}(\text{O}_2)_2\}_4]^{3-}$ which is identified and considered as the catalytically active species (Scheme 1).¹⁰⁴



Scheme 1 The degradation of $[\text{PW}_{12}\text{O}_{40}]^{3-}$ using H_2O_2 to form $[\text{PO}_4\{\text{WO}(\text{O}_2)_2\}_4]^{3-}$.

In addition to that, the choice of the cation can affect the catalytic properties, for example, the epoxidation reaction of lipophilic alkenes in an aqueous H_2O_2 by using phosphotungstate-functionalised IL in an amphipathic IL solution mixture which consists of $[\text{Bpy}]\text{BF}_4$ and $[\text{Dopy}]\text{BF}_4$. The IL-based catalytic system shown high activity, and efficient reusability.¹⁰⁵ Several transition metals have also been applied in order to increase activity and selectivity for sulfide oxidation.¹⁰⁶ The tungstate anion WO_4^{2-} has been shown to form a very effective species for the catalytic oxidation of sulfides as well as epoxidations of olefin (Scheme 2a)¹⁰⁷ and the oxidation of amines to nitrones (Scheme 2b).¹⁰⁸



Scheme 2 (a) Epoxidations of olefins and (b) Oxidation of secondary-amines.

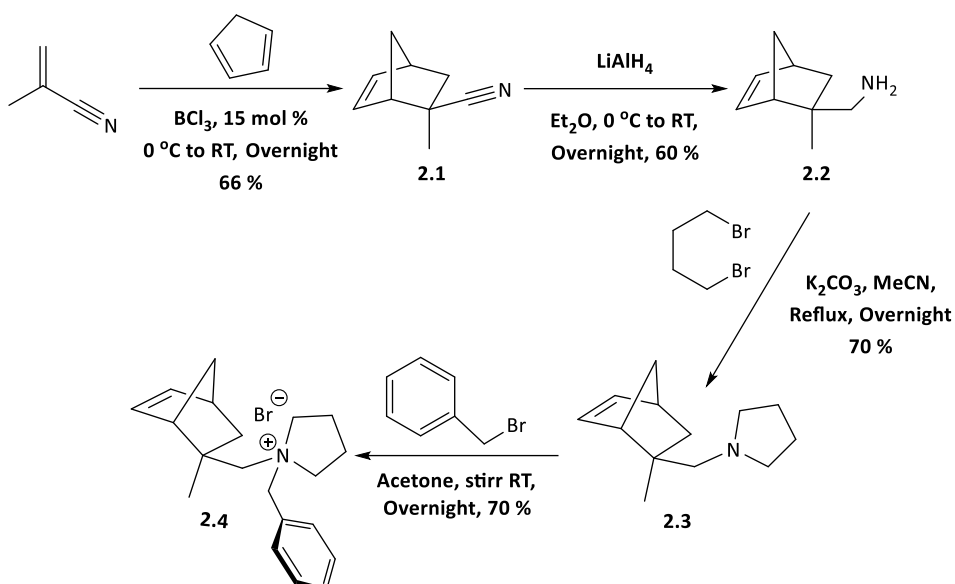
Due to the high activity and selectivity of tungstate and peroxoxometalate species, they have widely applied as combined catalytic systems consist of the catalyst based on catalytic active species and hydrogen peroxide.¹⁰⁹⁻¹¹² In this sense, hydrogen peroxide is considered to be a green and environmentally friendly, and economically oxidant as it is highly efficient and cheap, it has a high content of active oxygen and water is the only by-product. In 1998 Noyoroi was first to use an aqueous solution Na_2WO_4 and H_2O_2 as a homogeneous catalytic oxidation system.¹¹³ Although, this catalyst is considered to be a highly active and selective phase transfer catalyst,¹¹⁴ it still suffers from some drawbacks such as the difficulty of reuse and recycling. Hence the urgent need arose to stabilise the tungstate species onto a solid supporting such as mesoporous material,¹¹⁵ silica,¹¹⁶ polymers,¹¹⁷ or magnetic nanoparticles.¹¹⁸ Regarding the previous point of view, our project was to explore the possibility of loading the tungstate anion on a ROMP-derived cationic polymer to afford $[\text{WO}_4]^{-2}@\text{ROMP}$. The benefit from using ionic liquids in the supporting material design is to increase the stability of a catalyst and minimise tungstate anions leaching to the reaction solution or to the final product,^{119, 120} in addition to reducing the final product contamination with tungsten residues.¹²¹

2.2 Synthesis of Styrene Based Monomer

The Doherty group have previously used pyrrolidinium-tagged norbornene **2.4** as an IL-like monomer to prepare a PIILP support through ROMP (Scheme 3). The Diels-Alder cycloaddition between methacrylonitrile and freshly cracked cyclopentadiene catalysed by BCl_3 was conducted without solvent to give **2.1** as an 89:11 mixture of the *exo*- and

endo- diastereoisomers, respectively, as indicated by the integrals of the 3H singlets characteristic of methyl groups in the ^1H NMR spectrum of the adduct.¹²² As is reported in the literature the degree of diastereoselectivity is consistent with that observed in the BCl_3 -catalysed Diels-Alder reactions of methacrylonitrile.¹²³

The major diastereoisomer was the *endo*-isomer in which the larger nitrile group is pointing down from the norbornene ring as Schröder and co-workers suggested, which they claimed was due to favourable secondary orbital interactions between the HOMO of cyclopentadiene and the LUMO of methacrylonitrile. Due to the ease of pyrrolidinium bromide production, it was selected as an initial functional ionic liquid monomer; in addition, it is relatively straightforward to obtain different kind of counter anion by ion exchange. The unwanted β -elimination would be prevented by the quantisation of the pyrrolidine centre between the methyl group attached to the 2-position norbornene and benzyl group. We believe that the major isomer is, in fact, the *exo*-diastereoisomer with the nitrile group pointing up and away from the norbornene bicycle on the basis that the linear nature of the nitrile group prevents efficient HOMO-LUMO overlap in the *endo*-transition state. Referable to the larger nitrile group, which is coordinated to the large Lewis acid catalyst, the *exo*-transition state would be more favourable energetically due to the lower steric interaction as an outcome of looking away from the cyclopentadiene ring. The corresponding methylamine adduct **2.2** was obtained in 60 % yield by a reduction of **2.1** using lithium aluminium hydride. The base-mediated intramolecular dialkylation of compound **2.2** with 1,4-dibromobutane gave the desired pyrrolidine **2.3** in reasonable yield. This reaction was conducted under high dilution to limit the formation of dimers by intermolecular alkylation. The next step was the quaternisation of **2.3** with benzyl bromide in acetone to give the desired pyrrolidinium-based monomer **2.4**. Although, the synthesis of monomer **2.4** requires a linear four steps procedure each product was isolated in sufficiently high purity that column chromatography was not required (Scheme 3).

Scheme 3 Synthesis of pyrrolidinium-based monomer **2.4**.

These four synthesis steps to prepare monomer **2.4** are very simple in terms of cost reduction, whilst there is no need to use column chromatography for purification. Moreover, the synthetic approach described in (Scheme 3) is modular and highly versatile in that it will enable the norbornene unit to be functionalised through a judicious choice of dienophile used in the Diels-Alder reaction. On the other hand, the alkylation step could also be used to modify the architecture by altering the chain of dialkylbromide length or type. In addition to the possibility of produce a set of the Ionic Liquid library. The stereochemistry of monomer **2.4** was highly recommended to be *endo*-selective, due to the favourable interactions between secondary orbital (HOMO) of cyclopentadiene and (LUMO) of methacrylonitrile through the transition state formation reaction.¹²³ Despite this there are several reports that claim that the major product is the *exo*-diastereomer.¹²²

And because of all the above, it was necessary to undertake a single crystal X-ray structure determination of **2.4** (Figure 1) to determine precisely and unequivocally the stereochemistry of the final adduct; this is clear, the *exo*-isomer. The X-ray analysis was undertaken by Jack Ellison who was a member of the Doherty research group.

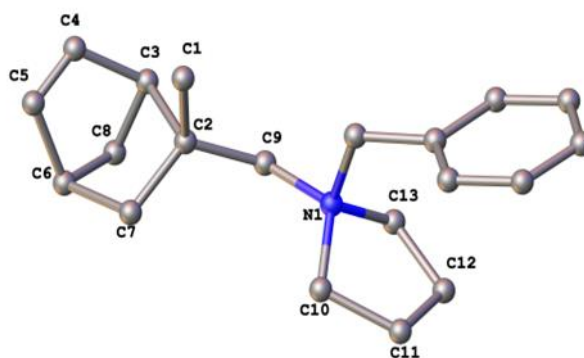
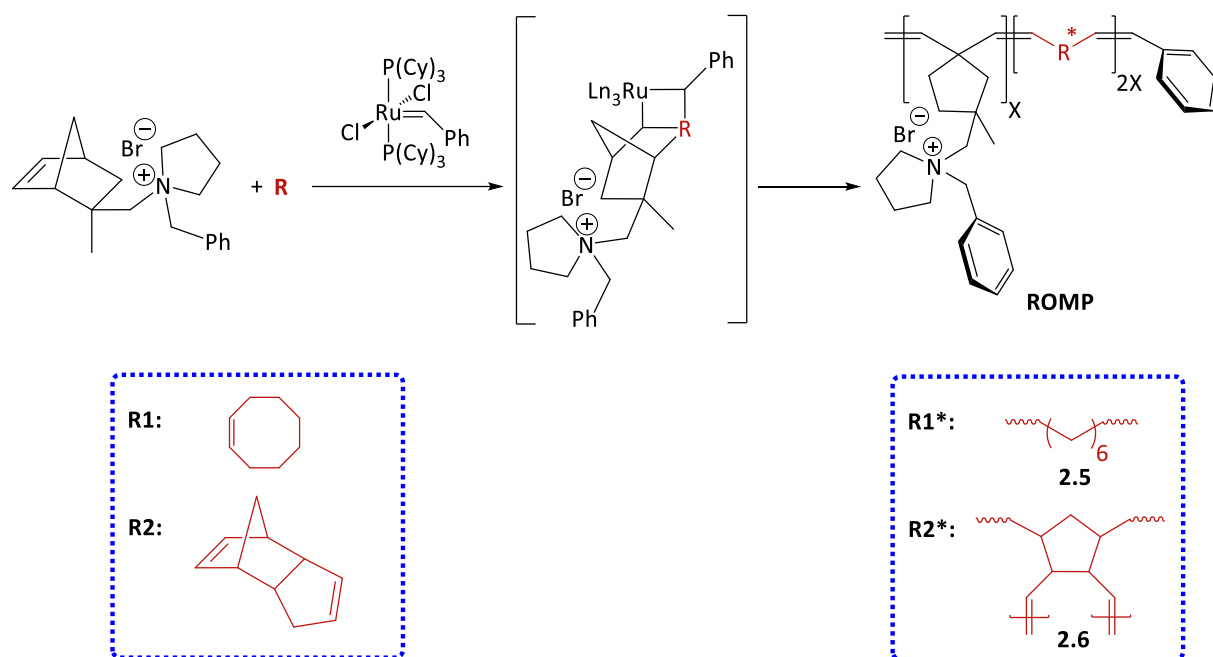


Figure 1 X-ray structure of 2.4 confirm the major stereoisomers is *exo*-isomer.¹

Monomer **2.4** was obtained in quite a good yield in each step of the synthesis, the minor product percentage was approximately 11% (determined by ¹H NMR), and as the major product in **2.4** was *exo*-isomer, it could be assumed that the same isomer would be the major product in **2.1**. As the nitrile group of methacrylonitrile is linear this would prevent the sufficient orbital overlapping between the (HOMO) and (LUMO) in the *endo*-transition state formation, therefore the thermodynamic drive to form the *endo*-isomer is sufficiently suppressed to favour formation of the *exo*-isomer as the major product.¹

2.3 Ring-Opening Polymerisation

Ring-opening metathesis polymerisation of monomer **2.4** with *cis*-cyclooctene afforded the target pyrrolidinium-based co-polymer **2.5** and afforded **2.6** when the *cis*-cyclooctene was replaced with dicyclopentadiene; both polymerisations were catalysed by the 1st generation Grubbs catalyst (Scheme 4).



Scheme 4 Synthesis of target pyrrolidinium-based polymers 2.5 and 2.6.

The reason behind using **2.4** co-monomer is the charged nature which would prevent the homo-polymerisation, so the producing of the undesirable soluble product would be also prevented, and this is what the study requires production an insoluble supporting material. In this study, two kinds of strained olefins were used as co-monomers in order to explore two different polymers, one has a linear alkyl spacer and another one has a cyclic alkyl spacer. In Ring-Opening Metathesis Polymerisation of **2.4** either with cis-cyclooctene or with dicyclopentadiene is catalysed by Grubbs 1st generation catalyst then followed by ruthenium end group removal from the chains of the polymer. We have chosen Grubbs 1st generation catalyst instead of the Grubbs 2nd generation to catalyse the ROMP due to its high activity towards the formation of linear polymers. An overnight polymerisation was carried out under mild conditions, the temperature was 40 °C in chloroform, followed by ethyl vinyl ether addition to quench and remove the active ruthenium carbene species from the chain.

Extraction with an aqueous solution of tris(hydroxymethyl)phosphine was employed to remove the cleaved ruthenium carbene. The *endo*-isomer form is less active with a different type of catalysts through the ROMP reaction.¹²⁴⁻¹²⁸ In this scene, some activity differences appeared as result of some steric effects of the reacting *endo*- form which could occur via one of three different modes (Figure 2).

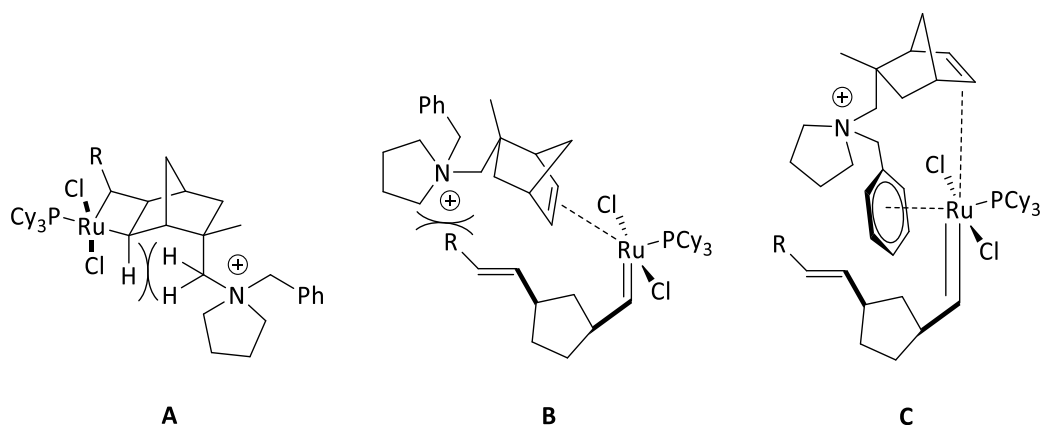


Figure 2 Three different modes of catalyst intermediates.

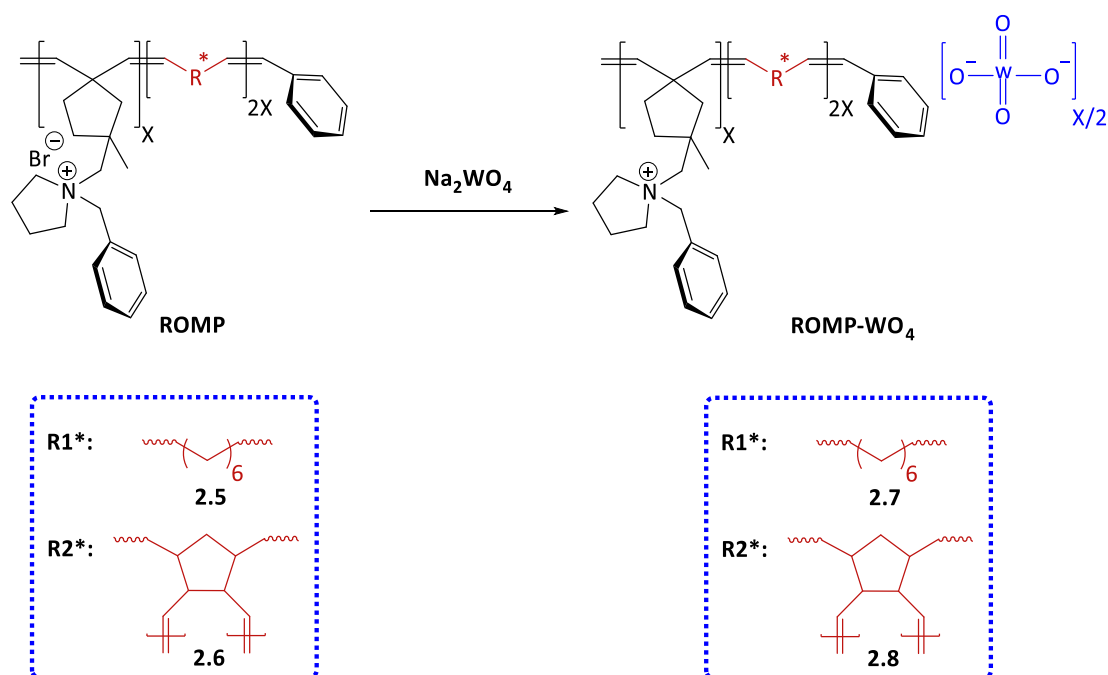
The rate-determining step of the ROMP reaction is metallacyclobutane ring formation. In this regard, (Figure 2A) also showed the protons steric interaction which may occur between the two protons the one on the newly formed sp^3 centre and a methylene proton of the ionic liquid group.^{129, 130} In the propagating step of ROMP, the propagated centre will coordinate with one of the favour places which is available on the site of cyclopentadiene terminal unit. While in (Figure 2B) the unfavourable interaction may occur between the polymer chain and the *endo*- group of the approaching substituted monomer.¹²⁶ Further deactivation affect the *endo*-isomer can happen during the chelate interactions where the ionic liquid species coordinates to the metal either during the initial metallacyclobutane intermediate ring opening or by the monomer approach as is shown in (Figure 2C).^{126, 131} From all mechanistic aspects that described previously, it can be assumed that the minor product (*endo*-form) of **2.4** monomer will be polymerised at a reduced rate in comparing with the *exo*-form producing, and as a result the percentage of the polymer produced from the *endo*-form would be negligible. However, due to the complexity of the ^1H and ^{13}C NMR polymer spectra, the determination of the *exo/endo* ratio would be complicated.

Pederson and co-workers have reported that the addition of ethyl vinyl ether quenched the polymerisation reaction, and the catalyst can be removed by extraction with an aqueous solution of tris(hydroxymethyl)phosphine. ICP-OES analysis showed that the content of ruthenium in the polymer was less than 0.001 wt % which was considered as evidence of the effectiveness of this protocol.¹ In spite of the efficiency of this method for the removal of the chain end ruthenium from the polymer other polymers produced

during the development of PIILP are likely to have different solubility, as evidenced by the water solubility of the imidazolium-based polymer developed by Dyson and co-workers; as such alternative methods of removing the Grubbs catalyst which does not employ an aqueous workup may well be required.¹

2.4 Immobilisation of Tungstate and Polyoxotungstate Species

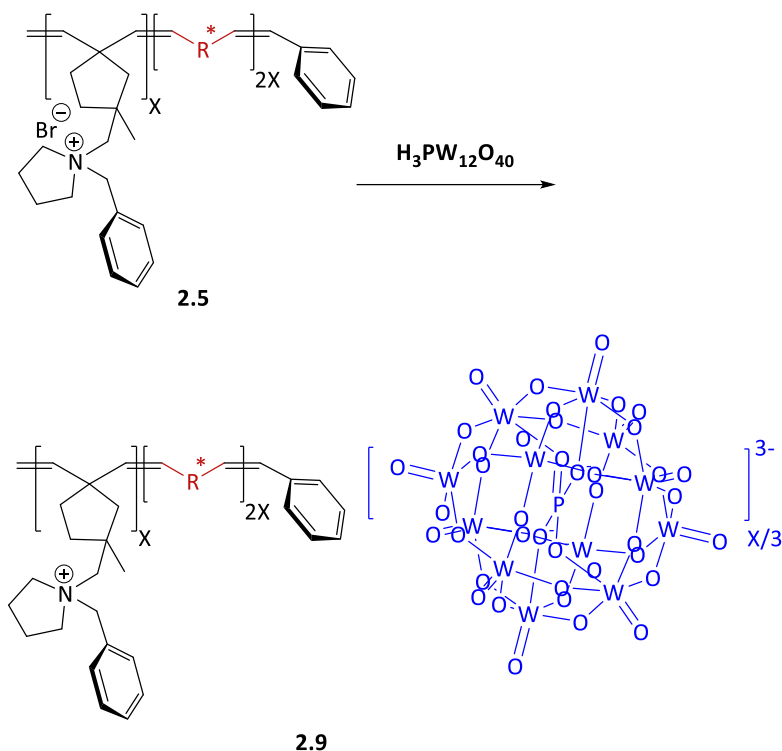
The heterogeneous tungstate-based catalyst **2.7** and **2.8** (Scheme 5) were prepared by stoichiometric exchange of the bromide anion with $[\text{WO}_4]^{-2}$; in both cases the catalyst precipitated as an off-white solid after the addition of an aqueous solution of sodium tungstate dihydrate to an ethanol suspension of polymer **2.5** or **2.6**; the product was isolated by filtration, washed with diethyl ether and dried to give an off-white powder.



Scheme 5 Synthesis of the heterogeneous tungstate-based catalyst 2.7 and 2.8.

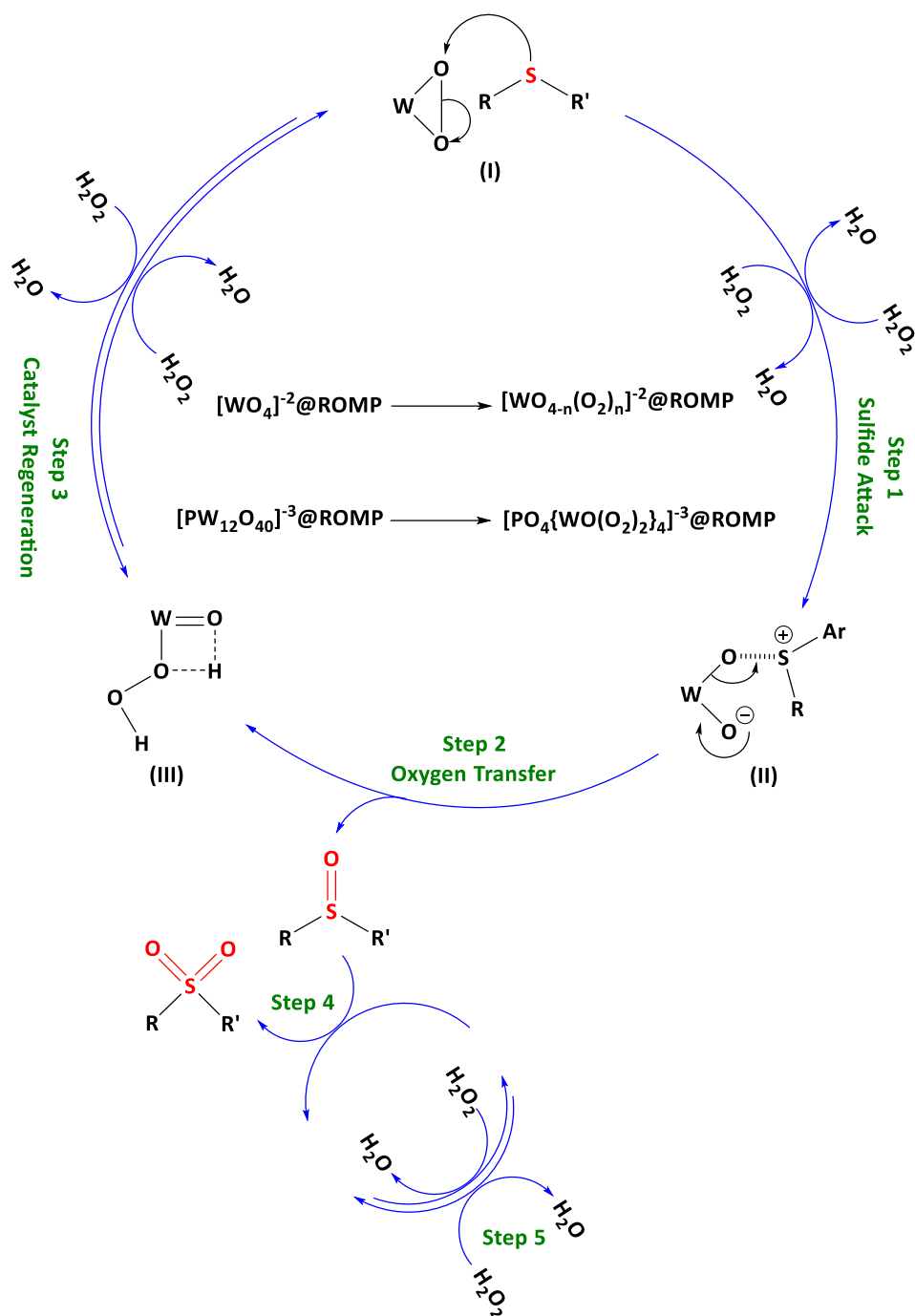
Another type of catalyst was prepared by using the Keggin phosphotungstic acid where the anion $[\text{PW}_{12}\text{O}_{40}]^{-3}$ formed and exchange with the bromide anions. Many studies refer to the Venturello peroxometalate as the active species for catalytic oxidations, however, there are reports that it suffers from decomposition in presence of H_2O_2 in the reaction media. For the purposes of overcoming this drawback, our group has worked on developing new catalyst system by immobilising $[\text{PW}_{12}\text{O}_{40}]^{-3}$ on the PIIL and generating the active Venturello peroxometalate $[\text{PO}_4\{\text{WO}(\text{O}_2)_2\}_4]^{3-}$ *in-situ* by treatment with

hydrogen peroxide immediately prior to addition of the substrate. Thus, pre-catalyst **2.9** was prepared by dissolving phosphotungstic acid in the minimum amount of water and stirring for half an hour at room temperature before transferring it to a solution of **2.5** in ethanol to afford **2.9** as an off-white solid which was isolated by filtration and dried under high vacuum (Scheme 6).¹



Scheme 6 Synthesis of the heterogeneous phosphotungstic acid-based pre-catalyst **2.9**.

The proposed mechanism for sulfoxidation catalysed by **2.9** is shown in (Scheme 7)¹³² and involves three major steps, the first is rate determining attack of sulfide at the tungsten activated peroxo in $[\text{PO}_4\{\text{WO}(\text{O}_2)_2\}_4]^{3-}$ @PIILP to afford **II**, the second is oxygen atom transfer to generate oxo-tungsten **III** via dissociation of sulfoxide and the third step regenerates the catalyst, between steps two and three there is a minor step based on conversion of sulfoxide to sulfone in presence of hydrogen peroxide. In this regard, the factors which could influence the catalyst efficiency would be possible to control via the accessibility of active site through immobilising the active species over the poly-ionic liquid, and this supporting material could be functionalised with a specific cross-linker.



Scheme 7 The proposed mechanism of sulfoxidation reaction by $\text{WO}_4@\text{ROMP}_x$, $\text{PW}_{12}\text{O}_{40}@\text{ROMP}_1$ as catalysts.

2.5 Experimental Studies on Optimisation of Sulfide Oxidation System Process Parameters

In recent years there has been a growing interest in the oxidation of sulfides to give the corresponding sulfoxide and sulfone, stimulated by applications as useful intermediates in several different transformations used in the pharmaceutical, agrochemical and fine chemicals industries¹³³⁻¹³⁶ as well as the synthesis of asymmetric chiral auxiliaries.^{134, 137, 138} In this regard, the hydrogen peroxide-mediated oxidation of a range of sulfides has previously been catalysed by tungstate species immobilised on IL-modified silica materials, poly-ionic liquid as well as embedded in meso-channels of SBA-15 and as such this reaction was deemed to be an ideal candidate with which to evaluate our new catalysts.¹¹⁵ Our group previous work were included using the Venturello peroxometalate catalytic active species anions which were preformed then supported on ROMP as $[\text{PO}_4\{\text{WO}(\text{O}_2)_2\}_4]^{3-}@\text{ROMP}_1$,⁵⁴ however, this project works on a comparative study with an *in-situ* generation version of Venturello peroxometalate from $\text{PW}_{12}\text{O}_{40}@\text{ROMP}_1$ (**2.9**), in addition to the new catalysts $\text{WO}_4@\text{ROMP}_x$ (**2.7**, **2.8**) (Figure 3).

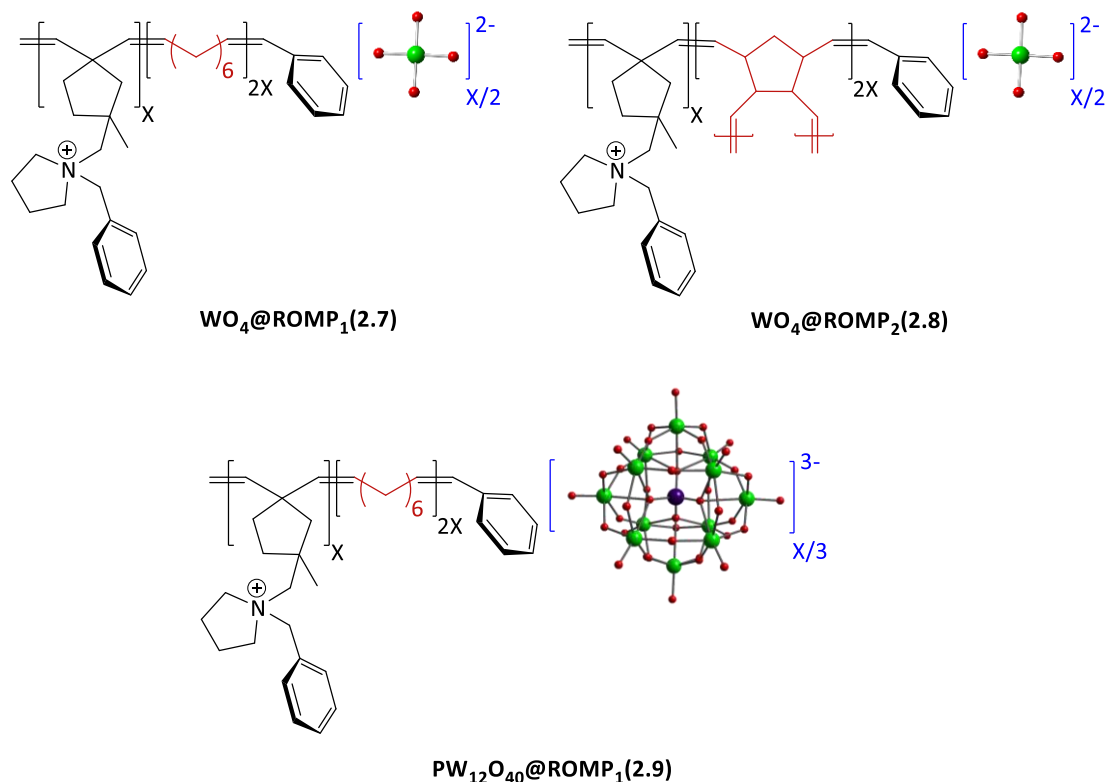


Figure 3 Tungstate and Polyoxotungstate Based-ROMP for the Catalytic Oxidation of Sulfides.

Thioanisole was selected for initial investigation due to its high boiling point and the distinct singlet in its ^1H NMR spectrum; this corresponds to the methyl group attached to sulfur and shifts downfield upon successive oxidation. This makes it possible to analyse reaction mixtures and quantify both conversion and selectivity using ^1H NMR spectroscopy based on an average of two runs (Figure 4).

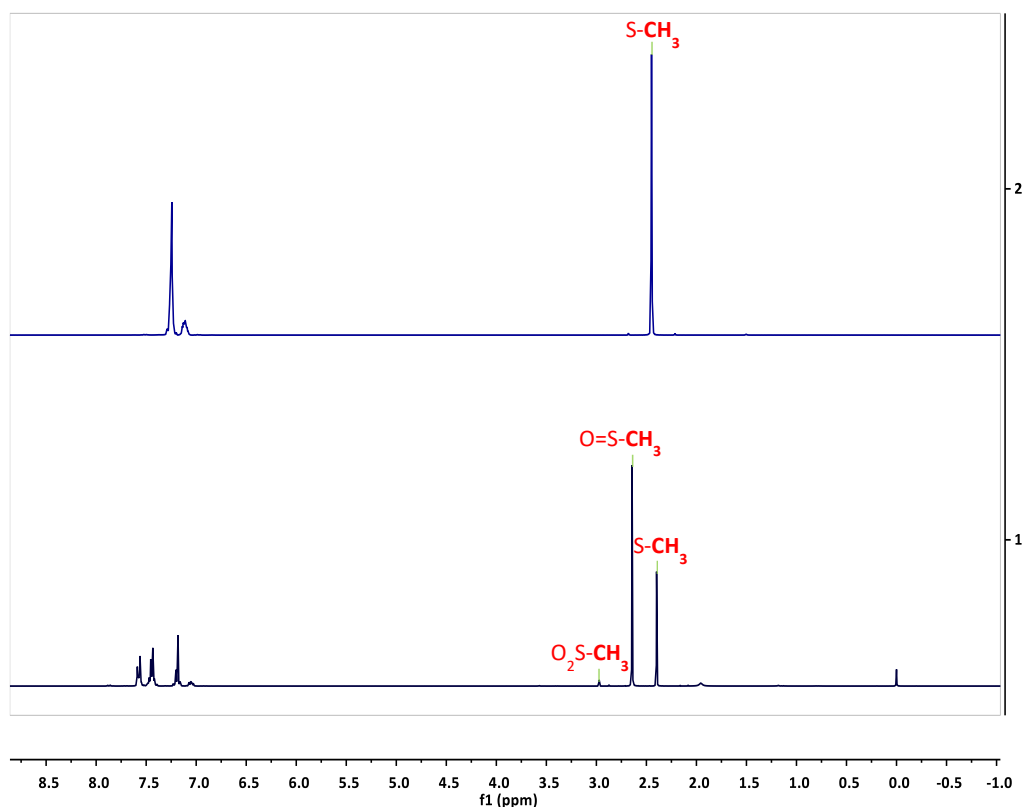
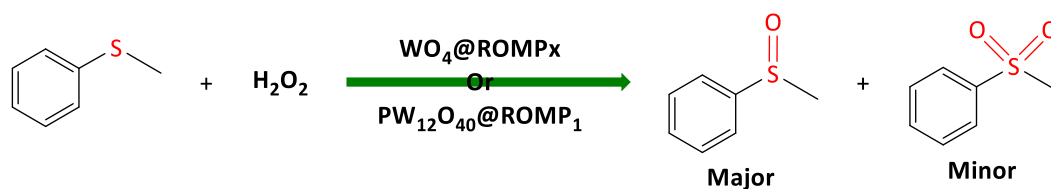


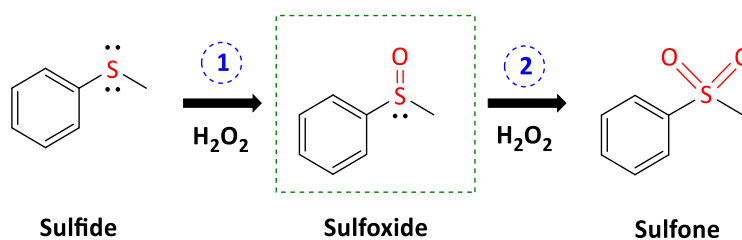
Figure 4 Stacked ^1H NMR spectra between thioanisole (purple) and sulfoxidation of thioanisole reaction mixture (navy).

The oxidation of thioanisole was conducted and the influence of hydrogen peroxide to substrate ratio and the reaction time and temperature were systematically investigated (Scheme 8).



Scheme 8 Typical oxidation of thioanisole with H_2O_2 catalysed by our prepared catalysts.

As sulfoxides and sulfones are both useful classes of compound, the conversion-selectivity profile was also monitored as a function of time and temperatures in methanol and acetonitrile using a catalyst loading of 0.3 mol % and a peroxide to substrate ratio of 2.5 with the aim of identifying optimum conditions for the formation of either methyl phenyl sulfoxide or sulfone.



Scheme 9 Typical reaction equation illustrating the two-oxidation steps of thioanisole with H_2O_2 .

The first oxidation to convert sulfide to sulfoxide is followed by the second oxidation to form sulfone. The objective of this project was to develop a robust catalyst that was selective for either product and to undertake comparative catalyst testing (Scheme 9).

2.5.1 Temperature Optimisation Studies

Sulfoxidations were carried out in two different solvents (methanol or acetonitrile) at a range of different temperatures starting from room temperature to 45 °C.

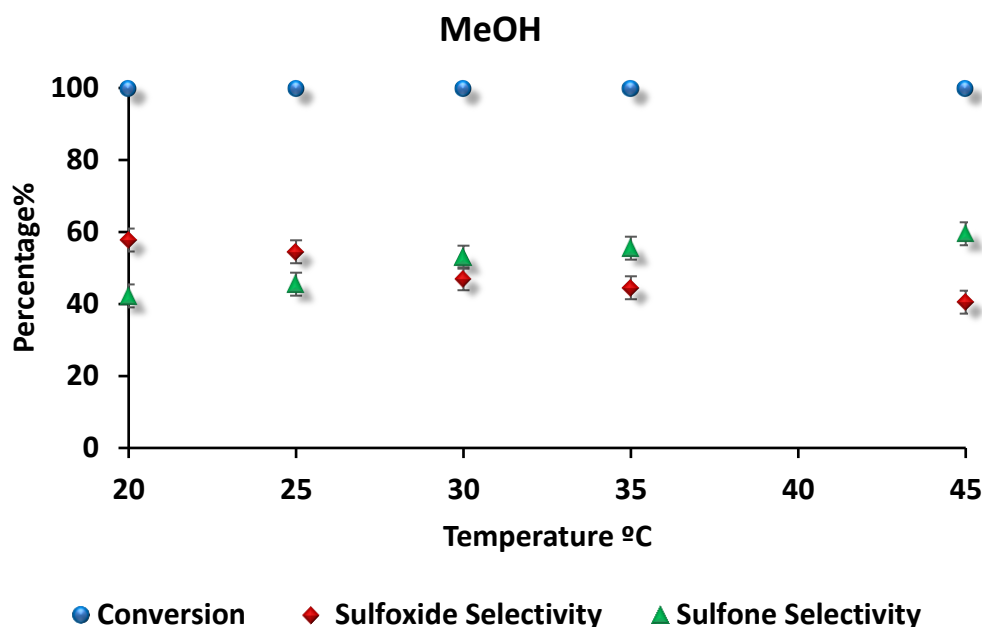


Figure 5 The Influence of temperature on conversion and selectivity for the oxidation of thioanisole catalysed by $\text{WO}_4\text{@ROMP}_1$.

Reaction conditions: 0.3 mol % catalyst; 1 mmol thioanisole; 3 mL methanol; 2.5 mmol of 35 % H_2O_2 ; 15 min; conversion measured by ^1H NMR (average of two runs); product selectivity = [% product / (% sulfoxide + % sulfone)].

Table 1 The Influence of temperature on conversion and selectivity for the oxidation of thioanisole in methanol catalysed by $\text{WO}_4\text{@ROMP}_1$ (average of two runs).

Temp. °C	%Conversion	%Sulfoxide Selectivity	%Sulfone Selectivity
20	100.0	56.5	43.5
25	100.0	54.5	45.5
30	100.0	47.0	53.0
35	100.0	44.5	55.5
45	100.0	40.5	59.5

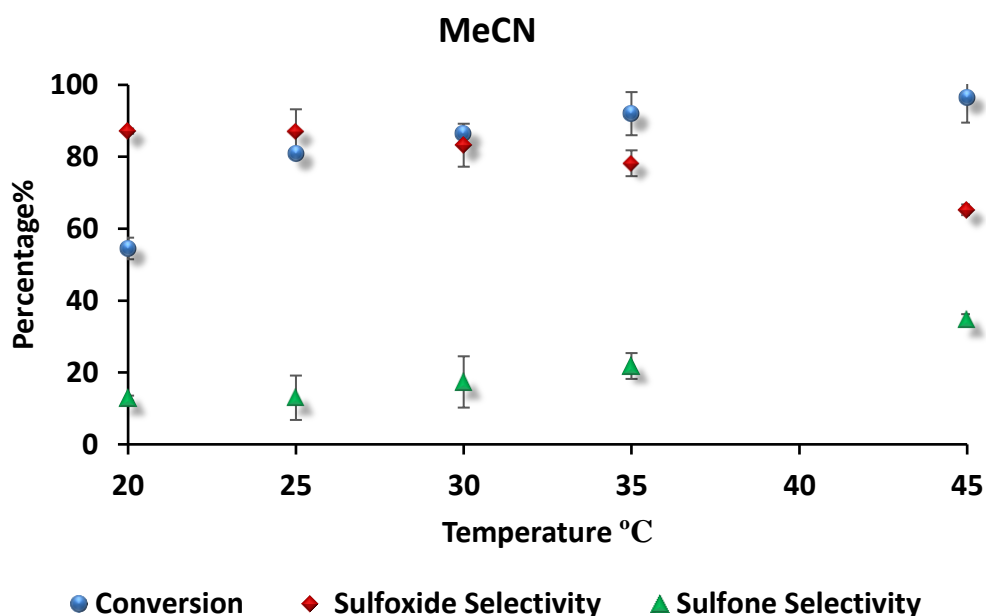


Figure 6 The Influence of temperature on conversion and selectivity for the oxidation of thioanisole catalysed by $\text{WO}_4\text{@ROMP}_1$.

Reaction conditions: 0.3 mol % catalyst; 1 mmol thioanisole; 3 mL acetonitrile; 2.5 mmol of 35 % H_2O_2 ; 15 min; conversion measured by ^1H NMR (average of two runs); product selectivity = [% product / (% sulfoxide + % sulfone)].

Table 2 The Influence of temperature on conversion and selectivity for the oxidation of thioanisole in acetonitrile catalysed by $\text{WO}_4\text{@ROMP}_1$ (average of two runs).

Temp. °C	%Conversion	%Sulfoxide Selectivity	%Sulfone Selectivity
20	54.5	87.1	12.9
25	81.0	87.0	13.0
30	86.5	83.2	17.4
35	92.0	78.2	21.8
45	96.0	65.3	34.7

The reaction is rapid and reaches completion when methanol is used as a solvent, whereas in acetonitrile the conversion gradually increases from 54.5 % at room temperature to 95 % at 45 °C. Varying the reaction temperature revealed that for both solvents the optimum selectivity for sulfoxide was obtained at 25 °C for a reaction time of 15 min. Moreover, selectivity for sulfoxide decreases as the temperature increases due to a second oxidation to sulfone. In this regard, selectivity for sulfone reached the maximum at 45 °C in methanol and at 30 °C in acetonitrile, details of which are shown in (Figures 5, and 6).

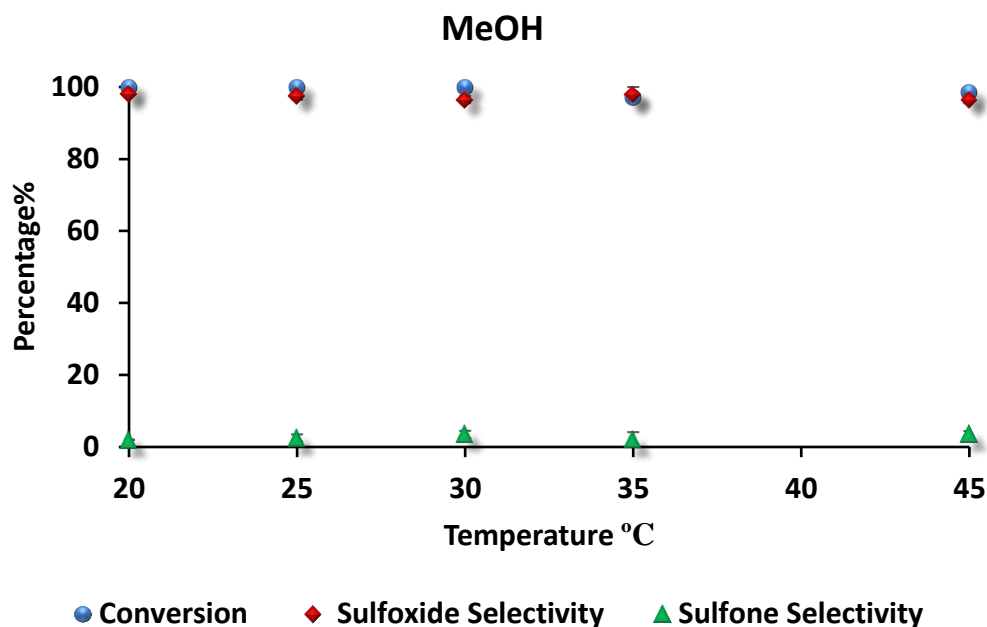


Figure 7 The Influence of temperature on conversion and selectivity for the oxidation of thioanisole catalysed by $PW_{12}O_{40}@ROMP_1$.

Reaction conditions: 0.3 mol % catalyst; 1 mmol thioanisole; 3 mL methanol; 2.5 mmol of 35 % H_2O_2 ; 15 min; conversion measured by 1H NMR (average of two runs); product selectivity = [% product / (% sulfoxide + % sulfone)].

Table 3 The Influence of temperature on conversion and selectivity for the oxidation of thioanisole in methanol catalysed by $PW_{12}O_{40}@ROMP_1$ (average of two runs).

Temp. °C	%Conversion	%Sulfoxide Selectivity	%Sulfone Selectivity
20	100.0	98.0	2.0
25	100.0	97.5	2.5
30	100.0	96.5	3.5
35	97.0	97.9	2.1
45	98.5	96.5	3.5

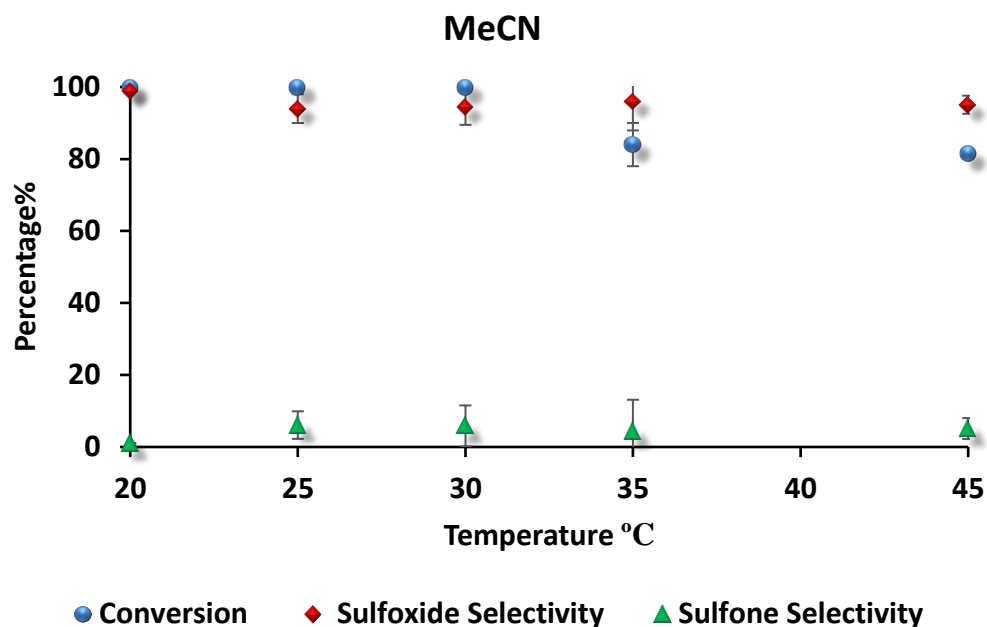


Figure 8 The Influence of temperature on conversion and selectivity for the oxidation of thioanisole catalysed by $PW_{12}O_{40}@ROMP_1$;

Reaction conditions: 0.3 mol % catalyst; 1 mmol thioanisole; 3 mL acetonitrile; 2.5 mmol of 35 % H_2O_2 ; 15 min; conversion measured by 1H NMR (average of two runs); product selectivity = [% product / (% sulfoxide + % sulfone)].

Table 4 The Influence of temperature on conversion and selectivity for the oxidation of thioanisole in acetonitrile catalysed by $PW_{12}O_{40}@ROMP_1$ (average of two runs).

Temp. °C	%Conversion	%Sulfoxide Selectivity	%Sulfone Selectivity
20	100.0	99.0	1.0
25	100.0	94.0	6.1
30	100.0	94.5	5.8
35	84.0	96.0	4.4
45	81.5	95.1	5.1

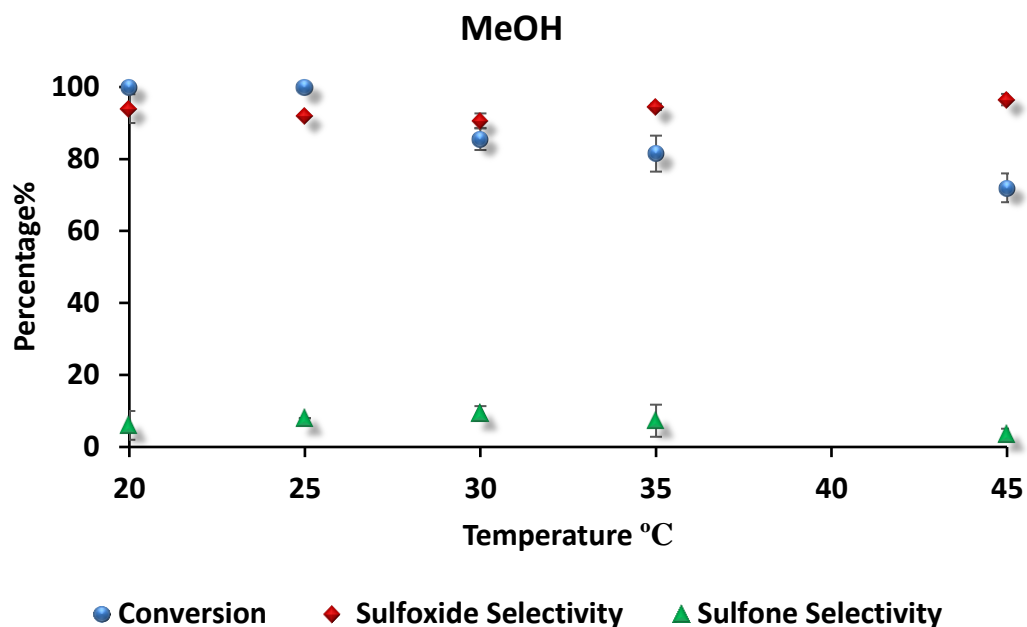


Figure 9 The Influence of temperature on conversion and selectivity for the oxidation of thioanisole catalysed by $\text{WO}_4\text{@ROMP}_2$.

Reaction conditions: 0.3 mol % catalyst; 1 mmol thioanisole; 3 mL methanol; 2.5 mmol of 35 % H_2O_2 ; 15 min; conversion measured by ^1H NMR (average of two runs); product selectivity = [% product / (% sulfoxide + % sulfone)].

Table 5 The Influence of temperature on conversion and selectivity for the oxidation of thioanisole in methanol catalysed by $\text{WO}_4\text{@ROMP}_2$ (average of two runs).

Temp. °C	%Conversion	%Sulfoxide Selectivity	%Sulfone Selectivity
20	100.0	94.0	6.0
25	100.0	92.0	8.0
30	85.5	90.7	9.3
35	81.5	94.5	7.3
45	72.0	96.5	3.5

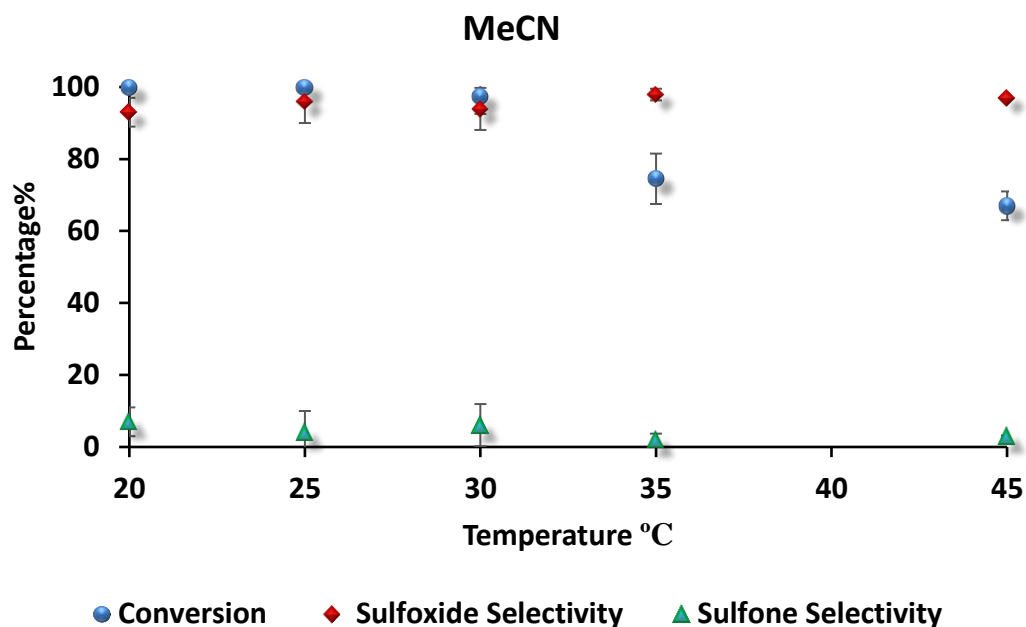


Figure 10 The Influence of temperature on conversion and selectivity for the oxidation of thioanisole catalysed by $\text{WO}_4@\text{ROMP}_2$.

Reaction conditions: 0.3 mol % catalyst; 1 mmol thioanisole; 3 mL acetonitrile; 2.5 mmol of 35 % H_2O_2 ; 15 min; conversion measured by ^1H NMR (average of two runs); product selectivity = [% product / (% sulfoxide + % sulfone)].

Table 6 The Influence of temperature on conversion and selectivity for the oxidation of thioanisole in acetonitrile catalysed by $\text{WO}_4@\text{ROMP}_2$ (average of two runs).

Temp. °C	%Conversion	%Sulfoxide Selectivity	%Sulfone Selectivity
20	100.0	93.0	7.0
25	100.0	96.0	4.0
30	97.5	93.9	6.1
35	74.5	97.9	2.1
45	67.0	97.1	2.9

From all the temperature profiles of the reactions which are catalysed by $\text{PW}_{12}\text{O}_{40}@\text{ROMP}_1$ or $\text{WO}_4@\text{ROMP}_2$ (Figure 7, 8, 9, and 10), both reactions reached 100% at room temperature and the selectivity also reached a maximum and stayed on the same level in methanol while it is slightly decreased in acetonitrile.

2.5.2 Time Optimisation Studies

The composition as a function of time shown using $\text{WO}_4\text{@ROMP}_1$ in (Figure 11) reveals that there is a dramatic decrease in selectivity from 94 % -22 % over 60 mins. For reactions conducted in methanol whereas there is only a slight drop in selectivity from 98 % - 81 % over the same time in acetonitrile.

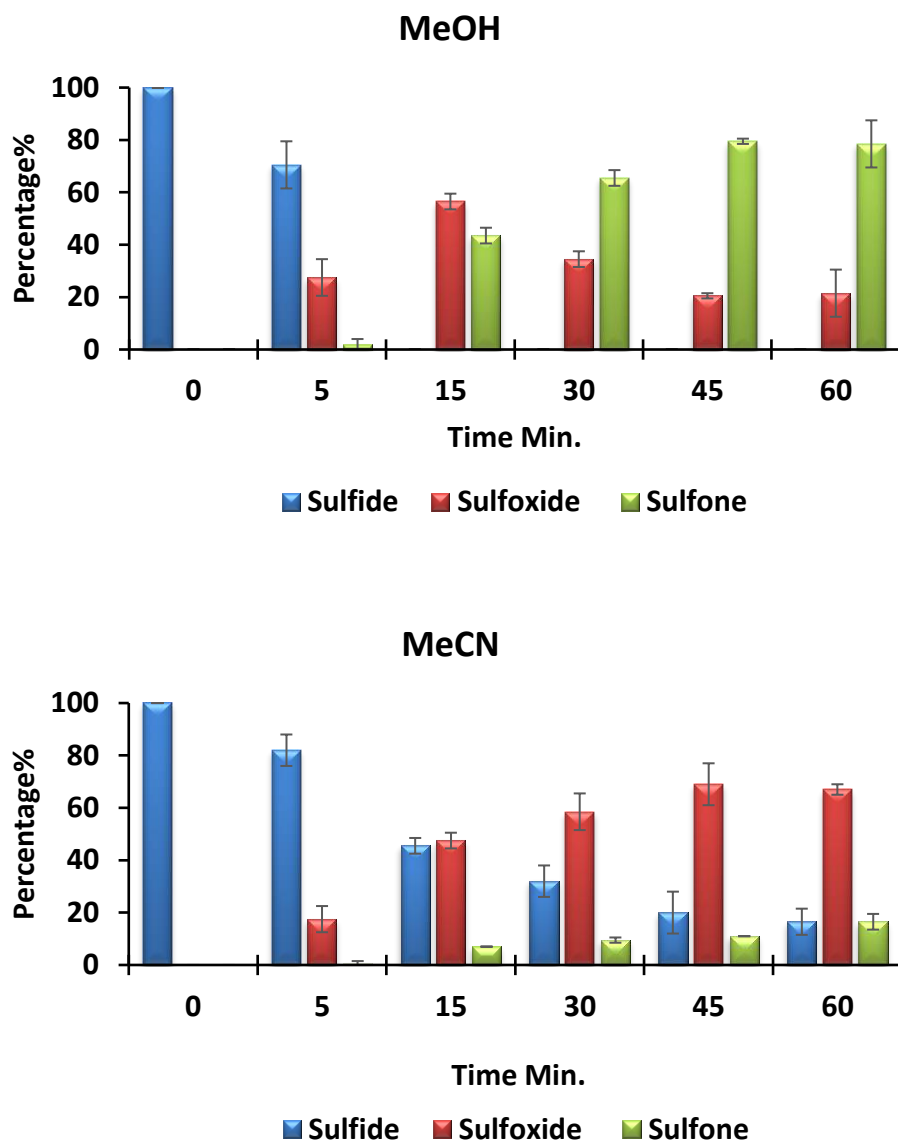


Figure 11 The influence of reaction time on the conversion of (sulfide, sulfoxide, and sulfone) in the oxidation of thioanisole catalysed by $\text{WO}_4\text{@ROMP}_1$.

Reaction conditions: 0.3 mol % catalyst; 1 mmol thioanisole; 3 mL solvent; 2.5 mmol of 35 % H_2O_2 ; rt; conversion measured by ^1H NMR (average of two runs); product selectivity = [% product / (% sulfoxide + % sulfone)].

Gratifyingly, complete conversion and high selectivity for sulfoxide were obtained in both methanol and acetonitrile after only 15 min with catalyst generated from $\text{PW}_{12}\text{O}_{40}@ \text{ROMP}_1$ (Figure 12); however, selectivity dropped at longer reaction times due to the formation of increasing amounts of sulfone.

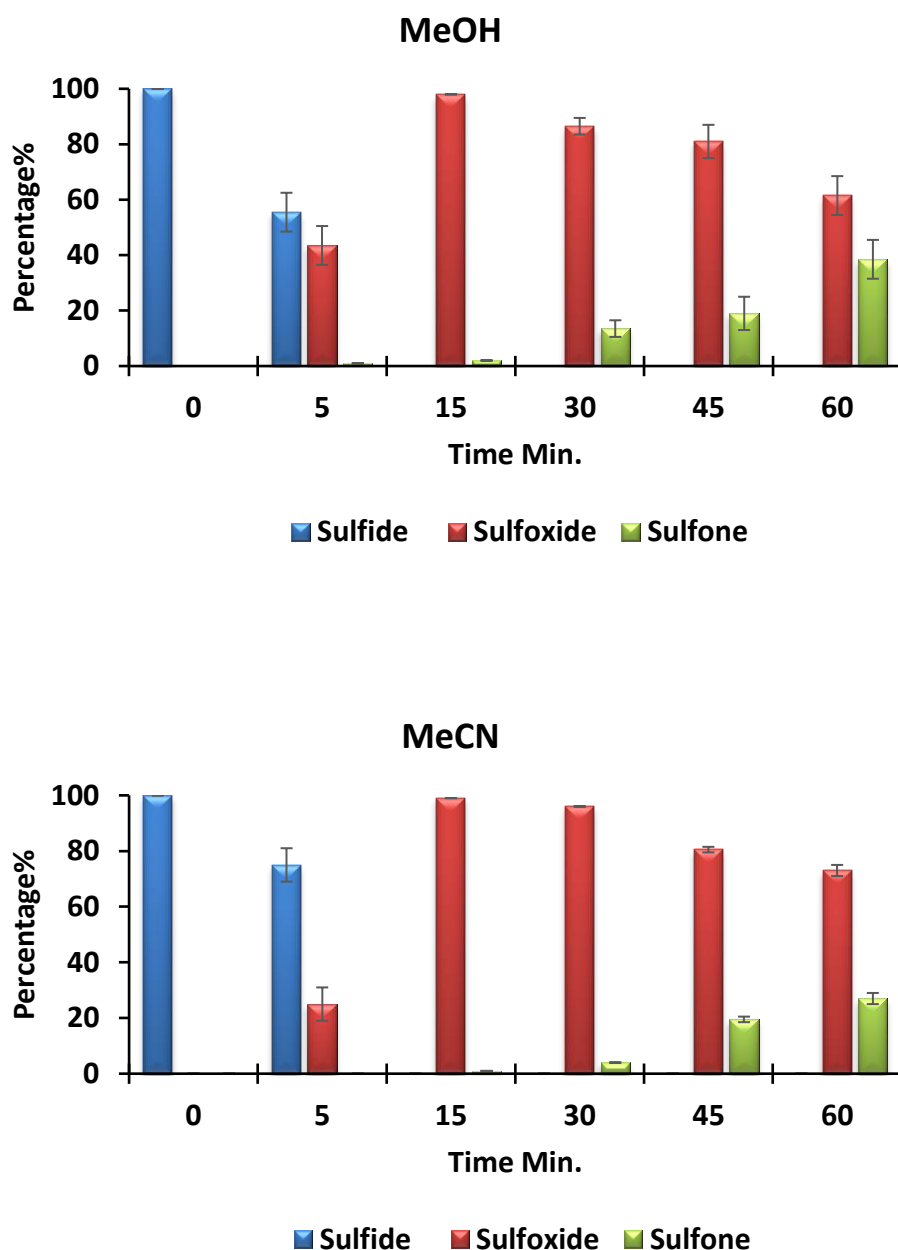


Figure 12 The Influence of reaction time on the conversion of (sulfide, sulfoxide, and sulfone) in the oxidation of thioanisole catalysed by $\text{PW}_{12}\text{O}_{40}@ \text{ROMP}_1$.

Reaction conditions: 0.3 mol % catalyst; 1 mmol thioanisole; 3 mL solvent; 2.5 mmol of 35 % H_2O_2 ; rt; conversion measured by ^1H NMR (average of two runs); product selectivity = [% product / (% sulfoxide + % sulfone)].

Similarly, $\text{WO}_4\text{@ROMP}_2$ gave complete conversion and high sulfoxide selectivity (Figure 13) in both methanol and acetonitrile up to 93 % after 15 min, and while the selectivities decreased at longer reaction times, this decrease was more dramatic in methanol.

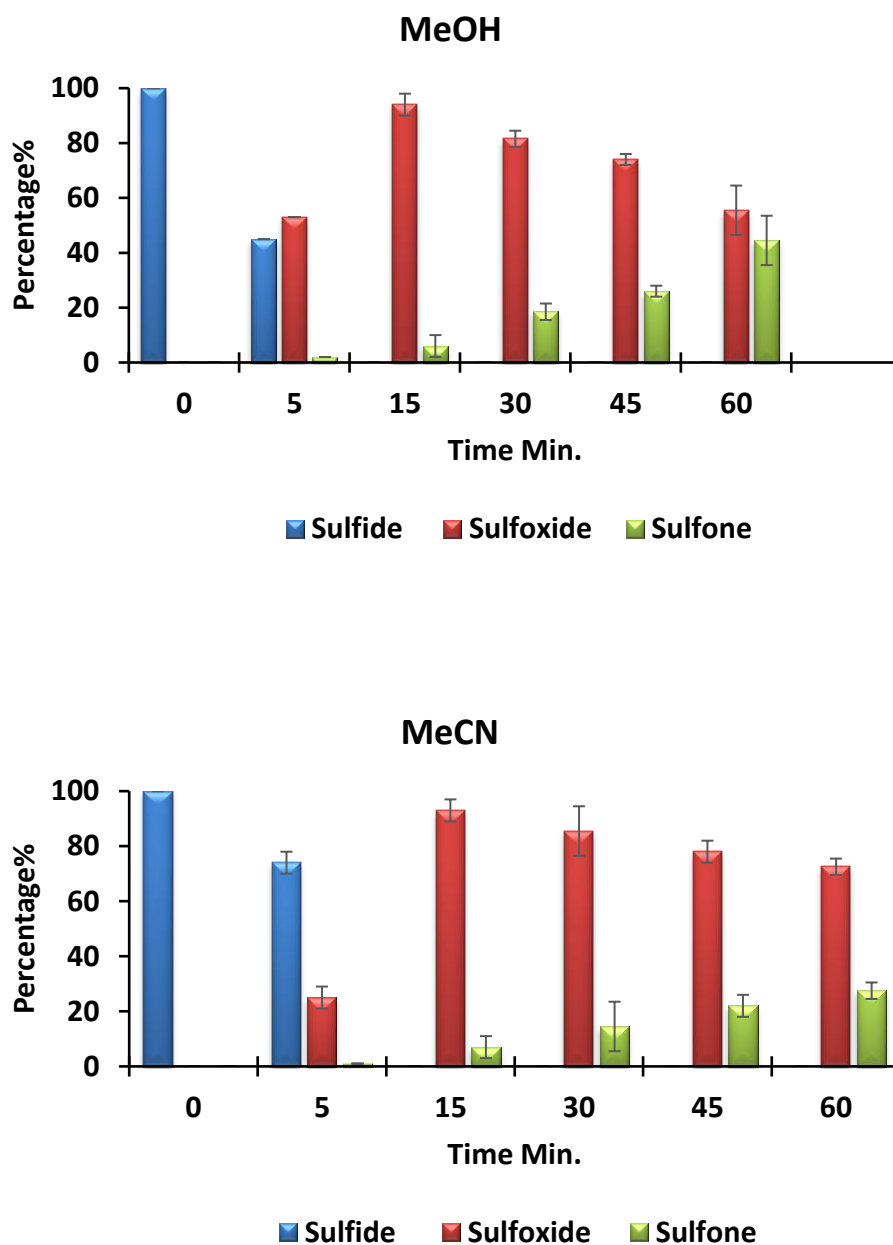


Figure 13 The Influence of reaction time on the conversion of (sulfide, sulfoxide, and sulfone) in the oxidation of thioanisole catalysed by $\text{WO}_4\text{@ROMP}_2$.

Reaction conditions: 0.3 mol % catalyst; 1 mmol thioanisole; 3 mL solvent; 2.5 mmol of 35 % H_2O_2 ; rt; conversion measured by ^1H NMR (average of two runs); product selectivity = [% product / (% sulfoxide + % sulfone)].

2.5.3 Hydrogen Peroxide Concentration Optimisation Studies

Initially, the effect of hydrogen peroxide on the selectivity of sulfoxidation was examined in both solvents (methanol and acetonitrile) by using 0.3 mol % of ROMP-based catalysts ($\text{WO}_4\text{@ROMP}_1$ (**2.7**), $\text{WO}_4\text{@ROMP}_2$ (**2.8**), $\text{PW}_{12}\text{O}_{40}\text{@ROMP}_1$ (**2.9**)) at room temperature and 15 minutes.

The behaviour of the reaction in terms of selectivity and effectiveness was different between methanol and acetonitrile when $\text{WO}_4\text{@ROMP}_1$ was used as a catalyst. A series of batch reactions were first conducted to explore the effect of the H_2O_2 : substrate ratio on selectivity in methanol and acetonitrile, details of which are shown in (Figures 14, and 15). In methanol, the best compromise of sulfoxide selectivity 57 % and conversion 100 % was achieved using a 0.3 mol % loading of $\text{WO}_4\text{@ROMP}_1$ with a H_2O_2 : S mole ratio of 2.5. In contrast, in acetonitrile, the highest sulfoxide selectivity of 87 % for the oxidation of thioanisole was obtained at 55 % conversion. Although, higher sulfoxide selectivities were obtained at lower H_2O_2 : S ratios, conversions were too low to be practical.

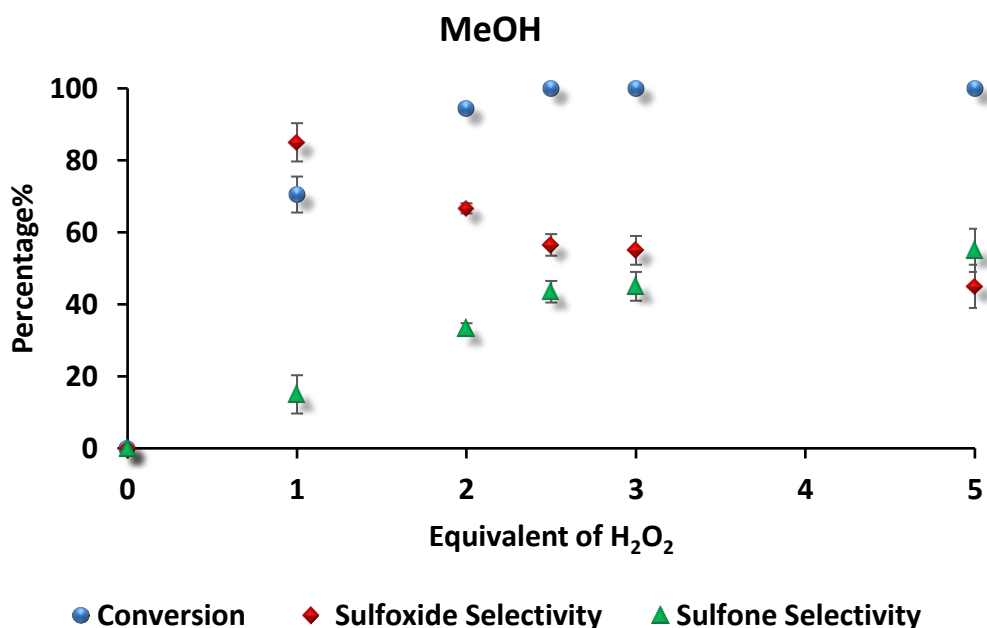


Figure 14 The Influence of hydrogen peroxide mole ratio on conversion and for the oxidation of thioanisole catalysed by $\text{WO}_4\text{@ROMP}_1$.

Reaction conditions: 0.3 mol % catalyst; 1 mmol thioanisole; 3 mL methanol; rt; 15 min; conversion measured by ^1H NMR (average of two runs); product selectivity = [% product / (% sulfoxide + % sulfone)].

Table 7 The Influence of hydrogen peroxide mole ratio on conversion and selectivity for the oxidation of thioanisole in methanol catalysed by $\text{WO}_4\text{@ROMP}_1$ (average of two runs).

H_2O_2 eq.	%Conversion	%Sulfoxide Selectivity	%Sulfone Selectivity
0	0.0	0.0	0.0
1	70.5	85.0	15.0
2	94.5	66.7	33.3
2.5	100.0	56.5	43.5
3	100.0	55.0	45.0
5	100.0	45.0	55.0

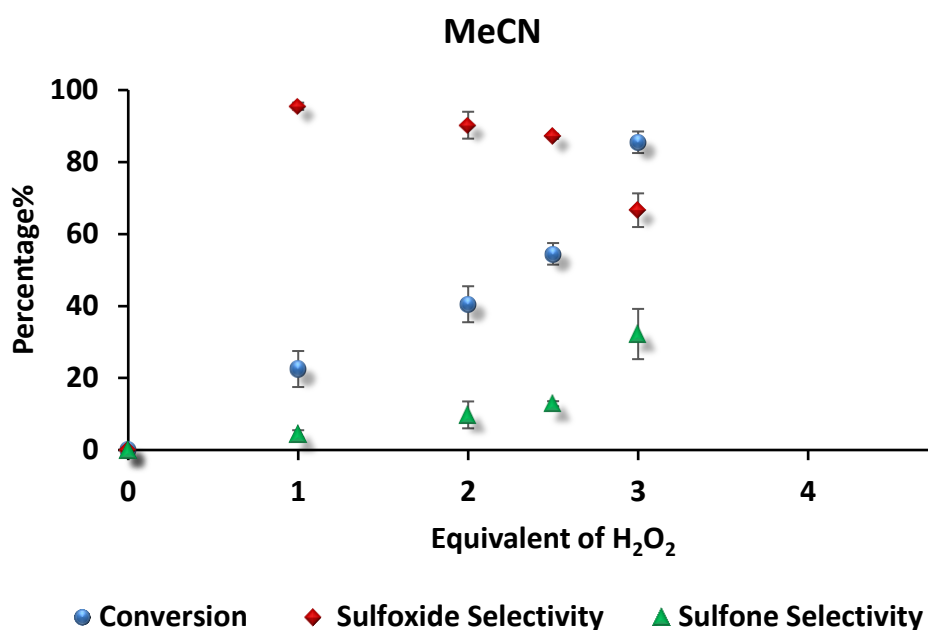


Figure 15 The Influence of hydrogen peroxide mole ratio on conversion and for the oxidation of thioanisole catalysed by $\text{WO}_4\text{@ROMP}_1$.

Reaction conditions: 0.3 mol % catalyst; 1 mmol thioanisole; 3 mL acetonitrile; rt; 15 min; conversion measured by ^1H NMR (average of two runs); product selectivity = [% product / (% sulfoxide + % sulfone)].

Table 8 The Influence of hydrogen peroxide mole ratio on conversion and selectivity for the oxidation of thioanisole in acetonitrile catalysed by $\text{WO}_4\text{@ROMP}_1$ (average of two runs).

H_2O_2 eq.	%Conversion	%Sulfoxide Selectivity	%Sulfone Selectivity
0	0.0	0.0	0.0
1	22.5	95.5	4.5
2	40.5	90.2	9.8
2.5	54.5	87.1	12.9
3	85.5	66.8	32.2
5	100.0	30.5	69.5

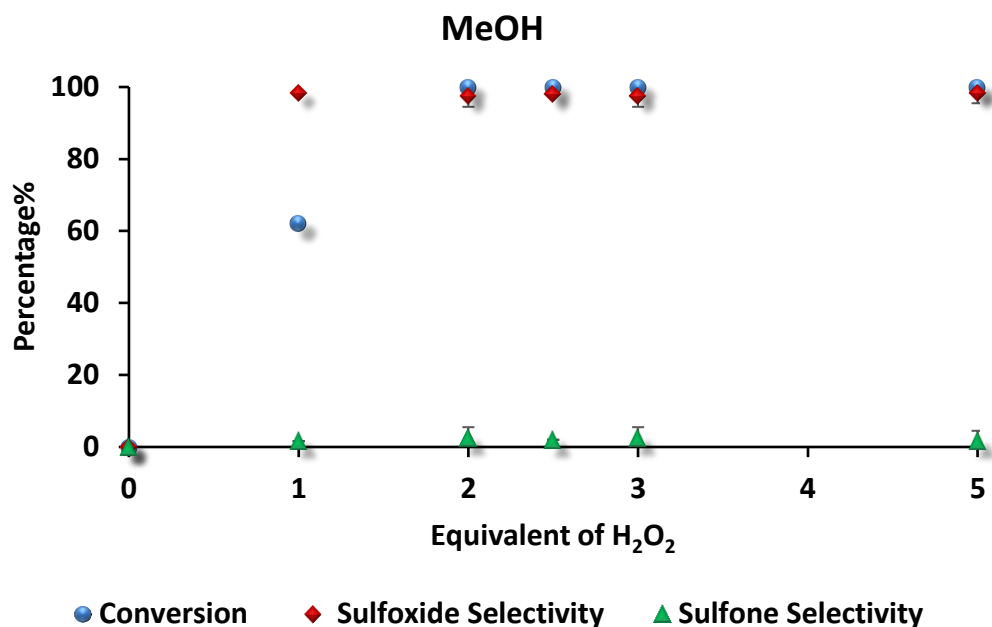


Figure 16 The Influence of hydrogen peroxide mole ratio on conversion and for the oxidation of thioanisole catalysed by $PW_{12}O_{40}@ROMP_1$.

Reaction conditions: 0.3 mol % catalyst; 1 mmol thioanisole; 3 mL methanol; rt; 15 min; conversion measured by 1H NMR (average of two runs); product selectivity = [% product / (% sulfoxide + % sulfone)].

Table 9 The Influence of hydrogen peroxide mole ratio on conversion and selectivity for the oxidation of thioanisole in methanol catalysed by $PW_{12}O_{40}@ROMP_1$ (average of two runs).

H ₂ O ₂ eq.	%Conversion	%Sulfoxide Selectivity	%Sulfone Selectivity
0	0.0	0.0	0.0
1	62.0	98.4	1.6
2	100.0	99.0	1.0
2.5	100.0	98.0	2.0
3	100.0	96.0	4.0
5	100.0	97.0	3.0

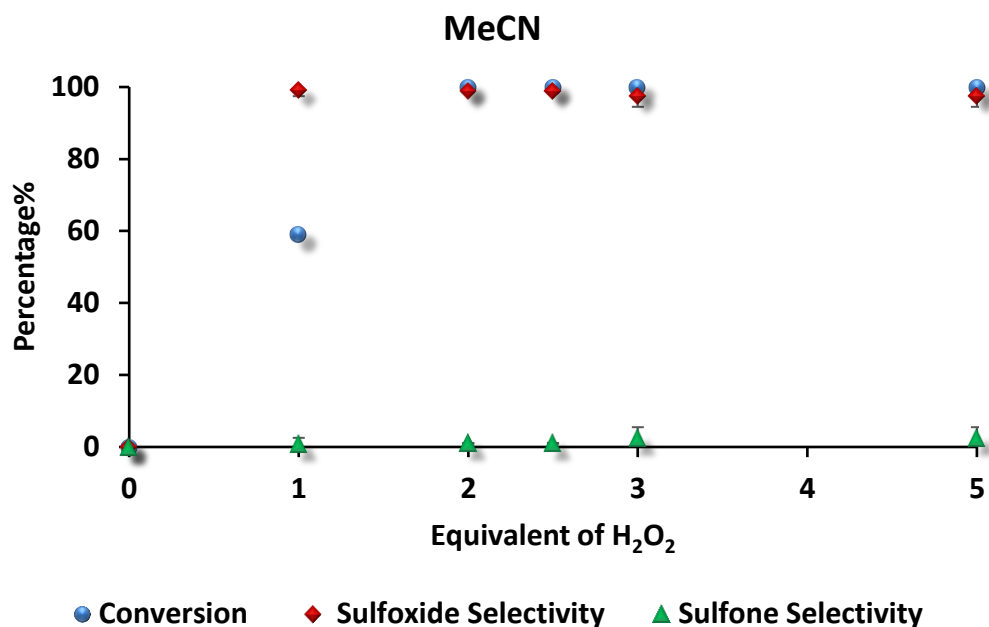


Figure 17 The Influence of hydrogen peroxide mole ratio on conversion and for the oxidation of thioanisole catalysed by $PW_{12}O_{40}@ROMP_1$.

Reaction conditions: 0.3 mol % catalyst; 1 mmol thioanisole; 3 mL acetonitrile; rt; 15 min; conversion measured by 1H NMR (average of two runs); product selectivity = [% product / (% sulfoxide + % sulfone)].

Table 10 The Influence of hydrogen peroxide mole ratio on conversion and selectivity for the oxidation of thioanisole in acetonitrile catalysed by $PW_{12}O_{40}@ROMP_1$ (average of two runs).

H ₂ O ₂ eq.	%Conversion	%Sulfoxide Selectivity	%Sulfone Selectivity
0	0.0	0.0	0.0
1	59.0	98.3	1.7
2	100.0	99.0	1.0
2.5	100.0	99.0	1.0
3	100.0	96.0	4.0
5	100.0	99.0	1.0

The results are shown in (Figures 16, and 17) reveals that complete conversion and a sulfoxide selectivity of 99 % can be achieved with $PW_{12}O_{40}@ROMP_1$ and two equivalents of hydrogen peroxide. Moreover, high sulfoxide selectivity is retained in both solvents even when the H₂O₂: S ratio is increased to five.

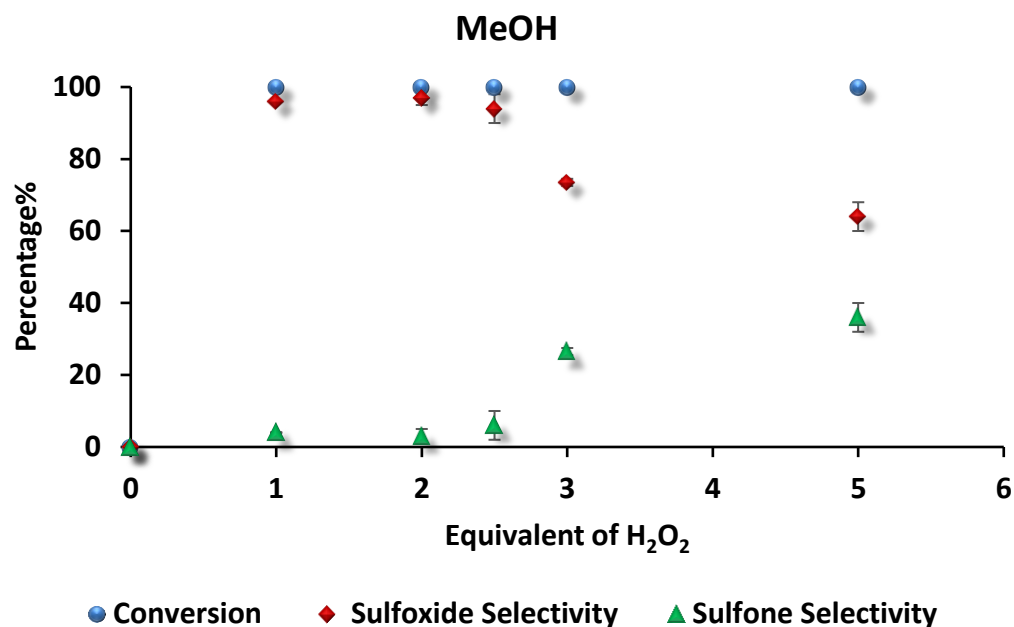


Figure 18 The Influence of hydrogen peroxide mole ratio on conversion and for the oxidation of thioanisole catalysed by WO₄@ROMP₂.

Reaction conditions: 0.3 mol % catalyst; 1 mmol thioanisole; 3 mL methanol; rt; 15 min; conversion measured by ¹H NMR (average of two runs); product selectivity = [% product / (% sulfoxide + % sulfone)].

Table 11 The Influence of hydrogen peroxide mole ratio on conversion and selectivity for the oxidation of thioanisole in methanol catalysed by WO₄@ROMP₂ (average of two runs).

H ₂ O ₂ eq.	%Conversion	%Sulfoxide Selectivity	%Sulfone Selectivity
0	0.0	0.0	0.0
1	100.0	96.0	4.0
2	100.0	97.0	3.0
2.5	100.0	94.0	6.0
3	100.0	73.5	26.5
5	100.0	64.0	36.0

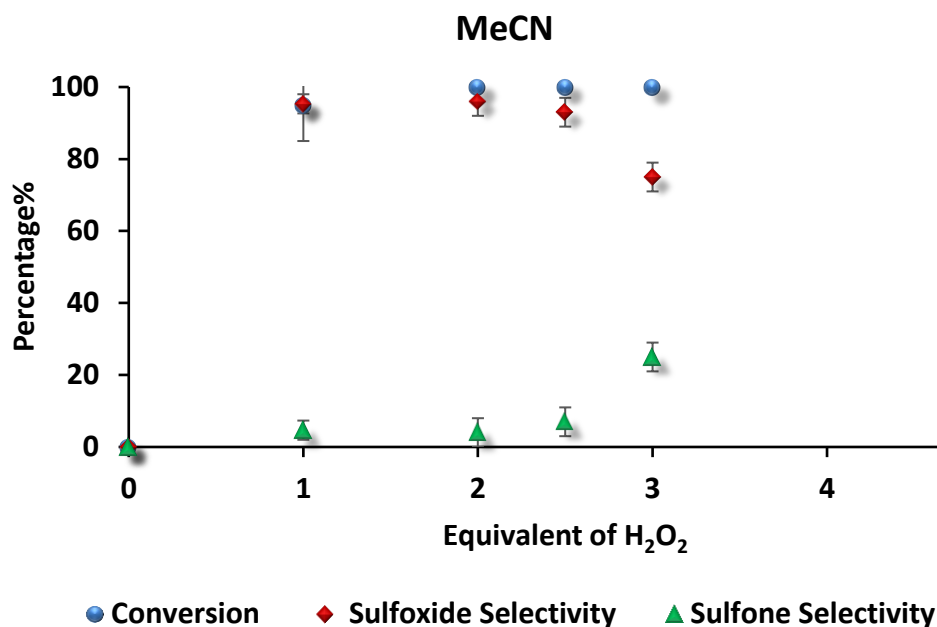


Figure 19 The Influence of hydrogen peroxide mole ratio on conversion and for the oxidation of thioanisole catalysed by WO₄@ROMP₂.

Reaction conditions: 0.3 mol % catalyst; 1 mmol thioanisole; 3 mL acetonitrile; rt; 15 min; conversion measured by ¹H NMR (average of two runs); product selectivity = [% product / (% sulfoxide + % sulfone)].

Table 12 The Influence of hydrogen peroxide mole ratio on conversion and selectivity for the oxidation of thioanisole in acetonitrile catalysed by WO₄@ROMP₂ (average of two runs).

H ₂ O ₂ eq.	%Conversion	%Sulfoxide Selectivity	%Sulfone Selectivity
0	0.0	0.0	0.0
1	95.0	95.3	4.7
2	100.0	96.0	4.0
2.5	100.0	93.0	7.0
3	100.0	75.0	25.0
5	100.0	80.0	20.0

Under the same conditions the sulfoxidation of thioanisole catalysed by WO₄@ROMP₂ reached complete conversion with 96 % selectivity for sulfoxide after 15 min with two equivalents of hydrogen peroxide, however, this decreased slightly to 75 % and 80 % with three and five equivalents, respectively, in the same time. For comparison, while the WO₄@ROMP₁ catalysed the oxidation of thioanisole reached completion with 2.5 equivalents of hydrogen peroxide in methanol, five equivalents of hydrogen peroxide were required for complete consumption of sulfide in acetonitrile, however, in both cases the sulfoxide selectivity was at best moderate (Tables 7 and 8). Regarding this, the

first oxidation reaction rate to convert sulfide to sulfoxide is faster than the second oxidation reaction rate to form sulfone from sulfoxide with both catalysts ($\text{PW}_{12}\text{O}_{40}@R\text{OMP}_1$, $\text{WO}_4@R\text{OMP}_2$) in both solvents (Scheme 8).

Earlier work undertaken in the Doherty group reported that immobilisation of the *pre-formed* active species, $[\text{PO}_4\{\text{WO}(\text{O}_2)_2\}_4]^{3-}$, on ROMP materials gives good yields and selectivity for the sulfoxidation of thioanisole to methyl phenyl sulfoxide. In MeOH (conversion 90 % and selectivity 88 %) is achievable at 0.5 mol %, however, the catalyst does not perform well in MeCN (68 % conversion and 65 % selectivity)⁵⁴. For comparison, this work demonstrates that immobilisation of the polyoxometallate precursor, $[\text{PW}_{12}\text{O}_{40}]^{3-}$, and generating $[\text{PO}_4\{\text{WO}(\text{O}_2)_2\}_4]^{3-}$ *in-situ* allows the sulfoxide products to be obtained in 99% selectivity at full conversion at catalyst loadings as low as 0.3 mol %. Furthermore, the catalyst also operates efficiently even on lowering the molar equivalents of the H_2O_2 oxidant to 2:1 with the substrate. On the other hand, if we compare our work with others where the tungstate or peroxotungstate anions are immobilised on modified silica containing IL¹¹⁵ or IL containing brushes¹³⁹ or Keggin heteropolycompounds¹⁴⁰, higher catalyst loadings, longer reaction times and/or higher temperatures were required to achieve similar performance.

As sulfones are also a useful class of compound, there is interest in generating these products in high yield and selectivity; this can be achieved either by increasing the mole ratio of hydrogen peroxide and/or raising the temperature and increasing the reaction time. A blank experiment conducted without catalyst gave no conversion under the same conditions and sulfide was recovered in quantitative yield; this clearly shows that either tungstate or phosphotungstate is required to achieve sulfide oxidation. Another blank experiment was run in order to investigate the effectiveness of the catalyst active species (WO_4^{2-} , $\text{PW}_{12}\text{O}_{40}^{3-}$), the oxidation reaction was conducted in the absence of the tungstate anion to determine its role in the catalytic system. ROMP_1 used to catalyse the reaction and the results were only a minor amount of sulfoxide (15 %) were observed when the reaction solvent was MeCN/water and (16 %) when the reaction was conducted in methanol at 30 °C; this indicates that the tungstate anion is required to catalyse sulfide oxidation.

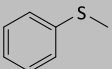
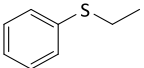
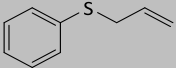
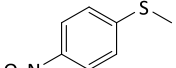
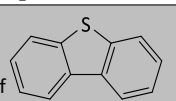
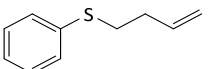
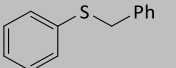
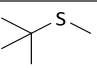
From the above optimisation studies, we have chosen a catalyst loading of 0.3 mol %, room temperature and a substrate: hydrogen peroxide ratio of 2.5 to undertake substrate screening in methanol and acetonitrile.

2.5.4 Sulfide Substrate Screening Studies

Due to the encouraging optimisation results for the sulfoxidation of thioanisole particularly with WO₄@ROMP₂ the oxidation of a range of alkyl and aryl alkyl sulfides was investigated under the optimum conditions described above. Gratifyingly, (Table 13) showing different range conversions and selectivity, which were obtained across the range of the examined substrates. The oxidation of allyl phenyl sulfide is less selective than the corresponding oxidation of homo allyl phenyl sulfide as the latter is more chemoselective towards sulfoxide 91 %. The moderate conversion of 74 % obtained for the WO₄@ROMP₁ catalysed sulfoxidation of dibenzothiophene (DBT) at 60 °C for 60 min (in methanol) is entirely consistent with the proposed electrophilic pathway due to the lower nucleophilicity of this substrate as well as previous reports that the rate of oxidation increases with increasing nucleophilicity of the sulfide.¹⁴¹

For comparison, there was no conversion of DBT in acetonitrile under the same conditions which may be due to the poor solubility of the substrate in acetonitrile. There is an obvious decrease in conversion with 4-nitrothioanisole (in acetonitrile) which may be caused by the strong electron withdrawing nitro group. In contrast, a conversion of 98 % was obtained in methanol.^{115, 142, 143} The results in (Table 13), clearly show that higher conversions were obtained in methanol (74 - 100 %) compared with acetonitrile (0 - 100 %).

Table 13 The sulfoxidation of sulfides to sulfoxides and sulfones with hydrogen peroxide catalysed by WO₄@ROMP₁

Entry	Substrate	Solvent	%Conv. ^b	%Sulfoxide ^b	%Sulfone ^b	Sulfoxide Selectivity ^{b,c}	Sulfone Selectivity ^{b,d}
1		CH ₃ CN	76	65	11	86	14
		CH ₃ OH	98	54	44	66	44
2		CH ₃ CN	67	60	7	90	10
		CH ₃ OH	98	54	44	55	45
3		CH ₃ CN	93	64	29	67	33
		CH ₃ OH	92	69	23	75	25
4		CH ₃ CN	29	26	3	90	10
		CH ₃ OH	98	30	68	31	69
5		CH ₃ CN	0	0	0	0	0
		CH ₃ OH	74	27	47	36	64
6		CH ₃ CN	57	52	5	91	09
		CH ₃ OH	97	59	38	61	39
7		CH ₃ CN	70	61	9	87	13
		CH ₃ OH	98	62	36	63	37
8		CH ₃ CN	100	82	18	82	18
		CH ₃ OH	100	73	27	73	27

^a **Reaction conditions:** 0.3 mol % catalyst; 1 mmol substrate; 3 mL solvent; 2.5 mmol of 35 % H₂O₂; ((3 mL) CH₃CN, 45 min) or ((3 mL) MeOH, 15 min) at rt.

^b Determined by ¹H NMR spectroscopy (average of two runs).

^c Sulfoxide selectivity = [% sulfoxide / (% sulfoxide + % sulfone)] × 100 %.

^d Sulfone selectivity = [% sulfone / (% sulfoxide + % sulfone)] × 100 %.

^f **Reaction conditions:** 0.3 mol % catalyst; 1 mmol substrate; 3 mL solvent; 2.5 mmol of 35 % H₂O₂; 60 °C, 60 min.

2.5.5 Recycle Studies

A series of recycling experiments were conducted using thioanisole to establish the efficacy of the catalyst as a function of its reuse. In a typical recycle experiment, when the reaction was completed, the catalyst was removed and isolated by centrifuge, washed with diethyl ether and reused again for another cycle by charging the reaction flask with more solvent and substrate.

The results in (Table 14) shown a dramatic reducing in the catalyst performance after the second cycle in terms of the percentages of conversion and the selectivity towards sulfone which may attribute to the high solubility of the WO₄@ROMP₁ in methanol.

Table 14 Comparative recycle studies for the sulfoxidation of thioanisole in methanol catalysed by $\text{WO}_4\text{@ROMP}_1$.

Run	%Conversion	% Sulfone Selectivity
1	100	90
2	65	18
3	42	2
4	16	0

Reaction conditions: 0.9 mol % catalyst; 3 mmol substrate; 9 mL methanol; 7.5 mmol of 35 % H_2O_2 ; rt; 45 min; conversion measured by ^1H NMR (average of two runs); product selectivity = [% product / (% sulfoxide + % sulfone)].

While, in acetonitrile (Table 15), the results did not show any significant decrease in the performance of the catalyst after six cycles in terms of the percentages of conversion and selectivity towards sulfoxide which may indicate that the tungstate active species is effectively stabilised on the ROMP.

Table 15 Comparative recycle studies for the sulfoxidation of thioanisole in acetonitrile catalysed by $\text{WO}_4\text{@ROMP}_1$.

Run	%Conversion	%Sulfoxide Selectivity
1	77	77
2	73	86
3	79	85
4	81	84
5	84	86
6	81	90
7	13	92
8	20	95

Reaction conditions: 0.9 mol % catalyst; 3 mmol substrate; 9 mL acetonitrile; 7.5 mmol of 35 % H_2O_2 ; rt; 60 min; conversion measured by ^1H NMR (average of two runs); product selectivity = [% product / (% sulfoxide + % sulfone)].

For comparison, the results of recycling experiments in acetonitrile and in methanol are shown in (Tables 14 and 15), the sulfoxide selectivity of thioanisole in acetonitrile increased from 77 – 95 % as a function of recycling while conversions decreased from 77 – 20 % after the 8th run (Table 15). In contrast, the catalyst recycled only very poorly in methanol as conversion and selectivity dropped quite dramatically after the first run (Table 14). We believe that the rapid drop in conversion for recycling sulfoxidations

reactions conducted in methanol is due to solubilisation and leaching of the tungstate during the catalyst recovery stage.

Table 16 Comparative recycle studies for the sulfoxidation of thioanisole in methanol catalysed by PW₁₂O₄₀@ROMP₁.

Run	%Conversion	%Sulfoxide Selectivity
1	100	98
2	89	82
3	37	78
4	17	94
5	21	100
6	20	100

Reaction conditions: 0.9 mol % catalyst; 3 mmol substrate; 9 mL methanol; 7.5 mmol of 35 % H₂O₂; rt; 15 min; conversion measured by ¹H NMR (average of two runs); product selectivity = [% product / (% sulfoxide + % sulfone)].

Table 17 Comparative recycle studies for the sulfoxidation of thioanisole in acetonitrile catalysed by PW₁₂O₄₀@ROMP₁.

Run	%Conversion	%Sulfoxide Selectivity
1	100	99
2	100	91
3	97	65
4	36	97
5	9	100
6	6	100

Reaction conditions: 0.9 mol % catalyst; 3 mmol substrate; 9 mL acetonitrile; 7.5 mmol of 35 % H₂O₂; rt; 15 min; conversion measured by ¹H NMR (average of two runs); product selectivity = [% product / (% sulfoxide + % sulfone)].

In comparison, recycle studies conducted under the same conditions with PW₁₂O₄₀@ROMP₁ resulted in a dramatic drop in conversion after the third recycle for reactions in both methanol and acetonitrile (Tables 16 and 17) conversion is dropped really quickly after third recycle.

Table 19 Comparative recycle studies for the sulfoxidation of thioanisole in methanol catalysed by WO₄@ROMP₂.

Run	%Conversion	%Sulfoxide Selectivity
1	100	96
2	97	99
3	91	97
4	88	98
5	81	100
6	82	100

Reaction conditions: 0.9 mol % catalyst; 3 mmol substrate; 9 mL methanol; 2.5 mmol of 35 % H₂O₂; rt; 15 min; conversion measured by ¹H NMR (average of two runs); product selectivity = [% product / (% sulfoxide + % sulfone)].

The results of recycling sulfoxidation experiments conducted with WO₄@ROMP₂ in methanol and acetonitrile are shown in (Tables 18 and 19) and surprisingly conversions dropped only very slowly in methanol over six runs 100 – 82 % and the selectivity remained high 96 – 100 %. On the other hand, conversions dropped quite dramatically after the 4th run for recycling reactions conducted in acetonitrile; this is in stark contrast to the corresponding recycle studies catalysed by WO₄@ROMP₁ which gave poor conversions even after the second run in methanol.

Table 18 Comparative recycle studies for the sulfoxidation of thioanisole in acetonitrile catalysed by WO₄@ROMP₂.

Run	%Conversion	%Sulfoxide Selectivity
1	100	92
2	83	88
3	81	89
4	79	92
5	23	96
6	21	90

Reaction conditions: 0.9 mol % catalyst; 3 mmol substrate; 9 mL acetonitrile; 2.5 mmol of 35 % H₂O₂; rt; 15 min; conversion measured by ¹H NMR (average of two runs); product selectivity = [% product / (% sulfoxide + % sulfone)].

Our preliminary evaluation and optimisation studies have shown that high selectivity for sulfoxide can be obtained through a judicious choice of solvent and reaction conditions, Moreover, recycle studies have shown that ROMP₂ is an effective support for tungstate-derived catalysts, for sulfoxidation in methanol.

Our catalysts have outperformed many of the heterogeneous systems published in literature especially regarding reaction conditions that are considered as mild conditions. For example, sulfoxidation reactions catalysed by peroxotungstate (VI) catalysts based on poly(acrylonitrile) $[W(O)_2(O_2)(CN)_2]$ -PAN (PANW) were conducted in aqueous media at room temperature for 35 min in methanol using 2 mole ratio of 30 % H_2O_2 . The authors report 72 % sulfoxide yield and 49 % with 1 molar equivalent, while when replacing methanol with acetonitrile, the reaction was slower, as more time was required to reach 67 % (45 minutes).¹⁴²

2.6 Characterisations Methods

2.6.1 Elemental Analysis (CHN)

Table 19 CHN analysis of the prepared materials.

Entry	Sample	%C	%H	%N
1	ROMP ₁	62.69	8.31	2.61
		62.75	8.41	2.67
2	WO ₄ @ROMP ₁	49.36	6.78	2.15
		49.44	6.90	2.23
3	PW ₁₂ O ₄₀ @ROMP ₁	33.18	4.61	1.31
		33.27	4.70	1.37
4	ROMP ₂	71.56	8.81	1.91
		71.43	8.88	1.97
5	WO ₄ @ROMP ₂	66.05	8.09	1.88

2.6.2 BET Surface Area Analysis

As the performance of the catalysts would be affected by the morphology and/or the porosity of the catalyst the Brunauer-Emmett-Teller (BET) method was used to measure the specific surface area from the adsorption curve and pore size distribution was measured by Barrett-Joyner-Halenda (BJH) method using the desorption curve. All samples were degassed at 90 °C for 30 hours prior to analysis.

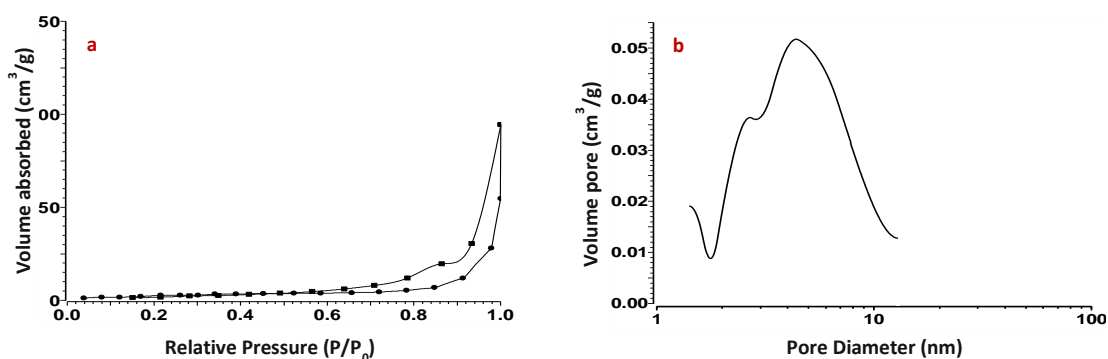


Figure 20 (a) Nitrogen adsorption-desorption isotherm profile, (b) Pore size distributions profile of ROMP₁.

The nitrogen adsorption varied considering the size and the shape of the anions and the structure of the ROMP, therefore, the pore size distribution would be varied also depending on the cations species size. In this regard, the nitrogen gas adsorption measurements would be detected the type of isotherm and the pore size which depends on the pore diameter where the micropores (pore diameter; < 2 nm), the mesopores (pore diameter; 2 ~ 50 nm), the macropores (pore diameter; > 50 nm). According to the nitrogen adsorption-desorption isotherms the specific surface area, pore size distributions, and total pore volume of the materials all increased after loading the ROMP-based support with tungstate or polyoxotungstate with the exception of WO₄@ROMP₁ (Table 20). Moreover, the isotherms for ROMP₁, PW₁₂O₄₀@ROMP₁, WO₄@ROMP₂ are type (IV) and the hysteresis loop is type H₃, while the isotherms for WO₄@ROMP₁, ROMP₂ are type (I) according to IUPAC.¹⁴⁴ In this regard, the material is classified as mesoporous if it is under type (IV) isotherm while it likely to be a microporous solid if its type (I).

Table 20 Specific surface and pore size distributions of the prepared materials.

Entry	Sample	Specific Surface Area (m ² /g)	Maximum Diameter (nm)	Average Diameter (nm)
1	ROMP ₁	10.75	3.13	14.99
2	WO ₄ @ROMP ₁	3.02	-	-
3	PW ₁₂ O ₄₀ @ROMP ₁	36.5	8.33	9.99
4	ROMP ₂	9.07	-	-
5	WO ₄ @ROMP ₂	30.65	-	14.99

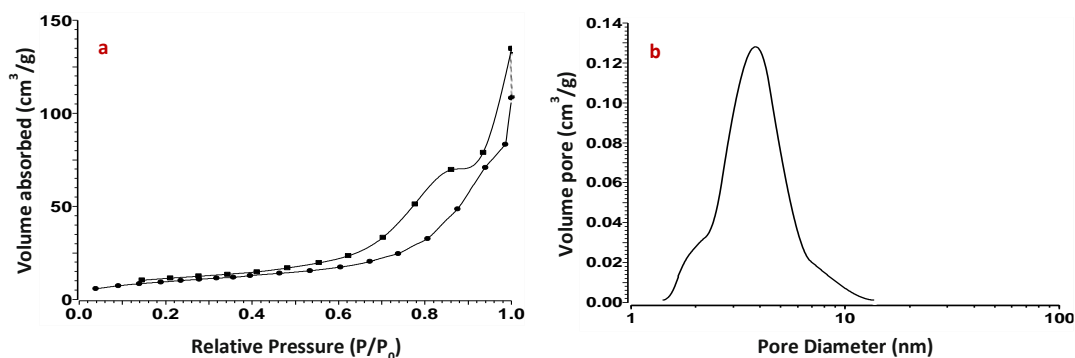


Figure 21(a) Nitrogen adsorption–desorption isotherm profile, (b) Pore size distributions profile of $PW_{12}O_{40}@ROMP_1$.

*See **Appendices** for all Nitrogen adsorption–desorption isotherm profiles and pore size distributions profiles traces.

2.6.3 Solid-State Nuclear Magnetic Resonance (SSNMR)

$PW_{12}O_{40}@ROMP_1$ was analysed by solid-state ^{31}P NMR spectroscopy. (Figure 22) shows a large peak at δ -11.97 ppm which can be assigned to the $[PW_{12}O_{40}]^{3-}@ROMP$. On comparison with the literature, the parent $H_3[PW_{12}O_{40}]$ has been reported at approximately δ -15¹⁴⁵, small shifts in the polymer immobilised material may well be due to interactions between the phosphorus and the cationic support, which suggests successful loading of the polymer with the phosphotungstate. The absence of peaks in the area between δ -5 and -10 suggest that no decomposition into the $[PO_4\{WO(O_2)_2\}_4]^{3-}$ species has occurred. In comparison with previous work in the Doherty/Knight group, in which the *pre-formed* $[PO_4\{WO(O_2)_2\}_4]^{3-}$ species was immobilised on ROMP, there is clear evidence of residual $H_3[PW_{12}O_{40}]$ and the decomposition product (Figure 23).¹

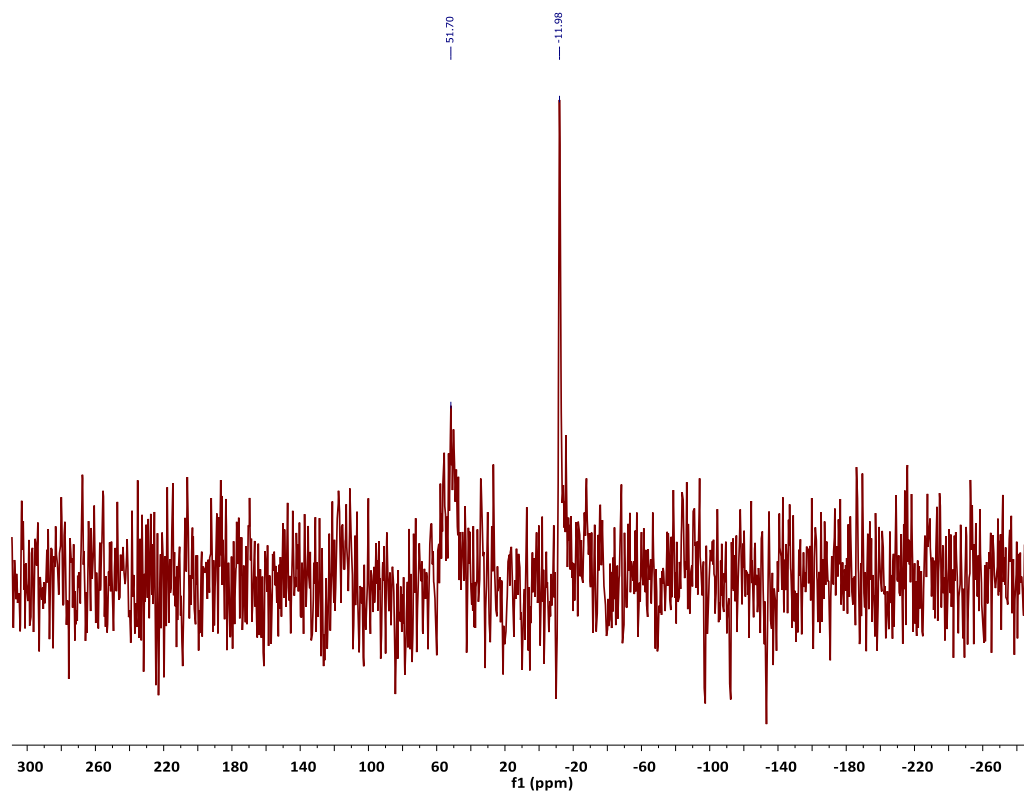


Figure 22 Solid-state ^{31}P NMR of $\text{PW}_{12}\text{O}_{40}@ROMP_1$.

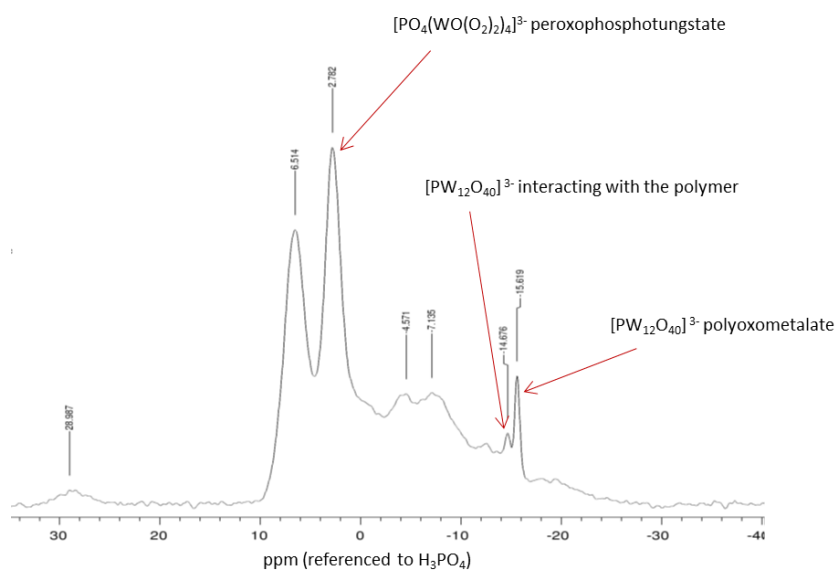


Figure 23 Solid-state ^{31}P NMR of $[\text{PO}_4(\text{WO}(\text{O}_2)_2)_4]^{3-}@ROMP_1$.¹

*See **Appendices** for all (SSNMR&NMR) spectrum traces.

2.6.4 Infrared Radiation (FT-IR)

The fresh catalysts were characterised by FT-IR and are shown in (Figure 24), which contain characteristic bands at 1077 cm^{-1} attributed to ν (P-O) stretching, a band at 974 cm^{-1} for ν (W=O), bands at 893 cm^{-1} , 803 cm^{-1} for O-O, and $900\text{--}725\text{ cm}^{-1}$ for ν (W-O-W). In addition bands at 595 cm^{-1} and 508 cm^{-1} were attributed to ν (W-O-O) symmetric and asymmetric vibrations for $\text{PW}_{12}\text{O}_{40}@ROMP_1$ catalyst.^{105, 146}

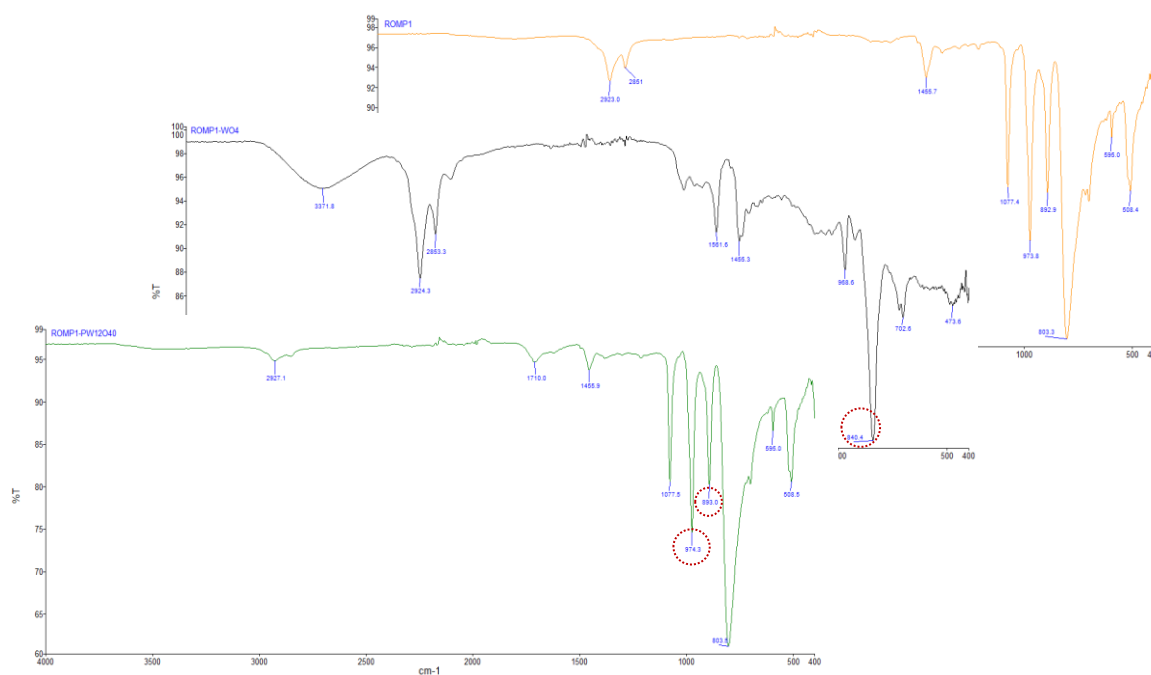


Figure 24 FT-IR of (a) ROMP_1 , (b) $\text{WO}_4@\text{ROMP}_1$, and (c) $\text{PW}_{12}\text{O}_{40}@\text{ROMP}_1$.

The new peaks in (Figure 25) appeared in $\text{WO}_4@\text{ROMP}_2$ at 827 cm^{-1} which confirmed the presence of (W=O) and successful exchange of bromide for tungstate on the ROMP based PIIL.

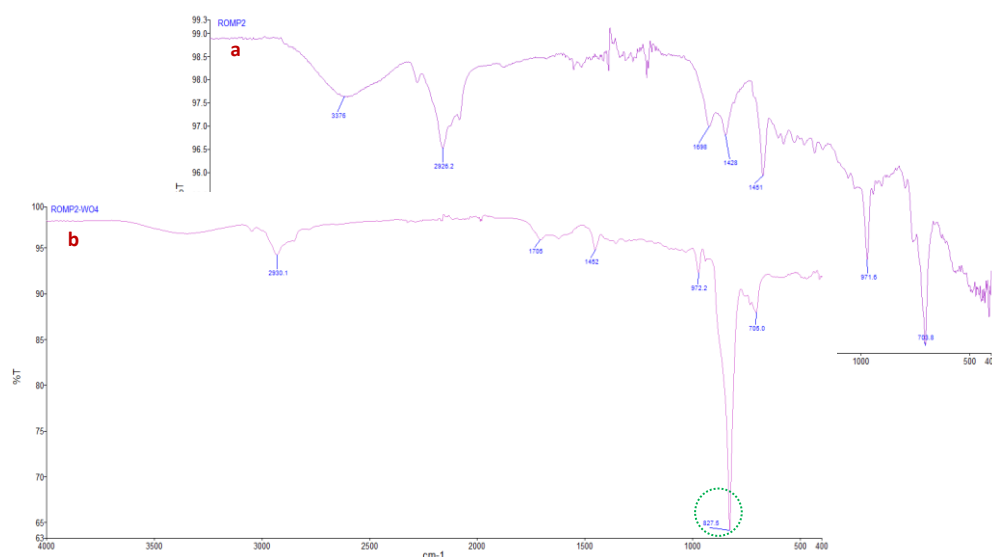


Figure 25 FT-IR of (a) ROMP₂, and (b) WO₄@ROMP₂.

2.6.5 Scanning Electron Microscope (SEM)

Further investigation was carried out on the morphology of both the polymers and their loaded materials by scanning electron microscopy (SEM).

SEM images of ROMP₁ (Figure 26) show different images with a range of size distributions. The pore diameter was in a good agreement with the result obtained by BET (Table 20). However, the images show some macropores in a range of 50 ~ 150 nm.

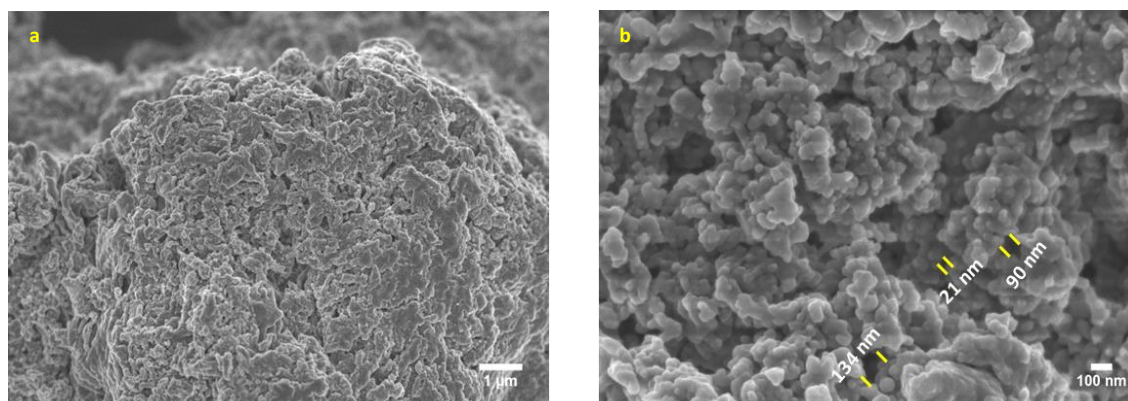


Figure 26 SEM images of ROMP₁ (a) 1 μ m, and (b) 100 nm.

While the SEM images in (Figure 27) show smooth surface of the polymer immobilised with $[\text{WO}_4]^{-2}$, there are small regions of granular-like structures (Figure 27 b, and c), which exhibit some porous features. This could be one possible reason why $\text{WO}_4@\text{ROMP}_1$ shows a low surface area in BET measurement which could, in turn, affect the catalyst performance.

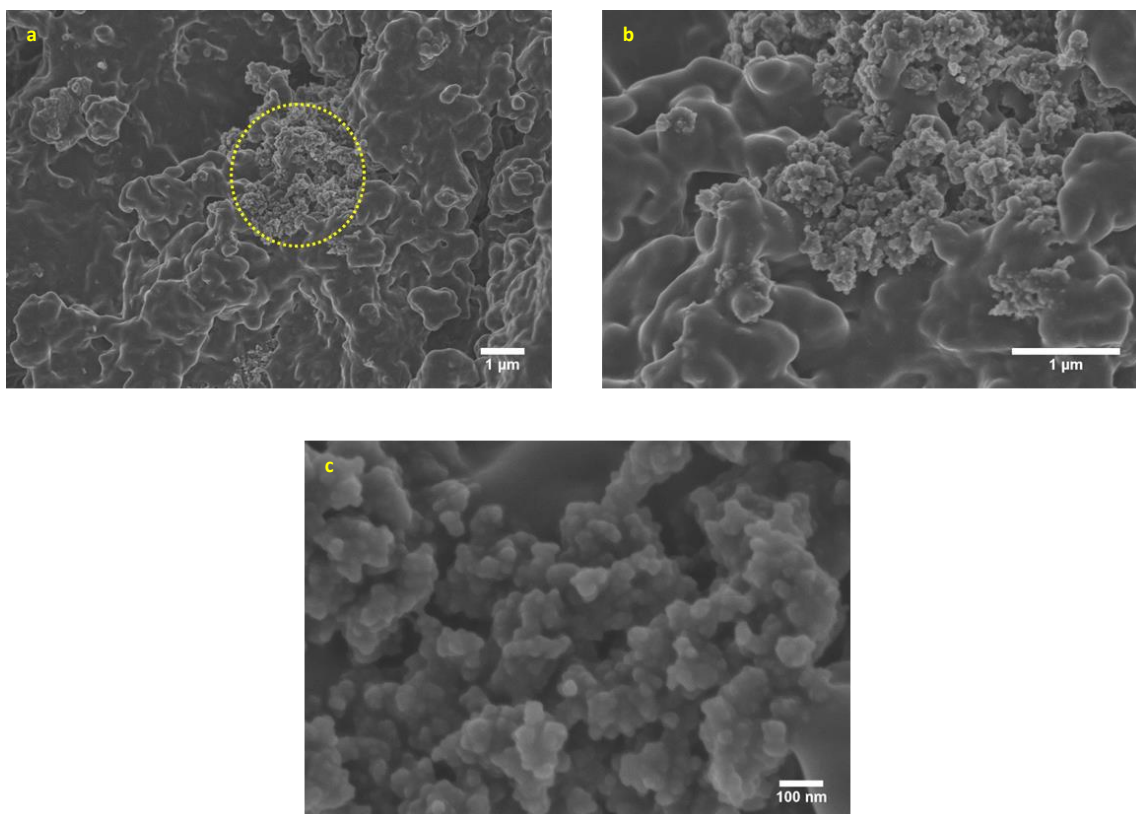


Figure 27 SEM images for $\text{WO}_4@\text{ROMP}_1$ (a) 1 μm, (b) 1 μm, and (c) 100 nm.

$\text{PW}_{12}\text{O}_{40}@\text{ROMP}_1$ shows a significant improvement in the surface area (Figure 28).

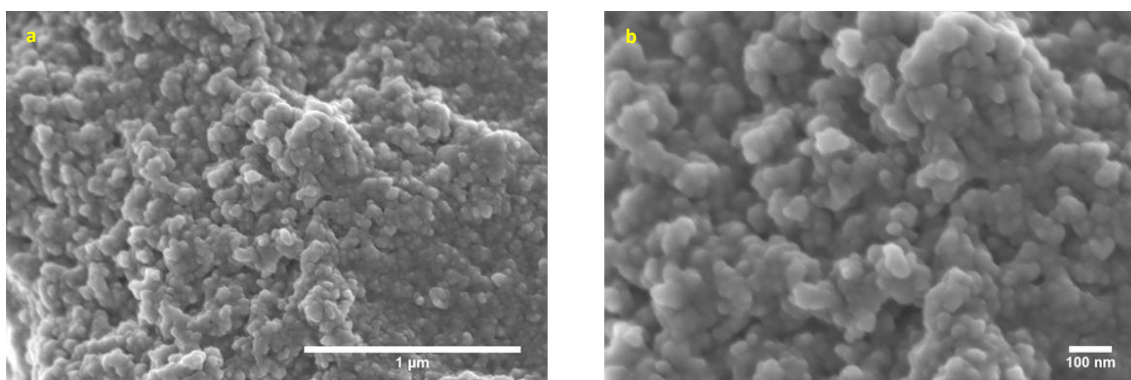


Figure 28 SEM images for $\text{PW}_{12}\text{O}_{40}@\text{ROMP}_1$ (a) 1 μm, and (b) 100 nm.

The differences in surface morphology between (Figure 26, and 29) could possibly be attributed to different monomers as ROMP₁ has a linear alkyl spacer and ROMP₂ features a cyclic alkyl spacer, this may affect the surface area ROMP₂ to be the uneven surface.

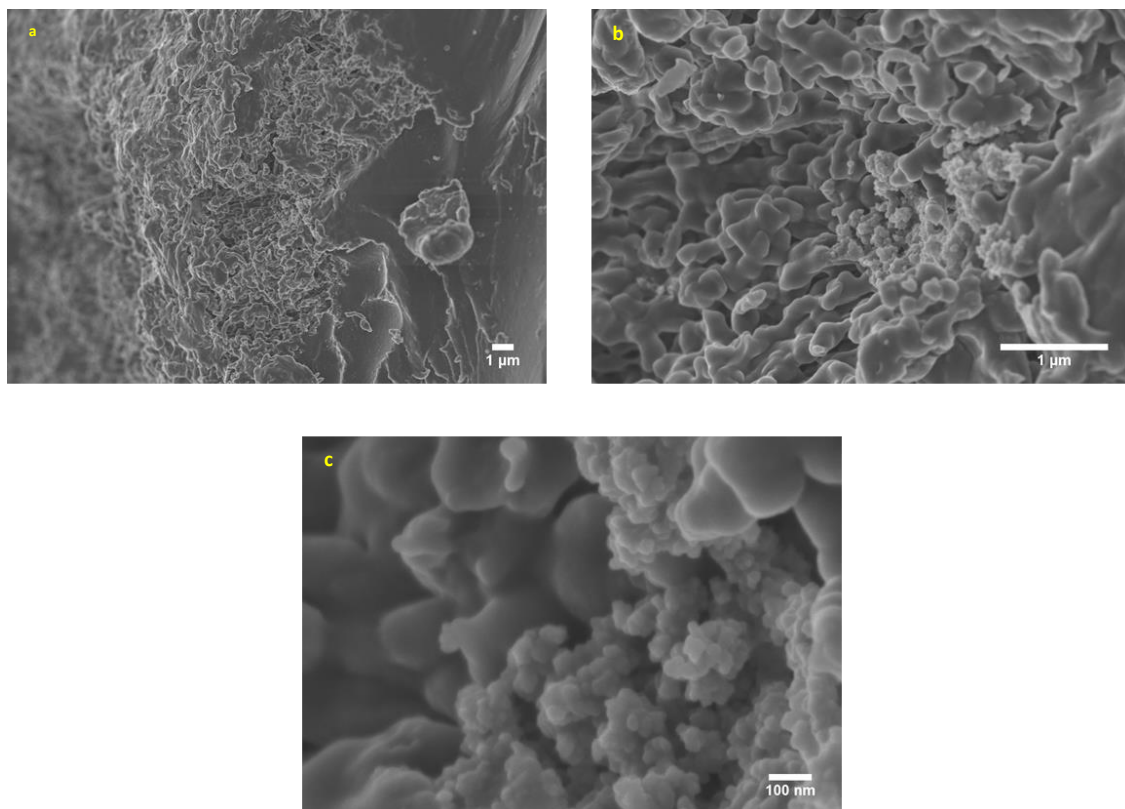


Figure 29 SEM images for ROMP₂ (a) 1 μm, (b) 1 μm, and (c) 100 nm.

(Figure 30) is shown the loaded version of ROMP₂, it is obvious, there is mesopores and macropores which working on increasing the surface area.

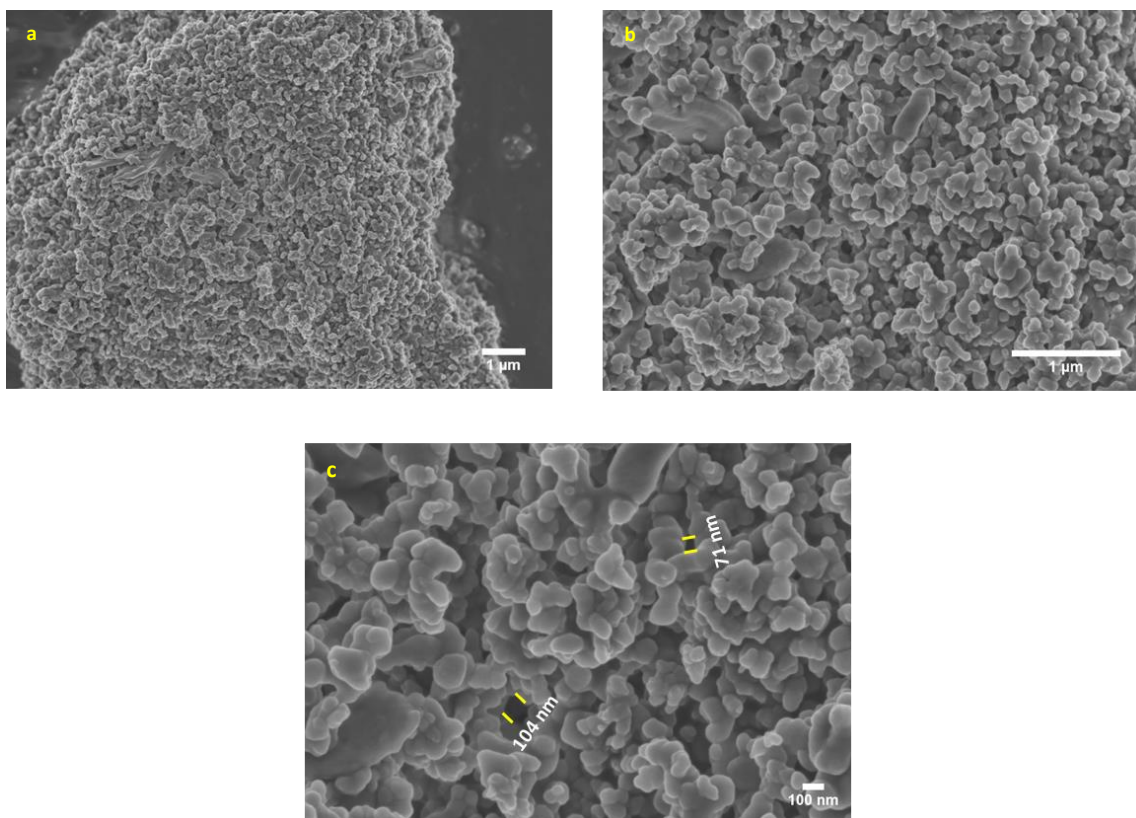


Figure 30 SEM images for $\text{WO}_4@\text{ROMP}_2$ (a) 1 μm , (b) 1 μm , and (c) 100 nm.

*See **Appendices** for all SEM images.

2.6.6 Scanning Electron Microscopy with Energy-Dispersive X-ray Spectroscopy (SEM/EDX)

To identify the content of elements in the prepared catalysts (SEM/EDX) spectroscopy was used (Figure 31). The pure ROMP_1 showed peaks for oxygen, nitrogen, carbon, and bromine, while the peaks of bromine were absent in the sample of $\text{WO}_4@\text{ROMP}_1$, which confirms that all the bromide has been replaced with tungstate and new peaks are attributed to tungsten and trace amounts of Na due to the Na_2WO_4 which was the source of WO_4^{2-} in the catalyst preparation steps.

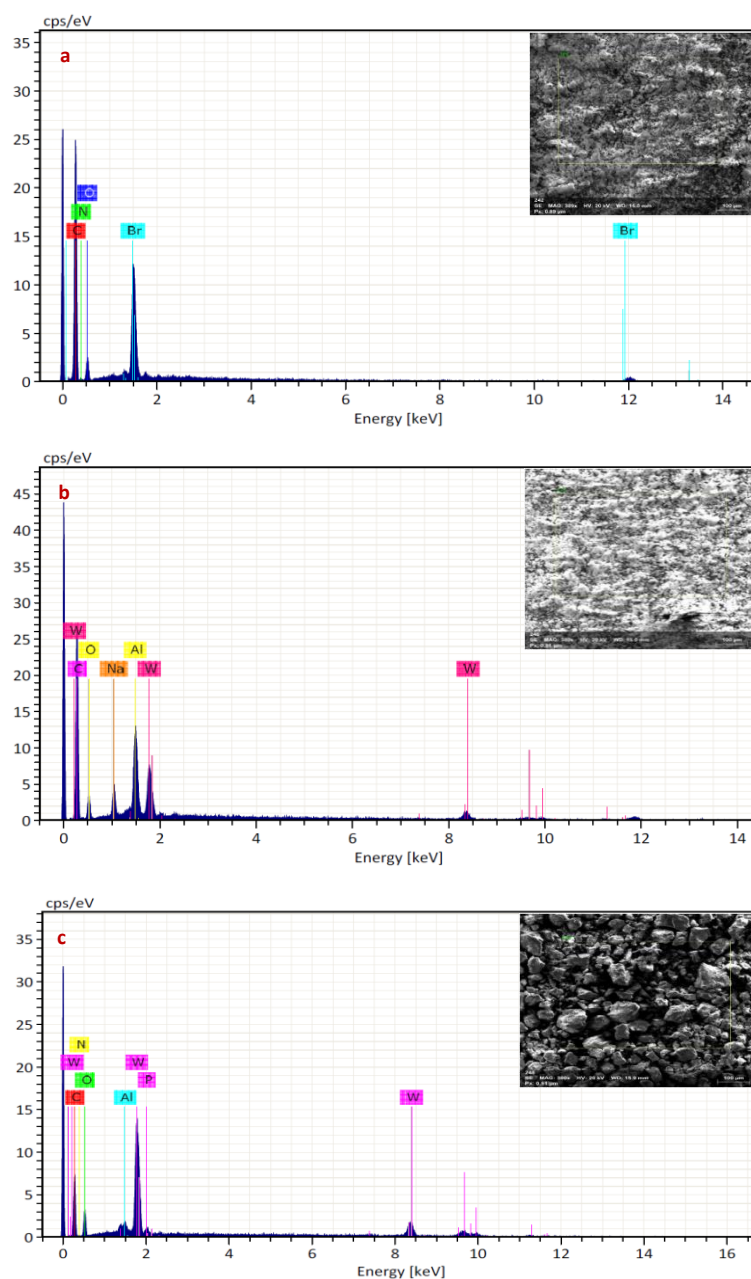


Figure 31 (SEM/EDX) spectroscopy of (a) ROMP₁, (b) WO₄@ROMP₁, and (c) PW₁₂O₄₀@ROMP₁.

In comparison, the EDX spectrum of WO₄@ROMP₂ (Figure 32), showed no evidence for sodium which indicating the exchanging process of the bromide anions with WO₄⁻² is complete and that there is unlikely to be excess Na₂[WO₄] in the product. The aluminium atom signal which should be alerted, it is attributed to the aluminium stubs used in EXD sample which is present in some of the spectra.

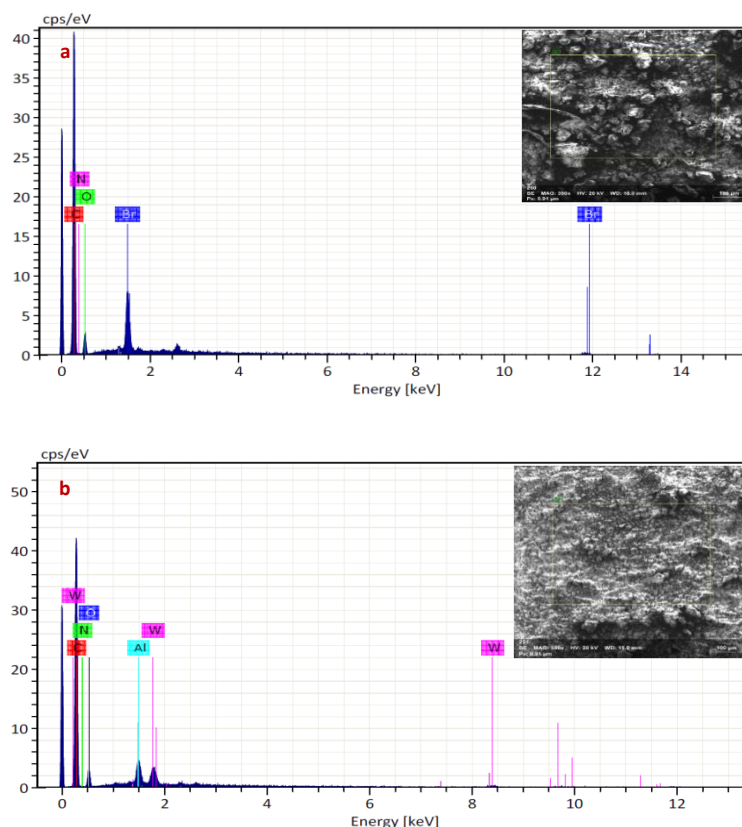


Figure 32 (SEM/EDX) spectroscopy of (a) ROMP₂, and (b) WO₄@ROMP₂.

2.6.7 Thermogravimetric Analysis (TGA)

The thermogravimetry analysis (TGA) (Figure 33) were used to evaluate the thermal stability of the prepared polymers (ROMP₁ and ROMP₂), and some of their loaded versions (PW₁₂O₄₀@ROMP₁ and WO₄@ROMP₂).

All the TGA traces of the polymers has not shown any initial loss in the percent weight while the loaded versions have shown about an initial loss less than ($\sim 2\%$). This could be attributed to the evaporation of some existence residual reaction solvent or water. All the measured samples were followed three main degradation steps, which occur from *c.a.* 200 °C, well above the temperature required for this type of catalysis, except the polymer (ROMP₂) which has followed two steps (Figure 33 b).

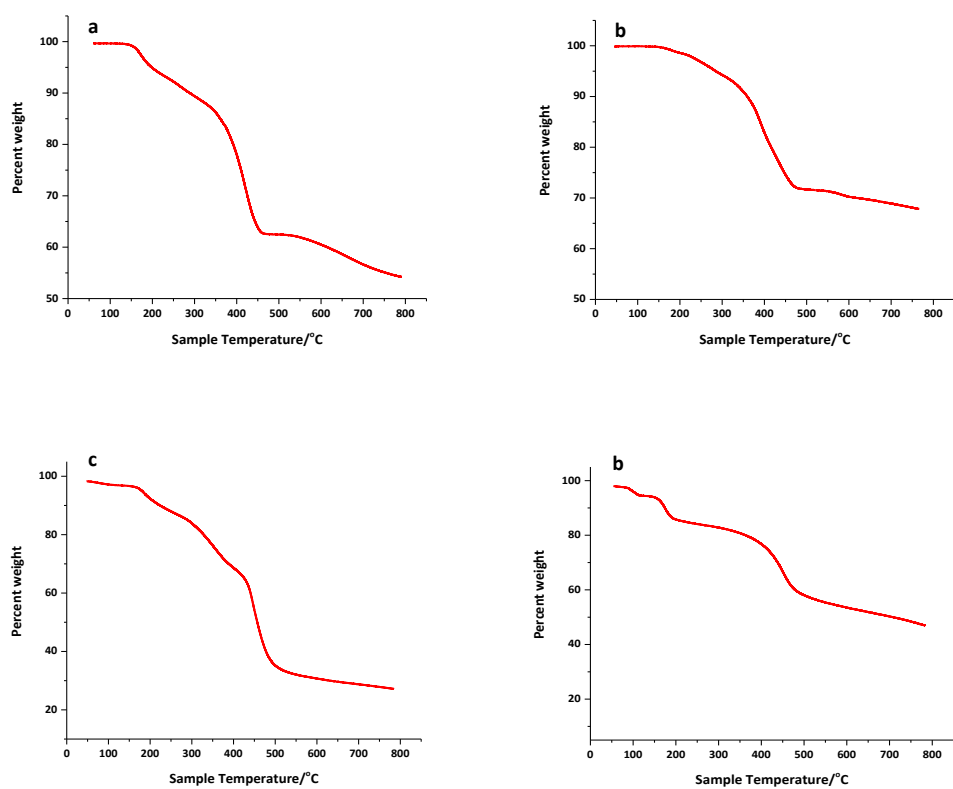


Figure 33 TGA traces of (a) ROMP₁, (b) PW₁₂O₄₀@ROMP₁, (c) ROMP₂, and (d) WO₄@ROMP₂.

2.7 Conclusions

Tungstate and polyoxotungstate anions have been successfully loaded onto ROMP-derived ionic liquid-based polymers through a simple anion exchange process. The monomers required for the polymerisation were prepared in a straightforward linear synthesis without the need for purification by column chromatography. Also, all materials were characterised by various physical techniques. ROMP was chosen as the monomers can be modified which will enable the nature of the architecture, microenvironment and charge distribution on polymer properties to be explored with the aim of identifying an optimum support for catalyst immobilisation.

The pyrrolidinium-functionalised ROMP based polymer has been used to immobilise tungstate $[\text{WO}_4]^{2-}$; and polyoxotungstate $[\text{PW}_{12}\text{O}_{40}]^{3-}$, the resulting Polymer Immobilised Ionic Liquid supported systems form efficient catalysts for the oxidation of sulfides. High selectivity for sulfoxide across a range of aryl alkyl sulfides was obtained in methanol and in acetonitrile, using 2.5 equivalents of hydrogen peroxide as a green oxidant for 15 minutes at room temperature.

Although, a profound difference in catalyst activity was observed between systems based on the nature of the cross-linker whether it is linear in ROMP₁ or cyclic in ROMP₂ which may affect the support structure and then the catalyst performance. In this sense, $\text{WO}_4@\text{ROMP}_1$ recycled only very poorly in methanol with both conversion and selectivity decreasing dramatically after the first run; in contrast, both conversion and selectivity remained relatively constant over six runs when acetonitrile was used as a solvent. More importantly, catalyst generated from $\text{WO}_4@\text{ROMP}_2$ was recovered and reused for up to six runs without any marked decrease in either activity or selectivity towards sulfoxide in both solvents. Furthermore, the efficacy of catalyst generated from $[\text{WO}_4]^{2-}@\text{ROMP}$ and $[\text{PW}_{12}\text{O}_{40}]^{3-}@\text{ROMP}$ was compared with $[\text{PO}_4\{\text{WO}(\text{O}_2)_2\}_4]^{3-}@\text{ROMP}$ which is based on the active Venterullo peroxometalate⁵⁴, and our catalysts showed remarkable efficacy under mild conditions and in a short reaction time at low catalyst loadings (0.3 mol %).

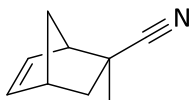
2.8 Laboratory Preparation Procedures

• General Comments

All manipulations involving air-sensitive compounds were carried out using standard Schlenk line techniques under an atmosphere of nitrogen in oven-dried glassware. All the solvents were dried and distilled under a nitrogen atmosphere, (chloroform and dichloromethane) were distilled from calcium hydride, and (diethyl ether and tetrahydrofuran) from sodium wire/benzophenone; (toluene and hexane) from sodium wire; acetonitrile from potassium carbonate; (methanol and ethanol) from magnesium; while (dimethylformamide) were distilled under vacuum. Cyclopentadiene was obtained by distillation of dicyclopentadiene over iron(III) oxide powder and was used without any further purification process. All chemicals were purchased from commercial suppliers and used as received without further purification. ^1H and $^{13}\text{C}\{^1\text{H}\}$ NMR spectra were recorded on either JEOL ECS-400 or a Bruker Avance III 300 spectrometer. CHN analysis was performed using Elemental Analysis Service of London Metropolitan University. Spectrum Two™ FT-IR Spectrometers by PerkinElmer were used to record the on FT-IR spectrums, and all the data were collected over a spectral range (4000-400) cm^{-1} . Specific surface area and pore size measurements were obtained from N_2 adsorption-desorption curves that characterise by Thermo Scientific™ SURFER at the Newcastle University. Brunauer-Emmett-Teller (BET) method was used to measure the specific surface area of the adsorption curve and pore size distribution was measured by Barrett-Joyner-Halenda (BJH) method using the desorption curve. All sample were outgassed at 90 °C for 30 hours prior to analysis. Also, we have used a high-speed centrifuge (Eppendorf™ 5804 Series Centrifuge) for the recycling study. The (SEM/ EDS) analysis was taken using a high-resolution imaging of surfaces by a Tescan Vega 3LMU scanning electron microscope fitted with a detector (Bruker XFlash® 6 | 30). Solid-state NMR were recorded using a Bruker Avance III HD, and a 4 mm HX MAS / magic-angle spinning probe. They were obtained using the type of measurement (cross-polarisation (CP), Direct excitation (DE)), Chemical shifts were referenced: Carbon to neat tetramethylsilane, Phosphorus to 85% H_3PO_4 , Proton to neat tetramethylsilane.

See **Appendices for all characterisation results.*

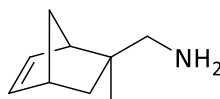
2.8.1 Synthesis of 2-methylbicyclo [2.2.1] hept-5-ene-2-carbonitrile (**2.1**)¹



2.1

An oven-dried three neck round-bottom flask was charged with boron trichloride (0.02 equivalent of 1.0 M in hexane, 0.034 mL, 0.034 mmol) and allowed to cool to 0 °C. To this was added methacrylonitrile (0.143 mL, 1.707 mmol) dropwise with rapid stirring. A white precipitate formed which re-dissolved upon slow addition of freshly cracked cyclopentadiene (0.181 mL, 2.05 mmol). The reaction was allowed to stir overnight then left to warm to room temperature to give a pale-yellow solution which was poured onto an ice-cold solution of saturated sodium bicarbonate which was subsequently extracted with diethyl ether (3 × 100 mL). The organic fractions were dried over magnesium sulfate, filtered, then the solvent was removed under reduced pressure to afford the desired product **2.1** as pale oil in (14.47 g, 108.6 mmol, 66 %, 133.19 g/mol).

¹H NMR (399.78 MHz, CDCl₃, δ): (94:6 *exo:endo* mixture, major *exo*) 6.18 (dd, *J* = 5.7, 3.0 Hz, 1H, *H_aC=CH_b*), 5.94 (dd, *J* = 5.7, 3.1 Hz, 1H, *H_aC=CH_b*), 3.00 (dd, *J* = 3.1, 1.6 Hz, 1H, bridgehead CH), 2.90 (td, *J* = 3.7, 1.8 Hz, 1H, bridgehead CH), 2.25 (dd, *J* = 12.1, 3.9 Hz, 1H, CH₂), 1.72 (dd, *J* = 9.0, 1.6 Hz, 1H, bridge CH₂), 1.63 – 1.54 (m, 1H, bridge CH₂), 1.15 (s, 3H, CH₃), 1.00 (dd, *J* = 12.0, 2.9 Hz, 1H, CH₂); ¹³C{¹H} NMR (100.52 MHz, CDCl₃, δ): 138.9, 131.8, 126.38, 51.81, 49.25, 42.83, 40.35, 35.92, 23.64.

2.8.2 Synthesis of (2-methylbicyclo[2.2.1]hept-5-en-2-yl)methylamine (2.2**)¹****2.2**

An oven-dried three neck round-bottom flask was charged with lithium aluminium hydride (8.9 g, 235 mmol) freshly distilled diethyl ether (100 mL) and cooled down to 0°C under a nitrogen atmosphere. A solution of **2.1** (14.00 g, 117 mmol) in *c.a.* 20 mL of diethyl ether was added dropwise resulting in a vigorous and instantaneous exotherm. The reaction mixture was allowed to cool down to room temperature and stirring was continued for an additional 20 hours. The resulting mixture was worked-up by slow addition of (1.0 M, ~ 12 mL) sodium hydroxide solution with vigorous stirring and then distilled water until there was no exotherm. The resulting reaction mixture was filtered through a pad of celite with an additional 150 mL of diethyl ether. The organic phase then washed with distilled water, separated and the solvent removed under high vacuum. The product was further purified by an acid-base extraction sequence which involved addition of (1.0 M, 180 mL, 180 mmol) hydrochloric acid extraction with diethyl ether (3 × 75 mL) and treatment of the aqueous layer with sodium hydroxide (1.0 M) to pH 12.0 to liberate the amine which was extracted into diethyl ether (3 × 100 mL). The organic phase was dried over magnesium sulfate and the solvent removed to afford **2.2** as a yellow-orange oil in (8.64 g, 62.96 mmol, 60 %, 137.23 g/mol).

¹H NMR (399.78 MHz, CDCl₃, δ): 6.06 (dd, *J* = 5.7, 2.9 Hz, 1H, *H*_aC=CH_b), 6.02 (dd, *J* = 5.9, 2.9 Hz, 1H, *H*_aC=CH_b), 2.70 (t, *J* = 2.4 Hz, 1H, bridgehead CH), 2.64 (s, 2H, CH₂NH₂), 2.42 – 2.34 (m, 1H, bridgehead CH), 1.52 (m, 1H, bridge CH₂), 1.42 (dd, *J* = 11.6, 3.8 Hz, 1H, CH₂), 1.31 (br d, *J* = 2.2 Hz, 1H, bridge CH₂), 1.13 (s, *J* = 1.13, Hz, 2H, NH₂), 0.80 (s, 3H, CH₃), 0.73 (dd, *J* = 11.7, 2.7Hz, 1H, CH₂); ¹³C{¹H} NMR (100.52 MHz, CDCl₃, δ): 136.62, 136.29, 53.28, 48.58, 47.54, 43.17, 42.63, 38.40, 22.88.

2.8.3 Synthesis of 1-(2-methylbicyclo[2.2.1]hept-5-en-2-yl)methylpyrrolidine (**2.3**)¹

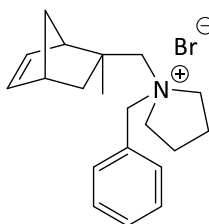


2.3

A round-bottom flask was charged with **2.2** (5.0 g, 37.0 mmol) 1,4-dibromobutane (4.42 mL, 37.0 mmol), potassium carbonate (10.23 g, 74 mmol) and acetonitrile (300 mL) and the resulting mixture refluxed with rapid stirring under nitrogen for 20 hours. The solvent was removed under high vacuum and the residue diluted with diethyl ether (100 mL) followed by hydrochloric acid (1.0 M, 74 mL, 74 mmol). The aqueous layer was extracted with (2 × 70 mL) diethyl ether, treated with a sodium hydroxide (1.0 M) until pH 12.0 and then the product extracted into diethyl ether (3 × 75 mL). The combined organic fractions were dried over magnesium sulfate, filtered and the solvent removed under reduced pressure to afford **2.3** as an orange oil in (5.4 g, 28.22 mmol, 70 %, 191.32 g/mol).

Exo-diastereoisomer: ¹H NMR (399.78 MHz, CDCl₃, δ): 6.07 (m, 2H, =CH), 2.71 (s, 1H), 2.66 – 2.49 (br m, 5H, pyrrolidine CH₂ + bridgehead CH), 2.47 (s, 2H, CH₂), 1.71 (td, *J* = 6.4, 2.9 Hz, 4H, pyrrolidine CH₂), 1.62 – 1.56 (m, 1H, bridgehead CH), 1.52 (dd, *J* = 11.7, 3.8 Hz, 1H, CH₂), 1.35 – 1.27 (m, 1H, bridge CH), 0.89 (s, 3H, CH₃), 0.78 (dd, *J* = 11.5, 2.7 Hz, 1H, bridge CH); ¹³C{¹H} NMR (100.52 MHz, CDCl₃, δ): 136.69, 135.99, 68.64, 56.63, 50.81, 47.75 43.51, 42.78, 39.79, 24.96, 23.78.

2.8.4 Synthesis of 1-benzyl-1-((2-methylbicyclo[2.2.1]hept-5-en-2-yl)methyl)pyrrolidin-1-ium bromide (**2.4**)¹

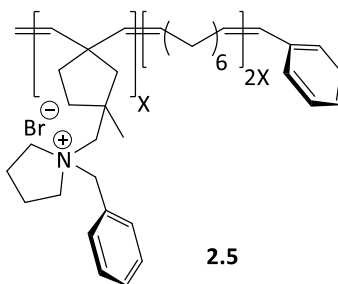


2.4

A round-bottom flask was charged with **2.3** (5.09 g, 27 mmol), benzyl bromide (12.6 mL, 81 mmol), and acetone (30 mL) and the mixture stirred at ambient temperature for 19 hours. The resulting white precipitate was filtrated, washed with hexane (20 mL), diethyl ether (2 × 40 mL) and acetone (20 mL) and dried under reduced pressure to give the desired product **2.4** as a pure white solid in (6.56 g, 18.1 mmol, 70 %, 362.35 g/mol).

Exo-diastereoisomer: ¹H NMR (300.13 MHz, CDCl₃, δ): 7.69 – 7.61 (m, 2H, Ar-*H*), 7.47 – 7.34 (m, 3H, Ar-*H*), 6.17 (dd, *J* = 5.7, 3.0 Hz, 1H, *H*_aC=CH_b), 6.03 (dd, *J* = 5.7, 3.2 Hz, 1H, *H*_aC=CH_b), 5.29 (d, *J* = 12.8 Hz, 1H, N-CH_aH_b-Ph), 4.74 (d, *J* = 12.8 Hz, 1H, NCH_aH_b-Ph), 4.14 (d, *J* = 13.8 Hz, 1H, CMeCH_cH_d-N), 4.07 (dt, *J* = 8.4, 5.0 Hz, 1H, pyrrolidine NCH₂CH₂), 3.94 (ddd, *J* = 12.2, 8.3, 6.6 Hz, 1H, pyrrolidine NCH₂CH₂), 3.86 (d, *J* = 4.0 Hz, 1H, CMeCH_cH_d-N), 3.84 – 3.69 (m, 2H, pyrrolidine NCH₂CH₂), 2.88 (s, 1H, bridgehead CH), 2.62 (dd, *J* = 3.2, 1.6 Hz, 1H, bridgehead CH), 2.10 (d, *J* = 3.9 Hz, 1H, pyrrolidine NCH₂CH₂), 2.06 (d, *J* = 3.8 Hz, 1H, CH_eH_f), 1.94 (s, 1H, pyrrolidine NCH₂CH₂), 1.92 – 1.73 (m, 2H, pyrrolidine NCH₂CH₂), 1.66 – 1.52 (m, 1H, bridge CH), 1.44 – 1.34 (m, 1H, bridge CH), 1.20 (s, 3H, CH₃), 0.97 (dd, *J* = 11.7, 2.6 Hz, 1H, CH_eH_f); ¹³C{¹H} NMR (75.48 MHz, CDCl₃, δ): 138.11, 134.76, 133.21, 130.68, 129.29, 128.45, 72.73, 65.35, 62.99, 60.75, 53.23, 48.37, 44.48, 42.83, 40.72, 25.73, 22.69, 21.95.

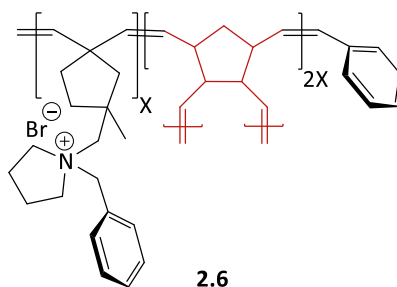
2.8.5 Ring Opening Metathesis Polymerisation of 1-benzyl-1-((2-methylbicyclo[2.2.1]hept-5-en-2-yl)methyl)pyrrolidin-1-ium bromide with cis-cyclooctene (2.5)¹



An oven-dried three neck round-bottom flask under a nitrogen atmosphere was charged with dry chloroform (80 mL) cis-cyclooctene (3.04 mL, 23.3 mmol) and **2.4** (4.23 g 11.7 mmol). To this was added a solution of $[\text{RuCl}_2(\text{PCy}_3)_2(=\text{CHPh})]$ (0.576 g, 0.7 mmol) in chloroform (*c.a.* 10 mL) and the resulting mixture heated at 40 °C and left for overnight stirring. The reaction mixture was allowed to cool to room temperature before adding ethyl vinyl ether (1.68 mL, 17.5 mmol, 10 eq. with respect to Grubbs catalyst); the solution was then left to stir for an additional hour. The polymer was precipitated by slowly adding the reaction mixture portion wise to diethyl ether (*c.a.* 600 mL) with vigorous stirring for a further 60 minutes. The resulting solid was filtered using a sintered frit washed with diethyl ether and dried to afford a pale green solid. A solution of tetrakis(hydroxymethyl)phosphonium chloride adding (2.5 mL, 17.5 mmol, 25 eq. with respect to Grubbs catalyst) in nitrogen-degassed 2-propanol was prepared and treated with potassium hydroxide (0.98 g, 17.5 mmol, 25 eq. with respect to Grubbs catalyst) to generate tris-(hydroxymethyl) phosphine. A white precipitate formed over 15 min after which time a chloroform solution of the polymer was added. The reaction mixture was heated at 60 °C for 19 hours after which sodium bromide (18.02 g, 175 mmol, 250 eq. with respect to Grubbs catalyst) was added and the resulting mixture stirred for an additional 3 hours at 60 °C. Then the reaction mixture was filtered, washed rigorously with distilled water (3 × 50 mL) and the organic layer added dropwise to diethyl ether (*c.a.* 500 mL) with rapid stirring for a minimum of 60 minutes. The polymer was isolated by filtration through a sintered frit, washed with diethyl ether (2 × 50 mL) and dried under high vacuum to afford **2.5** as a pale-green solid in (5.57 g, 7.58 mmol, 65 %, 735 g/mol).

FT-IR: $\tilde{\nu}$ = 2823, 2851, 1455, 1077, 973, 892, 803, 595, 508.

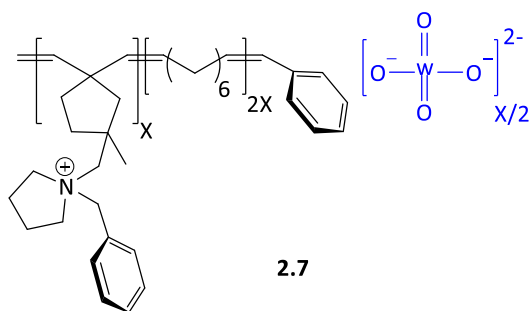
2.8.6 Ring Opening Metathesis Polymerisation of 1-benzyl-1-((2-methylbicyclo[2.2.1]hept-5-en-2-yl)methyl)pyrrolidin-1-ium bromide with dicyclopentadiene (2.6)



An oven-dried three neck round-bottom flask under a nitrogen atmosphere was charged with dry chloroform (80 mL) dicyclopentadiene (2.25 g, 17.0 mmol) and **2.4** (3.08 g, 8.5 mmol). To this was added a solution of $[\text{RuCl}_2(\text{PCy}_3)_2(=\text{CHPh})]$ (0.42 g, 0.51 mmol) in (*c.a.* 10 mL) chloroform and the mixture heated at 40 °C overnight stirring. The reaction was allowed to cool to room temperature, ethyl vinyl ether (0.92 mL, 12.8 mmol, 10 eq. with respect to Grubbs catalyst) added and the solution stirred for an additional hour. The polymer was precipitated by slowly adding the reaction mixture portion wise to diethyl ether (*c.a.* 600 mL) with vigorous stirring for a further 60 minutes. The polymer was then filtrated, using a sintered frit, washed with diethyl ether and dried to afford **2.6** as brown solid in (3.7 g, 5.6 mmol, 65 %, 666.93 g/mol).

FT-IR: ν = 3376, 2926, 1698, 1428, 1451, 971, 708.

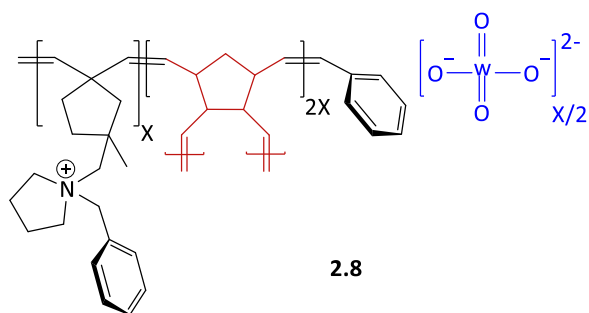
2.8.7 Synthesis of Polymer Supported Tungstate (2.7)



A beaker charged with a suspension of **2.5** (2.8 g, 3.8 mmol) dissolved in ethanol (20 ml) was stirred at room temperature and a solution of sodium tungstate dihydrate dissolved in a minimum volume of water (1.26 g, 3.8 mmol) was added portion wise. The reaction mixture was allowed to stir at room temperature for 2.5 hours after which time the precipitate was filtered through a sintered glass frit, washed with a minimum volume of water (1 × 5 mL), ethanol (1 × 10 mL), and diethyl ether (3 × 75 mL) and dried under vacuum to afford **2.7** as an off-white solid in (3.54 g, 4.12 mmol, 87 %, 859 g/mol).

FT-IR: ν = 3371, 2924, 2853, 1561, 1455, 968, 840 (W=O), 702, 473 W (O₂) sym, asym:.

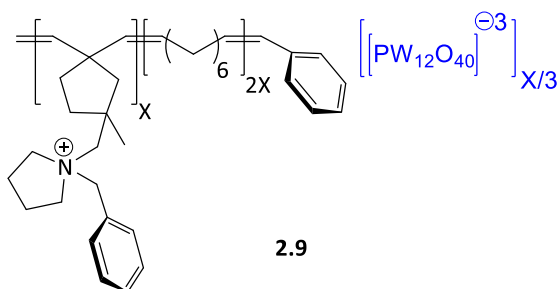
2.8.8 Synthesis of Polymer Supported Tungstate (2.8)



A beaker was charged with a suspension of **2.6** (2.5 g, 3.75 mmol) dissolved in ethanol (20 ml) and stirred at room temperature. A solution of sodium tungstate dihydrate (1.24 g, 3.75 mmol) dissolved in a minimum volume of water was then added portion wise and stirring continued at room temperature for 2.5 h, to afford a greenish-white precipitate. The reaction mixture was filtered through a sintered glass frit and the precipitate washed with a minimum volume of water, ethanol and then diethyl ether (3 × 75 mL) and dried under vacuum to afford **2.8** as an off-white powder in (3.74 g, 4.7 mmol, 92 %, 790.85 g/mol).

FT-IR: ν = 2930, 1705, 1452, 972, 827 (W=O), 705 W (O₂) sym, asym:.

2.8.9 Synthesis of Polymer Supported Polyoxotungstate (2.9)



A beaker was charged with a suspension of **2.5** (1 g, 1.36 mmol) dissolved in ethanol (15 mL) and stirred at room temperature. To this was added a solution of phosphotungstic acid (3.9 g, 1.36 mmol) dissolved in a minimum volume of water. The reaction mixture was allowed to stir at room temperature for 2.5 hours after which time the resulting precipitate was filtered through a sintered glass frit, washed with a minimum volume of water (1 × 5 mL), ethanol (1 × 10 mL), and diethyl ether (3 × 75 mL) and then dried under vacuum to afford **2.9** as an off-white solid in (4.27 g, 2.5 mmol, 87 %, 1694 g/mol).

FT-IR: ν = 2927, 1710, 1455, 1077 (P-O), 974 (W=O), 893 (W=O), 803 (O-O), 595, 508 W (O₂) sym, asym:.

2.8.10 Catalysts Applications and Optimisation Studies

- **Typical Procedure for Catalytic Sulfoxidation Reaction**

An oven-dried Schlenk flask equipped with a magnetic stirrer bar was cooled to room temperature under vacuum, subsequently refilled with nitrogen gas and then charged with sulfide (1.0 mmol), catalyst (0.003 mmol, 0.3 mol %) and solvent (3 mL) and then activated by the addition of 35 % hydrogen peroxide (0.24 mL, 2.5 mmol). The reaction mixture was allowed to stir at room temperature for 15 minutes after which time it was diluted with dichloromethane (25 mL) and washed with water (*c.a.* 50 mL). The organic phase was separated, dried over magnesium sulfate and the solvent removed under reduced pressure. The resulting residue was analysed by ^1H NMR spectroscopy to quantify the composition of starting material and products using 1, 3-dinitrobenzene as an internal standard.

- **Reaction Temperature Optimisation Studies**

An oven-dried Schlenk flask equipped with a magnetic stirrer bar allowed to cool to room temperature under vacuum, backfilled with nitrogen and then charged with thioanisole (0.13 mL, 0.97 g/mL, 1.0 mmol), catalyst (0.003 mmol, 0.3 mol %) and solvent (3 mL) and then activated by the addition of 35 % hydrogen peroxide (0.24 mL, 2.5 mmol). The reaction mixture was allowed to stir for 15 minutes at different temperatures (20, 25, 30, 35, 40, 45) °C after which time dichloromethane (25 mL) was added and the mixture washed with water (*c.a.* 50 mL). The organic phase was separated dried over magnesium sulfate and the solvent removed under reduced pressure. The resulting residue was analysed by ^1H NMR spectroscopy to quantify the composition of starting material and products with 1,3-dinitrobenzene as an internal standard.

- **Reaction Time Optimisation Studies**

An oven-dried Schlenk flask equipped with a magnetic stirrer bar was cooled to room temperature under vacuum, back with nitrogen, and charged with thioanisole (0.13 mL, 0.97 g/mL, 1.0 mmol), catalyst (0.003 mmol, 0.3 mol %) and solvent (3 mL) and then activated by the addition of 35 % hydrogen peroxide (0.24 mL, 2.5 mmol). The reaction mixture was stirred at room temperature for a series of different times after which dichloromethane was added (25 mL) and the mixture washed with water (*c.a.* 50 mL). The organic phase was separated, dried over magnesium sulfate and the solvent removed under reduced pressure. The resulting residue was analysed by ^1H NMR spectroscopy to quantify the composition of starting material and products using 1,3-dinitrobenzene as an internal standard. For each substrate tested ^1H NMR spectra were recorded with relaxation delays of 10, 20 and 30 seconds to establish the optimum time to ensure accurate integration of the signals chosen to determine the selectivity and conversion. Well-resolved resonances were used to calculate the yield and conversion by normalising the integration according to the number of protons.

- **Hydrogen Peroxide Concentration Optimisation Studies**

An oven-dried Schlenk flask equipped with a magnetic stirrer bar was cooled to room temperature under vacuum, backfilled with nitrogen and then charged with thioanisole (0.13 mL, 0.97 g/mL, 1.0 mmol) catalyst (0.003 mmol, 0.3 mol %) and solvent (3 mL) and then activated by addition of varying amounts of 35 % hydrogen peroxide equivalent (0, 1, 2, 2.5, 3, 5) mmol. The reaction mixture was stirred at room temperature for 15 minutes after which time it was diluted with dichloromethane (25 mL) and then washed with water (*c.a.* 50 mL). The organic phase was dried over magnesium sulfate and the solvent removed under reduced pressure. The resulting residue was analysed by ^1H NMR spectroscopy to quantify the composition of starting material and products using 1,3-dinitrobenzene as an internal standard.

- **General Procedure for Catalytic Sulfoxidation Recycle Studies with Catalyst (2.7)**

An oven-dried Schlenk flask was cooled to room temperature and charged sequentially with thioanisole (0.39 mL, 0.97 g/mL, 3.0 mmol) catalyst (0.018 g, 0.009 mmol, 0.9 mol %) solvent (9 mL) solvent. The reaction was initiated by addition of 35 % H₂O₂ (0.72 mL, 7.5 mmol) and the resulting mixture allowed to stir at room temperature for either 45 minutes (methanol) or 60 minutes (acetonitrile). After this time the solution was allowed to settle, then decanted using a pipette and the remaining catalyst washed with the reaction solvent and dried prior to reuse under the same conditions. The remaining solution was subject to the same work-up and analysis as described above.

- **General Procedure for Catalytic Sulfoxidation Recycle Studies with Catalyst (2.8 and 2.9)**

An oven-dried Schlenk flask was allowed to cool to room temperature and charged sequentially with thioanisole (0.39 mL, 0.97 g/mL, 3.0 mmol), catalyst (0.009 mmol, 0.9 mol %) and solvent (9 mL) solvent. The reaction was initiated by addition of 35 % H₂O₂ (0.72 mL, 7.5 mmol) and the resulting mixture allowed to stir at room temperature for 15 minutes. After this time the solution was allowed to settle, decanted using a pipette and the remaining catalyst washed with the reaction solvent and dried prior to reuse under the same conditions. The remaining solution was subject to the same work-up and analysis as described above.

Chapter 3

PALLADIUM AND PLATINUM NANOPARTICLES LOADED ON POLYMER-IMMOBILISED IONIC LIQUIDS

Chapter 3. PALLADIUM AND PLATINUM NANOPARTICLES LOADED ON POLYMER-IMMOBILISED IONIC LIQUIDS

3.1 Introduction

Nowadays, the process of producing fuels and chemicals using alternative energy sources and feedstocks has attracted a lot of attention, this led to an increased focus on green chemistry and the renewable sources. Green chemistry considered as a modern aspect of chemistry, has its significance in the manufacturing, using and design chemicals. The major purpose of using green chemistry principles is to reduce pollution and risk which affect the environment.¹⁴⁷ Most importantly, there are major problems facing the green production of fine chemicals because they often require multi-step reactions which necessarily results in the consumption of a large amount of solvents and the need to protect active groups and the use of expensive catalysts.¹⁴⁸ In the regard, many multistep reaction sequences involve at least one catalytic step¹⁴⁹ and therefore organometallic chemistry has attracted a lot of attention in preparation, design, and modification of catalysts to obtain high activity and selectivity.⁶⁰ One of the most common catalysts for hydrogenation and cross-coupling are metal nanoparticles based on palladium, rhodium, and ruthenium. However, since these metals are expensive, the cost usability issues must be considered. In this sense, the catalyst must be stable, efficient, and reusable in order to reduce the cost. Several issues limited the usage of the naked metal nanoparticle such as leaching during the purification which may also lead to heavy metal contamination of the product.¹⁵⁰ Due to their small size and high surface area metal nanoparticles (i.e. it is having more active sites to catalyse the reaction) are more favoured as catalysts than the corresponding bulk metal. The high activity of nanoparticles makes them have the ability to achieve catalysis reaction under milder conditions than the bulk. Furthermore, the (high surface area/volume) ratio of the nanoparticles makes them very reactive and unstable with respect to their bulk counterparts. In addition, the large surface tension of the nanoparticles makes the outer atoms highly reactive.

Again, the nanoparticles size is another factor has the same effect on nano-catalysis ability, where the smaller particles, the more reactive to catalyse reactions.

In this regard, small nanoparticles are thermodynamically unstable and are prone to agglomerate together undergoing the Ostwald ripening process.^{151, 152} The larger particles are more energetically favourable than smaller particles, the reason behind this is in the larger particle most of the atoms would be in full coordinate and in good order in the bulk. Thus, nanoparticles are often immobilised on a support material to control their size and distribution as well as prevent agglomeration by keeping the NPs highly dispersed.¹⁵³ Interestingly, there is several kinds of a stabilising agent such as heteroatom donors,¹⁵² polyvinylpyrrolidone (PVP)^{154, 155} and poly-ionic liquids.¹⁵⁶ Another factor that must be considered while stabilising the NPs is that the more stable nanoparticle is likely to be less active. To this end, a catalytically competent nanoparticle should have a good balance between stabilising interactions and accessibility of the reactant to the active site.^{152, 157} For stabilising nanoparticles on polymers, there are two main different ways: steric effects or electrostatic stabilisation for instance via heteroatoms (Figure 1).¹⁵⁶

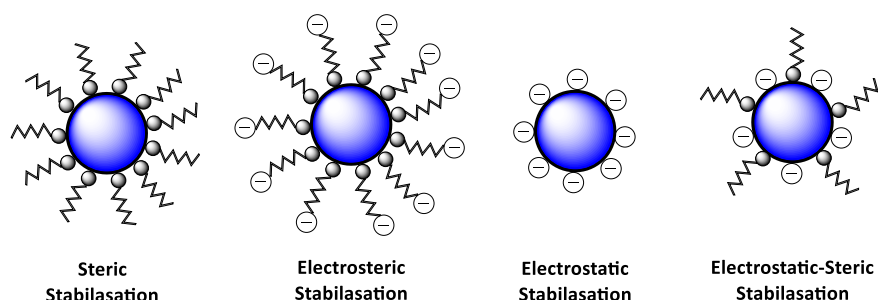


Figure 1 Type of nanoparticles stabilisation.

In order to design catalyst system combines the benefits of homogeneous and heterogeneous catalysis, while providing a suitable environment to immobilise nanoparticles, polymers would be a great choice.¹⁵⁰ Moreover, the polymers flexibility allow catalysts greater movement in the reaction media in comparison with other supporting materials such as silica (SiO₂)^{158, 159}, carbon materials^{160, 161}, zeolite^{162, 163}, metal oxide¹⁶⁴⁻¹⁶⁶, etc.), while the ability to graft heteroatom donors, functional groups and ionic liquids to polymers could be used to tune the properties and performance of metal nanoparticles.¹⁶⁷ Ionic liquids have been widely used to stabilise metal nanoparticles; popular ionic liquids are those based on a bulky substituted imidazolium cation, which stabilise nanoparticles through electrostatic effects.¹⁵⁶

Incorporation of an ionic liquid and a heteroatom donor into a single polymer would be expected to provide both steric and electrostatic stabilisation which might work synergistically to prevent nanoparticle agglomeration.¹¹⁵ An imidazole co-monomer would provide more stabilisation via coordination with the metal surface and in this regard, Dyson has reported that a styrene-based polymer containing imidazolium chloride stabilises transition metal nanoparticles by electrostatic effects.¹⁶⁸

It has been frequently reported that on the generation of metallic state metal, the resultant average particle size is dependent on the relative nucleation rate, with fast nucleation rates yielding smaller particles. Ionic liquids tend to exhibit low interfacial enabling fast nucleation in solution, therefore PIILP materials may prove to be a valuable tool for the synthesis of small nanoparticles (Figure 2).^{169, 170}

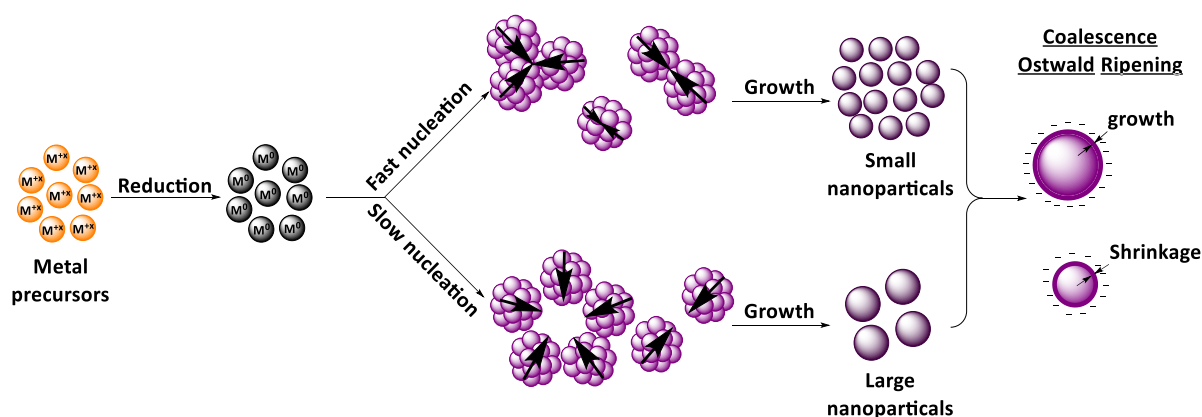


Figure 2 Schematic representation of the nucleation and the growth steps of nanoparticles.

The charge surrounding the nanoparticle ‘the first shell or protective shell’ would be anionic according to the Derjaguin-Landau-Verwey-Overbeek (DLVO) theory; this provides the metal nanoparticles with the necessary electrostatic effects for stabilisation as shown in (Figure 2).^{156, 170, 172-174}

3.2 Synthesis of Monomers and Cross-linker

This phase of the project is concerned with the design and synthesis of amino-, phosphino-, and pyrrolidino-decorated polymer immobilised ionic liquids (Figure 3), and of the effects of the heteroatom donor on the stability and dispersity of noble metal nanoparticles.

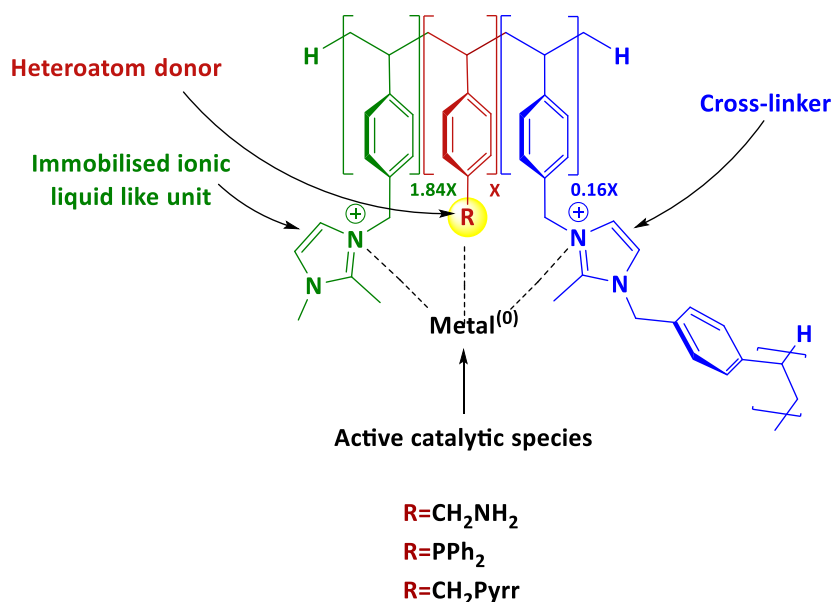
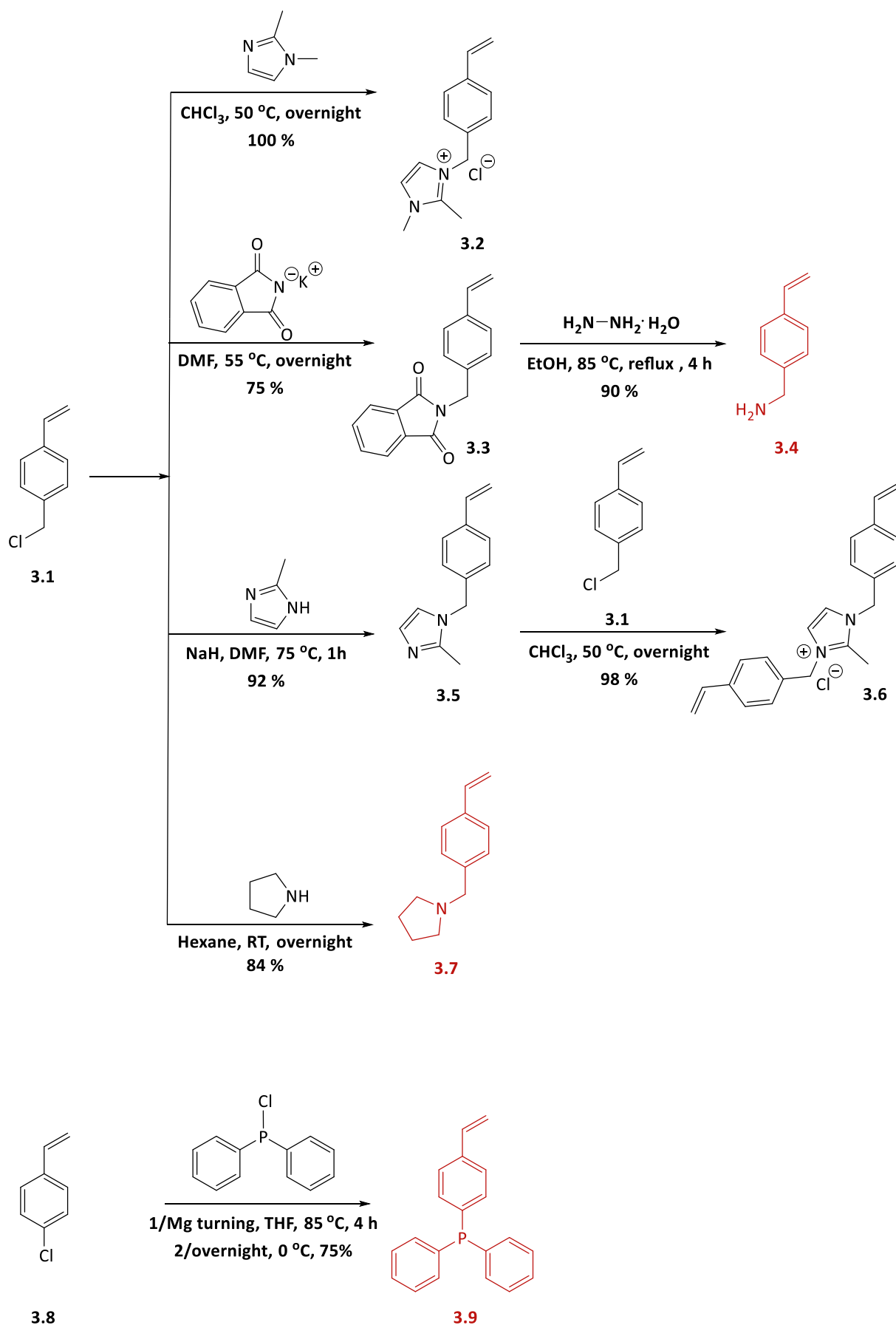


Figure 3 Schematic structure of the prepared catalysts.

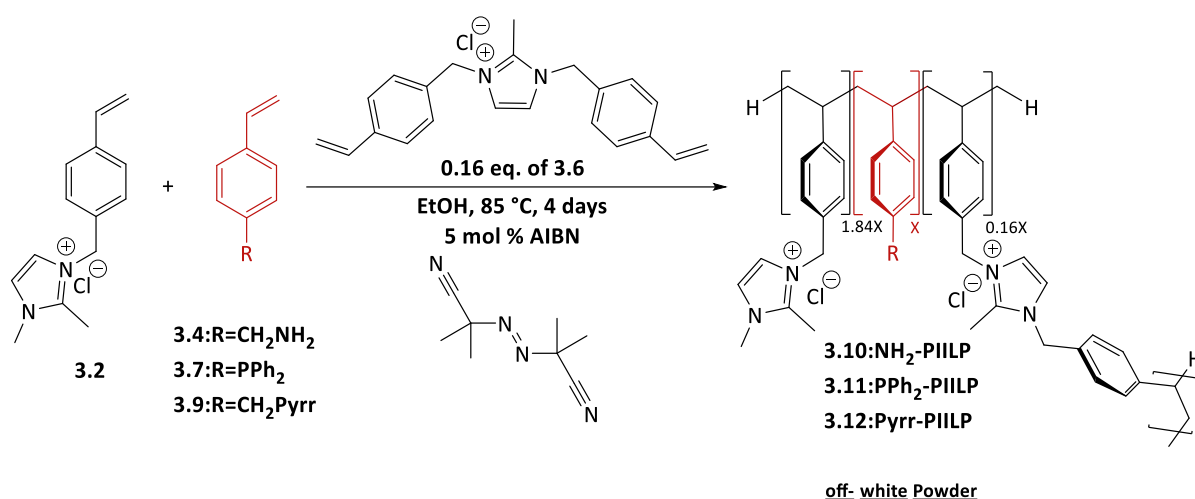
Monomer **3.2** was synthesised in an overnight reaction between 1,2-dimethyl imidazole and 4-chloromethyl styrene **3.1** at 50 °C and isolated in nearly quantitative yield by removing the solvent and washing the oily residue with ethyl acetate.¹⁷⁴ The synthesis of monomer **3.4** is a two steps sequence, the first step is the production of N-[(4-vinylphenyl)] phthalimide **3.3** from the reaction between 4-chloromethyl styrene **3.1** and potassium phthalimide in DMF. The second step involves hydrazinolysis of **3.3** to afford (4-vinylphenyl) methanamine **3.4**.¹⁷⁵ The preparation of the cross-linker **3.6** was adapted from Jingsong You *et.al*¹⁷⁴ and is a two-step reaction. First intermediate imidazole **3.5** was prepared by deprotonation of 2-methyl imidazole with sodium hydride in dry DMF, followed by the drop-wised addition of 4-chloromethyl styrene **3.1** to the solution; the desired product was isolated as a pale-yellow oil after work-up. Cross-linker **3.6** was then prepared from the reaction of 4-chloromethyl styrene **3.1** with **3.5** in an overnight reaction at 50 °C. In a 75 % yield, the pyrrolidino-monomer **3.7** was synthesised in one simple step overnight reaction, in dry hexane, by treating of 4-chloromethyl styrene **3.1** with pyrrolidine. Monomer **3.9** was synthesised from 4-chlorostyrene **3.8** according to the method of Leebrick and Marcus,¹⁷⁶ The Grignard preparation was modified by adding only 0.8 equivalents of chlorophosphine and because of the sensitivity of the phosphine, the entire reaction and work-up were *performed* under a nitrogen atmosphere. The crude product was purified by column chromatography and obtained as a white solid after crystallisation from dichloromethane/ethanol (Scheme 1).



Scheme 1 Synthesis of functionalised styrene monomers 3.2, 3.4, 3.6, 3.7, and 3.9.

3.3 Radical Polymerisation of Cross-linked Poly Ionic Liquid

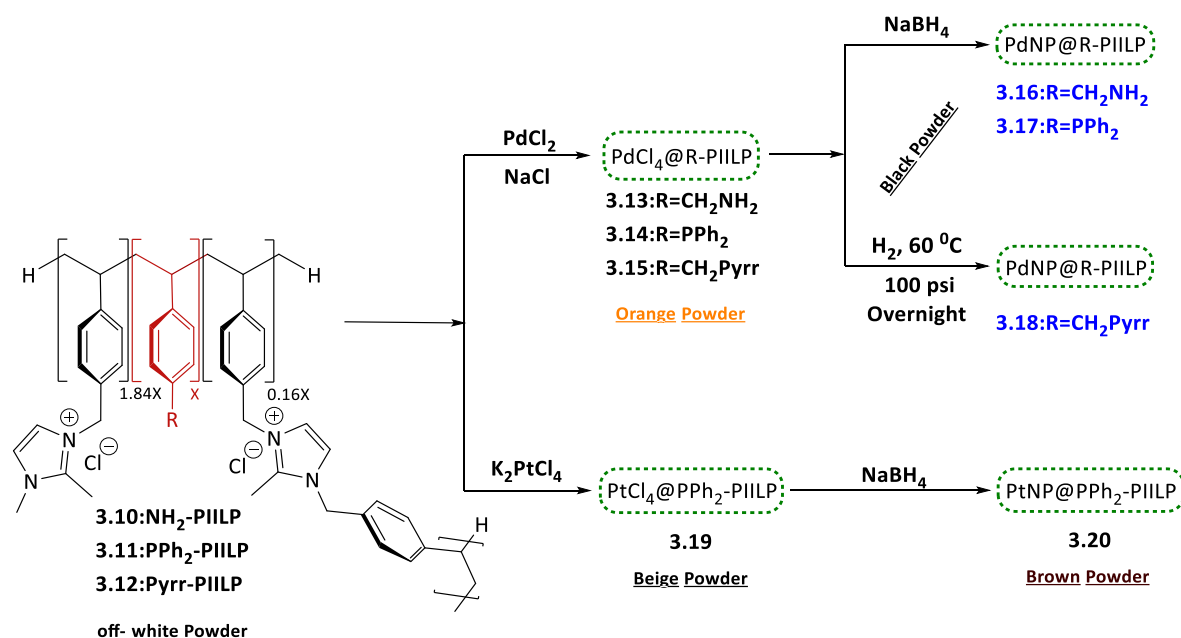
The polystyrene-based PIILs **3.10**, **3.11**, and **3.12** were synthesised by the free radical copolymerization of neutral co-monomers **3.2** with either **3.4**, **3.7**, or **3.9**, respectively, in the presence of 0.16 eq. of cross-linker **3.6** using 5 mol % azobisisobutyronitrile (AIBN) as initiator; all reactions were conducted in ethanol and heated at 85 °C for 4 days. An additional amount of 5 mol % AIBN after 4 days and the reaction extended for another day to ensure complete polymerisation. The solvent was removed under reduced pressure and the residue washed with diethyl ether then dried to give the polymer as an off-white fine powder (Scheme 2). This procedure is desirable as it is highly efficient, straightforward to execute and afford the desired polymer in high yield. However, re-dissolving the sample followed by re-precipitation in diethyl ether reduced the amount of unreacted monomer by about 5 % as the 1, 2-dimethyl-3-(4-vinylbenzyl) imidazolium chloride **3.2** was added in excess relative to the **3.4**, **3.7**, and **3.9**, respectively. The overall charge ratio of imidazolium-based monomer/cross-linker to neutral monomer is 2 such that the final polymer would have two positive charged imidazolium groups for each heteroatom donor and exchange of all the chloride for $[\text{PdCl}_4]^{2-}$ would afford a heteroatom donor to metal ratio of one.



Scheme 2 Synthesis of Cross-linked Polymer Immobilised Ionic Liquids.

3.4 Synthesis of Polymer Decorated with Palladium and Platinum Nanoparticles

All prepared polymers were impregnated by stoichiometric exchange of chloride with $[\text{PdCl}_4]^{2-}$ (Scheme 3). This was achieved by the addition of the polymer to an aqueous solution of $\text{Na}_2[\text{PdCl}_4]$ generated *in-situ* from PdCl_2 and excess NaCl at 80 °C. After stirring for 5 hours the desired $[\text{PdCl}_4]@\text{PIILP}$ was isolated by filtration as an orange powder.^{57, 177} Polymer immobilised ionic liquid-stabilised palladium nanoparticles **3.16**, and **3.17** were generated by reduction of **3.13**, and **3.14** with sodium borohydride in ethanol; the suspension turned from orange to black, which indicated a successful reduction of Pd^{II} to PdNP .^{57, 177} However, reduction for **3.15** was performed under 70 psi of hydrogen by stirring an ethanol solution overnight at 60 °C; the $\text{PdNP}@\text{Pyrr-PIILP}$ was isolated by reducing the volume of the solvent by vacuum, followed by addition of diethyl ether and filtering the resulting solid, which was dried under reduced pressure. The reason behind using hydrogenation to produce the $\text{PdNP}@\text{Pyrr-PIILP}$ instead of using NaBH_4 as a reducing agent is the low yield when the latter method was used.



Scheme 3 Synthesis of polymer stabilised palladium and platinum nanoparticles.

For comparison, the platinum nanoparticles of PPh₂ polymer were prepared following the same procedure, but instead of using PdCl₂, K₂PtCl₄ was used to afford PtCl₄@PPh₂PIILP which was then reduced with sodium borohydride.

3.5 Characterisations Methods

3.5.1 BET Surface Area Analysis

As it is mentioned in the previous chapter that the performance of the catalysts may well be affected by the morphology and/or the porosity of the catalytic species, the specific surface area of all the prepared sample was measured from the adsorption curve by using the Brunauer-Emmett-Teller (BET) method while the pore size distribution was determined from the nitrogen desorption curve using the Barrett-Joyner-Halenda (BJH) method.

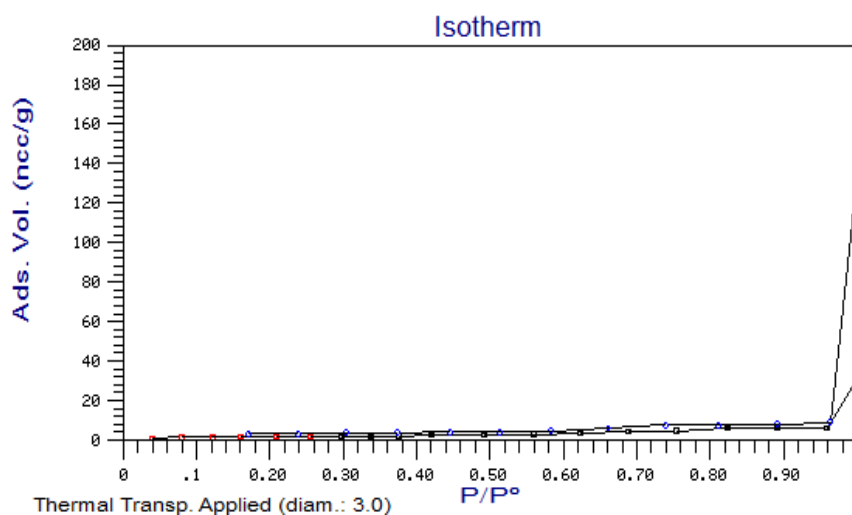
The specific surface area (Brunauer-Emmett-Teller (BET)) were determined by nitrogen adsorption-desorption isotherms (Table 1). The specific surface area of the polymers (NH₂-PIILP, Pyrr-PIILP) increased about three times after loading with [PdCl₄]²⁻ anions and increased even more after reduction to the palladium nanoparticles. Although PPh₂-PIILP has a high surface 62.4 (m²/g), this is decreases to 14.09 (m²/g) in the polymer loaded with [PdCl₄]²⁻, but then increases again to 54.65 (m²/g) when loaded with Pd nanoparticles. However, the corresponding [PtCl₄]²⁻ loaded PPh₂-PIILP as has a specific surface area of 10.08 (m²/g) which decreases to 6.3 (m²/g) after reduction with sodium borohydride, this it may attribute to the low loading of platinum nanoparticles 28.5% in PtNP@PPh₂-PIILP (Table 1).

Exchange of amino/ pyrrolidino with the PPh₂ functionalisation appears to dramatically alter the surface area of the material. This may alter the fundamental physicochemical properties of the support as the PPh₂ is more hydrophobic and may well interact very differently with solvent during processing enabling more facile solvent trapping/polymer swelling which could decrease the overall surface area. Evidenced by SEM analysis (See Appendices), it is clear that indeed the surface morphology of PPh₂PIILP is different to its amino and pyrrolidino counterparts. Furthermore, after the additional processing involved during impregnation and reduction steps, the SEM analysis of PPh₂ functionalised supports reveals a more granular surface which may be the reason for the increase in surface area.

Table 1 Specific surface and pore size distributions of the prepared materials.

Entry	Sample	Specific Surface Area (m ² /g)	Maximum Diameter (nm)	Average Diameter (nm)
1	NH ₂ -PIILP	5.56	-	-
2	PdCl ₄ @NH ₂ -PIILP	14.1	-	-
3	PdNP@NH ₂ -PIILP	49.41	2.82	5.92
4	Pyrr-PIILP	4.64	-	-
5	PdCl ₄ @Pyrr-PIILP	47.09	2.82	6.86
6	PdNP@Pyrr-PIILP	61.24	3.71	8.25
7	PPh ₂ -PIILP	62.4	-	-
8	PdCl ₄ @PPh ₂ -PIILP	14.09	-	-
9	PdNP@PPh ₂ -PIILP	54.65	-	-
10	PtCl ₄ @PPh ₂ -PIILP	10.08	-	-
11	PtNP@PPh ₂ -PIILP	6.3	-	-

Moreover, all isotherms are type (I) (Figure 4), except the isotherms for PdNP@NH₂-PIILP, PdCl₄@Pyrr-PIILP, PdNP@Pyrr-PIILP which are a mix between type (I and IV) hysteresis loop H₃ (Figure 5) according to IUPAC.¹⁴⁴ In this regard, the material would be a mixture of microporous and mesoporous if it is under type (I and IV) isotherm while it is likely to be microporous solid if it is type (I).

Figure 4 Nitrogen adsorption-desorption isotherm profile for NH₂-PIILP.

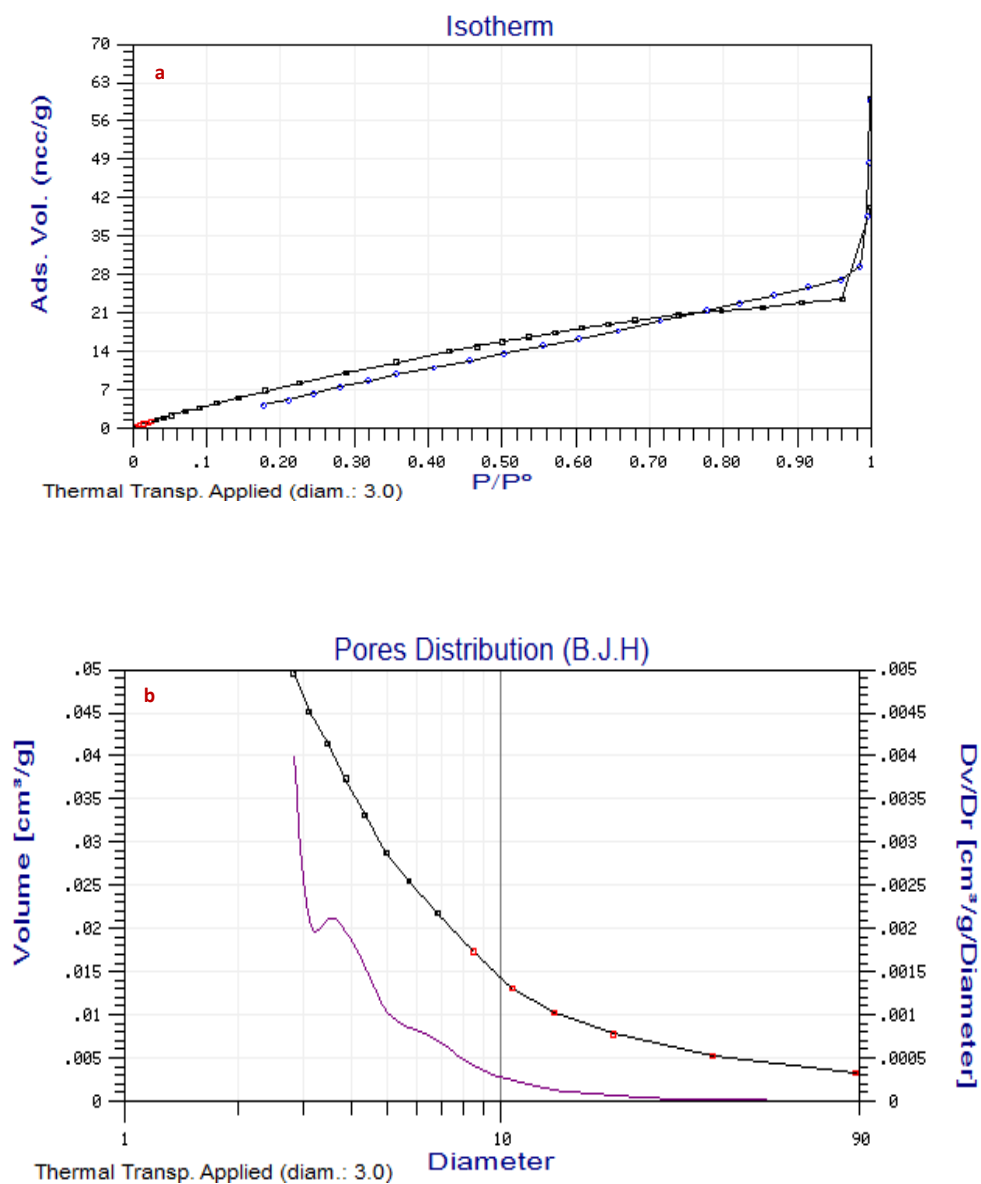


Figure 5 (a) Nitrogen adsorption–desorption isotherm profile, (b) Pore size distributions profile for PdNP@NH₂-PIILP.

*See **Appendices** for all Nitrogen adsorption–desorption isotherm profiles and pore size distributions profiles traces.

3.5.2 Solid-State (SSNMR) & Solution Nuclear Magnetic Resonance (NMR)

The solid-state ^{31}P NMR spectrum of $\text{PdCl}_4@\text{PPh}_2\text{-PIILP}$ (Figure 6 c) confirms the presence of a Pd–P interaction which is clearly evident from the change in the chemical shift from δ -5 to δ 28 ppm. In addition, the solid-state ^{31}P NMR spectrum of $\text{PdNP}@\text{PPh}_2\text{-PIILP}$ (Figure 6 d) does not contain any signals associated with uncoordinated PPh_2 ; this suggests that the surface of the palladium nanoparticles is decorated with phosphine groups. There are, however, multiple phosphorus environments between δ -7 and δ 30. This could be as a result of oxidation of the phosphine, generating the corresponding phosphine oxide or the multiple binding modes associated with polymer-tethered phosphines to a Pd surface rather than an isolated Pd atom. This effect has been observed by Iwai *et al.* where mono-, bi- and tridentate interactions between phosphorus and palladium were reported using crosslinked phosphine functionalised supports.¹⁷⁸ The same effect observed when the $\text{PPh}_2\text{-PIILP}$ loaded with PtCl_4 and PtNPs (Figures 6, and 7).

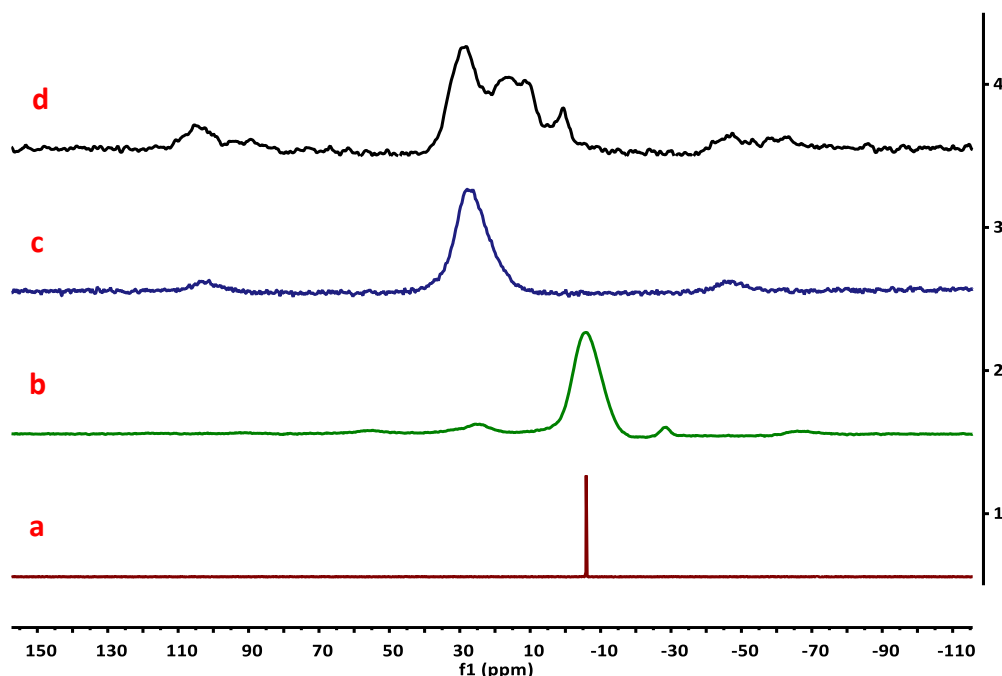


Figure 6 Stacked ^{31}P NMR spectra for: solution NMR (a) $\text{PPh}_2\text{-PIILP}$; solid-state NMR (b) $\text{PPh}_2\text{-PIILP}$; (c) $\text{PdCl}_4@\text{PPh}_2\text{-PIILP}$; and (d) $\text{PdNP}@\text{PPh}_2\text{-PIILP}$.

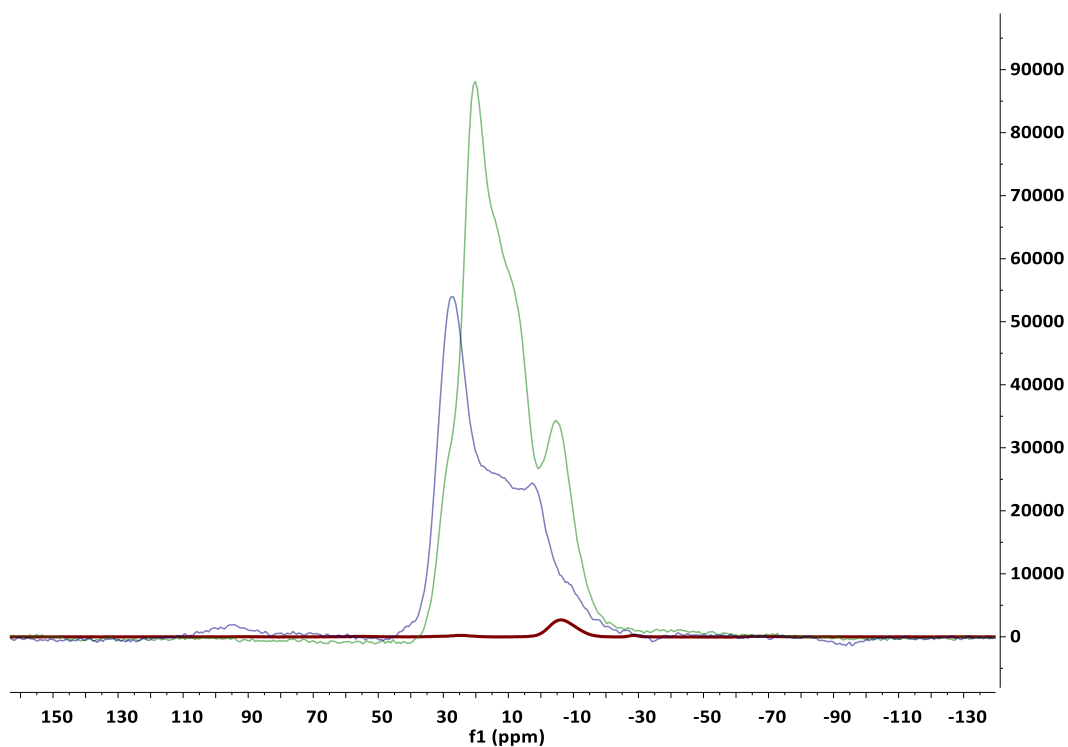


Figure 7 Superimposed Solid-state ^{31}P NMR for $\text{PPh}_2\text{-PIILP}$ red spectra, $\text{PtCl}_4\text{@PPh}_2\text{-PIILP}$ green spectra; and $\text{PtNP@PPh}_2\text{-PIILP}$ blue spectra.

A colour coded ^1H NMR spectrum of the phosphino-decorated polymer is shown in (Figure 8). The spectra show evidence that all the monomers were fully incorporated in the polymerisation, there are no sharp well-resolved signals characteristic of monomer.

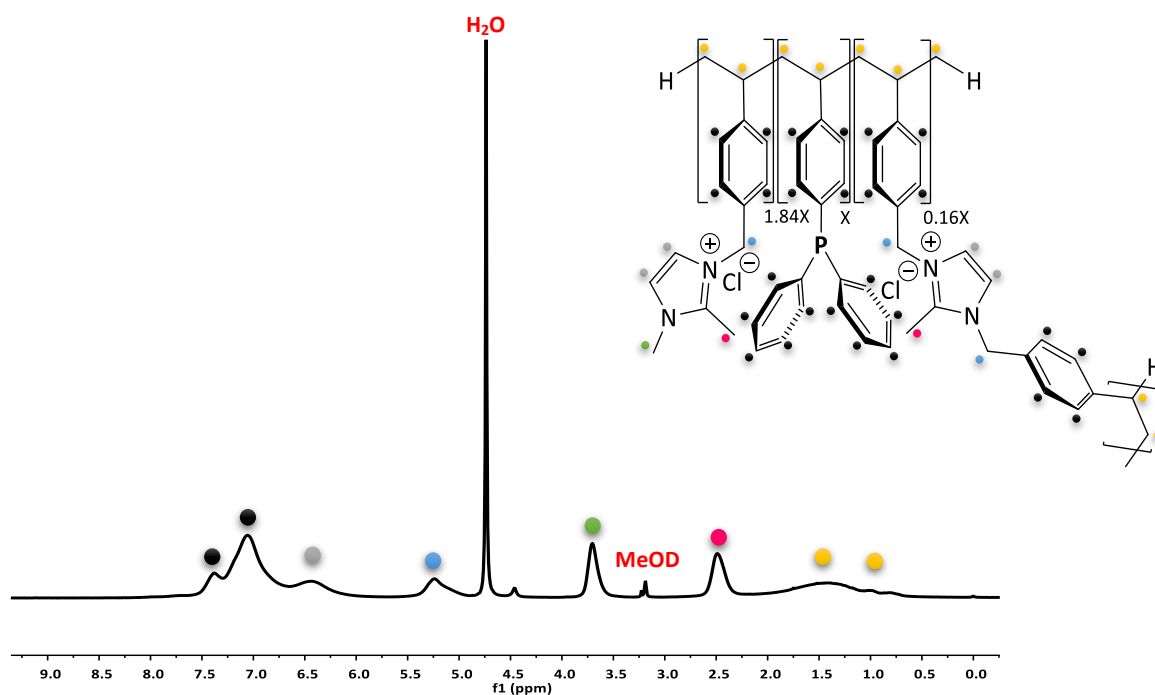


Figure 8 ^1H NMR spectra for polymer ($\text{PPh}_2\text{-PIILP}$) in MeOD.

*See **Appendices** for all (SSNMR&NMR) spectrum traces.

3.5.3 Transmission Electron Microscopy (TEM)

TEM analysis was performed for PdNP@NH₂-PIILP, PdNP@PPh₂-PIILP and PdNP@Pyrr-PIILP, and all the samples analysed consist of a small near monodisperse nanoparticles with an average diameter of 1.8 ± 0.525 nm, 2.87 ± 0.83 nm, and 1.57 ± 0.85 nm, respectively (Figures 9, 10, and 11).

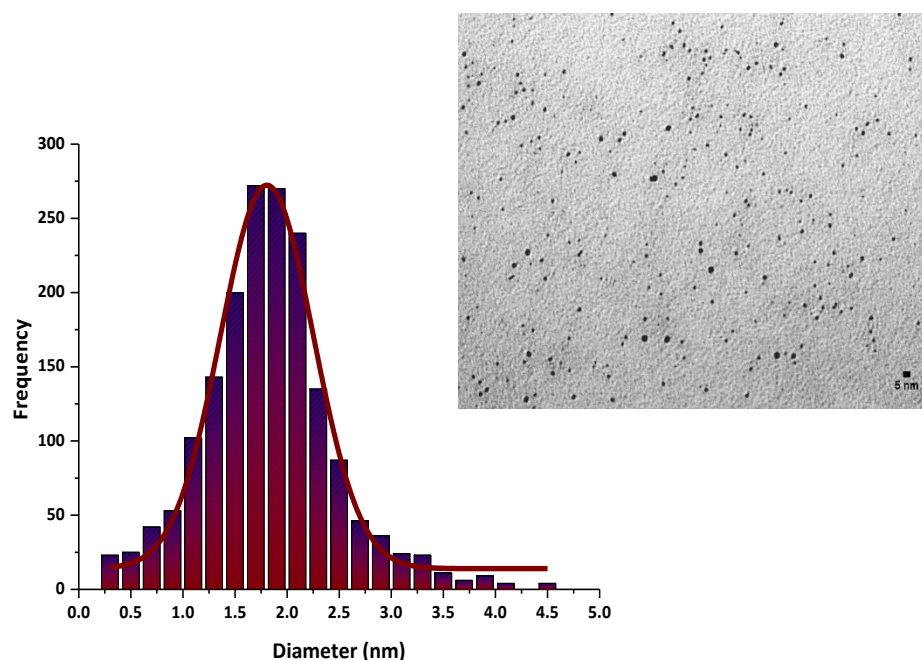


Figure 9 The calculated nanoparticles distribution of PdNP@NH₂-PIILP fitted by Gaussian equation.

The nanoparticles size distribution analysis (Figure 9) is demonstrated from a TEM image by ImageJ, then the frequency fitted by Gaussian equation.

Gaussian equation $\longrightarrow y = y_0 + \frac{Ae^{\frac{-4 \ln(2)(x-x_c)^2}{\omega^2}}}{\omega \sqrt{\frac{\pi}{4 \ln(2)}}}$

For example, the calculation for PdNP@NH₂-PIILP

> 1755 particles

Average NP size (χ_c) = 1.8 nm,

ω = 1.1 nm,

Standard deviation (σ) = $\omega/2$ = 0.55 nm

Average NP size with error = $\chi_c \pm \sigma$ = 1.8 \pm 0.55 nm

Polydispersity = (σ/χ_c) * 100% = (0.55/1.8) * 100% = 36.6%

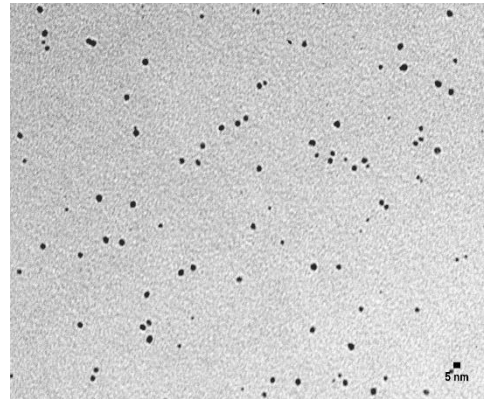
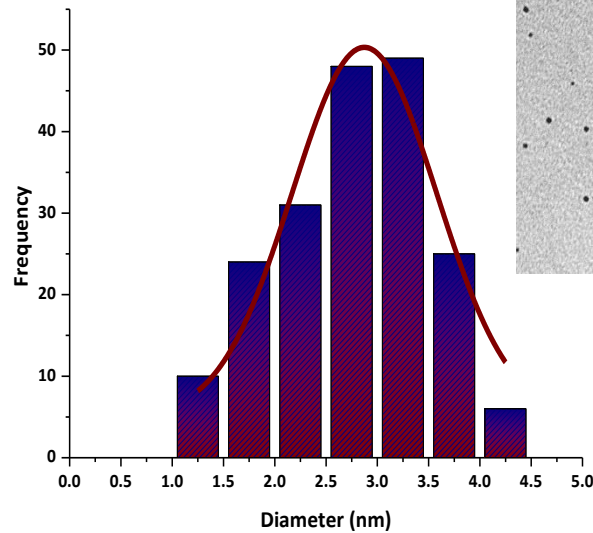
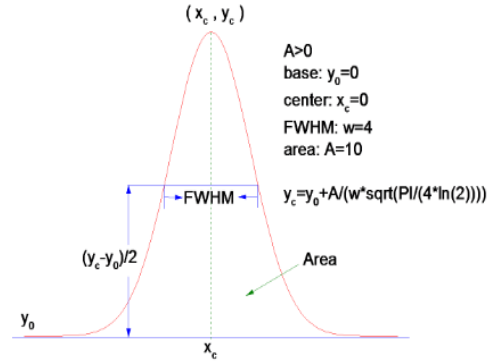


Figure 10 The calculated nanoparticles distribution for PdNP@PPh₂-PIILP fitted by Gaussian equation.

The TEM image of PdNP@PPh₂-PIILP shows that palladium nanoparticles are highly dispersed in the polymer matrix. The particle size distribution was determined by counting > 190 particles, and the average NP size was 2.87 ± 0.83 nm, with a polydispersity 28.9% (Figure 10).

However, the TEM images of PdNP@Pyrr-PIILP shows that palladium nanoparticles are large in comparison with the other two catalysts. The particle size distribution was determined by counting > 2900 particles which gave an average NP size of 1.57 ± 0.85 nm, with a polydispersity of 54.14 % (Figure 11).

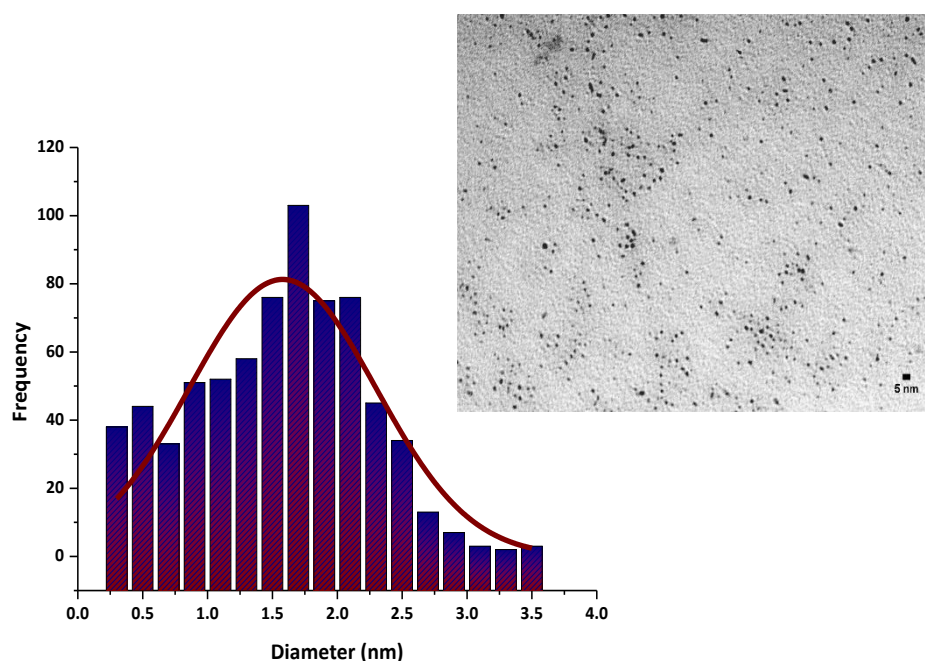


Figure 11 The calculated nanoparticles frequency of PdNP@Pyrr-PIILP fitted by Gaussian equation.

3.5.4 Energy-Dispersive X-Ray Spectroscopy (EDX)

To identify elements, present in the prepared catalysts each sample was analysed by SEM/EDX spectroscopy. The pure PPh₂-PIILP showed peaks for oxygen, nitrogen, carbon, phosphorus, and chlorine. New peaks appear attributed to palladium, chloride, and a trace of sodium, presumably due to the use of excess sodium chloride used to [PdCl₄]²⁻ in preparation of PdCl₄@PPh₂-PIILP. While the peaks of sodium disappeared with some traces of chloride in the sample of PdNP@PPh₂-PIILP, that's mean all the [PdCl₄] anions are reduced to produce PdNP, in addition to the intensity of the Pd increased which indicates high palladium content (Figure 12).

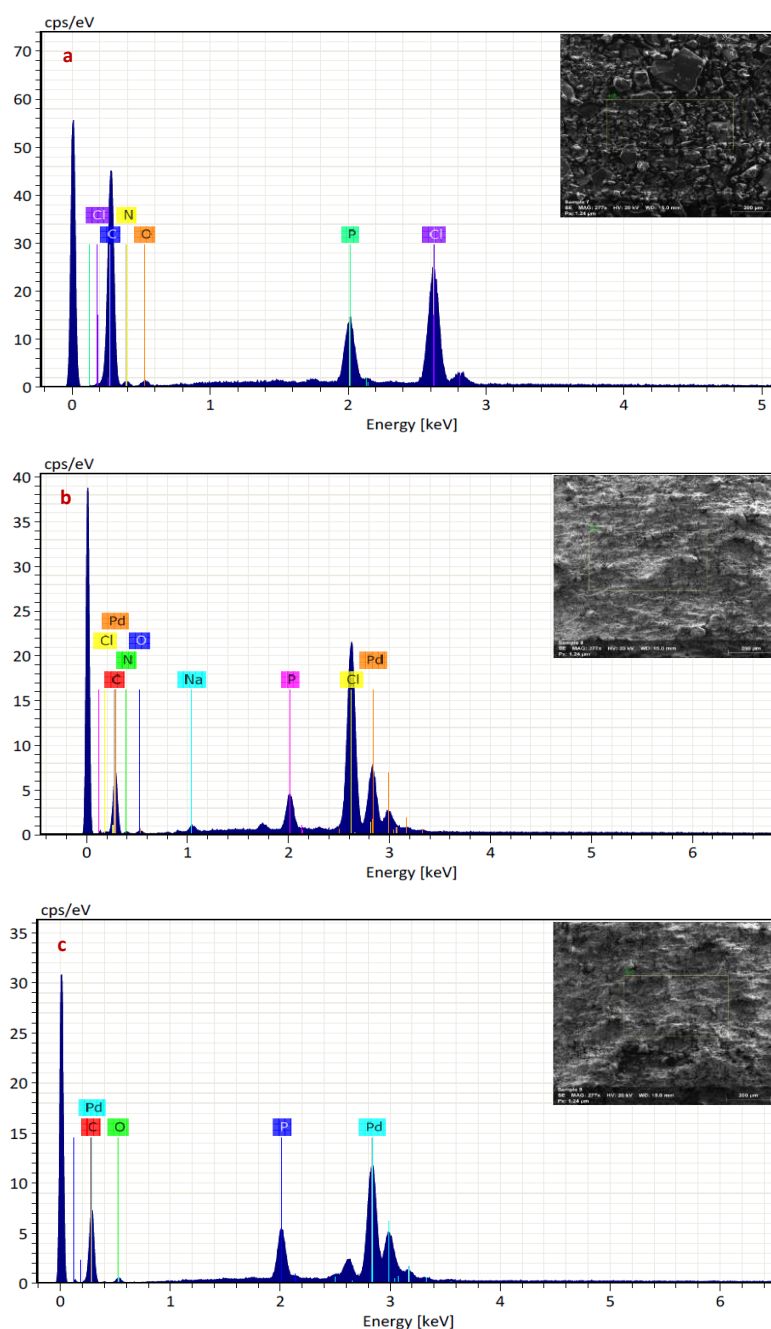


Figure 12 (SEM/EDX) spectroscopy of (a) PPh₂-PIILP, (b) PdCl₄@PPh₂-PIILP, and (c) PdNP@PPh₂-PIILP.

The EDX spectra of $\text{PtCl}_4@\text{PPh}_2\text{-PIILP}$, and $\text{PtNP}@\text{PPh}_2\text{-PIILP}$ are shown in (Figure 13). Again, there is a significant reduction in the intensity of chloride peak which may indicate the reduction process of the $[\text{PtCl}_4]^{2-}$ to PtNP has almost completely done.

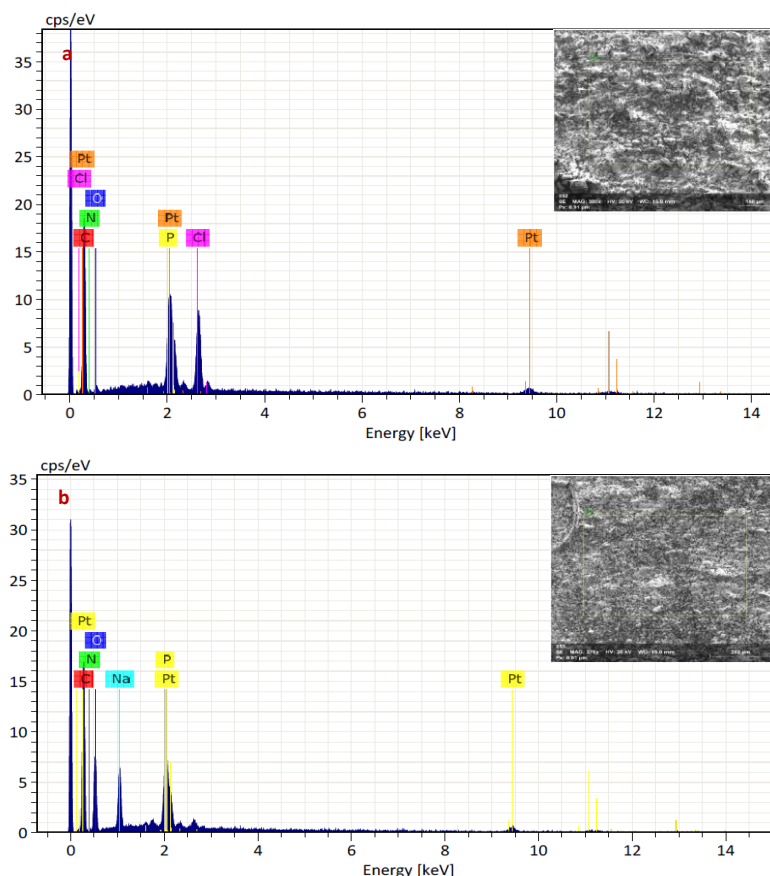


Figure 13 (SEM/EDX) spectroscopy of (a) $\text{PtCl}_4@\text{PPh}_2\text{-PIILP}$, and (b) $\text{PtNP}@\text{PPh}_2\text{-PIILP}$.

*See **Appendices** for all (SEM/EDX) spectra.

3.5.5 X-Ray Powder Diffraction (XRD)

In (Figures 15, and 16) the X-Ray powder diffraction patterns of all prepared catalysts ($\text{PdNP}@\text{NH}_2\text{-PIILP}$, $\text{PdNP}@\text{Pyr-PIILP}$, $\text{PdNP}@\text{PPh}_2\text{-PIILP}$, and $\text{PtNP}@\text{PPh}_2\text{-PIILP}$) are shown. All patterns (Figure 14) show broad peaks (the centre approximately at $2\theta = 20^\circ$) which belongs to the amorphous structure of the polymer. The expected sharp intensity of metals was lower in the immobilised samples due to the effect of a very large amount of polymeric material in those samples.

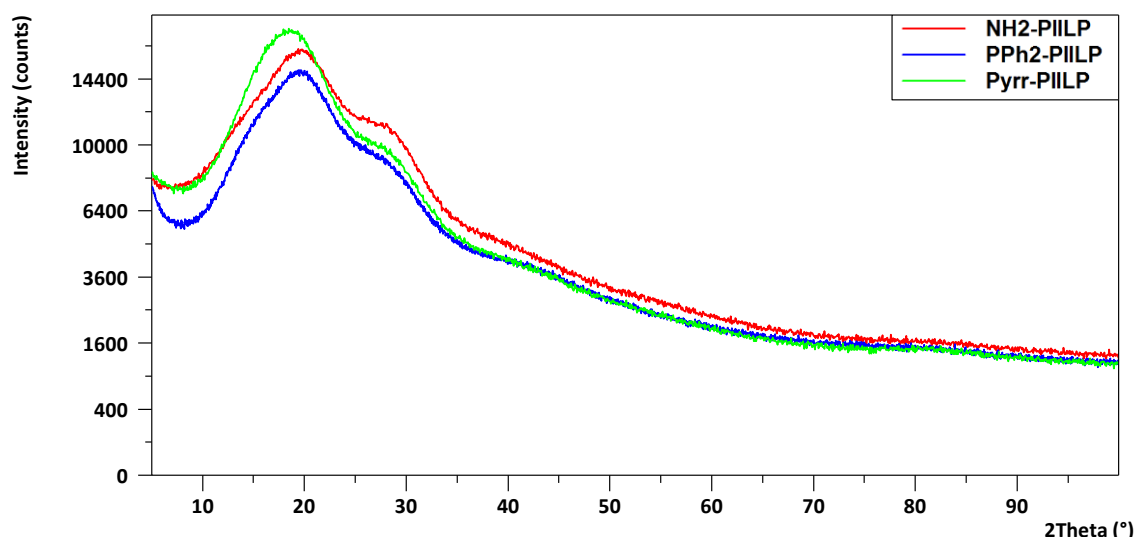


Figure 14 Powder XRD stacked patterns of $\text{NH}_2\text{-PIILP}$, $\text{PPh}_2\text{-PIILP}$, and Pyrr-PIILP .

Diffraction peaks at $2\theta = 40^\circ$ (111), $2\theta = 46.7^\circ$ (200), $2\theta = 68^\circ$ (220), $2\theta = 82^\circ$ (311), and $2\theta = 86.7^\circ$ (222) correspond to the palladium metal in $\text{PdNP@NH}_2\text{-PIILP}$ which confirms successful Pd loading and reduction, however, the peaks are less intense in PdNP@Pyrr-PIILP (Figure 15). In comparison, the powder XRD patterns for $\text{PdNP@PPh}_2\text{-PIILP}$, and $\text{PtNP@PPh}_2\text{-PIILP}$ (Figure 16) show some variation in the Bragg intensities, indicating the successful loading of Pd or Pt nanoparticles in the $\text{PPh}_2\text{-PIILP}$.¹⁷⁹ In addition, no diffraction peaks corresponding to Pd crystallite can be observed over the $\text{PdNP@PPh}_2\text{-PIILP}$ and $\text{PtNP@PPh}_2\text{-PIILP}$ which implies that the highly dispersed Pd or Pt species exist as nanoparticles or in an amorphous component.¹⁷⁹

The above diffraction peaks are consistent with face-centered cubic (fcc) crystalline palladium and platinum. According to the Debye-Scherrer equation,¹⁸⁰ the average palladium and platinum nanoparticle crystallite size for each sample was calculated using the (111) reflection as shown below.

Debye–Scherrer Equation $\longrightarrow \mathcal{T} = \frac{k\lambda}{(\beta_s \cos \theta)}$

k : Shape factor (a value of 0.9 assumes spherical crystallites).

λ : The wavelength of the x-ray radiation (Å).

β_s : $\beta_{\text{structural}} = \beta_{\text{observed}} - \beta_{\text{standard}}$ (the full-width at half-maximum (FWHM) of the peak).

θ : The angle of diffraction (half the Bragg angle in radians).

For example, the calculation for PdNP@NH₂-PIILP

$$\mathcal{T} = \frac{0.9 * 1.541874}{\left(\left(\frac{(2.34) * \pi}{180} \right) * \left(\cos \left(\left(\frac{39.9}{2} \right) * \pi / 180 \right) \right) \right)} = 36.10 \text{ Å} = 3.61 \text{ nm}$$

The size of the palladium nanoparticle in PdNP@NH₂-PIILP, PdNP@PPh₂-PIILP, and PdNP@Pyrr-PIILP were calculated to be 3.61, 3.01, and 1.79 nm, respectively, while the calculated platinum nanoparticle size for PtNP@PPh₂-PIILP was 6.11 nm. All the calculated average sizes were in good agreement with the analysed size measured by TEM. In this regard, it's important to take into an account the accuracy of the sizes determined using the Scherrer equation as it is affected by the uncertainties of k and β values, and the error percentage may well be as high 20 percent.¹⁸¹

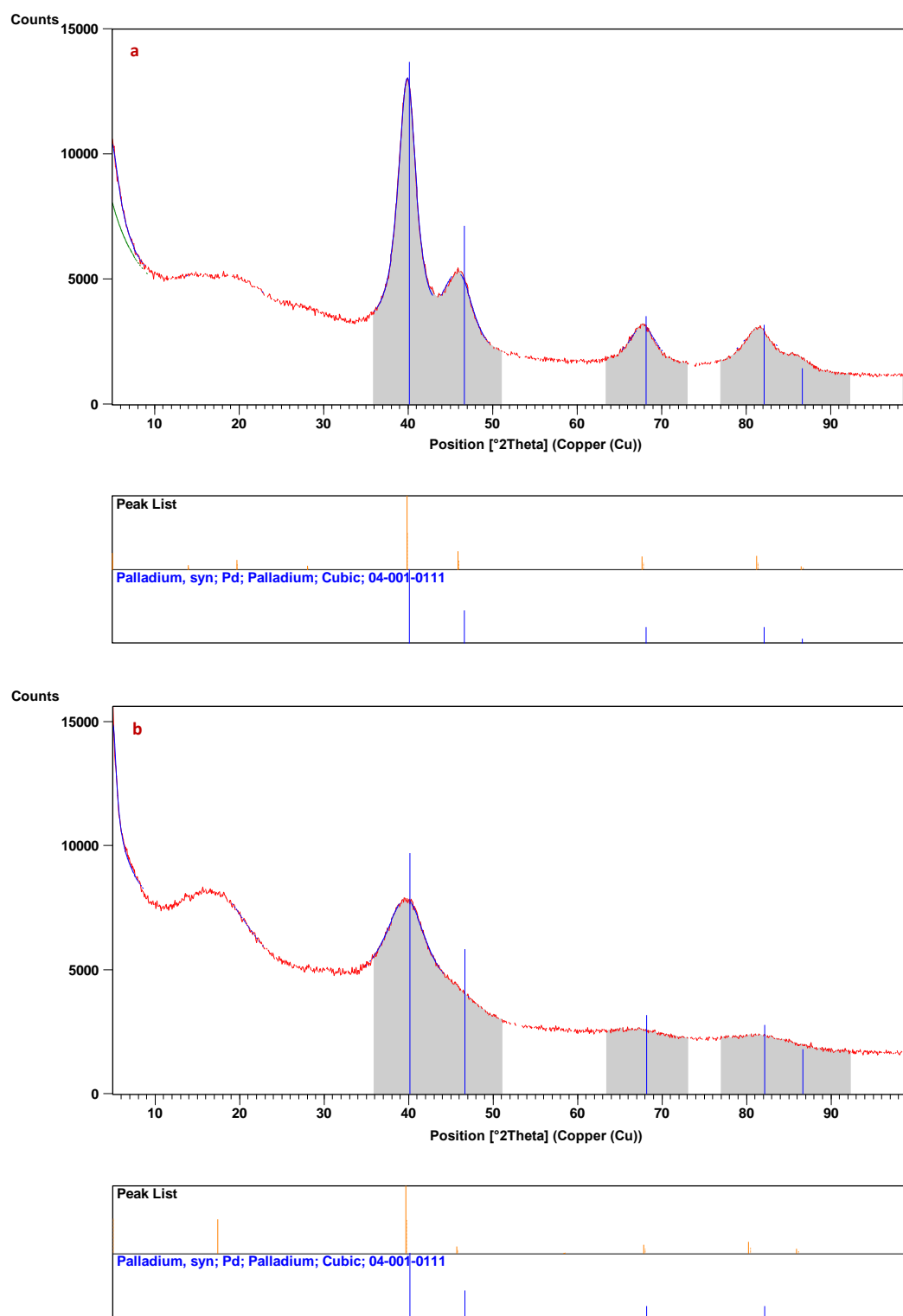


Figure 15 Powder XRD patterns of (a) PdNP@NH₂-PIILP, and (b) PdNP@Pyrr-PIILP.

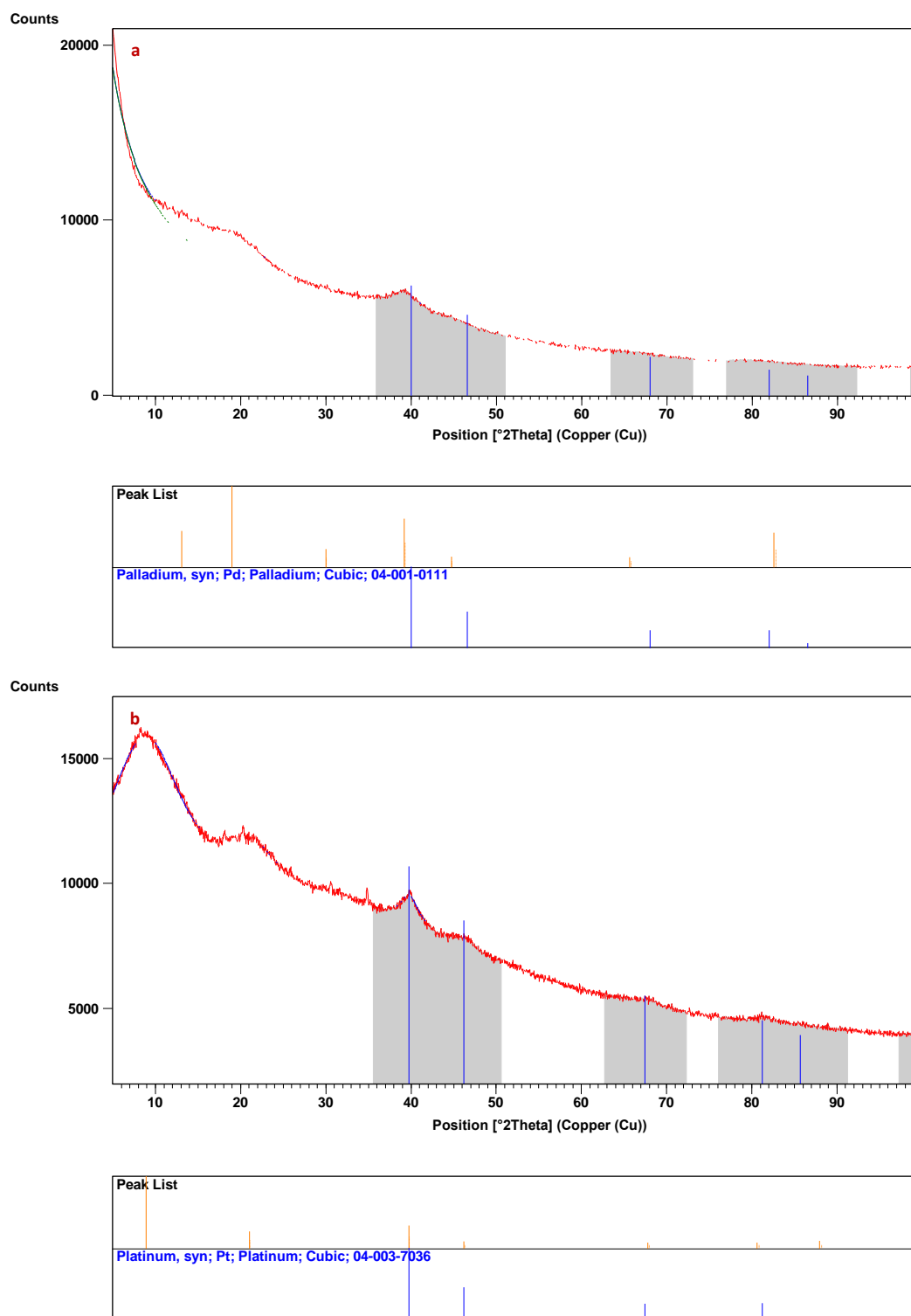


Figure 16 Powder XRD patterns of (a) PdNP@PPh₂-PIILP, and (b) PtNP@PPh₂-PIILP.

3.5.6 ICP Optical Emission Spectrometry (ICP-OES)

The palladium and platinum contents were determined by ICP-OES. (Table 2) shows the calculated amount of metal per gram of polymer and the metal percent loading based on repeating unit. Interestingly, the palladium content in the phosphine-based tetrachloropalladate and the corresponding PdNP was similar indicating negligible loss of palladium in the reduction step. However, in contrast, the palladium content in the tetrachloropalladate and PdNP amino-based systems were markedly disparate indicating significant leaching of the palladium in the reduction step.

Table 2 ICP Optical Emission Spectrometry (ICP-OES) results of the prepared catalysts.

Entry	Sample	Metal (mol/ g of polymer)	Metal content (wt %)
1	PdCl ₄ @NH ₂ -PIILP	1.109*10 ⁻³	11.8
2	PdNP@NH ₂ -PIILP	0.633*10 ⁻³	6.7
3	PdCl ₄ @Pyrr-PIILP	1.298*10 ⁻³	13.8
4	PdNP@Pyrr-PIILP	1.038*10 ⁻³	11.0
5	PdCl ₄ @PPh ₂ -PIILP	0.854*10 ⁻³	9.1
6	PdNP@PPh ₂ -PIILP	1.095*10 ⁻³	11.7
7	PtCl ₄ @PPh ₂ -PIILP	0.252*10 ⁻³	4.9
8	PtNP@PPh ₂ -PIILP	0.385*10 ⁻³	7.5

3.5.7 Thermogravimetry Analysis (TGA)

Thermogravimetric analysis (TGA) was used to evaluate the thermal stability of all prepared polymers and some of their loaded materials detail of which are shown in (Figures 17, and 18).

All the TGA traces showed an initial loss in the percent weight about (~ 5 %), and this could be attributed to the evaporation of some residual reaction solvent or water. The degradation of the amino-, phosphino-, and pyrrolidino-decorated polymer was characterised by three steps (Figure 17). The first degradation stage was around (~ 230 °C), then the degradation of the imidazole pendants around (~ 320 °C) followed with final large decomposition step around (~ 410 °C) which corresponds to the decomposition of the main polymer backbone, interestingly, by (~ 500 °C) about 20 % of the material weight remained even when the temperature reached (~ 800 °C).^{182, 183}

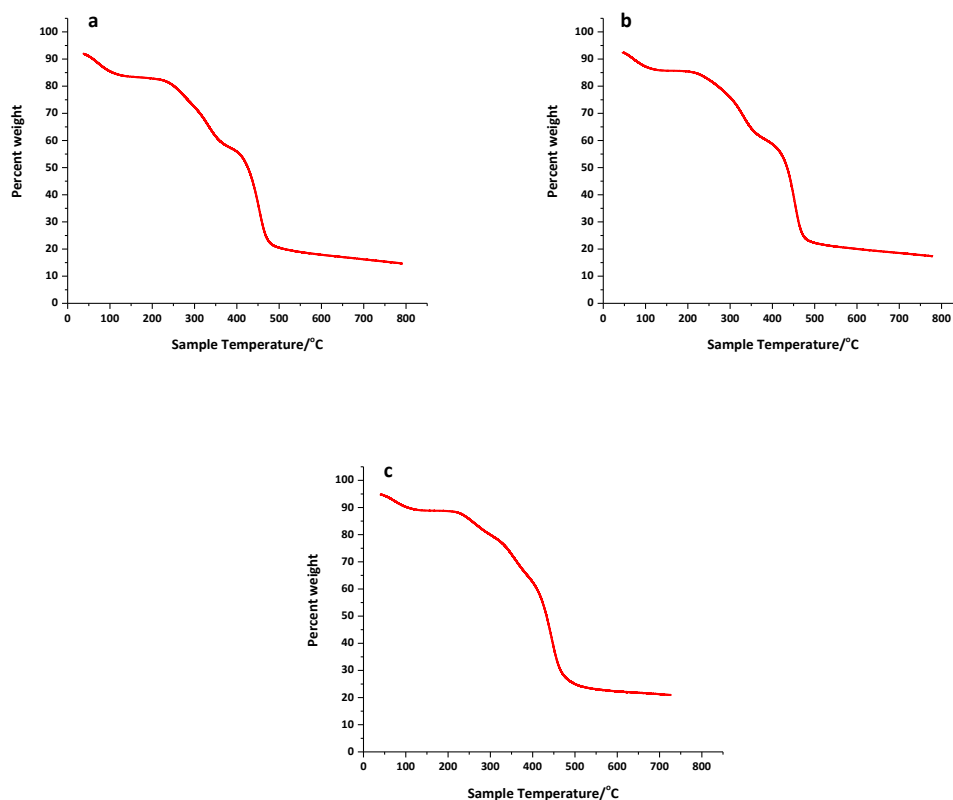


Figure 17 TGA traces of (a) NH₂-PIILP, (b) Pyrr-PIILP, and (c) PPh₂-PIILP.

In comparison (Figure 18) shows the TGA curves of PPh₂-PIILP polymer loaded with tetrachloropalladate and platinate as well as the corresponding PdNP and PtNP systems. Unlike, the free polymers and PdNP@PPh₂-PIILP which showed three main degradation stages, here there are only two steps around (~ 250 °C), then (~ 450 °C) corresponding to a weight loss of *c.a.* 50 %. This weight loss remained constant above 450 °C until the temperature reached (~ 800 °C); this suggests extremely high thermal stability which may well be affected by the metal contents.

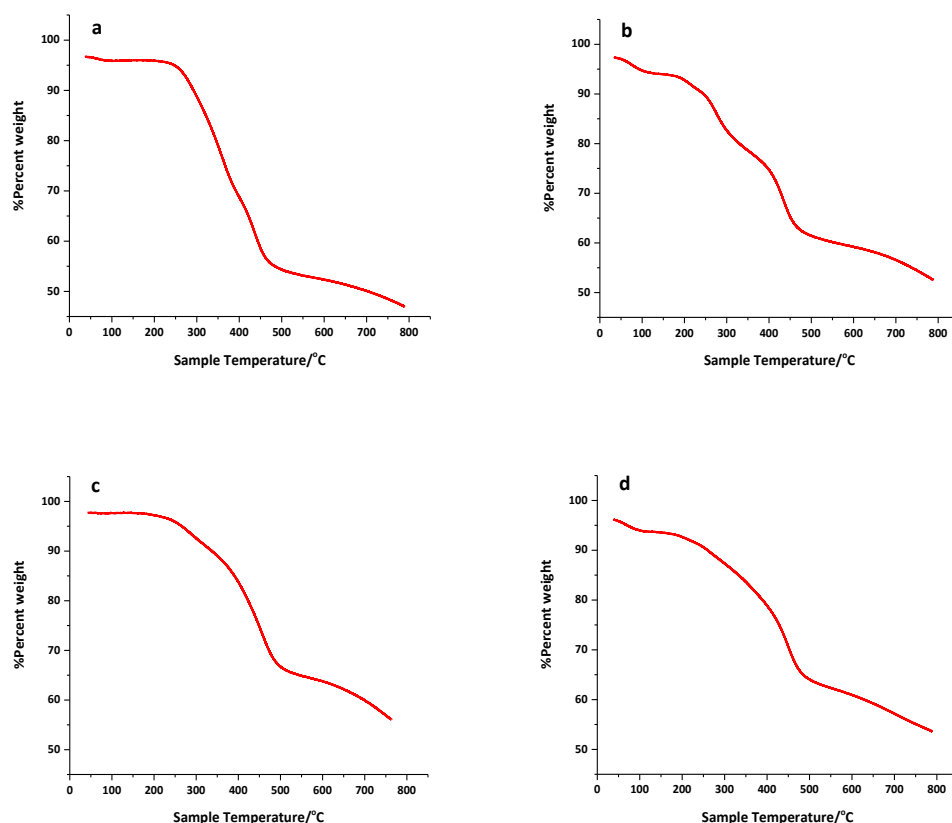


Figure 18 TGA traces of (a) PdCl₄@PPh₂-PIILP, (b) PdNP@PPh₂-PIILP, (c) PtCl₄@PPh₂-PIILP, and (d) PtNP@PPh₂-PIILP.

3.5.8 X-Ray Photoelectron Spectroscopy (XPS)

X-ray photoelectron spectroscopy (XPS) analysis was conducted on PdCl₄@R-PIILP, PdNP@R-PIILP (R=CH₂NH₂, PPh₂, CH₂Pyrr), PtCl₄@PPh₂-PIILP, and PtNP@PPh₂-PIILP to find out the oxidation state of palladium or platinum in the analysed samples. XPS spectra were calibrated based on the binding energy of the C 1s electron at 284.6 eV and were fitted by using CASAXPS software. XPS fitted spectra were obtained for each of Pd^{II}, PdNP two spin-orbital ($3d_{5/2}$, $3d_{3/2}$), and also for Pt^{II} and PtNP two spin-orbital ($4f_{7/2}$, $4f_{5/2}$).

All the PdNP samples have Pd^{II} doublet peaks and it has appeared in high composition, this may attribute to incomplete reduction of the sample; this agrees with studies published recently on the sodium borohydride reduction of polymer supported PdCl₄.^{184, 185} This was attributed to the lack of accessibility of the reducing agent to the Pd^{II} sites

which were dispersed within the matrix of polymer. Alternatively, the presence of Pd^{II} in PdNP based systems have been reported to arise from the oxidation of surface PdNP by exposure to air.¹⁸⁶

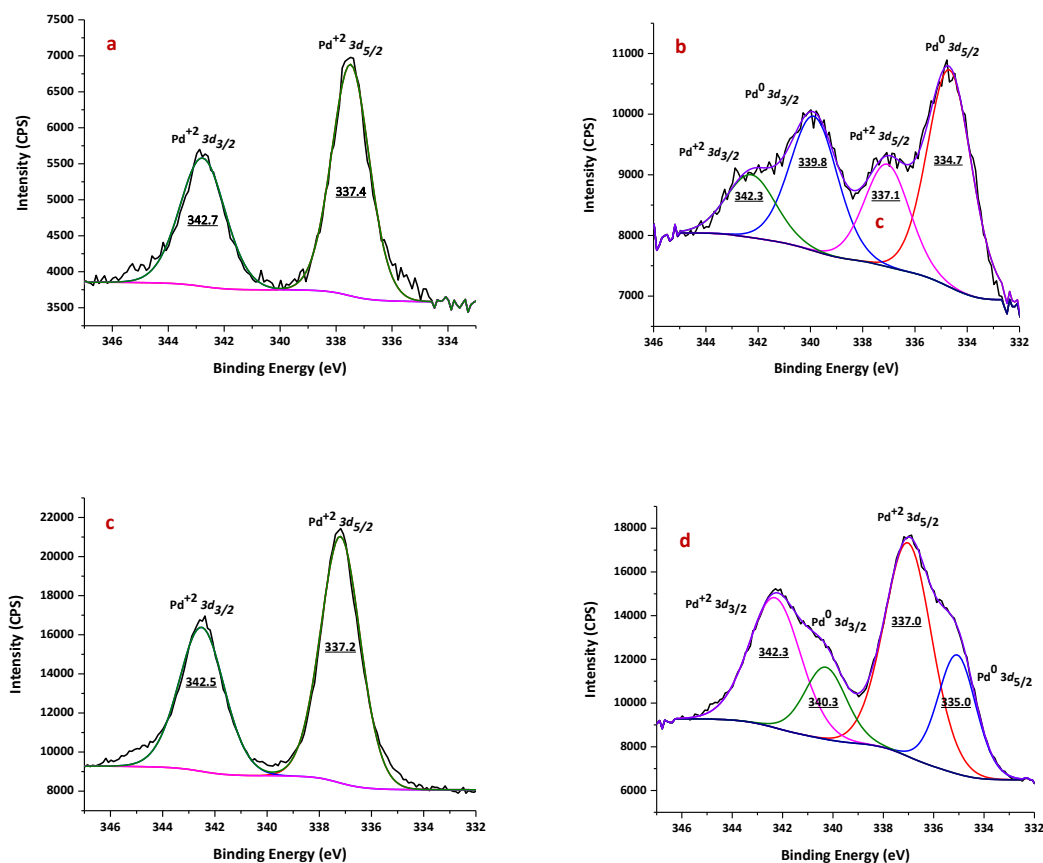


Figure 19 XPS spectra (a) PdCl₄@NH₂-PIILP, (b) PdNP@NH₂-PIILP, (c) PdCl₄@Pyrr-PIILP, and (d) PdNP@Pyrr-PIILP.

Although PdNP@Pyrr-PIILP sample was reduced using hydrogen gas it still had a high Pd^{II} content as shown in (Figure 19 d). The previous XPS results led us to do an extend studies by preparing samples of PdNP@PPh₂-PIILP for XPS samples freshly under vacuum and the results of this study are shown in (Figures 20-b, c, and d). Interestingly, the percentage of Pd^{II} and the area of the peak decreased, which strongly suggests that the Pd^{II} peaks in PdNP samples are associated with oxides, hydrides and/or carbenes species which are available in the reaction media or re-oxidation of the metal nanoparticle surface by exposure to air.^{56, 186, 187} (Figures 20-e, and f) clearly show that PtCl₄@PPh₂-PIILP contains both Pt^{IV} and Pt^{II} and that PtNP@PPh₂-PIILP also contains Pt^{IV} and Pt^{II} as

well as PtNP. Again, both the Pt^{IV} and Pt^{II} species appear upon exposure of the measured sample to air.¹⁸⁸⁻¹⁹⁰

*See **Appendices** for all XPS survey traces.

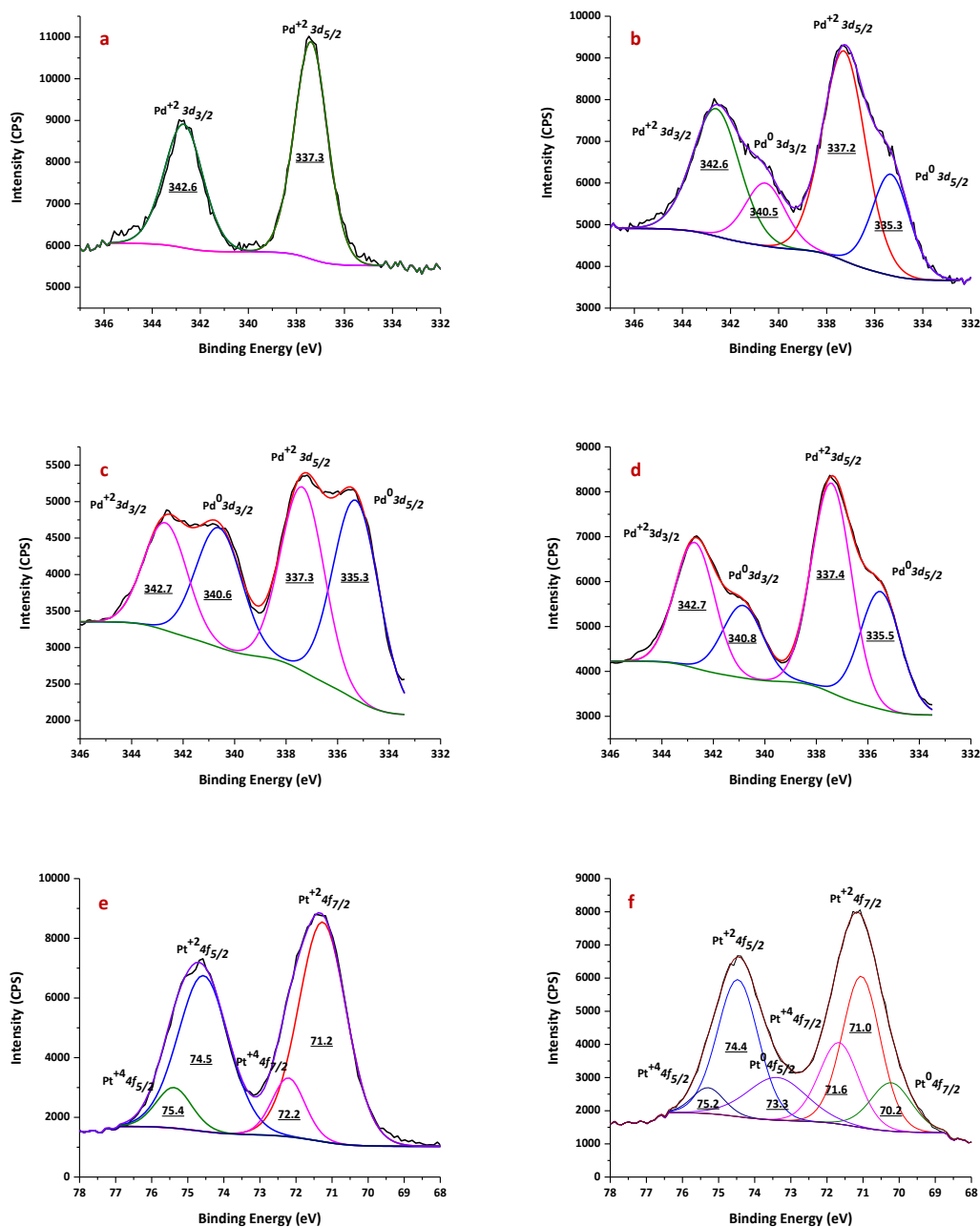


Figure 20 XPS spectra (a) PdCl₄@PPh₂-PIILP, (b) PdNP@PPh₂-PIILP 1, (c) PdNP@PPh₂-PIILP 2, (d) PdNP@PPh₂-PIILP 3, (e) PtCl₄@PPh₂-PIILP, and (f) PtNP@PPh₂-PIILP.

3.6 Conclusion

Amino-, phosphino- and pyrrolidino-decorated polystyrene-based PIILs were successfully synthesised by the free radical copolymerization. The PIILs were loaded with either Pd^{II} or Pt^{II} by anion exchange using an aqueous solution of Na₂PdCl₄ and K₂PtCl₄, respectively to afford MCl₄@R-PIILP (M = Pd, Pt, R = CH₂NH₂, PPh₂, CH₂Pyrr). Reduction of MCl₄@R-PIILP with either NaBH₄ or by hydrogenation gave the corresponding polymer immobilised ionic liquid supported nanoparticles PdNP@R-PIILP with average diameters of 1.8 ± 0.525 nm, 2.87 ± 0.83 nm, and 1.57 ± 0.85 nm, respectively. Interestingly, the nanoparticles in PdNP@PPh₂-PIILP were much more dispersed and had a noticeably smaller size distribution than those of their amino and pyrrolidino counterparts which suggests that it may well be possible to control the properties and thereby the performance of metal nanoparticles with heteroatoms donor modified polymer immobilised ionic liquids. The following two chapters evaluate the performance of the prepared catalysts for the selective reduction of α,β -unsaturated aldehydes, and the Suzuki-Miyaura cross coupling.

3.7 Laboratory Preparation Procedures

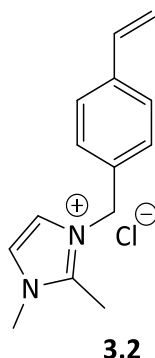
- **General Comments**

All manipulations involving air-sensitive compounds were carried out using standard Schlenk line techniques under an atmosphere of nitrogen in oven-dried glassware. All the solvents were dried and distilled under a nitrogen atmosphere, chloroform and dichloromethane were distilled from calcium hydride, and diethyl ether and tetrahydrofuran from sodium wire/benzophenone; toluene and hexane from sodium wire; acetonitrile from potassium carbonate; methanol and ethanol from magnesium; while dimethylformamide was distilled under vacuum. All chemicals were bought from commercial suppliers and used as received without further purification. ^1H and $^{13}\text{C}\{^1\text{H}\}$ NMR spectra were recorded on either JEOL ECS-400 or a Bruker Avance III 300 spectrometer. Spectrum Two™ FT-IR Spectrometers by PerkinElmer were used to record the on FT-IR spectrums, and all the data were collected over a spectral range (4000-400) cm^{-1} . Specific surface area and pore sizes were obtained from N_2 adsorption-desorption curves that obtained using Thermo Scientific™ SURFER at the Newcastle University. Brunauer-Emmett-Teller (BET) method was used to measure the specific surface area of the adsorption curve and pore size distribution was measured by Barrett-Joyner-Halenda (BJH) method via using the desorption curve. All sample were outgassed at 90 °C for 30 hours prior to analysis. The (SEM/EDS) analysis was taken using a high-resolution imaging of surfaces by a Tescan Vega 3LMU scanning electron microscope fitted with a detector (Bruker XFlash® 6 | 30). Solid-state NMR were recorded using a Bruker Avance III HD, and a 4 mm HX MAS/magic-angle spinning probe. They were obtained using the type of measurement (cross-polarisation (CP), direct excitation (DE)), Chemical shifts were referenced: carbon to neat tetramethylsilane, phosphorus to 85 % H_3PO_4 , proton to neat tetramethylsilane. Powder X-ray diffraction patterns (XRD) were recorded using a PANalytical X'Pert Pro Multipurpose Diffractometer (MPD) using $\text{Cu K}\alpha/\beta$ radiation of wavelength of 1.5418 Å. Thermogravimetric analysis (TGA) was *performed* using a Simultaneous Thermal Analyser (STA) 6000 instrument/Perkin Elmer, at a heating rate of 10 °C min^{-1} under argon gas atmosphere (BOC), argon flow 40ml/min. The onset of the weight loss in each thermogram was used as a measure of the decomposition temperature. The palladium loading was quantified using inductively coupled plasma optical emission spectroscopy (ICP-OES) ICP analysis was conducted using a Perkin-Elmer Optima 4300 ICP-OES analyser. SEM images were acquired on a

Tescan Vega 3LMU scanning electron microscope with digital image collection. TEM images were acquired in a bright field using a Tecnai 200 kV F20 Transmission Electron Microscope with a Field Emission Gun. A few drops of the sample were pipetted onto an Agar holey carbon film copper TEM grids and the prepared grid was set aside for *c.a.* 20 min prior to inserting it into the microscope, in order to allow the solvent to evaporate. Images were taken with a Gatan CCD digital camera attached to the microscope and processed using Image J software. XPS analysis was *per-formed* with a Kratos Axis Nova spectrometer. The solid catalysts were fixed on the support using a carbon double-sided adhesive tape. The spectra were excited by the monochromatized Al Ka source (1486.6 eV) run at 15 kV and 10 mA. For the individual peak regions, a pass energy of 20 eV was used. Survey spectrum was measured at 160 eV pass energy. Analysis of the peaks was *per-formed* with the CasaXPS software.

See **Appendices for all characterisation results.*

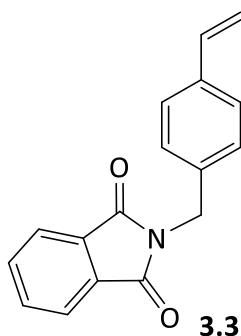
3.7.1 Synthesis of 1, 2-dimethyl-3-(4-vinylbenzyl) imidazolium chloride [DMVBIM][Cl] (3.2)¹⁷⁴



An oven-dried Schlenk flask was allowed to cool to room temperature and charged with a mixture of 1, 2-dimethyl imidazole (5.25 g, 54.6 mmol) and 4-chloromethyl styrene (10.84 g, 71.0 mmol) then stirred in (50 mL) of chloroform overnight at 50 °C. The solvent was then removed under vacuum. The residue washed with ethyl acetate (4 × 50 mL) to give a white solid that was filtered and dried under vacuum to afford **3.2** in (13.5 g, 54.27 mmol, 100 %, 248.75 g/mol).

¹H NMR (399.78 MHz, CDCl₃, δ): 7.72 – 7.57 (dd, *J* = 14.5, 2.0 Hz, 2H), 7.35 (d, *J* = 8.2 Hz, 2H), 7.26 (d, *J* = 9.0 Hz, 2H), 6.63 (dd, *J* = 17.6, 10.9 Hz, 1H), 5.71 (d, *J* = 17.7 Hz, 1H), 5.51 (s, 2H), 5.25 (d, *J* = 10.8 Hz, 1H), 3.92 (s, 3H), 2.73 (s, 3H); ¹³C{¹H} NMR (101 MHz, CDCl₃, δ): 144.33, 138.42, 135.84, 132.47, 128.58, 127.13, 122.95, 121.94, 115.39, 52.17, 35.91, 10.96.

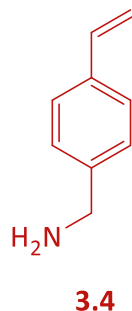
3.7.2 Synthesis of *N*-[(4-vinylphenyl) alkyl] phthalimide (**3.3**)¹⁷⁵



An oven-dried Schlenk flask was allowed to cool to room temperature and charged with a mixture of 4-chloromethyl styrene (26.6 mmol), potassium phthalimide (27.4 mmol) and dry DMF (25 mL). The reaction mixture was heated at 55 °C under nitrogen with stirring for 17 hours. The reaction solvent was reduced under low pressure, then DCM (350 mL) was added to the residue, washed with water (6 x 250 mL), and then dried over magnesium sulfate. The solvent was removed under reduced pressure, then the product was dissolved in chloroform (50 mL) and washed with 0.2 M sodium hydroxide (15 mL), washed with water (2 x 15 mL) and dried over magnesium sulfate. The removal of the solvent at reduced pressure afforded a crude solid which was crystallised from methanol to afford **3.3** in (5.2 g, 19.74 mmol, 75 %, 263.30 g/mol).

¹H NMR (300.13 MHz, CDCl₃, δ): 7.78 (dd, *J* = 5.5, 3.0 Hz, 2H), 7.64 (dd, *J* = 5.5, 3.0 Hz, 2H), 7.37 – 7.24 (m, 4H), 6.60 (dd, *J* = 17.6, 10.9 Hz, 1H), 5.64 (d, *J* = 18.5 Hz, 1H), 5.15 (d, *J* = 10.9 Hz, 1H), 4.76 (s, 2H); ¹³C{¹H} NMR (75 MHz, CDCl₃, δ): 168.14, 137.32, 136.24, 135.84, 134.01, 132.11, 128.87, 126.49, 123.37, 114.17, 41.35.

3.7.3 Hydrazinolysis of Phthalimides to Afford **3.4**¹⁷⁵

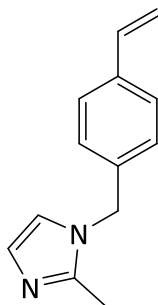


An oven-dried three neck round-bottom flask was allowed to cool to room temperature and charged with phthalimide **3.3** (38.3 mmol) and 95 % ethanol (100 mL) under nitrogen. A solution of hydrazine hydrate (2.74 g, 54.7 mmol) in 95 % ethanol (5 mL) was added and the resulting mixture was stirred and heated at reflux for 3.5 hours up to the disappearance of **3.3** (TLC, eluent benzene). The solvent was removed under reduced pressure the solid residue was taken into chloroform (50 mL) and treated with 20 % aqueous sodium hydroxide (50 mL). The aqueous phase was separated, extracted with chloroform (3 × 50 mL) and the extracts combined and dried over magnesium sulfate. The removal of chloroform afforded monomer **3.4** in (4.59 g, 34.5 mmol, 90 %, 133.19 g/mol) as a pale-yellow oil.

¹H NMR (300.13 MHz, CDCl₃, δ): 7.32 – 7.23 (m, 2H), 7.20 – 7.02 (m, 2H), 6.60 (dd, *J* = 17.6, 10.9 Hz, 1H), 5.63 (dd, *J* = 17.6, 1.0 Hz, 1H), 5.12 (dd, *J* = 10.9, 1.0 Hz, 1H), 3.72 (d, *J* = 5.7 Hz, 2H), 1.36 (br s, NH₂); ¹³C{¹H} NMR NMR (75 MHz, CDCl₃, δ): 142.95, 136.53, 136.21, 127.27, 126.40, 113.49, 46.25.

3.7.4 Synthesis of Cross-linker (3.6)

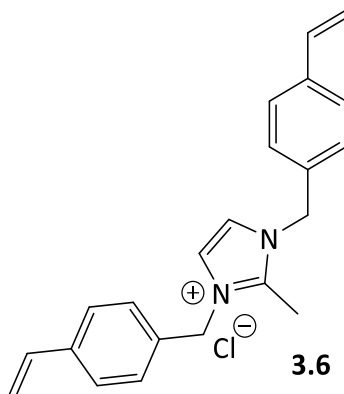
- **Synthesis of 2-methyl-1-(4-vinylbenzyl)-1H-imidazole (3.5)**

**3.5**

An oven-dried Schlenk flask was allowed to cool to room temperature and charged with sodium hydride (0.73 g, 30.4 mmol) and dry DMF (20 mL) and cooled to 0 °C. 2-methyl imidazole (3.0 g, 36.5 mmol) was added resulting in the liberation of gas and on exothermic reaction. The reaction mixture was cooled in an ice bath, and 4-chloromethyl styrene (4.29 mL, 30.4 mmol) was added drop-wise. The reaction was heated to 75 °C for 30 minutes. The reaction mixture was poured onto water (250 mL) and the product extracted with ethyl acetate (2 × 100 mL). The combined extracts were washed with water (180 mL) and brine (50 mL) before being extracted with 6N hydrochloric acid (2 × 25 mL). The aqueous layer was washed with diethyl ether (20 mL) then treated with sodium hydroxide solution (1.0 M) to pH 12.0 and the product extracted with diethyl ether (3 × 100 mL), dried over magnesium sulfate and the solvent removed under reduced pressure to afford **3.5** as a pale-yellow oil in (5.55 g, 28 mmol, 92 %, 198.27 g/mol).

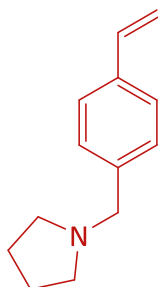
^1H NMR (300.13 MHz, CDCl_3 , δ): 7.30 (d, J = 8.2 Hz, 2H), 6.93 (d, J = 8.2 Hz, 2H), 6.82 (dd, J = 35.3, 1.3 Hz, 2H), 6.61 (dd, J = 17.6, 10.9 Hz, 1H), 5.66 (dd, J = 17.6, 0.8 Hz, 1H), 5.18 (dd, J = 10.9, 0.8 Hz, 1H), 4.95 (s, 2H), 2.25 (s, 3H). $^{13}\text{C}\{^1\text{H}\}$ NMR (75 MHz, CDCl_3 , δ): 144.92, 137.33, 136.05, 135.81, 127.36, 126.86, 126.73, 126.11, 119.89, 114.47, 49.50, 13.14.

- Synthesis of 2-methyl-1,3-bis(4-vinylbenzyl)-1H-imidazol-3-ium chloride (**3.6**)¹⁷⁴



An oven-dried Schlenk flask was allowed to cool to room temperature and charged with a solution of **3.5** (5.16 g, 26.0 mmol) in dry chloroform (50 mL) under a nitrogen atmosphere. 4-Chloromethyl styrene was added and the reaction mixture stirred and heated at 50 °C under nitrogen for 19 hours. After removal of the solvent under reduced pressure the solid residue was washed with ethyl acetate. The product was dried under reduced pressure and the resulting crude product dissolved in dichloromethane then added drop-wise to diethyl ether (*c.a.* 250 mL) with vigorous stirring. After stirring for a minimum of 60 minutes the product was allowed to settle, isolated by filtration through a frit, washed with diethyl ether (2 × 50 mL) and dried under high vacuum to afford **3.6** as a white powder in (8.961 g, 26 mmol, 98 %, 350.89 g/mol).

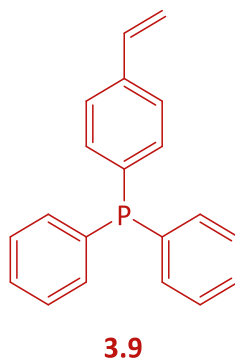
¹H NMR (399.78 MHz, CDCl₃, δ): 7.57 (s, 2H), 7.37 - 7.25 (m, 8H), 6.64 (dd, *J* = 17.6, 10.9 Hz, 2H), 5.72 (d, *J* = 17.5 Hz, 2H), 5.50 (s, 4H), 5.27 (d, *J* = 10.8 Hz, 2H), 2.76 (s, *J* = 22.6 Hz, 3H); ¹³C{¹H} NMR (75 MHz, CDCl₃, δ): 144.3, 138.3, 135.7, 132.2, 128.5, 127.1, 121.9, 115.3, 52.1, 11.2.

3.7.5 Synthesis of 1-[(4-ethenylphenyl) methyl]-pyrrolidine (3.7)**3.7**

An oven-dried Schlenk flask was charged with hexane (25 mL) and 4-chloromethyl styrene (4.6 mL, 32.9 mmol) and cooled using ice-bath. Dropwise addition of pyrrolidine (5.4 mL, 65.7 mmol) to the cooled solution resulted in an obvious colour change from white to yellow. The reaction mixture was allowed to warm to room temperature and left to stir for a further 18 h after which the solid product was isolated by filtration and washed with hexane. The sample was dried under vacuum to afford **3.7** as a yellow oil (5.17 g, 27.6 mmol, 84 %, 187.29 g/mol).

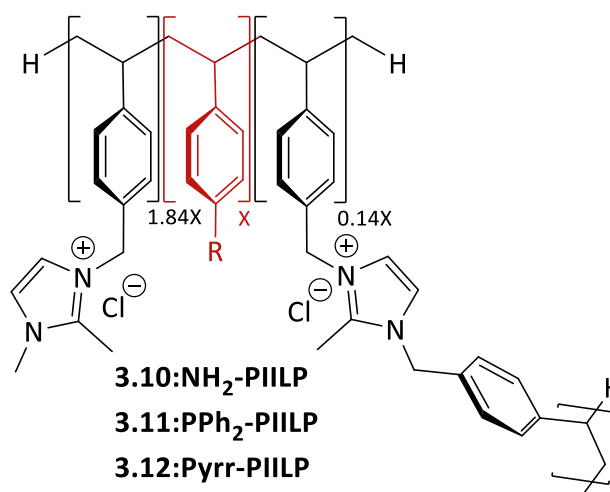
^1H NMR (CDCl_3 , 300.13 MHz, δ): 7.25 (d, $J = 8.2$ Hz, 2H), 7.18 (d, $J = 8.2$ Hz, 2H), 6.59 (dd, $J = 17.6, 10.9$ Hz, 1H), 5.61 (dd, $J = 17.6, 1.0$ Hz, 1H), 5.10 (dd, $J = 10.9, 1.0$ Hz, 1H), 3.48 (s, 2H), 2.44 – 2.34 (m, 4H), 1.75 – 1.62 (m, 4H); $^{13}\text{C}\{^1\text{H}\}$ NMR (75 MHz, CDCl_3 , δ): 139.10, 136.70, 136.29, 129.07, 126.11, 113.33, 60.44, 54.16, 23.51.

3.7.6 Synthesis of diphenyl (4-vinylphenyl) phosphine (**3.9**)¹⁷⁶



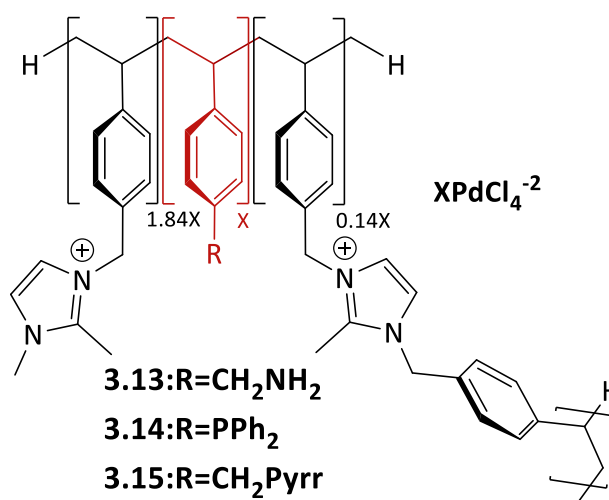
An oven-dried three neck round-bottom flask was allowed to cool to room temperature and charged with Mg turnings (1.77g, 72.84 mmol) and anhydrous THF (60 mL). A crystal of iodine was added, the mixture was cooled to 0 °C and *c.a.* 20 % of a solution of 4-chlorostyrene (4.70 mL, 39.34 mmol) in anhydrous THF (40 mL) was added under a nitrogen atmosphere using cannula transfer techniques. The solution was heated until Grignard formation initiated after which the remaining 4-chlorostyrene solution was added at such a rate as to maintain a gentle reflux. Once addition was completed the solution was heated at 65 °C for 4h. The resulting Grignard solution was added drop-wise using cannula transfer to a solution of chlorophosphine solution in anhydrous THF (30 mL) and the resulting mixture left to stir at room temperature overnight. The solution was then quenched by addition of degassed water (100 mL) and extracted with a large excess of diethyl ether (3 x 170 mL) whilst bubbling nitrogen through the solution. The organic extracts were combined dried over magnesium sulfate and the solvent removed via an external trap to give the **3.9** as a white crystalline solid in (5.43 g, 18.8 mmol, 75 %, 288.33 g/mol).

¹H NMR (300.13 MHz, CDCl₃, δ): 7.33 – 7.13 (m, 14H), 6.61 (dd, *J* = 17.6, 10.9 Hz, 1H), 5.68 (dd, *J* = 17.6, 0.9 Hz, 1H), 5.18 (dd, *J* = 10.8, 0.9 Hz, 1H); ¹³C{¹H} NMR (75 MHz, CDCl₃, δ): 137.93, 137.21, 137.07, 136.80, 136.66, 136.39, 134.09, 133.86, 133.83, 133.60, 128.76, 128.58, 128.49, 126.35, 126.26, 114.70; ³¹P NMR (121 MHz, CDCl₃, δ): -5.90.

3.7.7 Procedure for the Polymerization (3.10, 3.11, 3.12)

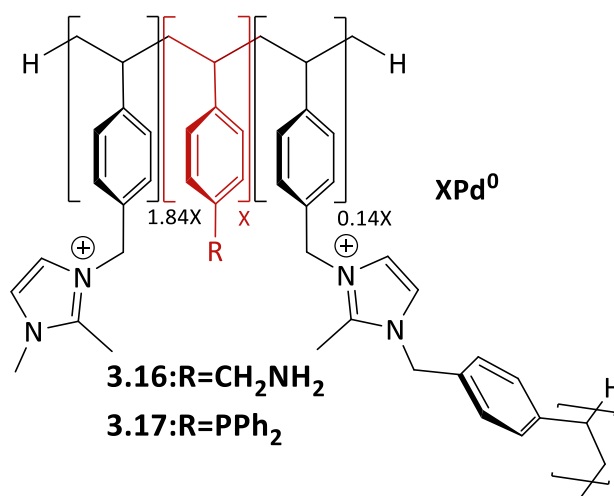
An oven-dried Schlenk flask was allowed to cool to room temperature and charged with a mixture of (5 g, 20.1 mmol) of **3.2** (10.92 mmol) of (**3.4, 3.7, 3.9**), (0.29 g, 1.75 mmol) azobisisobutyronitrile (AIBN), and (0.61 g, 1.75 mmol) of **3.6** followed by addition dry ethanol (100 mL) when monomer (**3.4, 3.7**), however in the case of **3.9**, the solvent choice was modified and a mixture of 1:1 THF/ethanol was used in order to solubilise the phosphine. Then the resulting mixture was degassed via freeze-thaw method (6 cycles), next allowed to warm to room temperature, after that the reaction mixture was heated at 85 °C for 96 hours, after cooling to room temperature and additional equivalent of AIBN was added to the mixture, which was then degassed again (5 times) as above before, stirring at 85 °C overnight. After cooling to room temperature, the solvent was removed under reduced pressure. Then we scratch using spatula the yellow puff product was washed with diethyl ether and filtered then dried under reduced pressure to afford an off-white powder of **3.10** (6.2 g, 9.6 mmol, 88 %, 647.03 g/mol), **3.11** (8.4 g, 10.5 mmol, 96 %, 802.17 g/mol), and **3.12** (7.1 g, 10.1 mmol, 93 %, 701.13 g/mol).

3.7.8 Procedure for Synthesis of Palladium Chloride Loaded on Polymer (**3.13**, **3.14**, **3.15**)



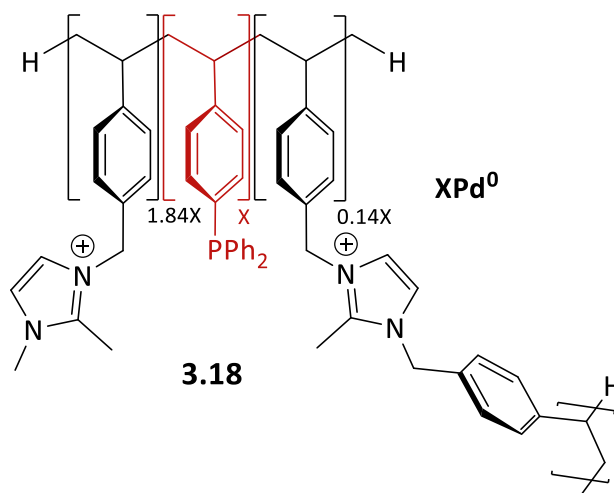
An oven-dried Schlenk flask was allowed to cool to room temperature and charged with palladium chloride (0.5 g, 2.82 mmol), sodium chloride (3.3 g, 56.4 mmol) and water (40 mL). The reaction mixture was heated at 80 °C until the $PdCl_2$ was fully dissolved. This resulting clear red solution of $Na_2[PdCl_4]$ was cooled to room temperature and a suspension of (2.82 mmol) of (**3.10**, **3.11**, or **3.12**) dissolved in water (20 mL). The mixture was stirred at room temperature for 4 h, filtered under reduced pressure and the solid washed with water, ethanol and then diethyl ether and dried to afford an orange powder of **3.13** (1.54 g, 1.72 mmol, 84 %, 895.25 g/mol), **3.14** (2.1 g, 2 mmol, 93 %, 1050.39 g/mol), and **3.15** (1.74 g, 1.83 mmol, 88 %, 949.35 g/mol).

3.7.9 Procedure for Synthesis of Palladium Nanoparticles Amino- And Phosphino-Decorated Polymer Immobilised Ionic Liquids (3.16, 3.17)



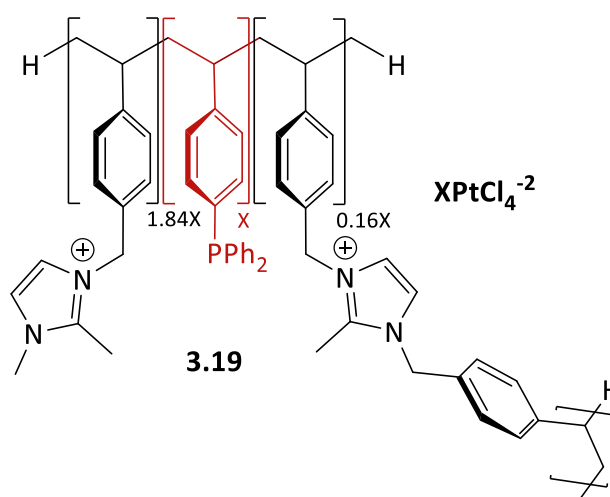
An oven-dried Schlenk flask was allowed to cool to room temperature and charged with **(3.13, 3.14)** (2.27 mmol) and ethanol (30 ml). To this suspension was added a solution of sodium borohydride (0.6 g, 15.86 mmol) in water (5 mL) drop-wise resulting in an immediate colour change to black. The resulting suspension was stirred at room temperature for 5 h. The reaction solvent was reduced under low pressure, then the residue washed with water, ethanol and then diethyl ether and dried overnight under reduced pressure to afford a black powder of **3.16** (1.3 g, 1.73 mmol, 64 %, 753.45 g/mol), and **3.17** (2.1 g, 2.3 mmol, 88 %, 908.59 g/mol).

3.7.10 Palladium Nanoparticles Loaded on Pyrrolidino- Decorated Polymer Immobilised Ionic Liquids (3.18)



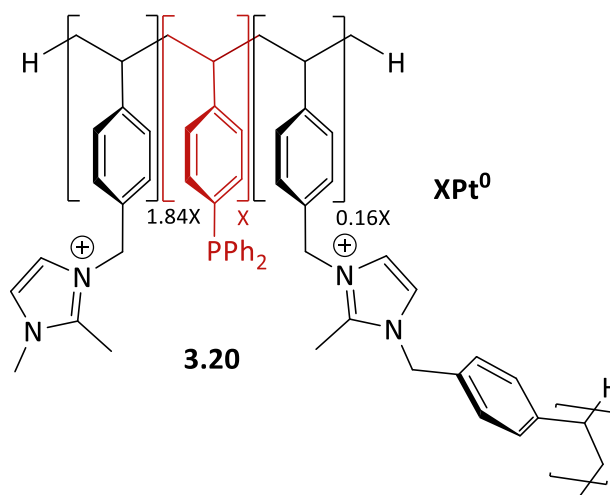
A reaction vessel and charged with **3.15** (0.5 g, 0.53 mmol) and ethanol (25 ml) and the suspension heated at 100 °C under hydrogen gas (65 psi) overnight. The reaction solvent was reduced under low pressure, then the residue washed with water, ethanol and then diethyl ether and dried overnight under reduced pressure to afford a black powder of **3.18** (0.42 g, 0.52 mmol, 84 %, 807.55 g/mol).

3.7.11 Synthesis of Platinum Chloride Loaded on Polymer (3.19)



An oven-dried Schlenk flask was allowed to cool to room temperature and charged with K_2PtCl_4 (0.52 g, 1.25 mmol) and water (15 mL). The reaction mixture was stirred at room temperature and a suspension of **3.11** (1.0 g, 1.25 mmol) in water (20 mL) was added. The mixture was stirred at room temperature for 4 h, filtered under reduced pressure and the solid washed with water, ethanol and then diethyl ether and dried to afford **3.19** as a beige powder (0.86 g, 0.76 mmol, 86 %, 1137.01 g/mol).

3.7.12 Platinum Nanoparticles Loaded on Amino- and Phosphino-Decorated Polymer Immobilised Ionic Liquids (3.20)



An oven-dried Schlenk flask was allowed to cool to room temperature and charged with **3.19** (0.75 g, 0.66 mmol) and ethanol (10 ml). To this suspension was added a solution of sodium borohydride (0.175 g, 4.62 mmol) in water (2 mL), resulting in the immediate appearance of a black colour. The resulting suspension was stirred at room temperature for 5 h. The reaction solvent was reduced under low pressure, then the residue washed with water, ethanol and then diethyl ether and dried overnight under reduced pressure to afford a brown powder of **3.20** (0.71 g, 0.71 mmol, 95 %, 997.26 g/mol).

Chapter 4

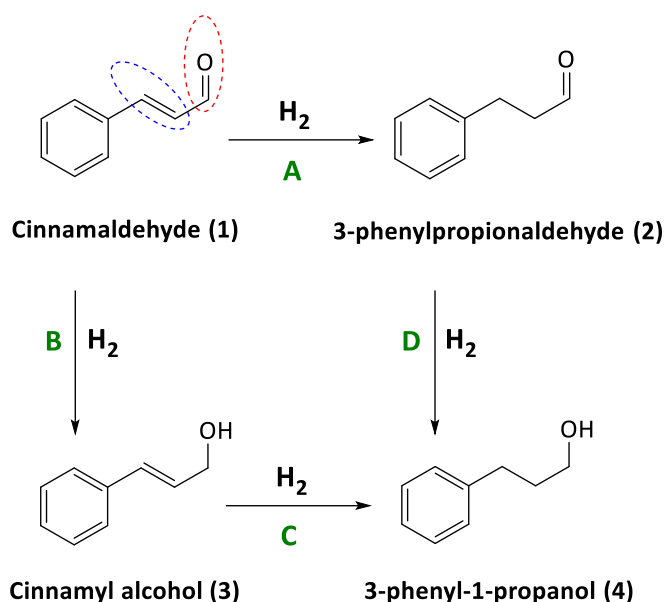
CATALYTIC HYDROGENATION OF α,β -UNSATURATED ALDEHYDES WITH POLYMER-IMMOBILISED IONIC LIQUIDS STABILISED PALLADIUM NANOPARTICLES

Chapter 4. CATALYTIC HYDROGENATION OF α,β -UNSATURATED ALDEHYDES WITH POLYMER-IMMOBILISED IONIC LIQUIDS STABILISED PALLADIUM NANOPARTICLES

4.1 Introduction

The selective hydrogenation of α,β -unsaturated aldehydes to their corresponding aldehyde is considered as one of the most challenging synthetic reactions in a field of fine-chemical production.^{191, 192}

This is a highly important transformation as the products of hydrogenated α,β -unsaturated aldehydes are important and valuable chemical intermediates especially in the production of fragrances and flavours.¹⁹³ In this regard, the chemo-selectivity of α,β -unsaturated aldehyde affected this type of chemistry. Trans-cinnamaldehyde is one of such substrate in this category; it is isolated for the first-time from cinnamon oil. An α,β -unsaturated aldehyde (Scheme 1) contains two functional groups conjugated to each other which is the alkene group (C=C) and the carbonyl group (C=O). As such it is important to be able to selectively reduce one of these functional groups while leaving the other intact, for example, to obtain (3-phenylpropanal **(2)**) by selective hydrogenation of the conjugated alkene group, whilst avoiding further reduction of the carbonyl group (C=O) to afford 3-phenyl-1-propanol **(4)** as these products are not easy to separate.¹⁹⁴ The reactivity and the unhindered nature of the aldehyde **(1)** made the selectivity towards hydrogenation very difficult in comparison with the corresponding ketone, further to undergoing competitive side reactions from **(1)** to **(2)** Path A and from **(1)** to **(3)** to **(4)** path B and C.



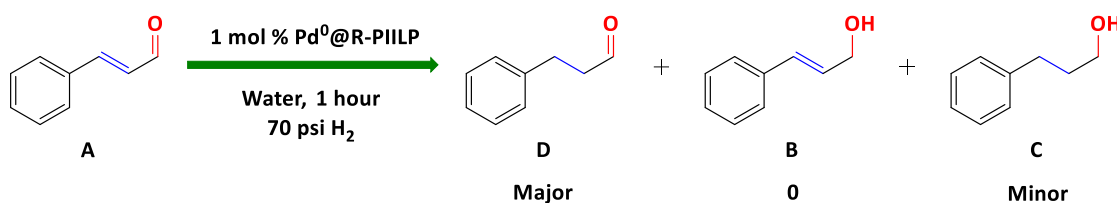
Scheme 1 The hydrogenation of trans-cinnamaldehyde.

The transition metal catalysts are usually used for this kind of reaction where the catalyst increases the reaction rate and/or modifies the reaction selectivity. Palladium, platinum, and ruthenium are the most notable transition metal catalysts used for this hydrogenation reaction. Conventionally palladium hydrogenates the alkene group while the platinum has been used for selective reduction of the carbonyl group.^{191, 195}

4.2 Optimisation Studies

All PdNP loaded amino-, phosphino-, and pyrrolidino- decorated PIILPs, **3.16**, **3.17**, and **3.18**, respectively, were initially examined as catalysts for hydrogenation of the model substrate trans-cinnamaldehydes to optimise selectivity and activity.

In the selective hydrogenation reaction of an α,β -unsaturated aldehyde, there are three possible products. The highly desirable reduction is the carbon-carbon double bond (C=C) to produce the corresponding saturated aldehyde (**2**), however, due to the probability of carbonyl hydrogenation is higher, so the main product is unsaturated alcohol. In this regard, there are many publications that report the thermodynamically favourable reduction of the C-C double bond of α,β -unsaturated carbonyl compounds with palladium catalysts.^{184, 191} In this project, we have examined the efficacy of the prepared PdNP@R-PIILP for the hydrogenation of trans-cinnamaldehyde (Scheme 2).



Scheme 2 Selective hydrogenation of trans-cinnamaldehyde catalysed by PdNP@R-PIILP.

Catalysts efficiencies were tested on the hydrogenation of carbon-carbon bond of trans-cinnamaldehyde to afford hydrocinnamaldehyde. All the catalytic hydrogenation reactions were conducted in a Parr bench top pressure reactor equipped with a magnetically coupled stirrer and a gas ballast. Reactions were conducted in a glass vessel charged with trans-cinnamaldehyde (1 mmol) and 1 mol % of catalyst MNP@R-PIILP (M=Pd, Pt; R=CH₂NH₂, PPh₂, CH₂Pyrr) dissolved in (13 mL) solvent under (70 psi) hydrogen gas atmosphere for one hour at room temperature. The conversion and selectivity of each reaction were determined by analysing the ¹H NMR spectrum of the crude reaction mixture. The calculation depends on the integral of the highlighted proton in each compound which is the best choice to avoid overlap with other signals. The conversion was calculated depends on the difference between cinnamaldehyde and the products, while the selectivity was calculated using the difference between one of the products (the desired) and all other as shown in (Figure 1).

$$\text{Conversion} = (B + C + D) / (2A + B + C + D)$$

$$\text{Selectivity} = D / (B + C + D)$$

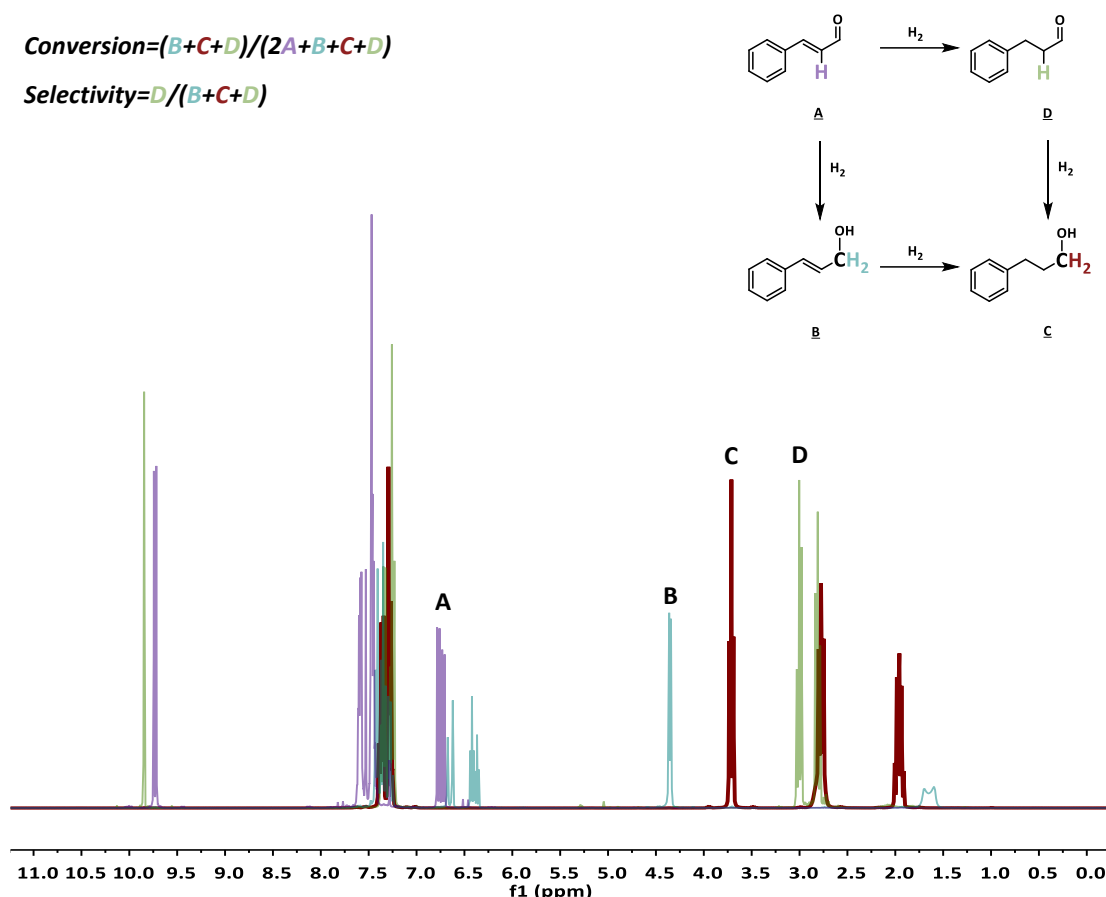


Figure 1 Stacked ¹H NMR spectra of cinnamaldehyde (CA) (purple); 3-phenyl propanol (PPL) (blue); cinnamyl alcohol (CAL) (red); hydrocinnamaldehyde (HCA) (green).

4.2.1 Solvent Screening Studies

As the solvent is known to have a dramatic influence on reaction selectivity and activity, the hydrogenation of cinnamaldehyde was catalysed by PdNP@NH₂-PIILP in a range of different solvents (polar, non-polar, protic and aprotic) at room temperature and 60 °C, and each of which is summarised in (Figure 2).

**All the catalysts have higher performance at 60 °C than at room temperature.*

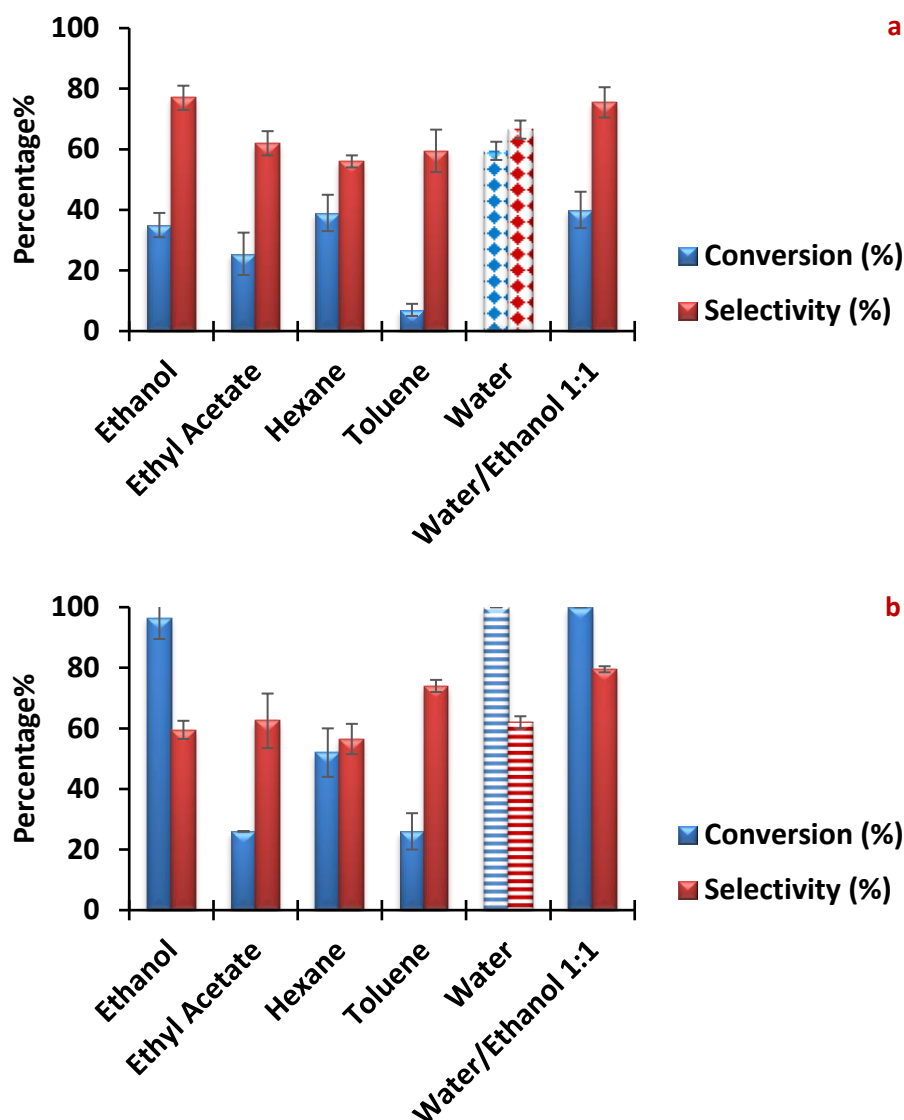


Figure 2 Solvent-screening studies using PdNP@NH₂-PIILP (a) at room temperature (b) at 60 °C.

Reaction Conditions: 0.1 mol % PdNP@NH₂-PIILP; 1 mmol *trans*-cinnamaldehyde; 13 mL solvent; 70 psi H₂; 1 h; determined by ¹H NMR spectroscopy (average of 2 runs).

Generally, at both temperatures, PdNP@NH₂-PIILP appears to perform well in hydrogen bonding solvents ethanol, water, and a water/ethanol solvent mixture while it is performing poorly in the organic solvents. Although the conversion varied widely depending on the solvent used, the selectivity remained high.

Many reasons make water the best choice as a reaction solvent such as the greenest solvent, environmentally friendly, non-hazardous, accessible, cheap alternative for any other organic solvents, easy product isolation by extraction and the ease of recycling.^{196,}

In this sense, water as used as the solvent of choice even though the highest conversion (100 %) and selectivity (80 %) were obtained in a water/ethanol mixture at 60 °C.

As there was only a minor drop in selectivity from 67 % to 62 % between reactions conducted at 60 °C and room temperature (Figure 2), all further optimisation studies and substrate screening were performed at room temperature.

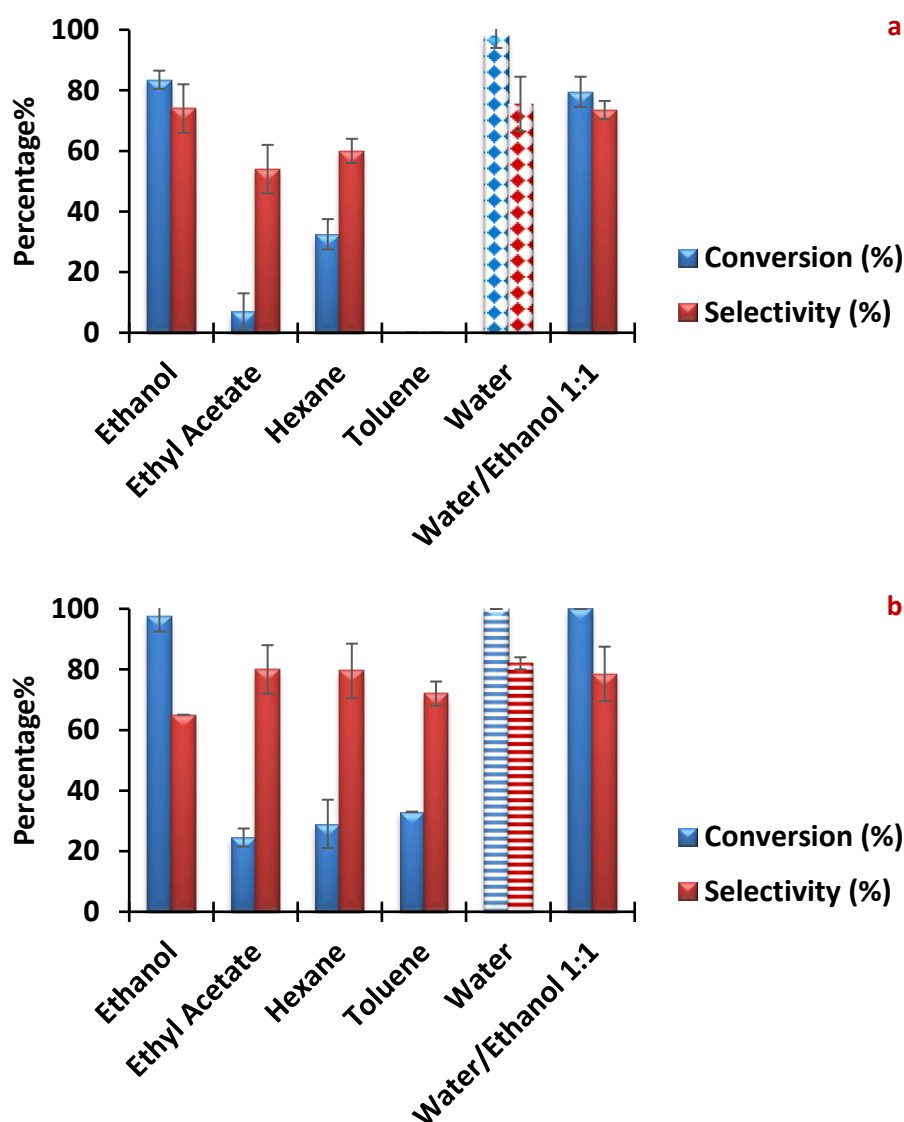


Figure 3 Solvent-screening studies using PdNP@PPh₂-PIILP(a) at room temperature (b) at 60 °C.

Reaction Conditions: 0.1 mol % PdNP@PPh₂-PIILP; 1 mmol trans-cinnamaldehyde; 13 mL solvent; 70 psi H₂; 1 h; determined by ¹H NMR spectroscopy (average of 2 runs).

Again, the PdNP@PPh₂-PIILP performs well in ethanol, water and a water/ethanol mixture at both temperatures, with a slightly higher selectivity of 82 % at 60 °C compared with 76 % at room temperature (Figure 3).

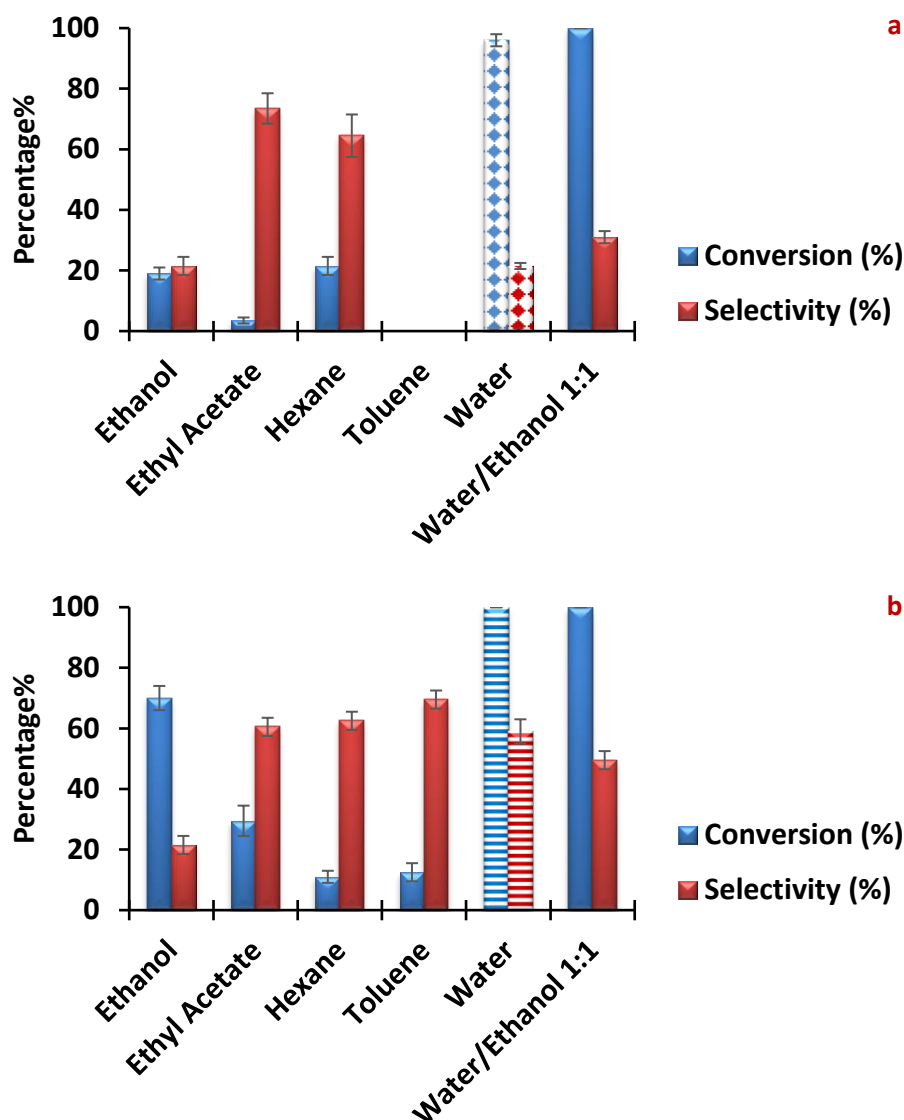


Figure 4 Solvent-screening studies using PdNP@Pyrr-PIILP(a) at room temperature (b) 60 °C.

Reaction Conditions: 0.1 mol % PdNP@Pyrr-PIILP; 1 mmol trans-cinnamaldehyde; 13 mL solvent; 70 psi H_2 ; 1 h; determined by 1H NMR spectroscopy (average of 2 runs).

In contrast, PdNP@Pyrr-PIILP gave a much lower selectivity for hydrocinnamaldehyde in ethanol, water or water/ethanol mixture than its amino-, and phosphino-based counterpart at room temperature. However, selectivity improved quite dramatically to 69.5 % at the higher temperature (Figure 4).

From all above studies, both PdNP@NH₂-PIILP and PdNP@PPh₂-PIILP showed a similar trend in conversion and selectivity, while PdNP@Pyrr-PIILP was markedly less selective across the range of solvents examined.

4.2.2 Temperature Optimisation Studies

The hydrogenation reactions of each catalyst were carried out in water, under 70 psi hydrogen at a range of different temperatures from room temperature to 60 °C. (Figure 5) shows the effect of increasing the temperature on the conversion and the selectivity of PdNP@NH₂-PIILP. The conversion reached 100 % at 30 °C, however, the selectivity obtained at 60 °C was 60 % while it was 67 % at 20 °C, this means the selectivity of the catalyst has not affected by rising temperature.

The trend appears to show that at the higher temperatures, the selectivity is higher, however for the reaction conducted at 20 °C, there is an obvious difference in selectivity. This may well be due to the fact that at the higher conversion of the starting material, there is intrinsically a high concentration of saturated aldehyde that can react further to form the saturated alcohol. Further studies at a predetermined conversion would allow for a more accurate temperature dependence on selectivity.

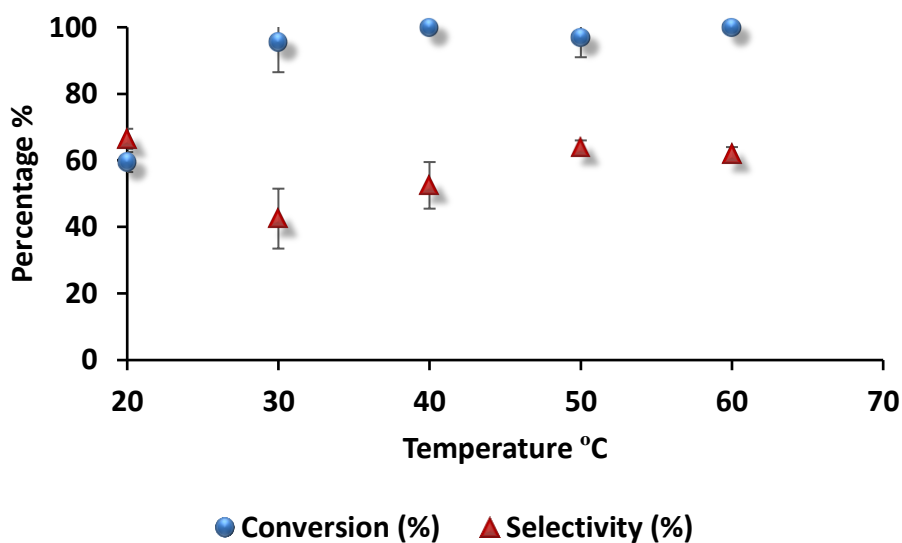


Figure 5 Temperature optimisation profile using PdNP@NH₂-PIILP.

Reaction Conditions: 0.1 mol % PdNP@NH₂-PIILP; 1 mmol trans-cinnamaldehyde; 13 mL water; 70 psi H₂; 1 h; determined by ¹H NMR spectroscopy (average of 2 runs).

In contrast, the conversion/selectivity profile for PdNP@PPh₂-PIILP showed less variation with temperature than PdNP@NH₂-PIILP and the optimum conversion of 82 % was a significant improvement on that obtained with its amino counterpart (Figure 6).

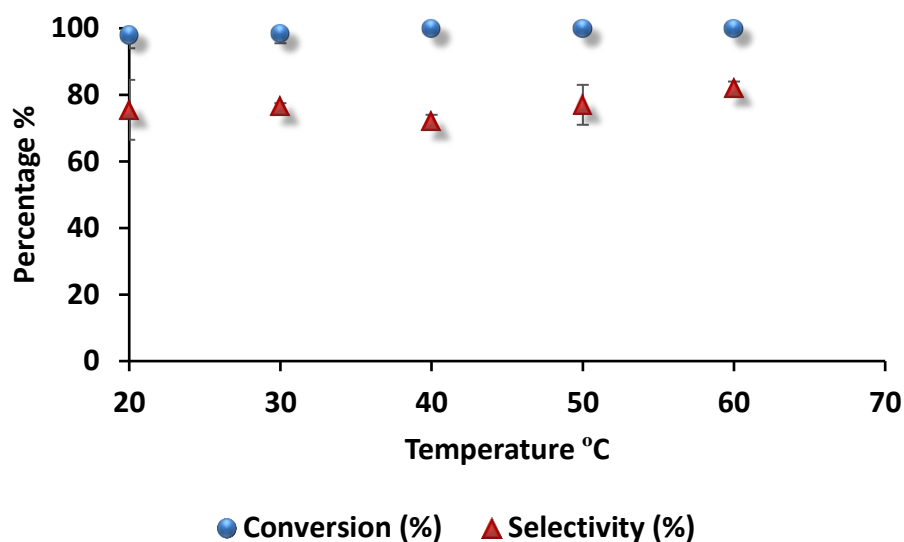


Figure 6 Temperature optimisation profile using PdNP@PPh₂-PIILP.

Reaction Conditions: 0.1 mol % PdNP@PPh₂-PIILP; 1 mmol *trans*-cinnamaldehyde; 13 mL water; 70 psi H₂; 1 h; determined by ¹H NMR spectroscopy (average of 2 runs).

Interestingly, selectivity increased with increasing temperature from 21.5 % at room temperature to 78 % at 50 °C for pyrrolidine-based catalyst PdNP@Pyrr-PIILP, while complete conversion was obtained at each temperature (Figure 7).

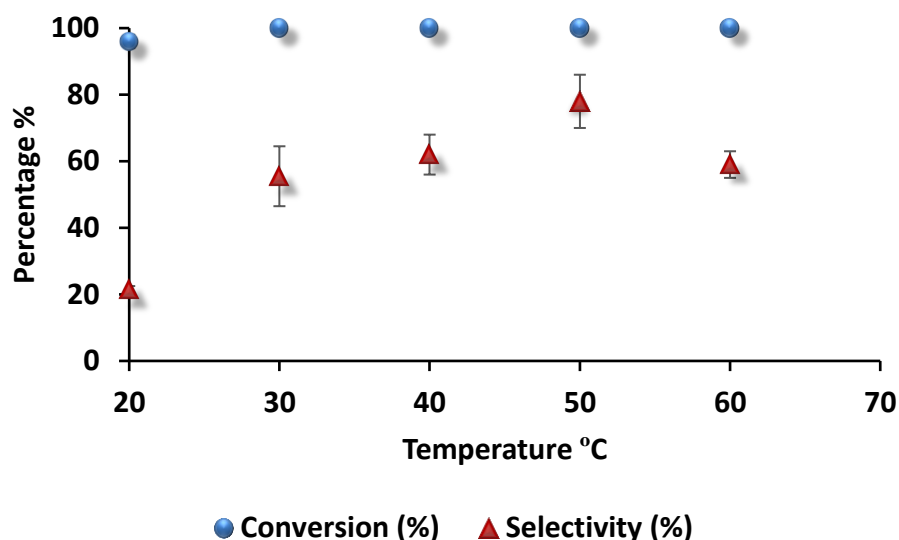


Figure 7 Temperature optimisation profile using PdNP@Pyrr-PIILP.

Reaction Conditions: 0.1 mol % PdNP@Pyrr-PIILP; 1 mmol trans-cinnamaldehyde; 13 mL water; 70 psi H₂; 1 h; determined by ¹H NMR spectroscopy (average of 2 runs).

The mild reaction conditions using PdNP@R-PIILP are ideal as catalyst lifetimes would be affected by the reaction temperatures and nanoparticles tend to aggregate at higher temperatures, which lowers surface area and activity. In addition, the ambient reaction condition would reduce the reaction costs and safety risks management.

4.2.3 Pressure Experiment Optimisation Studies

The effect of the reaction pressure on catalyst performance was investigated as it could affect activity through the concentration of dissolved hydrogen. Thus, a series of reactions were conducted in which the hydrogen pressure was varied between 8 - 800 psi in water at room temperature in order to explore the influence of pressure on the catalytic performance. (Figure 8) shows that conversions increased quite dramatically with increasing pressure for reactions catalysed by PdNP@NH₂-PIILP whereas selectivity increased slightly from 60.5 % at 8 psi to a maximum of 68.5 % at 40 psi; above this pressure selectivity decreased slowly with increasing pressure.

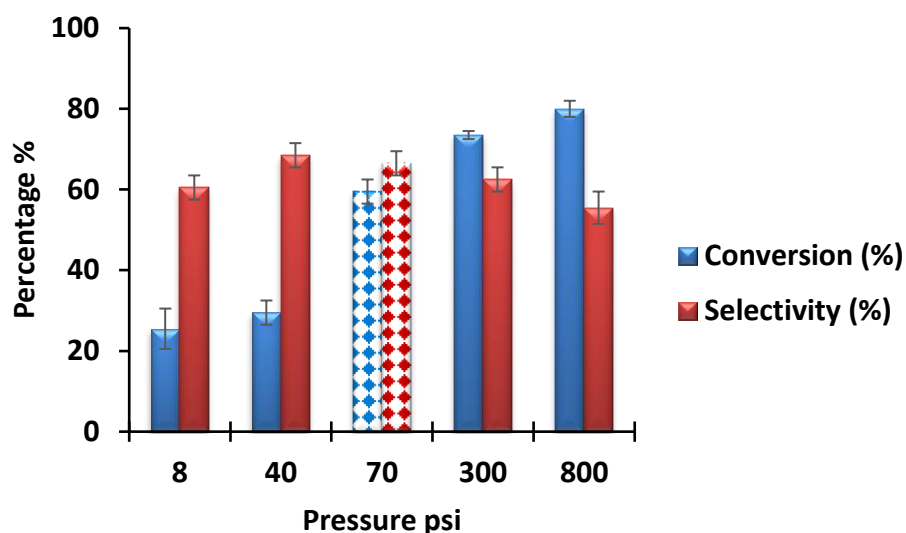


Figure 8 Pressure optimisation profile using PdNP@NH₂-PIILP.

Reaction Conditions: 0.1 mol % PdNP@NH₂-PIILP; 1 mmol trans-cinnamaldehyde; 13 mL water; 70 psi H₂; rt; 1 h; determined by ¹H NMR spectroscopy (average of 2 runs).

In comparison, PdNP@PPh₂-PIILP gave a low conversion at 8 psi whereas complete conversion of cinnamaldehyde was obtained at 70 psi and above (Figure 9). While selectivity varied erratically between 8 and 800 psi the changes were relatively small.

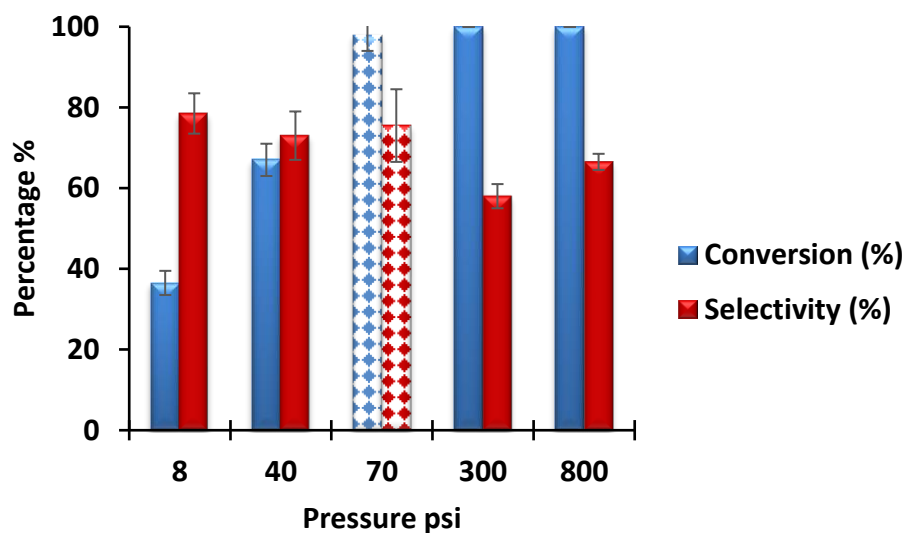


Figure 9 Pressure optimisation profile using PdNP@PPh₂-PIILP.

Reaction Conditions: 0.1 mol % PdNP@PPh₂-PIILP; 1 mmol trans-cinnamaldehyde; 13 mL water; 70 psi H₂; rt; 1 h; determined by ¹H NMR spectroscopy (average of 2 runs).

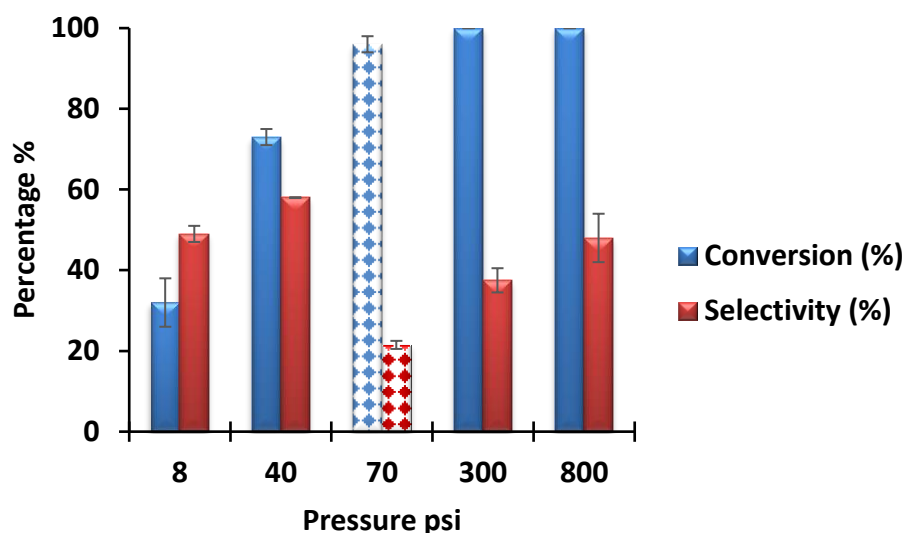


Figure 10 Pressure optimisation profile using PdNP@Pyrr-PIILP.

Reaction Conditions: 0.1 mol % PdNP@Pyrr-PIILP; 1 mmol trans-cinnamaldehyde; 13 mL water; 70 psi H₂; rt; 1 h; determined by ¹H NMR spectroscopy (average of 2 runs).

The conversion pressure profile for PdNP@Pyrr-PIILP (Figure 10) was qualitatively similar to that for PdNP@PPh₂-PIILP in that low conversions were obtained below 70 psi with complete conversion above this pressure. While selectivity also varied erratically, it was significantly lower than that obtained with its phosphino- counterpart at each pressure tested.

4.2.4 Effect of Additives Studies (Base Addition)

Recently, many studies on the hydrogenation of C=C double bonds have suggested that the presence of the base in the reaction mixture could increase the selectivity. From this point of view, the effect of introducing a range of inorganic and organic bases was examined.

1. Sodium hydroxide (NaOH)

Addition of sodium hydroxide to reactions catalysed by PdNP@NH₂-PIILP or PdNP@PPh₂-PIILP resulted in a decrease in conversion with increasing amount of base and a slight increase in selectivity details of which are shown graphically in (Figures 11, and 12).

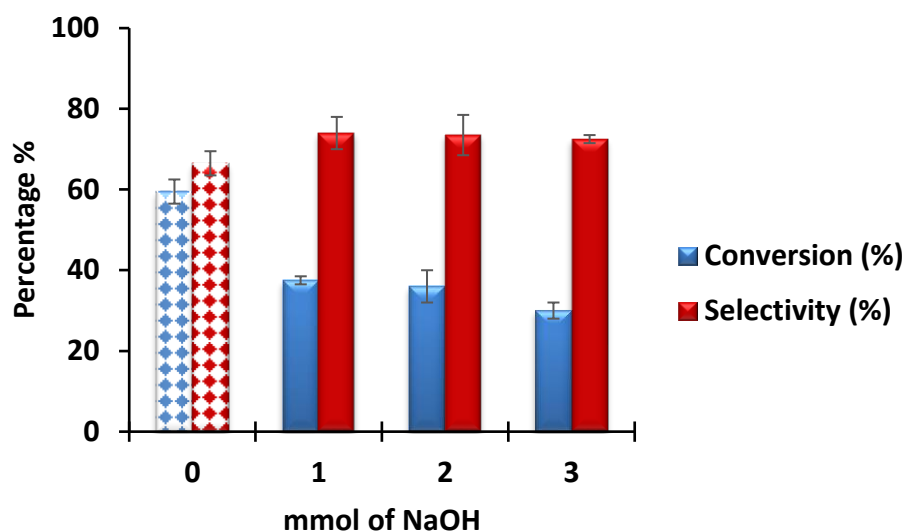


Figure 11 The effect of addition NaOH for PdNP@NH₂-PIILP.

Reaction Conditions: 0.1 mol % PdNP@NH₂-PIILP; 1 mmol trans-cinnamaldehyde; 13 mL water; 70 psi H₂; rt; 1 h; determined by ¹H NMR spectroscopy (average of 2 runs).

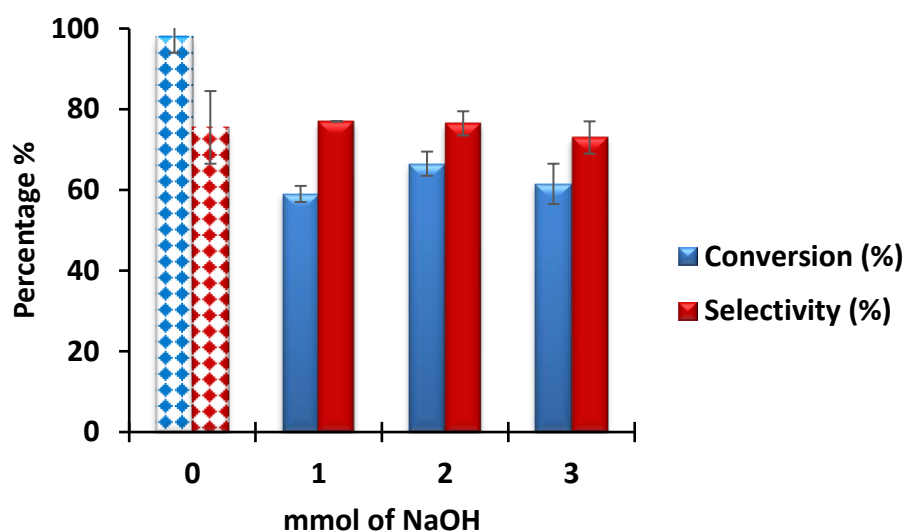


Figure 12 The effect of addition NaOH for PdNP@PPh₂-PIILP.

Reaction Conditions: 0.1 mol % PdNP@PPh₂-PIILP; 1 mmol trans-cinnamaldehyde; 13 mL water; 70 psi H₂; rt; 1 h; determined by ¹H NMR spectroscopy (average of 2 runs).

In contrast, the addition of base to the reaction catalysed by PdNP@Pyrr-PIILP resulted in a dramatic drop in the conversion from 96 % to 29 %, whereas selectivity increased from 21.5 % to 73 % upon addition of one equivalent of sodium hydroxide but decreased slightly in the presence of an additional base (Figure 13).

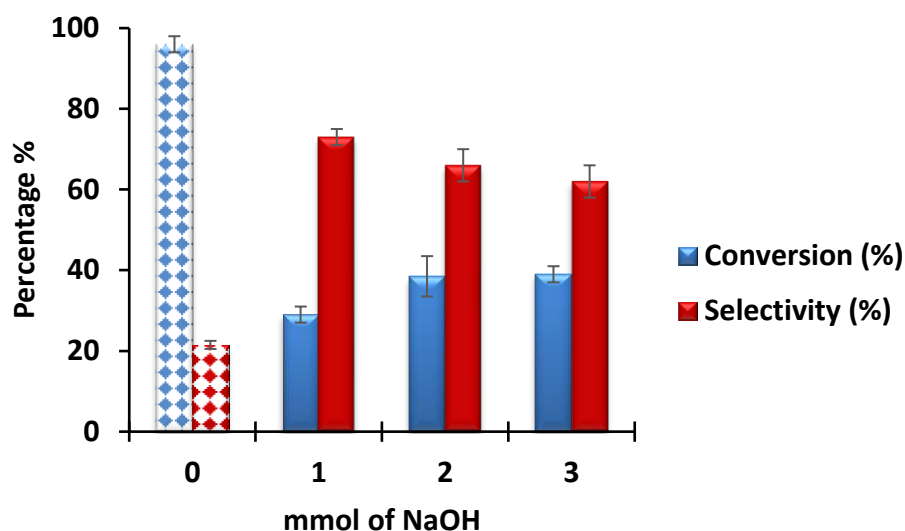


Figure 13 The effect of addition NaOH for PdNP@Pyrr-PIILP.

Reaction Conditions: 0.1 mol % PdNP@Pyrr-PIILP; 1 mmol trans-cinnamaldehyde; 13 mL water; 70 psi H₂; rt; 1 h; determined by ¹H NMR spectroscopy (average of 2 runs).

2. Potassium carbonate (K₂CO₃)

The addition of varying amounts of potassium carbonate from 0.1 to 1.0 equivalents was next examined. Reactions catalysed by amino- modified catalyst showed a steady decrease in conversion as the amount of base was increased from 0 to 1.0 while selectivity increased quite sharply from 66.5 % to 84.5 % in the presence of 0.1 mol % K₂CO₃ (Figure 14). The conversion/selectivity profile as a function of added potassium carbonate for reactions catalysed by PdNP@Pyrr-PIILP was qualitatively similar to its amino counterpart but the improvement in selectivity from 21.5 % to 78 % upon addition of 0.1 equivalents of K₂CO₃ was more dramatic (Figure 16).

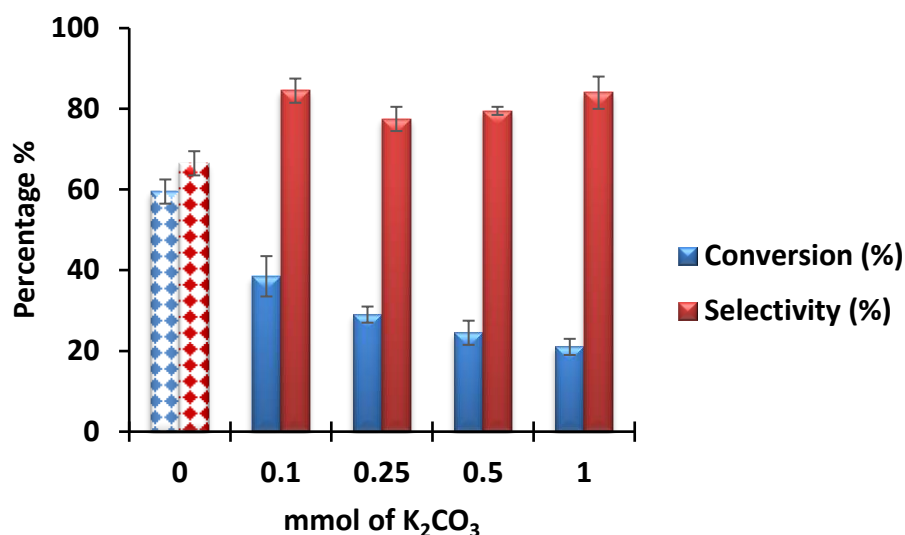


Figure 14 The effect of addition K_2CO_3 for PdNP@NH₂-PIILP.

Reaction Conditions: 0.1 mol % PdNP@NH₂-PIILP; 1 mmol trans-cinnamaldehyde; 13 mL water; 70 psi H₂; rt; 1 h; determined by ¹H NMR spectroscopy (average of 2 runs).

Gratifyingly, there was a marked improvement in selectivity from 76 % to 90 % on addition of one equivalent of potassium carbonate to the PdNP@PPh₂-PIILP catalysed hydrogenation of cinnamaldehyde (Figure 15). Surprisingly, an addition of 0.1 equivalents of base resulted in a marked decrease in the conversion from 98 % to 46.5 % while the addition of an additional base up to one equivalent improved conversions.

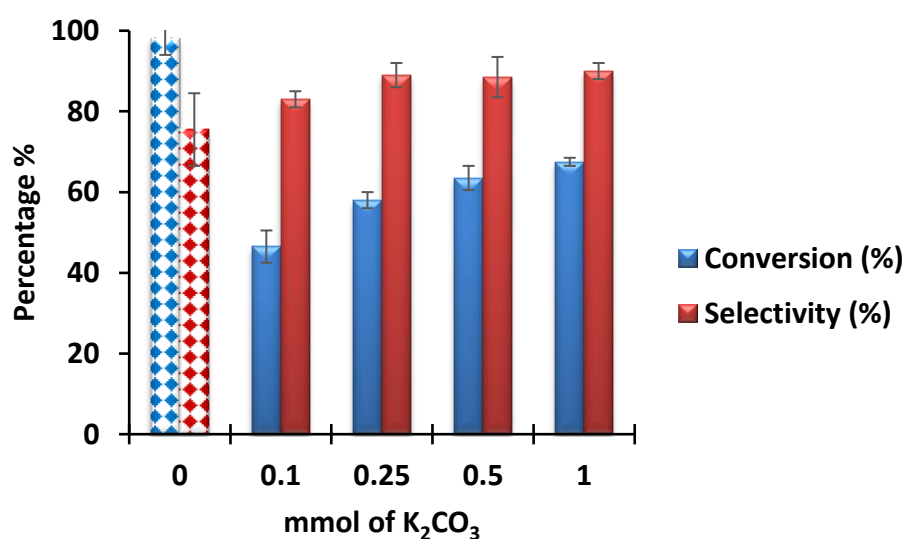


Figure 15 The effect of addition K_2CO_3 for PdNP@PPh₂-PIILP.

Reaction Conditions: 0.1 mol % PdNP@PPh₂-PIILP; 1 mmol trans-cinnamaldehyde; 13 mL water; 70 psi H₂; rt; 1 h; determined by ¹H NMR spectroscopy (average of 2 runs).

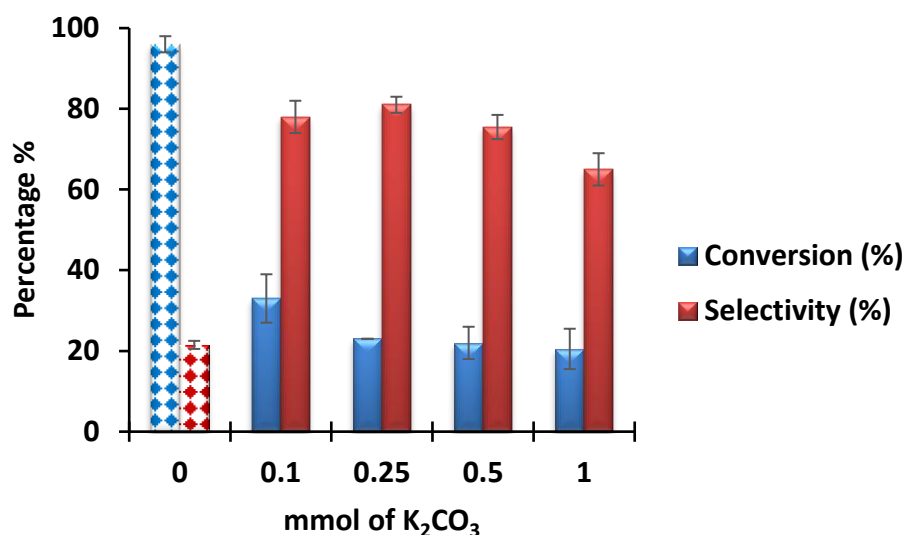


Figure 16 The effect of addition K_2CO_3 for PdNP@Pyrr-PIILP.

Reaction Conditions: 0.1 mol % PdNP@Pyrr-PIILP; 1 mmol trans-cinnamaldehyde; 13 mL water; 70 psi H_2 ; rt; 1 h; determined by 1H NMR spectroscopy (average of 2 runs).

3. Potassium phosphate (K_3PO_4)

Similarly, the addition of one equivalent of potassium phosphate resulted in a drop in conversion for each of the catalysts examined (Figure 17) while in all cases selectivity increased, quite significantly for reactions catalysed by PdNP@Pyrr-PIILP.

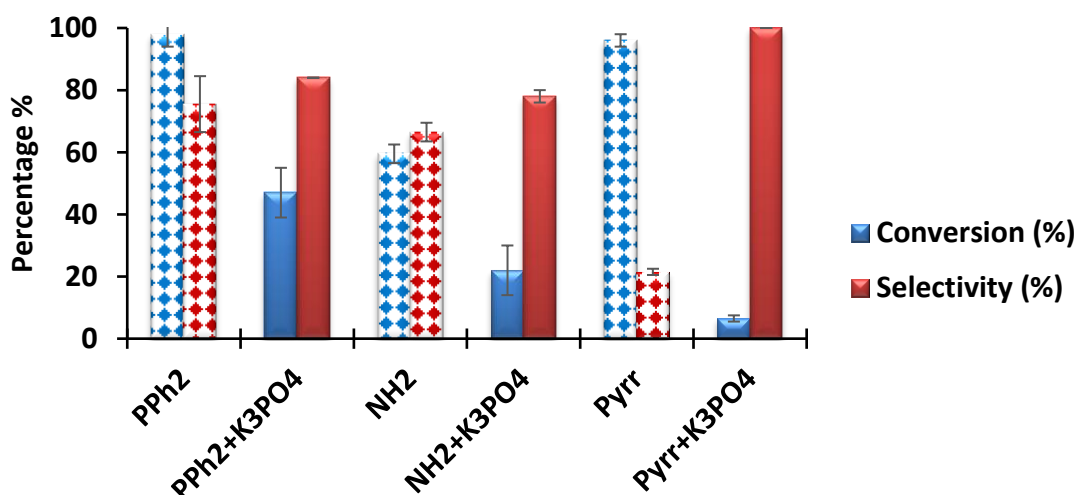


Figure 17 The effect of addition (1 mmol) K_3PO_4 for PdNP@R-PIILP.

Reaction Conditions: 0.1 mol % PdNP@R-PIILP; 1 mmol trans-cinnamaldehyde; 13 mL water; 70 psi H_2 ; rt; 1 h; determined by 1H NMR spectroscopy (average of 2 runs).

4. Triethylamine (NEt₃)

Addition of triethylamine (Figure 18) also resulted in a decrease in conversion and a concomitant increase in selectivity with reactions catalysed by PdNP@Pyrr-PIILP showing the most disparate changes.

Although the role of the base within the reaction mixture is currently unknown it appears that the increase in selectivity is intrinsically linked to a drop in conversion, which is consistent for competing reactions. Further studies were applied by using the addition of 0.1 mL of (1M) HCl which appear to show a dramatic drop in both of conversion and selectivity.

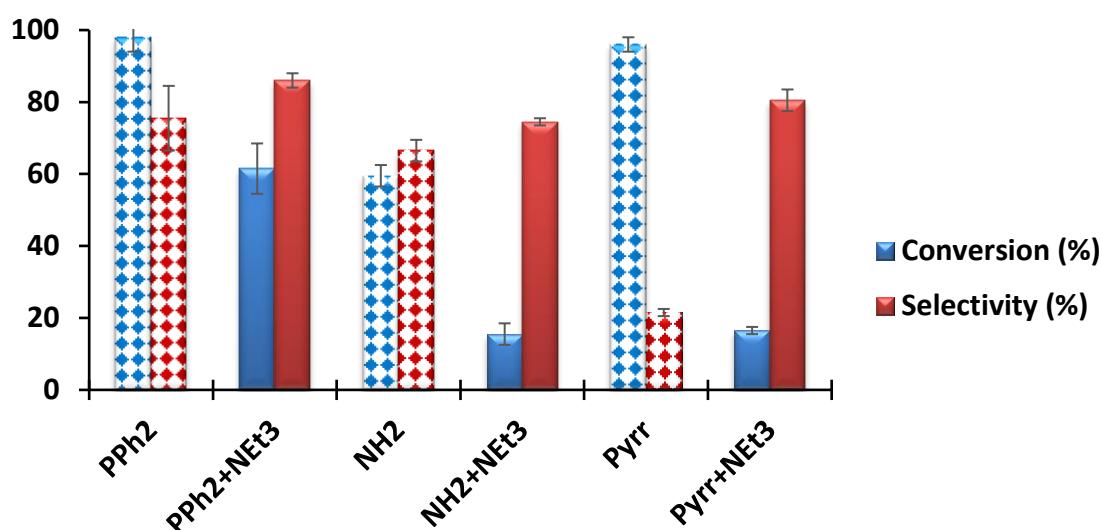


Figure 18 The effect of addition (1 mmol) NEt₃ PdNP@R-PIILP.

Reaction Conditions: 0.1 mol % PdNP@R-PIILP; 1 mmol trans-cinnamaldehyde; 13 mL water; 70 psi H₂; rt; 1 h; determined by ¹H NMR spectroscopy (average of 2 runs).

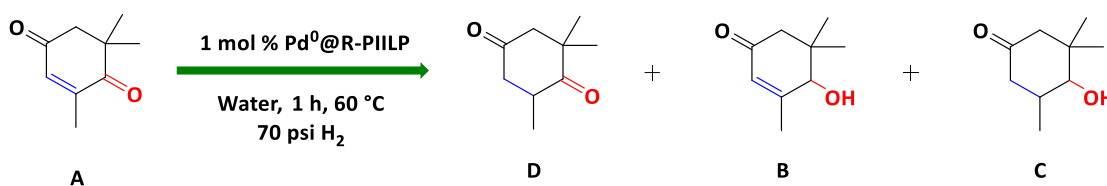
4.2.5 α,β -unsaturated Compounds Screening Studies

The studies were extended to examine a range of α,β -unsaturated aldehydes, and ketones including trans-chalcone, cis-citral, 4-phenyl-3-butene-2-one, 2,6,6-trimethyl-2-cyclohexene-1,4-dione, and trans-2-pentenal (Table 1).

The hydrogenation of α,β -unsaturated ketones was generally slower than for cinnamaldehyde, possibly due to the increased steric hindrance of the R group attached to the carbonyl fragment (Entries 1, 3, and 4) however, high selectivity for the C=C reduction is achievable. Of these substrates, trans-chalcone was particularly slow, which

is perhaps not surprising due to the high steric encumbrance of the phenyl ring of the substrate, which may decrease access to the catalyst active site. Generally, quantitative amounts of saturated ketones were recovered however the phosphino-functionalised catalyst appears to yield small amounts of the saturated alcohol for entry 1, highlighting the effect that heteroatom donors may have on catalyst activity. High selectivity was achieved for the selective C=C reduction of 4-phenyl-3-butene-2-one (Entry 3), most likely again due to the fact that the carbonyl bond of the ketone bearing substrates is less reactive than the corresponding aldehydes.

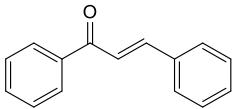
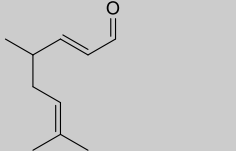
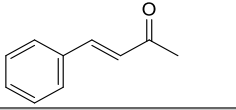
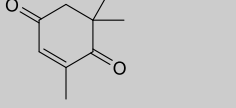
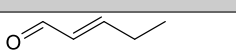
Interestingly, ketoisopherone (Entry 4) gave high selectivity for reduction of both the C=C and the C=O group shown in (Scheme 3) below for NH₂ and PPh₂ functionalised catalysts but high selectivity for the only C=C reduction in the case of the pyrrolidine functionalised catalyst, again demonstrating the complexity of the system and possible heteroatom-metal interactions.



Scheme 3 Selective hydrogenation of 2,6,6-Trimethyl-2-Cyclohexene-1,4-dione catalysed by PdNP@R-PIILP.

Trans-2-pentenal also gives high selectivities at quantitative conversions (Entry 5), and the hydrogenation of cis-citral (Entry 2) gave 3,7-dimethyloct-6-enal as the sole product in all cases suggesting that the less hindered and conjugated C=C bond is more accessible for hydrogenation than the isolated one.

Table 1 The hydrogenation of profile α,β -unsaturated compounds catalysed by PdNP@NH₂-PIILP; PdNP@PPh₂-PIILP, and PdNP@Pyrr-PIILP, respectively.

Entry	Substrate	PdNP@NH ₂ -PIILP				PdNP@PPh ₂ -PIILP				PdNP@Pyrr-PIILP			
		%Conv.	%Selec.	TON	TOF h ⁻¹	%Conv.	%Selec.	TON	TOF h ⁻¹	%Conv.	%Selec.	TON	TOF h ⁻¹
1		31	100	310	310	33	87 ^a	387	387	68	97	690	690
2		100	100	1001	1001	100	100	1171	1171	100	100	1014	1014
3		100	100	1001	1001	100	94	1171	1171	100	100	1014	1014
4		100	85 ^b	1001	1001	100	84 ^c	1171	1171	82	75 ^b	832	832
5		100	96	1001	1001	100	92	1171	1171	100	96	1014	1014

Reaction Conditions: 0.1 mol % PdNP@R-PIILP; 1 mmol α,β -unsaturated compounds; 13 mL water; 70 psi H₂; at 60 °C; 1 h; determined by ¹H NMR spectroscopy (average of 2 runs).

^a Selective hydrogenation towards saturated alcohol (1,3-diphenylpropan-1-ol).

^b Selective hydrogenation towards unsaturated alcohol (Levodione).

^c Selective hydrogenation towards unsaturated alcohol (4-hydroxy-3,5,5-trimethylcyclohex-2-en-1-one).

4.2.6 Recycling Studies

As the ability of a catalyst to be recycled without any loss of activity and selectivity are an important feature, recycle studies were conducted on trans-cinnamaldehyde under the optimum reaction conditions using each of the prepared catalysts PdNP@R-PIILP. As only a small amount of catalyst was used it was extremely difficult to recover the entire sample, simply because of the nature of the physical protocol. After running the experiment, the pressure was released; the diethyl ether was removed, followed by recharging the reaction system with further water and cinnamaldehyde. (Figure 19) shows that PdNP@NH₂-PIILP recycles with a slight decrease in selectivity from 68 % to 51 % after six runs and a gradual but significant drop in the conversion from 58 % to 17 %.

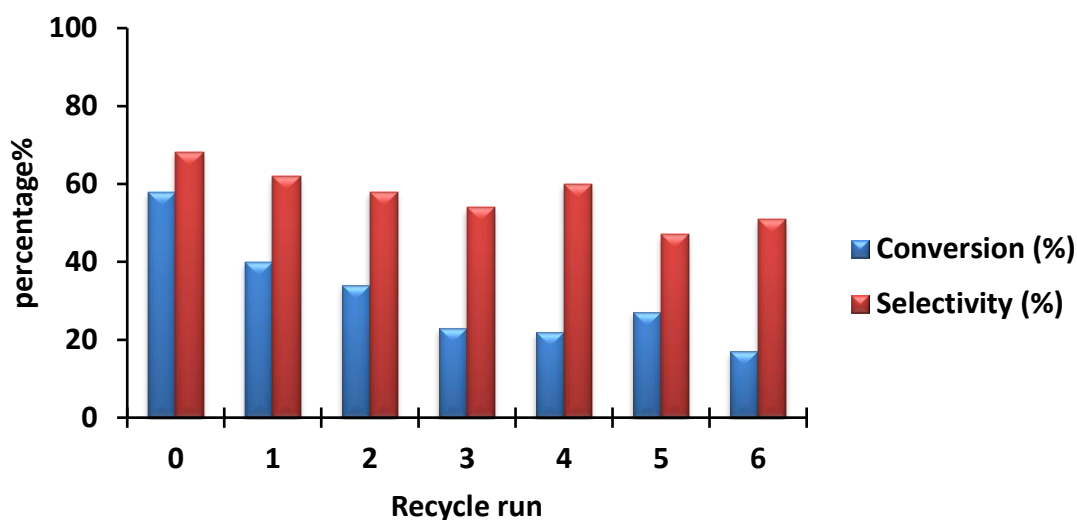


Figure 19 Recycling studies using PdNP@NH₂-PIILP catalysed hydrogenation of cinnamaldehyde.

Reaction Conditions: 0.1 mol % PdNP@NH₂-PIILP; 1 mmol *trans*-cinnamaldehyde; 13 mL water; 70 psi H₂; rt; 1 h; determined by ¹H NMR spectroscopy.

Interestingly, selectivity remained relatively stable for the first five recycles with PdNP@PPh₂-PIILP after which there was a significant increase to 100 %, however, this was accompanied by a dramatic drop in conversion (Figure 20). The gradual drop in conversion may be attributed to catalyst attrition during the workup of each individual run. In this regard, ICP analysis of the aqueous phase after recycling with similar systems developed by the Doherty Knight group has shown a decrease in Pd content. However, catalyst deactivation cannot be discounted in which TEM analysis of the spent catalyst may show aggregation of the NPs after multiple runs.

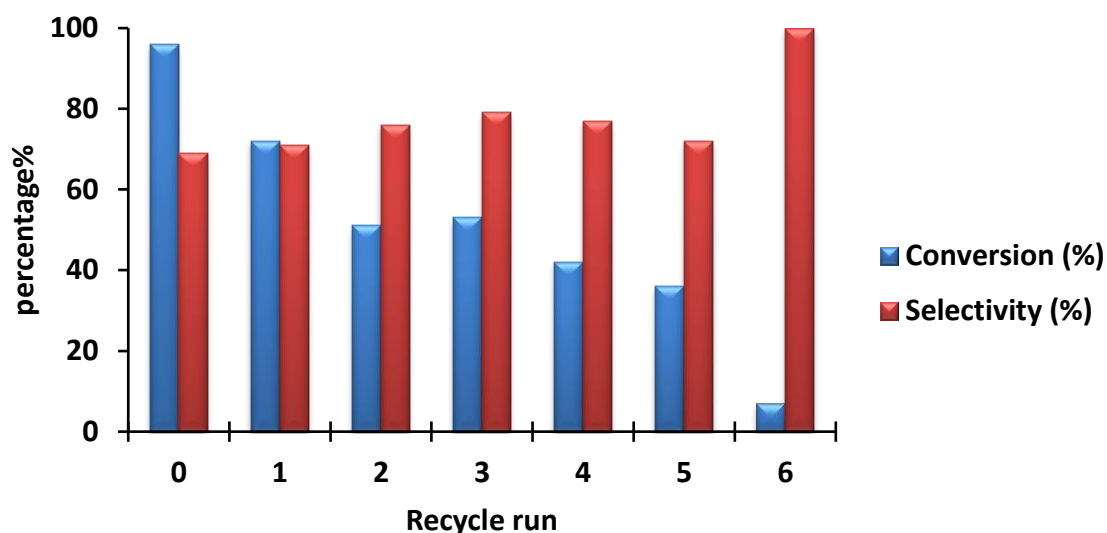


Figure 20 Recycling studies using PdNP@PPh₂-PIILP catalysed hydrogenation of cinnamaldehyde.

Reaction Conditions: 0.1 mol % PdNP@PPh₂-PIILP; 1 mmol trans-cinnamaldehyde; 13 mL water; 70 psi H₂; rt; 1 h; determined by ¹H NMR spectroscopy.

In general, the gradual decrease in conversion overruns 1-3 may be attributed to poisoning of the active sites, nanoparticle agglomeration, or leaching during the work-up, all of which are known to decrease activity. Interestingly, there is an increase in conversion after recycle No. 3. This may be due to the reduction of any residual PdCl₄ precursor or PdO from surface oxidation over the first three cycles generating a higher concentration of metallic Pd⁰. Indeed, this phenomenon has been reported for other transition metal nanoparticle systems.¹⁹⁸

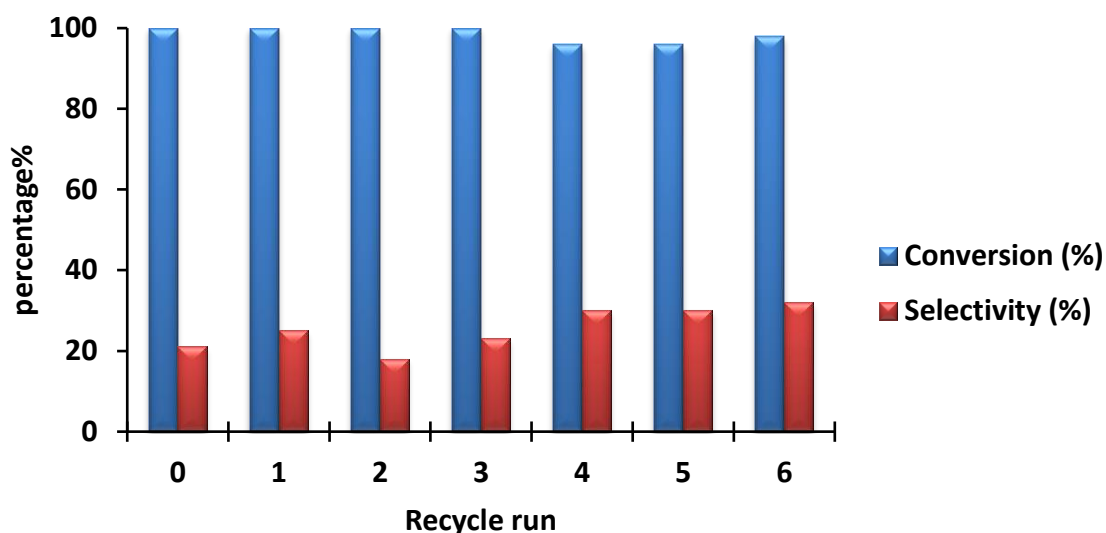


Figure 21 Recycling studies using PdNP@Pyrr-PIILP catalysed hydrogenation of cinnamaldehyde.

Reaction Conditions: 0.1 mol % PdNP@Pyrr-PIILP; 1 mmol trans-cinnamaldehyde; 13 mL water; 70 psi H₂; rt; 1 h; determined by ¹H NMR spectroscopy.

Surprisingly, the corresponding recycling studies with PdNP@Pyrr-PIILP (Figure 21) gave complete conversion for each run and a stable selectivity profile, however, the selectivity is very low rendering the system impractical even though conversions were high.

4.2.7 Transmission Electron Microscopy (TEM)

Comparative TEM analysis were performed for some of the newly prepared catalysts (PdNP@NH₂-PIILP and PdNP@Pyrr-PIILP) before and after recycling, to establish whether the decreases in conversions were related to any change in the nanoparticle size as a result of aggregation which would decrease the surface area of the nanoparticles and the number of active sites (Figures 22, and 23).

As described in **Chapter 3** the nanoparticle size distribution analysis is demonstrated from a TEM image by ImageJ, then the frequency fitted by Gaussian equation. The TEM image of PdNP@NH₂-PIILP after recycling shows that palladium nanoparticles were still highly dispersed in the polymer matrix and not significantly affected during recycling. The particle size distributions determined by counting > 1373 particles revealed a mean NP diameter of 1.54 ± 0.46 nm, with 29.9 % of polydispersity. However, the particle size

before recycling by counting > 1755 particles was 1.8 ± 0.525 nm, and the polydispersity was 29.2 %, which mean there was not any indication of nanoparticles aggregation (Figure 22).

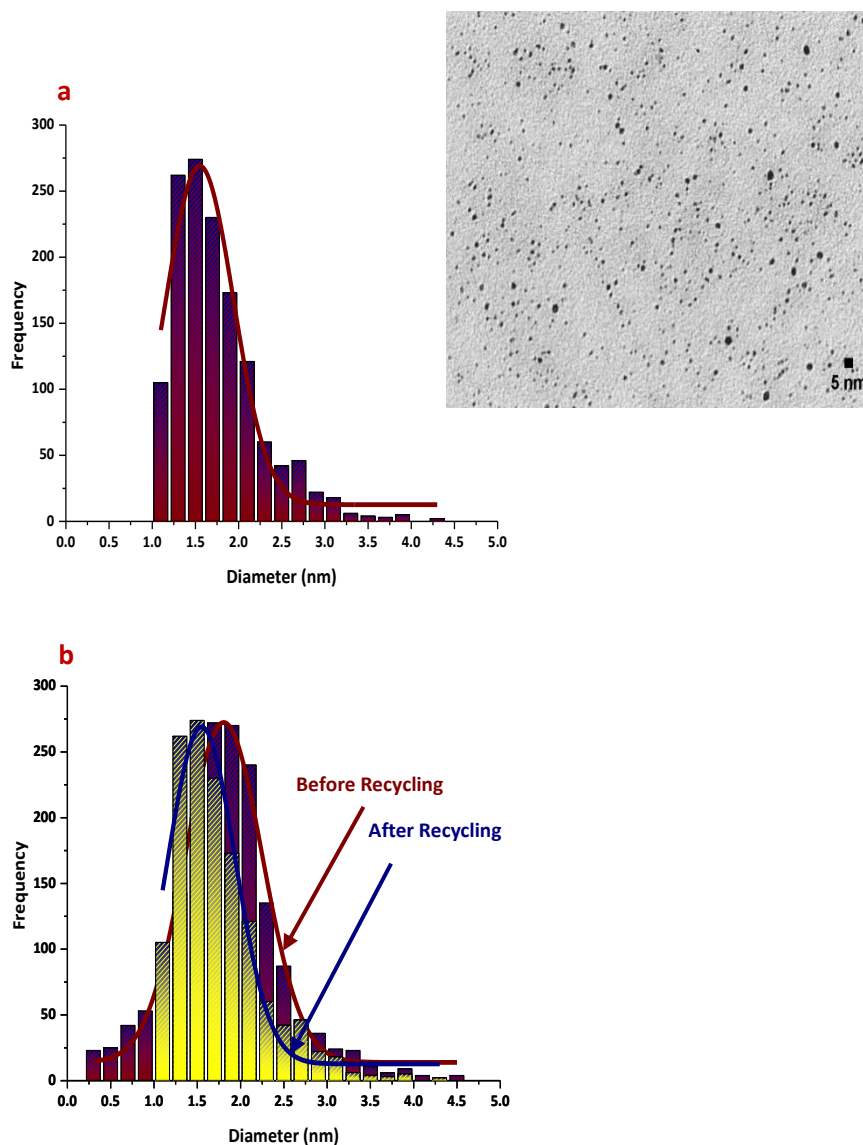


Figure 22 The calculated nanoparticles frequency of (a) recycled sample; (b) stacked diagram before and after recycling of PdNP@NH₂-PIILP fitted by Gaussian equation.

For comparison, the palladium size calculated from the TEM image of PdNP@Pyrr-PIILP after recycling by counting > 237 particles were 1.56 ± 0.43 nm, which is closely similar to before recycling which was 1.57 ± 0.85 nm by counting > 2900 particles. While the polydispersity increased from 54.1 % before recycling sample to 78 % after recycling, which indicates a significant change in the nanoparticles dispersity; this may be attributed to catalyst aging in the reaction mixture (Figure 23).

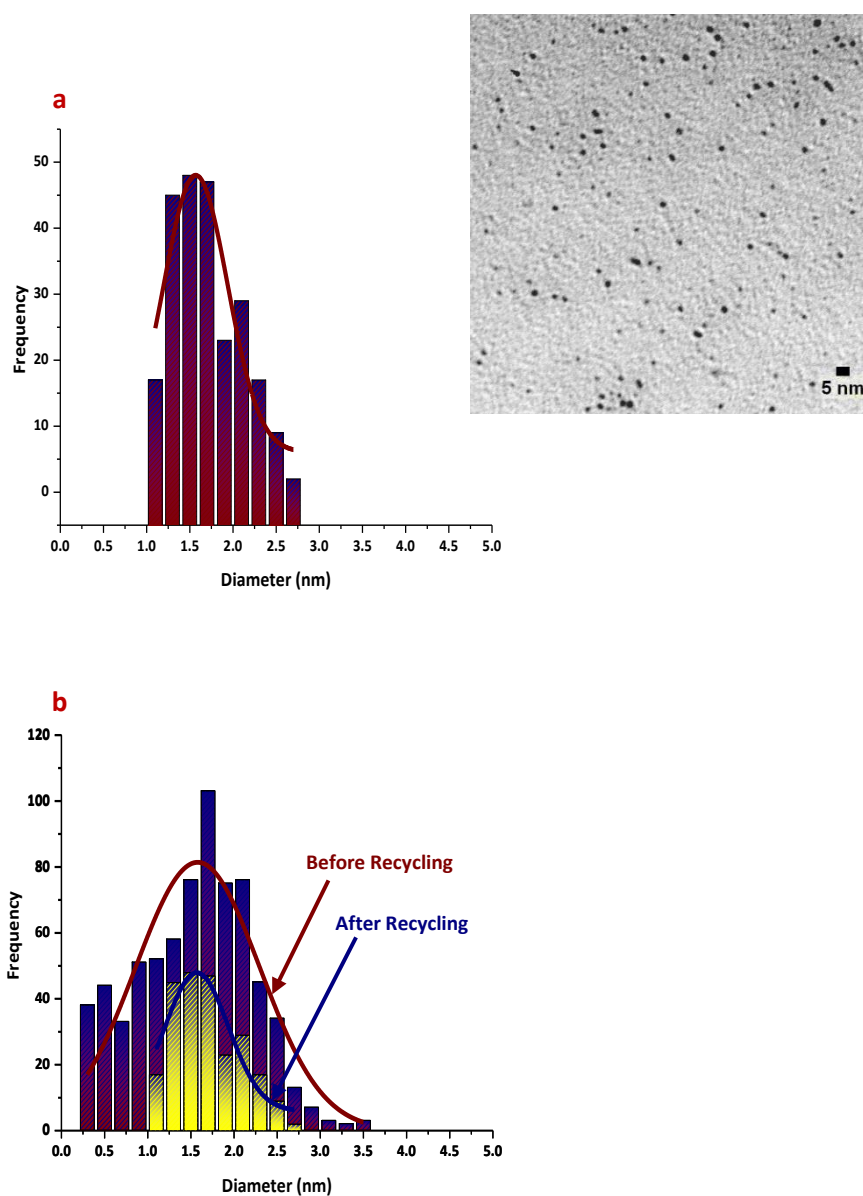
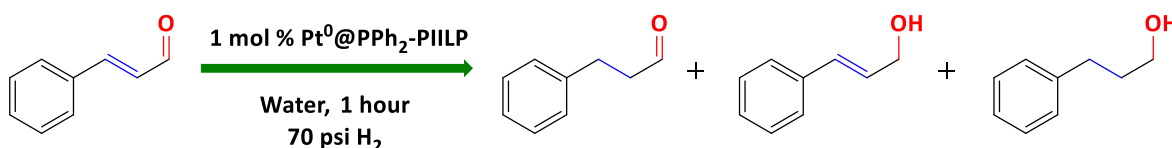


Figure 23 The calculated nanoparticles frequency of (a) recycled sample; (b) stacked diagram before and after recycling of PdNP@Pyrr-PIILP fitted by Gaussian equation.

4.2.8 Further Comparison Investigation Using Platinum Nanoparticles Loaded PIILP

As platinum catalysed hydrogenations are widely preceded in the literature diphenylphosphino modified polymer immobilised ionic liquid stabilised PtNPs were also prepared and their efficacy as catalysts for the hydrogenation of cinnamaldehyde examined for comparison with its palladium counterpart (Scheme 4).



Scheme 4 hydrogenation of *trans*-cinnamaldehyde hydrogenation catalysed by PtNP@PPh₂-PIILP.

From several initial experiments (Table 2), unfortunately, the results were discouraging and PtNP@PPh₂-PIILP was a poor catalyst for the hydrogenation of *trans*-cinnamaldehyde giving 30 % conversion with 64 % selectivity for hydrocinnamaldehyde. Even after extending to reaction time to 2 h the conversion only increased to 64 % with a selectivity of 69 % while the reaction at 60 °C increased the conversion to 78 % with 69 % selectivity. From the literature, the desired selectivity of PtNPs is cinnamyl alcohol, through the reorientation of cinnamaldehyde wherein hydrogenation of the C=O bond would be favoured over the C=C bond.^{192, 199}

Table 2 The hydrogenation results of *trans*-cinnamaldehyde catalysed by PtNP@PPh₂-PIILP.

Reaction Condition	%Conversion	%Selectivity
Water	30	64
Ethanol:Water (1:1)	32	51
Ethanol	37	70
Water; 60 °C	78	56
Water; 2 Hours	64	69
(1 mmol) K ₂ CO ₃	20	78

4.3 Conclusion

Two systems palladium and platinum nanoparticles stabilised by a heteroatom donor modified PIIL support were applied as catalysts for the selective hydrogenation of α,β -unsaturated aldehydes. Solvents screening studies revealed that the catalysts performed most efficiently in protic solvents, with reactions in water giving the best balance of conversion and selectivity. This may be attributed to the dissolution of the catalyst in water resulting in efficient dispersion and access to the active site.

The study of the effect of reaction temperature on catalyst efficacy between 20 - 60 °C showed that selectivity typically increased with increasing temperature, albeit by only a small amount, and that highest selectivity was obtained at 50 °C. TEM analysis of the catalyst recovered after recycling revealed that the mean diameter of the NPs was similar to that of the unspent catalyst. As discussed earlier in **Chapter 3**, although there is no specific trend with regard to particle size and surface morphology, changing the heteroatom donor does seem to result in a dramatic change in the catalysts performances. In order to deduce whether this is a direct result of the many possible metal-heteroatom donor interactions or due to differences in particle size distributions, more studies on the electronic effects of the donors, which may well dominate catalyst activity would be needed.

4.4 Laboratory Preparation Procedures

- **General Comments**

All manipulations involving air-sensitive compounds were carried out using standard Schlenk line techniques under an atmosphere of nitrogen in oven-dried glassware. All solvents dried and distilled under a nitrogen atmosphere, (chloroform and dichloromethane) were distilled from calcium hydride, and (diethyl ether and tetrahydrofuran) from sodium wire / benzophenone; (toluene and hexane) from sodium wire; acetonitrile from potassium carbonate; (methanol and ethanol) from magnesium; while (dimethylformamide) were distilled under vacuum. All chemicals were purchased from commercial suppliers and used as received without further purification. ^1H and $^{13}\text{C}\{^1\text{H}\}$ NMR spectra were recorded on either JEOL ECS-400 or a Bruker Avance III 300 spectrometer.

See **Appendices for all characterisation results.*

4.4.1 General Procedure for Catalytic Hydrogenation of α,β -Unsaturated Aldehydes in Batch

A glass flask insert was charged with (139 μ l, 1 mmol) of trans-cinnamaldehyde, catalyst (1 mmol) and solvent (13 mL) and placed in a reactor equipped with a magnetically coupled stirrer and gas ballast. The reactor was assembled, pressurised with 70 psi of hydrogen, left to stand for 10 seconds and then the gas released through an outlet valve. This sequence was repeated ten times after which the reactor was pressurized to the desired pressure and the solution stirred vigorously at room temperature for 1 hour (unless otherwise stated). The product was extracted with ethyl acetate (3 x 25 mL) the organic fractions combined, dried over MgSO_4 , filtered and the solvent removed. The resulting residue was analysed by ^1H NMR spectroscopy to quantify the composition of starting material and products and to determine the selectivity; for each substrate tested an internal standard of 1,3-dinitrobenzene was initially employed to ensure mass balance.

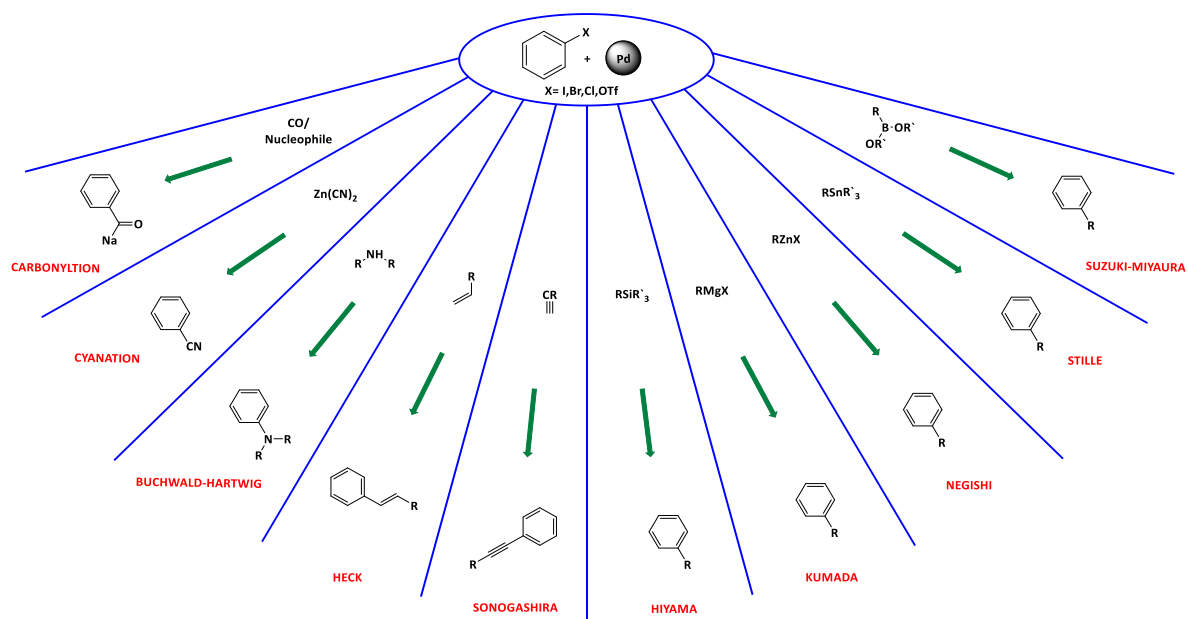
Chapter 5

PIILP PALLADIUM NANOPARTICLES- CATALYSED SUZUKI-MIYaura CROSS-COUPling REACTION

Chapter 5. PIILP PALLADIUM NANOPARTICLES-CATALYSED SUZUKI-MIYAUURA CROSS-COUPLING REACTION

5.1 Introduction

Palladium catalysed cross-couplings have attracted considerable attention recently and the area is still evolving, particularly, when it was acknowledged by the Nobel Prize in 2010 which was awarded to Heck, Negishi, and Suzuki for their work in this field. This field includes a diverse range of carbon-carbon and carbon-heteroatom bond forming reactions which now form an important component of organic synthetic methodology (Scheme 1).^{152, 200}

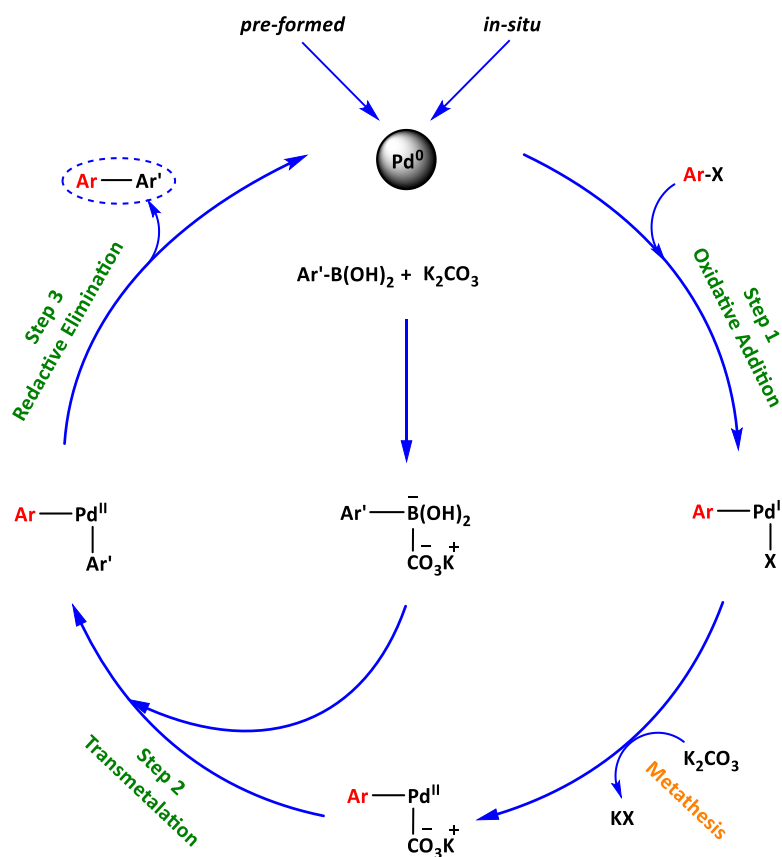


Scheme 1 Representative of palladium catalysed cross-couplings.

The Suzuki-Miyaura reaction is one of the most important and widely used cross-couplings for construction of the biaryl motif. Many reasons behind the success of this synthesis such as the functional groups tolerance and the availability of boronic acid and its stability.²⁰¹ Both Pd^{2+} and Pd^0 complexes typically form highly active catalysts for these types of reactions especially when the reaction contains phosphines or any other ligands in an organic or aqueous reaction media.²⁰²

The mechanism of PdNP catalysed cross-coupling remains unclear and may occur at palladium atoms leached from the nanoparticle or on the surface of the nanoparticle. In this sense, several different theories have appeared in the past decade which try to discuss this matter. Rothenburg *et.al* suggested that catalysis occurs on the leached Pd atoms in case of the Heck and Suzuki-Miyaura cross-coupling,^{182, 203} similarly Vries *et.al*^{204, 205} proposed that nanoparticles catalysed the reaction by working as a reservoir of palladium atoms. As there are numerous examples of palladium nanoparticles immobilised on a range of supports for the Suzuki-Miyaura cross-coupling the efficacy of PdNP@R-PIILP for this transformation was also examined to compare their efficacy and evaluate the relative merits of an ionic liquid decorated heteroatom modified support.

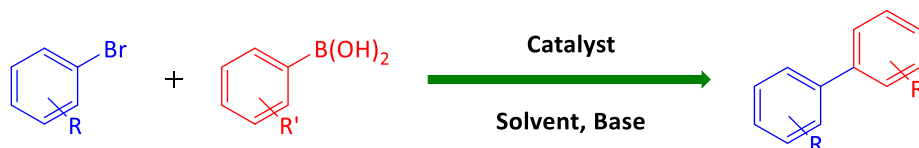
The proposed catalytic cycle for Suzuki-Miyaura cross-coupling reaction catalysed by palladium nanoparticles is shown in (Scheme 2). Palladium nanoparticles would either be *pre-formed*, in this case, it will involve the reaction cycle directly or generated *in-situ* by reduction of PdCl₄@R-PIILP. The reaction then follows three essential steps: the first step is an oxidative addition; this step comprises the addition of Pd⁰ species to the aryl halide (Ar-X). In the second step, the base K₂CO₃ will either exchange with halide on the palladium to afford a Pd-CO₃⁻K⁺ after metathesis, which assists transmetalation with ArB(OH)₂ to afford the [ArB-(OH)₂CO₃⁻K⁺] anion which is activated towards transmetalation.²⁰⁶ The reductive elimination is the final step which generates the desired product and reproduces the Pd⁰ catalyst. As mentioned previously, the rate of the first and final steps of the catalytic cycle can be increased by using bulky electron-donating ligands.^{207, 208}



Scheme 2 The proposed catalytic cycle for the palladium catalysed Suzuki-Miyaura cross-couplings.

5.2 Experimental Studies on Optimisation of Suzuki-Miyaura Cross-Coupling System Process Parameters

For this phase of the project, we chose to examine the efficacy of amino- and phosphino-based PdNP@R-PIILP as catalysts for the Suzuki-Miyaura cross-coupling with the aim of exploring whether the presence of a heteroatom donor affects catalyst performance (Scheme 3).



Scheme 3 Suzuki-Miyaura cross-coupling reaction between aryl halides and aryl boronic acids.

As there are numerous literature reports of highly efficient cross-coupling with metal nanoparticles immobilised on supporting material,^{14, 77, 85, 182, 209} so the comparison with

the efficiency of PdNP@R-PIILP (R = CH₂NH₂, PPh₂) may well be highly informative towards future design and modifications.

It should be noted that reaction optimisation studies for PdNP@PIILP (namely PdNP@OMe-PIILP) systems have previously been conducted by other members of the Doherty/Knight group.²¹⁰ The optimum conditions were identified from the data shown below, which have been employed for this study. Solvent screening studies using EtOH, H₂O, toluene, THF; DMF; EtOH:H₂O; toluene:H₂O; THF:H₂O were carried out, and the best solvent was identified as a 1:1 mixture of EtOH:H₂O (Table 1).²¹⁰

Table 1 Solvent screening studies using catalysed by (PdNP@OMe-PIILP).¹⁶

Entry	Solvent	%Conversion
1	EtOH	24
2	H ₂ O	14
3	Toluene	2
4	THF	5
5	DMF	13
6	EtOH:H ₂ O	84
7	Toluene:H ₂ O	3
8	THF:H ₂ O	17

Reaction Conditions: 0.1 mol % catalysts; 1 mmol aryl halide; 1.13 mmol phenylboronic acid; 1.2 mmol K₂CO₃; 30 °C; 0.5 h; (50:50) solvent mixture; determined by GC with 1 mmol GC standard n-decane; determined by ¹H NMR spectra (average of 2 runs).

In addition to previous studies, further experiments on choosing the best solvent volume ratios. In this sense, catalyst efficacy as a function of the ethanol to water ratio was examined (100:0; 75:25; 50:50; 25:75; 0:100) and the best conversion was achieved with a 50:50 mixtures (Table 2).²¹⁰

Table 2 Optimisation of solvent water content catalysed by (PdNP@OMe-PIILP).¹⁶

Entry	EtOH: H ₂ O	%Conversion
1	100:0	24
2	75:25	71
3	50:50	84
4	25:75	82

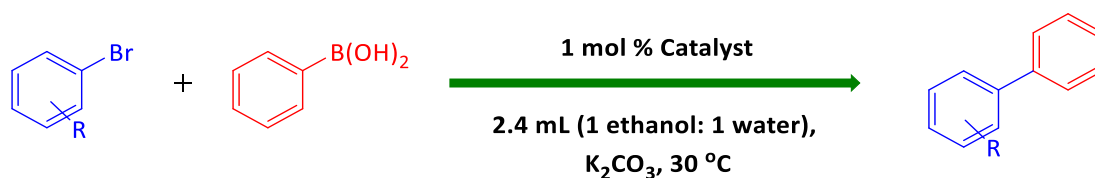
Reaction Conditions: 0.1 mol % catalysts; 1 mmol aryl halide; 1.13 mmol phenylboronic acid; 1.2 mmol K₂CO₃; 30 °C; 0.5 h; (50:50) solvent mixture; determined by GC with 1 mmol GC standard *n*-decane; determined by ¹H NMR spectra (average of 2 runs).

Thus, all further optimisation studies and substrate screening was undertaken in a 50:50 mixture of ethanol and water. The high-performance of the catalyst in this solvent system is most likely due to the ability to dissolve the organic reagents including aryl halides and aryl boronic acids at the same time as dissolving the inorganic base in the reaction mixture.⁵⁷ Base screening studies were conducted with a range of bases (NaOAc, CsOAc, NBU₃, K₃PO₄, CsF, NaHCO₃, K₂CO₃, Cs₂CO₃) and the best was K₂CO₃ and this agreed with the literature presented.^{184, 210-213}

From all previous studies above, the optimum conditions for all further Suzuki-Miyaura cross-couplings in this study are one to one ratio of the co-solvent (ethanol:water) and the base is potassium carbonate.

5.2.1 Aryl Bromide Substrate Screening Studies

With the aim of evaluating the influence of the heteroatom donor on catalyst performance, the efficiency of PdNP@NH₂-PIILP and PdNP@PPh₂-PIILP was examined in the Suzuki-Miyaura reaction between the phenylboronic acid and a series of aryl bromides in ethanol:water at 30 °C in the presence of K₂CO₃ as a base (Scheme 4). All the reactions were run at different times depending on the conversion starting with 19 hours. The catalysts were used in 0.1 mol % loading and reactions were conducted at 30 °C. Comparative catalysts testing was also undertaken with nanoparticles generated *in-situ* from the tetrachloropalladate-based precursors PdCl₄@NH₂-PIILP and PdCl₄@PPh₂-PIILP (Table 3).⁵⁹



Scheme 4 Suzuki-Miyaura cross-coupling reaction.

Interestingly, the *pre-reduced* PdNP@NH₂-PIILP was inactive for the Suzuki-Miyaura cross-coupling across the entire range of substrates tested, whereas those generated *in-situ* from PdCl₄@NH₂-PIILP gave good to excellent conversions across a range of electron rich and electron poor electrophiles.

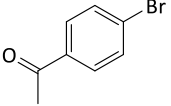
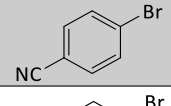
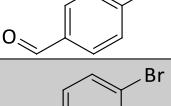
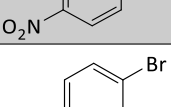
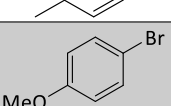
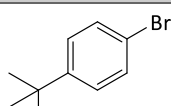
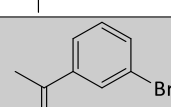
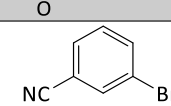
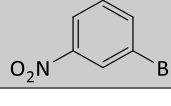

The performance of each catalyst system with a range of aryl bromides substituted with electron withdrawing groups was first examined. The high conversion was obtained with 4-bromoacetophenone and 4-bromobenzonitrile in only 30 min (Entries 1, and 2) whereas 4-bromobenzaldehyde only required 5 min to conversions of 70 – 95 % (Entry 3). For each substrate, catalyst generated *in-situ* from PdCl₄@PPh₂-PIILP was the most efficient. In contrast, 4-bromonitrobenzene required longer reactions times with *in-situ* generated and *pre-formed* PdNP@PPh₂-PIILP both giving conversions of 98 % after 4 h whereas catalyst generated *in-situ* from PdCl₄@NH₂-PIILP only reached 32 % conversion in the same time (Entry 4). In comparison, aryl bromide decorated with mild electron donating groups are slightly deactivated and more challenging. For example, 4-bromotoluene required a longer reaction time of 6 h to reach good conversions and in this case, the most efficient catalyst was generated *in-situ* from PdCl₄@PPh₂-PIILP. Similarly, 4-bromoanisole required a reaction time of 5 h but, in contrast, catalyst generated *in-situ* from PdCl₄@NH₂-PIILP gave higher conversions than its phosphino-counterpart. Substrates substituted with an electron withdrawing group at the 3-position such as 3-bromoacetophenone, 3-bromobenzonitrile, 3-bromonitrobenzene and 3-bromobenzaldehyde all required longer reaction times than their 4-substituted counterparts. For example, 3-bromobenzonitrile and 3-bromonitrobenzene required reactions time of 1 h and 2 h, respectively, and in both cases, PdNP@PPh₂-PIILP was more efficient than *in-situ* generated PdNP@NH₂-PIILP. In contrast, 3-bromoacetophenone and 3-bromobenzaldehyde required a reaction time of 19 h, and in both cases, the highest TOFs were obtained with catalyst generated *in-situ* from PdCl₄@PPh₂-PIILP. Good conversions were also obtained for 3-bromotoluene after 6 h

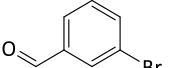
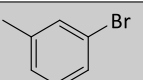
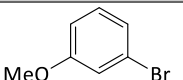
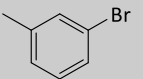
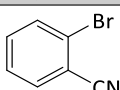
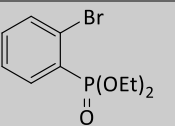
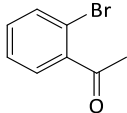
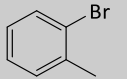
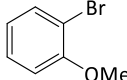
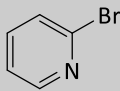
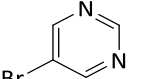
and whereas much lower conversions were obtained for 3-bromoanisole in the same time; however, in both cases catalyst generated *in-situ* from PdCl₄@PPh₂-PIILP proved to be the most efficient. Surprisingly, 5-bromo-*m*-xylene proved to be an extremely challenging substrate and while a conversion of 29 % could be obtained after 19 h with *in-situ* generated PdNP@NH₂-PIILP, both *in-situ* generated and *pre-formed* PdNP@PPh₂-PIILP were inactive. The reason behind the extreme reduction in the activity of the *meta*-substituents may be attributed to a decrease of the *ipso*- carbon positive charge, resulting in a stronger C-Br bond and a slower oxidative addition. While good conversions could be obtained with 2-bromobenzonitrile (81 – 95 %) and diethyl (2-bromophenyl)phosphonate (57 – 99 %) after 1 h and 6 h, respectively, each catalyst was inactive towards 2-bromoacetophenone. Gratifyingly, reasonable conversions could also be obtained with 2-bromotoluene, albeit after a reaction time of 16 h, and the highest TOF was obtained with *in-situ* generated PdNP@PPh₂-PIILP.

Interestingly, for the majority of substrates *in-situ* generated and *pre-formed* PdNP@PPh₂-PIILP give comparable conversions which are generally higher than those obtained with *in-situ* generated PdNP@NH₂-PIILP, with the exception of 4-bromoanisole.

Low conversions were obtained with heteroaromatic substrates 2-bromopyridine and 5-bromopyrimidine (Entries 20, and 21) for all catalysts, even after prolonged reaction times. This suggests that PdNP@PIILP systems are slow with this class of substrate. This could suggest a potential poisoning of the catalyst although further studies would be required to validate this.

Table 3 Aryl bromide Substrate Screening Studies catalysed by PdCl₄@NH₂-PIILP, PdCl₄@PPh₂-PIILP, and PdNP@PPh₂-PIILP.

Entry	Electrophile	Time (h)	PdCl ₄ @NH ₂ -PIILP			PdCl ₄ @PPh ₂ -PIILP			PdNP@PPh ₂ -PIILP		
			%Conv.	TON	TOF h ⁻¹	%Conv.	TON	TOF h ⁻¹	%Conv.	TON	TOF h ⁻¹
1		0.5	78	781	1562	99	1160	2320	99	1004	2008
2		0.5	100	1000	2000	100	1171	2343	100	1014	2029
3		5 Min.	70	701	8446	95	1113	13409	79	801	9655
4		4	32	320	80	98	1148	287	98	994	249
5		6	89	891	149	96	1125	187	85	862	144
6		5	80	801	160	62	726	145	45	456	91
7		19	6	60	3	0	0	0	0	0	0
8		19	96	961	51	95	1113	59	41	416	22
9		1	97	971	971	81	949	949	98	994	994
10		2	100	1001	501	99	1160	580	100	1014	507

Entry	Electrophile	Time (h)	PdCl ₄ @NH ₂ -PIILP			PdCl ₄ @PPh ₂ -PIILP			PdNP@PPh ₂ -PIILP		
			%Conv.	TON	TOF h ⁻¹	%Conv.	TON	TOF h ⁻¹	%Conv.	TON	TOF h ⁻¹
11		16	98	981	61	93	1089	68	83	842	53
12		6	75	751	125	80	937	156	87	882	147
13		6	23	230	38	33	387	64	31	314	52
14		19	29	290	15	0	0	0	0	0	0
15		1	90	901	901	81	949	949	95	964	964
16		6	63	631	105	99	1160	193	57	578	96
17		16	0	0	0	0	0	0	0	0	0
18		16	57	571	36	67	785	49	60	609	38
19		19	80	801	42	99	1160	61	100	1014	53
20		19	10	100	5	22	258	14	17	172	9
21		19	32	320	17	34	398	21	28	284	15

Reaction Conditions: 0.1 mol % catalysts; 1 mmol aryl halide; 1.13 mmol phenylboronic acid; 1.2 mmol K₂CO₃; 2.4 mL (1 ethanol: 1 water); 30 °C; determined by GC with 1 mmol GC standard n-decane; determined by ¹H NMR spectra (average of 2 runs).

5.3 Further Studies on the Suzuki-Miyaura Cross-Coupling Catalyzed by PdNP@R-PIILP

5.3.1 Kinetic Studies

The aryl bromides for these studies were selected depending on their reaction times ranging from long to short and reactions were catalysed by PdCl₄@NH₂-PIILP (**3.13**), PdCl₄@PPh₂-PIILP (**3.14**), and PdNP@PPh₂-PIILP (**3.17**).

➤ Kinetic Studies with 4-bromotoluene

A kinetic study on the Suzuki-Miyaura cross-coupling between phenyl boronic acid and 4-bromotoluene (Figure 1) was performed by sampling a reaction and monitoring progress by ¹H NMR spectroscopy. Qualitatively, each of the catalysts showed similar conversion time profiles, and all reactions reached maximum conversion after *c.a.* 360 min. However, close inspection of the profiles for **3.13** and **3.14** revealed subtle differences in the early stages (0 - 20 min) which may well be attributed to an induction associated with the reduction of the tetrachloropalladate precursor.

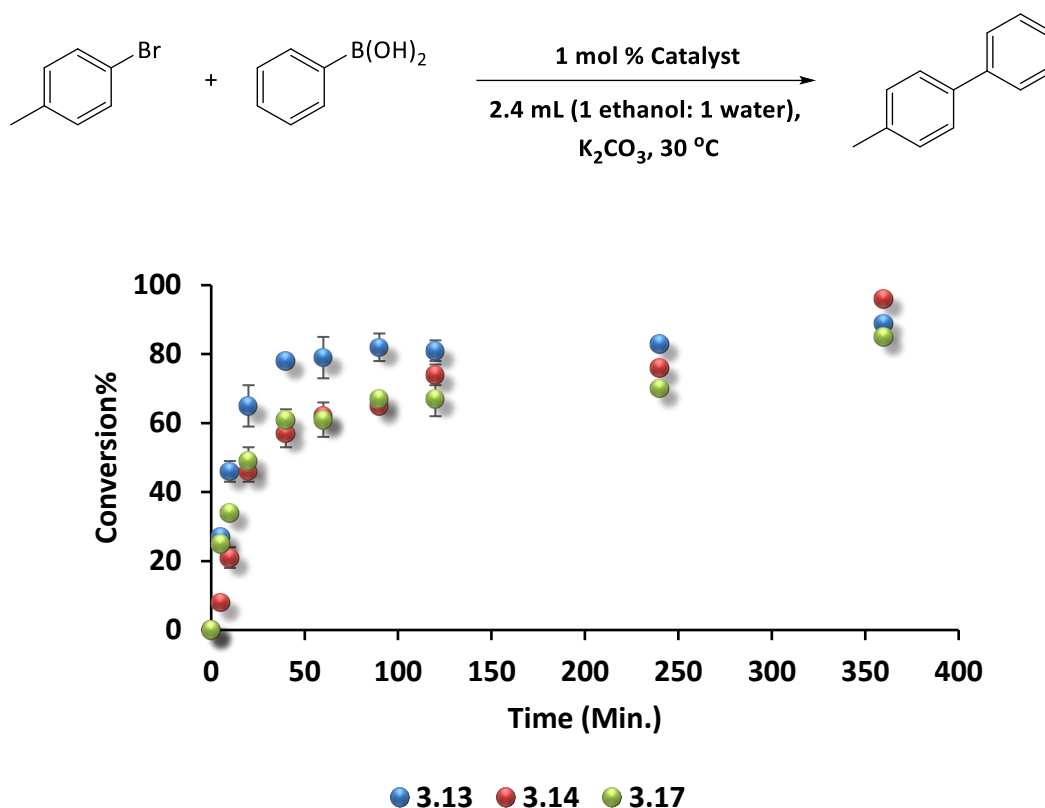


Figure 1 Kinetic profiles of 4-bromotoluene catalysed by PdCl₄@NH₂-PIILP (**3.13**); PdCl₄@PPh₂-PIILP (**3.14**); and PdNP@PPh₂-PIILP (**3.17**).

Reaction Conditions: 0.1 mol % catalysts; 1 mmol aryl halide; 1.13 mmol phenylboronic acid; 1.2 mmol K₂CO₃; 2.4 mL (1 ethanol: 1 water); 30 °C; determined by GC with 1 mmol GC standard *n*-decane; determined by ¹H NMR spectra (average of 2 runs).

The conversion-time profile was subsequently studied as a function of catalyst loading using 0.1 and 0.5 mol % $\text{PdCl}_4\text{@PPh}_2\text{-PIILP}$. As expected, the reaction catalysed by 0.1 mol % **3.14** was markedly slower than that with a loading of 0.5 mol % initial reaching 8 % and 25 % conversion respectively after 5 min, however, both reached near complete conversion after the same time (Figure 2).

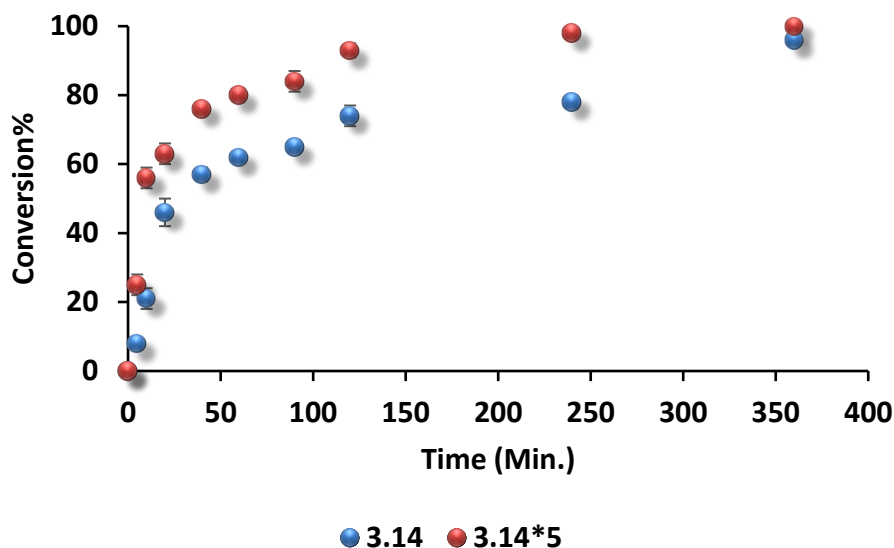


Figure 2 Kinetic profiles of 4-bromotoluene catalysed by) 0.1 mol %) $\text{PdCl}_4\text{@PPh}_2\text{-PIILP}$ (**3.14**), and 0.5 mol %) $\text{PdCl}_4\text{@PPh}_2\text{-PIILP}$ (**3.14 *5**).

Reaction Conditions: 0.1 mol % catalysts; 1 mmol aryl halide; 1.13 mmol phenylboronic acid; 1.2 mmol K_2CO_3 ; 2.4 mL (1 ethanol: 1 water); 30 °C; determined by GC with 1 mmol GC standard *n*-decane; determined by ^1H NMR spectra (average of 2 runs).

➤ Kinetic Studies of 4-bromobenzonitrile

Interestingly while the conversion-time profiles for the highly activated 4-bromobenzonitrile were qualitatively similar for each catalyst, $\text{PdNP@PPh}_2\text{-PIILP}$ showed a short induction period; this may well be associated with the different dispersibility and/or slower solvation preventing access to the active site. While all reaction was complete within 15 min $\text{PdCl}_4\text{@NH}_2\text{-PIILP}$ slightly more active than its phosphino-counterpart (Figure 3).

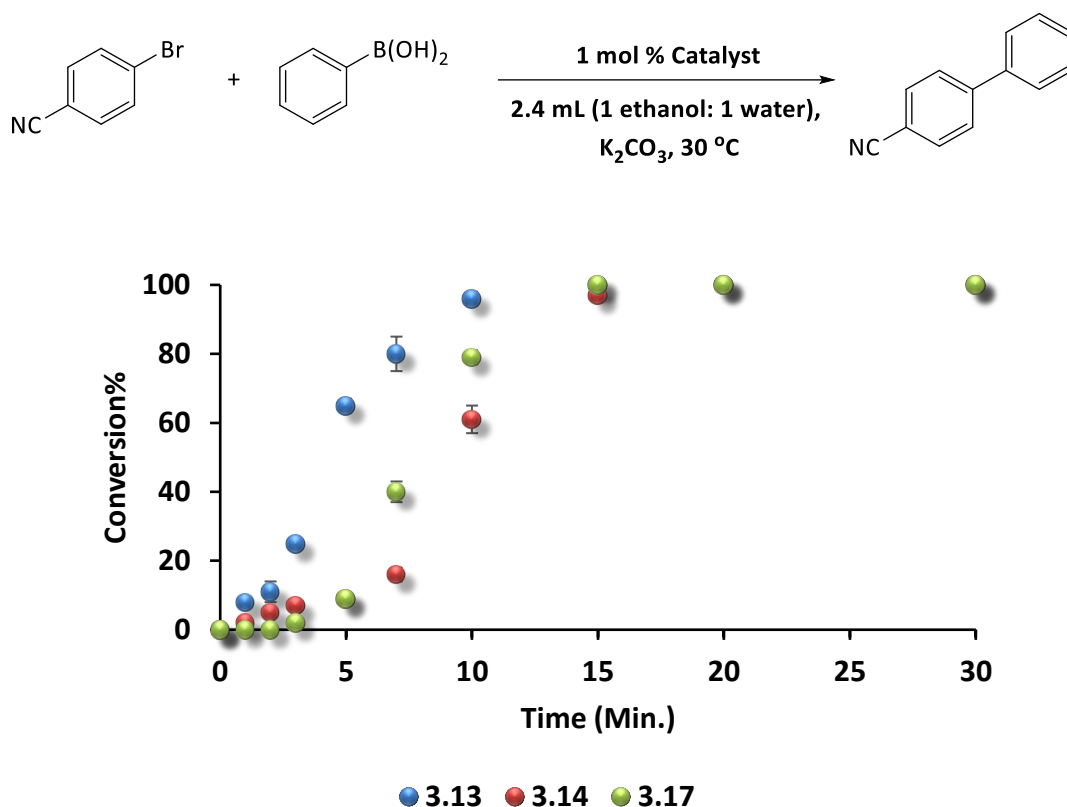
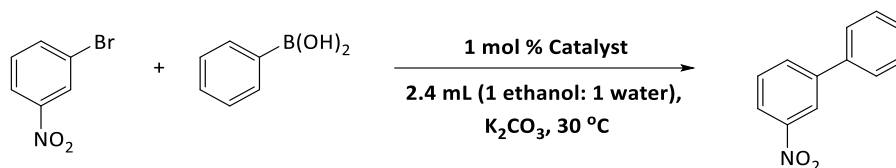


Figure 3 Kinetic profiles of 4-bromobenzonitrile catalysed by $\text{PdCl}_4@\text{NH}_2\text{-PIILP}$ (**3.13**); $\text{PdCl}_4@\text{PPh}_2\text{-PIILP}$ (**3.14**); and $\text{PdNP}@\text{PPh}_2\text{-PIILP}$ (**3.17**).

Reaction Conditions: 0.1 mol % catalysts; 1 mmol aryl halide; 1.13 mmol phenylboronic acid; 1.2 mmol K_2CO_3 ; 2.4 mL (1 ethanol: 1 water); 30 °C; determined by GC with 1 mmol GC standard n-decane; determined by ^1H NMR spectra (average of 2 runs).

➤ Kinetic Studies of 1-bromo-3-nitrobenzene

The conversion-time profile for the Suzuki-Miyaura coupling with 1-bromo-3-nitrobenzene showed a similar trend to 4-bromobenzonitrile in that catalyst generated from $\text{PdCl}_4@\text{NH}_2\text{-PIILP}$ was the most active while both phosphine-based systems showed a short but definite induction, which may be due to solvation and/or swelling effects (Figure 4).



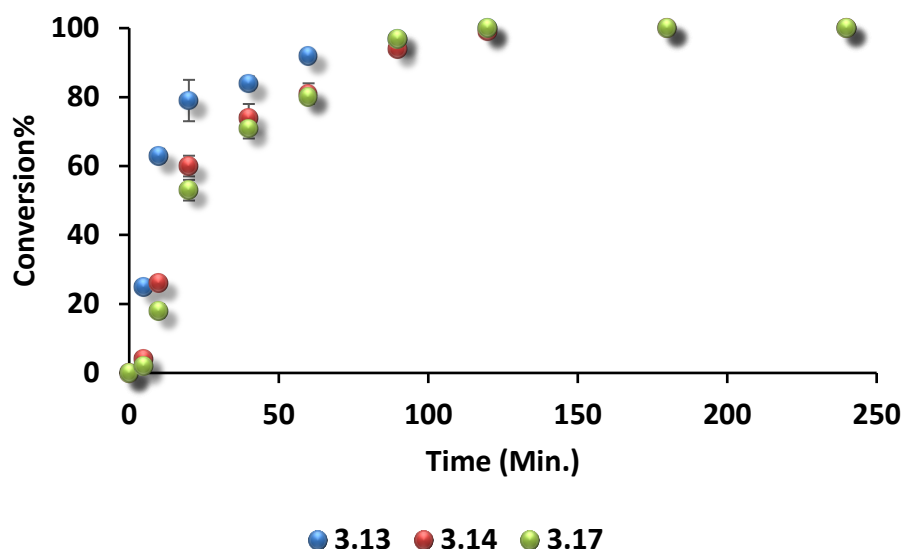


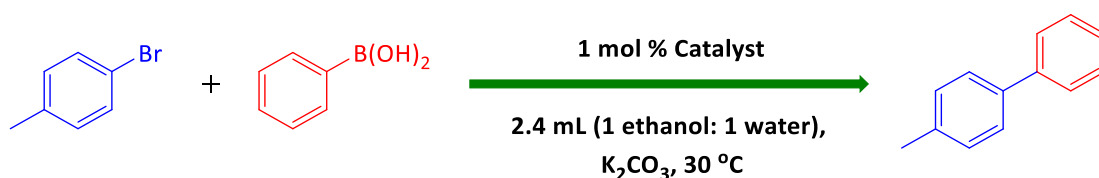
Figure 4 Kinetic profiles of 1-bromo-3-nitrobenzene catalysed by $\text{PdCl}_4@\text{NH}_2\text{-PIILP}$ (**3.13**); $\text{PdCl}_4@\text{PPh}_2\text{-PIILP}$ (**3.14**); and $\text{PdNP}@\text{PPh}_2\text{-PIILP}$ (**3.17**).

Reaction Conditions: 0.1 mol % catalysts; 1 mmol aryl halide; 1.13 mmol phenylboronic acid; 1.2 mmol K_2CO_3 ; 2.4 mL (1 ethanol: 1 water); 30 °C; determined by GC with 1 mmol GC standard *n*-decane; determined by ^1H NMR spectra (average of 2 runs).

In general, all the reactions with all the substrates (4-bromotoluene, 4-bromobenzonitrile and 1-bromo-3-nitrobenzene) showing the high average of the initial reactions rates with all catalysts through the early stages of the reactions.

Further studies have also been undertaken to explore the effect of catalyst loading, reaction dilution and mercury on catalyst performance with the aim of establishing whether catalysis occurs via a heterogeneous or homogenous pathway.

The Suzuki coupling of 4-bromotoluene (Scheme 5) was chosen to be a model reaction for these studies.



Scheme 5 The Suzuki-Miyaura cross-coupling between 4-bromotoluene and phenylboronic acid.

5.3.2 Catalyst Loading Studies

The effect of catalyst concentration from 0.025 to 3 mol % was first investigated for each of the catalysts. Conversions increased with increasing the catalyst loading up to 0.5 mol % for each catalytic system (Figure 5). Above 0.5 mol % conversions reached a plateau and then ultimately decreased as the loading reached 3 mol %. If the reaction rate is controlled at 0.025 mol %, one would expect conversions to increase with increasing catalyst loading and the plateau above 0.5 mol % may well signify the onset of diffusion control while the decrease in conversion at high catalyst loadings may well be due to agglomeration of nanoparticles. However, this agglomeration may well be interpreted either as catalysis at the nanoparticle due to a reduction in the number of active sites or catalysis by a soluble species as the agglomeration may well effect leaching or release of active palladium from the surface of the nanoparticle.

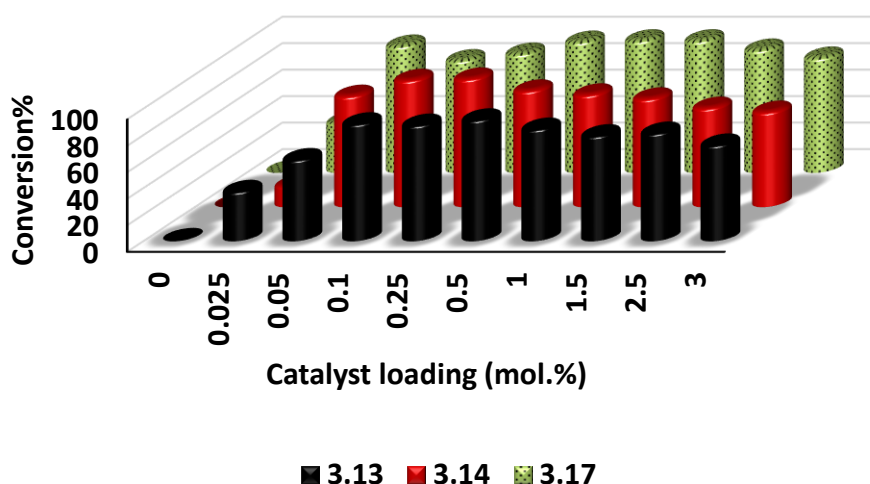


Figure 5 Catalyst loading studies of 4-bromotoluene catalysed by $\text{PdCl}_4@\text{NH}_2\text{-PIILP}$ (**3.13**); $\text{PdCl}_4@\text{PPh}_2\text{-PIILP}$ (**3.14**); and $\text{PdNP}@\text{PPh}_2\text{-PIILP}$ (**3.17**).

Reaction Conditions: 0.1 mol % catalysts; 1 mmol aryl halide; 1.13 mmol phenylboronic acid; 1.2 mmol K_2CO_3 ; 2.4 mL (1 ethanol: 1 water); 30 °C; 6 h; determined by GC with 1 mmol GC standard *n*-decane; determined by ^1H NMR spectra (average of 2 runs).

5.3.3 Reaction Dilution Studies

In a similar manner, the effect of reaction dilution was also investigated (Figure 6). The total reaction volume was varied from 1.2 mL to 250 mL while maintaining a 1:1 ratio of water to ethanol. For each catalyst, the increase in conversion when the reaction volume was diluted from 1.2 mL to 2.4 mL may be due to complete solubilisation of the substrate

or may indicate catalysis by nanoparticles as agglomeration-based deactivation is less likely in dilute solution. Interestingly, while PdNP@PPh₂-PIILP also showed an increase in conversion for the first dilution to 2.4 mL, conversions plateaued between 2.4 mL and 6 mL increased again in 10 mL and then remained constant up to a dilution of 80 mL.

Furthermore, the effect of the reaction dilution would behave differently based on the nature of the catalytic system, if the system were homogeneous, i.e. leaching of soluble Pd species was responsible for the activity, and the reaction rate would decrease with increasing reaction dilution. However, the opposite effect would be expected for a heterogeneous catalytic system, i.e. the activity would decrease under more concentrated conditions due to an increase in agglomeration of the nanoparticles leading to catalyst deactivation.

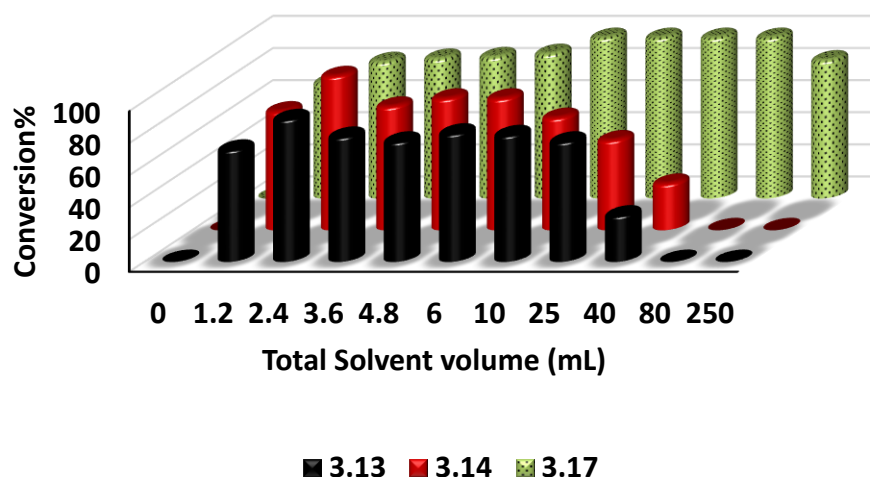


Figure 6 Reaction dilution studies for 4-bromotoluene catalysed by PdCl₄@NH₂-PIILP (**3.13**); PdCl₄@PPh₂-PIILP (**3.14**); and PdNP@PPh₂-PIILP (**3.17**).

Reaction Conditions: 0.1 mol % catalysts; 1 mmol aryl halide; 1.13 mmol phenylboronic acid; 1.2 mmol K₂CO₃; solvent (1 ethanol: 1 water); 30 °C; 6 h; determined by GC with 1 mmol GC standard n-decane; determined by ¹H NMR spectra (average of 2 runs).

5.3.4 Comparison with Commercially Available Pd/C

To determine the viability and relative merits of the newly prepared PdNP@PIILP, several comparative studies were run by using the most popular heterogeneous catalyst used for Suzuki coupling which is palladium on activated charcoal catalyst²³ (5 % Pd

basis) supplied from different commercial sources. Satisfyingly, under the same conditions, the conversions of 85 – 96 % obtained with PdNP@PIILP were significantly higher than those of 45 – 57 % obtained with three commercial samples of Pd/C; full details are illustrated in (Figure 7).

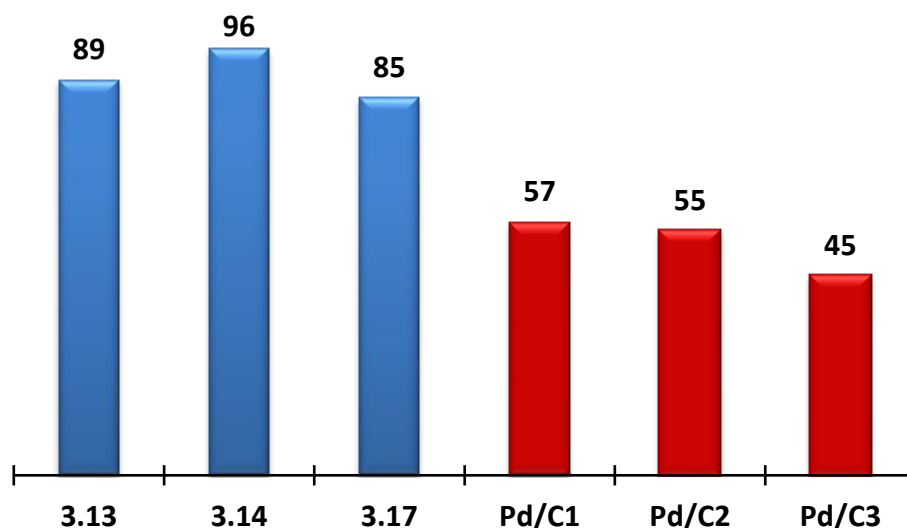


Figure 7 Comparisons studies of 4-bromotoluene catalysed by PdCl₄@NH₂-PIILP (**3.13**); PdCl₄@PPh₂-PIILP (**3.14**); PdNP@PPh₂-PIILP (**3.17**); (Pd/C1): Aldrich 276707; (Pd/C2): Aldrich 75992; and (Pd/C3): Palladium-on-Charcoal catalysts/Johnson Matthey.

Reaction Conditions: 0.1 mol % catalysts; 1 mmol aryl halide; 1.13 mmol phenylboronic acid; 1.2 mmol K₂CO₃; 2.4 mL (1 ethanol: 1 water); 30 °C; 6 h; determined by GC with 1 mmol GC standard *n*-decane; determined by ¹H NMR spectra (average of 2 runs).

5.3.5 Mercury Poisoning Experiments

Mercury poisoning experiments were undertaken in order to investigate whether catalysis occurs via a homogeneous or heterogeneous pathway (Figure 8).¹⁸ The role of mercury is to poison the surface of the nanoparticle by forming an amalgam which blocks the active sites and quenches the reaction. While the mercury poisoning test has conventionally been used to distinguish between heterogeneous and homogeneous catalysis on the basis that mercury does not form an amalgam with metal-ligand complexes, more recent evidence suggests that “naked” molecular palladium species are examples of homogeneous catalysts that should be affected by Hg(0), as a consequence of their lack of strong protecting ligands and their M(0) state and a such this test may lead to false positive result and should be treated with caution.

The reaction vessel charged with all the reactants (the catalyst, phenylboronic acid, K_2CO_3) and pre-stirred with mercury (200 eq. to the catalyst, ~ 0.008 mL) for a range of times as shown in (Figure 8) prior to adding the aryl bromide. The phenylboronic acid was added to the reaction mixture from the beginning of the reaction to reduce the tetrachloropalladate precursor and form the PdNPs *in-situ*. The obtained results showed the conversions decreased with increasing pre-stirring time and complete deactivation was only obtained with **3.14** and **3.17** after 24 h, whereas $PdCl_4@NH_2-PIILP$ remained active. As mercury poisoning tests as generally performed by adding mercury to a reaction mixture and observing an immediate effect on activity, it is difficult to confidently assign such a pre-stirring conversion profile to catalysis by a heterogeneous system. However, mercury may well influence leaching of palladium from the NP surface and such a process may well be time-dependent, i.e. the profile may well be explained by the NPs acting as a source of soluble palladium, but such an interpretation should be treated with caution.

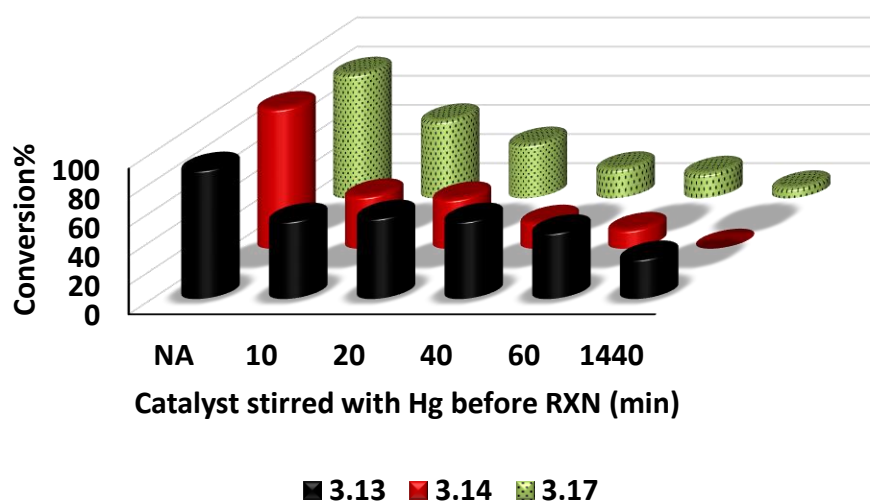


Figure 8 Mercury poisoning studies of 4-bromotoluene catalysed by $PdCl_4@NH_2-PIILP$ (**3.13**); $PdCl_4@PPh_2-PIILP$ (**3.14**); and $PdNP@PPh_2-PIILP$ (**3.17**).

Reaction Conditions: 0.1 mol % catalysts; 1 mmol aryl halide; 1.13 mmol phenylboronic acid; 1.2 mmol K_2CO_3 ; 2.4 mL (1 ethanol: 1 water); 30 °C; 6 h; determined by GC with 1 mmol GC standard *n*-decane; determined by 1H NMR spectra (average of 2 runs).

Comparative mercury studies were run by using palladium on activated charcoal catalysts (5 % Pd basis) and a similar trend was observed (Figure 9).

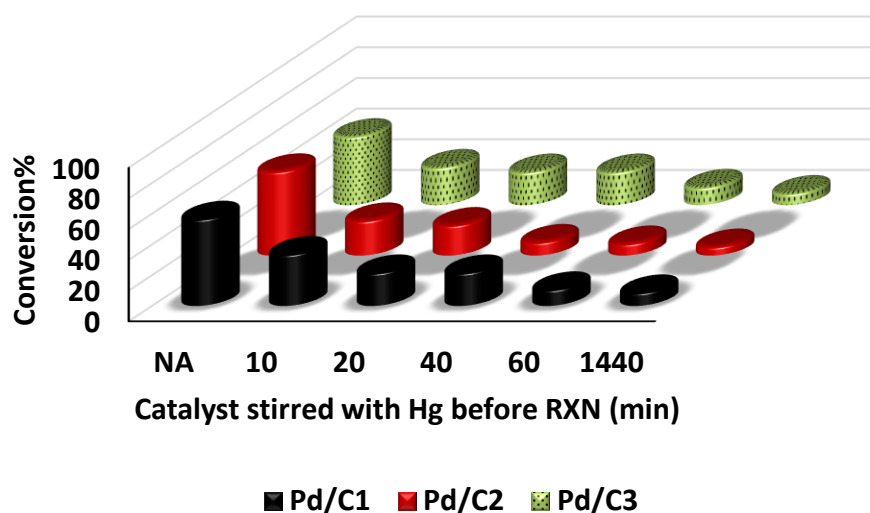


Figure 9 Mercury poisoning studies of 4-bromotoluene catalysed by (Pd/C1): Aldrich 276707; (Pd/C2): Aldrich 75992; and (Pd/C3): Palladium-on-Charcoal catalysts/Johnson Matthey.

Reaction Conditions: 0.1 mol % catalysts; 1 mmol aryl halide; 1.13 mmol phenylboronic acid; 1.2 mmol K_2CO_3 ; 2.4 mL (1 ethanol: 1 water); 30 °C; 6 h; determined by GC with GC standard *n*-decane (1 mmol), determined by 1H NMR spectra (average of 2 runs).

The graduated performance of the prepared catalysts reduction upon mercury poisoning might imply that a portion of the reaction has behaved as homogeneous reaction system via the palladium nanoparticles leached into the reaction mixture, while the other portion would behave as heterogeneous, as a result of Hg blocking of the PdNps immobilised within the PIILP matrix. From all the previous studies, we tentatively suggest that catalysts occur by both homogeneous and heterogeneous pathways.

5.4 Mechanism of the Palladium Nanoparticle Catalysed Suzuki-Miyaura Cross-Coupling

All the studies observations are strongly suggested that the catalytic activity may attribute to a combination of both homogeneous and heterogeneous catalytic reaction systems which is in agreement with the mechanism proposed by Pérez-Lorenzo (Figure 10).¹⁵²

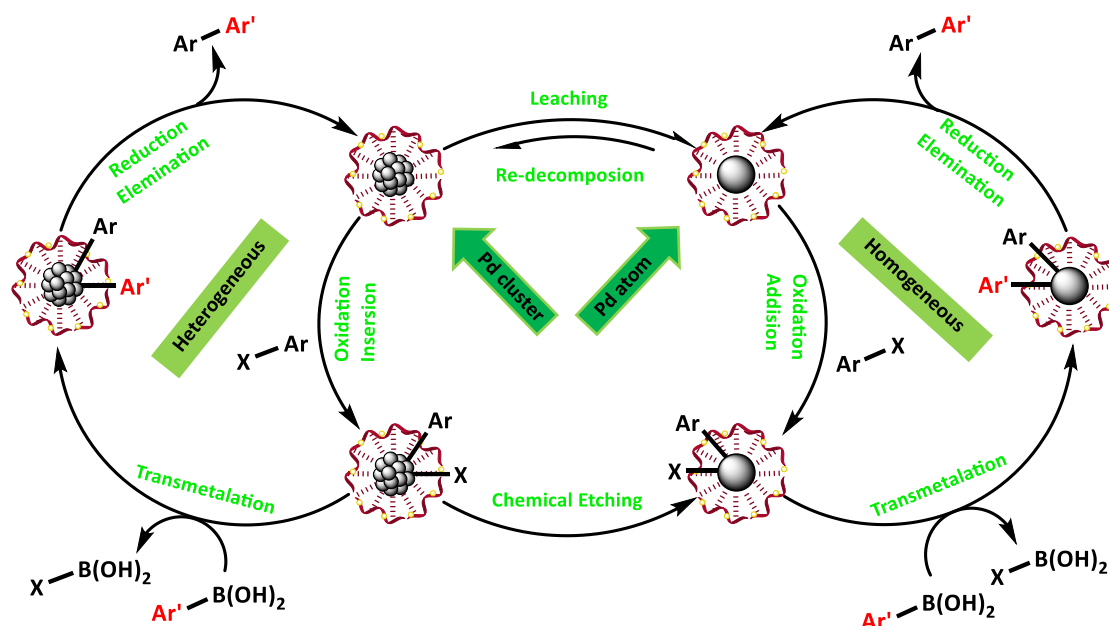


Figure 10 The proposed homogeneous and heterogeneous mechanisms for Suzuki-Miyaura cross-coupling catalysed by PdNP@PIILP.

The true nature and the exact mechanism of the active palladium species remain unclear, there are two different possible pathways for nanoparticles loaded on PIILP (PdNP@PIILP). In one case the NPs act as a reservoir for soluble palladium atoms which leach from the surface and act as a homogenous catalyst.^{152,205} Conversely, in the heterogenous pathway the catalytic steps occurs on the surface of the nanoparticle and activity will be affected by agglomeration.^{152, 215, 216}

However, the reactions may be occurring simultaneously, and the dominant pathway would be determined depending on the nature of the stabilising agent of the nanoparticles. In this regard, the hetero-atom donor decorated PIILP materials may well operate as a “catch and release” system in which leached molecular palladium interacts with and is stabilised by a heteroatom donor; this may well be the active species which is deactivated in the mercury poisoning experiments. Alternatively, the leached palladium may well redeposit on the NP surface.²¹⁷⁻²¹⁹

5.5 Conclusion

Hetero-atom decorated styrene-based poly-ionic liquid stabilised palladium nanoparticles have been tested in the Suzuki–Miyaura cross-coupling. Interestingly, while *pre-reduced* PdNP@NH₂-PIILP was completely inactive across the range of substrates tested, the corresponding catalyst generated *in-situ* by reduction of PdCl₄@NH₂-PIILP gave good conversions under mild conditions and competed with the *in-situ* generated and *pre-formed* phosphine stabilised counterparts.

A study of the conversion time profile for several electronically disparate substrates revealed that *in-situ* generated PdNP@PPh₂-PIILP displays similar trends to that of the *pre-formed* NPs, in that they both achieve high conversions after prolonged reactions times. There appears to be no prolonged induction period for the Pd²⁺ precursor in comparison with the *pre-reduced* PPh₂ functionalised catalyst indicating that reduction of this species to form the active catalyst is fast. The NH₂ functionalised catalyst appears to have a shorter induction period than that of the PPh₂ catalyst however as the course of the reaction proceeds, all of the catalysts seem to reach similar conversions.

A comparison with the literature reveals that PdNP@R-PIILP is highly efficient under mild conditions (30 °C), while the other system need reaction temperatures in excess of 70 °C.²⁰⁹ The results obtained from a mercury poisoning studies suggest that catalysis may be occurring both at the NP surface and leaching of soluble palladium which may be ‘captured’ and stabilised by interaction with the heteroatom donor.

5.6 Laboratory Preparation Procedures

- **General Comments**

All manipulations involving air-sensitive compounds were carried out using standard Schlenk line techniques under an atmosphere of nitrogen in oven-dried glassware. All solvents were dried and distilled under a nitrogen atmosphere, chloroform and dichloromethane was distilled from calcium hydride, and diethyl ether and tetrahydrofuran from sodium wire/benzophenone; toluene and hexane from sodium wire; acetonitrile from potassium carbonate; methanol and ethanol from magnesium while dimethylformamide was distilled under vacuum. All chemicals were purchased from commercial suppliers and used as received without further purification. ^1H and $^{13}\text{C}\{^1\text{H}\}$ NMR spectra were recorded on either JEOL ECS-400 or a Bruker Avance III 300 spectrometer. Gas chromatography was performed using a Shimadzu 2010 series gas chromatograph with a Supelco Beta DEX column. Total flow 92.5 mL/min; column flow 1.76 mL/min; pressure 21.2 psi; makeup flow 30 mL/min; H_2 flow 40 mL/min; air flow 400 mL/min.

See **Appendices for all characterisation results.*

- ***General Procedure for Catalytic Suzuki-Miyaura Couplings in Batch***

An oven-dried Schlenk flask was allowed to cool to room temperature and charged sequentially with catalyst (0.001 mmol, 0.1 mol %), aryl bromide (1 mmol), phenylboronic acid (0.138 g, 1.13 mmol), K₂CO₃ (0.166 g, 1.2 mmol), a mixture of 50:50 (ethanol:water) (2.4 mL). The reaction mixture was stirred at 30 °C for the desired time of reaction after which decane (0.195 mL, 1 mmol), water (5 mL) and diethyl ether (10 mL) were added, the mixture was shaken vigorously, and the organic phase separated and passed through a short plug of silica. A small portion of the organic extract was diluted with diethyl ether for analysis by GC and the remaining solvent was removed under reduced pressure and the resulting residue analysed by ¹H NMR spectroscopy.

Chapter 6

SUMMARY

Chapter 6. Summary

Drawing from previous work in the Doherty group, the results presented in this thesis demonstrate that concept of Polymer Immobilised Ionic Liquid Phase (PIILP) catalysis is a powerful and extremely versatile catalyst technology. Under this concept, two PIILP materials have been successfully synthesised using a modular synthesis and well characterised by a range of techniques including solid-state NMR spectroscopy, SEM, TEM, XRD, XPS, EDX, ICP, TGA and BET analysis.

Molecular catalysts were successfully immobilised within pyrrolidinium-decorated polymers prepared via ROMP and both tungstate and polyoxotungstate based catalysts were shown to be extremely active and selective catalysts for the oxidation of sulfides. The high activity of the catalysts which can be used either *pre-formed* or *in-situ* allows the reaction to proceed under extremely mild conditions and the catalysts recycled well. Furthermore, by applying the appropriate conditions, either sulfoxide or sulfone can be obtained in high selectivity.

The use of imidazolium functionalised styrene based monomers combined with various heteroatom donor modified monomers allows the fabrication of a new class of PIILP materials via free radical polymerisation which were shown to successfully support and stabilise Pd and Pt nanoparticles. PdNP@PIILP catalysts were shown to be highly active for the hydrogenation of α,β -unsaturated aldehydes and it was shown that the heteroatom donor had a strong influence on the catalyst activity and selectivity. In this regard, it may be possible to optimise these systems further and introduce other functionality via the simple PIILP synthesis to generate highly active and selective catalysts. Furthermore, the versatility of these systems is evident as the same catalysts are also extremely active for the Suzuki-Miyaura cross-coupling reaction under extremely mild conditions and low catalyst loadings (0.5 mol %). Again, the heteroatom donor showed a strong influence on the catalysis with the PPh₂ catalyst outperforming its amino- and pyrrolidino- counterparts.

The concept of PIILP catalysis has span across a range of chemical transformations and as a result of the work presented here, the group are now continuing to harness the idea to extend the applications of PIILP. In this regard, immobilisation of different catalytically

active metals can expand the potential applications, in particular, RuNPs have shown excellent potential as candidates for the production of platform and fuel chemicals from bio derived sources. Furthermore, bimetallic NPs have been shown to modulate activity and selectivity of catalyst systems in order to achieve optimum systems for the selective formation of reactant intermediates that may not have been accessible via monometallic NPs. The efficacy and facile synthesis of recyclable PIILP catalysts also highlights them as ideal materials for large scale catalysis and this methodology may enable us to develop systems suitable for continuous flow processes.

REFERENCES

REFERENCES

1. S. Doherty, J. G. Knight, J. R. Ellison, D. Weekes, R. W. Harrington, C. Hardacre and H. Manyar, *Green Chem.*, 2012, **14**, 925.
2. R. D. Rogers and G. A. Voth, *Acc. Chem. Res.*, 2007, **40**, 1077-1078.
3. J. Dupont, *J. Braz. Chem. Soc.*, 2004, **15**, 341-350.
4. V. P. Chris Hardacre, *Catalysis in Ionic Liquids : From Catalyst Synthesis to Application* Royal Society of Chemistry, 2014.
5. M. Koel, *Ionic Liquids in Chemical Analysis*, CRC Press, Boca Raton, Florida, 2008.
6. Z. Ma, J. Yu and S. Dai, *Adv. Mater.*, 2010, **22**, 261-285.
7. M. I. Burguete, F. Galindo, E. Garcia-Verdugo, N. Karbass and S. V. Luis, *Chem. Commun.*, 2007, **0**, 3086-3088.
8. J. S. Yadav, B. V. S. Reddy, G. Kondaji, S. Sowjanya and K. Nagaiah, *J. Mol. Catal. A: Chem.*, 2006, **258**, 361-366.
9. K. Ghandi, *GSC*, 2014, **04**, 44-53.
10. K. R. S. Annegret Stark, in *Kirk-Othmer Encyclopedia of Chemical Technology*, ed. A. Seidel, John Wiley & Sons, Inc., Hoboken, New Jersey, Editon edn., 2007, vol. 26, pp. 836-924.
11. J.-C. Xiao, B. Twamley and J. n. M. Shreeve, *Org. Lett.*, 2004, **6**, 3845-3847.
12. J. Bargon and L. T. Kuhn, *In situ NMR Methods in Catalysis (Topics in Current Chemistry)*, Springer, Berlin, 2007.
13. R. Giernoth, in *In situ NMR Methods in Catalysis*, eds. J. Bargon and L. T. Kuhn, Springer Berlin Heidelberg, Berlin, Heidelberg, 2007, pp. 1-23.
14. H. Olivier-Bourbigou, L. Magna and D. Morvan, *Appl. Catal., A*, 2010, **373**, 1-56.
15. A. Mele, G. Romanò, M. Giannone, E. Ragg, G. Fronza, G. Raos and V. Marcon, *Angew. Chem. Int. Ed.*, 2006, **45**, 1123-1126.
16. P. Wasserscheid and T. Welton, *Ionic Liquids in Synthesis*, 2nd edn., Wiley-VCH, Weinheim, 2008.
17. P. Wasserscheid and W. Keim, *Angew. Chem. Int. Ed.*, 2000, **39**, 3772-3789.
18. M. Smiglak, J. D. Holbrey, S. T. Griffin, W. M. Reichert, R. P. Swatloski, A. R. Katritzky, H. Yang, D. Zhang, K. Kirichenko and R. D. Rogers, *Green Chem.*, 2007, **9**, 90-98.
19. H. Srou, H. Rouault, C. C. Santini and Y. Chauvin, *Green Chem.*, 2013, **15**, 1341.
20. J. A. Boon, J. A. Levisky, J. L. Pflug and J. S. Wilkes, *J. Org. Chem.*, 1986, **51**, 480-483.
21. Y. Xiao and S. V. Malhotra, *J. Organomet. Chem.*, 2005, **690**, 3609-3613.
22. Y. Xiao and S. V. Malhotra, *J. Mol. Catal. A: Chem.*, 2005, **230**, 129-133.
23. R. Rinaldi, R. Palkovits and F. Schüth, *Angew. Chem. Int. Ed.*, 2008, **47**, 8047-8050.
24. J. Peng, F. Shi, Y. Gu and Y. Deng, *Green Chem.*, 2003, **5**, 224-226.
25. H. F. D. Almeida, M. G. Freire and I. M. Marrucho, *Green Chem.*, 2016, **18**, 2717-2725.
26. J. van den Broeke, F. Winter, B.-J. Deelman and G. van Koten, *Org. Lett.*, 2002, **4**, 3851-3854.
27. J. M. Fraile, J. I. García, C. I. Herrerías, J. A. Mayoral, O. Reiser and M. Vaultier, *Tetrahedron Lett.*, 2004, **45**, 6765-6768.

References

28. R. Sebesta, I. Kmentova and S. Toma, *Green Chem.*, 2008, **10**, 484-496.
29. S. Doherty, P. Goodrich, C. Hardacre, J. G. Knight, M. T. Nguyen, V. I. Pârvulescu and C. Paun, *Adv. Synth. Catal.*, 2007, **349**, 951-963.
30. R. L. Vekariya, *J. Mol. Liq.*, 2017, **227**, 44-60.
31. V. P. Ananikov and I. P. Beletskaya, *Organometallics*, 2012, **31**, 1595-1604.
32. Y. S. Chun, J. Y. Shin, C. E. Song and S.-g. Lee, *Chem. Commun.*, 2008, **0**, 942-944.
33. M. D. Rossell, F. J. Caparrós, I. Angurell, G. Muller, J. Llorca, M. Seco and O. Rossell, *Catal. Sci. Technol.*, 2016, **6**, 4081-4085.
34. R. Fareghi-Alamdari, N. Zekri, A. J. Moghadam and M. R. Farsani, *Catal. Commun.*, 2017, **98**, 71-75.
35. C. P. Mehnert, R. A. Cook, N. C. Dispenziere and M. Afeworki, *J. Am. Chem. Soc.*, 2002, **124**, 12932-12933.
36. C. P. Mehnert, *Chemistry*, 2004, **11**, 50-56.
37. S. Martín, R. Porcar, E. Peris, M. I. Burguete, E. García-Verdugo and S. V. Luis, *Green Chem.*, 2014, **16**, 1639.
38. A. Riisager, R. Fehrmann, M. Haumann and P. Wasserscheid, *Eur. J. Inorg. Chem.*, 2006, **4**, 695-706.
39. L. Alaerts, J. Wahlen, P. A. Jacobs and D. E. De Vos, *Chem. Commun.*, 2008, **10**, 1727-1737.
40. C. Coperet and R. v. Santen, *Dalton Trans.*, 2010, **39**, 8354-8354.
41. P. S. Campbell, A. Podgoršek, T. Gutel, C. C. Santini, A. A. H. Pádua, M. F. Costa Gomes, F. Bayard, B. Fenet and Y. Chauvin, *J. Phys. Chem. B*, 2010, **114**, 8156-8165.
42. C. Van Doorslaer, J. Wahlen, P. Mertens, K. Binnemans and D. De Vos, *Dalton Trans.*, 2010, **39**, 8377-8390.
43. C. Sievers, O. Jimenez, T. E. Müller, S. Steuernagel and J. A. Lercher, *J. Am. Chem. Soc.*, 2006, **128**, 13990-13991.
44. M. H. Valkenberg, C. deCastro and W. F. Hölderich, *Green Chem.*, 2002, **4**, 88-93.
45. M. Gruttadauria, S. Riela, C. Aprile, P. L. Meo, F. D'Anna and R. Noto, *Adv. Synth. Catal.*, 2006, **348**, 82-92.
46. O. D. Pavel, I. Podolean, V. I. Parvulescu, S. F. R. Taylor, H. G. Manyar, K. Ralphs, P. Goodrich and C. Hardacre, *Faraday Discuss.*, 2018, **206**, 535-547.
47. Y. Gu and G. Li, *Adv. Synth. Catal.*, 2009, **351**, 817-847.
48. J. C. Salamone, S. C. Israel, P. Taylor and B. Snider, *Polymer*, 1973, **14**, 639-644.
49. M. Yoshizawa, M. Hirao, K. Ito-Akita and H. Ohno, *J. Mater. Chem.*, 2001, **11**, 1057-1062.
50. F. Giacalone and M. Gruttadauria, *ChemCatChem*, 2016, **8**, 664-684.
51. H. Li, P. S. Bhadury, B. Song and S. Yang, *RSC Adv.*, 2012, **2**, 12525-12551.
52. B. Jahanbin, A. Davoodnia, H. Behmadi and N. Tavakoli-Hoseini, *Bull. Korean Chem. Soc.*, 2012, **33**, 2140-2144.
53. S. Doherty, J. G. Knight, J. R. Ellison, P. Goodrich, L. Hall, C. Hardacre, M. J. Muldoon, S. Park, A. Ribeiro, C. A. N. de Castro, M. J. Lourenço and P. Davey, *Green Chem.*, 2014, **16**, 1470-1479.
54. S. Doherty, J. G. Knight, M. A. Carroll, J. R. Ellison, S. J. Hobson, S. Stevens, C. Hardacre and P. Goodrich, *Green Chem.*, 2015, **17**, 1559-1571.
55. H. Chen, G. Wei, A. Ispas, S. G. Hickey and A. Eychmüller, *J. Phys. Chem. C*, 2010, **114**, 21976-21981.

56. G. Liu, M. Hou, J. Song, T. Jiang, H. Fan, Z. Zhang and B. Han, *Green Chem.*, 2010, **12**, 65-69.
57. C. Pavia, E. Ballerini, L. A. Bivona, F. Giacalone, C. Aprile, L. Vaccaro and M. Gruttadauria, *Adv. Synth. Catal.*, 2013, **355**, 2007-2018.
58. T. Nishikata, H. Tsutsumi, L. Gao, K. Kojima, K. Chikama and H. Nagashima, *Adv. Synth. Catal.*, 2014, **356**, 951-960.
59. C. M. Marrodan, D. Berti, F. Liguori and P. Barbaro, *Catal. Sci. Technol.*, 2012, **2**, 2279.
60. C. Moreno-Marrodan, P. Barbaro, M. Catalano and A. Taurino, *Dalton Trans.*, 2012, **41**, 12666-12669.
61. J. Yuan, D. Mecerreyes and M. Antonietti, *Prog. Polym. Sci.*, 2013, **38**, 1009-1036.
62. J. Lu, F. Yan and J. Texter, *Prog. Polym. Sci.*, 2009, **34**, 431-448.
63. B. M. L. D'Almeida, I. F. J. Vankelecom and P. A. Jacobs, *Adv. Synth. Catal.*, 2006, **348**, 1413-1446.
64. Q. Zhao, S. Soll, M. Antonietti and J. Yuan, *Polym. Chem.*, 2013, **4**, 2432.
65. S. M. Morozova, A. S. Shaplov, E. I. Lozinskaya, P. S. Vlasov, H. Sardon, D. Mecerreyes and Y. S. Vygodskii, *High Perform. Polym.*, 2017, **29**, 692-703.
66. M. W. Urban, *Stimuli-responsive Materials: From Molecules to Nature Mimicking Materials Design*, The Royal Society of Chemistry, Edinburg, 2016.
67. R. J. Young and P. A. Lovell, *Introduction to Polymers, 3rd edn.*, CRC Press, Boca Raton, Florida, 2011.
68. W. Sommer, *Aldrich ChemFiles*, 2009, **9**, 8.
69. H. Lu, J. Wang, Y. Lin and J. Cheng, *J. Am. Chem. Soc.*, 2009, **131**, 13582-13583.
70. U. Frenzel and O. Nuyken, *J. Polym. Sci. Part A: Polym. Chem.*, 2002, **40**, 2895-2916.
71. S. Sutthasupa, M. Shiotsuki and F. Sanda, *Polym. J.*, 2010, **42**, 905.
72. C. Slugovc, *J. Mol. Catal. A: Chem.*, 2004, **213**, 107-113.
73. J. Feng, S. S. Stoddart, K. A. Weerakoon and W. Chen, *Langmuir*, 2007, **23**, 1004-1006.
74. M. Crespo-Quesada, A. Yarulin, M. Jin, Y. Xia and L. Kiwi-Minsker, *J. Am. Chem. Soc.*, 2011, **133**, 12787-12794.
75. E. Schmidt, A. Vargas, T. Mallat and A. Baiker, *J. Am. Chem. Soc.*, 2009, **131**, 12358-12367.
76. J. Arras, E. Paki, C. Roth, J. Radnik, M. Lucas and P. Claus, *J. Phys. Chem. C*, 2010, **114**, 10520-10526.
77. R. Narayanan and M. A. El-Sayed, *J. Phys. Chem. B*, 2005, **109**, 12663-12676.
78. X. Yang, Z. Fei, D. Zhao, W. H. Ang, Y. Li and P. J. Dyson, *Inorg. Chem.*, 2008, **47**, 3292-3297.
79. K. L. Luska and A. Moores, *ChemCatChem*, 2012, **4**, 1534-1546.
80. Y. M. A. Yamada, S. M. Sarkar and Y. Uozumi, *J. Am. Chem. Soc.*, 2012, **134**, 3190-3198.
81. K. L. Luska and A. Moores, *Adv. Synth. Catal.*, 2011, **353**, 3167-3177.
82. X. Yang, N. Yan, Z. Fei, R. M. Crespo-Quesada, G. Laurenczy, L. Kiwi-Minsker, Y. Kou, Y. Li and P. J. Dyson, *Inorg. Chem.*, 2008, **47**, 7444-7446.
83. H. Lee, S. E. Habas, S. Kweckin, D. Butcher, G. A. Somorjai and P. Yang, *Angew. Chem. Int. Ed. Engl.*, 2006, **45**, 7824-7828.
84. X.-d. Mu, J.-q. Meng, Z.-C. Li and Y. Kou, *J. Am. Chem. Soc.*, 2005, **127**, 9694-9695.

References

85. D. Mecerreyes, *Applications of Ionic Liquids in Polymer Science and Technology*, Springer-Verlag Berlin Heidelberg, 2015.
86. C. Janiak, *Z. Naturforsch., ChemInform*, 2013, **68**, 1059-1089.
87. K. L. Luska and A. Moores, *Green. Chem.*, 2012, **14**, 1736-1742.
88. Y. Yabe, Y. Sawama, Y. Monguchi and H. Sajiki, *Catal. Sci. Technol.*, 2014, **4**, 260-271.
89. W. Long, N. A. Brunelli, S. A. Didas, E. W. Ping and C. W. Jones, *ACS Catal.*, 2013, **3**, 1700-1708.
90. S. J. Connon, A. M. Dunne and S. Blechert, *Angew. Chem. Int. Ed.*, 2002, **41**, 3835-3838.
91. G. Salas, C. C. Santini, K. Philippot, V. Colliere, B. Chaudret, B. Fenet and P. F. Fazzini, *Dalton Trans.*, 2011, **40**, 4660-4668.
92. C. Moreno-Marrodan, P. Barbaro, M. Catalano and A. Taurino, *Dalton Trans.*, 2012, **41**, 12666-12669.
93. J. Muzart, *Adv. Synth. Catal.*, 2006, **348**, 275-295.
94. L. Protesescu, M. Tudorache, S. Neatu, M. N. Grecu, E. Kemnitz, P. Filip, V. I. Parvulescu and S. M. Coman, *J. Phys. Chem. C*, 2011, **115**, 1112-1122.
95. F. Liu, Z. Fu, Y. Liu, C. Lu, Y. Wu, F. Xie, Z. Ye, X. Zhou and D. Yin, *Ind. Eng. Chem. Res.*, 2010, **49**, 2533-2536.
96. A. A. Lindén, M. Johansson, N. Hermanns and J.-E. Bäckvall, *J. Org. Chem.*, 2006, **71**, 3849-3853.
97. M. Ciclosi, C. Dinoi, L. Gonsalvi, M. Peruzzini, E. Manoury and R. Poli, *Organometallics*, 2008, **27**, 2281-2286.
98. M. Amini, H. Naslhajian, S. M. F. Farnia and M. Hołyńska, *Eur. J. Inorg. Chem.*, 2015, **2015**, 3873-3878.
99. T. Soundiressane, S. Selvakumar, S. Ménage, O. Hamelin, M. Fontecave and A. P. Singh, *J. Mol. Catal. A: Chem.*, 2007, **270**, 132-143.
100. Q. Zeng, W. Weng and X. Xue, *Inorg. Chim. Acta*, 2012, **388**, 11-15.
101. P. Pitchen, E. Dunach, M. N. Deshmukh and H. B. Kagan, *J. Am. Chem. Soc.*, 1984, **106**, 8188-8193.
102. C. Jahier, S. S. Mal, R. Al-Oweini, U. Kortz and S. Nlate, *Polyhedron*, 2013, **57**, 57-63.
103. M. V. Vasylyev and R. Neumann, *J. Am. Chem. Soc.*, 2004, **126**, 884-890.
104. C. Venturello and R. D'Aloisio, *J. Org. Chem.*, 1988, **53**, 1553-1557.
105. S.-S. Wang, W. Liu, Q.-X. Wan and Y. Liu, *Green Chem.*, 2009, **11**, 1589.
106. H. Srour, P. Le Maux, S. Chevance and G. Simonneaux, *Coord. Chem. Rev.*, 2013, **257**, 3030-3050.
107. A. Mouret, L. Leclercq, A. Muhlbauer and V. Nardello-Rataj, *Green Chem.*, 2014, **16**, 269-278.
108. B. M. Choudary, B. Bharathi, Ch. V. Reddy and M. L. Kantam, *Green Chem.*, 2002, **4**, 279-284.
109. X.-Y. Shi and J.-F. Wei, *J. Mol. Catal. A: Chem.*, 2008, **280**, 142-147.
110. T. Yamaura, K. Kamata, K. Yamaguchi and N. Mizuno, *Catal. Today*, 2013, **203**, 76-80.
111. N. Mizuno, K. Kamata and K. Yamaguchi, *Catal. Today*, 2012, **185**, 157-161.
112. L. Fan, Y. Hong, J. Cao and C. Hu, *RSC Adv.*, 2016, **6**, 56656-56660.
113. K. Sato, M. Aoki and R. Noyori, *Science*, 1998, **281**, 1646-1647.
114. K. Sato, J. Takagi, M. Aoki and R. Noyori, *Tetrahedron Lett.*, 1998, **39**, 7549-7552.

115. B. Karimi and M. Khorasani, *ACS Catal.*, 2013, **3**, 1657-1664.
116. K. Kawamura, T. Yasuda, T. Hatanaka, K. Hamahiga, N. Matsuda, M. Ueshima and K. Nakai, *Chem. Eng. J.*, 2016, **285**, 49-56.
117. A. Pourjavadi, M. Nazari-Chamazkoti and S. H. Hosseini, *New J. Chem.*, 2015, **39**, 1348-1354.
118. J. Zhu, P. C. Wang and M. Lu, *New J. Chem.*, 2012, **36**, 2587.
119. B. Karimi, F. B. Rostami, M. Khorasani, D. Elhamifar and H. Vali, *Tetrahedron*, 2014, **70**, 6114-6119.
120. T. Lu, L. Zhang, Z. Ge, Y. Ji and M. Lu, *Appl. Organomet. Chem.*, 2015, **29**, 276-279.
121. N. Zohreh, S. H. Hosseini, A. Pourjavadi, R. Soleyman and C. Bennett, *JIEC*, 2016, **44**, 73-81.
122. W. L. Dilling, R. D. Kroening and J. C. Little, *J. Am. Chem. Soc.*, 1970, **92**, 928-948.
123. A. Borosy, G. Frater, U. Müller and F. Schröder, *Tetrahedron*, 2009, **65**, 10495-10505.
124. C. Larroche, J. P. Laval, A. Lattes and J. M. Basset, *J. Org. Chem.*, 1984, **49**, 1886-1890.
125. J. D. Rule and J. S. Moore, *Macromolecules*, 2002, **35**, 7878-7882.
126. J. P. Mathew, A. Reinmuth, J. Melia, N. Swords and W. Risse, *Macromolecules*, 1996, **29**, 2755-2763.
127. P. S. Wolfe and K. B. Wagener, *Macromolecules*, 1999, **32**, 7961-7967.
128. S. Sutthasupa, M. Shiotsuki and F. Sanda, *Polym. J.*, 2010, **42**, 905-915.
129. E. L. Dias, S. T. Nguyen and R. H. Grubbs, *J. Am. Chem. Soc.*, 1997, **119**, 3887-3897.
130. M. S. Sanford, J. A. Love and R. H. Grubbs, *J. Am. Chem. Soc.*, 2001, **123**, 6543-6554.
131. F. Stelzer, J. K. Brunthaler, G. Leising and K. Hummel, *J. Mol. Catal.*, 1986, **36**, 135-143.
132. S. Doherty, J. G. Knight, M. A. Carroll, A. R. Clemmet, J. R. Ellison, T. Backhouse, N. Holmes, L. A. Thompson and R. A. Bourne, *RSC Adv.*, 2016, **6**, 73118-73131.
133. M. C. Carreno, *Chem. Rev.*, 1995, **95**, 1717-1760.
134. I. Fernández and N. Khair, *Chem. Rev.*, 2003, **103**, 3651-3706.
135. S. Caron, R. W. Dugger, S. G. Ruggeri, J. A. Ragan and D. H. B. Ripin, *Chem. Rev.*, 2006, **106**, 2943-2989.
136. R. Bentley, *Chem. Soc. Rev.*, 2005, **34**, 609-624.
137. Q.-A. Chen, X. Dong, M.-W. Chen, D.-S. Wang, Y.-G. Zhou and Y.-X. Li, *Org. Lett.*, 2010, **12**, 1928-1931.
138. B. Karimi, M. Ghoreishi-Nezhad and J. H. Clark, *Org. Lett.*, 2005, **7**, 625-628.
139. X. Shi, X. Han, W. Ma, J. Wei, J. Li, Q. Zhang and Z. Chen, *J. Mol. Catal. A: Chem.*, 2011, **341**, 57-62.
140. G. P. Romanelli, P. I. Villabrille, C. V. Cáceres, P. G. Vázquez and P. Tundo, *Catal. Commun.*, 2011, **12**, 726-730.
141. D. A. Bennett, H. Yao and D. E. Richardson, *Inorg. Chem.*, 2001, **40**, 2996-3001.
142. S. P. Das, J. J. Boruah, N. Sharma and N. S. Islam, *J. Mol. Catal. A: Chem.*, 2012, **356**, 36-45.
143. B. M. Choudary, B. Bharathi, Ch. V. Reddy and M. L. Kantam, *J. Chem. Soc., Perkin Trans. 1*, 2002, **0**, 2069-2074.

References

144. K. S. W. Sing, R. A. W. Haul, L. Moscou, R. A. Pierotti, J. Rouquero and T. Siemieniewska, *Pure & Appl. Chem.*, 1985, **57**, 603-619.
145. F. Lefebvre, *J. Chem. Soc., Chem. Commun.*, 1992, **0**, 756-757.
146. X. Lang, Z. Li and C. Xia, *Synth. Commun.*, 2008, **38**, 1610-1616.
147. F. Cavani, G. Centi, S. Perathoner and F. Trifirò, *Sustainable Industrial Chemistry: Principles, Tools and Industrial Examples*, Wiley, 2009.
148. J. H. Clark and D. J. Macquarrie, *Handbook of Green Chemistry and Technology*, Wiley-Blackwell, Oxford-London, 2002.
149. J. G. de Vries and S. D. Jackson, *Catal. Sci. Technol.*, 2012, **2**, 2009-2009.
150. D. C. Sherrington and A. P. Kybett, *Supported Catalysts and Their Applications*, The Royal Society of Chemistry, Editon edn, 2001.
151. G. Nichols, S. Byard, M. J. Bloxham, J. Botterill, N. J. Dawson, A. Dennis, V. Diart, N. C. North and J. D. Sherwood, *J. Pharm. Sci.*, 2002, **91**, 2103-2109.
152. M. Pérez-Lorenzo, *J. Phys. Chem. Lett.*, 2012, **3**, 167-174.
153. Z. Wang, H.i Wang, J. Yan, Y. Ping, O. Song-Il, S. Li and Q. Jiang, *Chem. Commun.*, 2014, **50**, 2732-2734.
154. S. Doherty, in *Catalysis in Ionic Liquids: From Catalyst Synthesis to Application*, The Royal Society of Chemistry, Editon edn, 2014, ch. 3, pp. 44-308.
155. C. Janiak, in *Catalysis in Ionic Liquids: From Catalyst Synthesis to Application*, The Royal Society of Chemistry, Editon edn, 2014, ch. 11, pp. 537-577.
156. D. Astruc, F. Lu and J. R. Aranzaes, *Angew. Chem. Int. Ed.*, 2005, **44**, 7852-7872.
157. W. Zhang, in *Nanomaterial: Impacts on Cell Biology and Medicine*, eds. D. G. Capco and Y. Chen, Springer Netherlands, Dordrecht, Editon edn., 2014, pp. 19-43.
158. Q.-L. Zhu and Q. Xu, *Chem*, 2016, **1**, 220-245.
159. A. Peled, M. Naddaka and J.-P. Lellouche, *J. Mater. Chem.*, 2012, **22**, 7580-7583.
160. B. Liu, H. Yao, W. Song, L. Jin, I. M. Mosa, J. F. Rusling, S. L. Suib and J. He, *J. Am. Chem. Soc.*, 2016, **138**, 4718-4721.
161. Q.-L. Zhu, N. Tsumori and Q. Xu, *Chem. Sci.*, 2014, **5**, 195-199.
162. J. Yao and Y. Yao, *Int. J. Hydrogen Energy*, 2017, **42**, 18560-18567.
163. X. Zhang, X. Ke and H. Zhu, *Chem. Eur. J.*, 2012, **18**, 8048-8056.
164. S. Chettibi, Y. Benguedouar and N. Keghouche, *Physics Procedia*, 2009, **2**, 707-712.
165. J. Seth, P. Dubey, V. R. Chaudhari and B. L. V. Prasad, *New J. Chem.*, 2018, **42**, 402-410.
166. N. Zheng and G. D. Stucky, *J. Am. Chem. Soc.*, 2006, **128**, 14278-14280.
167. S. Mahouche-Chergui, M. Guerrouache, B. Carbonnier and M. M. Chehimi, *Colloids Surf., A*, 2013, **439**, 43-68.
168. D. Zhao, Z. Fei, W. H. Ang and P. J. Dyson, *Small*, 2006, **2**, 879-883.
169. A. Elaiwi, P. B. Hitchcock, K. R. Seddon, N. Srinivasan, Y.-M. Tan, T. Welton and J. A. Zora, *J. Chem. Soc. Dalton Trans.*, 1995, 3467-3472.
170. W. Ostwald, *Z. Phys. Chem.*, 1901, **37**, 385.
171. R. A. Alvarez-Puebla, E. Arceo, P. J. G. Goulet, J. J. Garrido and R. F. Aroca, *J. Phys. Chem. B*, 2005, **109**, 3787-3792.
172. E. J. W Verwey and J. Th. G. Overbeek, *Theory of the Stability of Lyophobic Colloids (Dover Books on Chemistry)*, Dover Publications, 1999.
173. P. Migowski, D. Zanchet, G. Machado, M. A. Gelesky, S. R. Teixeira and J. Dupont, *PCCP*, 2010, **12**, 6826-6833.

174. W. Chen, Y. Zhang, L. Zhu, J. Lan, R. Xie and J. You, *J. Am. Chem. Soc.*, 2007, **129**, 13879-13886.
175. V. Bertini, S. Alfei, M. Pocci, F. Lucchesini, N. Picci and F. Iemma, *Tetrahedron*, 2004, **60**, 11407-11414.
176. R. Rabinowitz and R. Marcus, *J. Org. Chem.*, 1961, **26**, 4157-4158.
177. Y. M. A. Yamada and Y. Uozumi, *Tetrahedron*, 2007, **63**, 8492-8498.
178. T. Iwai, T. Harada, K. Hara and M. Sawamura, *Angew. Chem. Int. Ed. Engl.*, 2013, **52**, 12322-12326.
179. J. Chen, R. Liu, Y. Guo, L. Chen and H. Gao, *ACS Catal.*, 2015, **5**, 722-733.
180. P. Scherrer, *Göttinger Nachrichten Gesell.*, 1918, **2**, 98-100.
181. L. Alexander and H. P. Klug, *J. Appl. Phys.*, 1950, **21**, 137-142.
182. A. V. Gaikwad, A. Holuigue, M. B. Thathagar, J. E. ten Elshof and G. Rothenberg, *Chem. Eur. J.*, 2007, **13**, 6908-6913.
183. M. B. Thathagar, J. E. ten Elshof and G. Rothenberg, *Angew. Chem. Int. Ed. Engl.*, 2006, **45**, 2886-2890.
184. N. Jiao, Z. Li, Y. Wang, J. Liu and C. Xia, *RSC Adv.*, 2015, **5**, 26913-26922.
185. S. Kidambi and M. L. Bruening, *Chem. Mater.*, 2005, **17**, 301-307.
186. R. W. J. Scott, H. Ye, R. R. Henriquez and R. M. Crooks, *Chem. Mater.*, 2003, **15**, 3873-3878.
187. J. D. Scholten, B. C. Leal and J. Dupont, *ACS Catal.*, 2012, **2**, 184-200.
188. D. P and S. Ramaprabhu, *PCCP*, 2014, **16**, 26725-26729.
189. B. Keita, T. Liu and L. Nadjo, *J. Mater. Chem.*, 2009, **19**, 19-33.
190. H. Hagiwara, M. Nagatomo, C. Seto, S. Ida and T. Ishihara, *Catalysts*, 2013, **3**, 614-624.
191. K. Anderson, P. Goodrich, C. Hardacre and D. W. Rooney, *Green Chem.*, 2003, **5**, 448-453.
192. H. G. Manyar, B. Yang, H. Daly, H. Moor, S. McMonagle, Y. Tao, G. D. Yadav, A. Goguet, P. Hu and C. Hardacre, *ChemCatChem*, 2013, **5**, 506-512.
193. K. R. Kahsar, D. K. Schwartz and J. W. Medlin, *J. Am. Chem. Soc.*, 2014, **136**, 520-526.
194. A. B. da Silva, E. Jordão, M. J. Mendes and P. Fouilloux, *Appl. Catal., A*, 1997, **148**, 253-264.
195. P. Barbaro, L. Gonsalvi, A. Guerriero and F. Liguori, *Green Chem.*, 2012, **14**, 3211-3219.
196. M. Castro-Puyana, M. L. Marina and M. Plaza, *Current Opinion in Green and Sustainable Chemistry*, 2017, **5**, 31-36.
197. R. Breslow, *Handbook of Green Chemistry, Volume 5: Reactions in Water*, Wiley-VCH, Weinheim, 2010, ch. 1, pp. 1-29.
198. S. Iqbal, S. A. Kondrat, D. R. Jones, D. C. Schoenmakers, J. K. Edwards, L. Lu, B. R. Yeo, P. P. Wells, E. K. Gibson, D. J. Morgan, C. J. Kiely and G. J. Hutchings, *ACS Catal.*, 2015, **5**, 5047-5059.
199. L. J. Durndell, C. M. Parlett, N. S. Hondow, M. A. Isaacs, K. Wilson and A. F. Lee, *Scientific reports*, 2015, **5**, 9425.
200. C. Torborg and M. Beller, *Adv. Synth. Catal.*, 2009, **351**, 3027-3043.
201. A. Fihri, M. Bouhrara, B. Nekoueishahraki, J.-M. Basset and V. Polshettiwar, *Chem. Soc. Rev.*, 2011, **40**, 5181-5203.
202. V. Polshettiwar, A. Decottignies, C. Len and A. Fihri, *ChemSusChem*, 2010, **3**, 502-522.

References

203. M. B. Thathagar, J. E. ten Elshof and G. Rothenberg, *Angew. Chem. Int. Ed.*, 2006, **45**, 2886-2890.
204. A. H. M. de Vries, J. M. C. A. Mulders, J. H. M. Mommers, H. J. W. Henderickx and J. G. de Vries, *Org. Lett.*, 2003, **5**, 3285-3288.
205. J. G. de Vries, *Dalton Trans.*, 2006, **0**, 421-429
206. C. Amatore, A. Jutand and G. Le Duc, *Chem. Eur. J.*, 2011, **17**, 2492-2503.
207. I. Maluenda and O. Navarro, *Molecules*, 2015, **20**, 7528.
208. C. A. Tolman, *Chem. Rev.*, 1977, **77**, 313-348.
209. T. Chen, F. Mao, Z. Qi, Y. Li, R. Chen, Y. Wang and J. Huang, *RSC Adv.*, 2016, **6**, 16899-16903.
210. A. R. Clemmet, PhD thesis, Newcastle University, 2016.
211. D. D. Dolliver, B. T. Bhattarai, A. Pandey, M. L. Lanier, A. S. Bordelon, S. Adhikari, J. A. Dinser, P. F. Flowers, V. S. Wills, C. L. Schneider, K. H. Shaughnessy, J. N. Moore, S. M. Raders, T. S. Snowden, A. S. McKim and F. R. Fronczek, *J. Org. Chem.*, 2013, **78**, 3676-3687.
212. A. El Kadib, K. McEleney, T. Seki, T. K. Wood and C. M. Crudden, *ChemCatChem*, 2011, **3**, 1281-1285.
213. S. MacQuarrie, J. H. Horton, J. Barnes, K. McEleney, H.-P. Looock and C. M. Crudden, *Angew. Chem. Int. Ed.*, 2008, **47**, 3279-3282.
214. L. S. Liebeskind and E. Peña-Cabrera, *Org. Synth.*, 2000, **77**, 135.
215. S. Li, J. Wang, Y. Kou and S. Zhang, *Chem. Eur. J.*, 2010, **16**, 1812-1818.
216. R. Narayanan and M. A. El-Sayed, *Langmuir*, 2005, **21**, 2027-2033.
217. A. A. Kurokhtina and A. F. Schmidt, *ARKIVOC*, 2009, **xi**, 185-203.
218. M. Gruttadauria, F. Giacalone and R. Noto, *Green Chem.*, 2013, **15**, 2608-2618.
219. B. D. Briggs, N. M. Bedford, S. Seifert, H. Koerner, H. Ramezani-Dakhel, H. Heinz, R. R. Naik, A. I. Frenkel and M. R. Knecht, *Chem. Sci.*, 2015, **6**, 6413-6419.

➤ PUBLICATIONS

➤ APPENDICES

➤ VITA



Cite this: DOI: 10.1039/c6gc03528k

Received 21st December 2016,
Accepted 25th January 2017

DOI: 10.1039/c6gc03528k

rsc.li/greenchem

Highly efficient aqueous phase chemoselective hydrogenation of α,β -unsaturated aldehydes catalysed by phosphine-decorated polymer immobilized IL-stabilized PdNPs†‡

S. Doherty,^{*a} J. G. Knight,^{*a} T. Backhouse,^a E. Abood,^a H. Alshaikh,^a
I. J. S. Fairlamb,^{*b} R. A. Bourne,^c T. W. Chamberlain^c and R. Stones^c

Phosphino-decorated polymer immobilised ionic liquid phase stabilised palladium nanoparticles (PdNP@PPh₂-PIILP) and their PEGylated counterparts (PdNP@PPh₂-PEGPIILP) are remarkably active and exceptionally selective catalysts for the aqueous phase hydrogenation of α,β -unsaturated aldehydes, ketones, esters and nitriles with PdNP@PPh₂-PEGPIILP giving complete conversion and 100% selectivity for reduction of the C=C bond, under mild conditions. This is the most selective PdNP-based system to be reported for the aqueous phase hydrogenation of this class of substrates.

Ionic liquids are an intriguing class of solvents that have been widely used in catalysis as a result of their low vapour pressure, chemical and thermal stability, wide electrochemical window, excellent solvation properties and potential green credentials.¹ In particular, their dual role as both a solvent and stabilizer, and the ability to modify and tune their physiochemical properties and functionality, has fuelled their development in the synthesis of metal nanoparticles for use in catalysis.² Even though there has been considerable progress in this area and our understanding of these systems is now reasonably well-advanced, the use of ionic liquids suffers a number of practical limitations including their high cost compared with traditional solvents, high viscosity, leaching of the ionic liquid

during work-up and recovery and aggregation of metal nanoparticles under catalytic conditions.

The concept of supported ionic liquid phase (SILP) catalysis was introduced to reduce the volume of ionic liquid required and facilitate catalyst separation and recovery.³ However, these systems suffer drawbacks such as pore blocking and leaching of ionic liquid and/or catalyst. In a more recent development, ionic liquids have been covalently immobilised on to polymers, either as a single or multi-layer, which further reduces the amount of ionic liquid and prevents leaching while retaining the advantageous properties of an ionic liquid environment such as catalyst stabilisation, facile catalyst activation, enhancements in rate and selectivity and efficient recyclability.⁴ In this regard, there have been numerous successful applications of this strategy to the immobilisation and stabilisation of metal nanoparticles. Examples include aqueous phase Suzuki–Miyaura coupling and Heck reactions with multi-layered supported ionic liquid phase palladium nanoparticles^{5,6} as well as tris-imidazolium salt-stabilised PdNPs,⁷ carbonylative Suzuki–Miyaura coupling with supported ionic liquid phase-stabilised PdNPs,⁸ Heck reactions catalysed by palladium immobilised on a gel-supported ionic liquid-like phase,⁹ selective hydrogenations with ion exchange resin stabilised PdNPs¹⁰ and aqueous phase oxidation of 1-phenyl-ethanol with SIILP-stabilised gold nanoparticles.¹¹

The stabilisation of nanoparticles by ionic liquids has been thoroughly explored and is believed to result from weak electrostatic interactions that are easily displaced to generate the active site.¹² However, while these interactions must be efficiently displaced to achieve high activity they are often not sufficient to prevent nanoparticle aggregation under the conditions of catalysis. One potential solution to this problem has been to incorporate a metal-binding heteroatom donor group such as an amine,¹³ nitrile,¹⁴ thiolate,¹⁵ bipyridine,¹⁶ hydroxyl¹⁷ or phosphine¹⁸ on to the ionic liquid on the basis that an additional covalent interaction will improve the long-

^aNUCAT, School of Chemistry, Bedson Building, Newcastle University, Newcastle upon Tyne, NE1 7RU, UK. E-mail: simon.doherty@ncl.ac.uk; Tel: +44 (0) 191 208 6537

^bDepartment of Chemistry, University of York, Heslington, York YO10 5DD, UK

^cInstitute of Process Research & Development, School of Chemistry, University of Leeds, Woodhouse Lane, Leeds LS2 9JT, UK

†This paper is dedicated to the memory of Professor Malcolm H. Chisholm (FRS).

‡Electronic supplementary information (ESI) available: Synthesis and characterisation of imidazolium-based monomers, co-polymers **1a–4a**, PdCl₂-loaded co-polymers **1b–4b** and polymer immobilised ionic liquid stabilised PdNPs **1c–4c**; TGA and DSC curves for **2a–c** and **3a–c**, SEM images of **1a–4a**, **1b–4b** and **1c–4c**, TEM images of **1c–4c**, FTIR traces and X-ray photoelectron spectra of **1b–4b** and **1c–4c**. See DOI: 10.1039/c6gc03528k

term stability of the nanoparticles and/or control the kinetics of nanoparticle formation. As this approach has been reported to improve stability, solubility, activity and recyclability of NP catalysts we became interested in extending this concept and developing heteroatom donor-decorated polymer immobilised ionic liquids with the intention of combining the favourable properties and characteristics of an immobilised ionic liquid with heteroatom donor functionalisation. Moreover, there may well be additional benefits associated with incorporating heteroatom donors into polymer immobilised ionic liquids arising from changes to the electronic structure of the metal surface and/or hydrophilicity of the ligand environment as the presence of an amino or thiol group has been reported to improve or switch the chemoselectivity of NP-catalysed hydrogenations¹⁹ as has a secondary phosphine oxide²⁰ and tertiary phosphines;^{18a} the former two appear to operate *via* specific noncovalent molecular interactions and the latter *via* a metal-ligand cooperative mechanism. In addition, P-containing ionophilic ligands have been reported to generate smaller PdNPs than when a ligand was not present and the resulting catalysts were markedly more selective for the hydrogenation of 2-pentyne and cyclohexadiene.^{18a} Herein we report the first example of phosphino-decorated PIILP-stabilised palladium nanoparticles (PdNP@PPh₂-PIILP) and their PEGylated counterparts (PdNP@PPh₂-PEGPIILP) and their use as catalysts for the aqueous phase chemoselective hydrogenation of α,β -unsaturated aldehydes and ketones. To this end, the stabilisation of palladium nanoparticles for use in aqueous phase catalysis is currently a burgeoning area of interest as it offers immense potential for developing greener sustainable processes.²¹ The nomenclature chosen to describe these polymers and the corresponding NP-loaded systems attempts to identify their composition and/or modification according to Fig. 1. The most noteworthy developments in this project include (i) the highest selectivities to be reported for the aqueous phase PdNP-catalysed hydrogenation of α,β -unsaturated aldehydes with up to 100% selectivity for addition to the C=C bond under mild conditions and (ii) a marked improvement in

performance for PEGylated PPh₂-decorated polymer immobilised ionic liquid stabilised PdNPs (PdNP@PPh₂-PEGPIILP) compared with PdNP@PPh₂-PIILP.

Phosphino-decorated PIILP **1a** was prepared by AIBN-initiated radical polymerisation of the corresponding imidazolium-modified monomer, dicationic cross-linker and 4-diphenylphosphino styrene in the desired ratio ($x = 1.84$, $y = 1$, $z = 0.16$) and its PEGylated counterpart **2a** was prepared in a similar manner with the intention of introducing additional weak NP-stabilising interactions and improving water solubility for aqueous phase catalysis;²² full details and the corresponding characterisation data are provided in the ESI.†

A 1 : 2 ratio of PPh₂-based monomer to imidazolium comonomer and cross-linker was chosen such that complete exchange of halide in polymers **1a** and **2a** for [PdCl₄]²⁻ would correspond to a palladium to heteroatom ratio of one. Thus, both polymers were impregnated with [PdCl₄]²⁻ to afford **1b** and **2b** (**1b**, PdCl₄@PPh₂-PIILP; **2b**, PdCl₄@PPh₂-PEGPIILP) as red-brown solids in near quantitative yield; full characterisation data are provided in the ESI.† The solid state ³¹P NMR spectra of PdCl₄@PPh₂-PIILP **1b** and PdCl₄@PPh₂-PEGPIILP **2b** confirm the presence of a Pd–P interaction which is clearly evident from the change in the chemical shift from δ –8 and –10 ppm, respectively, to δ 29 and 32 ppm, respectively. The corresponding PIILP-stabilised nanoparticles **1c** and **2c** (**1c**, PdNP@PPh₂-PIILP; **2c**, PdNP@PPh₂-PEGPIILP) were prepared by sodium borohydride reduction of **1b** and **2b**, respectively, in ethanol and isolated as black powder in good yield. As for **1b** and **2b**, the solid state ³¹P NMR spectra of **1c** and **2c** do not contain signals associated with uncoordinated PPh₂; this suggests that the surface of the palladium nanoparticles is decorated with phosphino groups. TEM analysis showed that **1c** and **2c** consist of small near monodisperse nanoparticles with average diameters of 2.29 ± 0.96 nm (**1c**) and 1.93 ± 0.67 nm (**2c**) (Fig. 2 and the ESI.†), XPS analysis confirmed that

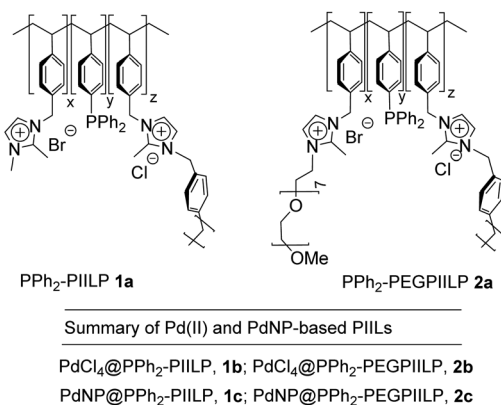


Fig. 1 Composition and formulation of polymer immobilised ionic liquids **1a–2a** and their [PdCl₄]²⁻ loaded counterparts (**1b–2b**) and PdNP (**1c–2c**).

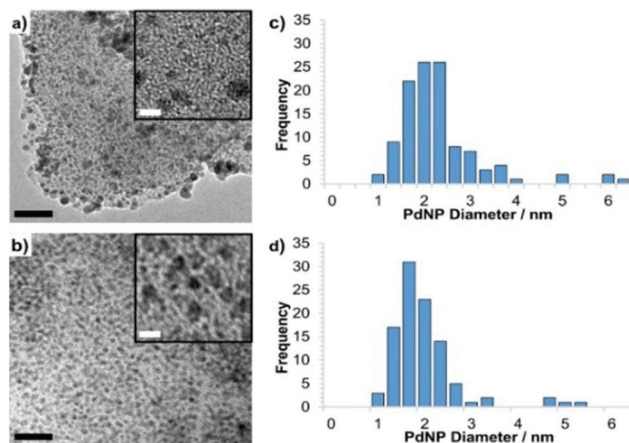


Fig. 2 HRTEM images of (a) PdNP@PPh₂-PIILP (**1c**) and (b) PdNP@PPh₂-PEGPIILP (**2c**) and particle size distributions determined by counting >100 particles revealing mean NP diameters of 2.29 ± 0.96 nm and 1.93 ± 0.67 nm for (c) **1c** and (d) **2c** respectively. Scale bars are 25 nm (black) and 5 nm (white).

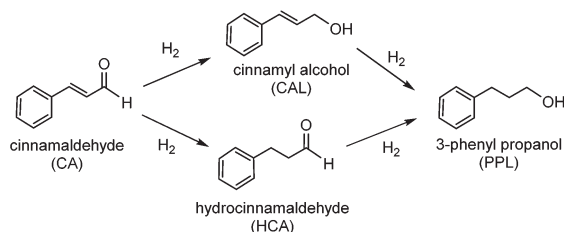


Fig. 3 Reaction pathways for the hydrogenation of *trans*-cinnamaldehyde.

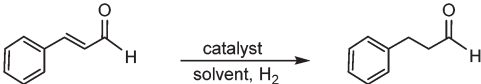
both **1c** and **2c** were composed of mixtures of Pd(II) and Pd(0) and the palladium content was determined by ICP-OES.

The hydrogenation of cinnamaldehyde was identified as an initial benchmark transformation for catalyst evaluation as the products of this reaction are valuable intermediates for the synthesis of fine chemicals, pharmaceuticals and perfumes (Fig. 3).²³ Furthermore, numerous palladium nanoparticle based systems have been reported to be highly selective for hydrocinnamaldehyde and as such will be suitable benchmarks for comparison. For example, palladium-decorated carbon nanotubes/charcoal composites gave hydrocinnamaldehyde in 96% selectivity albeit at a relatively low conversion of 41% as did AuPd on ordered mesoporous carbon (OMC),^{24a,b} palladium nanoparticles deposited on nitrogen-doped mesoporous carbon gave 93% selectivity at complete conversion²⁵ and palladium nanoparticles supported on ZIF-8 were 90% selective for hydrocinnamaldehyde.²⁶

Preliminary catalytic reactions were conducted in a stirred bench-top reactor using 0.5–1.0 mol% **1c** or **2c** and varying the temperature, pressure and solvent in order to identify an optimum system and conditions. Table 1 reveals that the solvent has quite a dramatic effect on both selectivity and conversion with **1c** and **2c** both giving high conversions and good selectivity in water and water/ethanol while reactions conducted in conventional organic solvents gave lower conversions and/or selectivities. The potential green benefits and practical advantages associated with aqueous phase catalysis promoted us to use this solvent for the remainder of our studies. For comparison, 1 mol% Pd/C catalysed this hydrogenation under the same conditions but only reached 60% conversion and 67% selectivity after 1 h at 60 °C.

Further optimisations explored the effect of temperature and pressure on performance. Interestingly, the selectivity for hydrocinnamaldehyde increased with temperature from 85% at 20 °C to 92% at 60 °C with 0.5 mol% PdNP@PPh₂-PEGPIILP under 70 psi of hydrogen in water; a similar improvement in selectivity was also obtained for PdNP@PPh₂-PIILP under the same conditions (Table S1, ESI†). While these selectivities compare favourably with the vast majority of polymer and mesoporous carbon or silica-stabilised PdNP systems they fall short of the 96% obtained with AuPd-ordered mesoporous carbon. However, the overwhelming majority of these studies have been conducted in either isopropanol or a conventional organic solvent whereas PdNP@PPh₂-PEGPIILP has the distinct advantage of operating most efficiently in water.

Table 1 Selective hydrogenation of cinnamaldehyde to hydrocinnamaldehyde as a function of catalyst, solvent and temperature^a

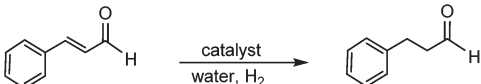


Catalyst	Solvent	Temp. (°C)	Conv. ^b (%)	TOF ^c (h ⁻¹)	Selectivity ^b (%)
1c	Toluene	25	0	0	0
2c	Toluene	25	23	46	78
1c	Ethanol	25	57	57	69
2c	Ethanol	25	54	108	76
1c	Hexane	25	35	35	58
2c	Hexane	25	52	104	82
1c	Ethyl acetate	25	10	10	58
2c	Ethyl acetate	25	29	58	85
1c	2-MeTHF	25	22	22	48
2c	2-MeTHF	25	35	70	62
1c	Water	25	75	75	74
2c	Water	25	81	162	85
1c	Water/ethanol ^d	25	82	82	72
2c	Water/ethanol ^d	25	75	150	74
Pd/C	Water ^e	60	60	60	67

^a Reaction conditions: 1 mmol cinnamaldehyde, **1c** (1.0 mol%), **2c** (0.5 mol%), 10 mL solvent, 70 psi H₂, time = 1 h, temperature. ^b Yields and selectivities determined by ¹H NMR spectroscopy using 1,3-dinitrobenzene as an internal standard. Average of three runs. ^c Moles product per mole catalyst per hour based on the total palladium content. ^d 1/1 water/ethanol. ^e 1 mol% Pd/C, reaction run at 60 °C.

Interestingly, addition of a base to the catalytic reaction mixture resulted in a marked and substantial improvement in the selectivity for hydrocinnamaldehyde such that reactions catalysed by **2c** in the presence of either potassium carbonate, potassium phosphate or sodium hydroxide gave complete conversion with 100% selectivity for hydrocinnamaldehyde at room temperature in short reaction times (Table 2). This is the

Table 2 Selective hydrogenation of cinnamaldehyde to hydrocinnamaldehyde as a function of base catalysed by PdNP@PPh₂-PIILP (**1c**) and PdNP@PPh₂-PEGPIILP (**2c**)^a



Catalyst	Base	Conversion ^b (%)	TOF ^c (h ⁻¹)	Selectivity ^b (%)
1c	NaOH	27	27	90
2c	NaOH	>99	200	100
1c	K ₂ CO ₃	43	43	95
2c	K ₂ CO ₃	>99	200	100
Pd/C	K ₂ CO ₃	42	44	93
1c	K ₃ PO ₄	49	49	93
2c	K ₃ PO ₄	100	200	100
1c	NEt ₃	24	24	91
2c	NEt ₃	90	180	88

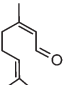
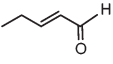
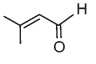
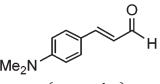
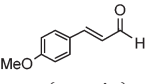
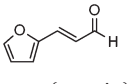
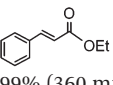
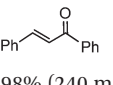
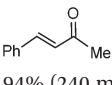
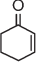
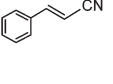
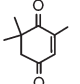
^a Reaction conditions: 1.0 mmol cinnamaldehyde, 1.0 mmol base, **1c** (1.0 mol%), **2c** (0.5 mol%) or Pd/C (1.0 mol%), 12 mL water, 70 psi H₂, reaction time = 1 h, 25 °C. ^b Yields and selectivities determined by ¹H NMR spectroscopy using 1,3-dinitrobenzene as an internal standard. Average of three runs. ^c Moles product per mole catalyst per hour based on the total palladium content.

highest selectivity to be reported for the aqueous phase hydrogenation of cinnamaldehyde and even though near 100% selectivity has been obtained with Pd/C in ionic liquids, reactions were slower than in conventional solvents and the ionic liquid was extremely expensive.²⁷ A survey of the conversion as a function of the amount of base revealed that high activity and selectivity were retained even in the presence of as little as 10 mol% base. Although an increase in selectivity was also obtained for reactions catalysed by **1c** the conversion dropped quite significantly for each base tested, reinforcing the value of the PEGylated design feature.

A marked improvement in the activity and selectivity has previously been reported for the hydrogenation of cinnamaldehyde over CeO₂-ZrO₂-supported platinum in the presence of an added base; in this case the selectivity for cinnamyl alcohol increased from 60% to 97% while TOFs increased from 586 to 1233 h⁻¹.²⁸ A benchmark comparison with Pd/C achieved 93% selectivity for hydrocinnamaldehyde under the optimum conditions but a much lower conversion of 42%; although markedly less efficient than PdNP@PPh₂-PEGPIILP this represents a significant improvement on the 67% selectivity and 60% conversion obtained at 60 °C in the absence of a base (Table 1).

The optimum conditions identified above have also been applied to the hydrogenation of a selection of other α,β -unsaturated aldehydes including citral, *trans*-pental, 3-methylcrotonaldehyde 4-dimethylaminocinnamaldehyde, 4-methoxycinnamaldehyde and 3-(furan-2-yl)acrolein (Table 3).

Table 3 Selective hydrogenation of α,β -unsaturated aldehydes and ketones catalysed by PdNP@PPh₂-PEGPIILP (**2c**)

Substrate ^a			
Conversion ^b	99% (75 min)	98% (75 min)	99% (75 min)
Selectivity ^b	100% ^c	100%	100%
Substrate ^b			
Conversion ^b	98% (75 min)	99% (75 min)	97% (75 min)
Selectivity ^b	97%	98%	67%
Substrate ^a			
Conversion ^b	99% (360 min)	98% (240 min)	94% (240 min)
Selectivity ^b	100%	100%	100%
Substrate ^a			
Conversion ^b	99% (120 min)	96% (120 min)	100% (240 min)
Selectivity ^b	100%	100%	92%

^a Reaction conditions: 1.0 mmol substrate, 1.0 mmol K₂CO₃, **2c** (0.5 mol%), 12 mL water, 70 psi H₂, reaction time given in parentheses after conversion (min), reaction temp = 25 °C. ^b Yields and selectivities determined by ¹H NMR spectroscopy using 1,3-dinitrobenzene as an internal standard. Average of three runs. ^c Selectivity of the α,β -unsaturated double bond.

The first three gave the saturated aldehyde as the sole product in excellent yield while 4-dimethylaminocinnamaldehyde and 4-methoxycinnamaldehyde gave high conversions with 98% and 99% selectivity for the corresponding hydrocinnamaldehyde. However, 3-(furan-2-yl)acrolein reached 97% conversion but only 67% selectivity for the desired saturated aldehyde with 3-tetrahydrofuran-2-yl-propionaldehyde as the only other significant product. In this regard, high selectivities for 3-(2-furyl)propanal have recently been reported with a RuNP catalyst stabilised by a poly(citric acid- β -cyclodextrin) polymer but in each case the conversion was very low (8–38%).²⁹ Similarly, ethyl cinnamate, benzylidene acetone, chalcone and cyclohexenone all gave the corresponding saturated ketone as the sole product in high yield (94–99%) albeit after longer reaction times of 2–4 h. The same protocol was successfully extended to cinnamonnitrile to afford the corresponding saturated nitrile as the sole product in high yield after only 2 h at room temperature. Finally, ketoisophorone gave 2,6,6-trimethyl-1,4-cyclohexanedione (levodione) as the major product in 92% selectivity together with minor amounts of 4-hydroxy-3,3,5-trimethylcyclohexanone and 4-hydroxy-3,5,5-trimethylcyclohex-2-enone.

The effect of the base on selectivity was particularly dramatic for the hydrogenation of ketoisophorone as the selectivity dropped to 50% when the reaction was run under identical conditions in the absence of potassium carbonate. High selectivity for the C=C bond in ketoisophorone has previously been reported for alumina-supported platinum in the presence of tertiary amine bases whereas its palladium counterpart was more selective for reduction of the sterically hindered carbonyl group.³⁰ Gratifyingly, **2c** is also a highly efficacious catalyst for the aqueous phase reduction of aromatic nitro compounds giving the corresponding amines as the sole product in quantitative yields under mild conditions; further details will be disclosed in a subsequent report.

Reasoning that an aqueous phase compatible catalyst should lend itself to facile separation and recovery, recycle experiments were conducted on the hydrogenation of cinnamaldehyde with 0.5 mol% PdNP@PPh₂-PEGPIILP under optimum conditions by extracting the product and unreacted substrate and recharging the catalyst solution with cinnamaldehyde. The data in Fig. 4 are encouraging as the catalyst retained its high selectivity over the first five runs with only a minor drop in conversion; the latter is most likely due to catalyst attrition during the separation and catalyst recovery protocol rather than deactivation. To this end, ICP analysis of the aqueous phase collected after the fifth run revealed that the palladium content had decreased from 44 ppm (0.5 mol%) to 28 ppm; this corresponds to a 38% decrease in catalyst across five recycles which would account for the gradual decrease in conversion. TEM analysis of the catalyst solutions after the fifth run confirmed that the palladium nanoparticles in **2c** remained monodisperse with a mean diameter of 1.97 \pm 0.38 nm (see the ESI for details[†]).

Finally, we have recently begun to examine the influence on catalyst performance of each component and started by comparing PdNP@PPh₂PEGstyrene (**3c**) and PdNP@PEGPIILP (**4c**)

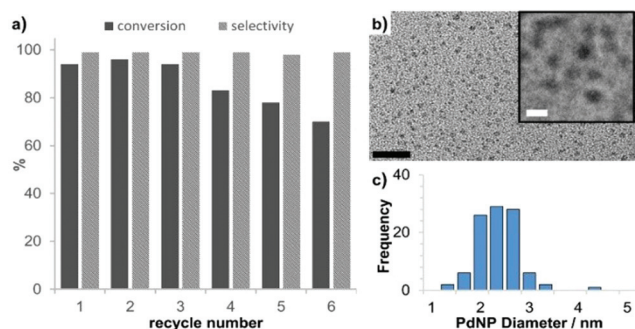


Fig. 4 (a) Recycling study for the hydrogenation of cinnamaldehyde in water catalysed by PdNP@PPh₂-PEGPIILP (**2c**) and (b) HRTEM images and (c) particle size distribution for PdNP@PPh₂-PEGPIILP (**2c**) after five recycles revealing an average NP size of 1.97 ± 0.38 nm. Scale bars are 25 nm (black) and 5 nm (white).

Table 4 Selective hydrogenation of cinnamaldehyde as a function of catalyst composition

Catalyst ^a		
	PdNP@PPh ₂ PEGstyrene (3c)	
Conversion ^b	72%	93%
TOF ^c (h ⁻¹)	144	132
Selectivity ^b	96%	82%

^a Reaction conditions: 1.0 mmol substrate, 1.0 mmol K₂CO₃, **3c** (0.5 mol%) or **4c** (0.7 mol%), 12 mL water, 70 psi H₂, reaction time = 1 h, 25 °C. ^b Yields and selectivities determined by ¹H NMR spectroscopy using 1,3-dinitrobenzene as an internal standard. Average of three runs. ^c Moles product per mole catalyst per hour based on the total palladium content.

in order to systematically explore the effect of the immobilised ionic liquid and the PPh₂, respectively (Table 4). Although our initial study has been restricted to two modifications, removal of the imidazolium appears to reduce the activity while removal of phosphine reduces the selectivity. A series of additional modifications are currently underway to further elucidate the role of each component, full details of which will be reported in due course.

Conclusions

Phosphino-decorated polymer immobilised ionic liquid stabilised PdNPs are highly efficient catalysts for aqueous phase chemoselective hydrogenation of α,β -unsaturated aldehydes and ketones. Modification of the support with PEG improved catalyst performance such that near quantitative conversions and 100% selectivity for addition to the C=C double bond

could be achieved under mild conditions and in short reaction times; these are the highest selectivities to be reported for the aqueous phase hydrogenation of this class of substrates. At this stage we do not have sufficient data to speculate about the mechanism of catalysis but *in situ* investigations on modified catalysts are now underway to explore the role of the phosphine, imidazolium and PEG. We are currently extending this family of catalysts to include a range of protic and aprotic heteroatom donors in order to explore their influence on the properties of the NP and their performance as catalysts, engineering a continuous flow process for aqueous phase chemoselective hydrogenation and developing a parallel approach based on tailor made heteroatom donor-modified mesoporous ionic liquid functionalised silica.

Notes and references

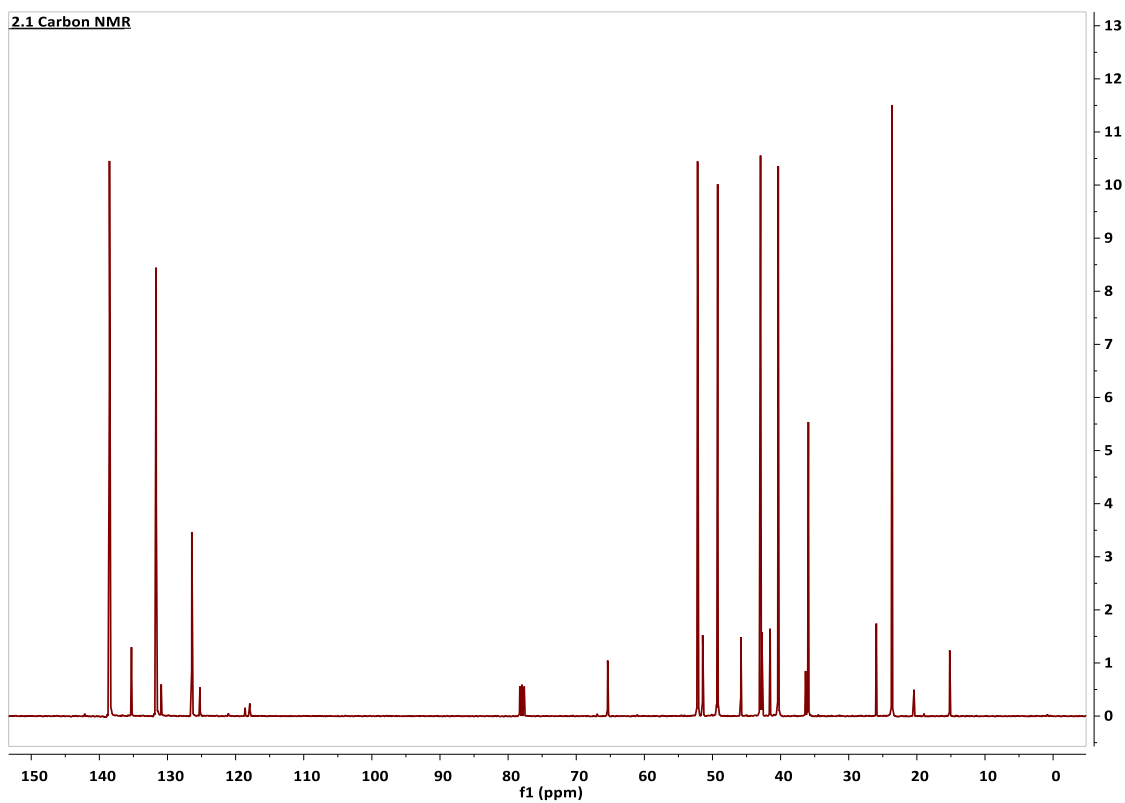
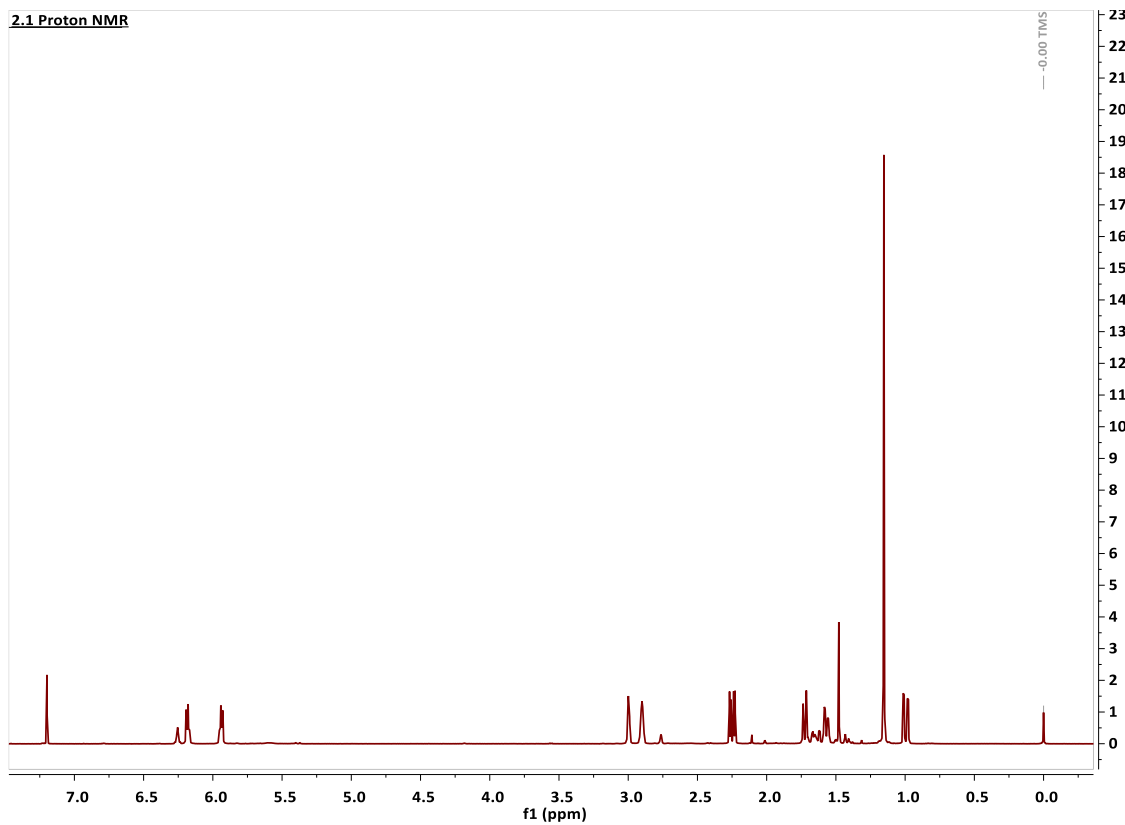
- (a) J. Dupont, *Acc. Chem. Res.*, 2011, **44**, 1223–1231; (b) P. Wasserscheid and T. Welton, *Ionic Liquids in Synthesis*, Wiley-VCH, Weinheim, 2007; (c) S. Doherty, in *Catalysis in Ionic Liquids: From Catalyst Synthesis to Applications*, ed. C. Hardacre and V. Parvulescu, RSC Catalysis Series, The Royal Society of Chemistry, 2014, pp. 44–308.
- (a) D. Astruc, *Nanoparticles and Catalysis*, Wiley-VCH, Weinheim, Germany, 2008; (b) J. Dupont and J. D. Scholten, *Chem. Soc. Rev.*, 2010, **39**, 1780–1804; (c) C. Vollmer and C. Janiak, *Coord. Chem. Rev.*, 2011, **255**, 2039–2057.
- (a) C. P. Mehnert, *Chem. – Eur. J.*, 2005, **11**, 50–56; (b) A. Riisager, R. Fehrmann, M. Haumann and P. Wasserscheid, *Eur. J. Inorg. Chem.*, 2006, 695–706; (c) Y. Gu and G. Liu, *Adv. Synth. Catal.*, 2009, **351**, 817–847; (d) C. van Doorslaer, J. Wahlen, P. Merlens, K. Binnemans and D. De Vos, *Dalton Trans.*, 2010, **39**, 8377–8390.
- For a highly informative up-to-date perspective on this area see: (a) F. Giacalone and M. Gruttadauria, *ChemCatChem*, 2016, **8**, 664–684; see also: H. Li, P. S. Bhadury, B. Song and S. Yang, *RSC Adv.*, 2102, 2, 12525–12551.
- (a) M. Gruttadauria, L. F. Liotta, A. M. P. Salvo, F. Giacalone, V. La Parola, C. Aprile and R. Noto, *Adv. Synth. Catal.*, 2011, **353**, 2119–2130; (b) V. Sans, F. Gelat, N. Karbass, M. I. Burguete, E. Garcíia-Verdego and S. V. Luis, *Adv. Synth. Catal.*, 2010, **352**, 3013–3021; (c) C. Pavia, E. Ballerini, L. A. Bivona, F. Giacalone, C. Aprile, L. Vaccaro and M. Gruttadauria, *Adv. Synth. Catal.*, 2013, **355**, 2007–2018; (d) M. Gruttadauria, L. A. Bivona, P. Lo Meo, S. Riela and R. Noto, *Eur. J. Org. Chem.*, 2012, 2635–2642.
- (a) X. Liu, X. Zhao and M. Lu, *Catal. Lett.*, 2015, **145**, 1549–1556; (b) C. Pavia, F. Giacalone, L. A. Bivona, A. M. P. Salvo, C. Petrucci, G. Strappaveccia, L. Vaccaro, C. Aprile and M. Gruttadauria, *J. Mol. Catal. A: Chem.*, 2014, **387**, 57–62; (c) G. Liu, M. Hou, J. Song, T. Jiang, H. Fan, Z. Zhang and B. Han, *Green Chem.*, 2010, **12**, 65–69.

- 7 M. Planellas, R. Pleixars and A. Shafir, *Adv. Synth. Catal.*, 2012, **354**, 651–662.
- 8 N. Jiao, Z. Li, Y. Wang, J. Liu and C. Xia, *RSC Adv.*, 2015, **5**, 26913–26922.
- 9 M. I. Burguete, E. García-Verdugo, I. Garcia-Villar, F. Gelat, P. Licence, S. V. Luis and V. Sans, *J. Catal.*, 2010, **269**, 150–160.
- 10 (a) C. Moreno-Marrodan, P. Barbaro, M. Catalano and A. Taurino, *Dalton Trans.*, 2012, **41**, 12666–12669; (b) F. Liguori and P. Barbaro, *Catal. Sci. Technol.*, 2014, **4**, 3835–3839.
- 11 J. Restrepo, P. Lozano, M. I. Burguete, E. García-Verdugo and S. V. Luis, *Catal. Today*, 2015, **255**, 97–101.
- 12 (a) A. P. Umpierre, P. F. P. Fichtner, S. R. Teixeira and J. Dupont, *Chem. – Eur. J.*, 2003, **9**, 3263–3269; (b) F. Bellina, *Molecules*, 2010, **15**, 2211–2245.
- 13 (a) A. Zhang and H. Cui, *Langmuir*, 2009, **25**, 2604–2612; (b) Z. Wang, Q. Zhang, D. Kuehner, A. Ivaska and L. Niu, *Green Chem.*, 2008, **10**, 907–909.
- 14 (a) D. B. Zhao, Z. F. Fei, T. J. Geldbach, R. Scopelliti and P. J. Dyson, *J. Am. Chem. Soc.*, 2004, **126**, 15876–15882; (b) C. Chiappe, D. Pieraccini, D. Zhao, Z. Fei and P. J. Dyson, *Adv. Synth. Catal.*, 2006, **348**, 68–74; (c) Z. Fei, D. Zhao, D. Pieraccini, W. H. Ang, T. J. Geldbach, R. Scopelliti, C. Chiappe and P. J. Dyson, *Organometallics*, 2007, **26**, 1588–1598; (d) X. Yang, Z. Fei, D. Zhao, W. H. Ang, Y. Li and P. J. Dyson, *Inorg. Chem.*, 2008, **47**, 3292–3297; (e) M. H. G. Precht, J. D. Scholten and J. Dupont, *J. Mol. Catal. A: Chem.*, 2009, **313**, 74–78.
- 15 (a) H. Itoh, K. Maki and Y. Chujo, *J. Am. Chem. Soc.*, 2004, **126**, 3026–3027; (b) N. Kocharova, J. Leiro, J. Lukkari, M. Heinonen, T. Skala, F. Sutara, M. Skoda and M. Vondracek, *Langmuir*, 2008, **24**, 3235–3242.
- 16 (a) B. Léger, A. Denicourt-Nowicki, A. Roucoux and H. Olivier-Bourbigou, *Adv. Synth. Catal.*, 2008, **350**, 153–159; (b) B. Léger, A. Denicourt-Nowicki, H. Olivier-Bourbigou and A. Roucoux, *Inorg. Chem.*, 2007, **47**, 9090–9096; (c) A. Denicourt-Nowicki, B. Léger and A. Roucoux, *Phys. Chem. Chem. Phys.*, 2011, **13**, 13510–13517; (d) R. R. Dykeman, N. Yan, R. Scopelliti and P. J. Dyson, *Inorg. Chem.*, 2011, **50**, 717–719.
- 17 (a) N. Yan, X. Yang, Z. Fei, Y. Li, Y. Kou and P. J. Dyson, *Organometallics*, 2009, **28**, 937–939; (b) X. Yuan, N. Yan, S. A. Katsyuba, E. E. Svereva, Y. Kou and P. J. Dyson, *Phys. Chem. Chem. Phys.*, 2012, **14**, 6026–6033.
- 18 (a) B. C. Leal, C. S. Consorti, G. Machado and J. Dupont, *Catal. Sci. Technol.*, 2015, **5**, 903–909; (b) K. L. Luska and A. Moores, *Adv. Synth. Catal.*, 2011, **353**, 3167–3177; (c) S. Bahadorikhalili, L. Ma'mani, H. Mahdavi and A. Shafiee, *RSC Adv.*, 2015, **5**, 71297–71305.
- 19 (a) S. G. Kwon, G. Krylova, A. Sumer, M. M. Schwartz, E. E. Bunel, C. L. Marshall, S. Chattopadhyay, B. Lee, J. Jellinek and E. V. Shevchenko, *Nano Lett.*, 2012, **12**, 5382–5388; (b) Z. Guo, C. Xiao, R. V. Maligal-Ganesh, L. Zhou, T. W. Goh, X. Li, D. Tesfagaber, A. Thiel and W. Huang, *ACS Catal.*, 2014, **4**, 1340–1348; (c) K. R. Kahsar, D. K. Schwartz and J. W. Medlin, *J. Am. Chem. Soc.*, 2014, **136**, 520–526.
- 20 I. Cano, A. M. Chapman, A. Urakawa and P. W. N. M. van Leeuwen, *J. Am. Chem. Soc.*, 2014, **136**, 2520–2528.
- 21 For examples of aqueous phase catalysis by surfactant-stabilised palladium nanoparticles see: (a) B. S. Souza, E. C. Leopoldino, D. W. Tondo, J. Dupont and F. Nome, *Langmuir*, 2012, **28**, 833–840; (b) G. La Sorella, P. Canton, G. Strukul and A. Scarso, *ChemCatChem*, 2014, **6**, 1575–1578; (c) J. Feng, S. Handa, F. Gallou and B. H. Lipshutz, *Angew. Chem., Int. Ed.*, 2016, **55**, 8979–8983; (d) S. Handa, Y. Wang, F. Gallou and B. H. Lipshutz, *Science*, 2015, **349**, 1087–1091; (e) B. H. Lipshutz and S. Ghorai, *Aldrichimica Acta*, 2008, **41**, 59–72; (f) J.-H. Noh and R. Meijboom, *Appl. Catal., A*, 2015, **497**, 107–120; (g) W. Zhu, H. Yang, Y. Yu, L. Hua, H. Li, B. Feng and Z. Hou, *Phys. Chem. Chem. Phys.*, 2011, **13**, 13492–13500; (h) N. Iranpoor, S. Rahimi and F. Panahi, *RSC Adv.*, 2016, **6**, 3084–3090; (i) N. Iranpoor, S. Rahimi and F. Panahi, *RSC Adv.*, 2015, **5**, 69559–49567; (j) B. L. Albuquerque, A. Denicourt-Nowicki, C. Meriadec, J. B. Domingos and A. Roucoux, *J. Catal.*, 2016, **340**, 144–153; (k) C. Deraedt and D. Astruc, *Acc. Chem. Res.*, 2014, **47**, 494–503. For examples of aqueous phase catalysis with surfactant-free palladium nanoparticles see: (l) M. Hyotanishi, Y. Isomura, H. Yamamoto, H. Kawasaki and Y. Obora, *Chem. Commun.*, 2011, **47**, 5750–5752; (m) M. Nasrollahzadeh, S. Mohammad Sajadi, M. Maham and A. Ehsani, *RSC Adv.*, 2015, **5**, 2562–2567; (n) A. Aijaz, Q.-L. Zhu, N. Tsumori, T. Akita and Q. Xu, *Chem. Commun.*, 2015, **51**, 2577–2580. For examples of aqueous phase catalysis by polymer-stabilised palladium nanoparticles see: (o) D. Damodara, R. Arundhati, T. Venkata Ramesh Babu, M. K. Legan, H. J. Kumpaty and P. R. Likhar, *RSC Adv.*, 2014, **4**, 22567–22574; (p) Y. Lee, S. Shabbir, S. Lee, H. Ahn and H. Rhee, *Green Chem.*, 2015, **17**, 3579–3583. For examples of aqueous phase catalysis by palladium nanoparticles stabilised in metal organic frameworks see: (q) F. Zhang, S. Zheng, Q. Xiao, Y. Zhong, W. Zhu, A. Lin and M. S. El-Shall, *Green Chem.*, 2016, **18**, 2900–2908.
- 22 Astruc and co-workers have recently reported a similar approach for the preparation of transition metal nanoparticles for highly efficient aqueous phase catalysis. C. Wang, R. Ciganda, L. Salmon, D. Gregurec, J. Irigoyen, S. Moya, J. Ruiz and D. Astruc, *Angew. Chem., Int. Ed.*, 2016, **55**, 3091–3095.
- 23 (a) E. Bus, R. Prins and J. A. van Bokhoven, *Catal. Commun.*, 2007, **8**, 1397–1402; (b) P. Virtanen, J. Mikkola and T. Salmi, *Ind. Eng. Chem. Res.*, 2009, **48**, 10335–10342; (c) P. Maki-Arvela, J. Hajeoh, T. Salmi and D. Y. Murzin, *Appl. Catal., A*, 2005, **292**, 1–49; (d) B.-H. Zhao, J.-G. Chen, X. Liu, Z.-W. Liu, Z. Hao, J. Xiao and Z.-T. Liu, *Ind. Eng. Chem. Res.*, 2012, **51**, 11112–11121.

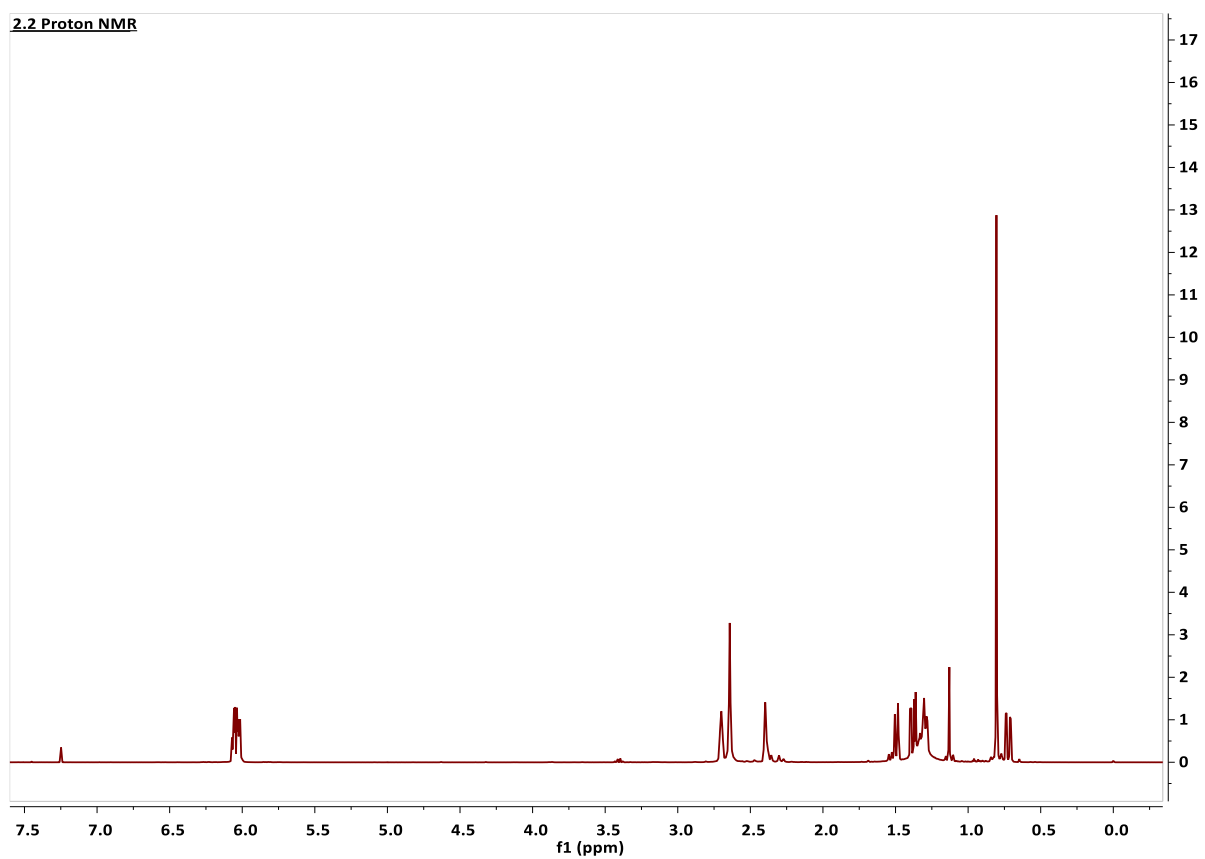
- 24 (a) P. H. Z. Ribeiro, E. Y. Matsubara, J. M. Rosolen, P. M. Donate and R. Gunnella, *J. Mol. Catal. A: Chem.*, 2015, **410**, 34–40; (b) H. Gu, X. Xu, A. Chen, P. Ao and X. Yan, *Catal. Commun.*, 2013, **41**, 65–69.
- 25 A. S. Nagpure, L. Gurrula, P. Gogoi and S. V. Chilukuri, *RSC Adv.*, 2016, **6**, 44333–44340.
- 26 Y. Zhao, M. Lui, B. Fan, Y. Chen, W. Lv, N. Lu and R. Li, *Catal. Commun.*, 2014, **57**, 119–123.
- 27 K. Anderson, P. Goodrich, C. Hardacre and D. W. Rooney, *Green Chem.*, 2003, **5**, 448–453.
- 28 S. Bhogeswararao and D. Srinivas, *J. Catal.*, 2012, **285**, 31–40.
- 29 R. Herbios, S. Noël, B. Léger, S. Tilloy, S. Menuel, A. Addad, B. Martel, A. Ponchel and E. Monflier, *Green Chem.*, 2015, **17**, 2444–2454.
- 30 M. von Arx, T. Mallat and A. Baiker, *J. Mol. Catal. A: Chem.*, 1999, **148**, 275–283.

APPENDICES

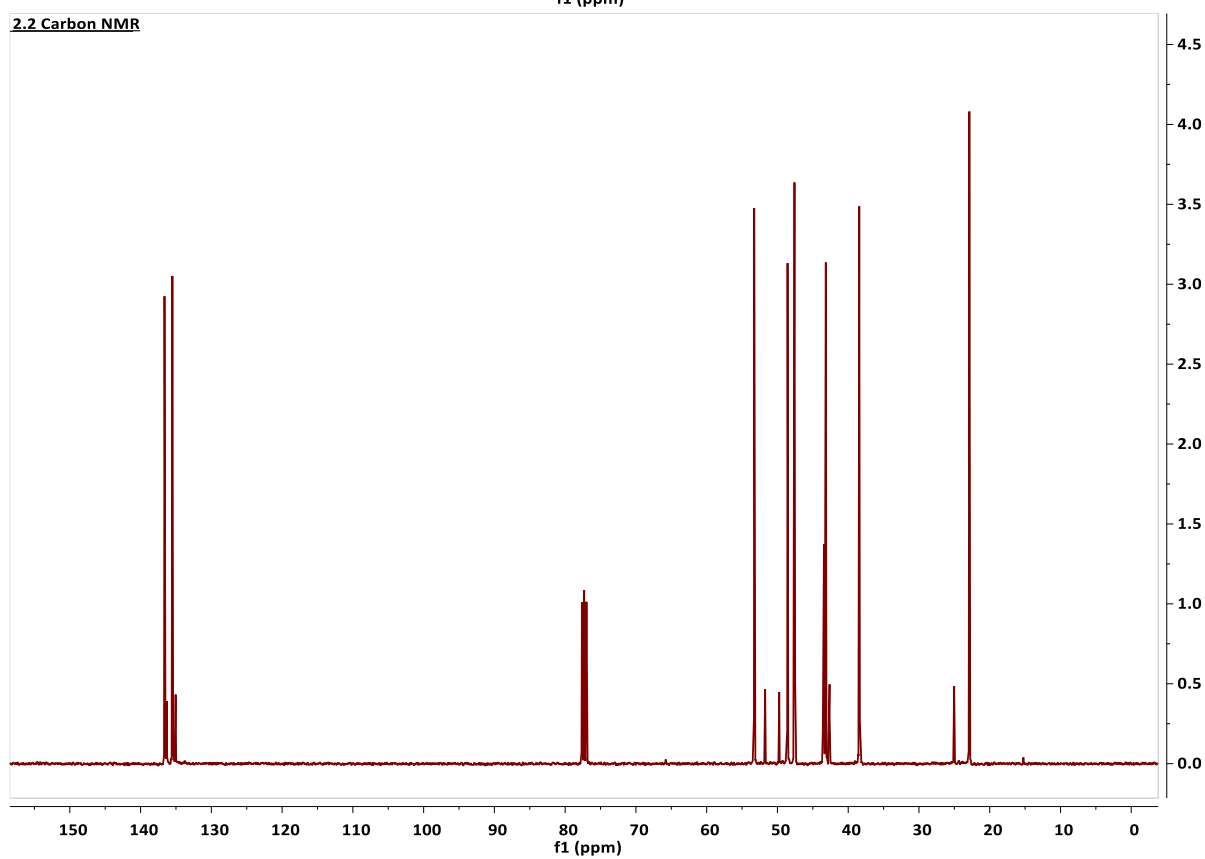
Appendix A. Nuclear magnetic resonance spectra (NMR)

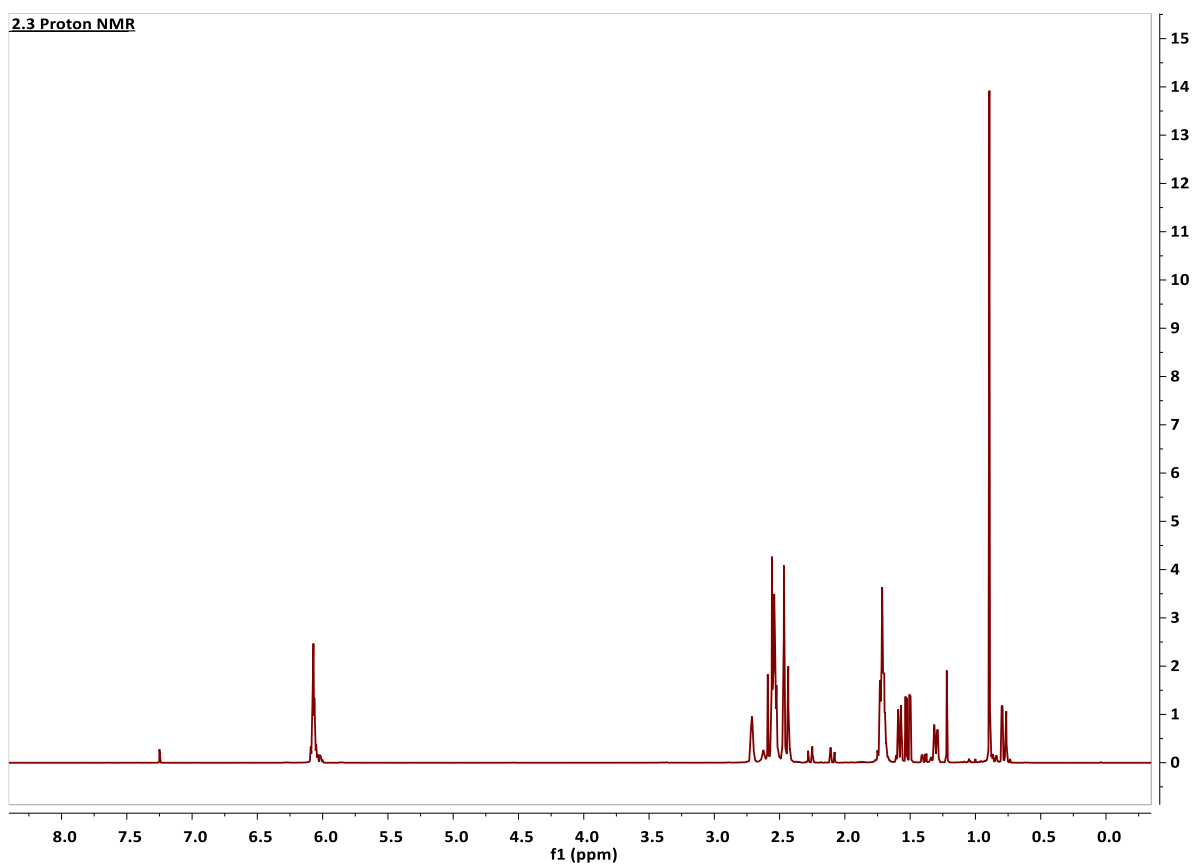
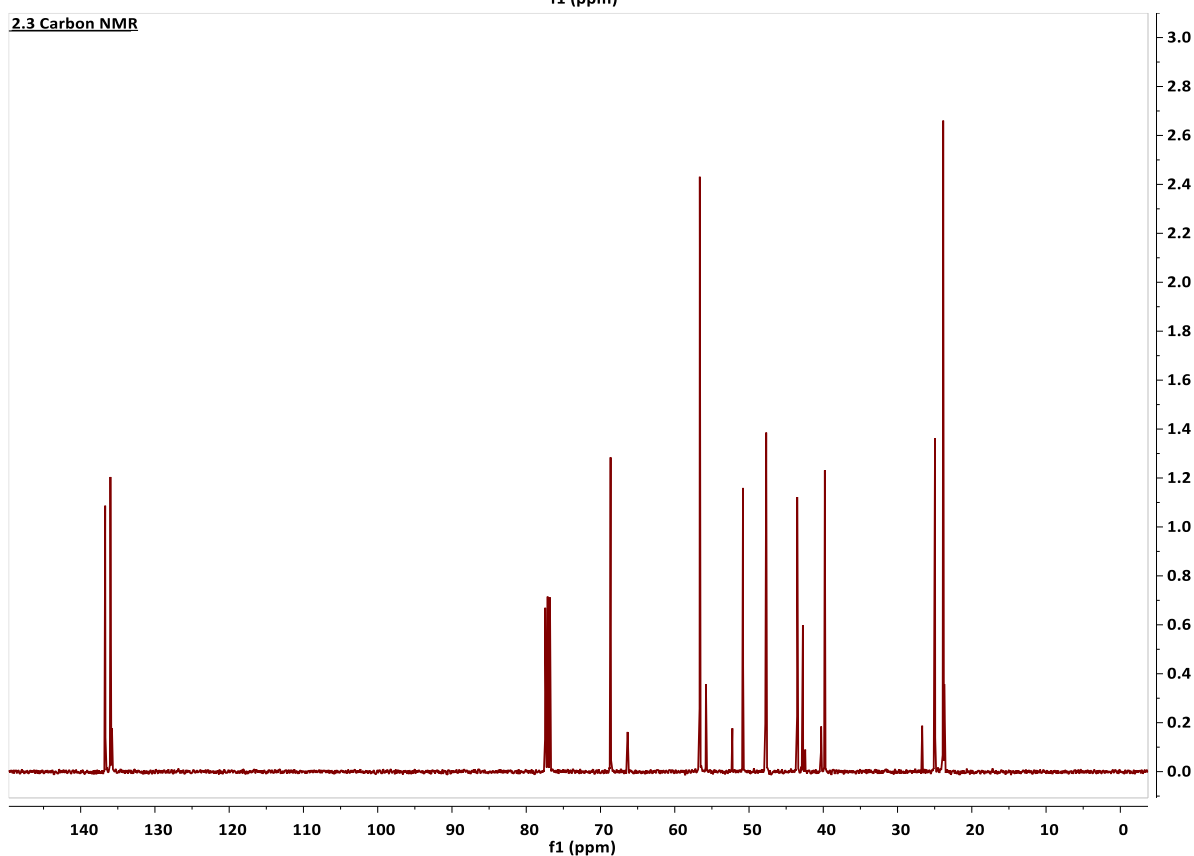


2.2 Proton NMR

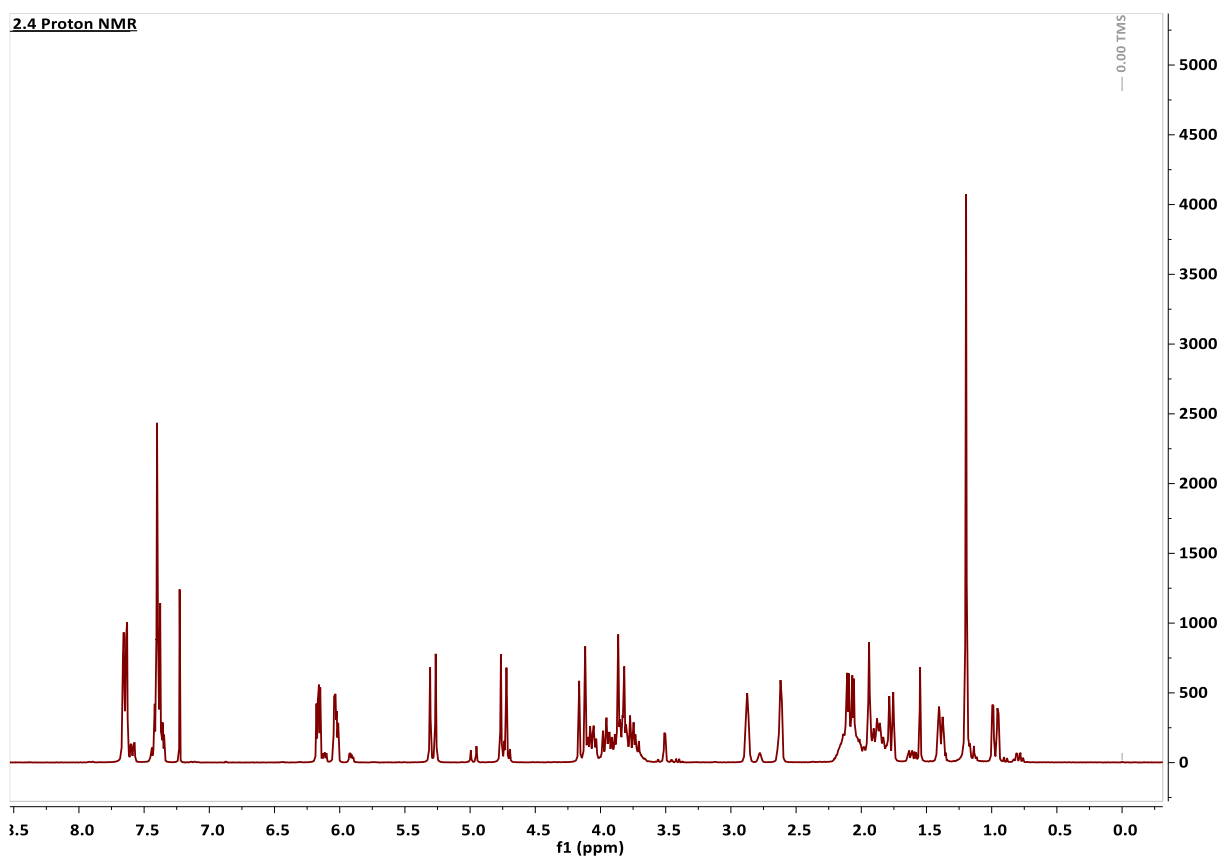


2.2 Carbon NMR

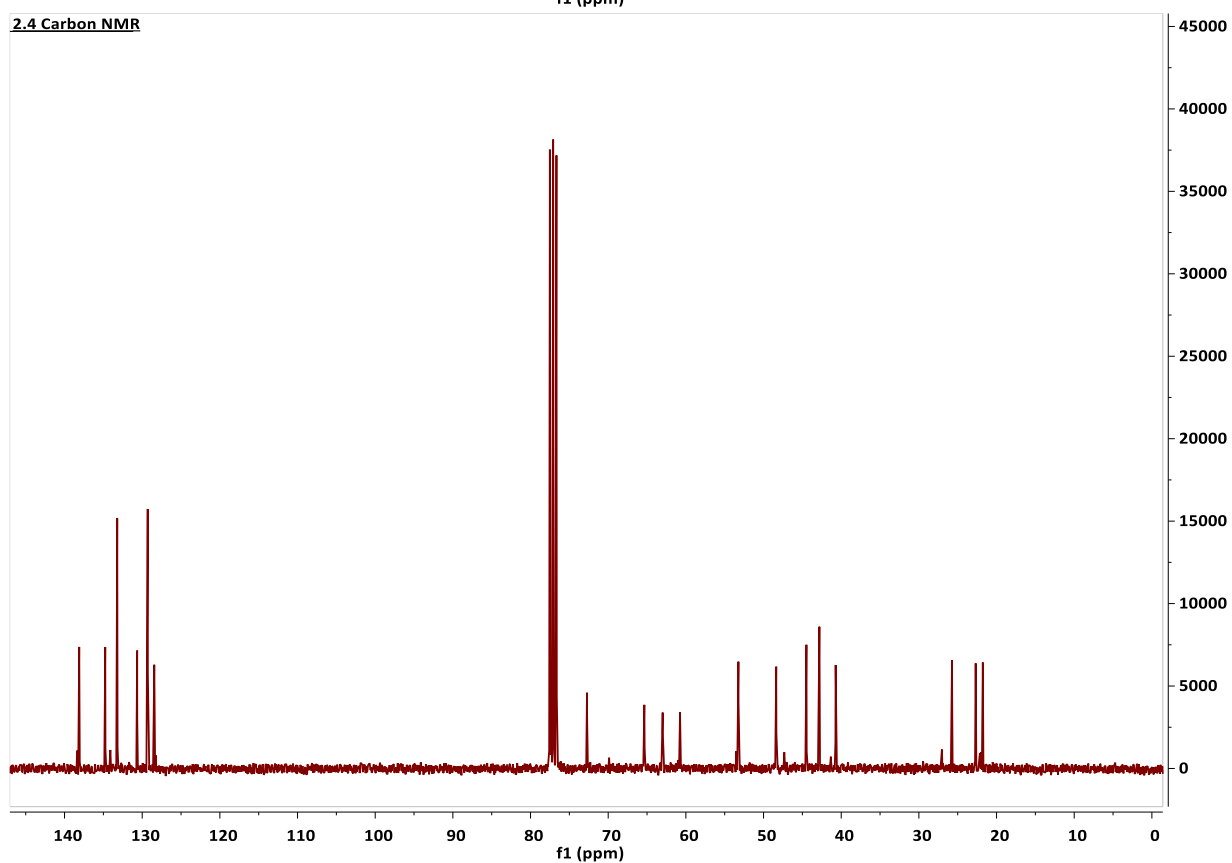


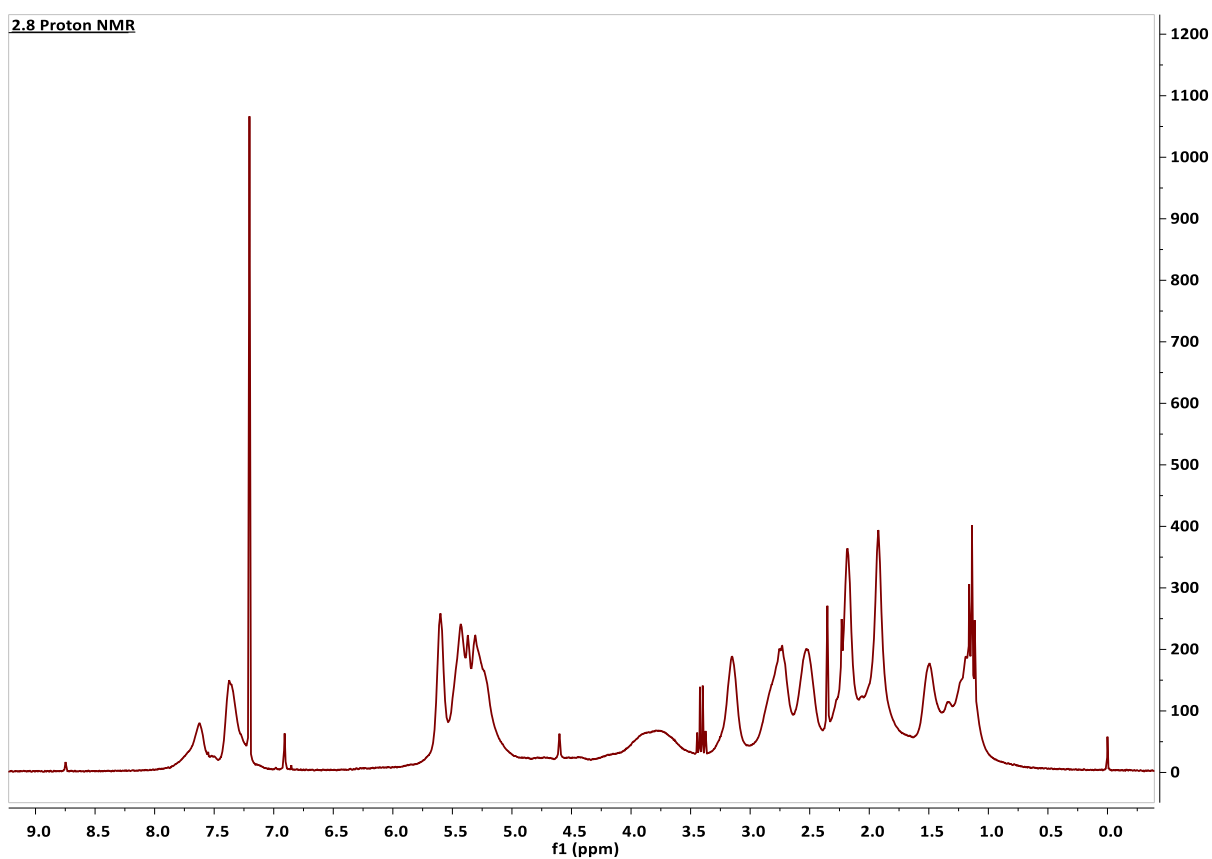
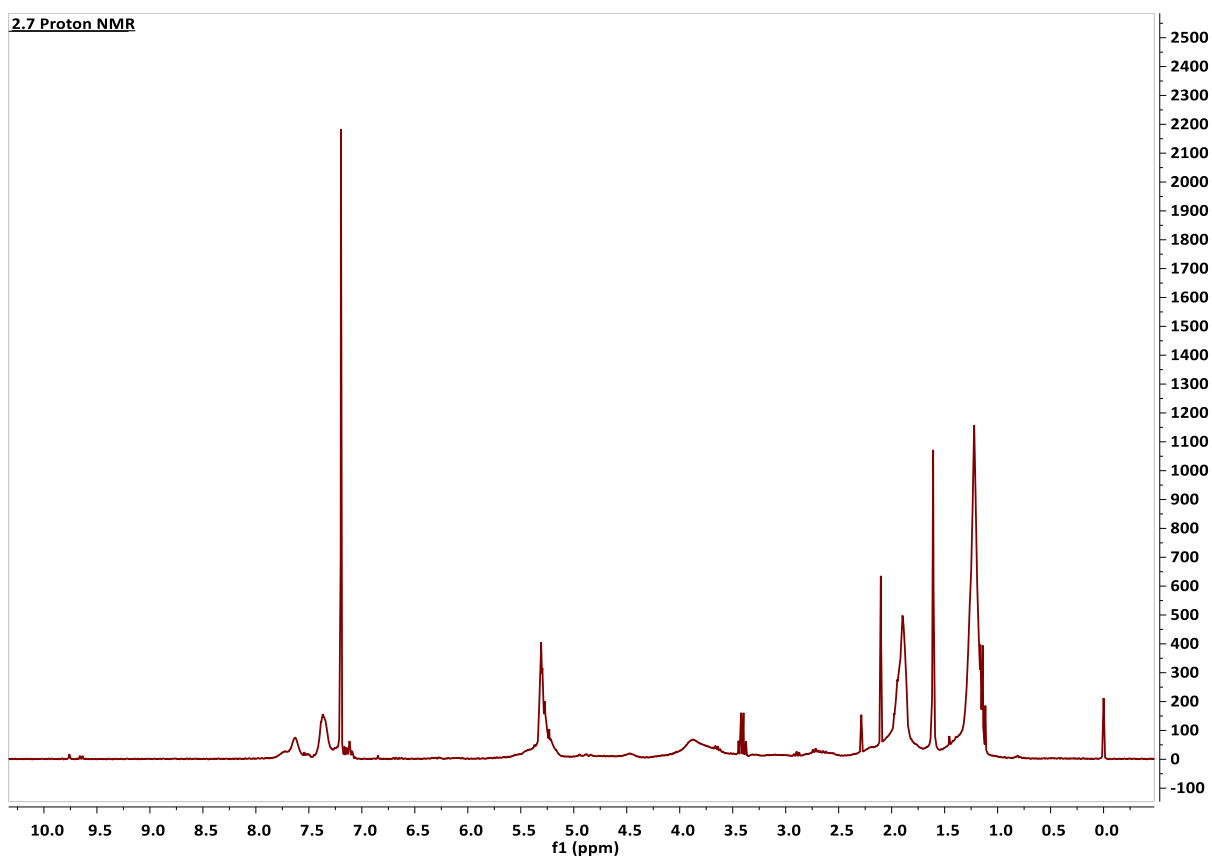
2.3 Proton NMR**2.3 Carbon NMR**

2.4 Proton NMR

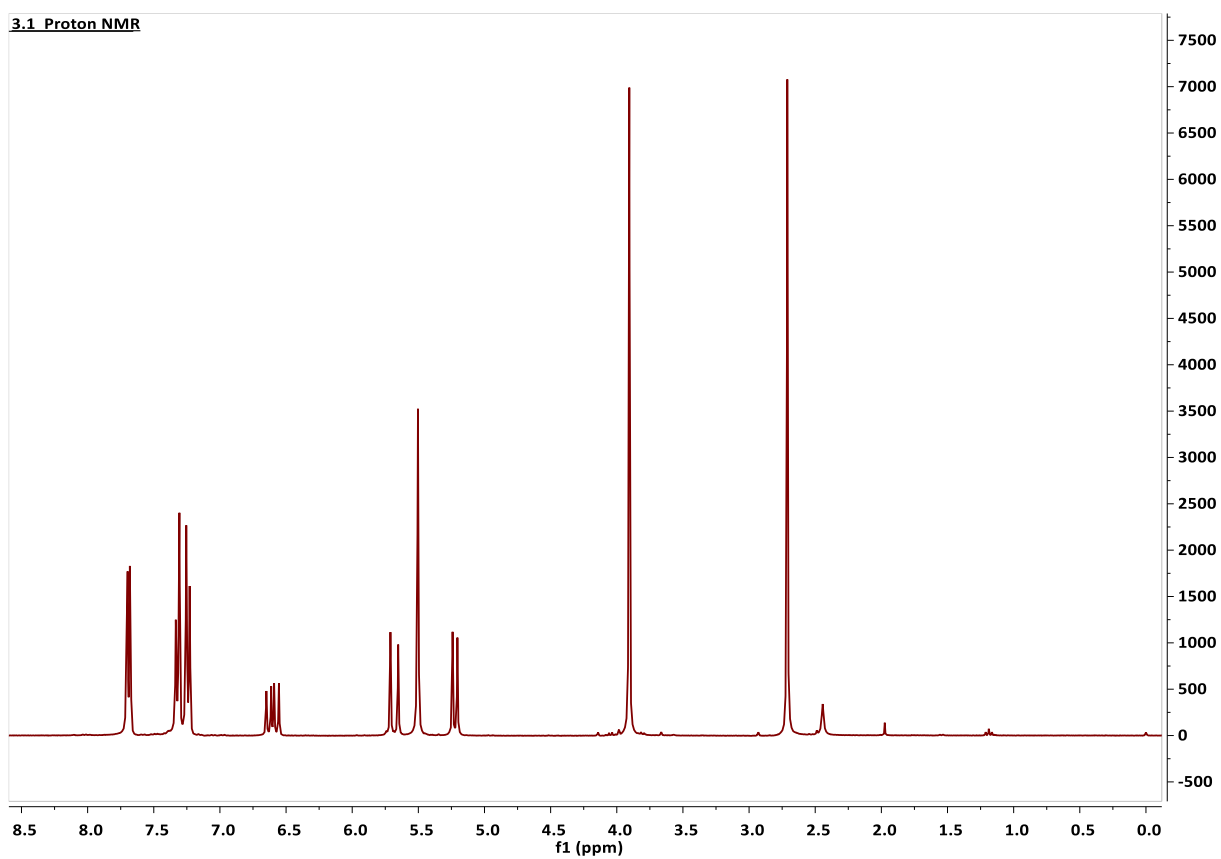


2.4 Carbon NMR

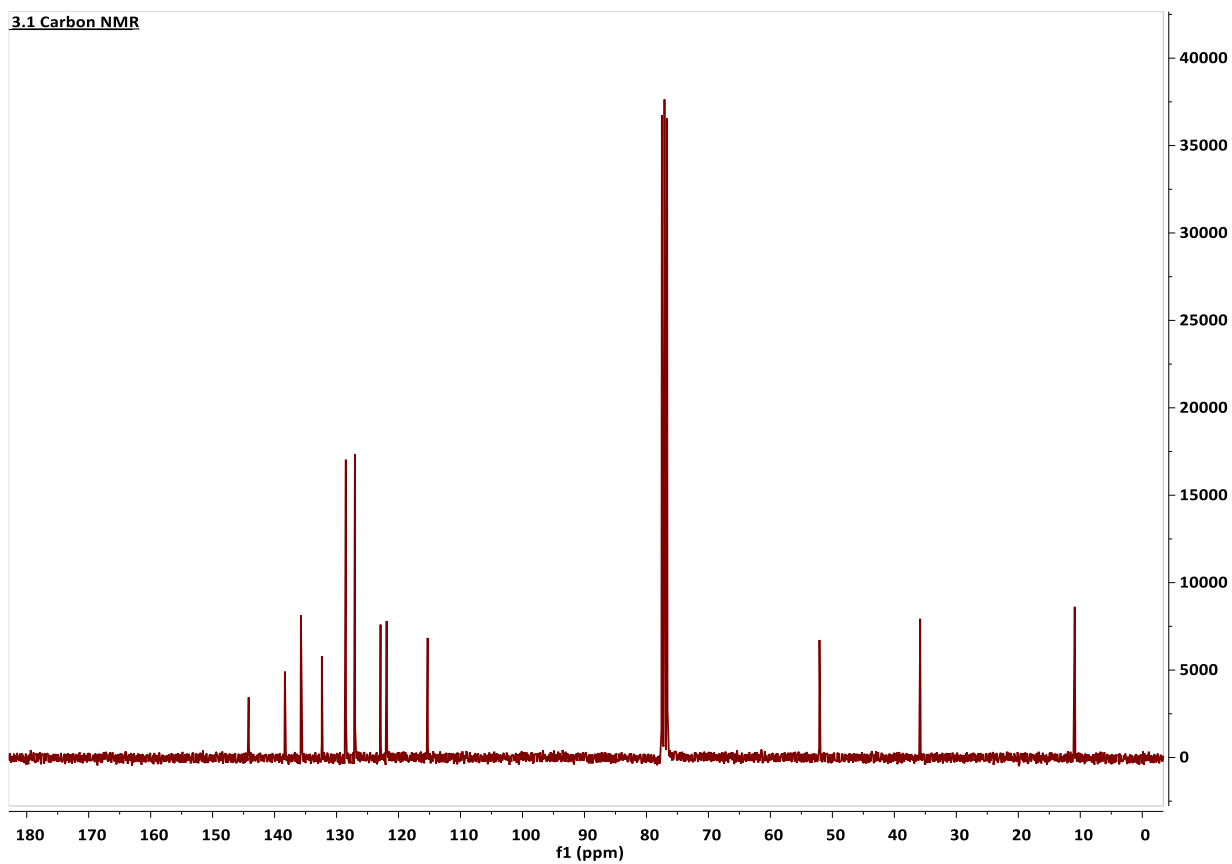


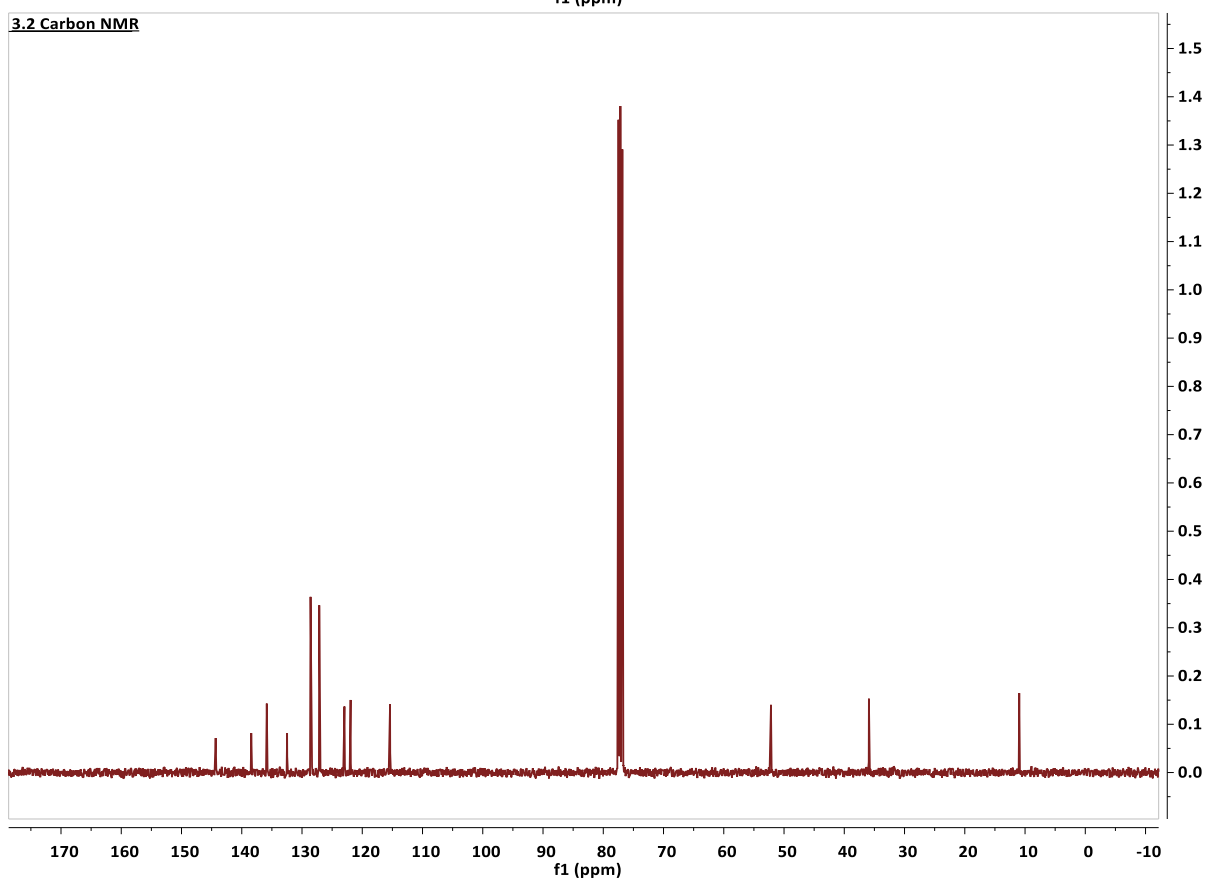
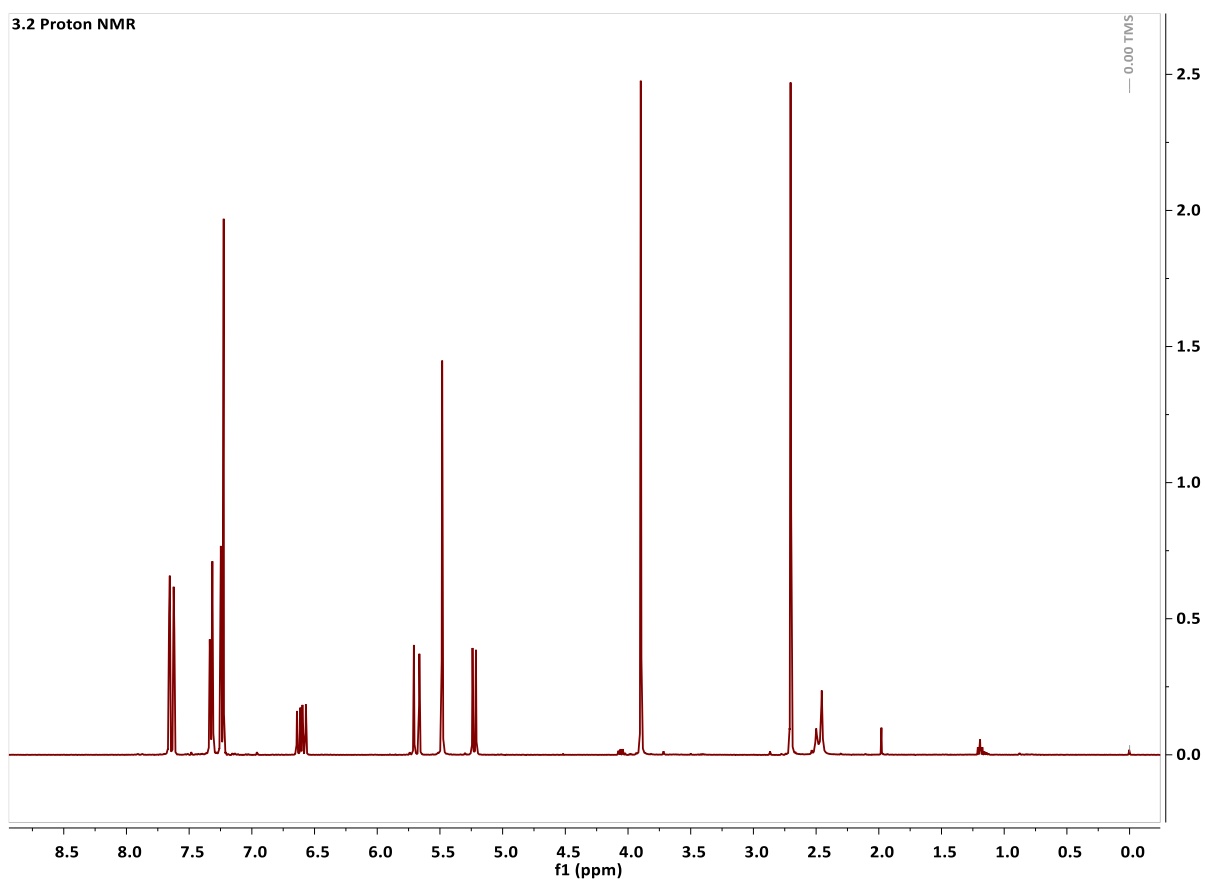


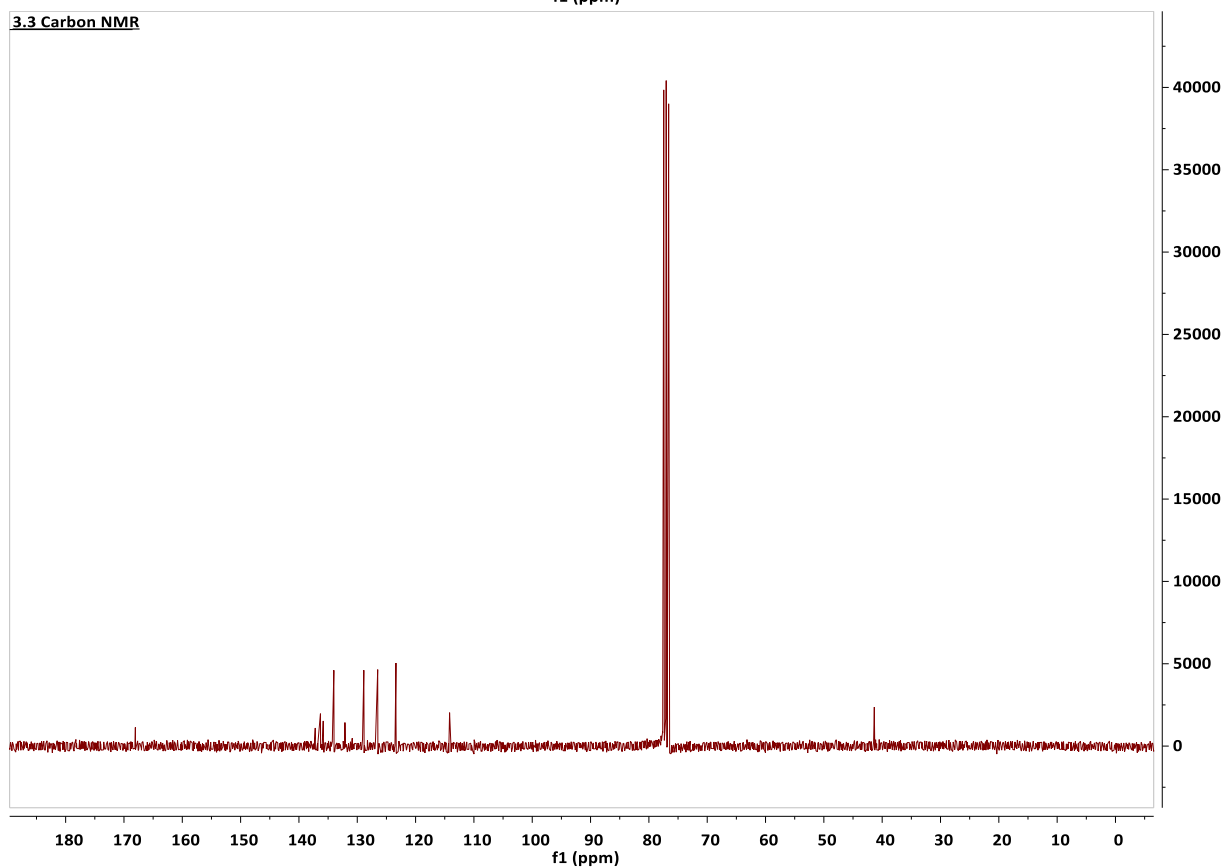
3.1 Proton NMR



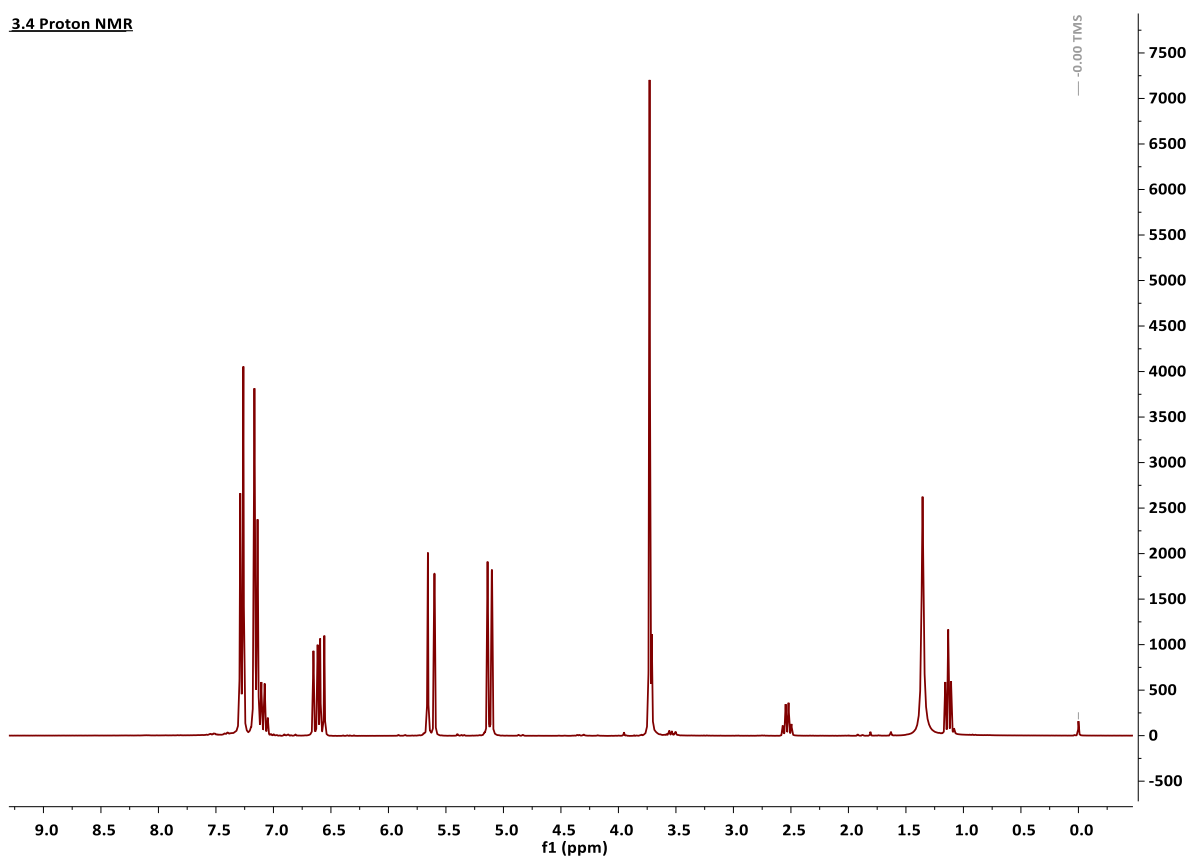
3.1 Carbon NMR



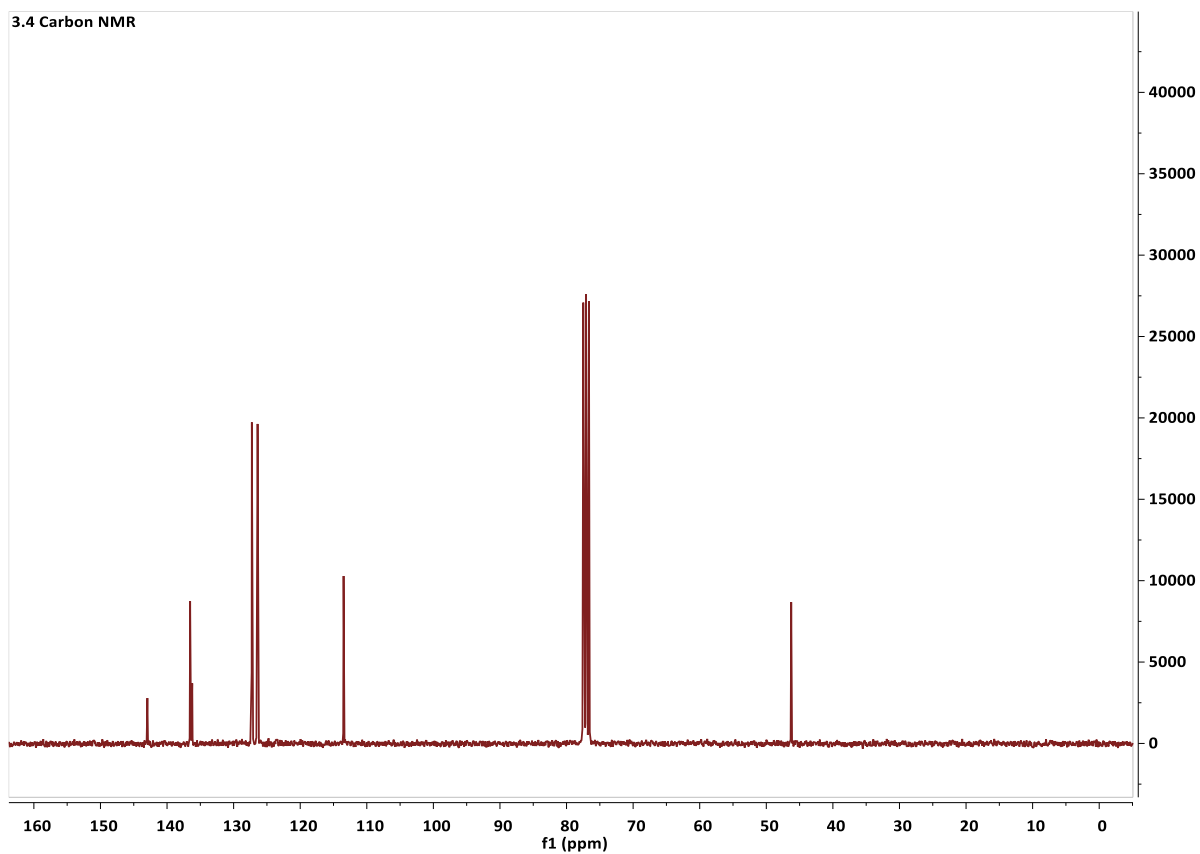




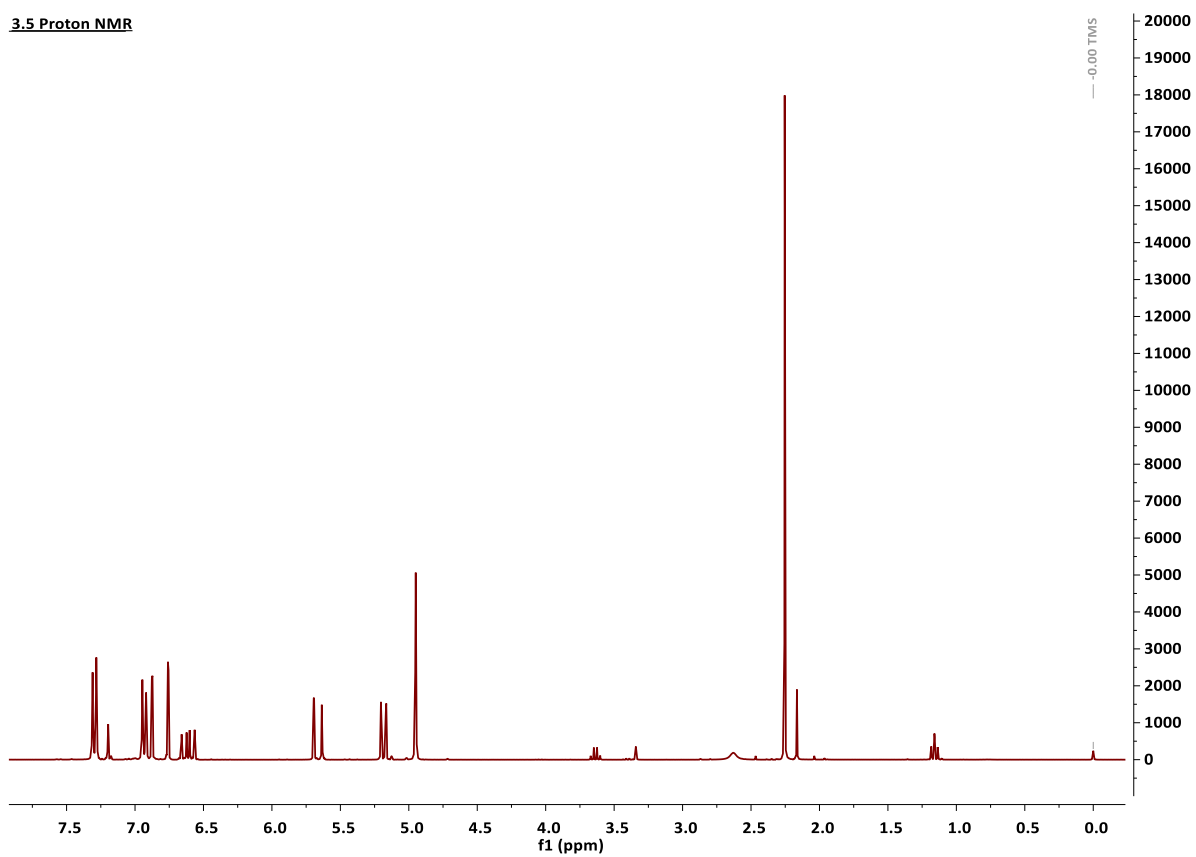
3.4 Proton NMR



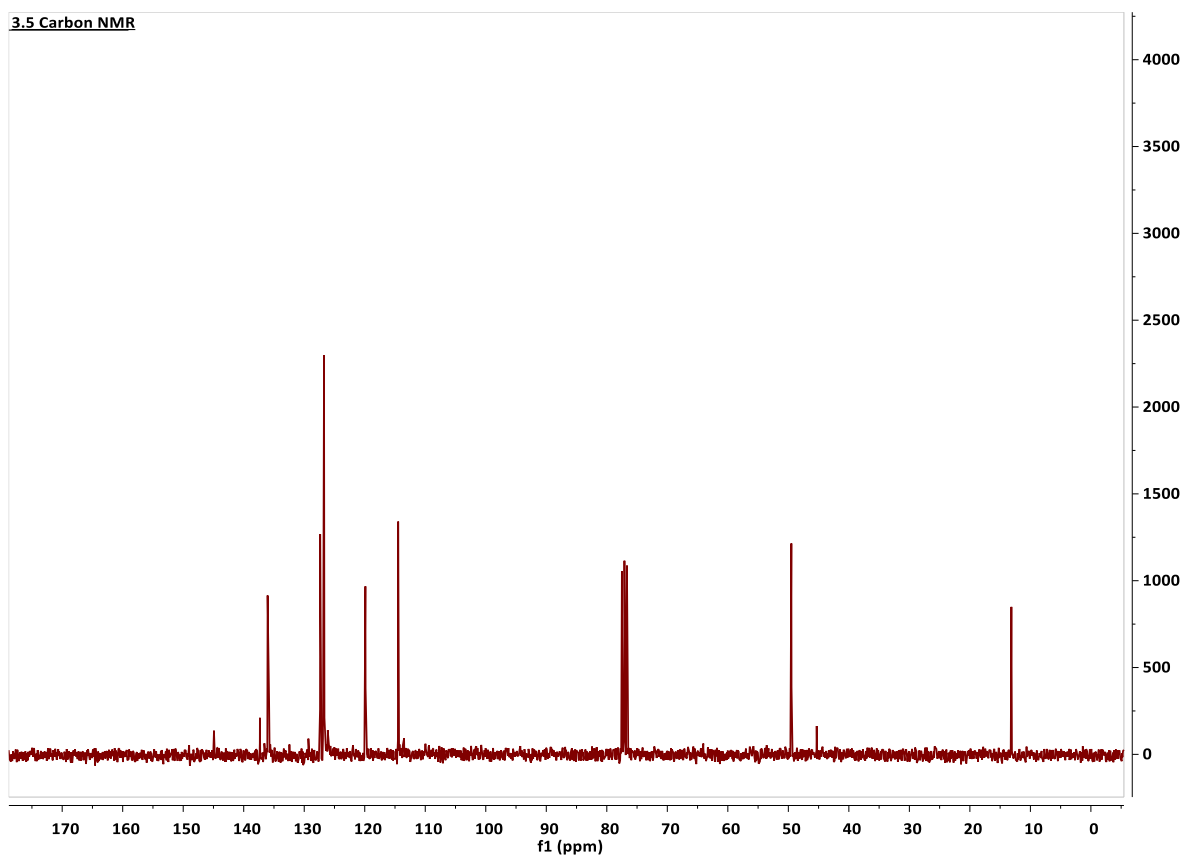
3.4 Carbon NMR

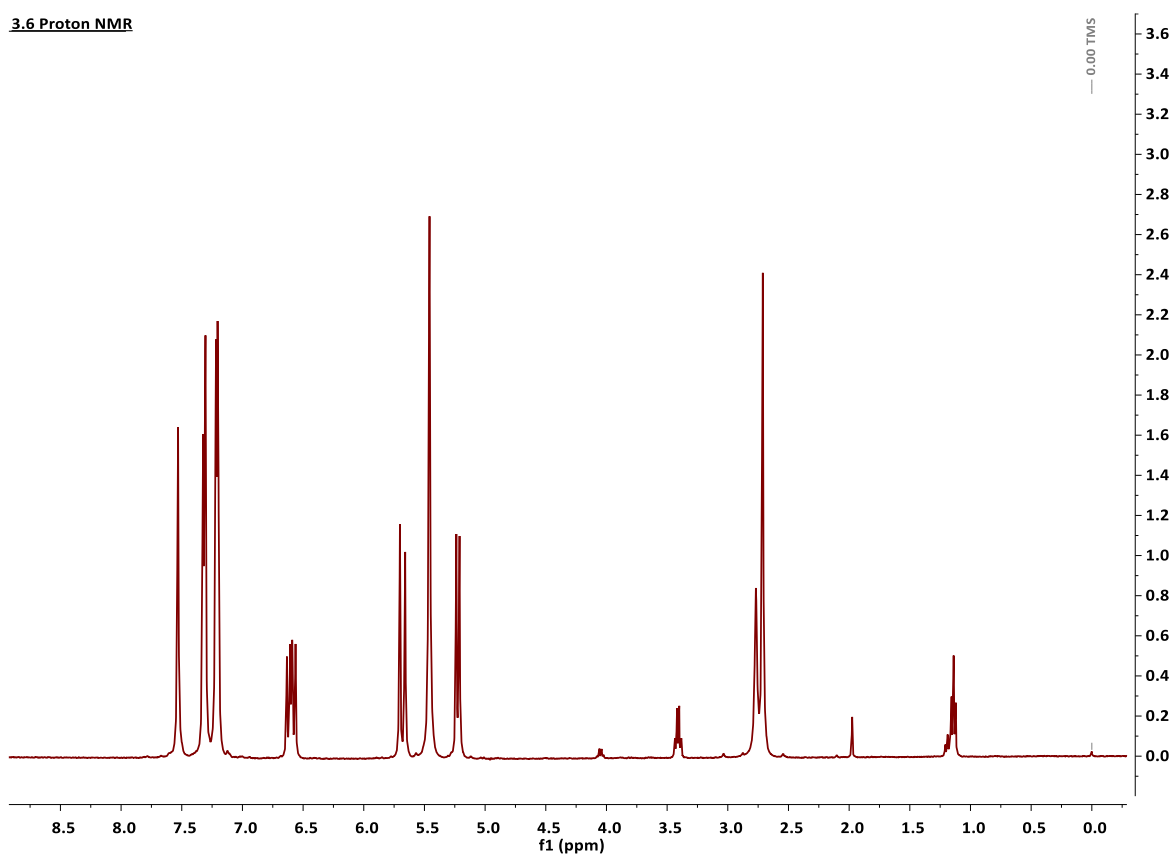
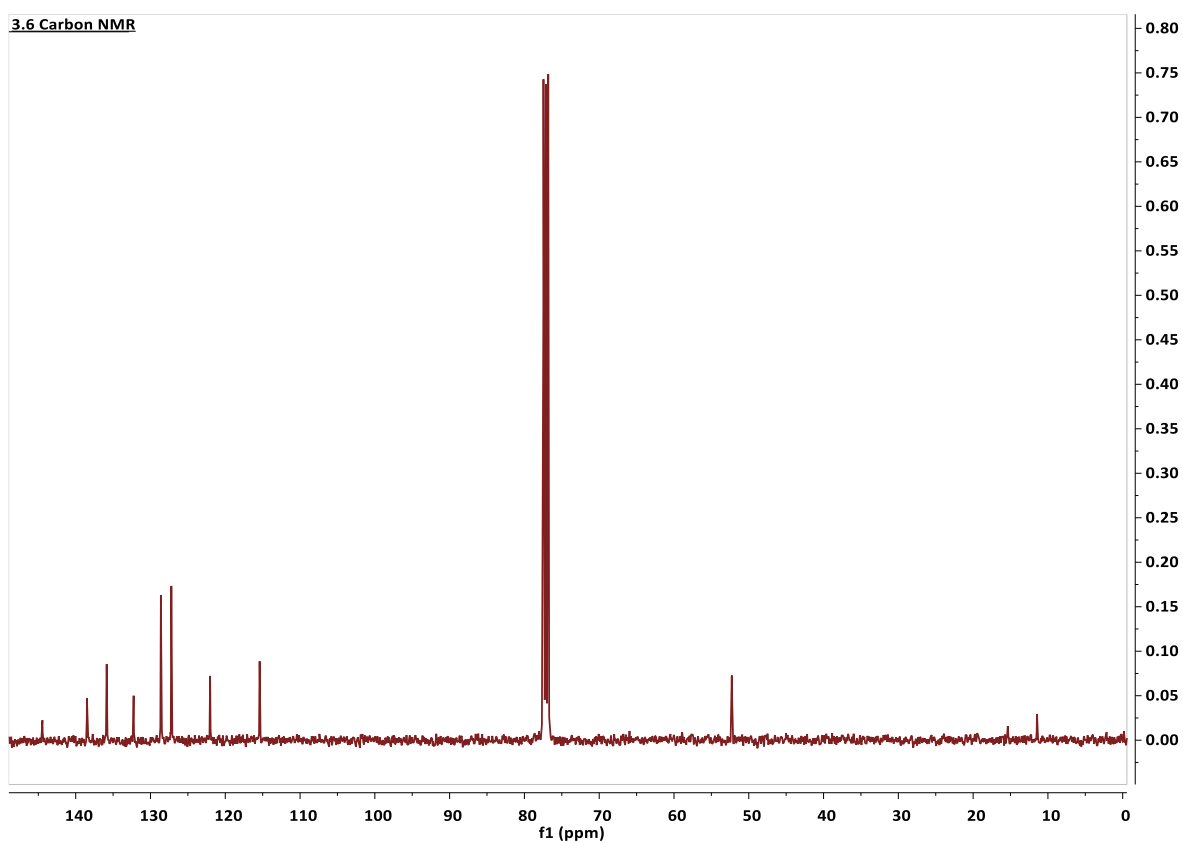


3.5 Proton NMR

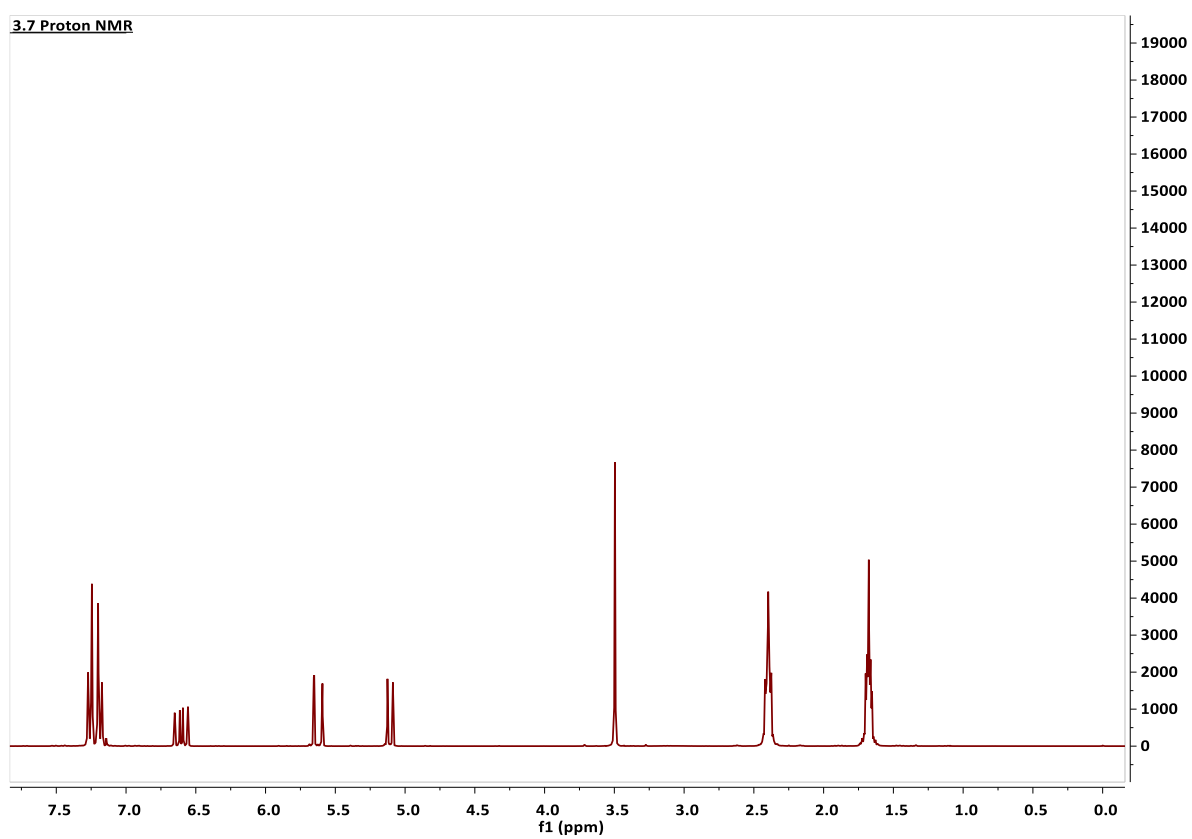


3.5 Carbon NMR

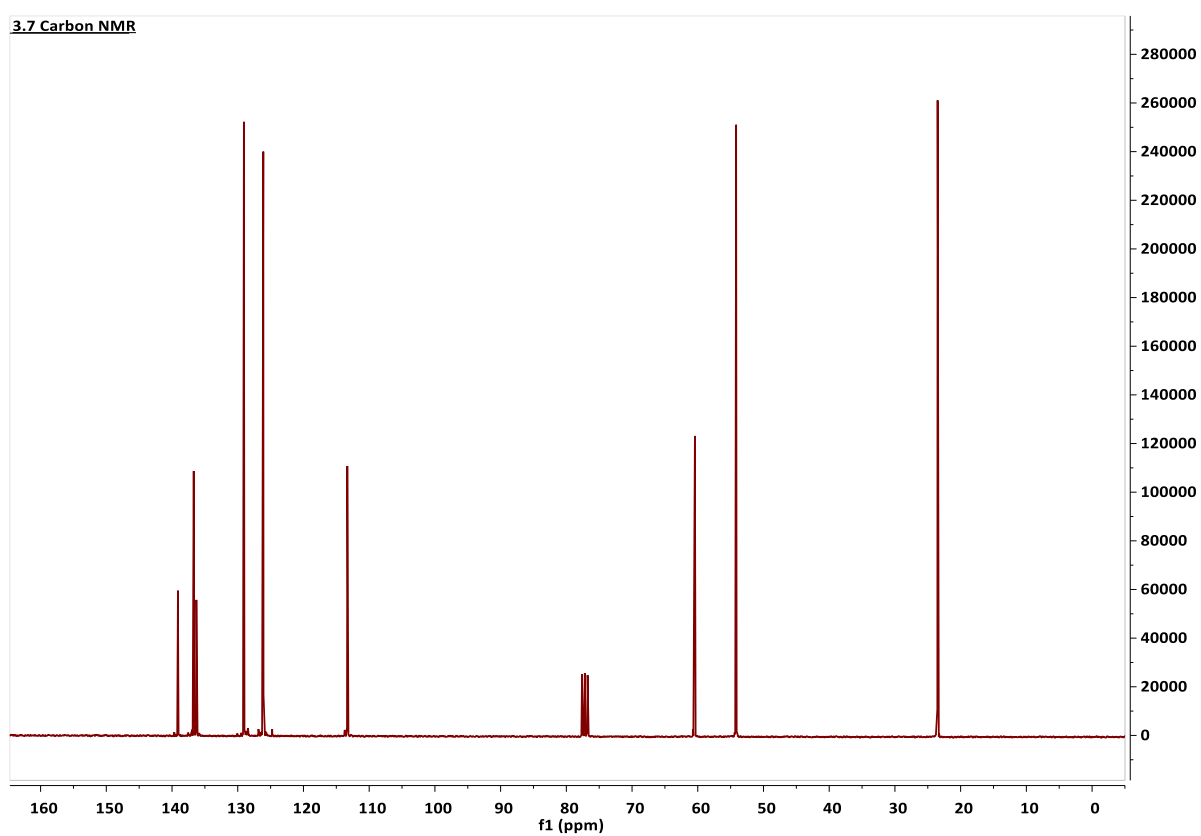


3.6 Proton NMR**3.6 Carbon NMR**

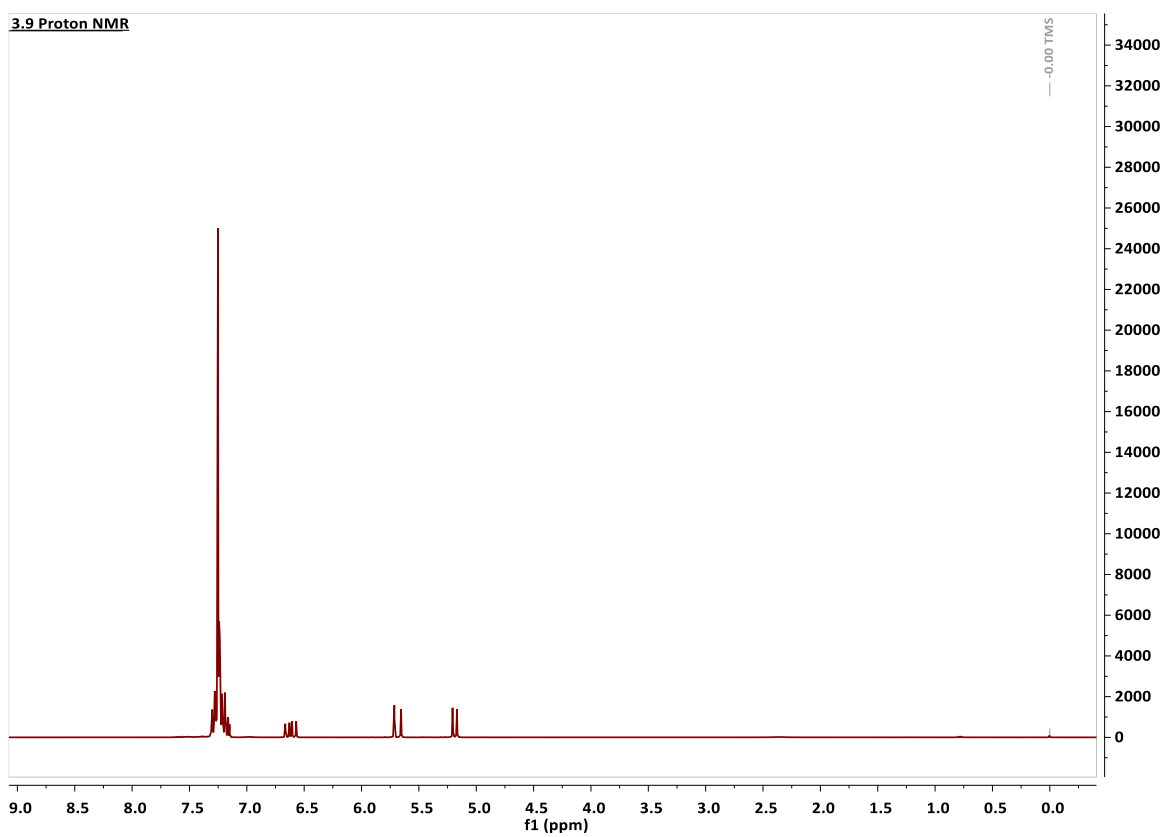
3.7 Proton NMR



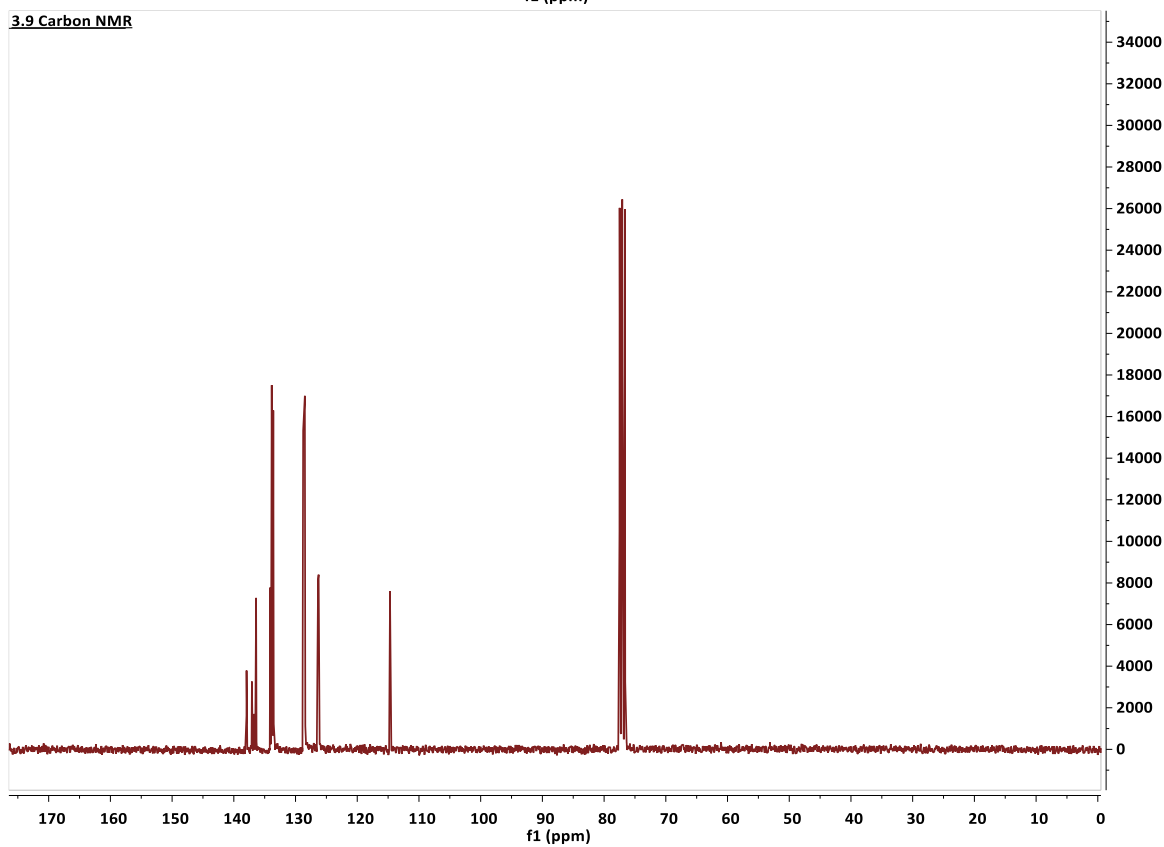
3.7 Carbon NMR

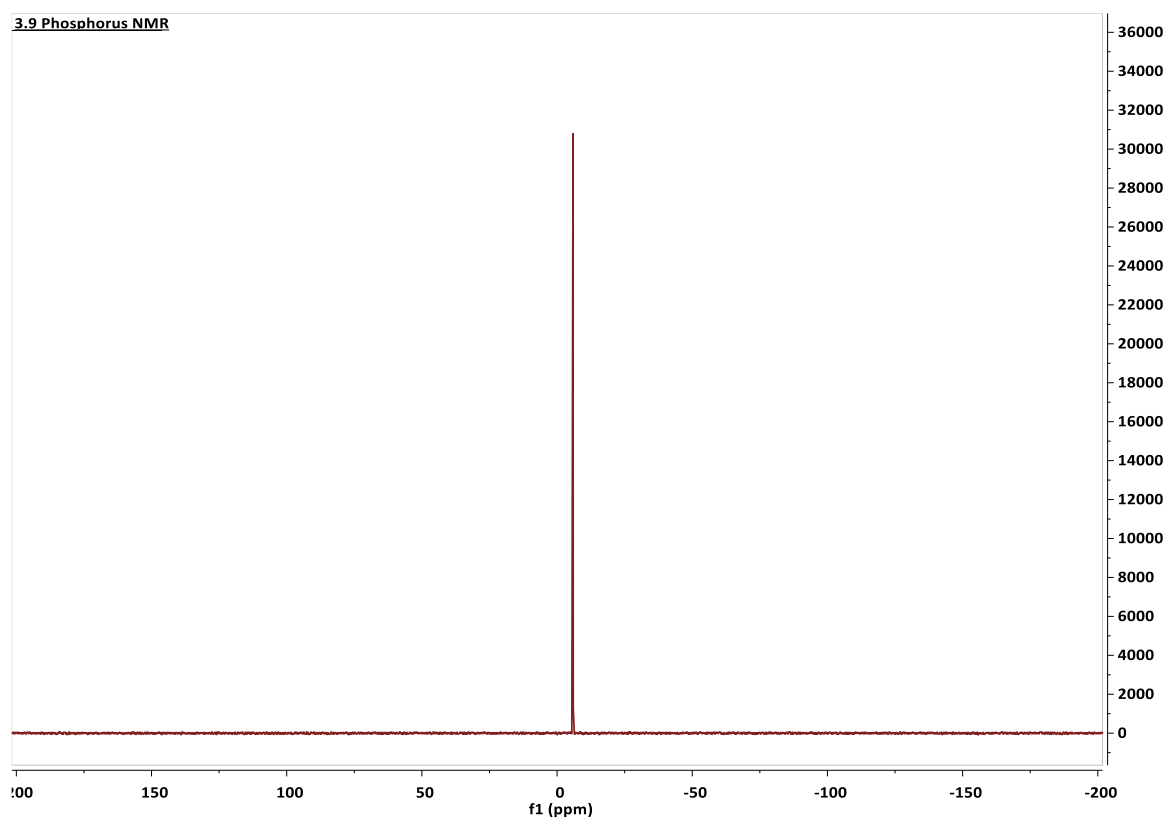


3.9 Proton NMR

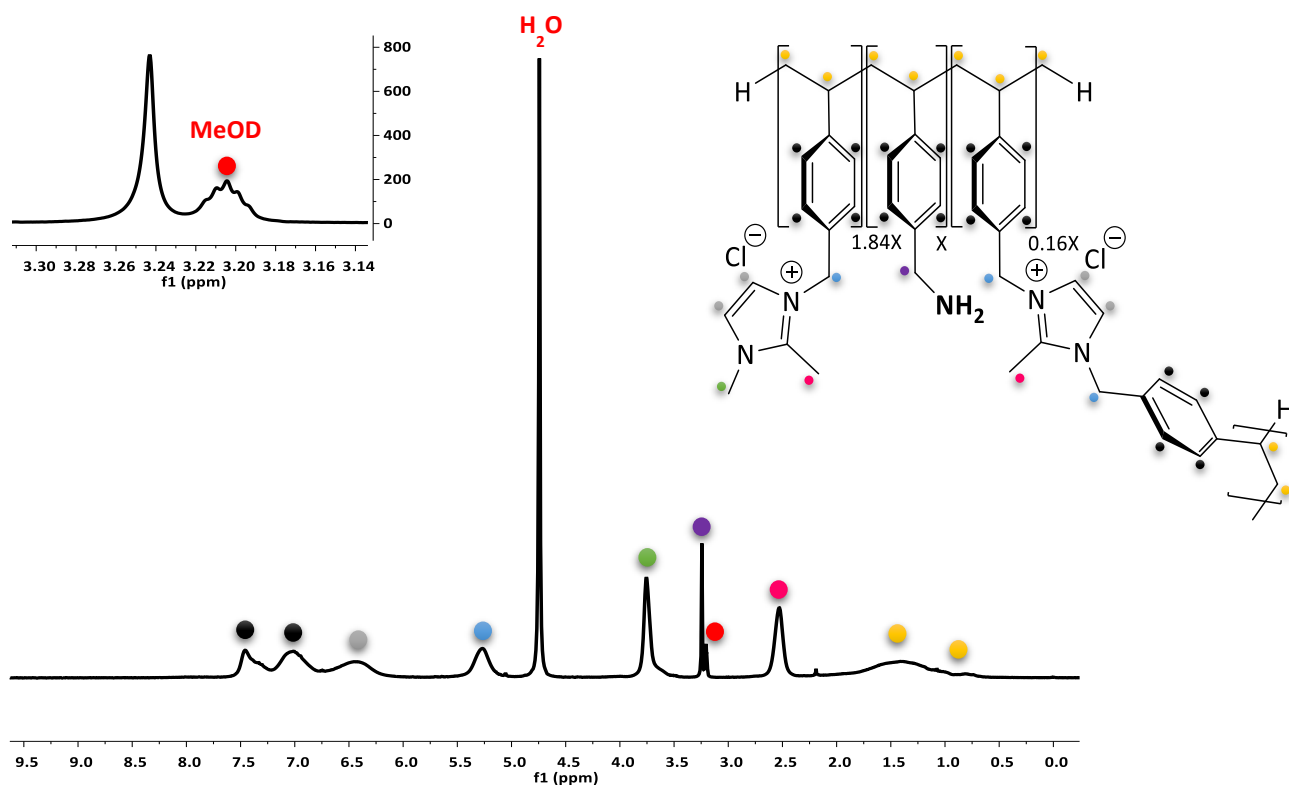


3.9 Carbon NMR

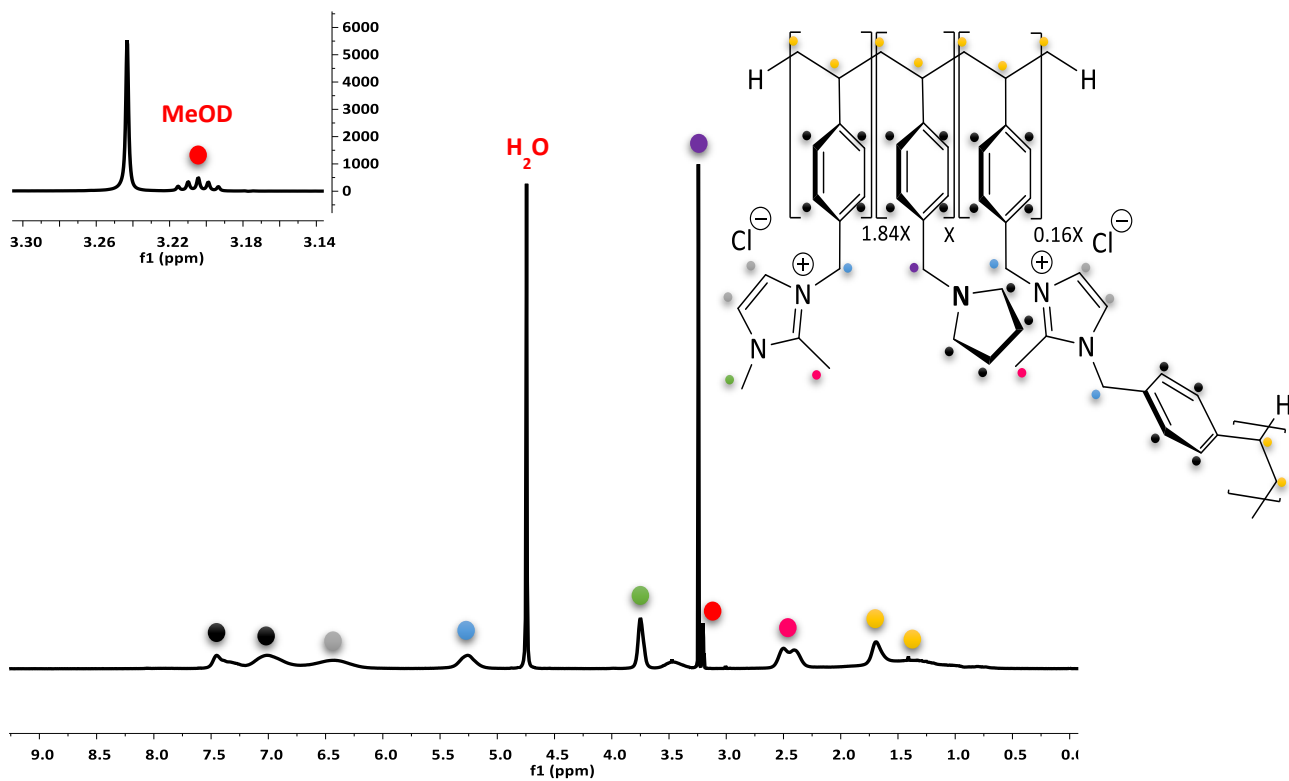




3.10 Proton NMR

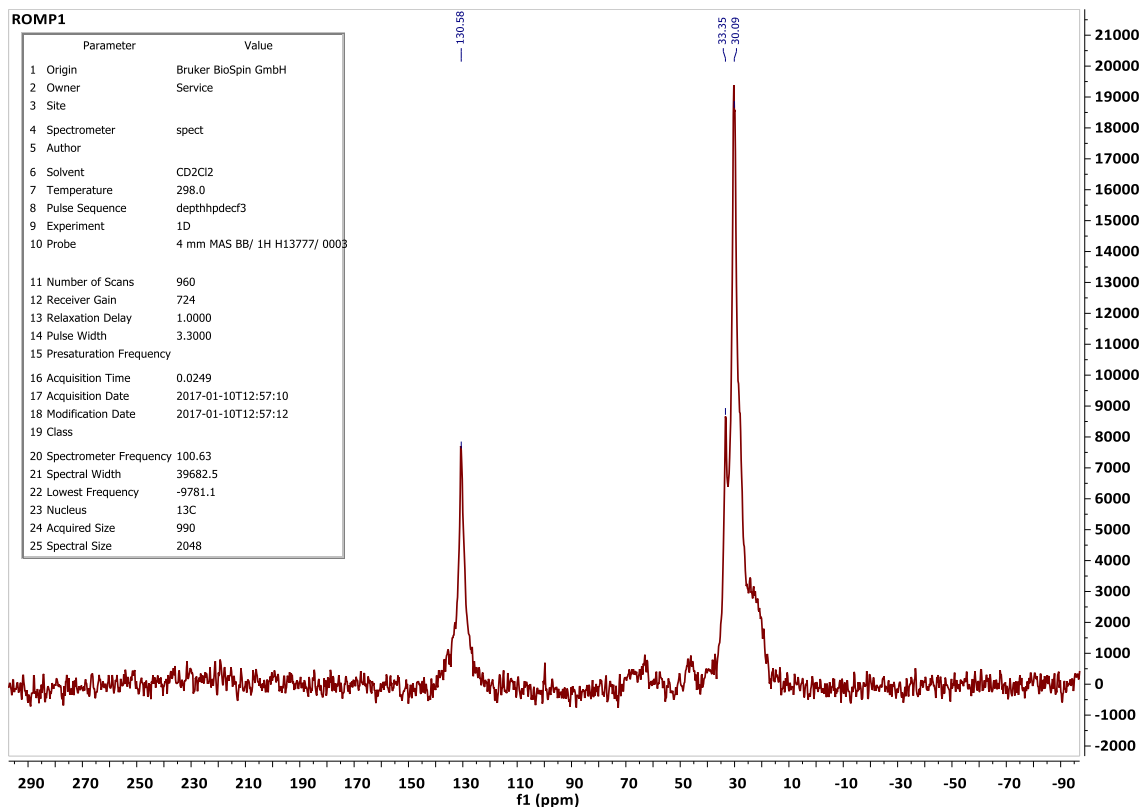
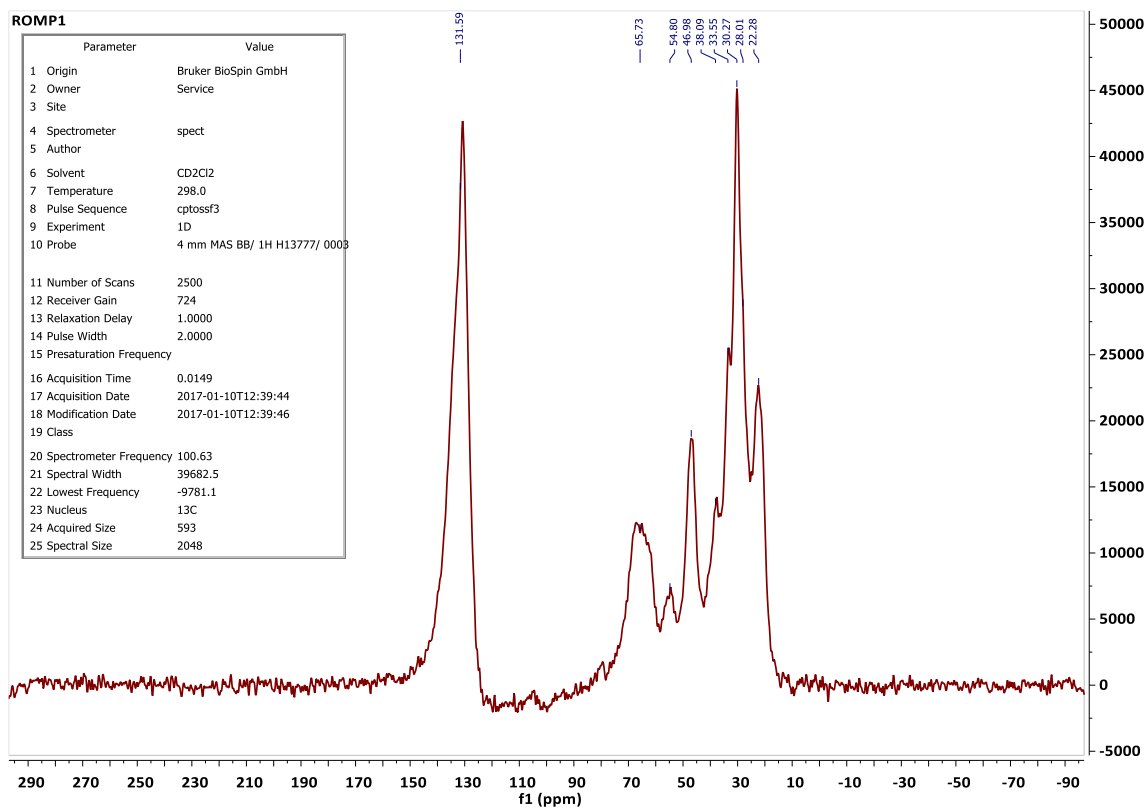


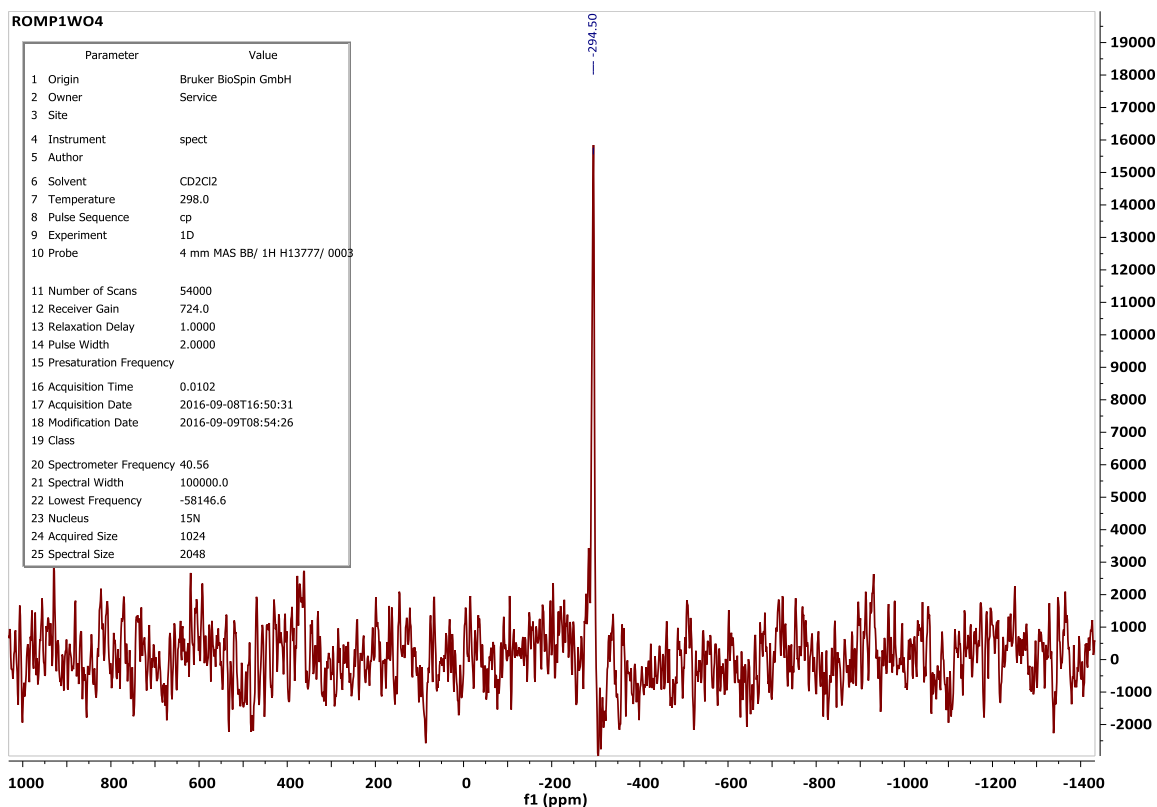
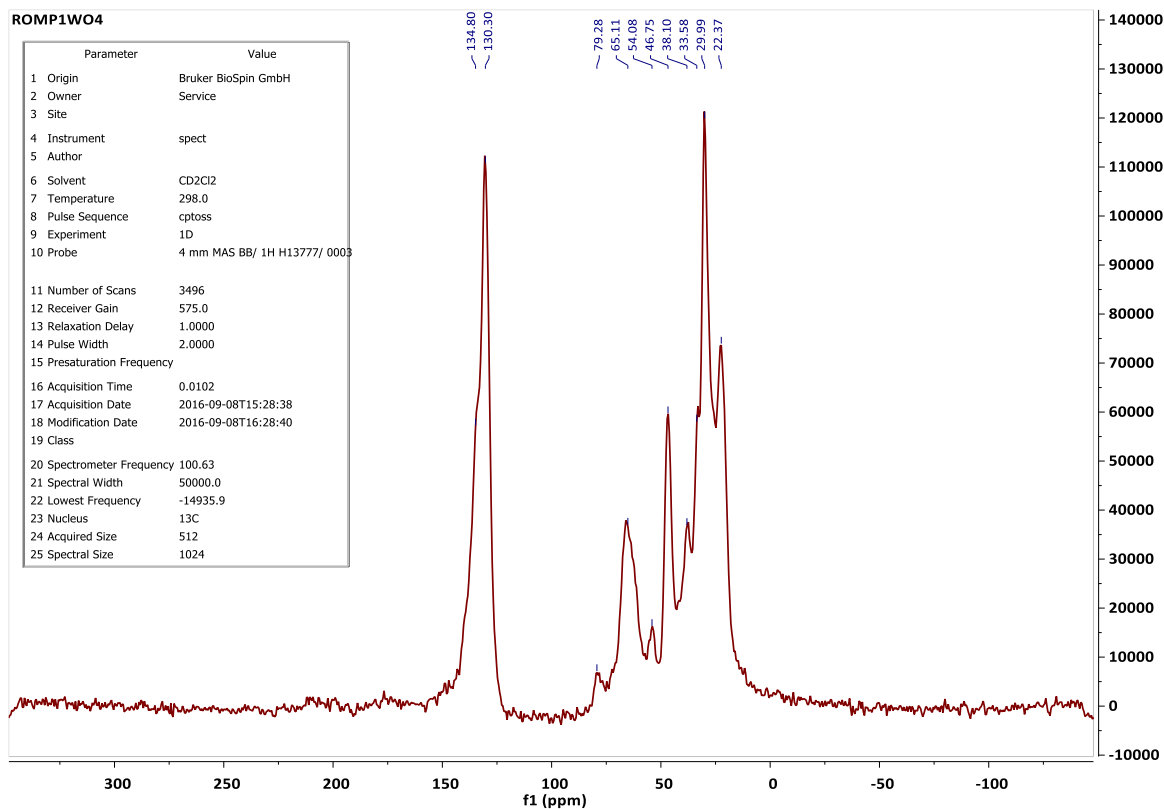
3.12 Proton NMR

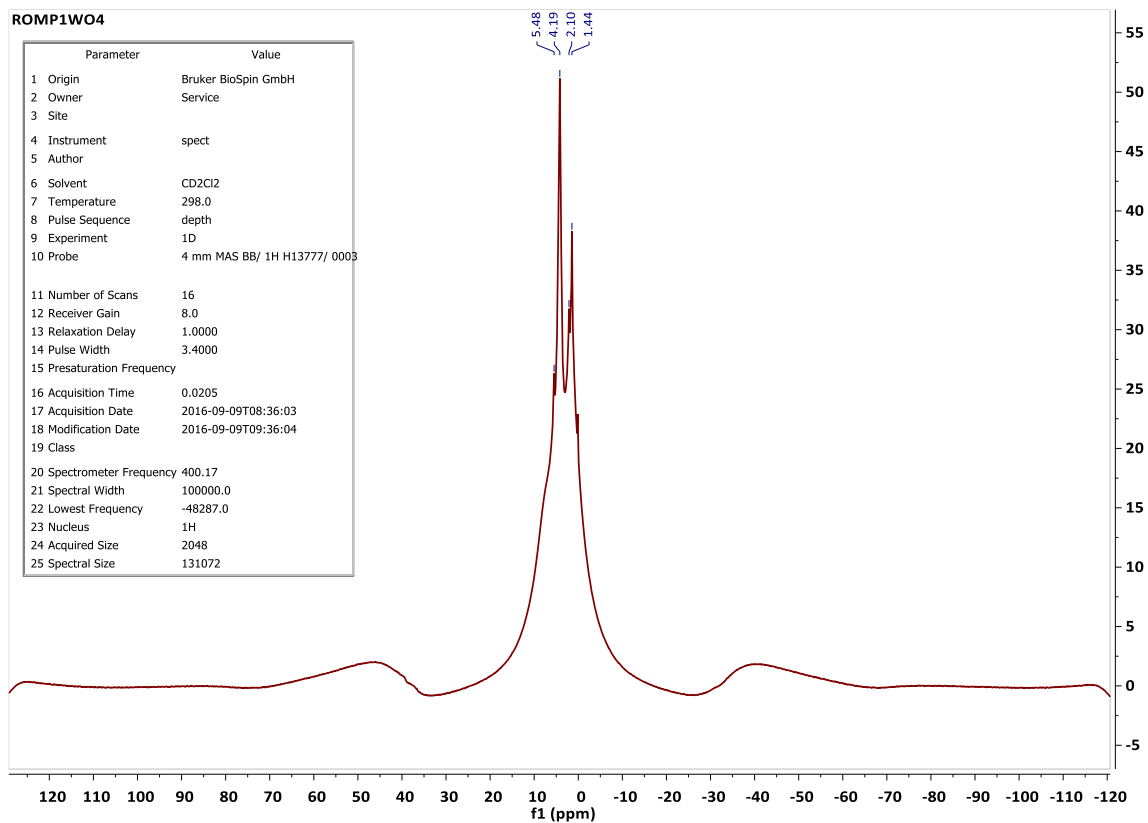
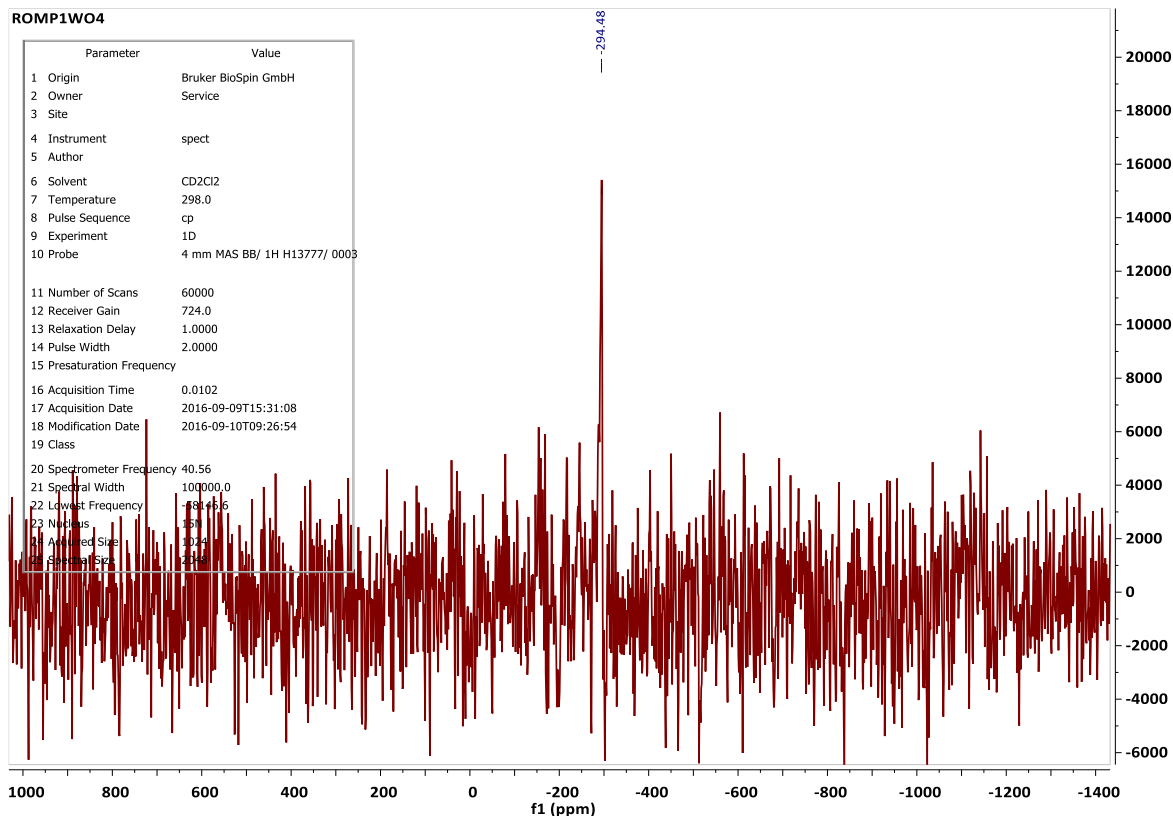


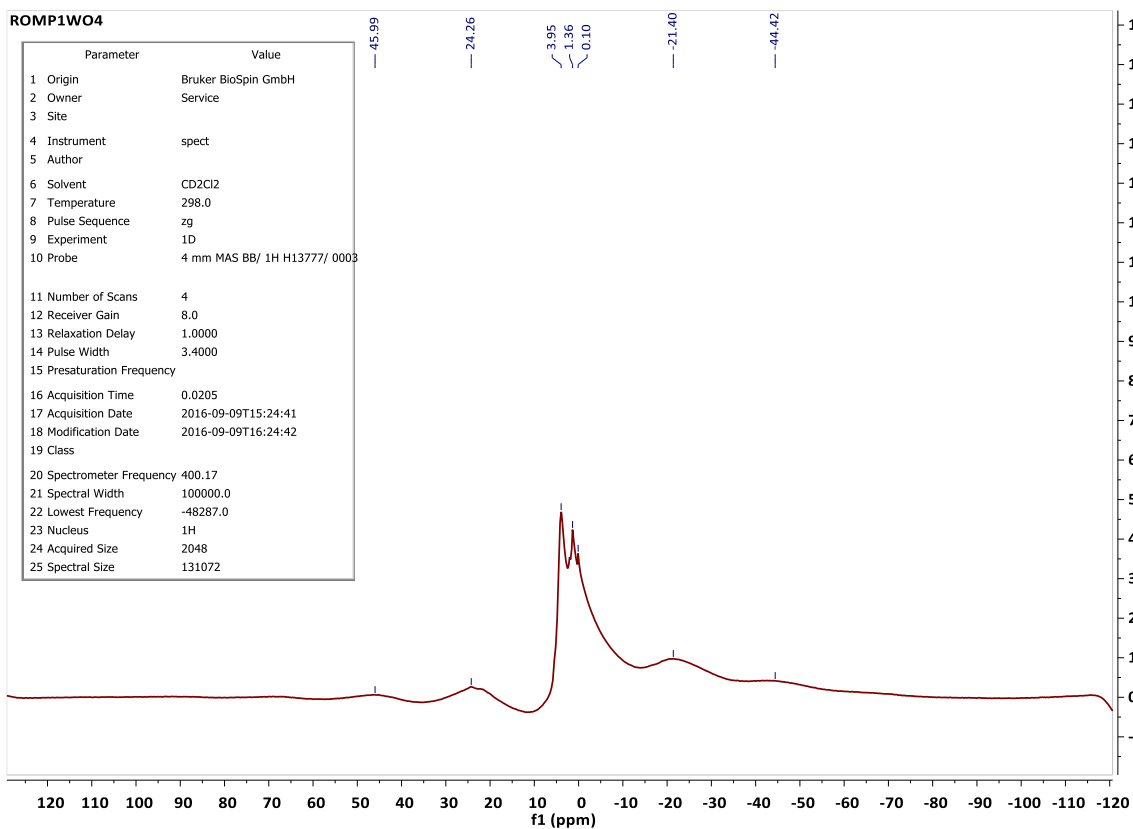
Appendix B. Solid-State Nuclear Magnetic Resonance (SSNMR)

1. ROMP1

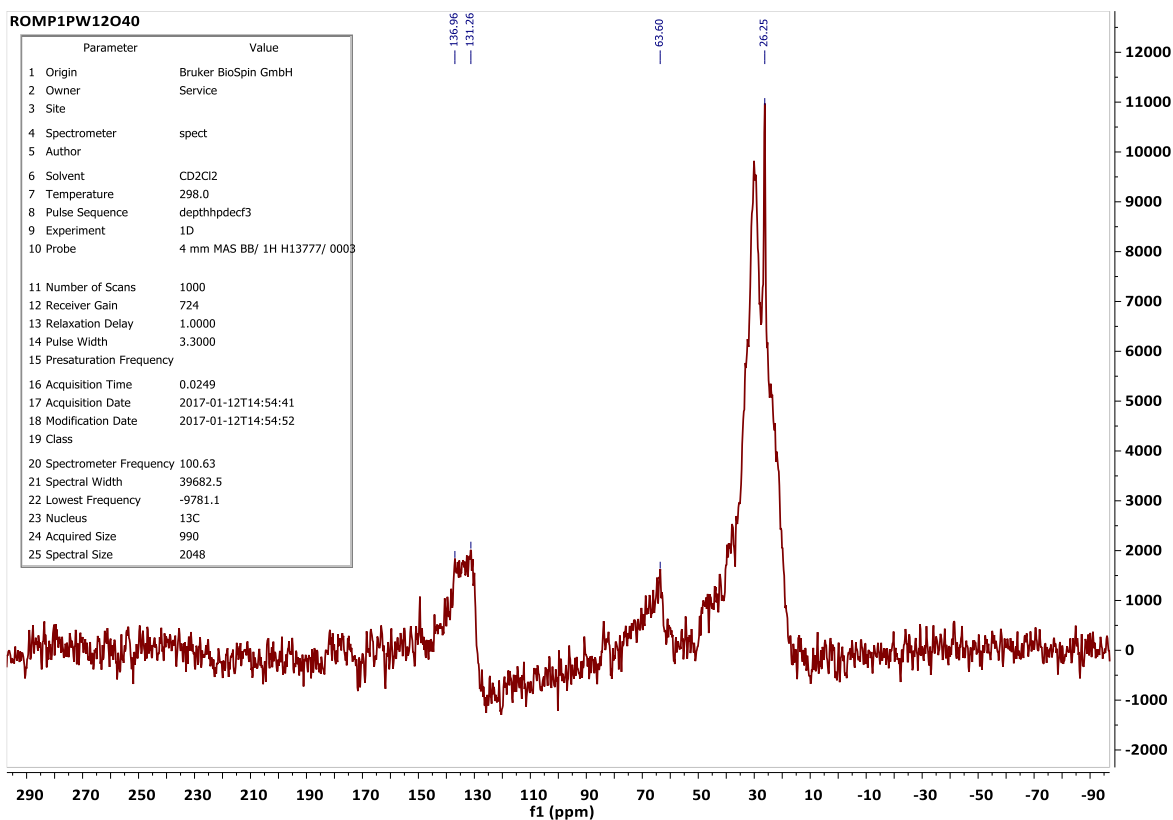


2. WO₄@ROMP₁

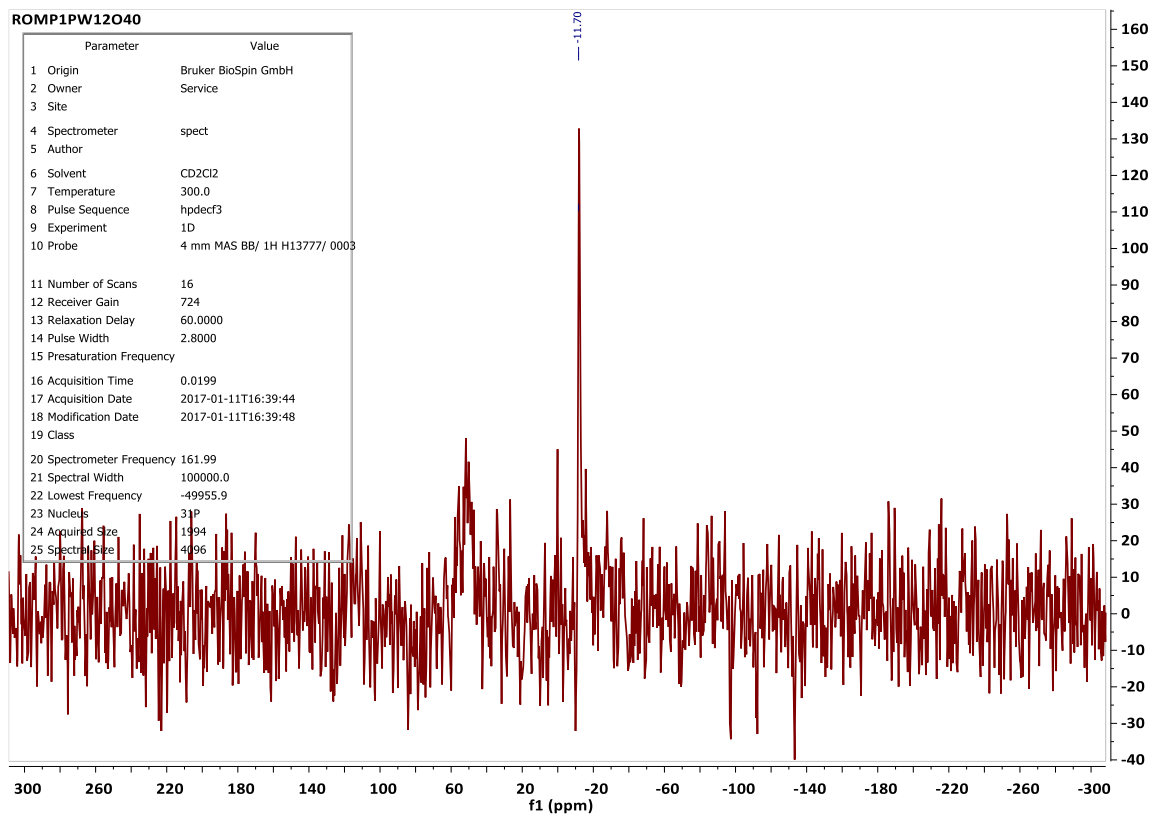
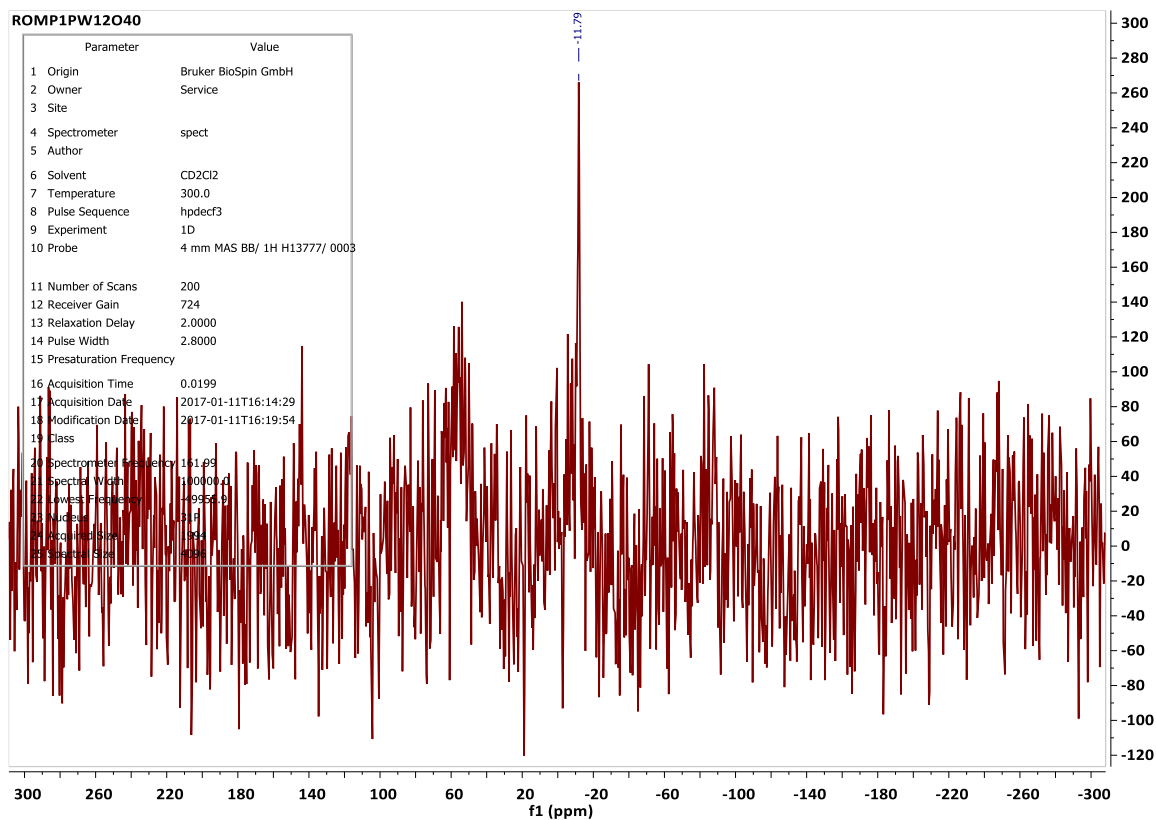


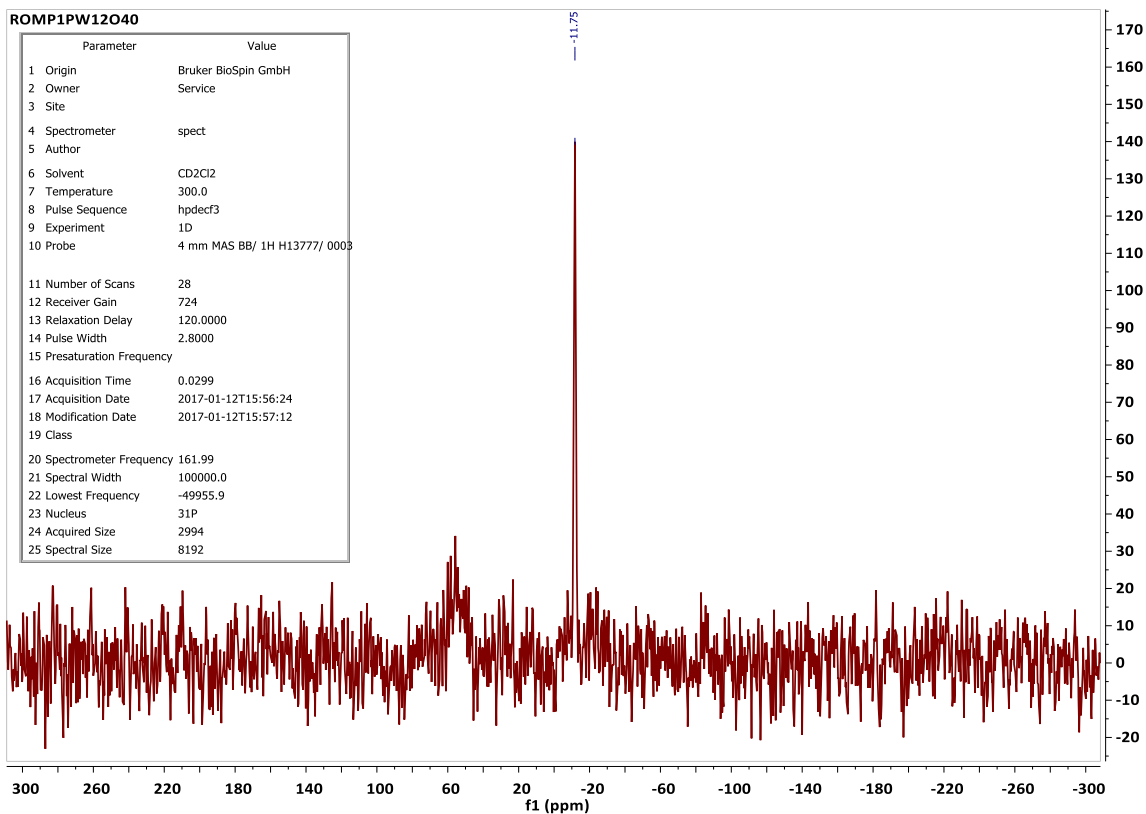
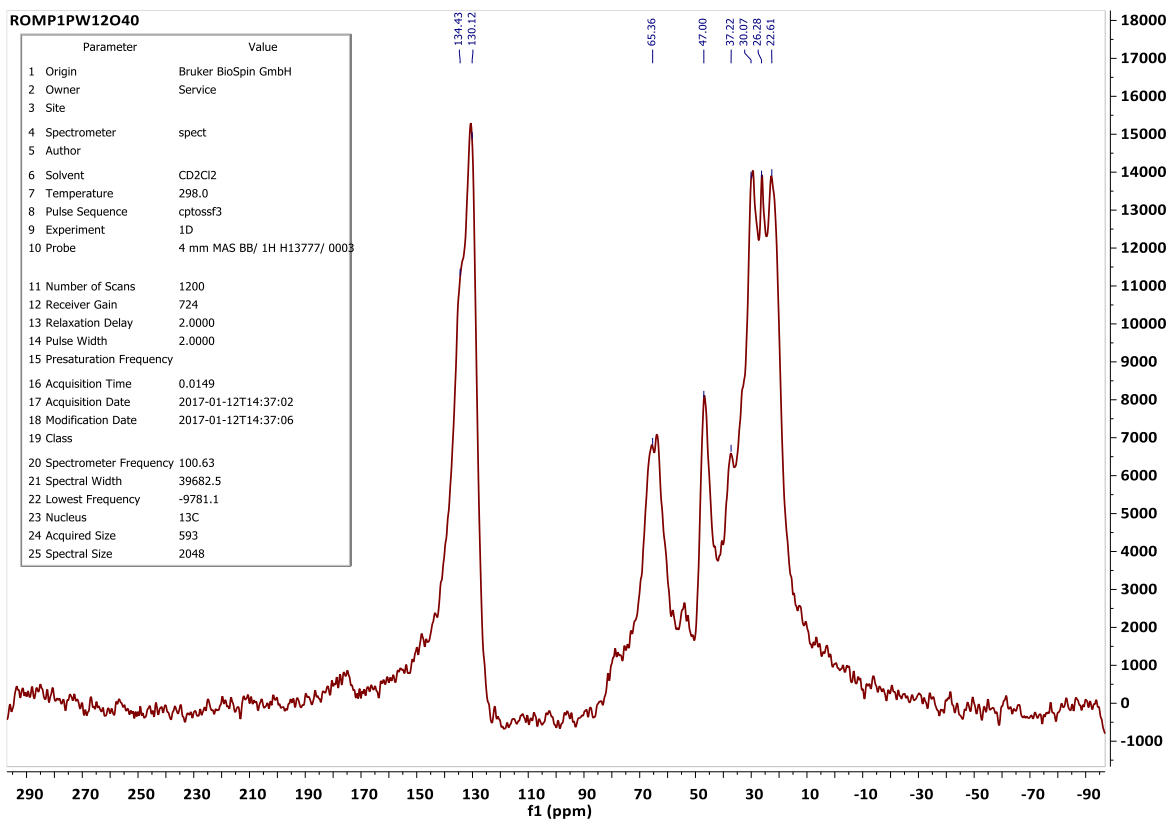


3. $PW_{12}O_{40}@ROMP_1$



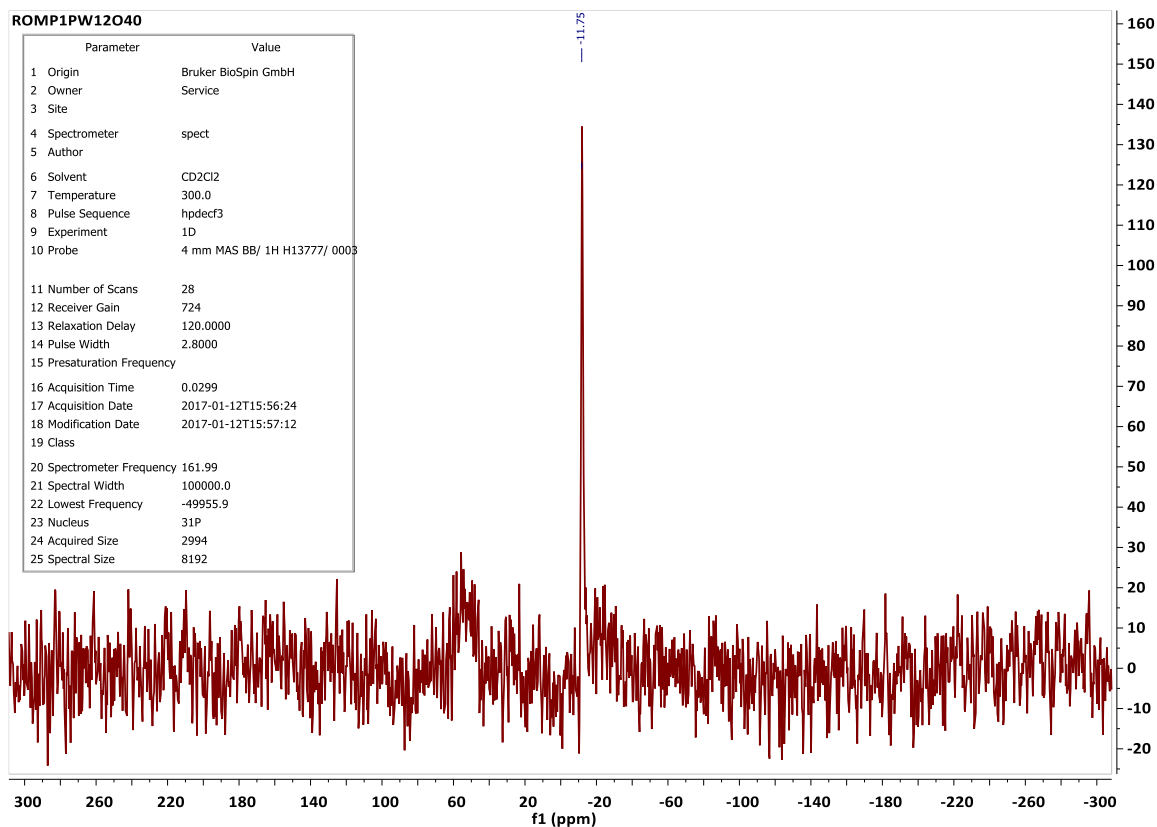
Appendices





ROMP1PW12O40

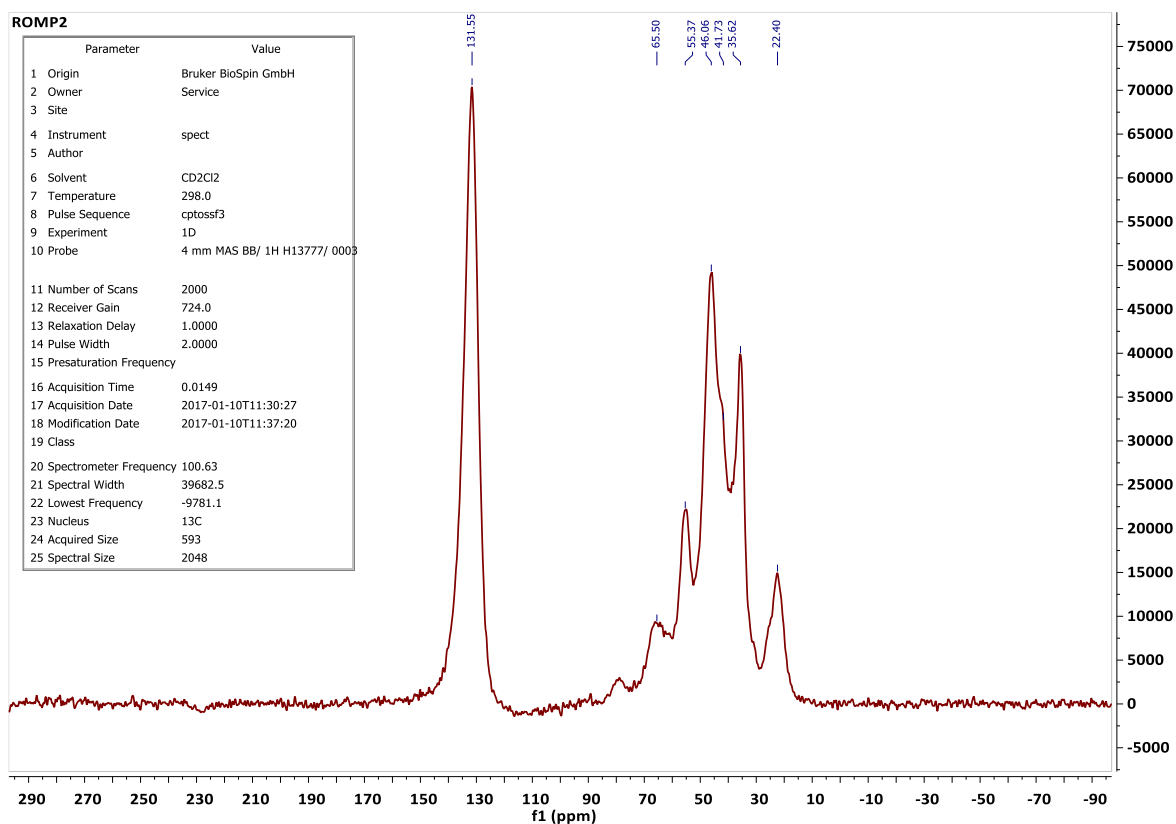
Parameter	Value
1 Origin	Bruker BioSpin GmbH
2 Owner	Service
3 Site	
4 Spectrometer	spect
5 Author	
6 Solvent	CD ₂ Cl ₂
7 Temperature	300.0
8 Pulse Sequence	hpdect3
9 Experiment	1D
10 Probe	4 mm MAS BB/ 1H H13777/ 0003
11 Number of Scans	28
12 Receiver Gain	724
13 Relaxation Delay	120.0000
14 Pulse Width	2.8000
15 Presaturation Frequency	
16 Acquisition Time	0.0299
17 Acquisition Date	2017-01-12T15:56:24
18 Modification Date	2017-01-12T15:57:12
19 Class	
20 Spectrometer Frequency	161.99
21 Spectral Width	100000.0
22 Lowest Frequency	-49955.9
23 Nucleus	31P
24 Acquired Size	2994
25 Spectral Size	8192

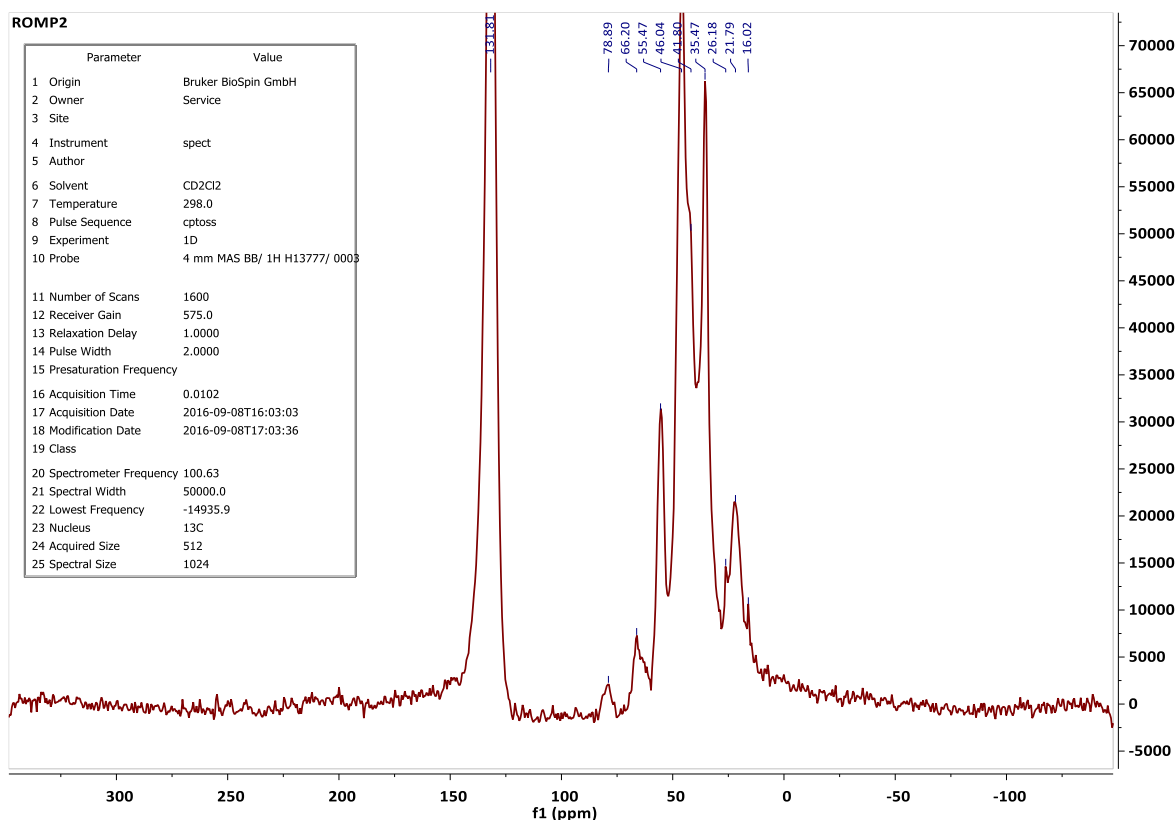
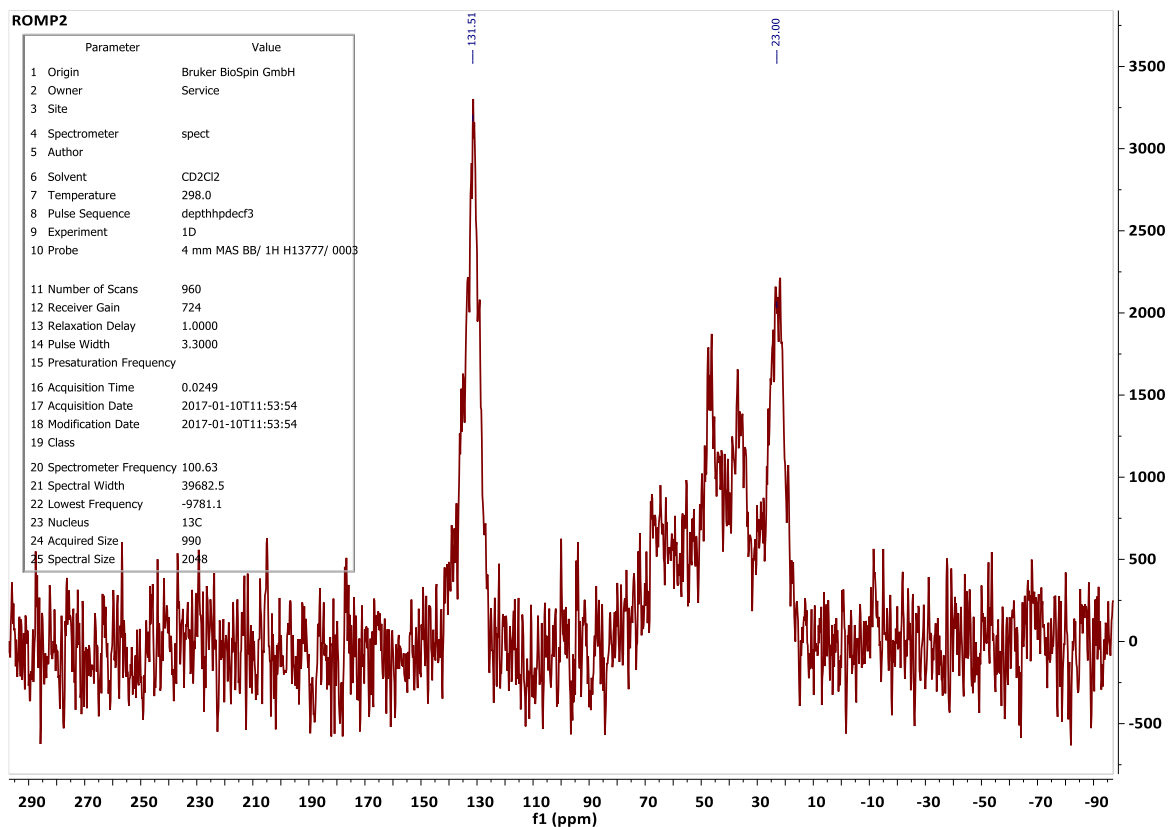


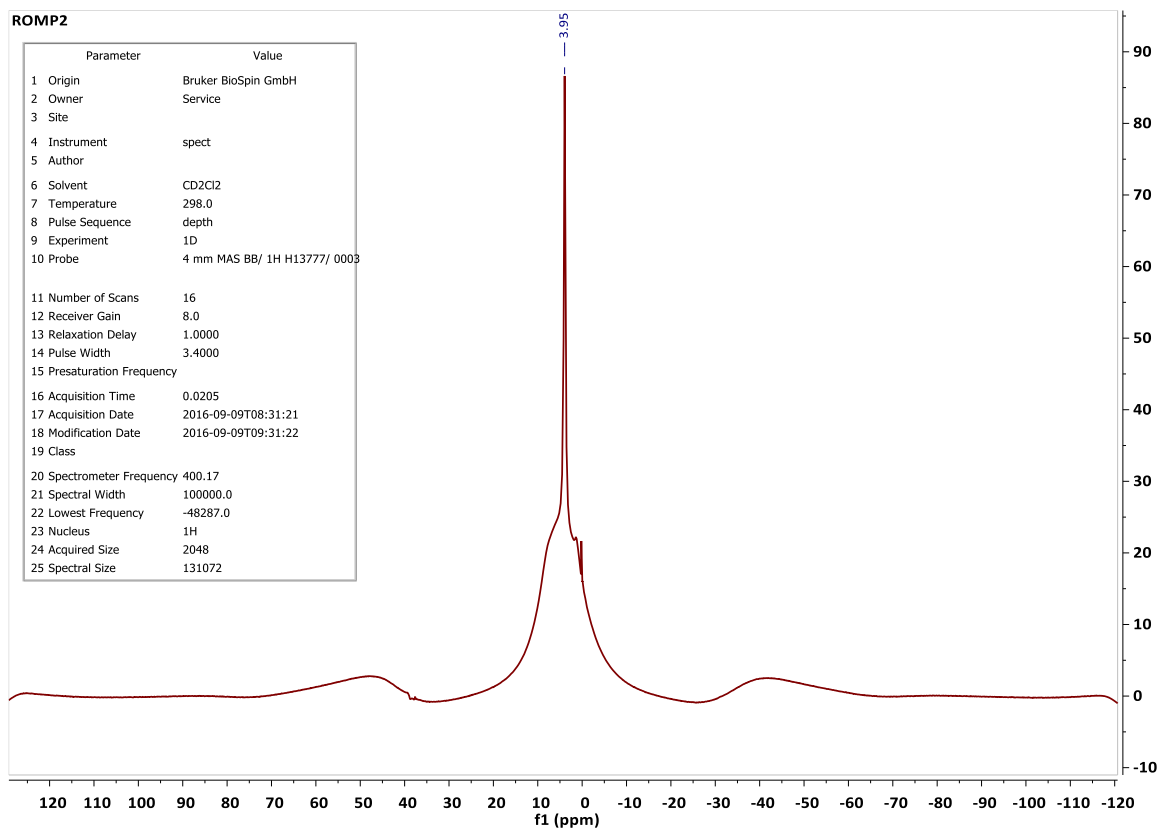
4. ROMP₂

ROMP2

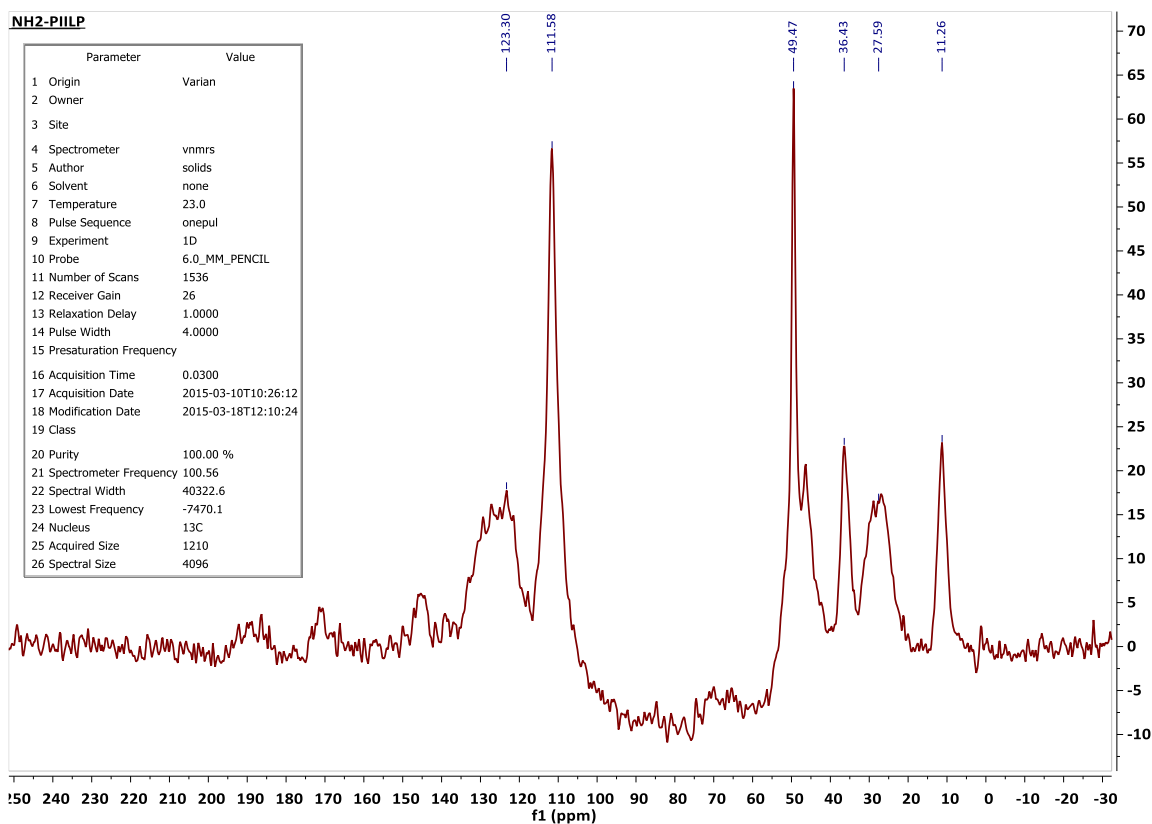
Parameter	Value
1 Origin	Bruker BioSpin GmbH
2 Owner	Service
3 Site	
4 Instrument	spect
5 Author	
6 Solvent	CD ₂ Cl ₂
7 Temperature	298.0
8 Pulse Sequence	cptossf3
9 Experiment	1D
10 Probe	4 mm MAS BB/ 1H H13777/ 0003
11 Number of Scans	2000
12 Receiver Gain	724.0
13 Relaxation Delay	1.0000
14 Pulse Width	2.0000
15 Presaturation Frequency	
16 Acquisition Time	0.0149
17 Acquisition Date	2017-01-10T11:30:27
18 Modification Date	2017-01-10T11:37:20
19 Class	
20 Spectrometer Frequency	100.63
21 Spectral Width	39682.5
22 Lowest Frequency	-9781.1
23 Nucleus	13C
24 Acquired Size	593
25 Spectral Size	2048

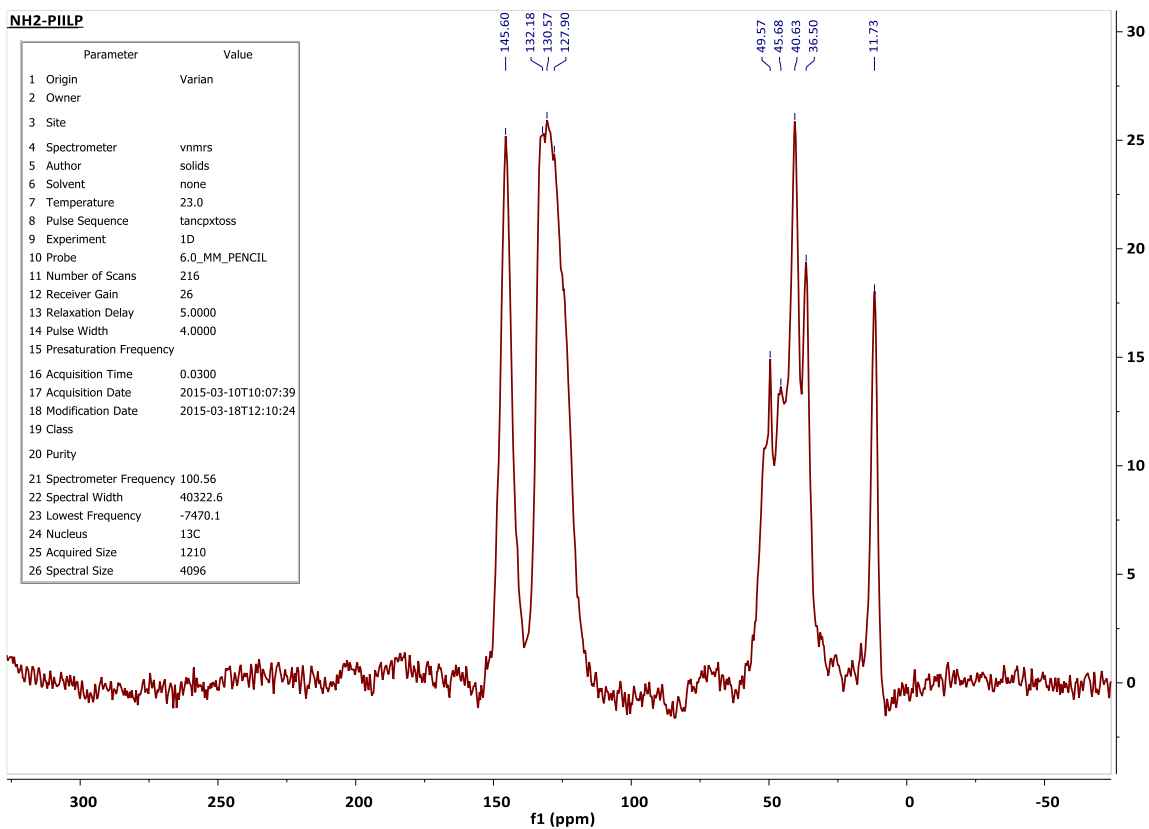




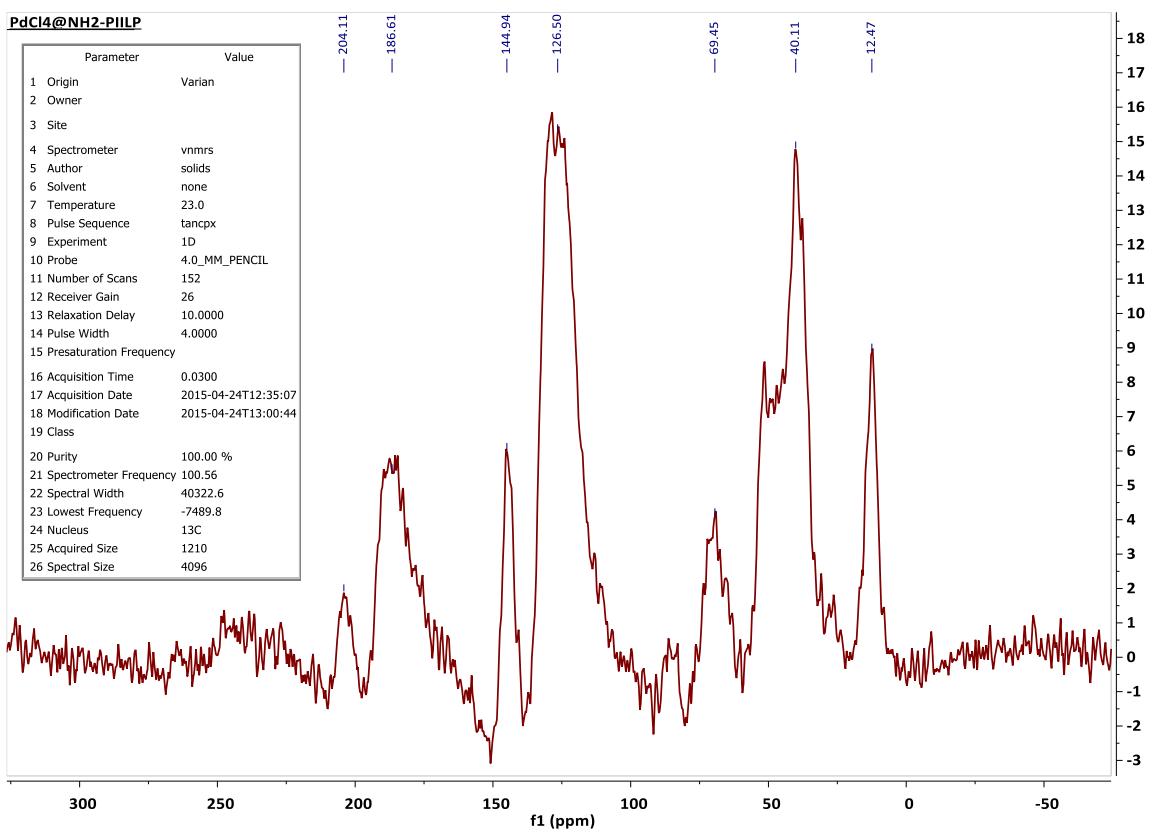


5. $\text{NH}_2\text{-PIILP}$

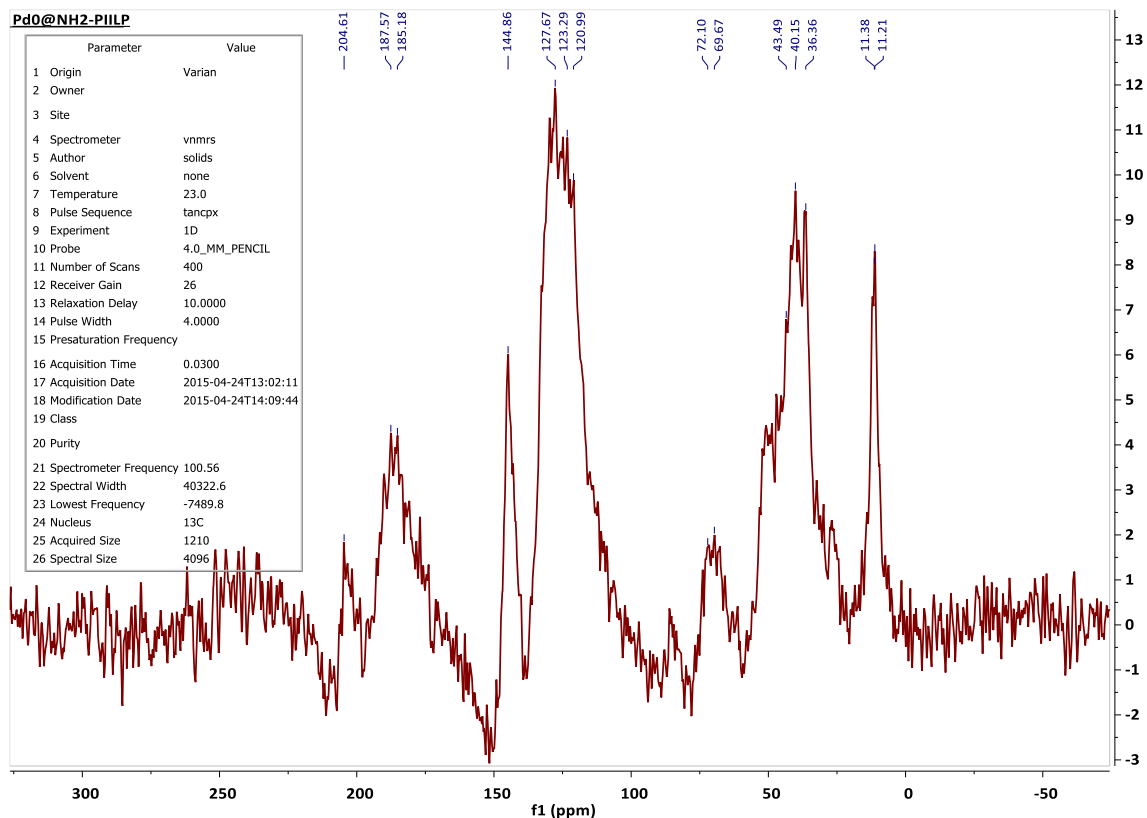




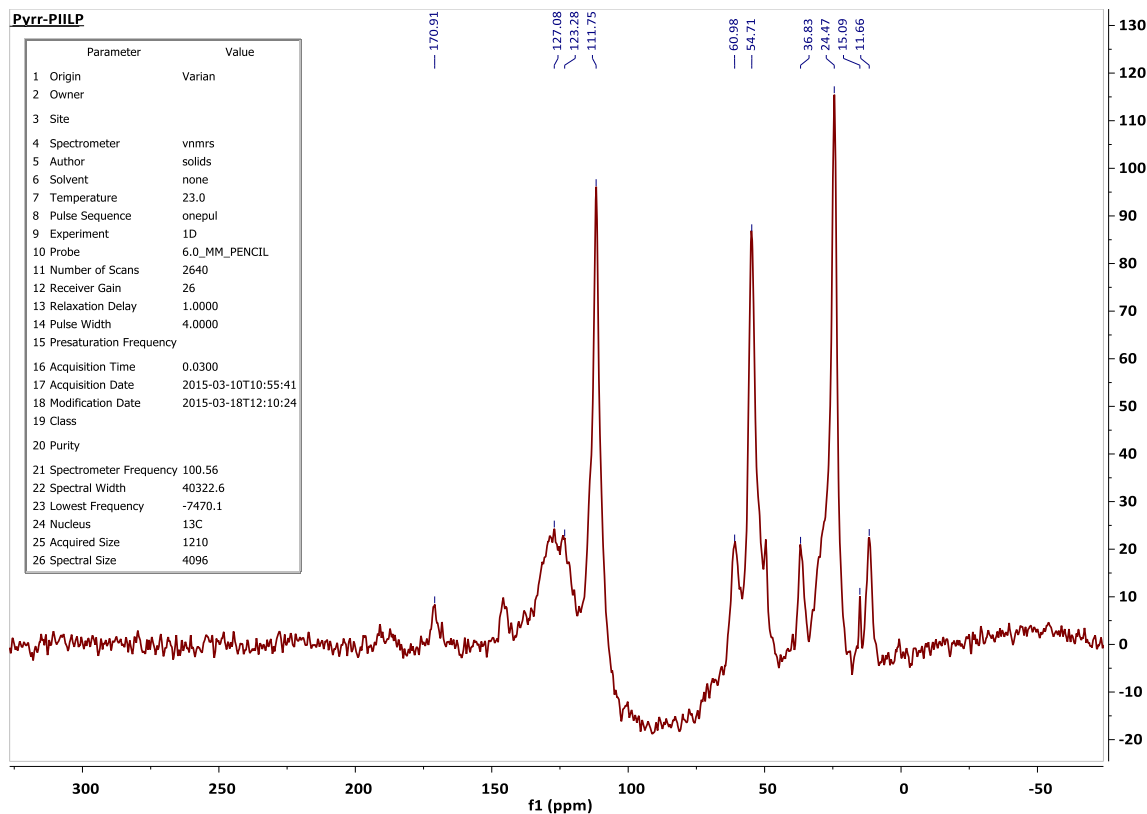
6. PdCl₄@NH₂-PIILP

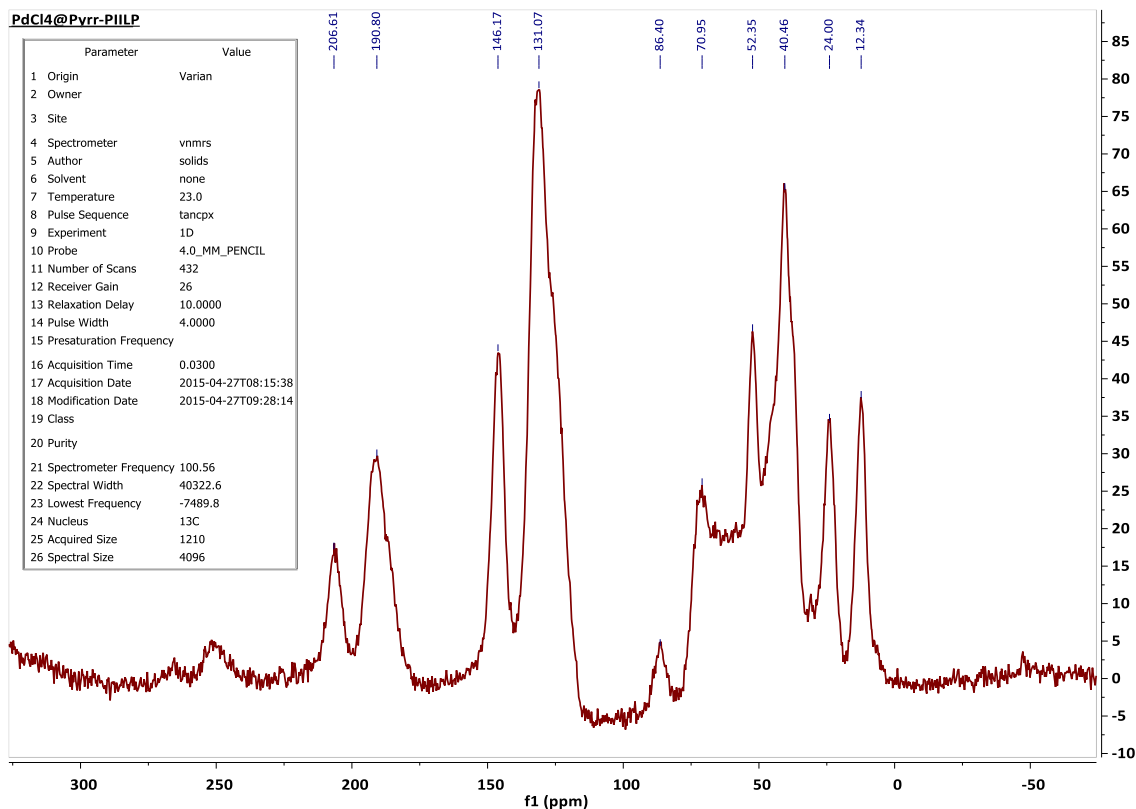
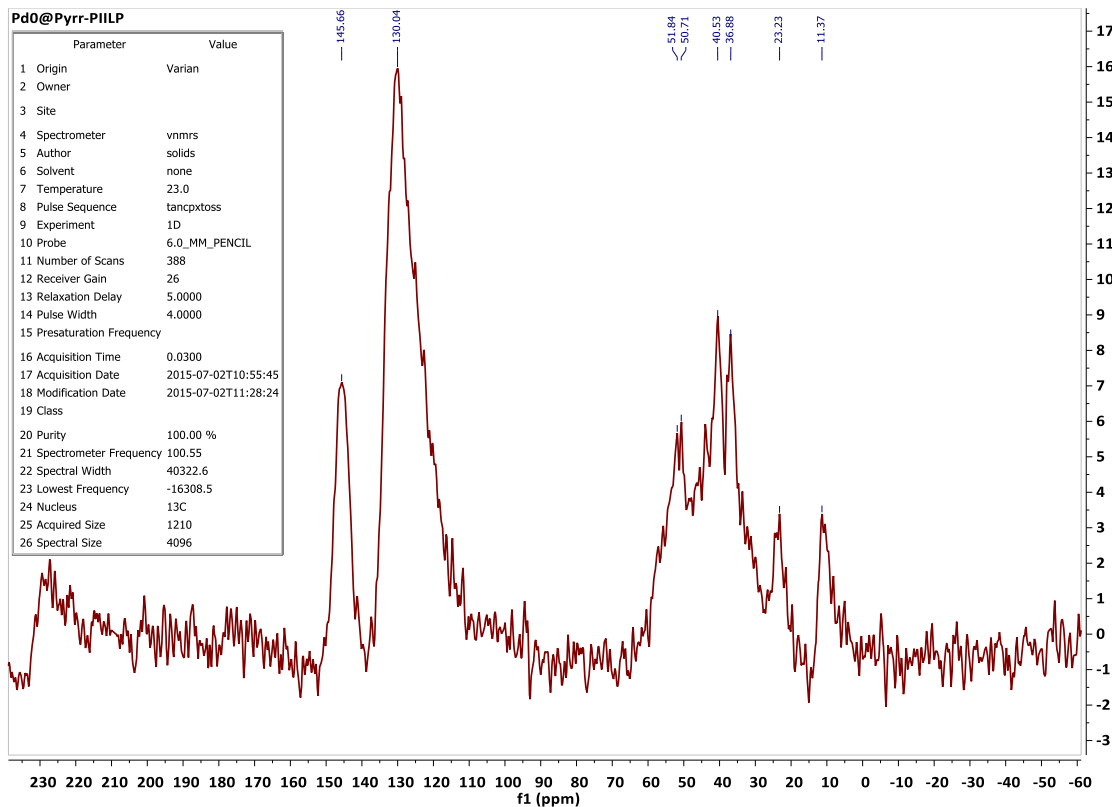


7. PdNP@NH₂-PIILP

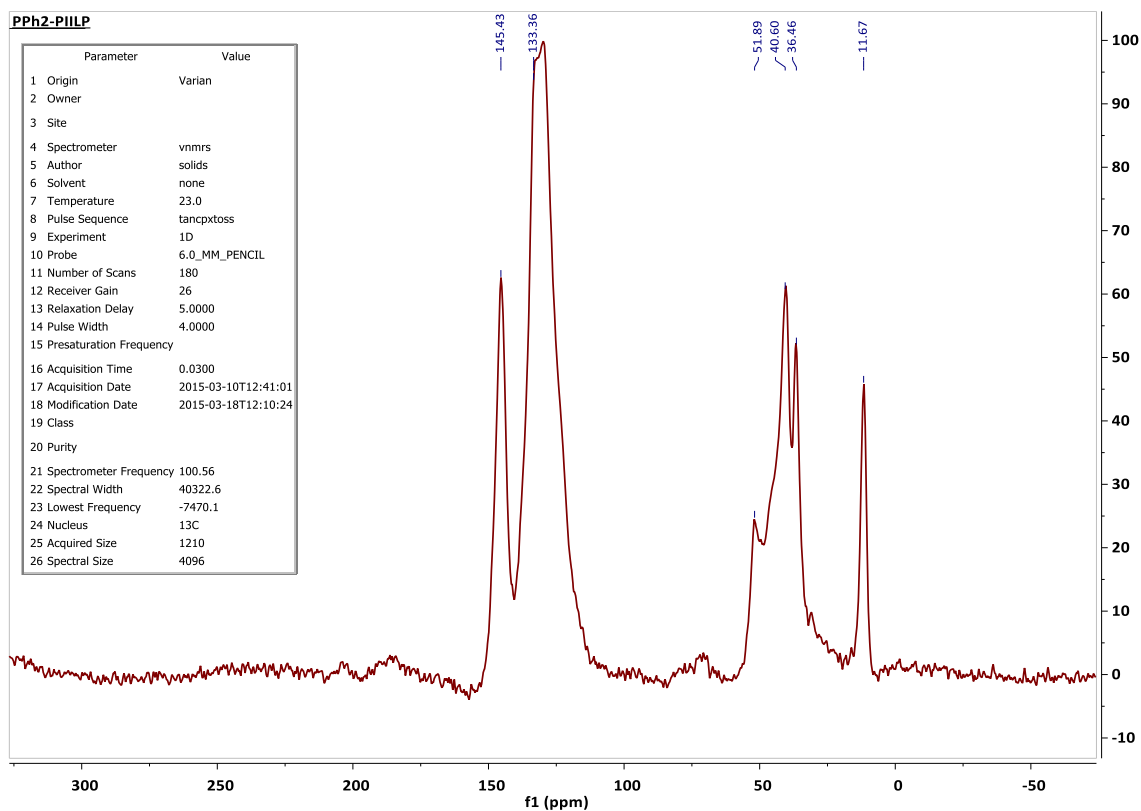
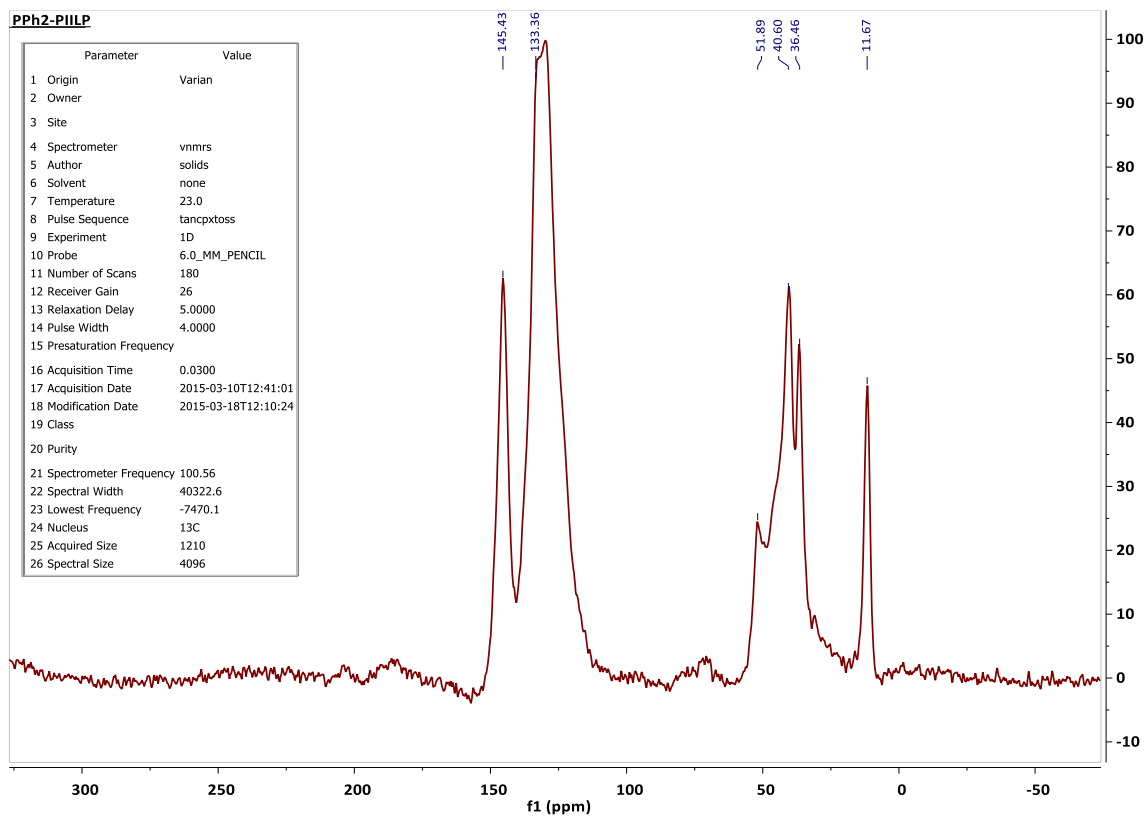


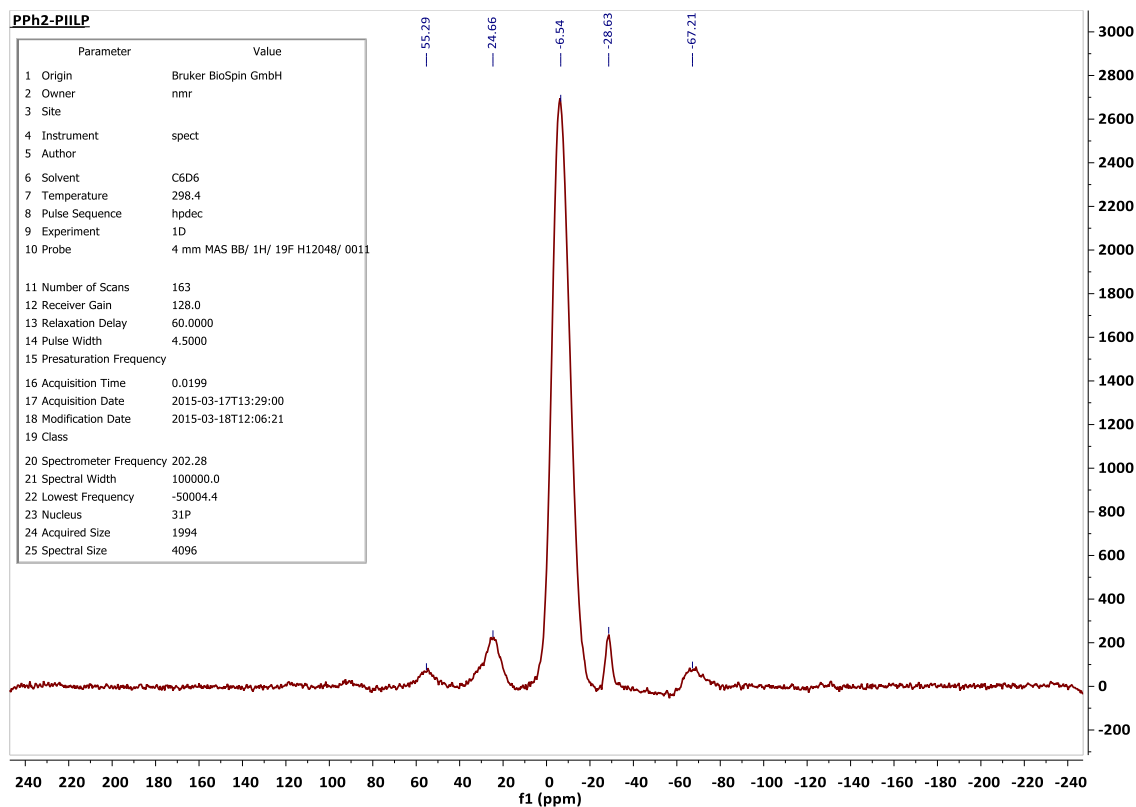
8. Pyrr-PIILP



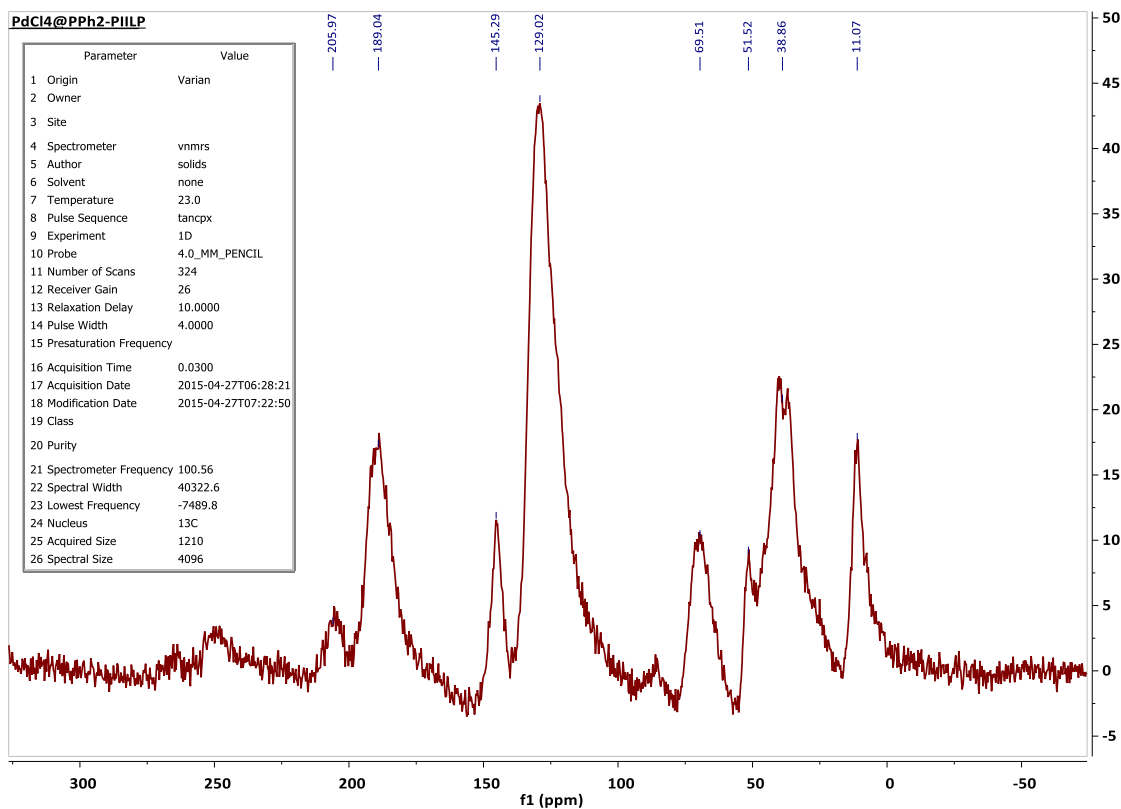
9. $\text{PdCl}_4\text{@Pyrr-PIILP}$ 10. PdNP@Pyrr-PIILP 

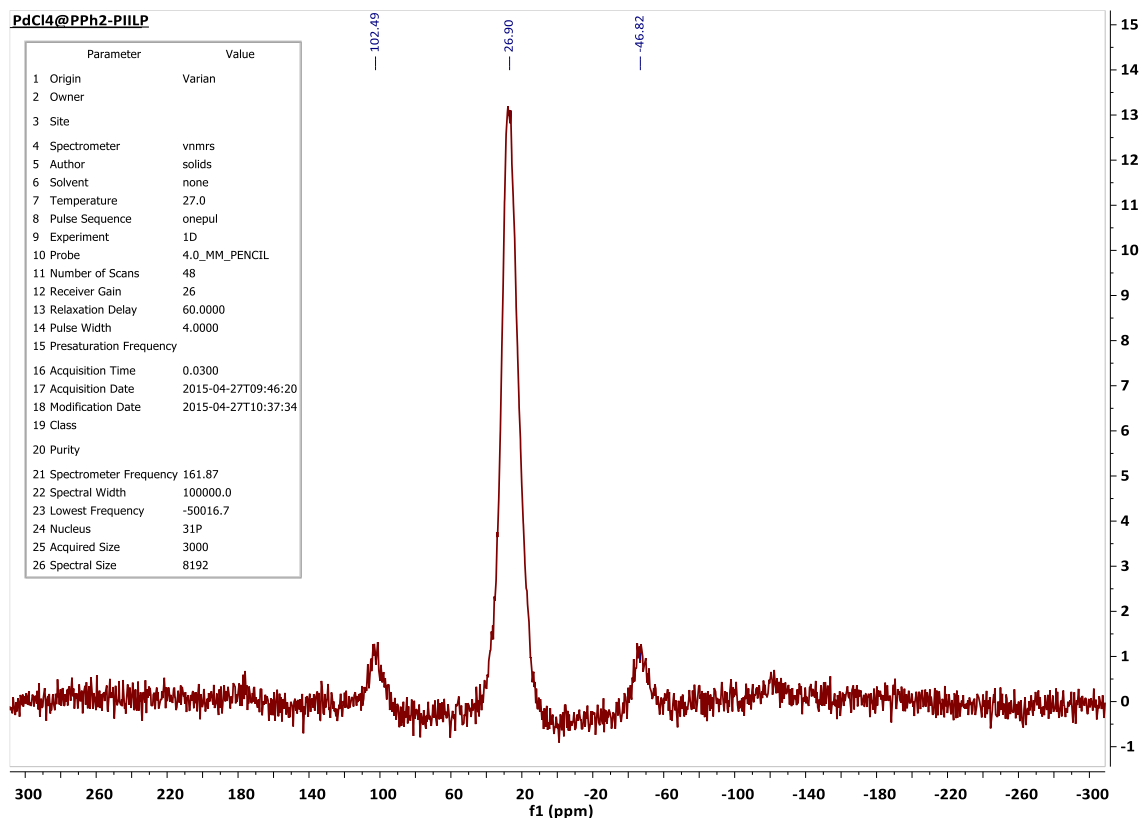
11.PPh₂-PIILP



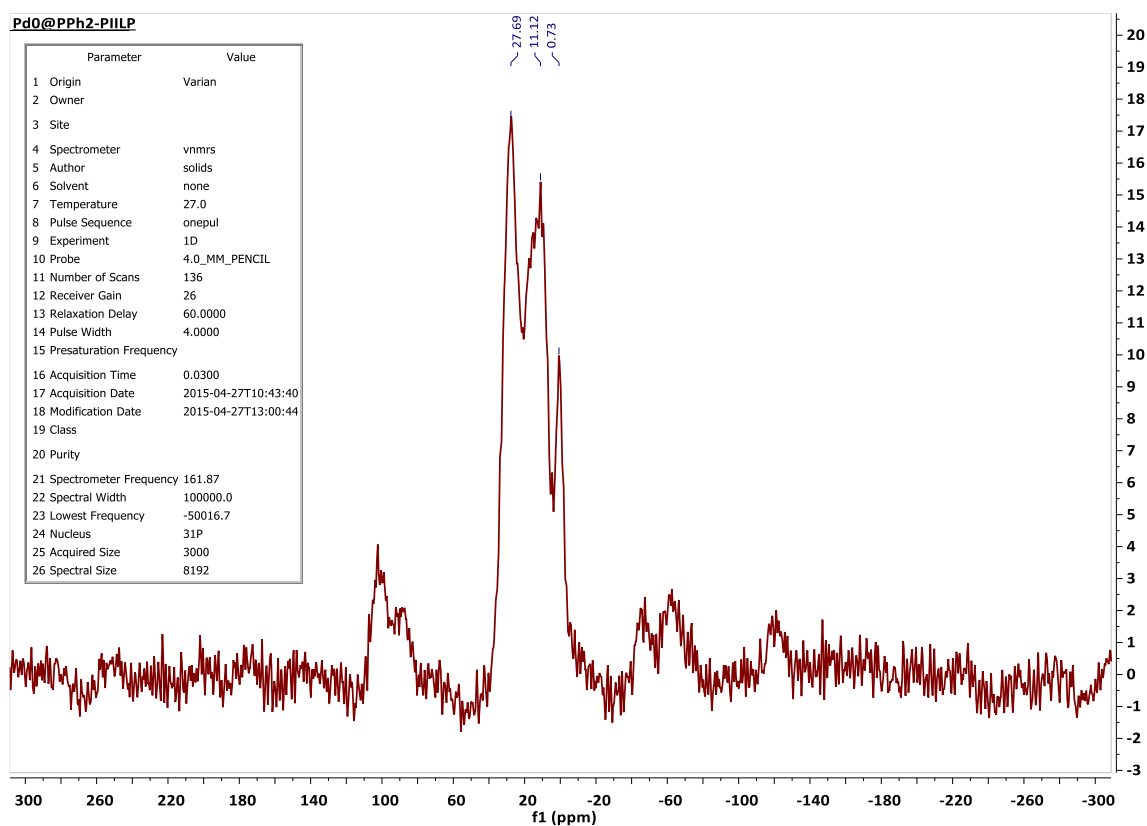


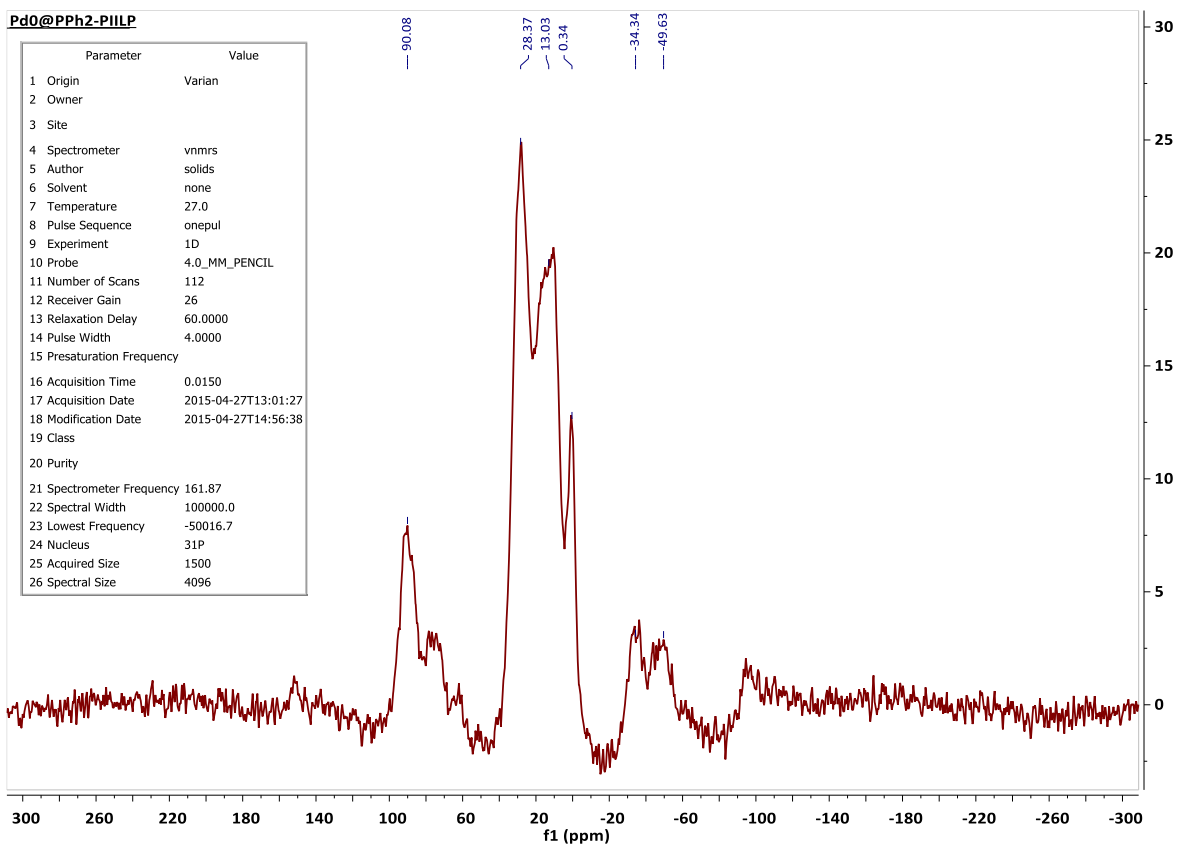
12. PdCl₄@PPh₂-PIILP



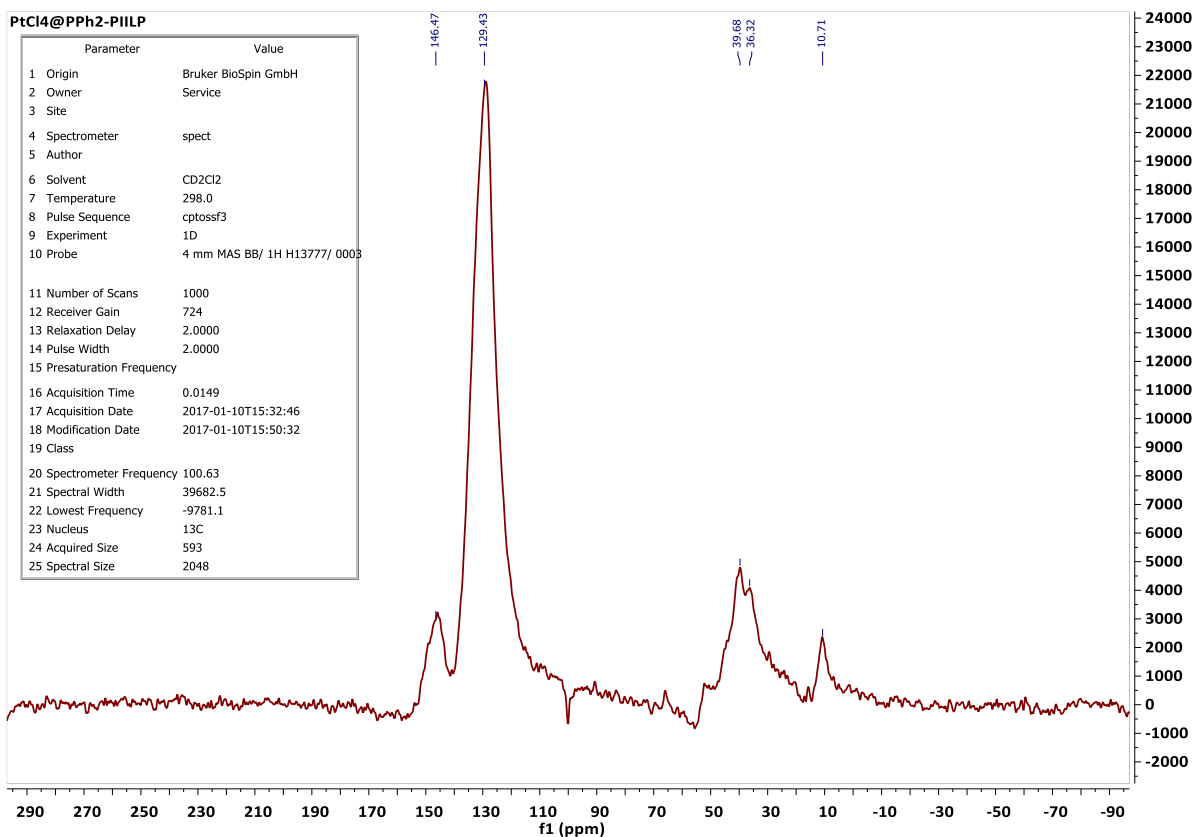


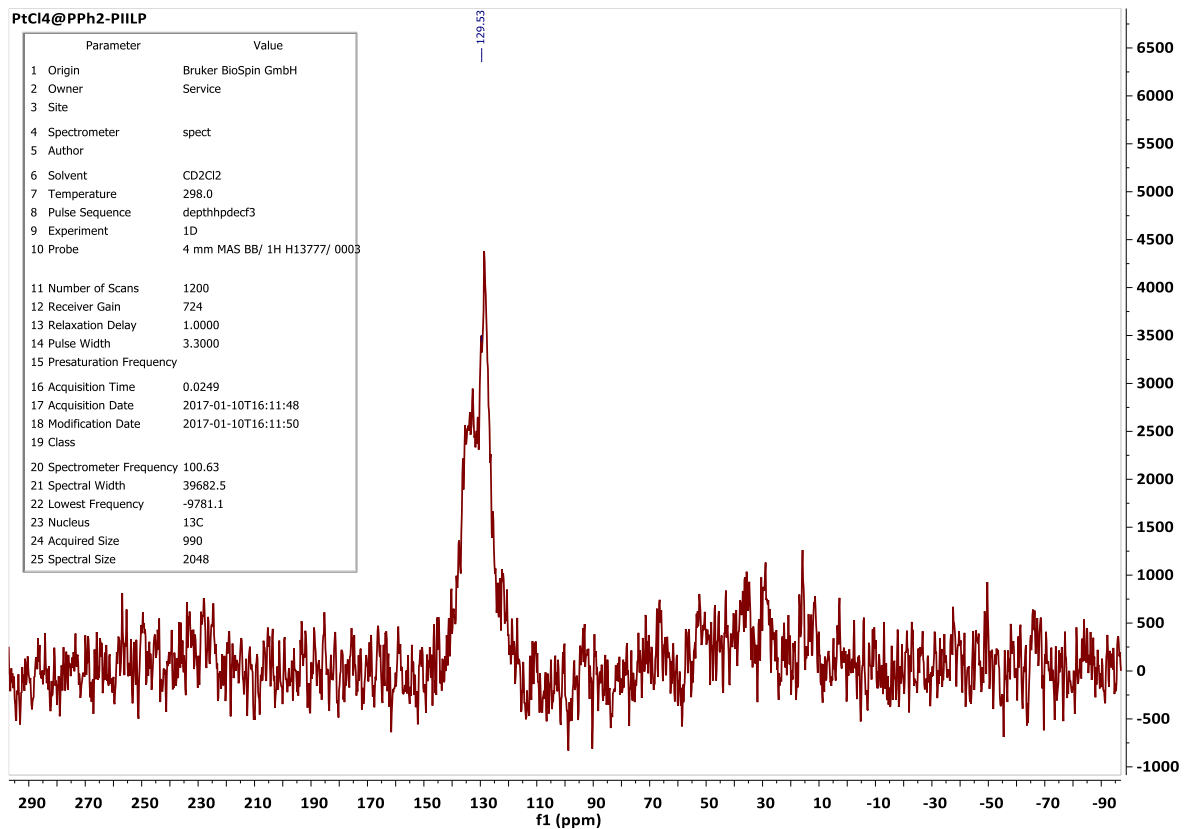
13. PdNP@PPh₂-PIILP



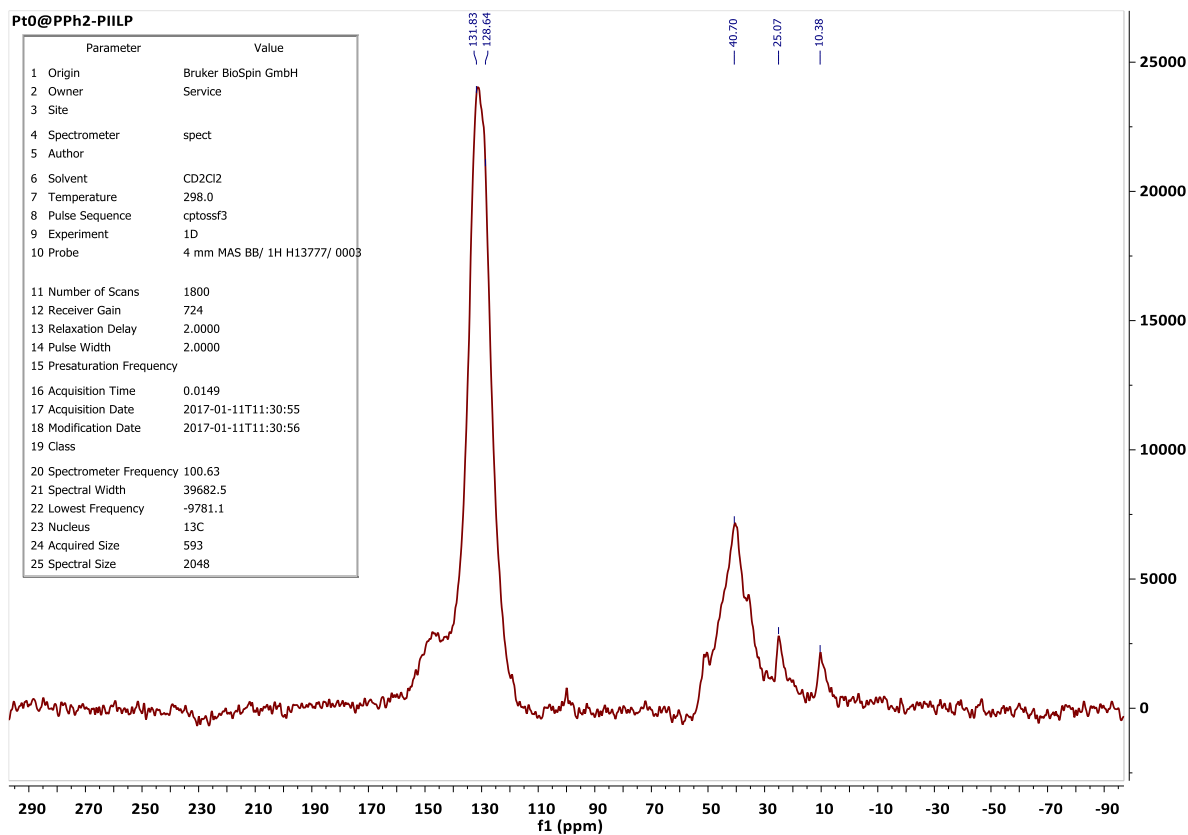


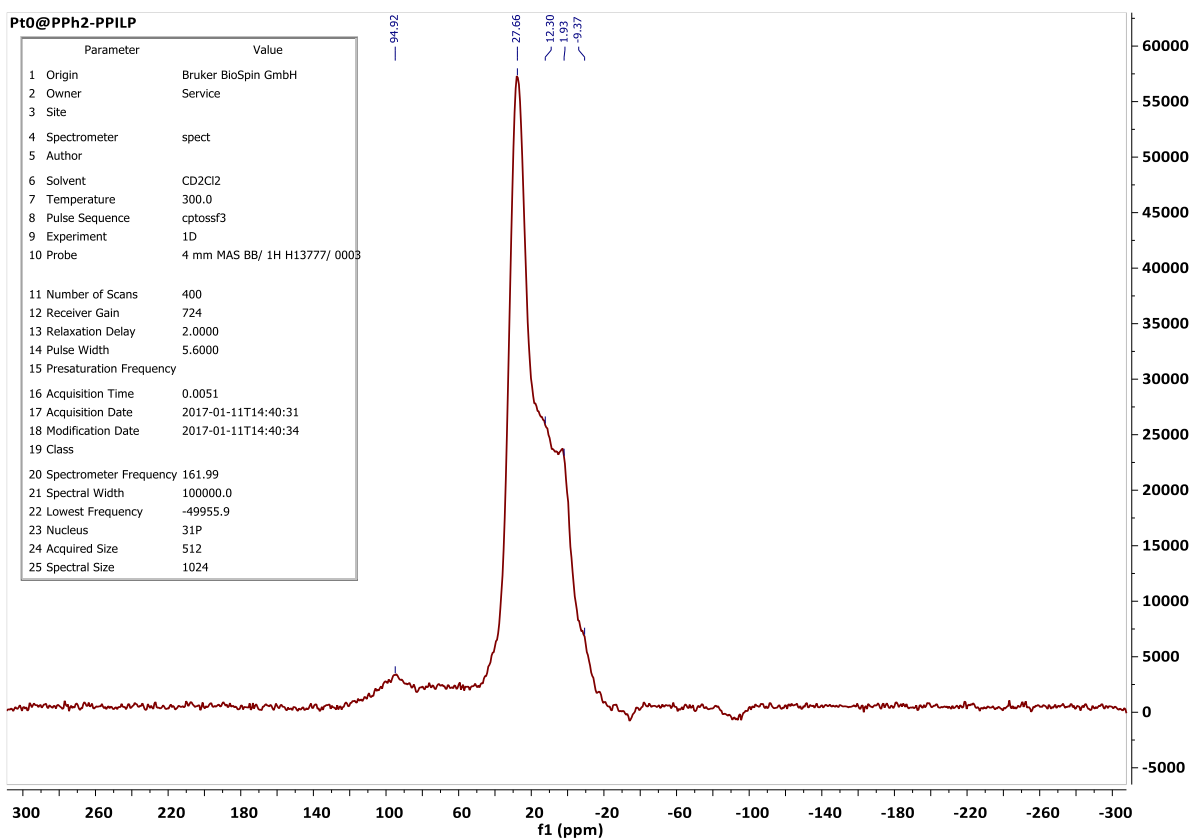
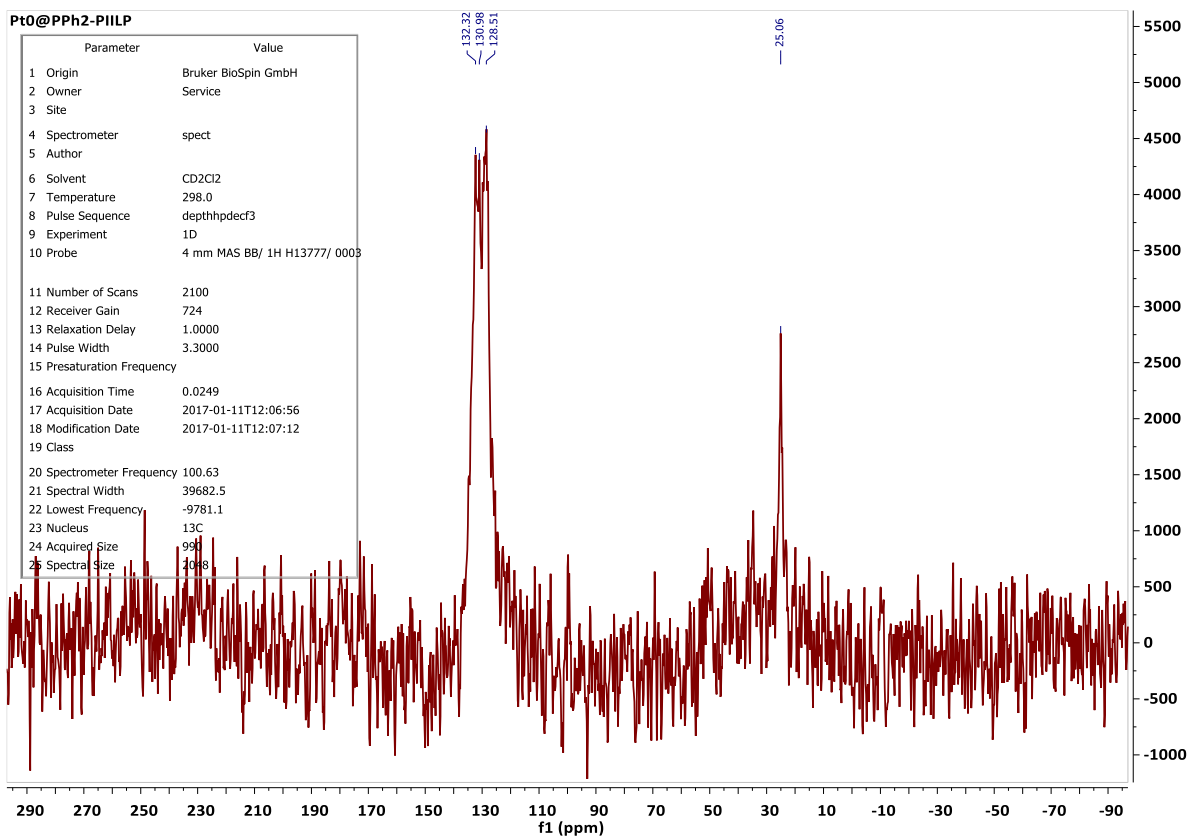
14. PtCl₄@PPh₂-PIILP





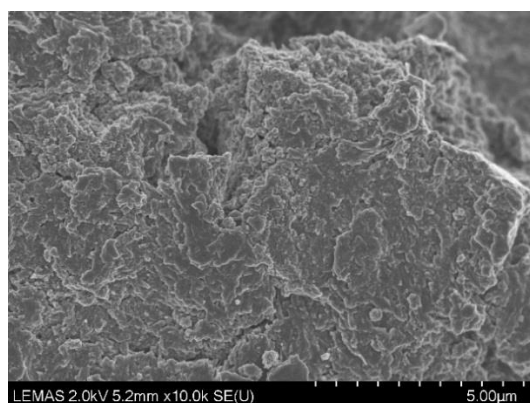
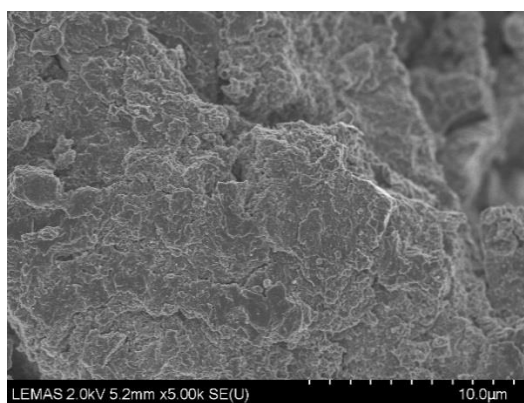
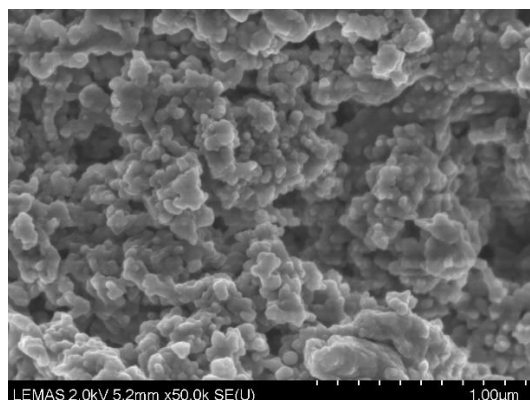
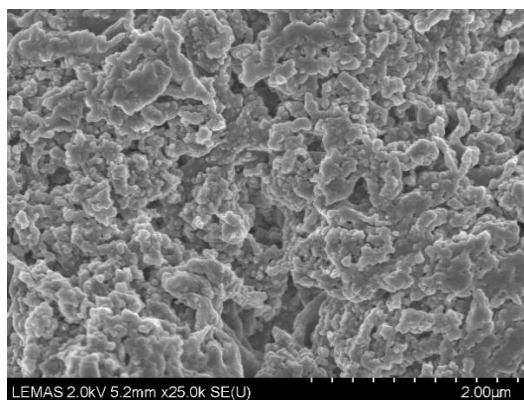
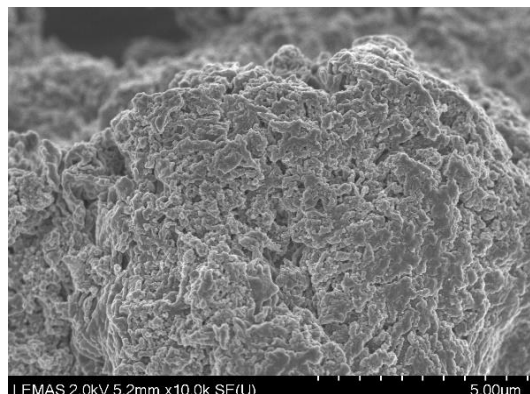
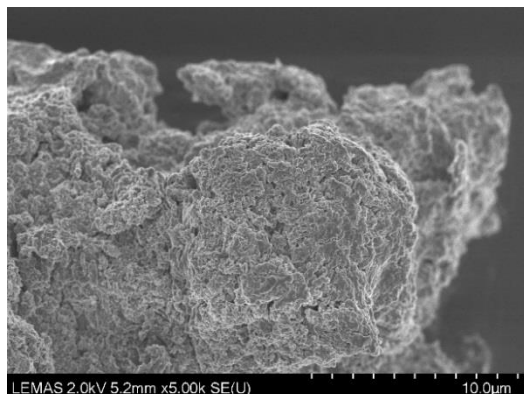
15. PtNP@PPh₂-PIILP

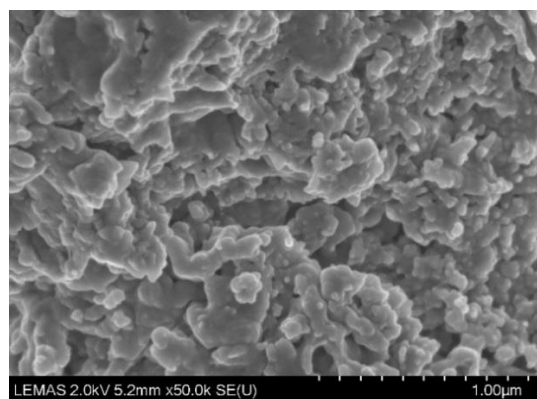
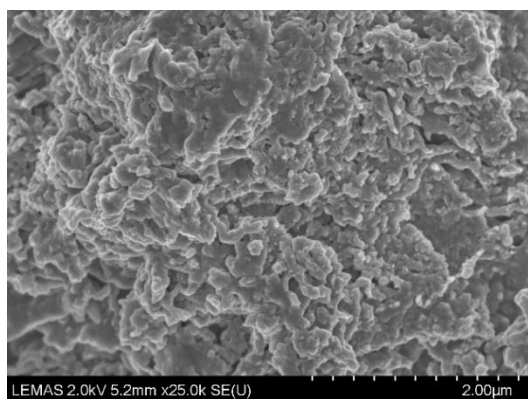
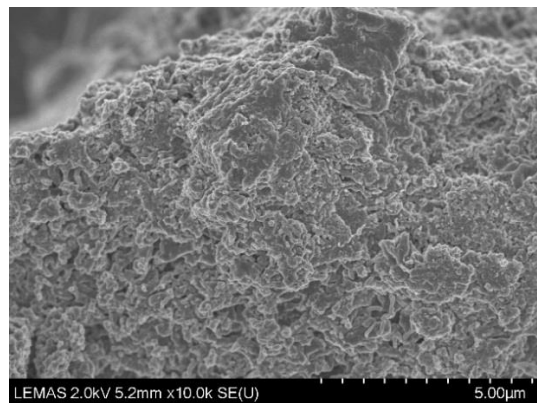
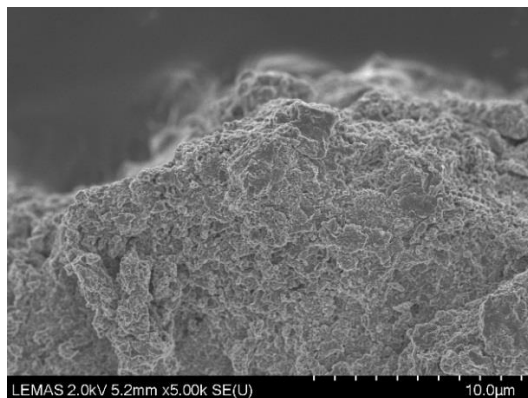
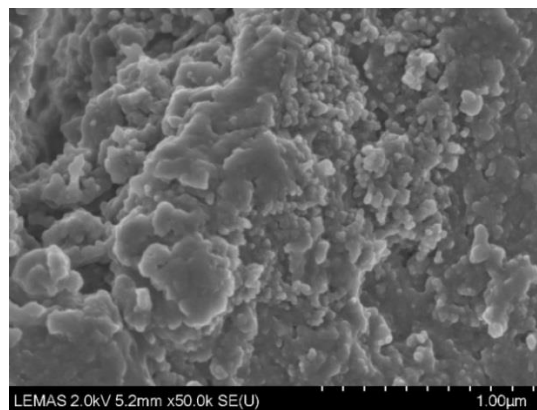
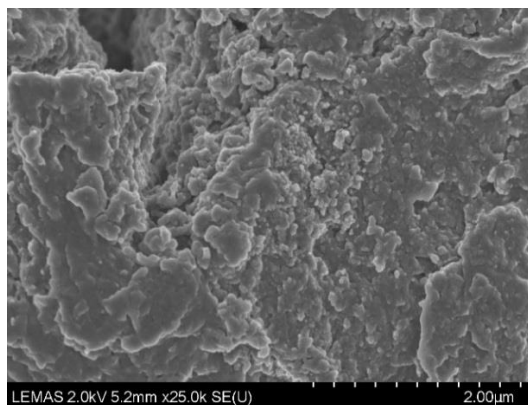




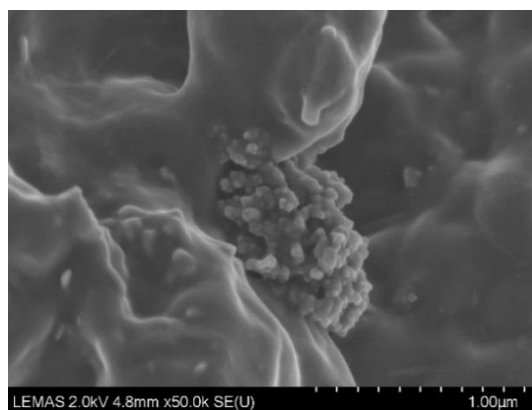
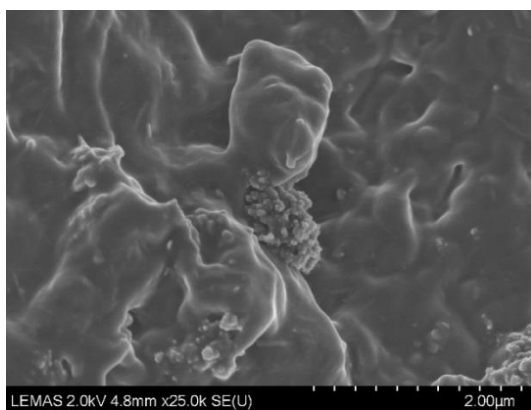
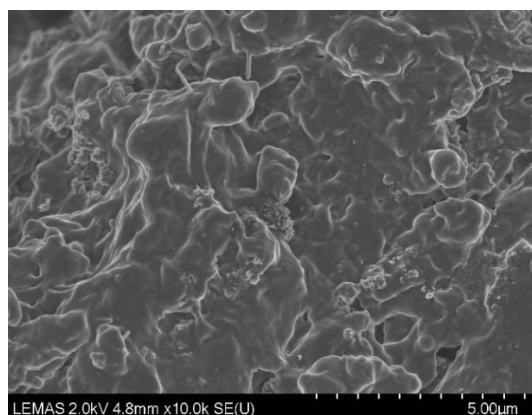
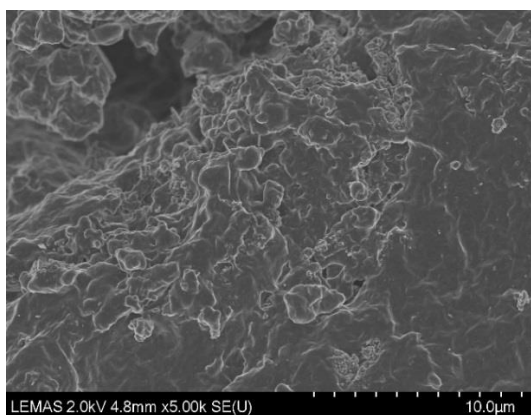
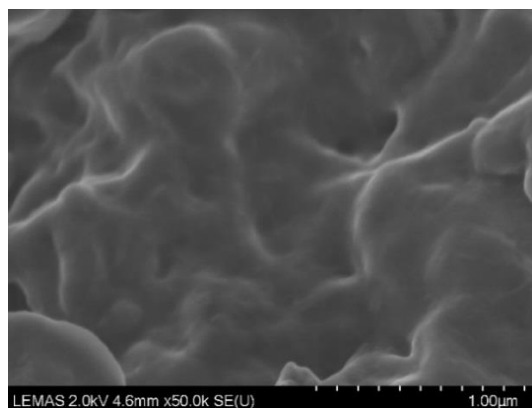
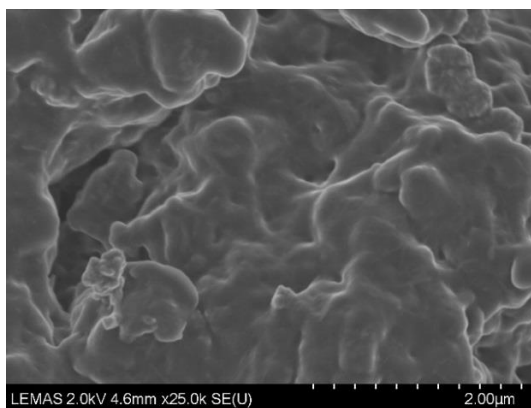
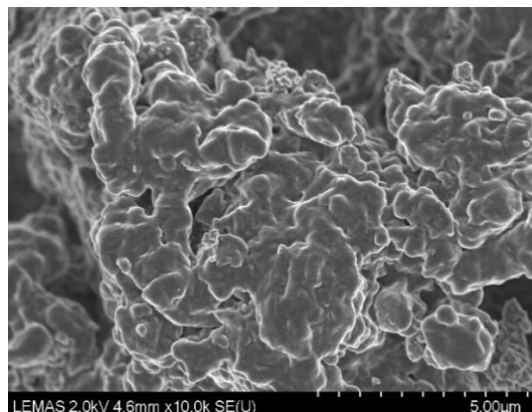
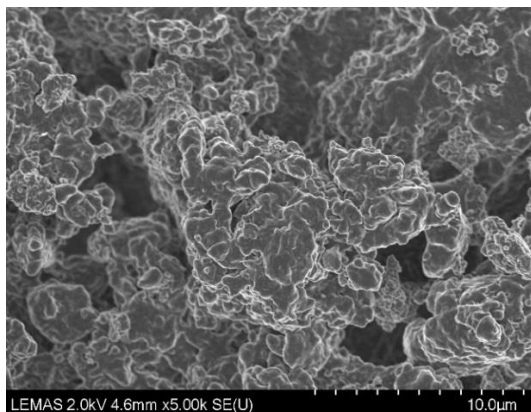
Appendix C. Scanning Electron Microscope (SEM)

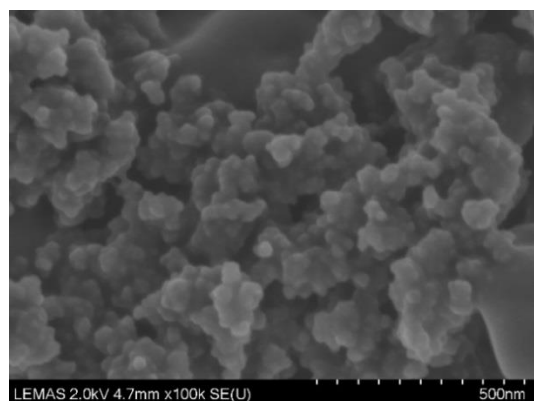
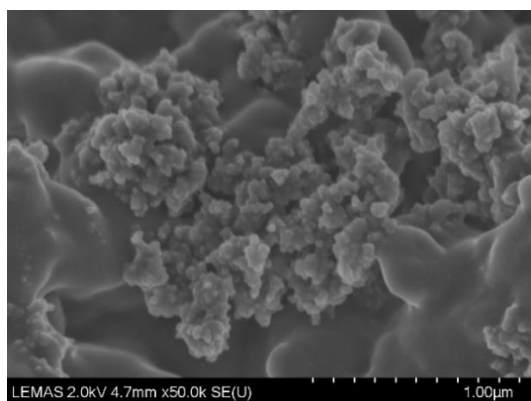
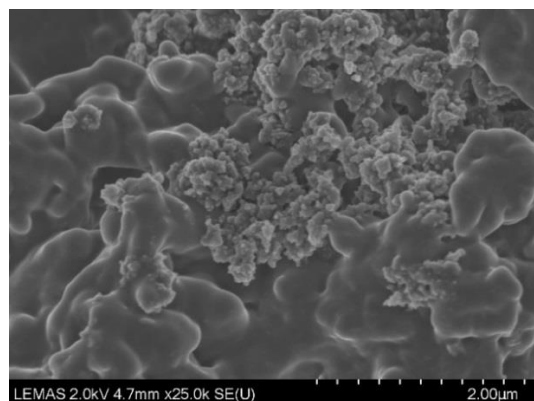
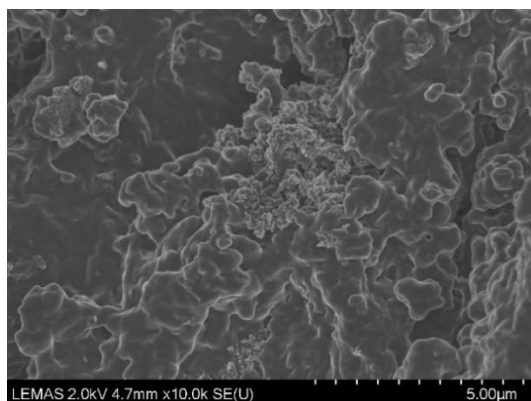
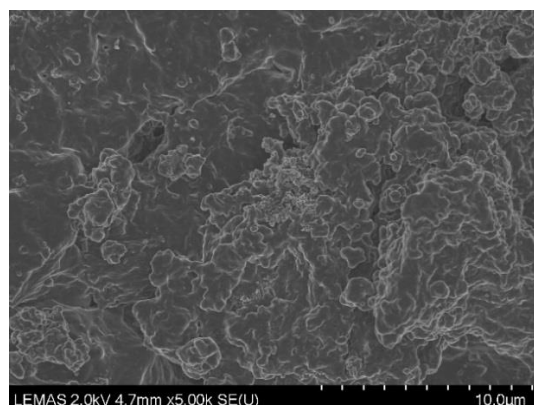
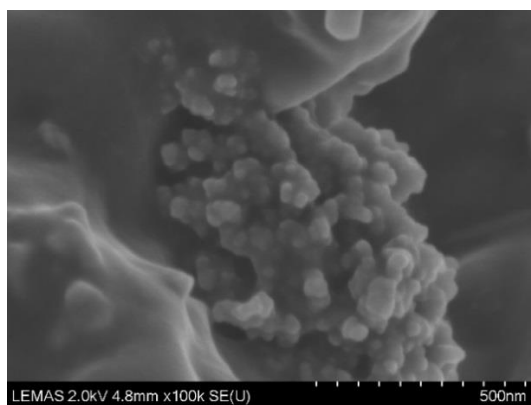
1. *ROMP₁*



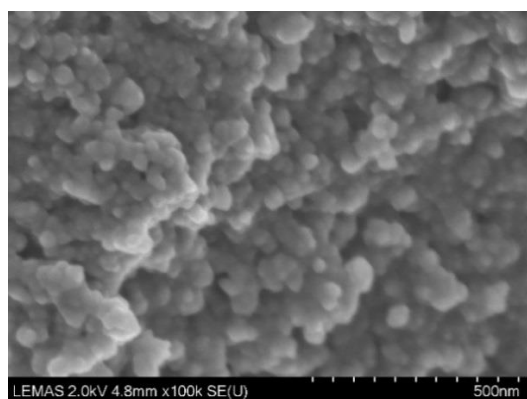
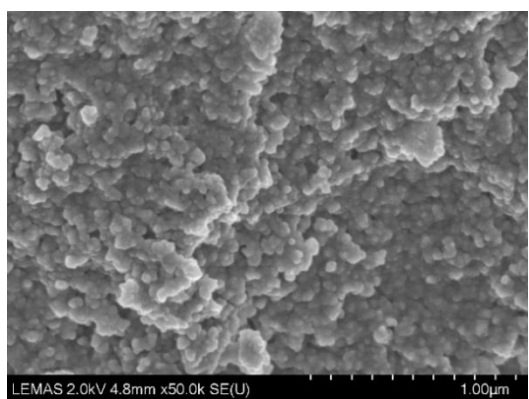
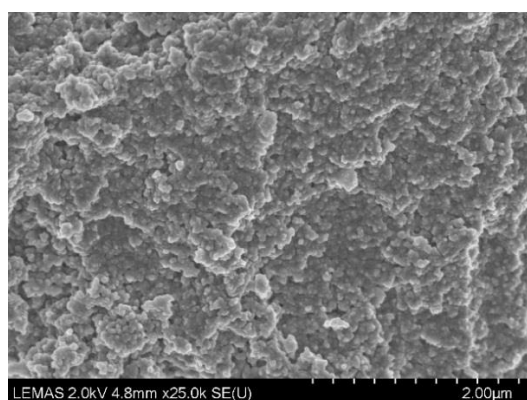
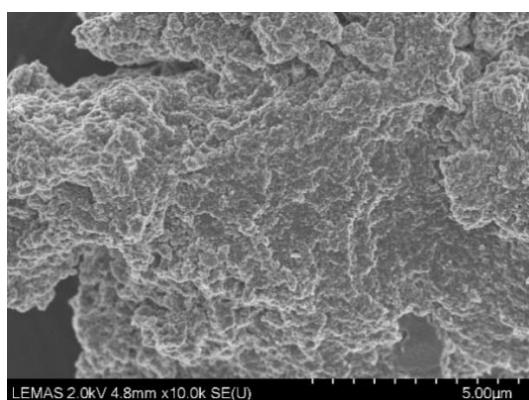
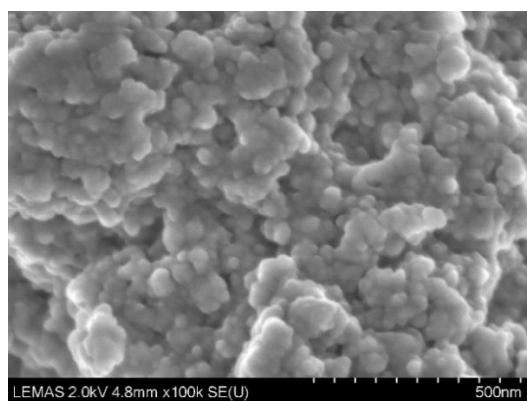
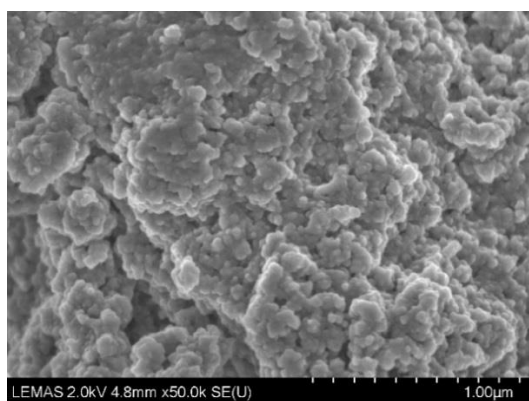
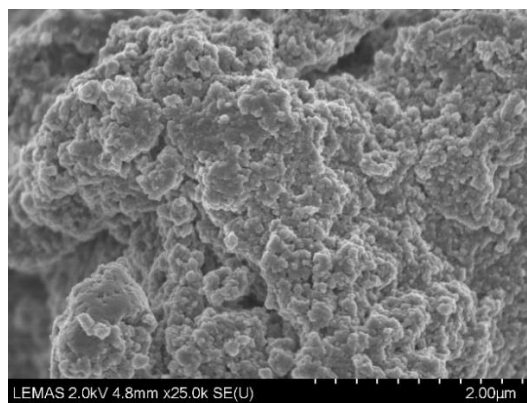
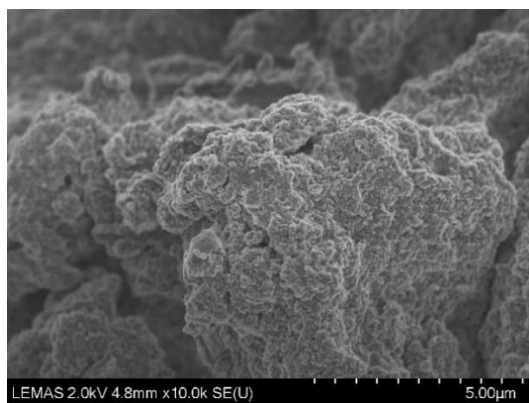


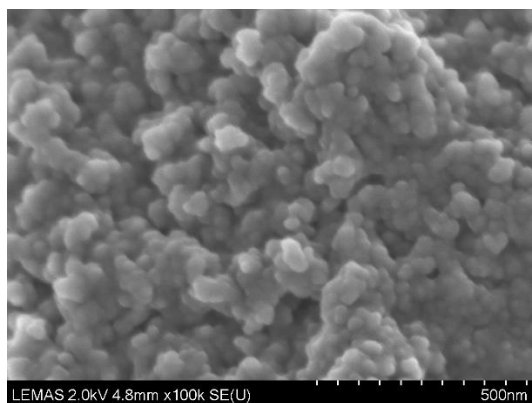
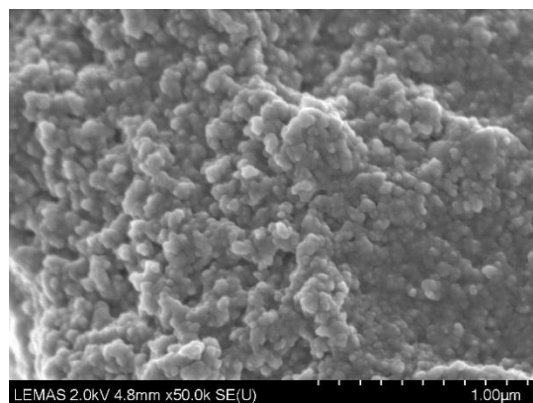
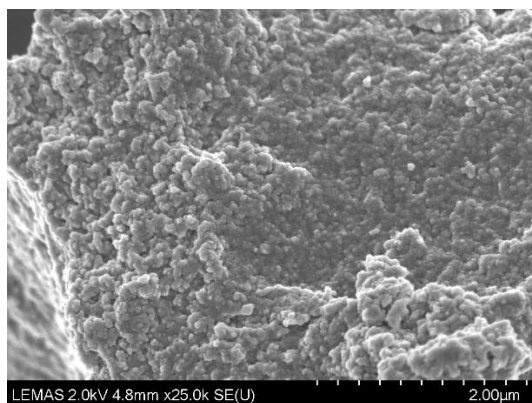
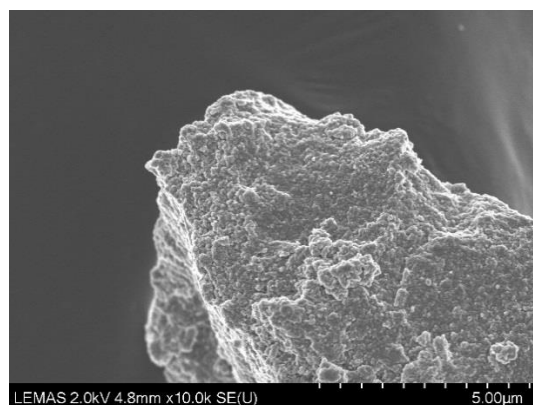
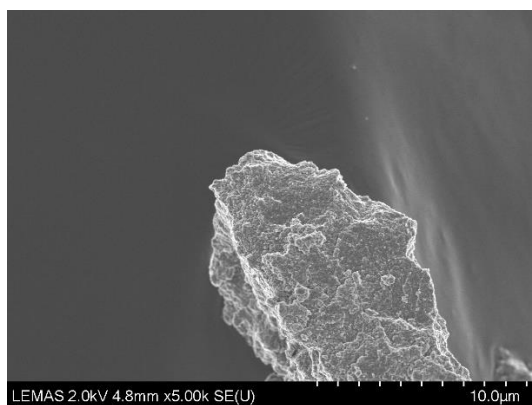
2. $WO_4@ROMP_1$



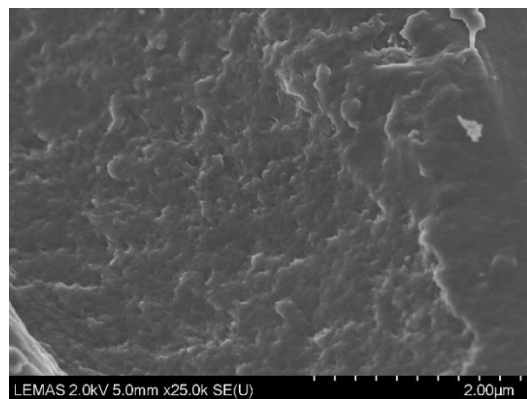
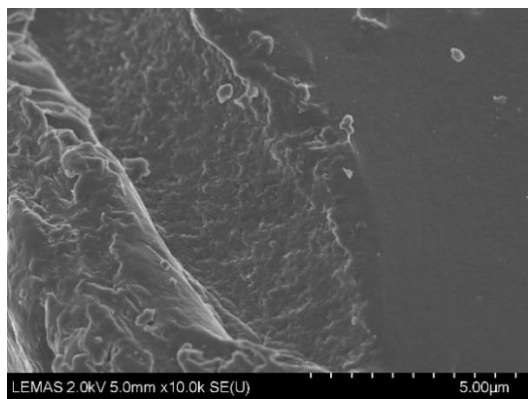
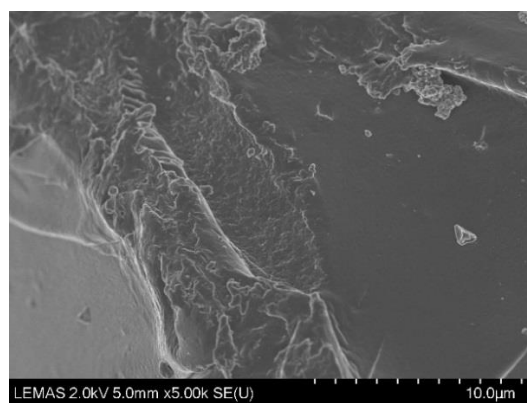
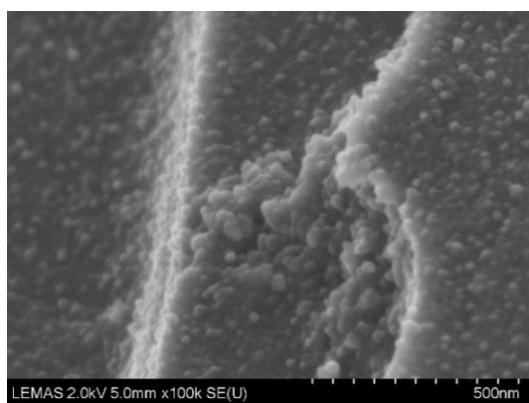
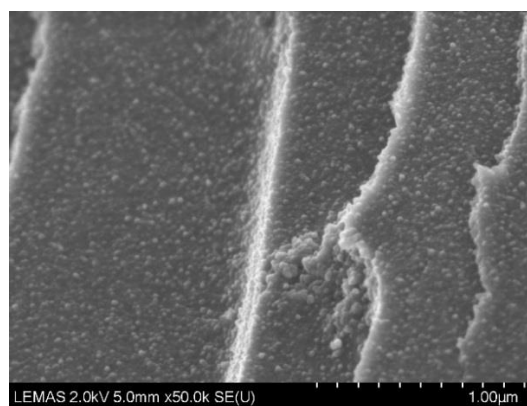
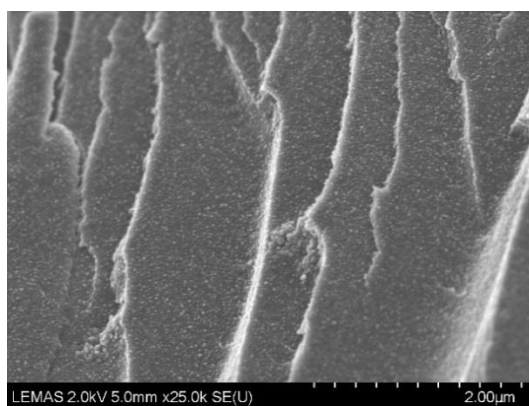
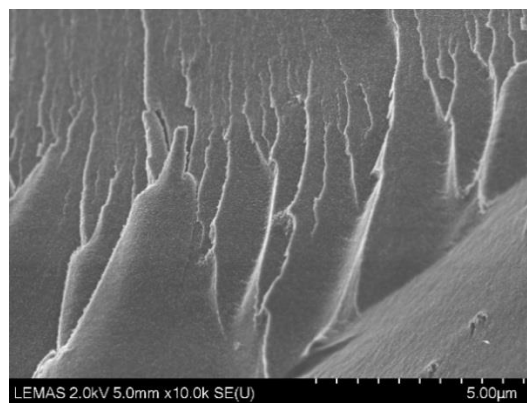
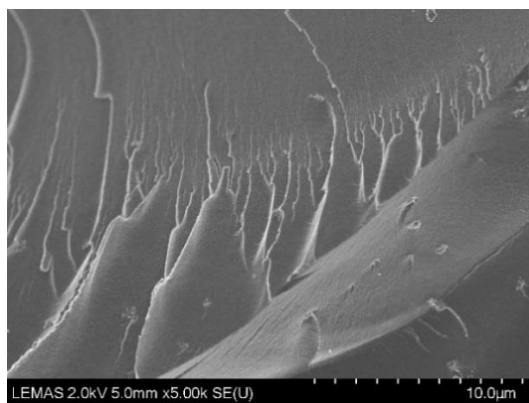


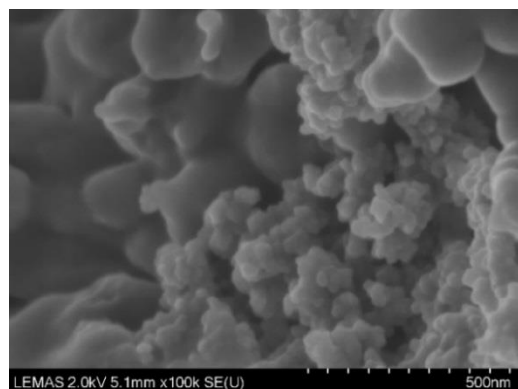
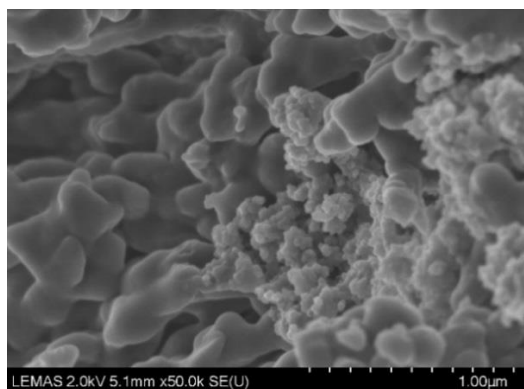
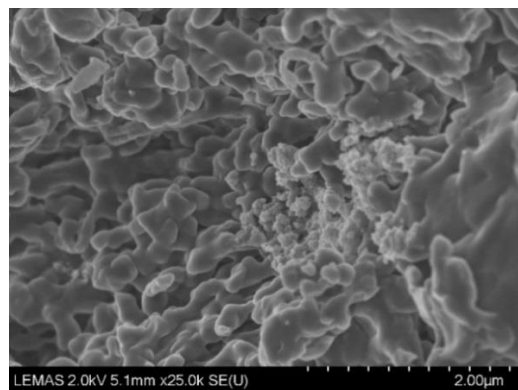
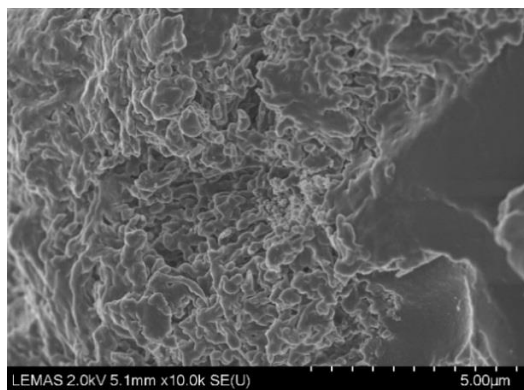
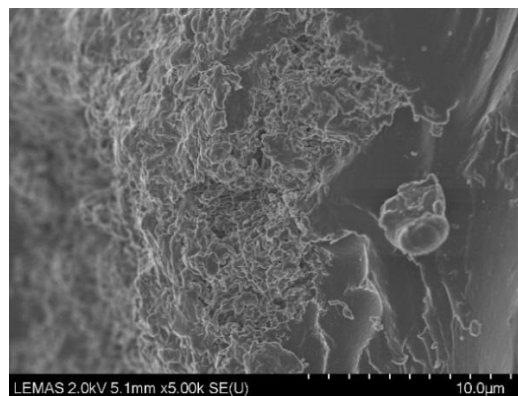
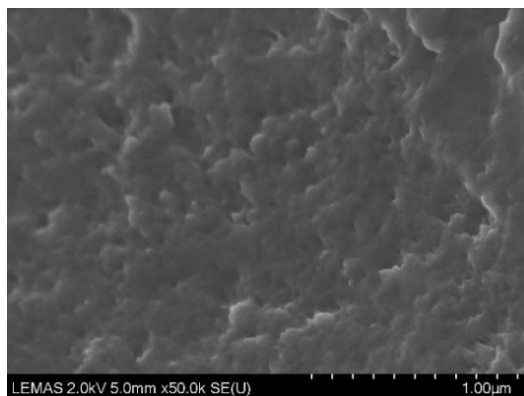
3. $PW_{12}O_{40}@ROMP_1$



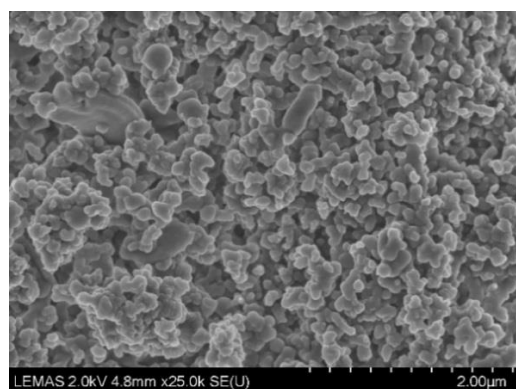
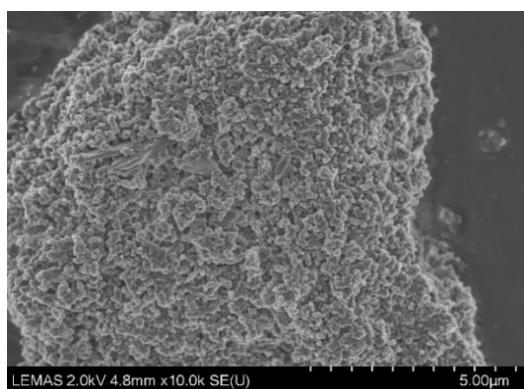
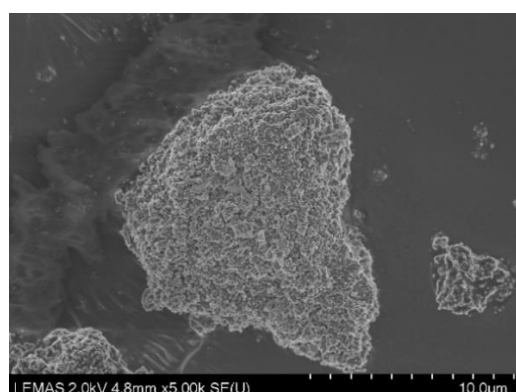
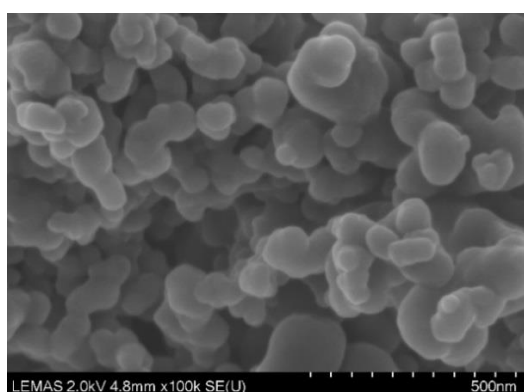
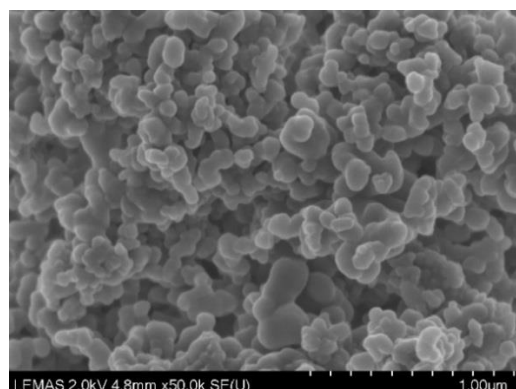
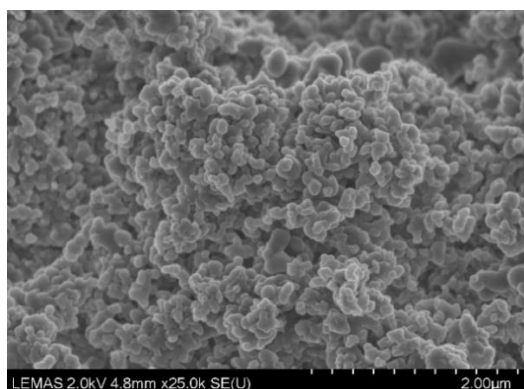
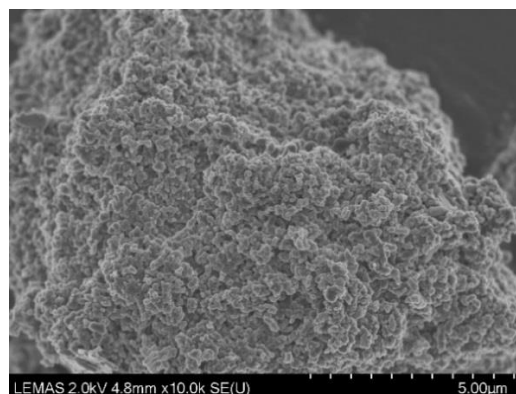
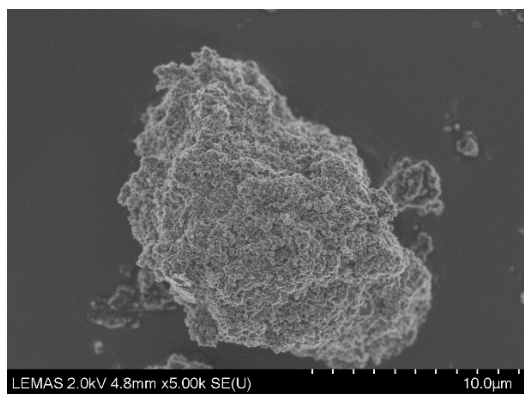


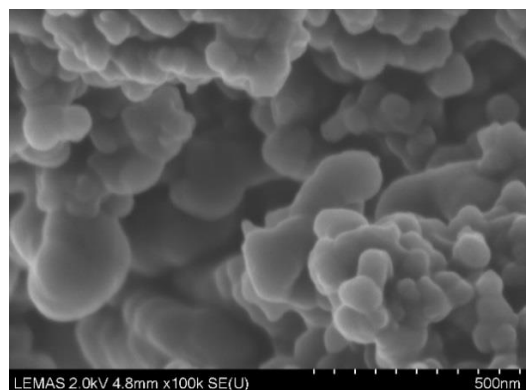
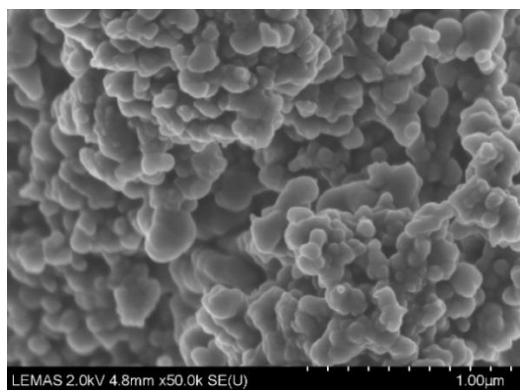
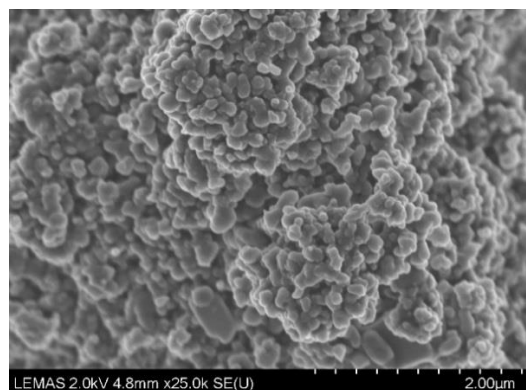
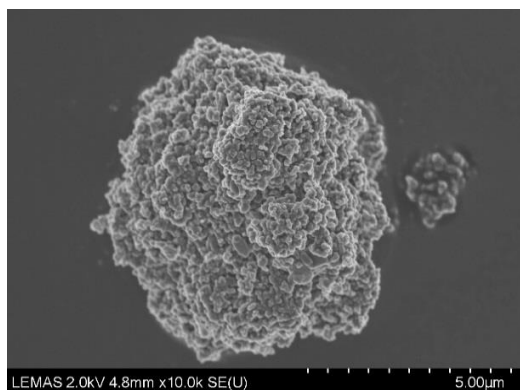
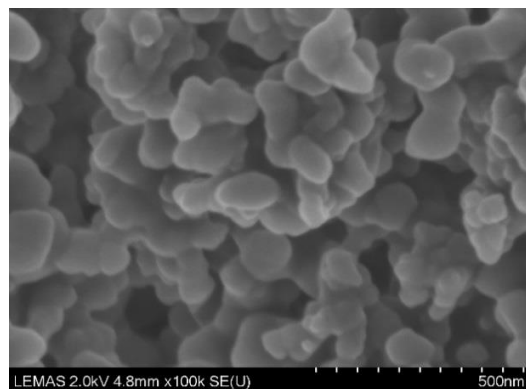
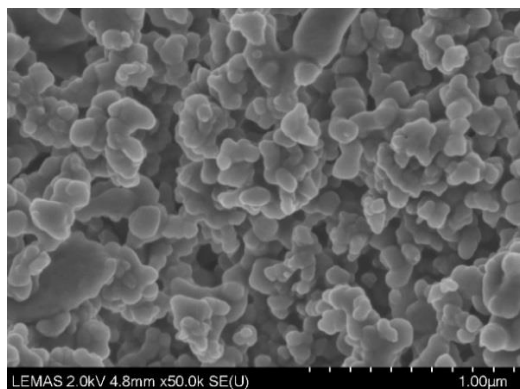
4. ROMP₂



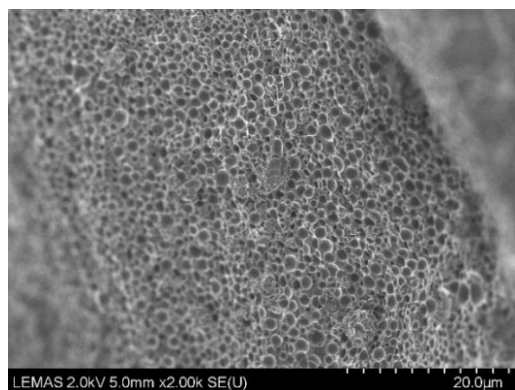
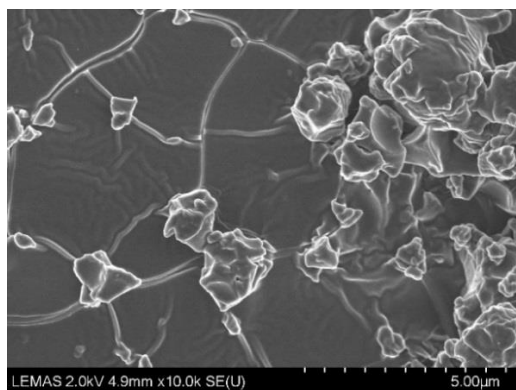
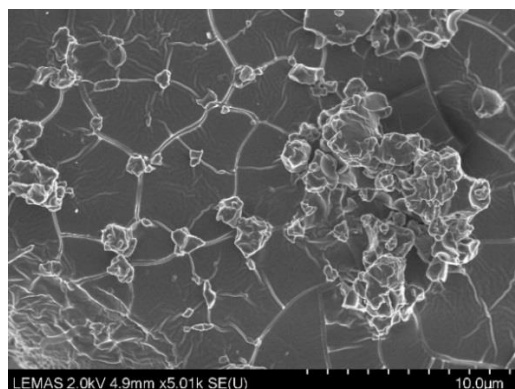
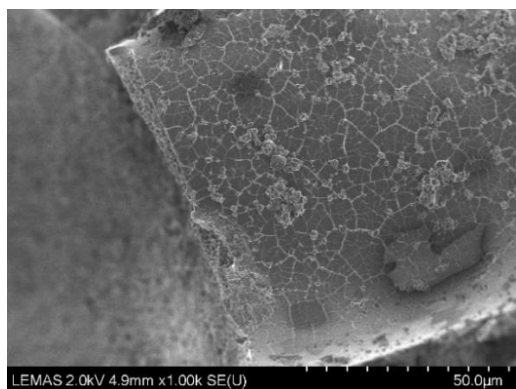
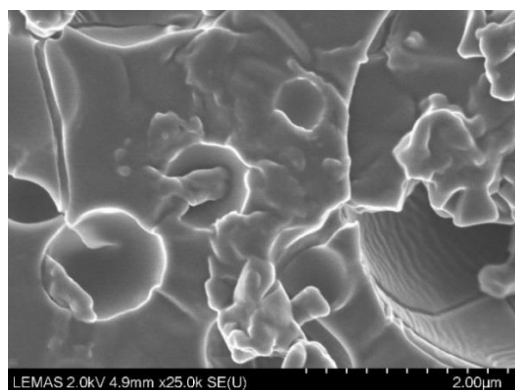
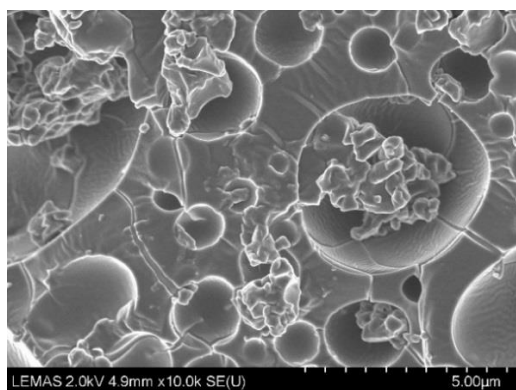
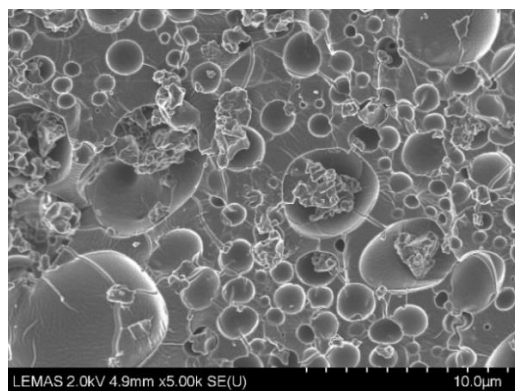
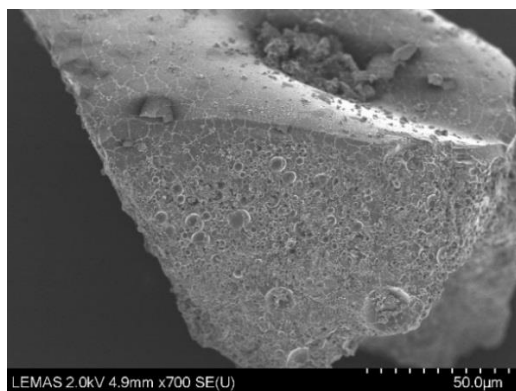


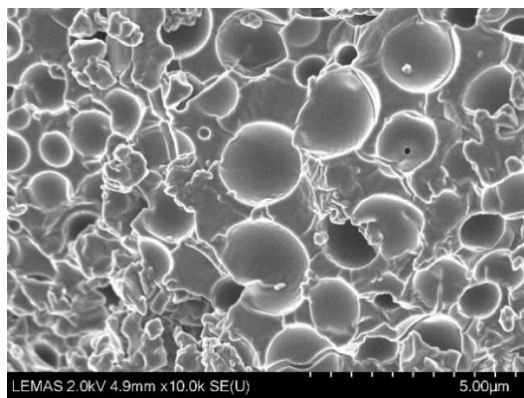
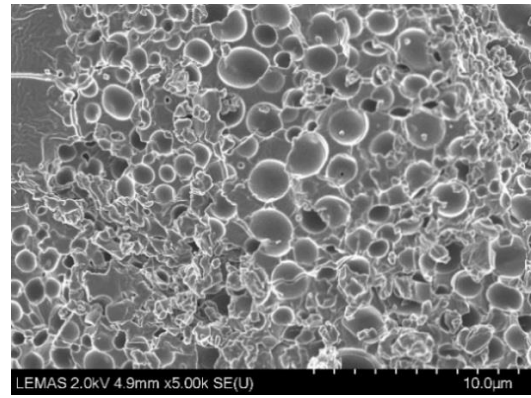
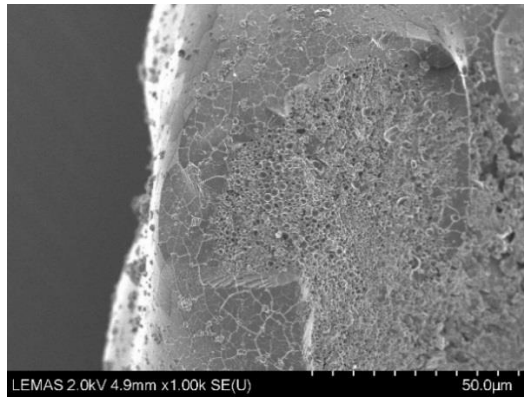
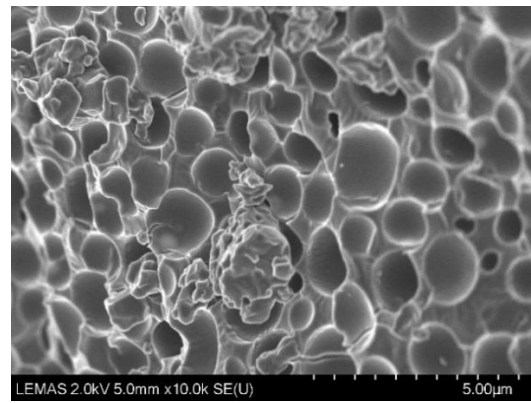
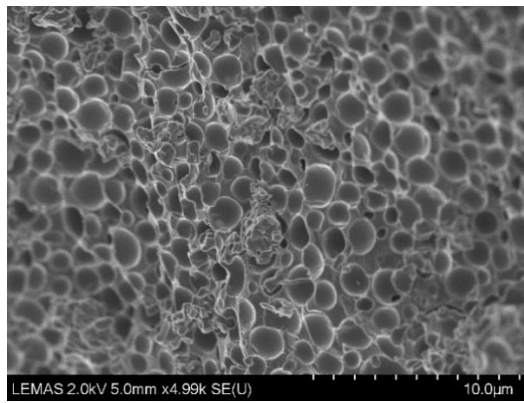
5. $\text{WO}_4\text{@ROMP}_2$



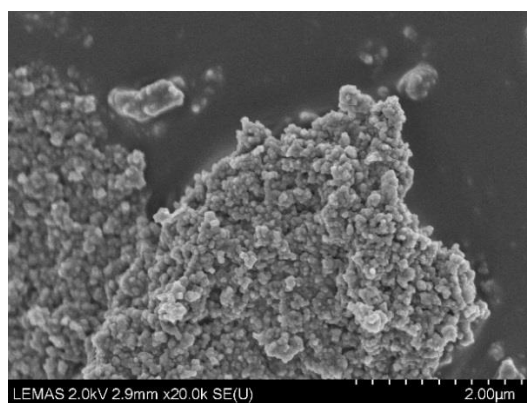
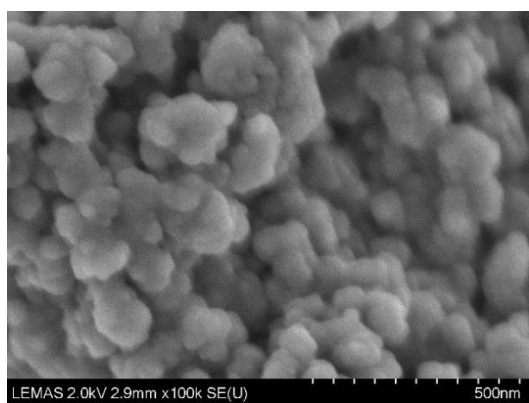
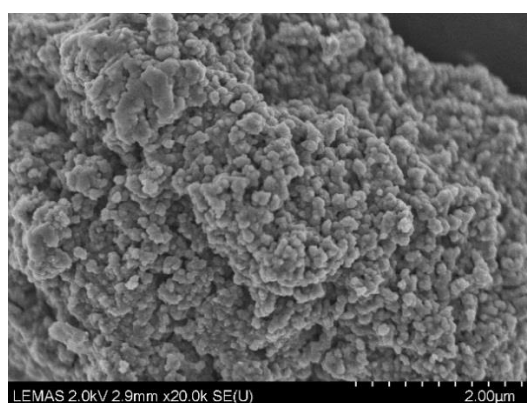
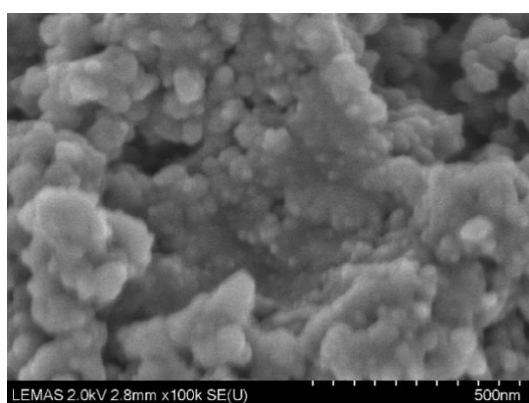
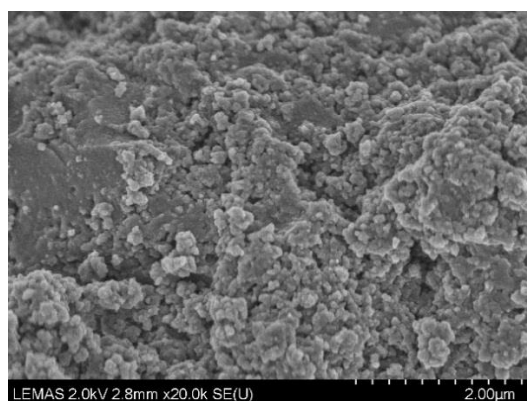
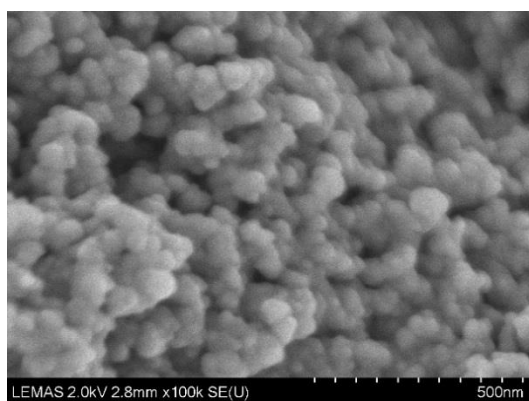
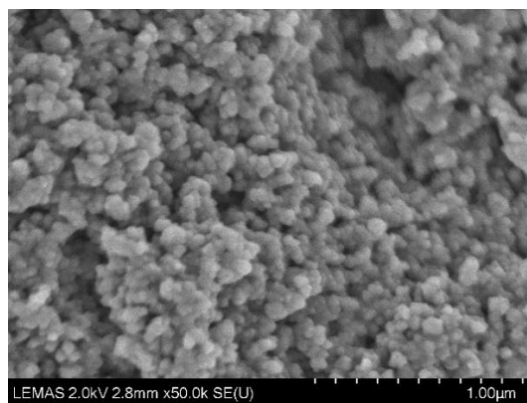
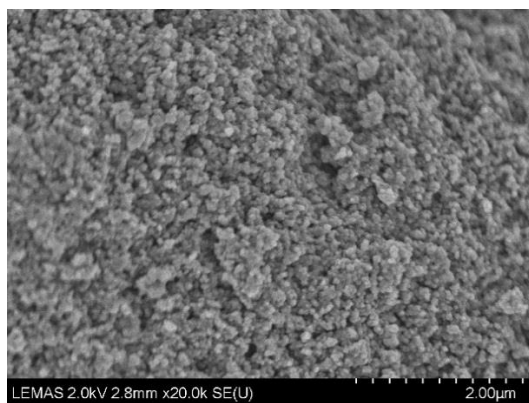


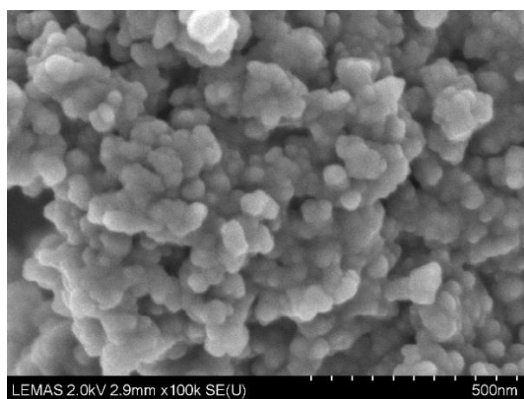
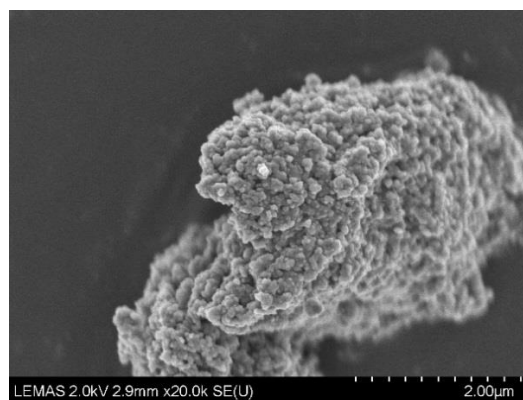
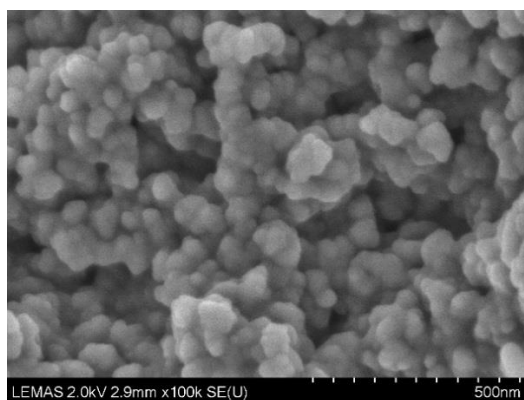
6. $\text{NH}_2\text{-PIILP}$



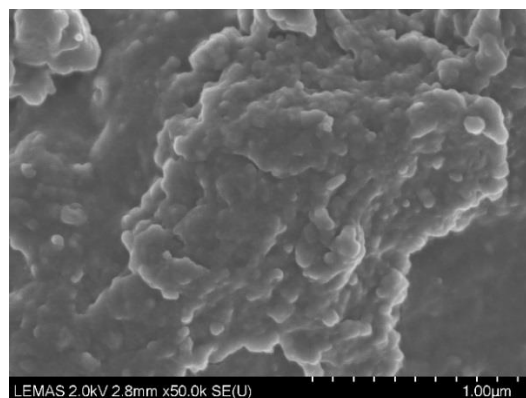
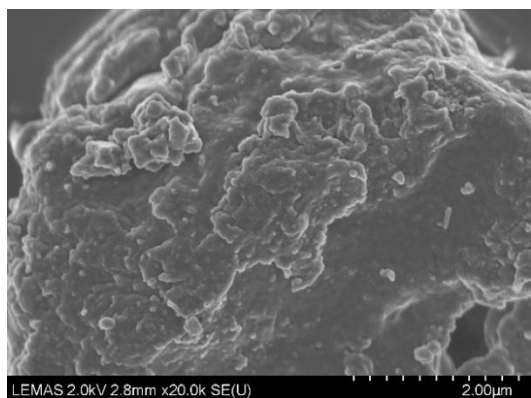
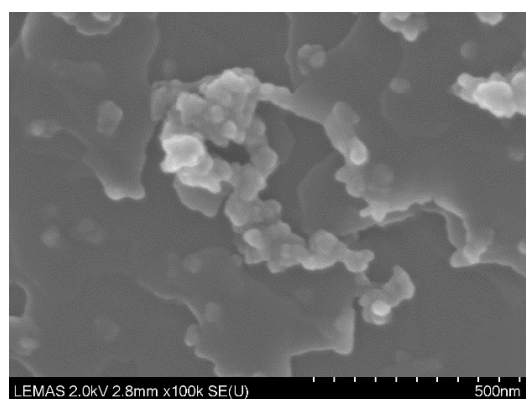
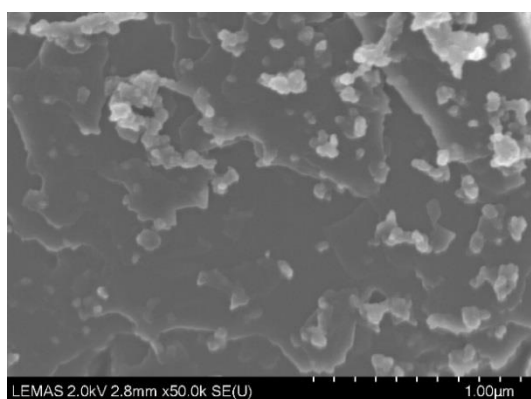
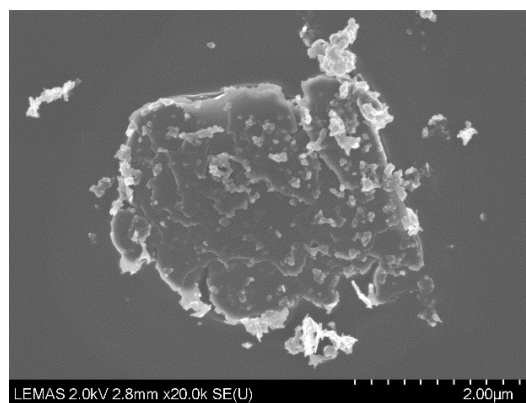
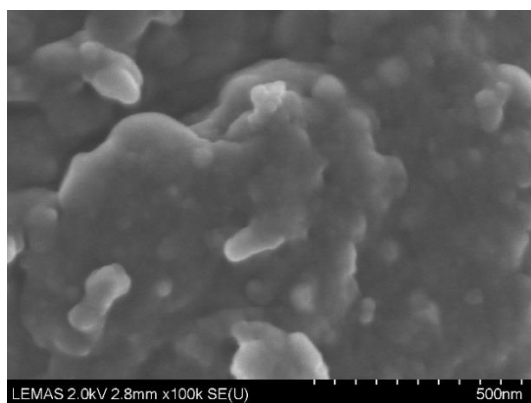
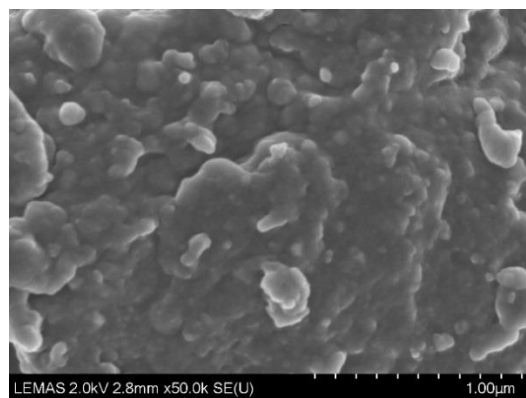
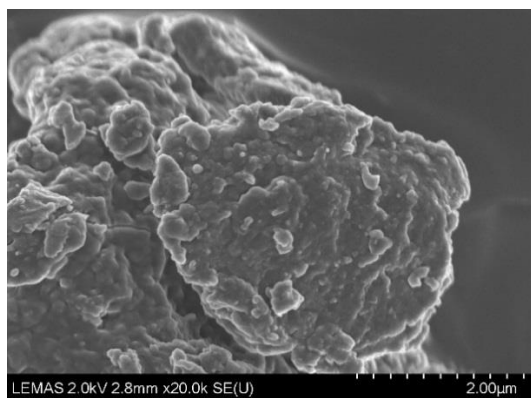


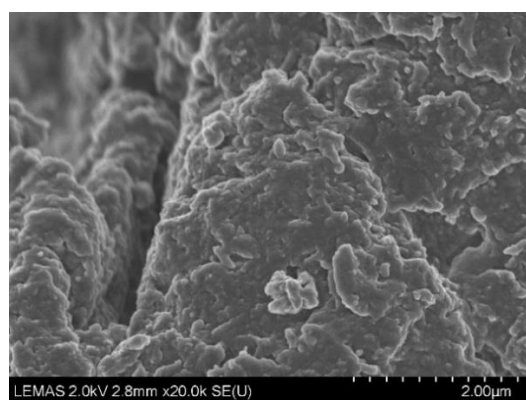
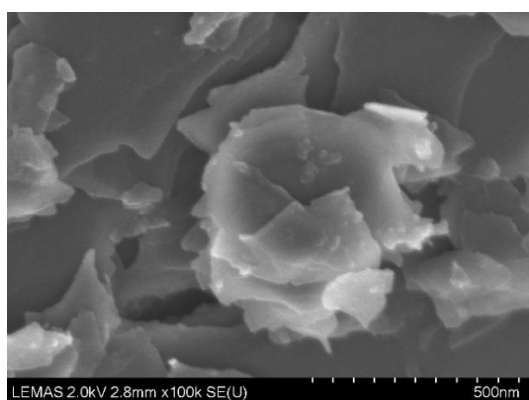
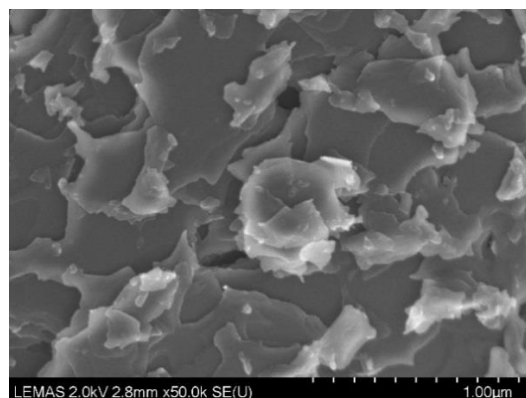
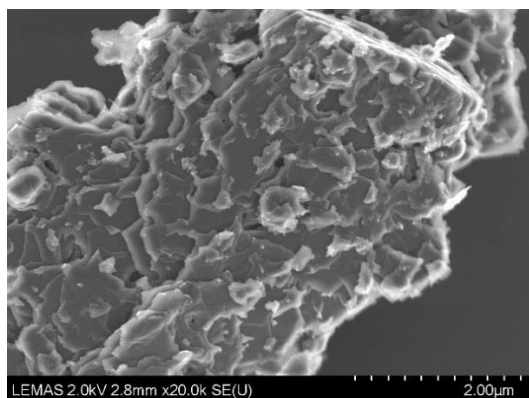
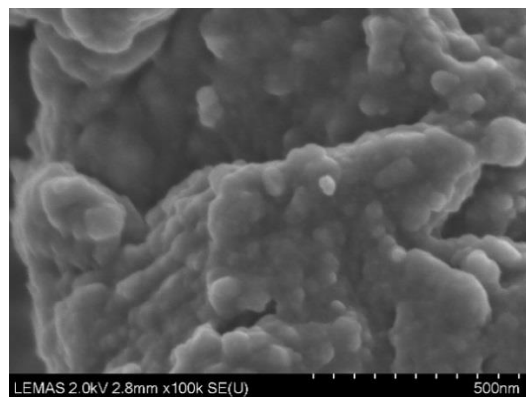
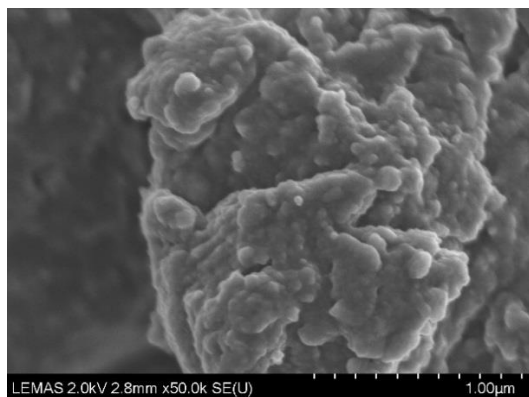
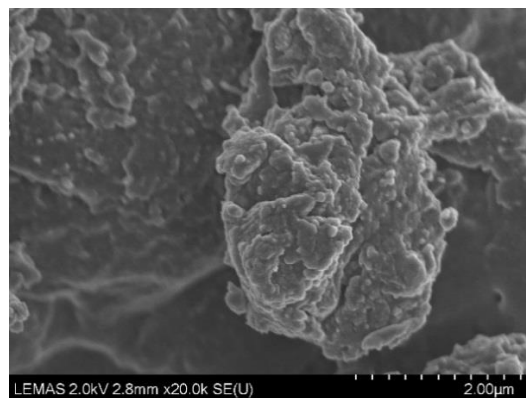
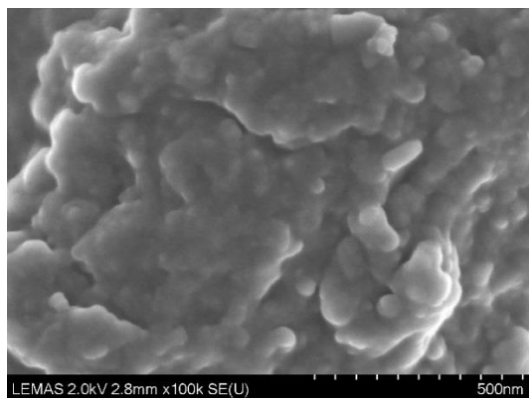
7. $\text{PdCl}_4@\text{NH}_2\text{-PIILP}$

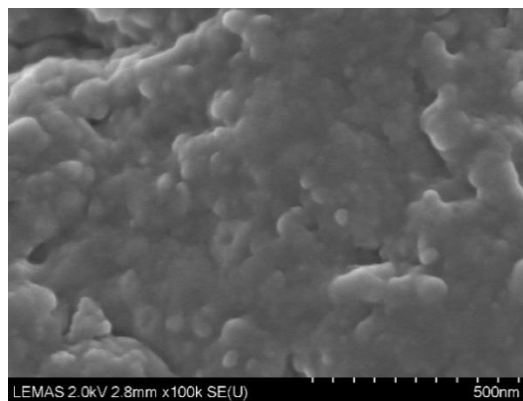
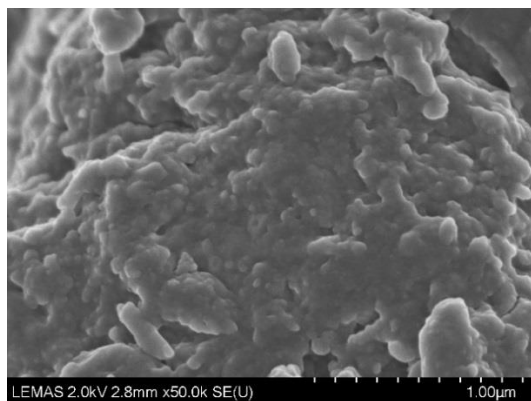




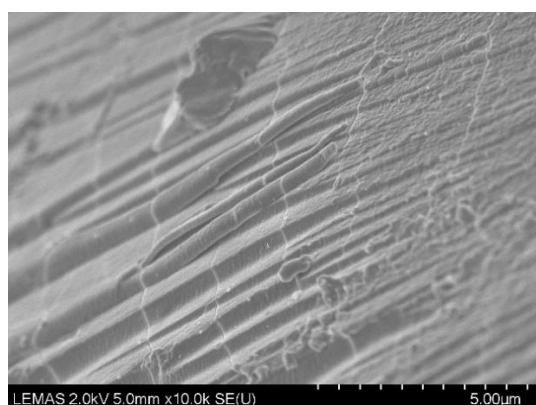
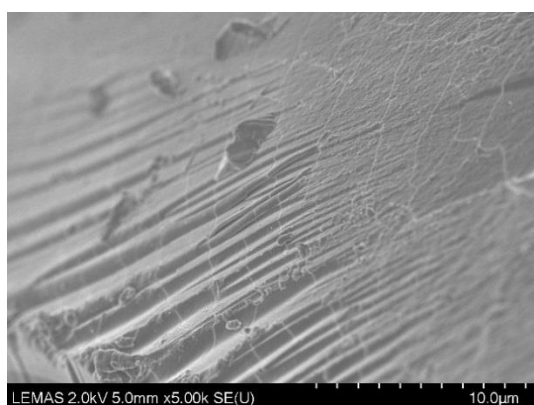
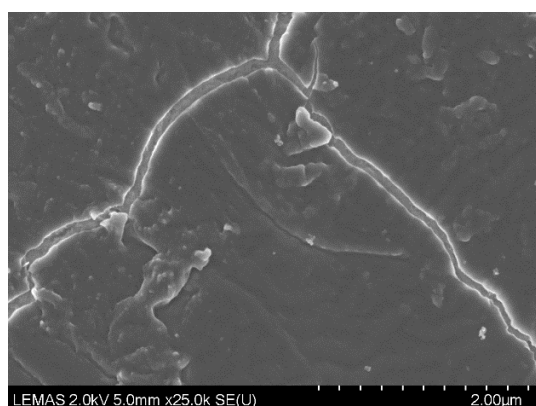
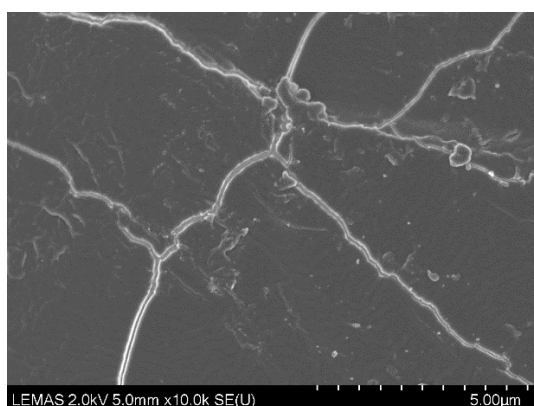
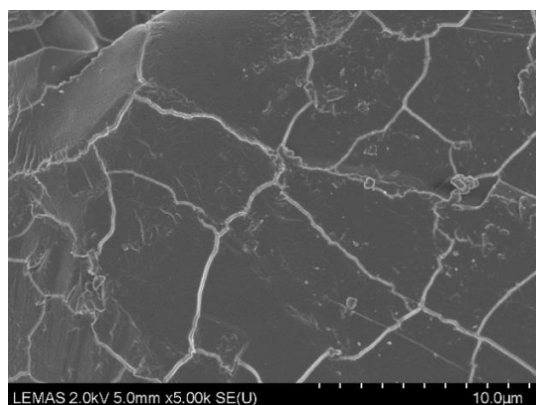
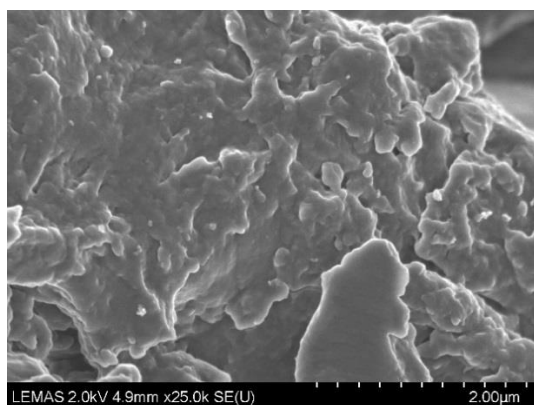
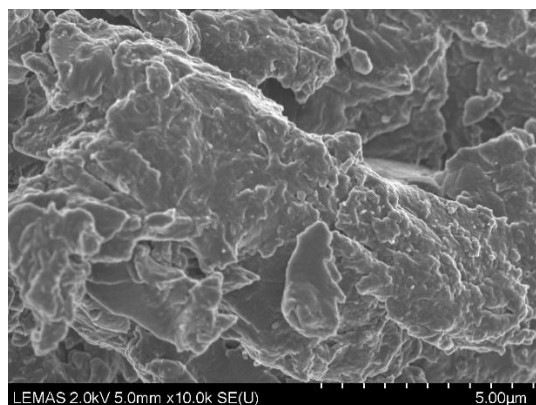
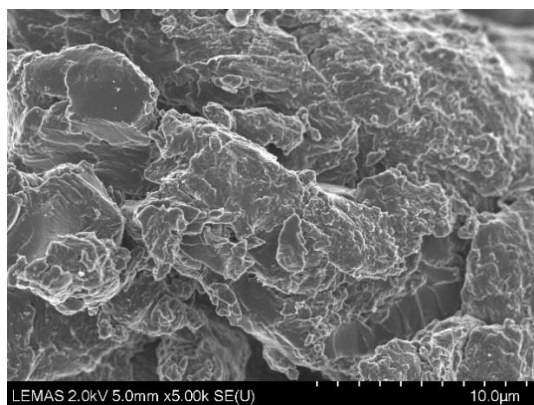
8. PdNP@NH₂-PIILP



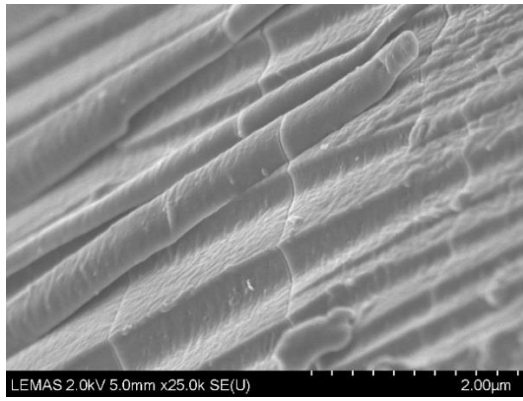




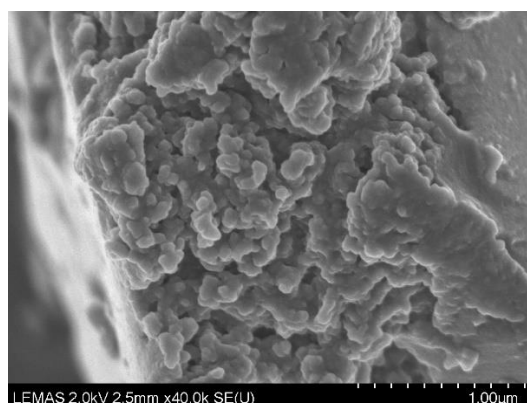
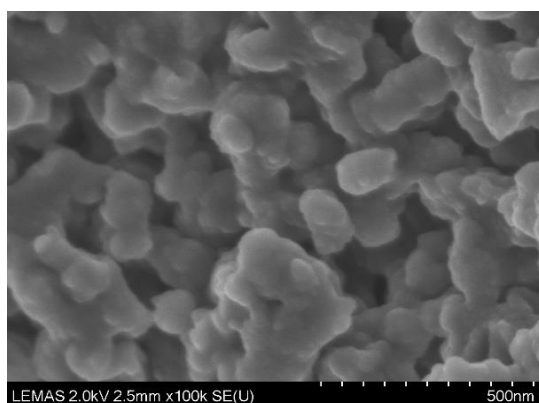
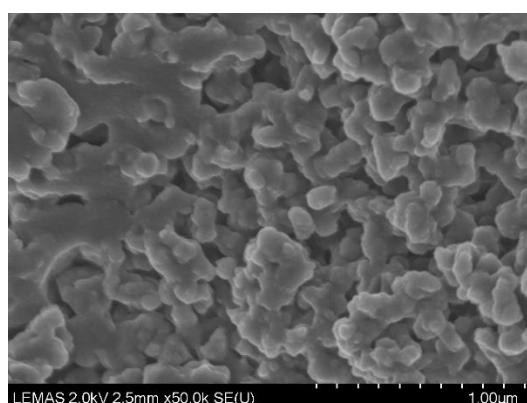
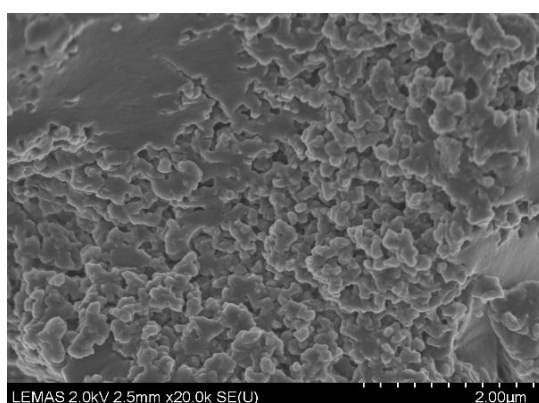
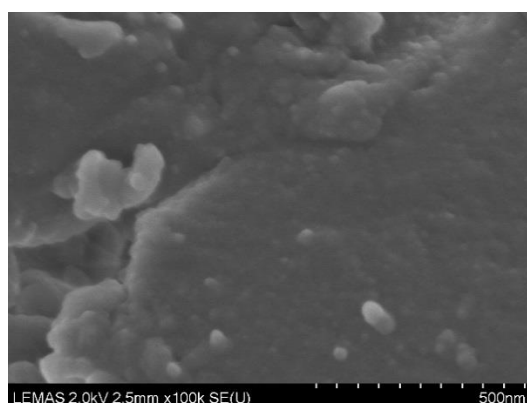
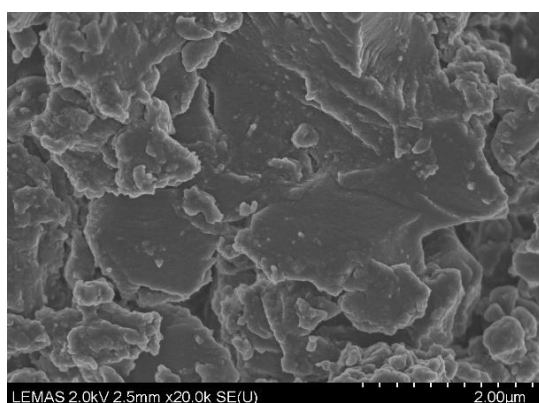
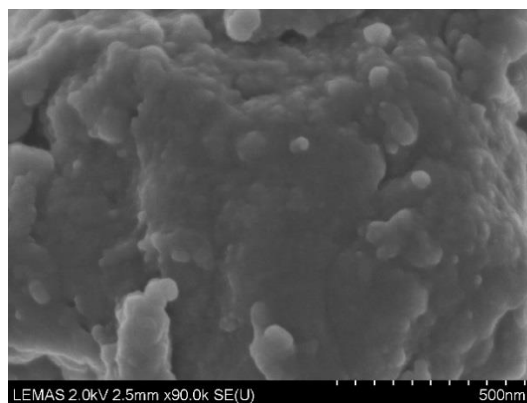
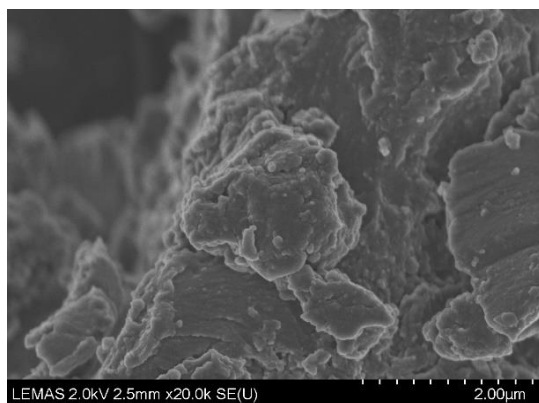
9. Pyrr-PIILP

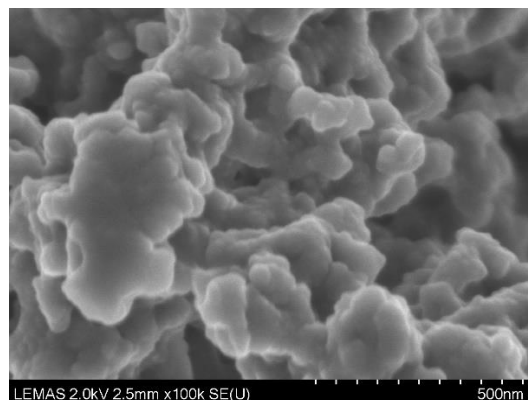
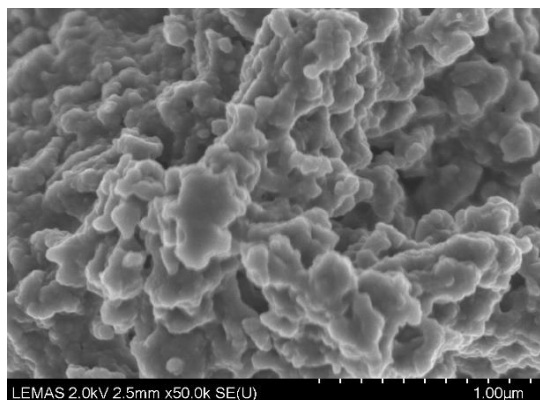
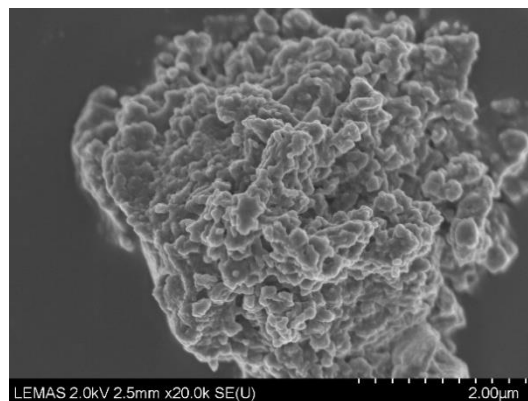
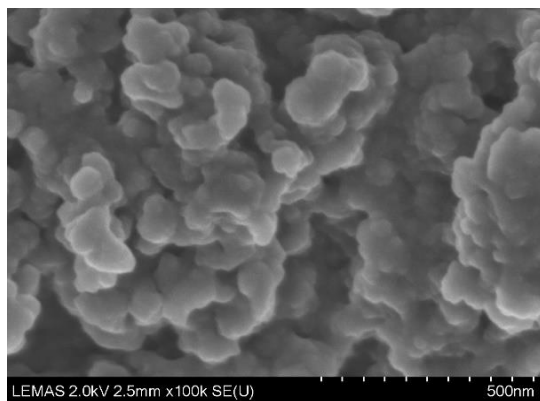


Appendices

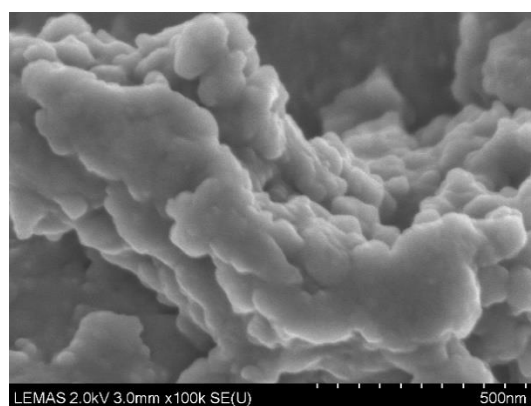
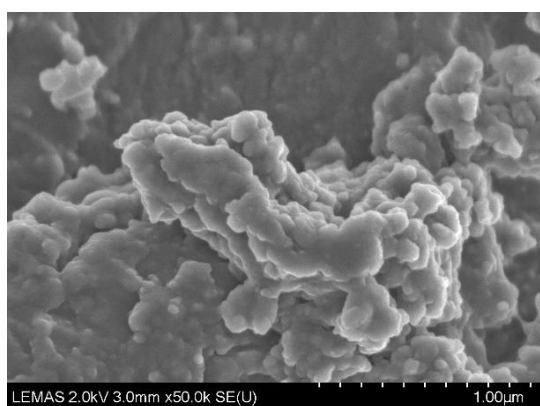
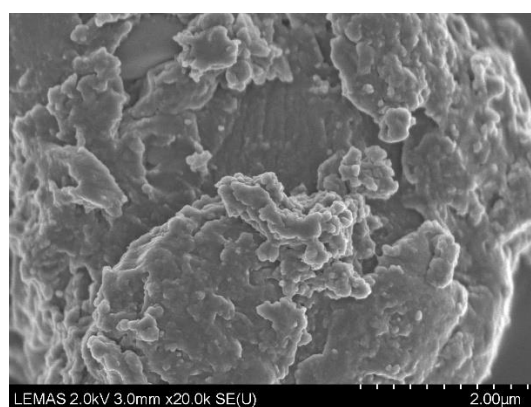
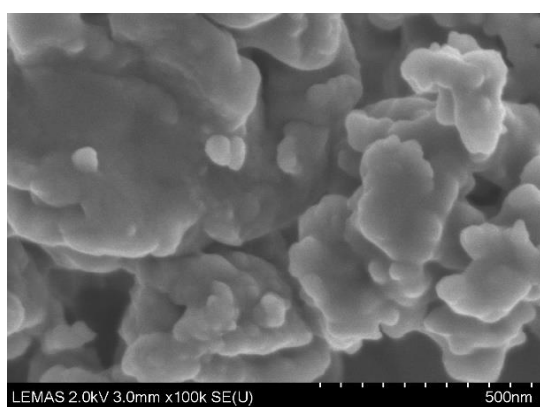
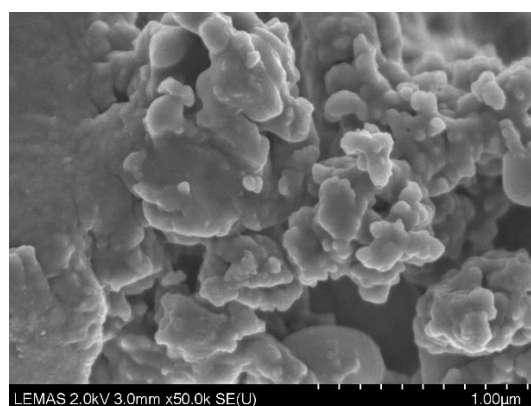
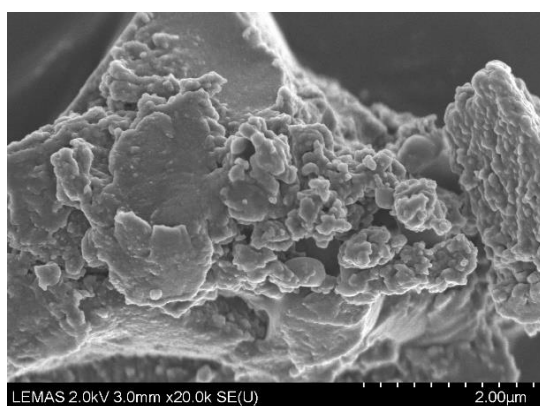
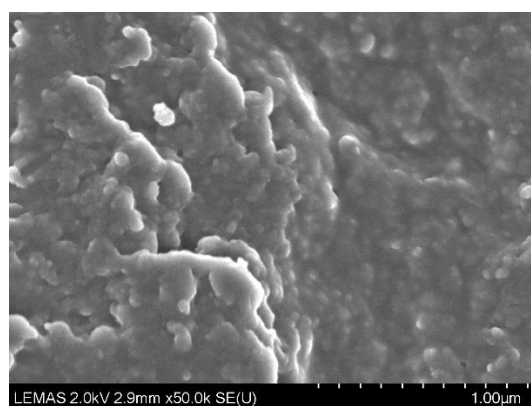
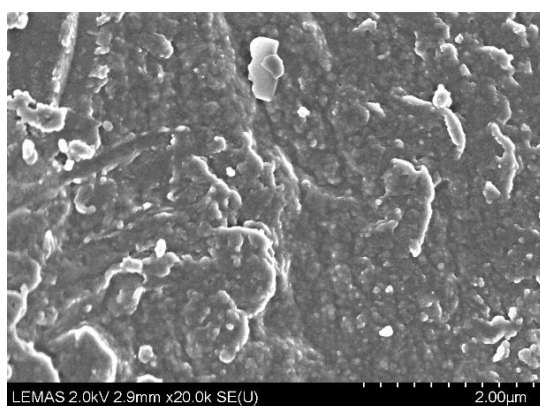


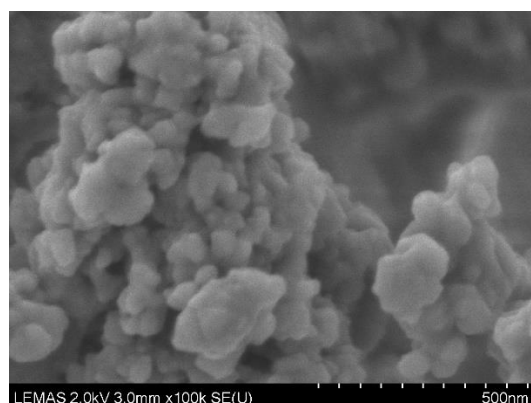
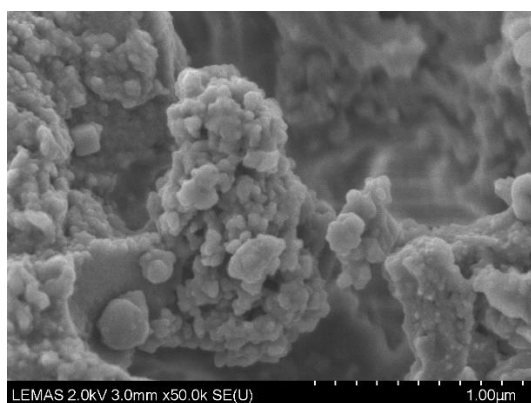
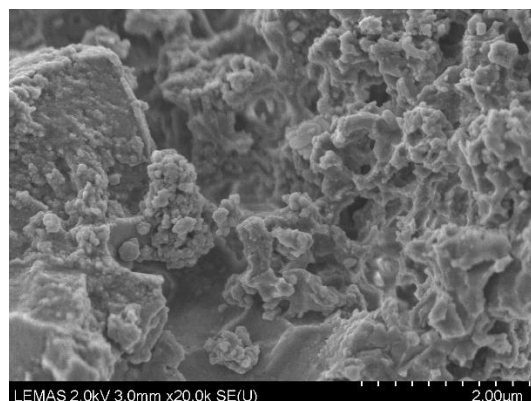
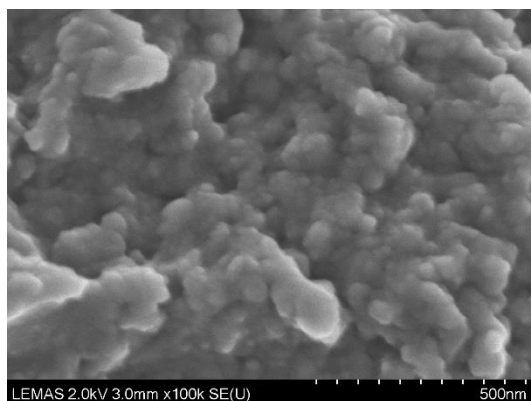
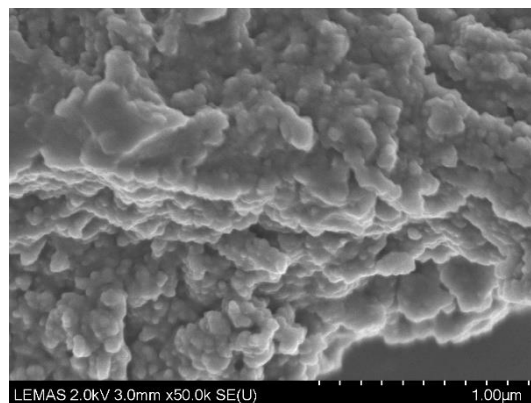
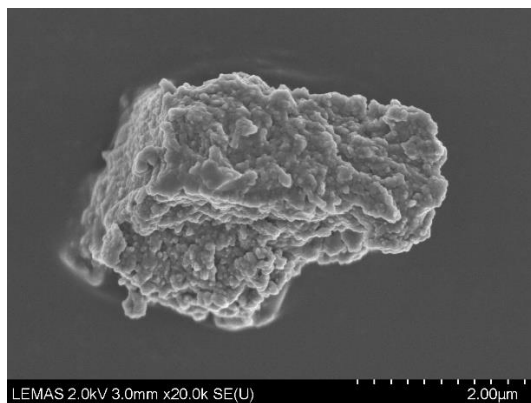
10. PdCl₄@Pyrr-PIILP



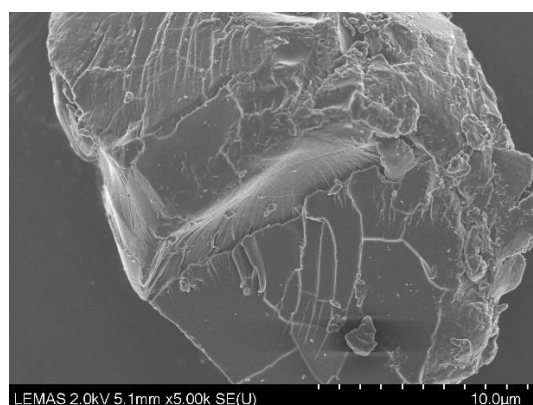
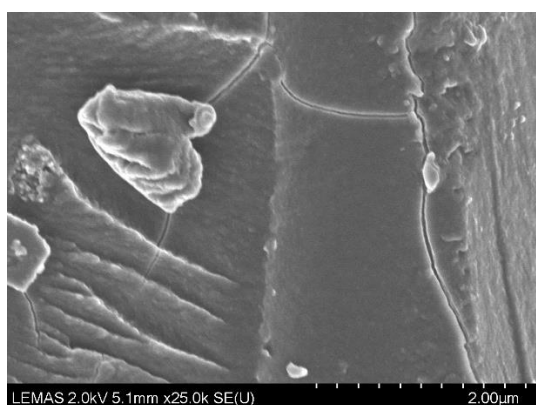
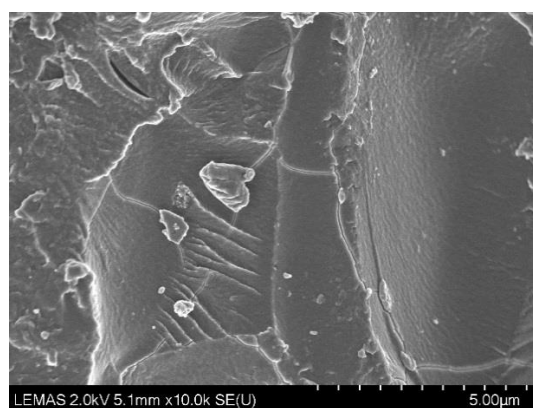
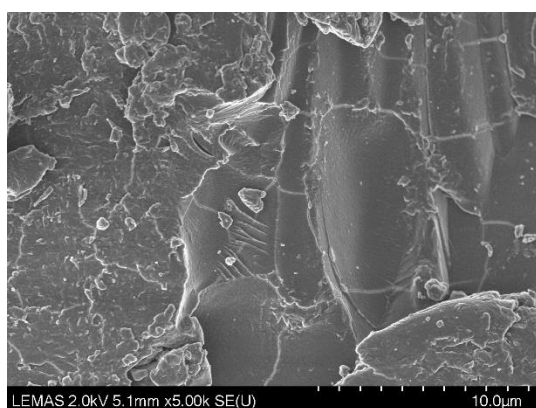
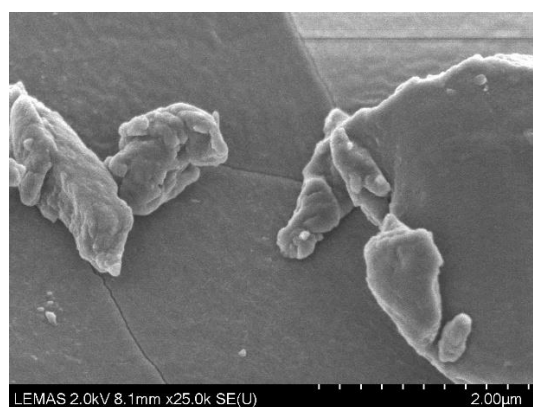
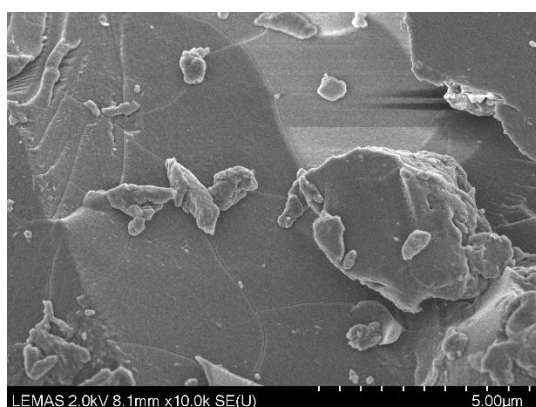
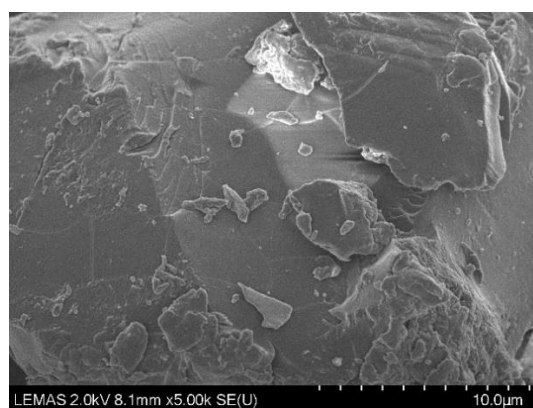
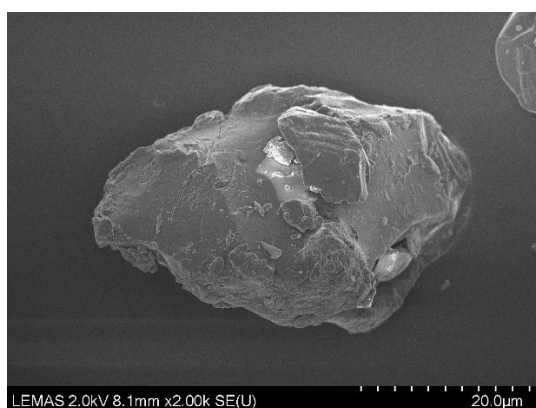


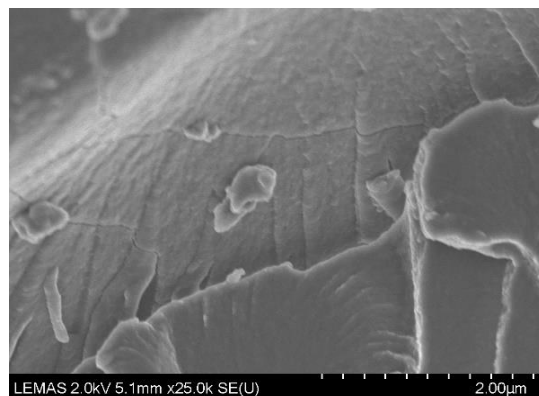
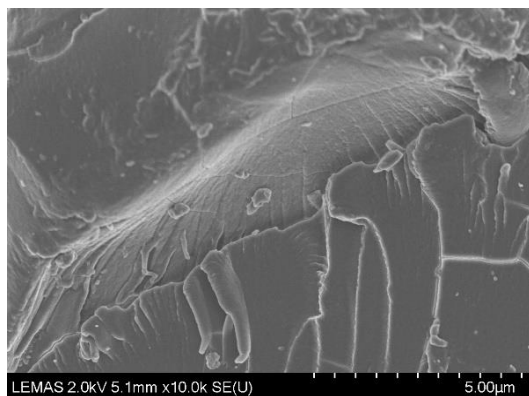
11. PdNP@Pyrr-PIILP



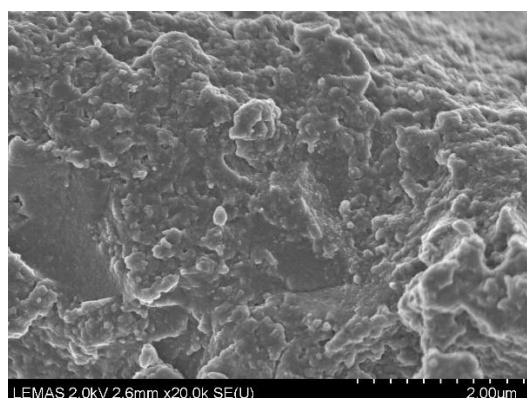
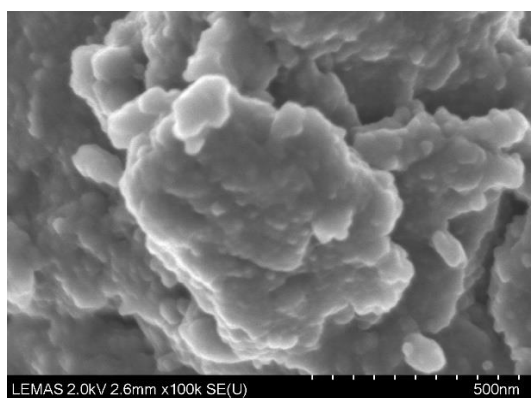
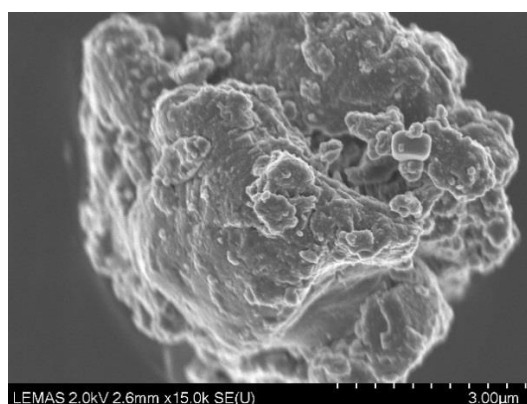
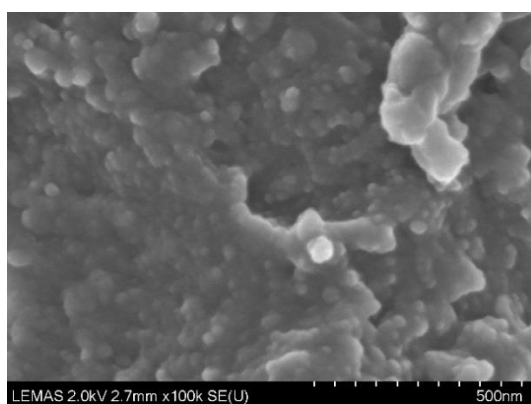
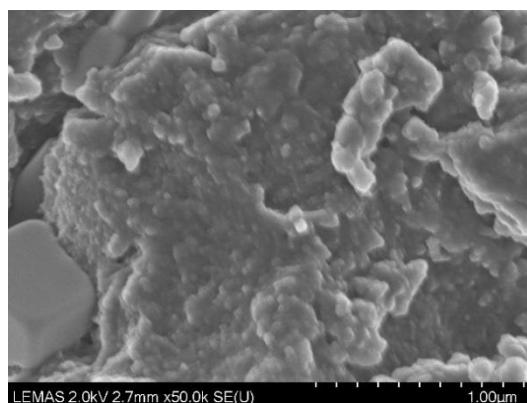
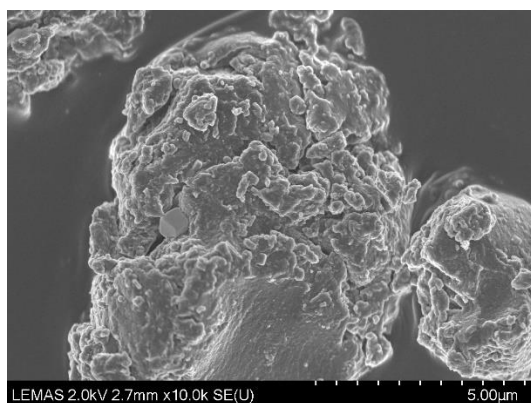
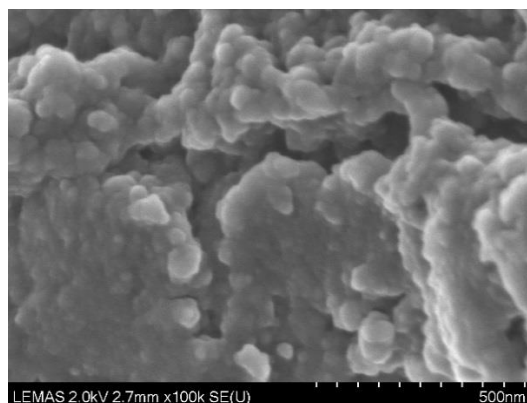
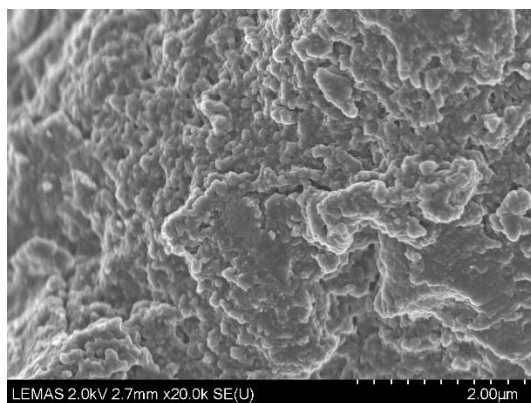


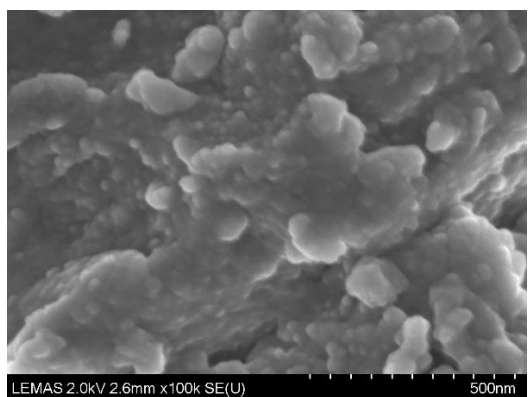
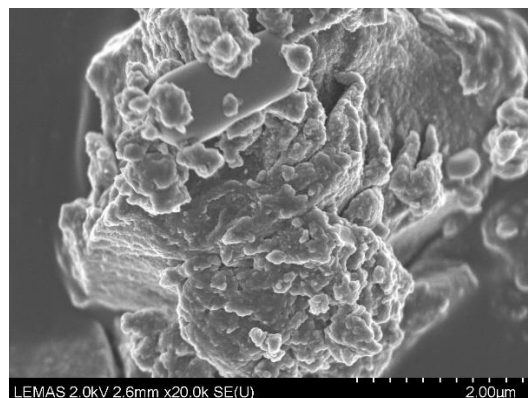
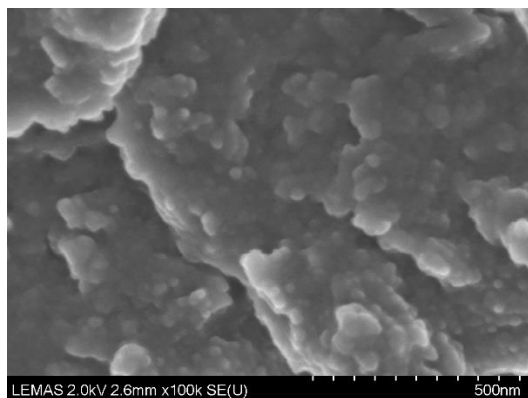
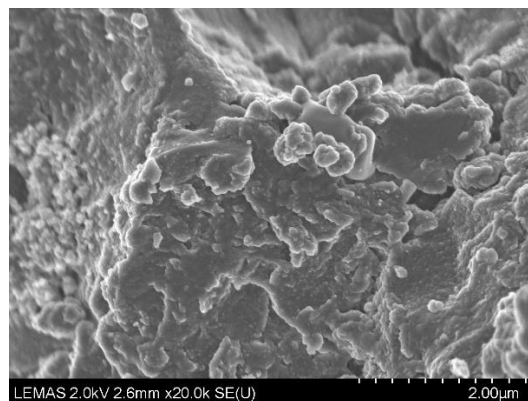
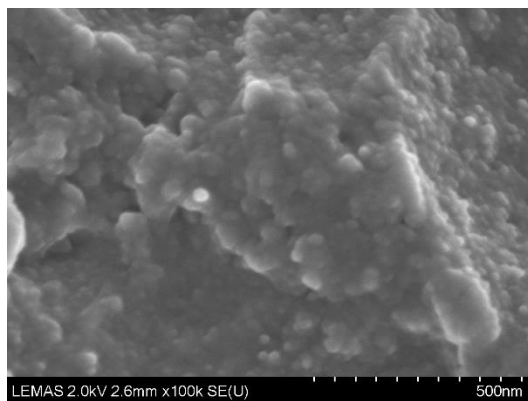
12. PPh_2 -PIILP



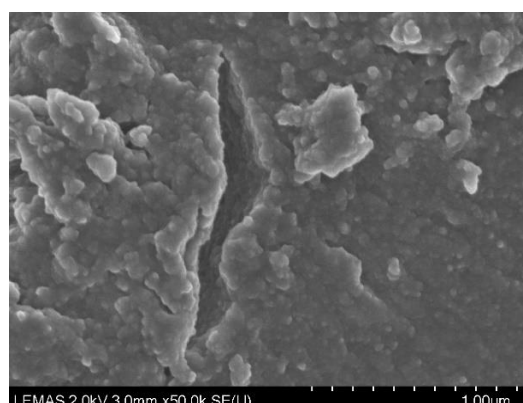
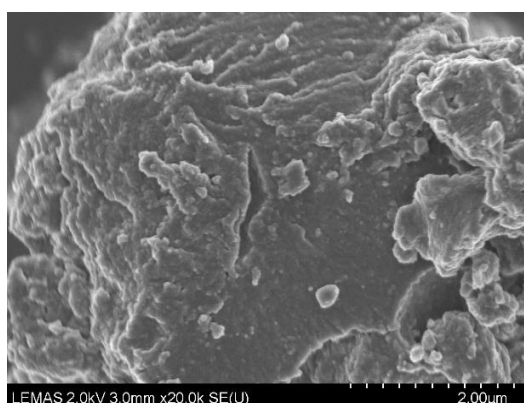
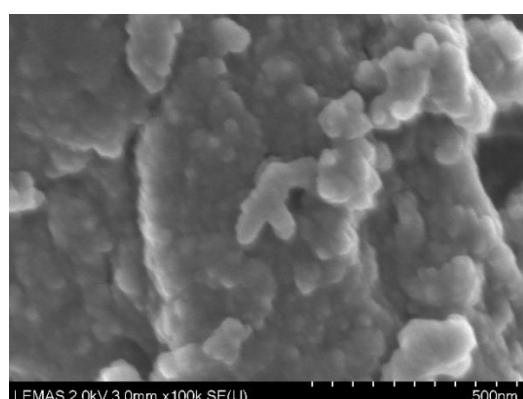
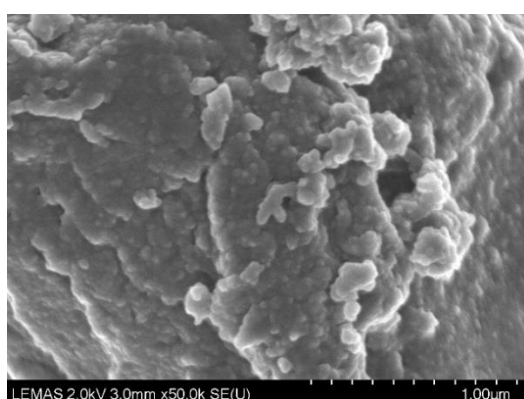
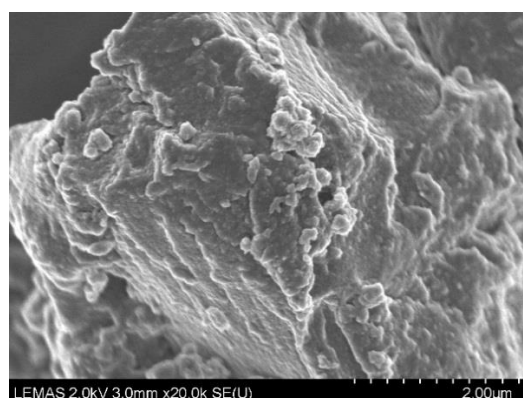
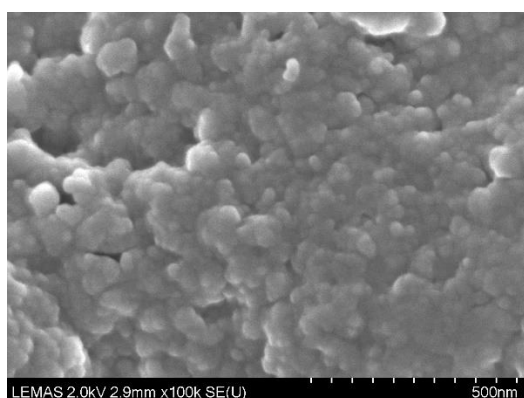
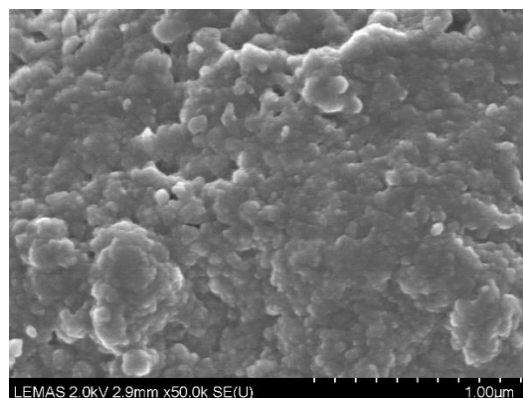
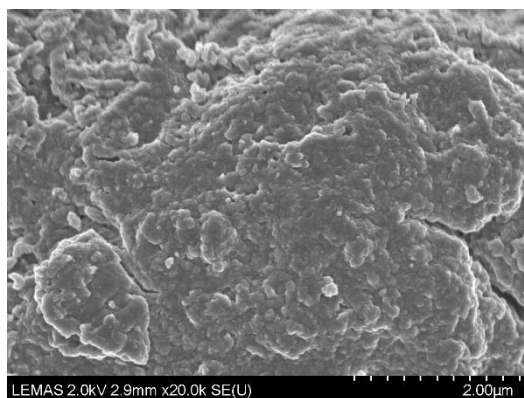


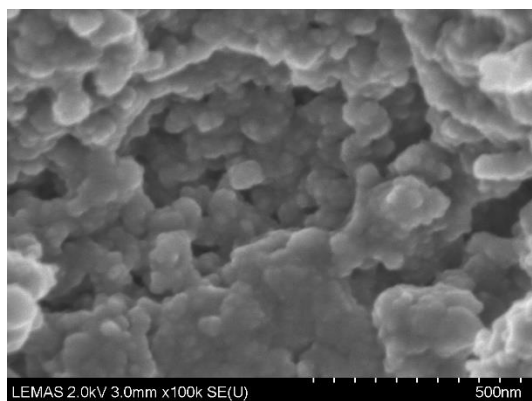
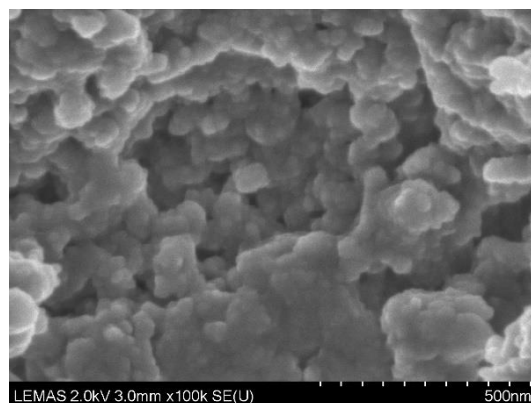
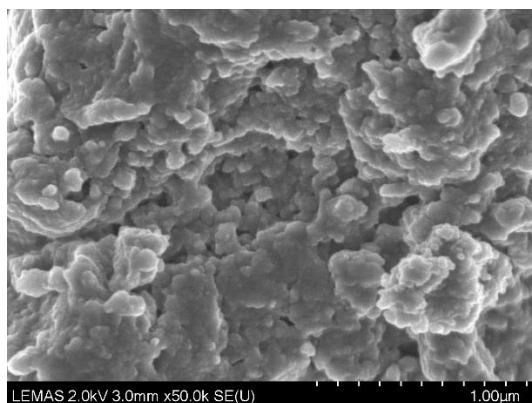
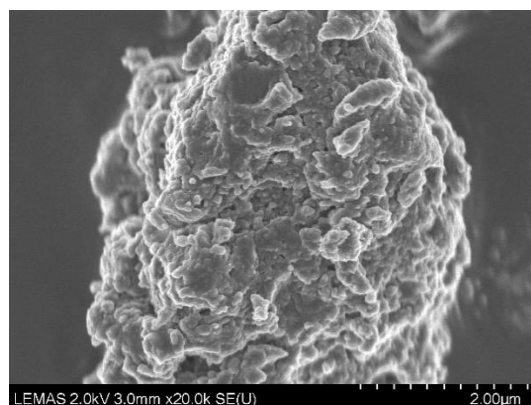
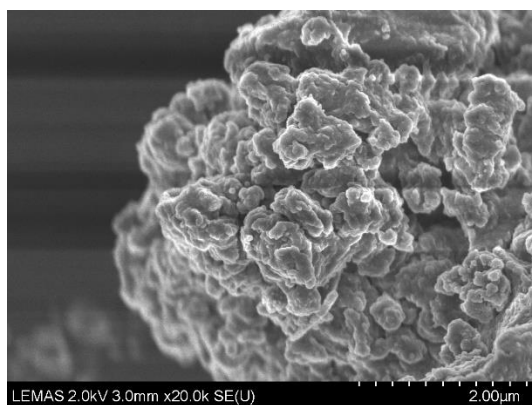
13. $\text{PdCl}_4\text{@PPh}_2\text{-PIILP}$



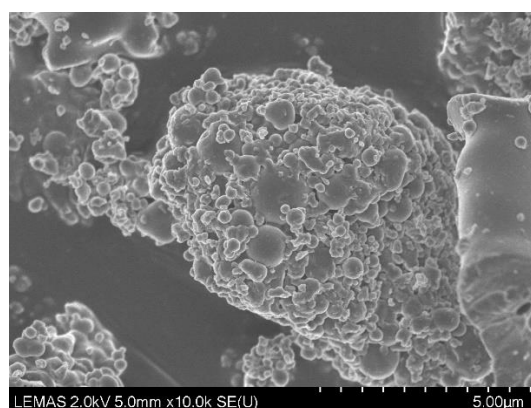
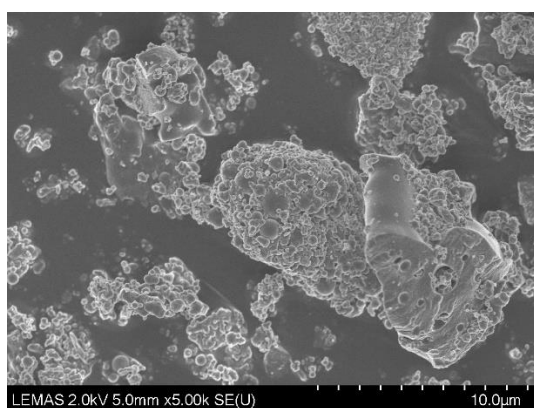
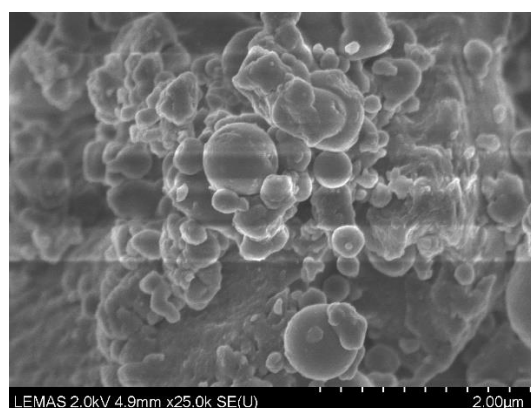
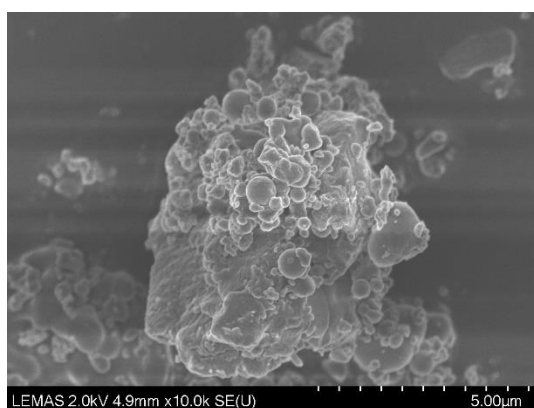
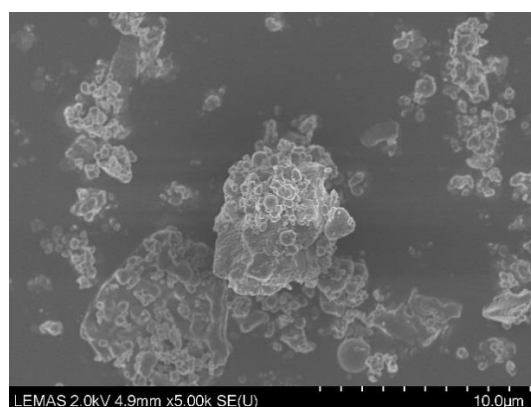
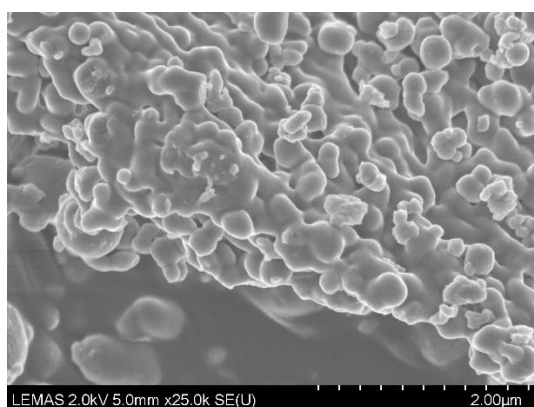
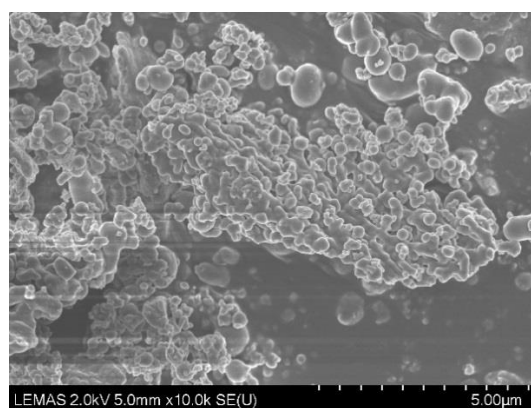
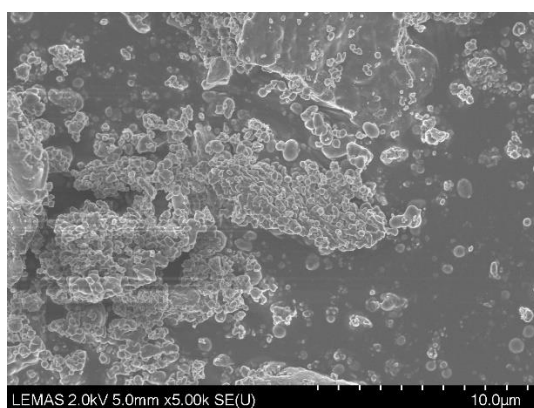


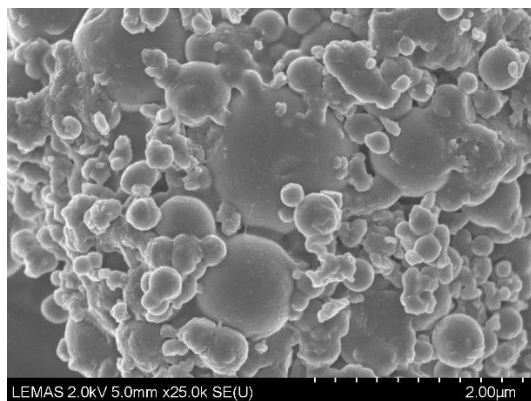
14. PdNP@PPh₂-PIILP

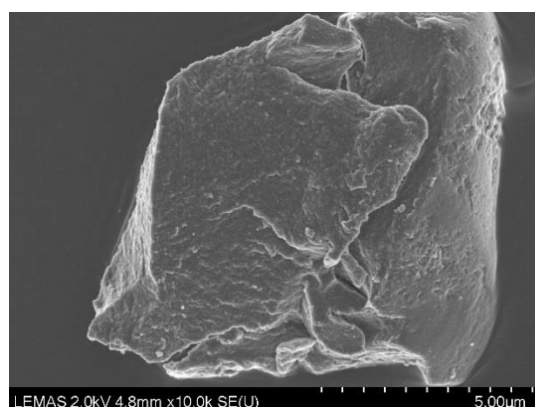
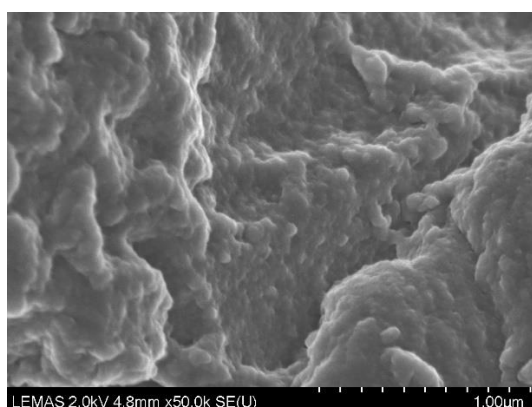
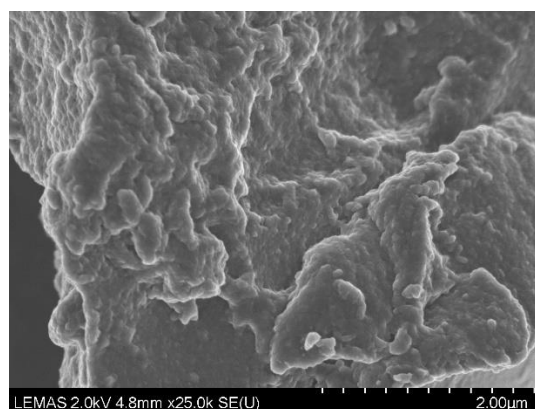
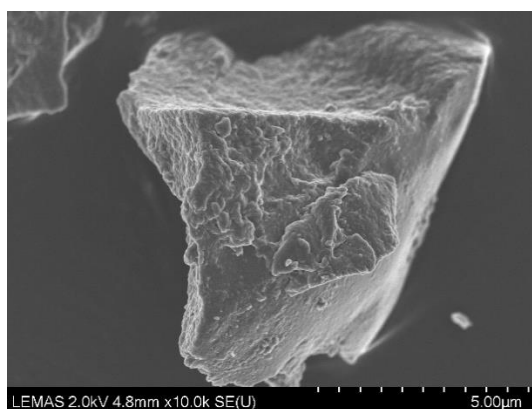
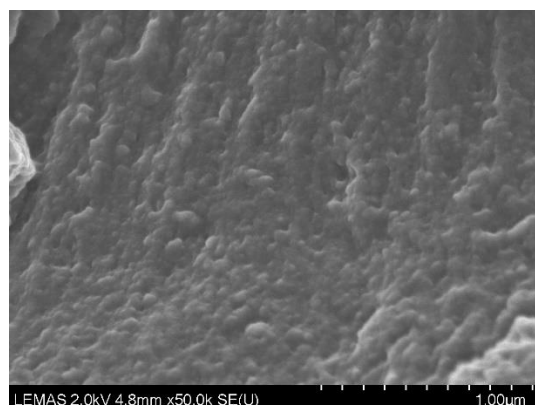
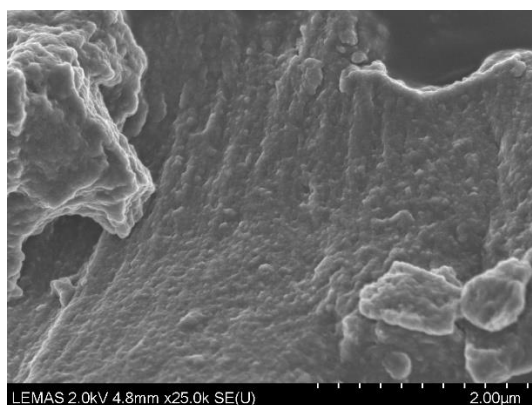
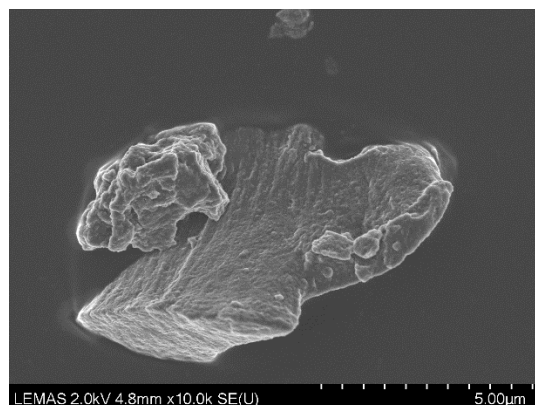
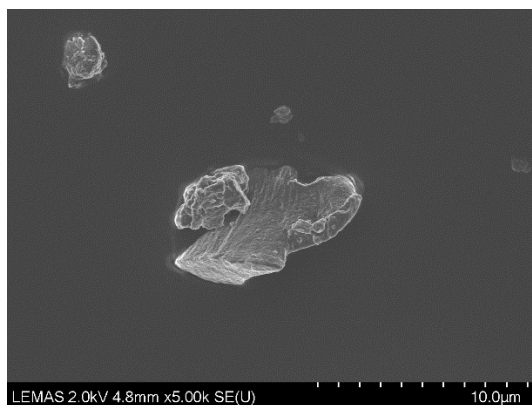


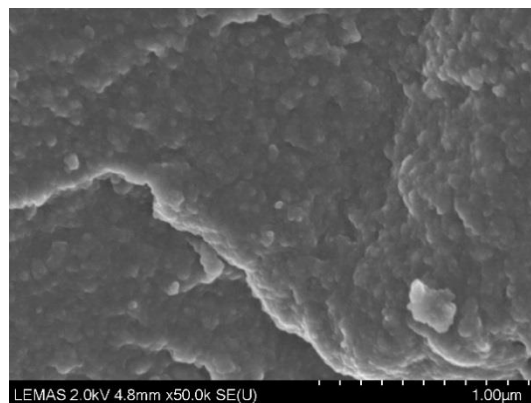
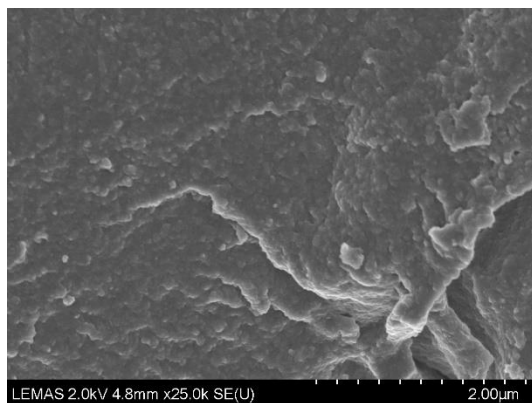


15. $\text{PtCl}_4@\text{PPh}_2\text{-PIILP}$

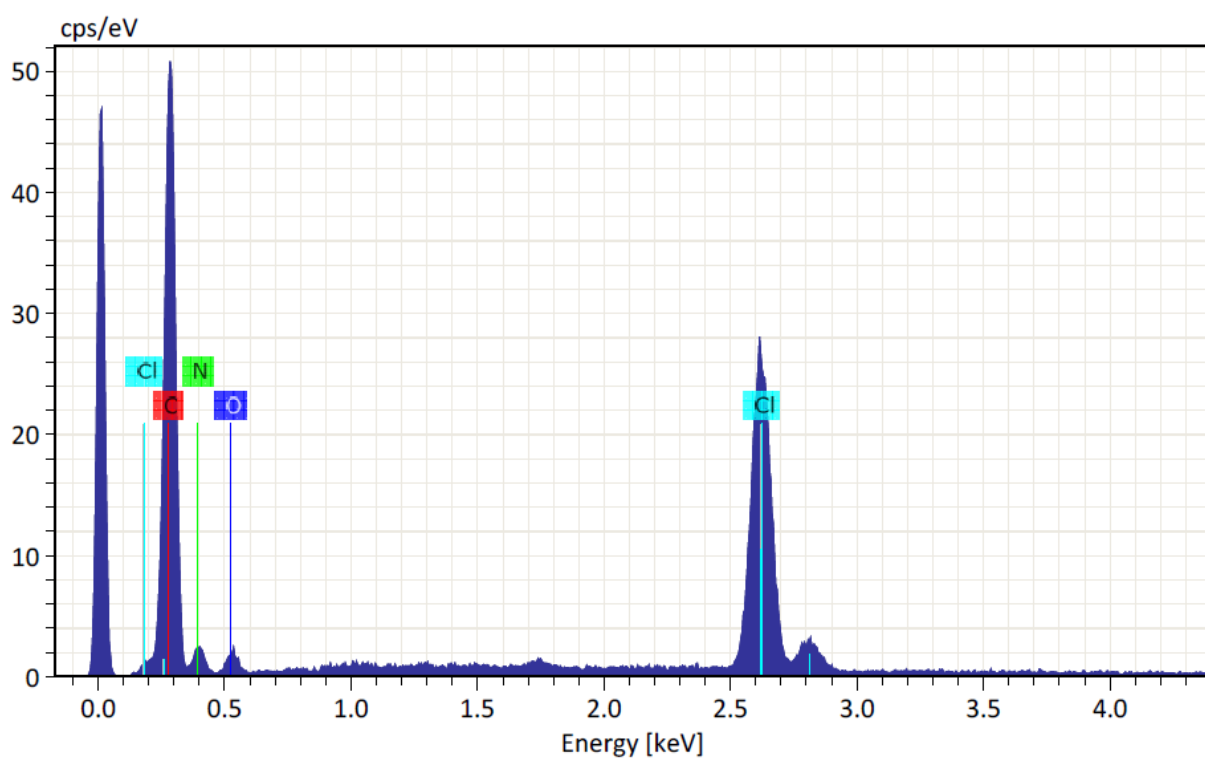
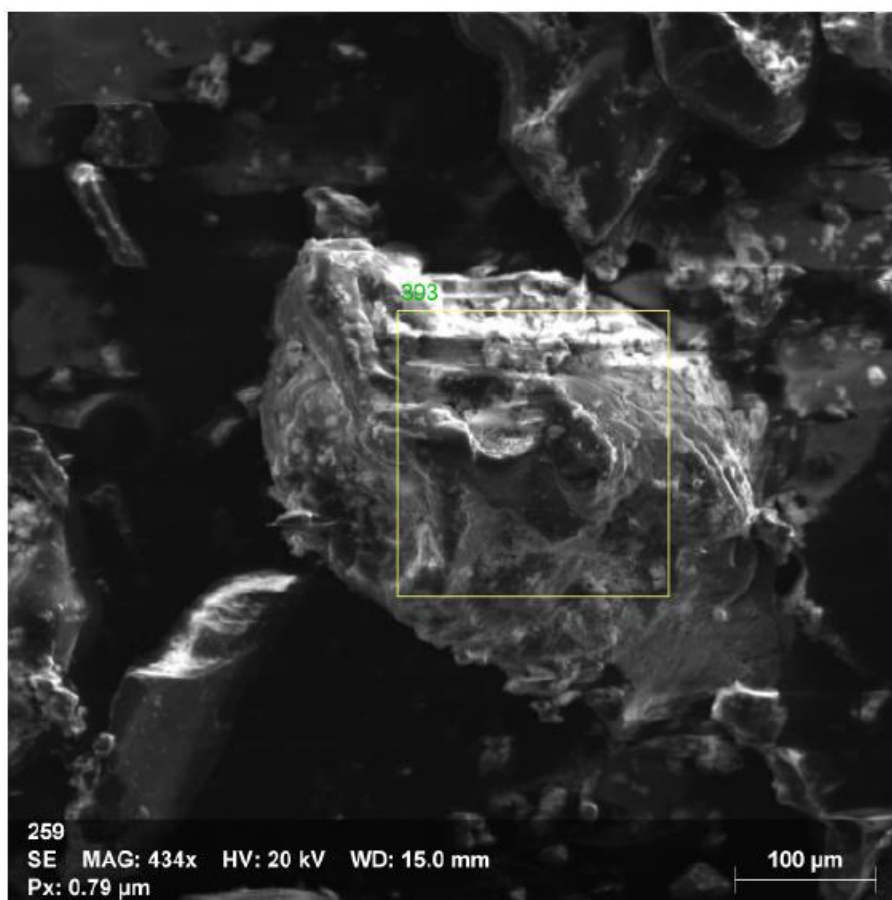




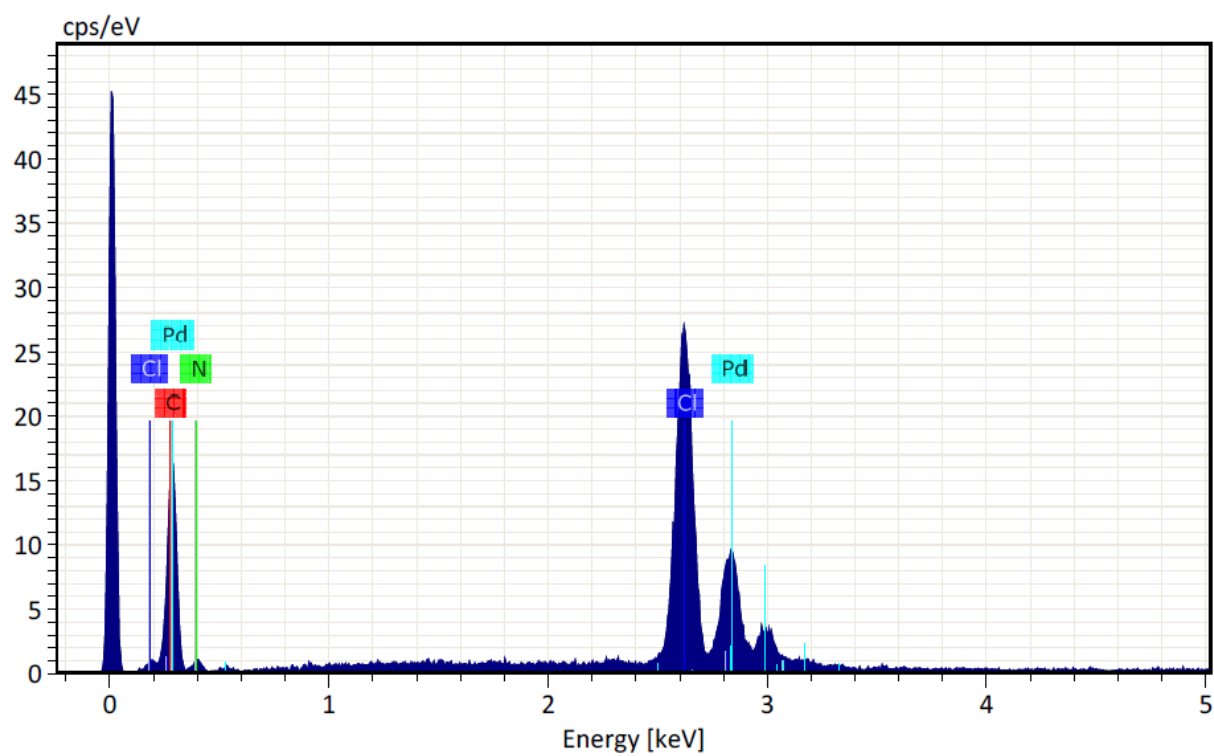
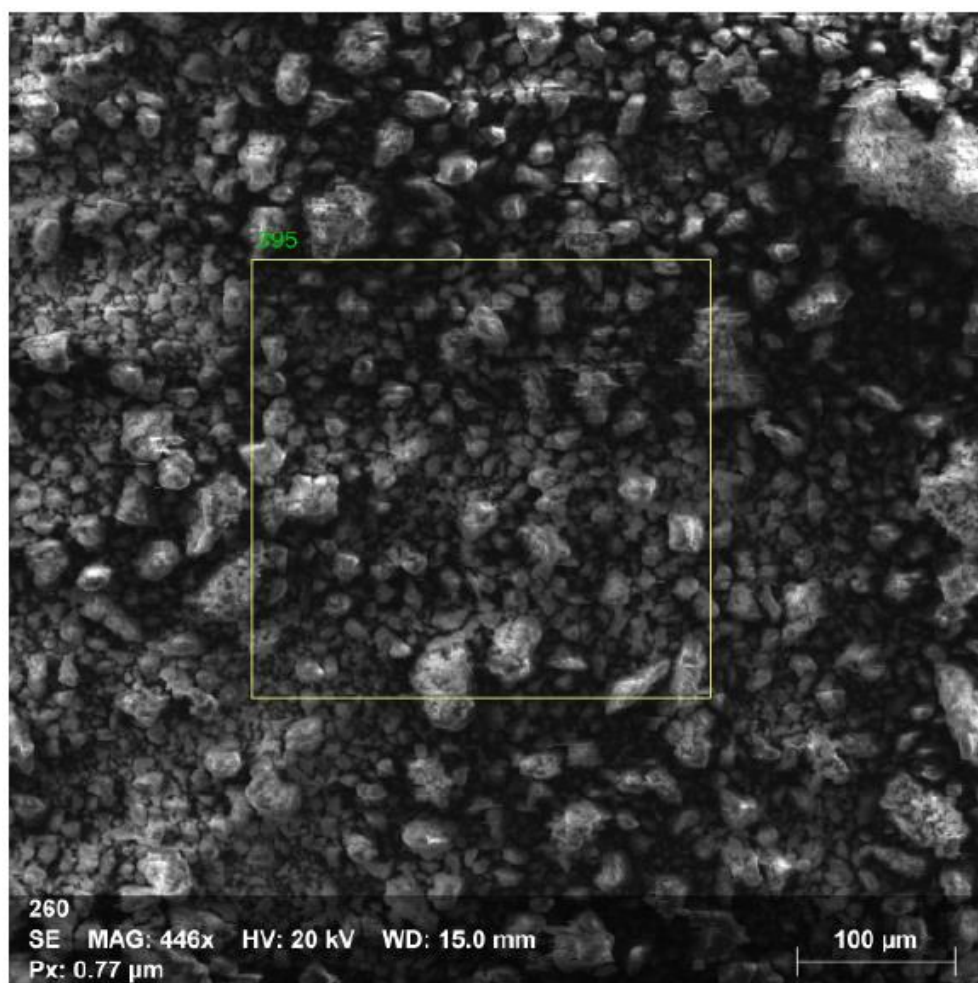
16. PtNP@PPh₂-PIILP

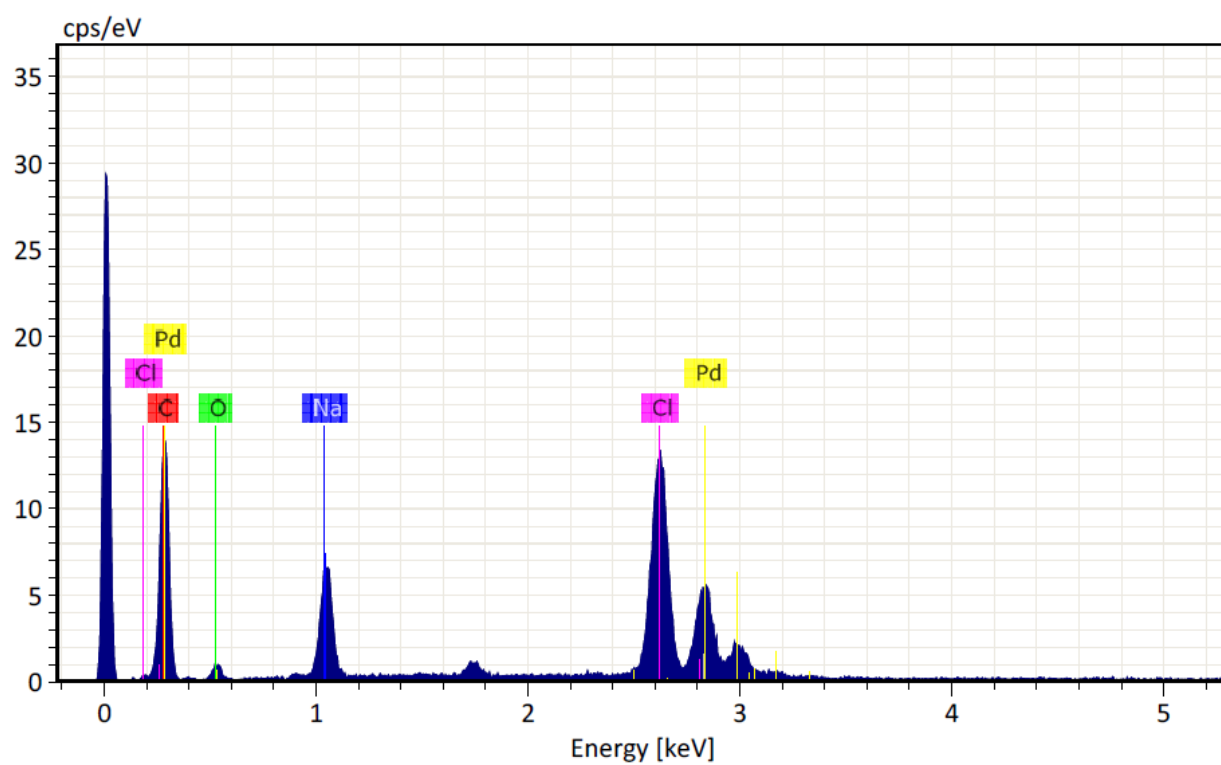
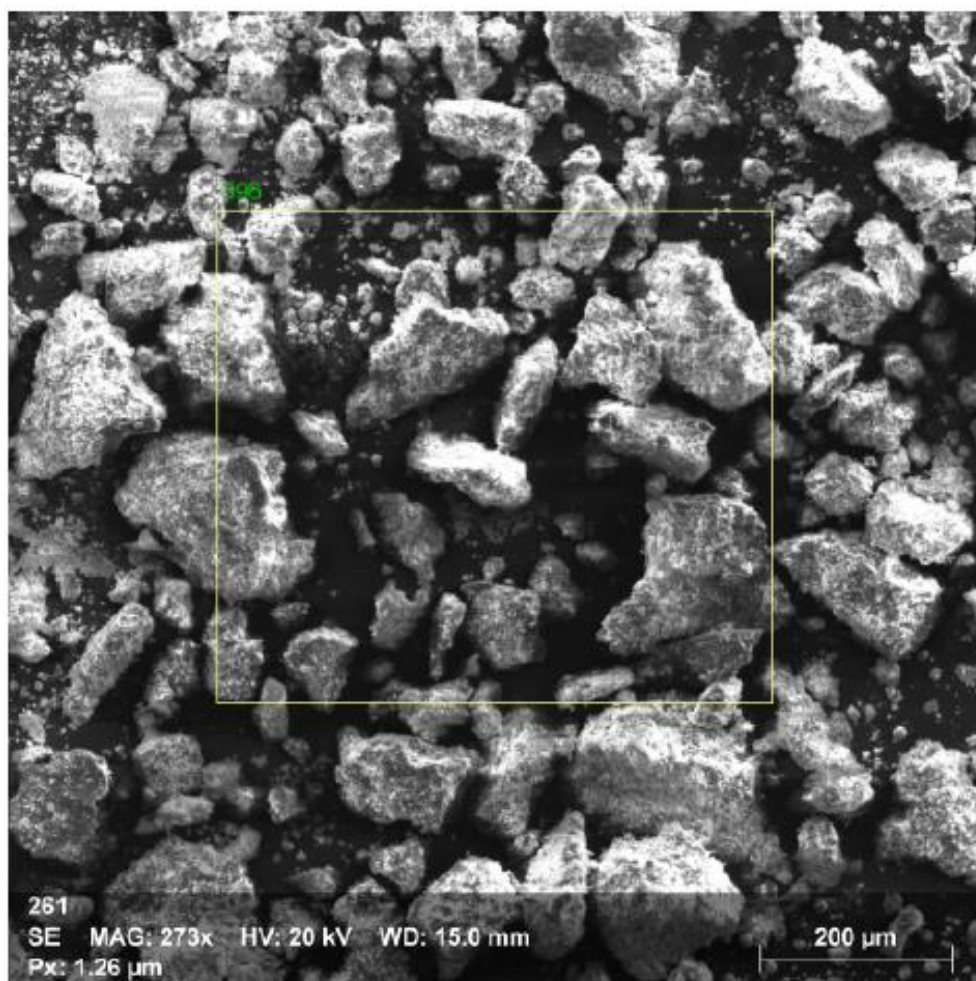


Appendix D. Energy-Dispersive X-Ray Spectroscopy (EDX)

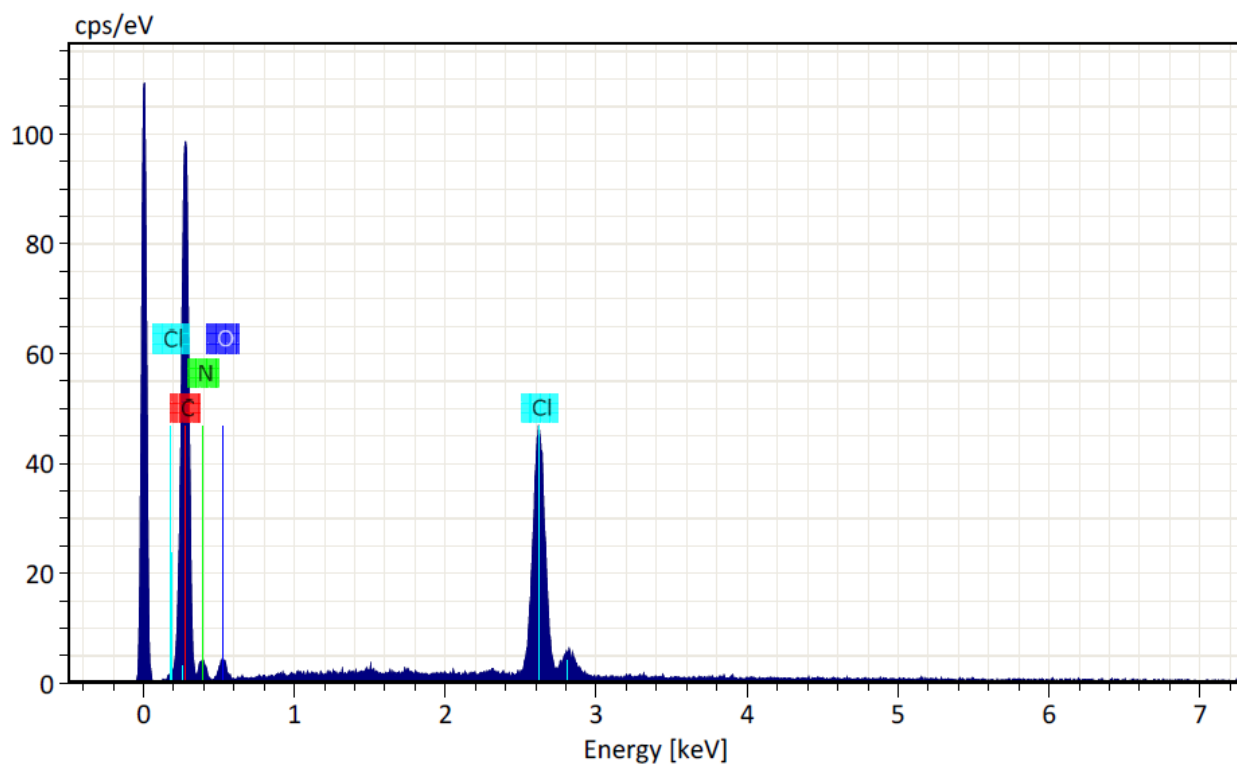
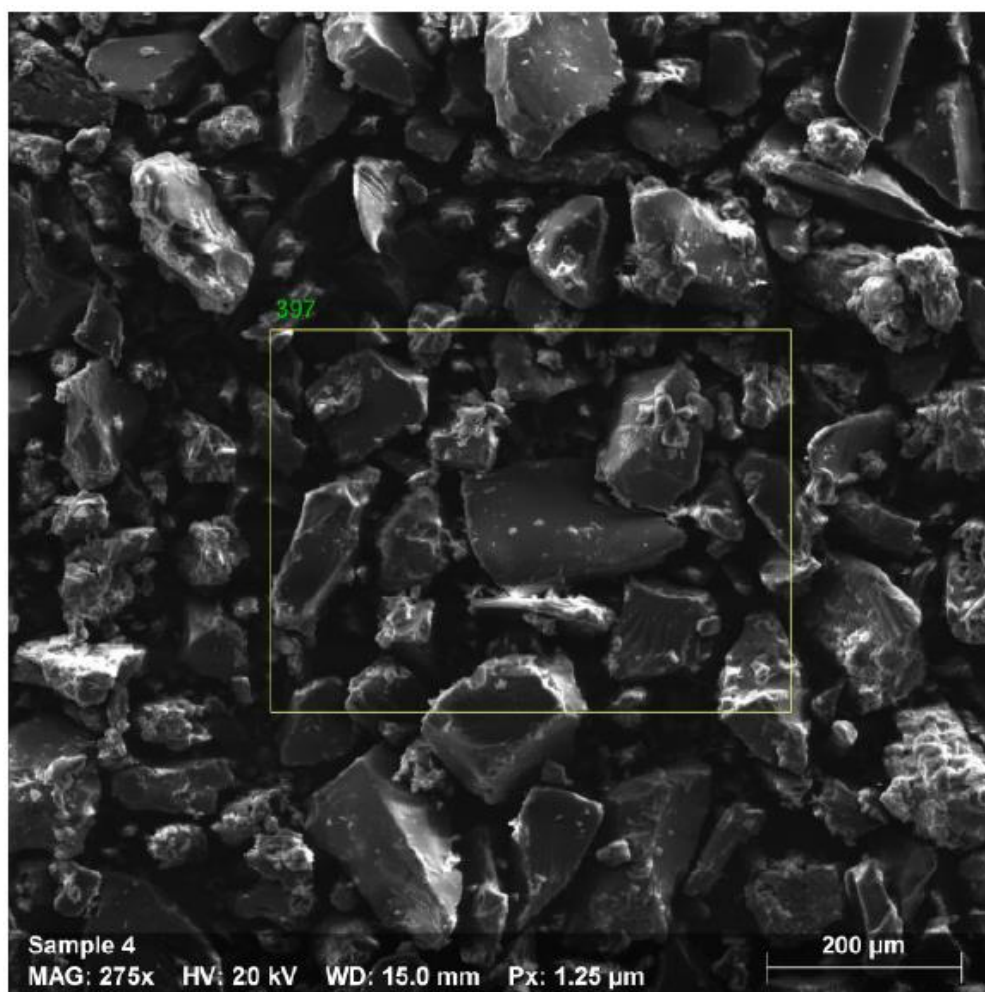
1. $\text{NH}_2\text{-PIILP}$ 

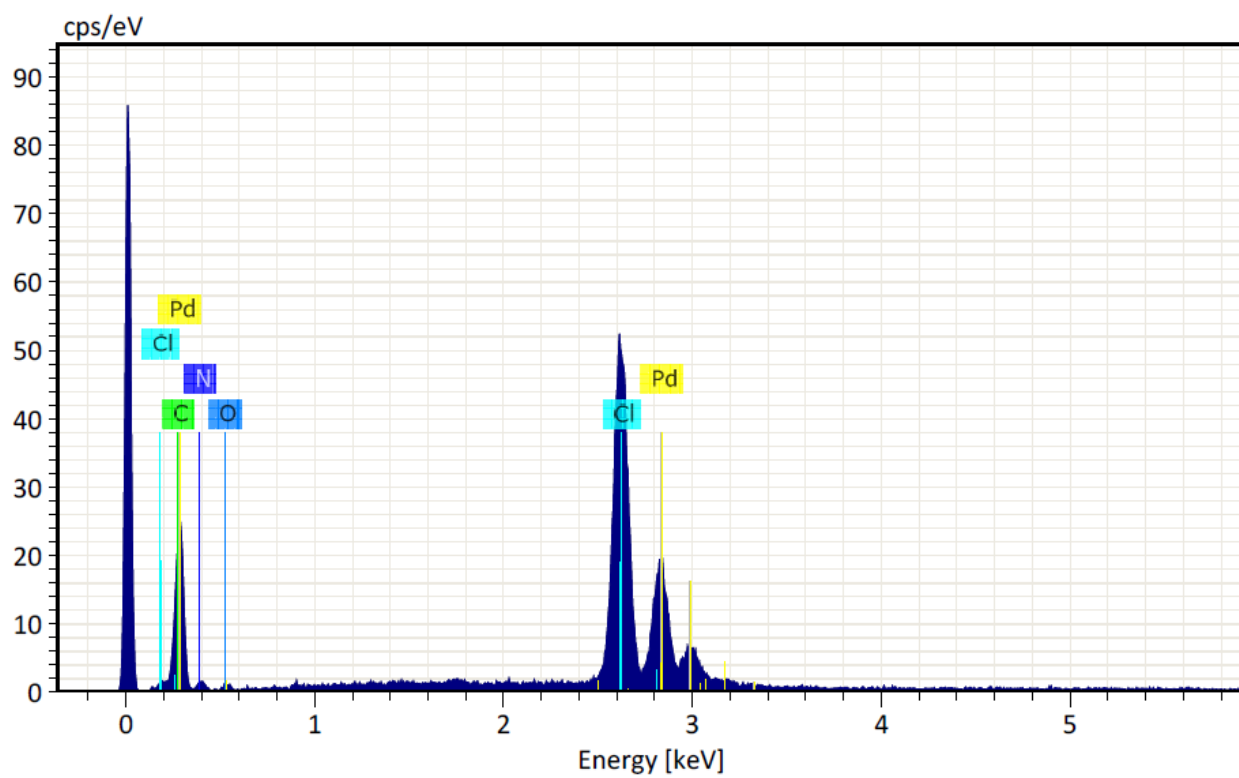
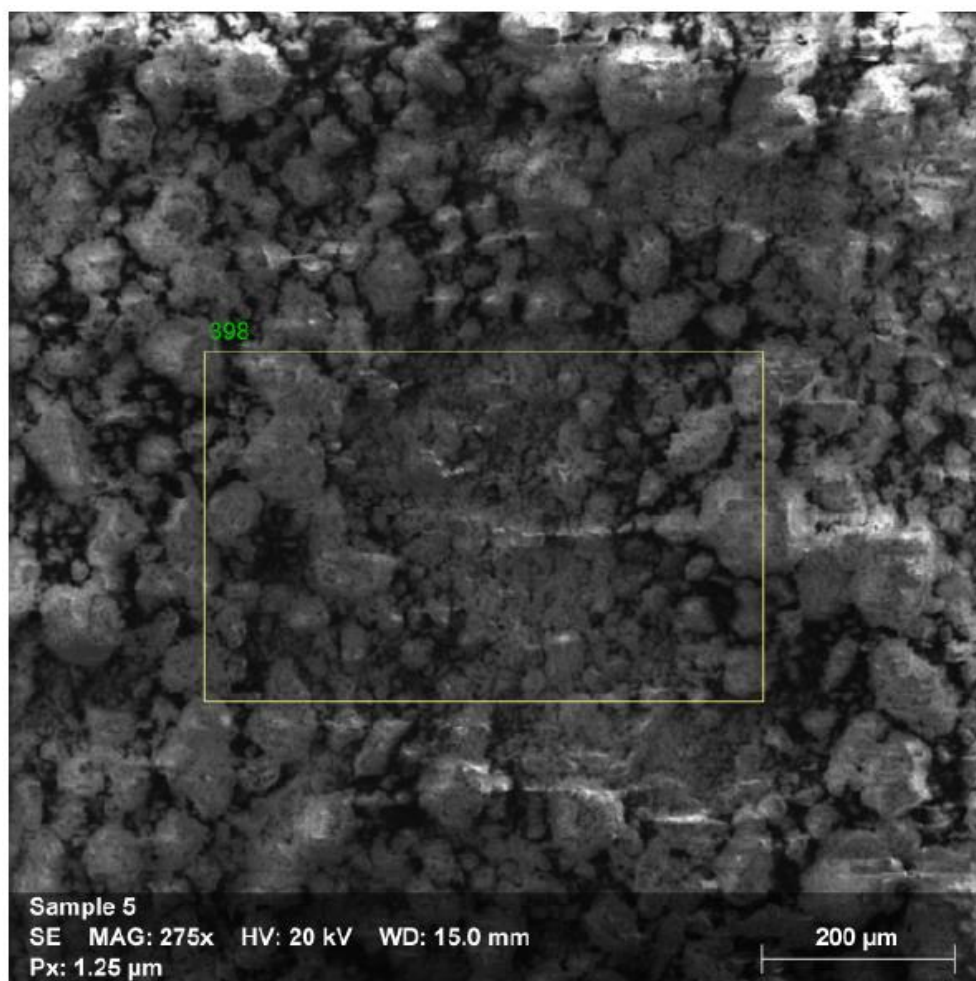
2. $\text{PdCl}_4@\text{NH}_2\text{-PIILP}$



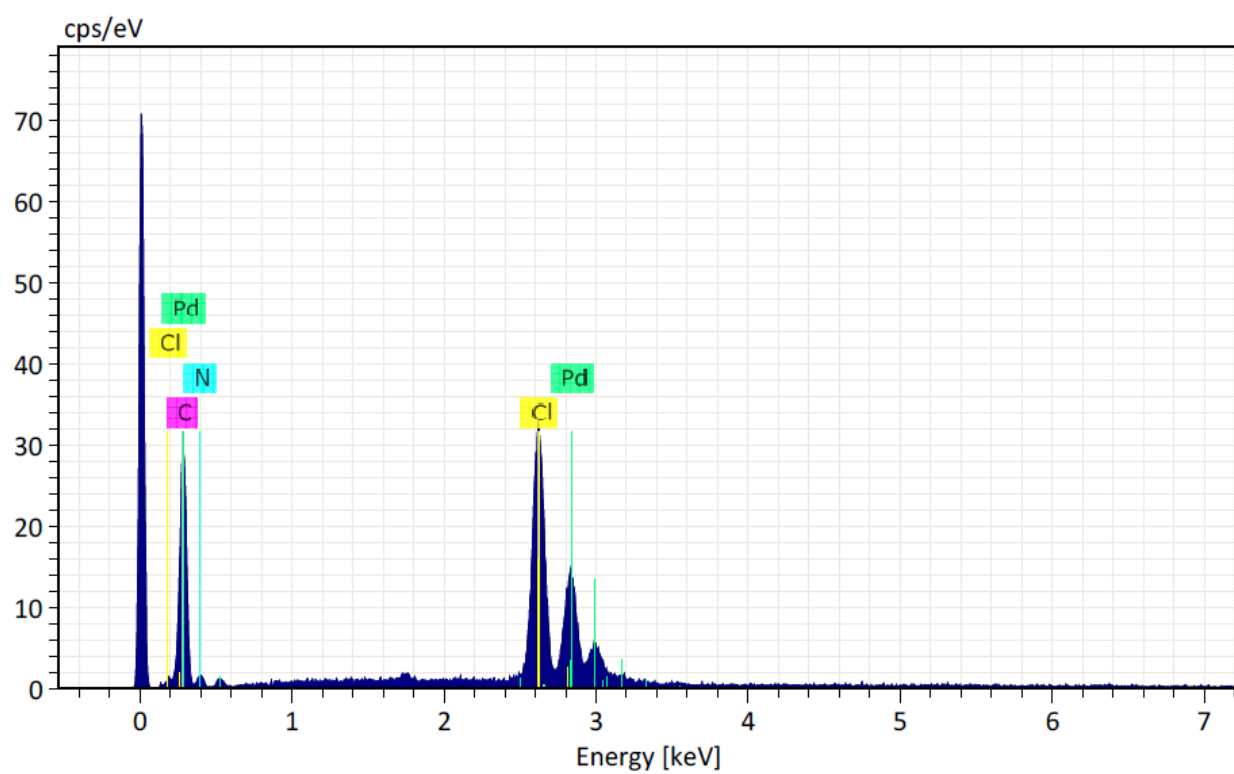
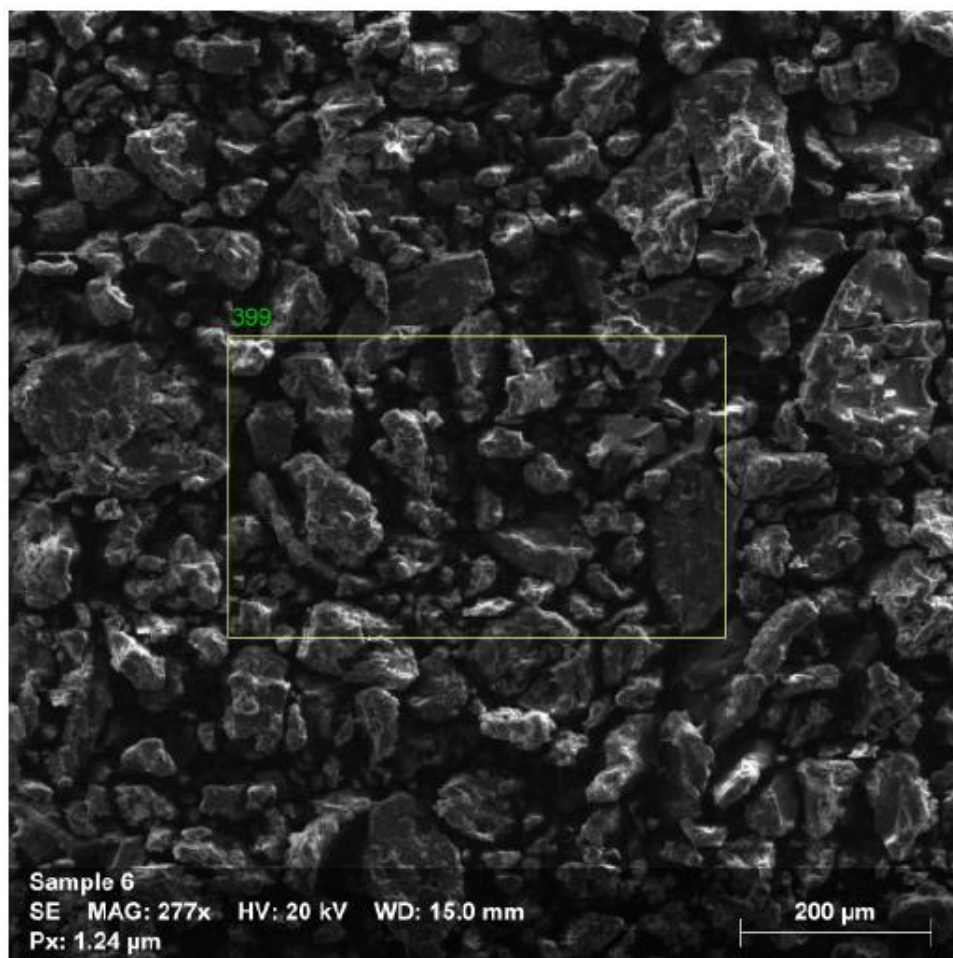
3. PdNP@NH₂-PIILP

4. Pyrr-PIILP



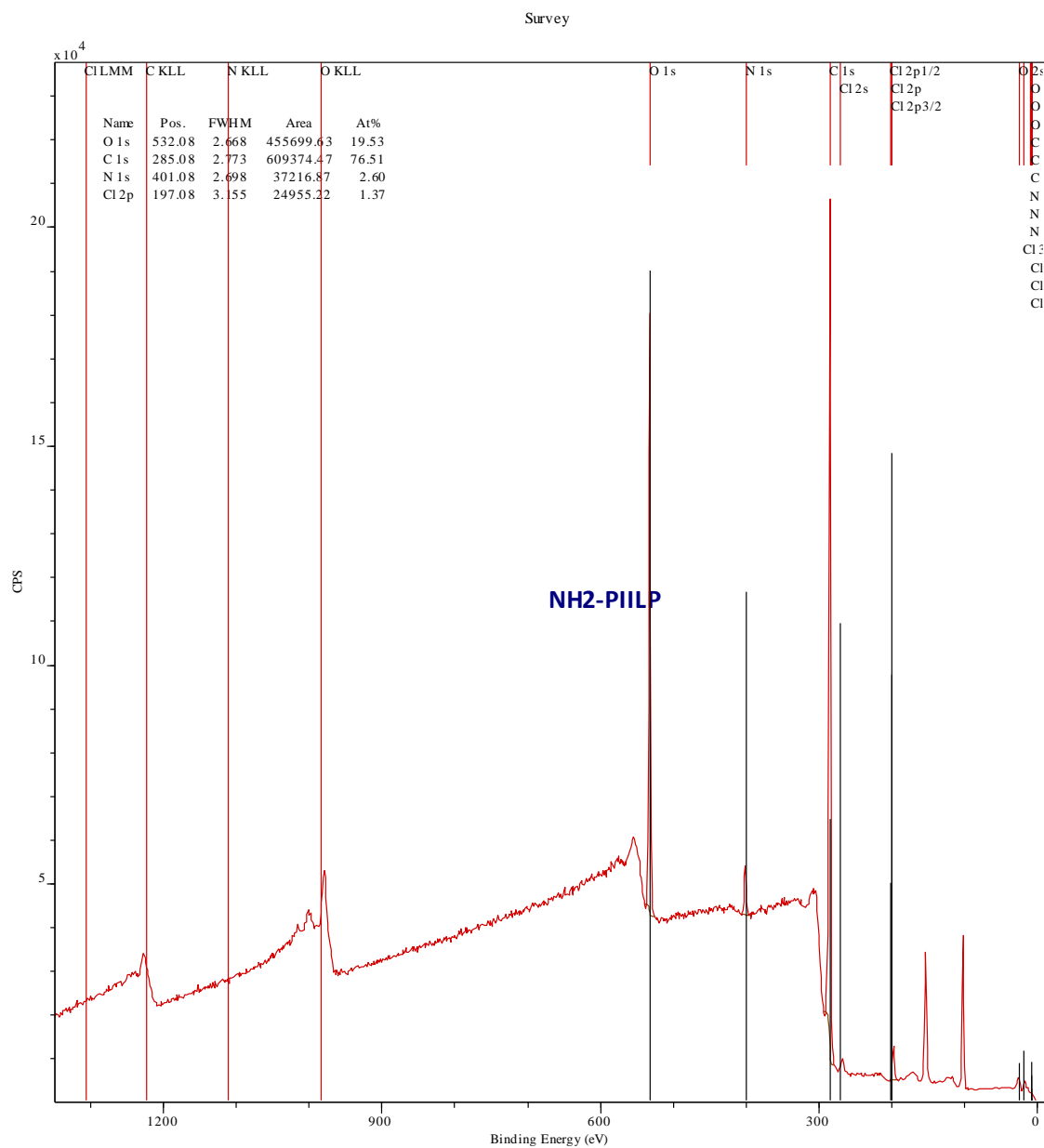
5. $\text{PdCl}_4\text{@Pyrr-PIILP}$ 

6. PdNP@Pyrr-PIILP

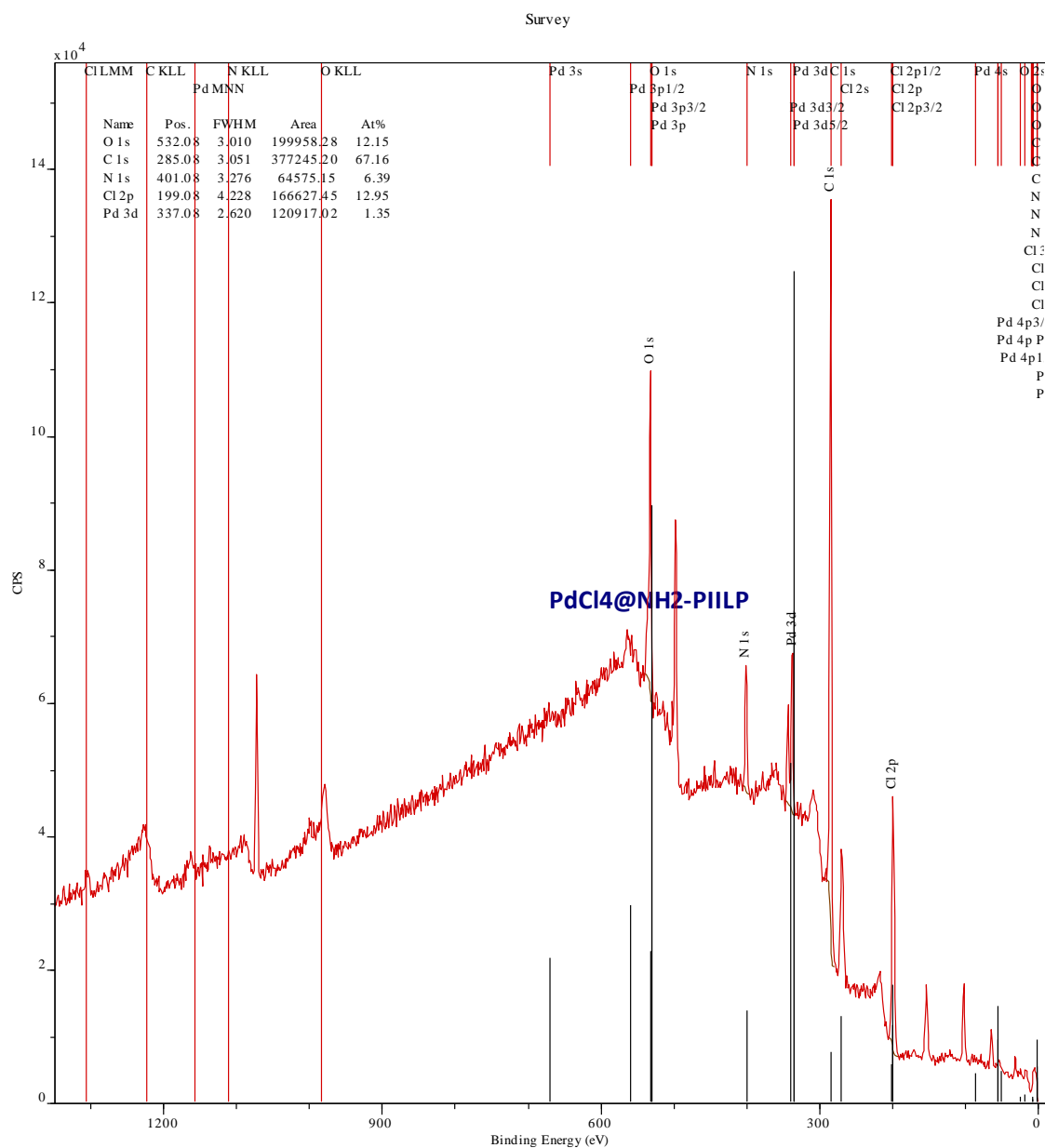


Appendix E. X-Ray Photoelectron Spectroscopy (XPS)

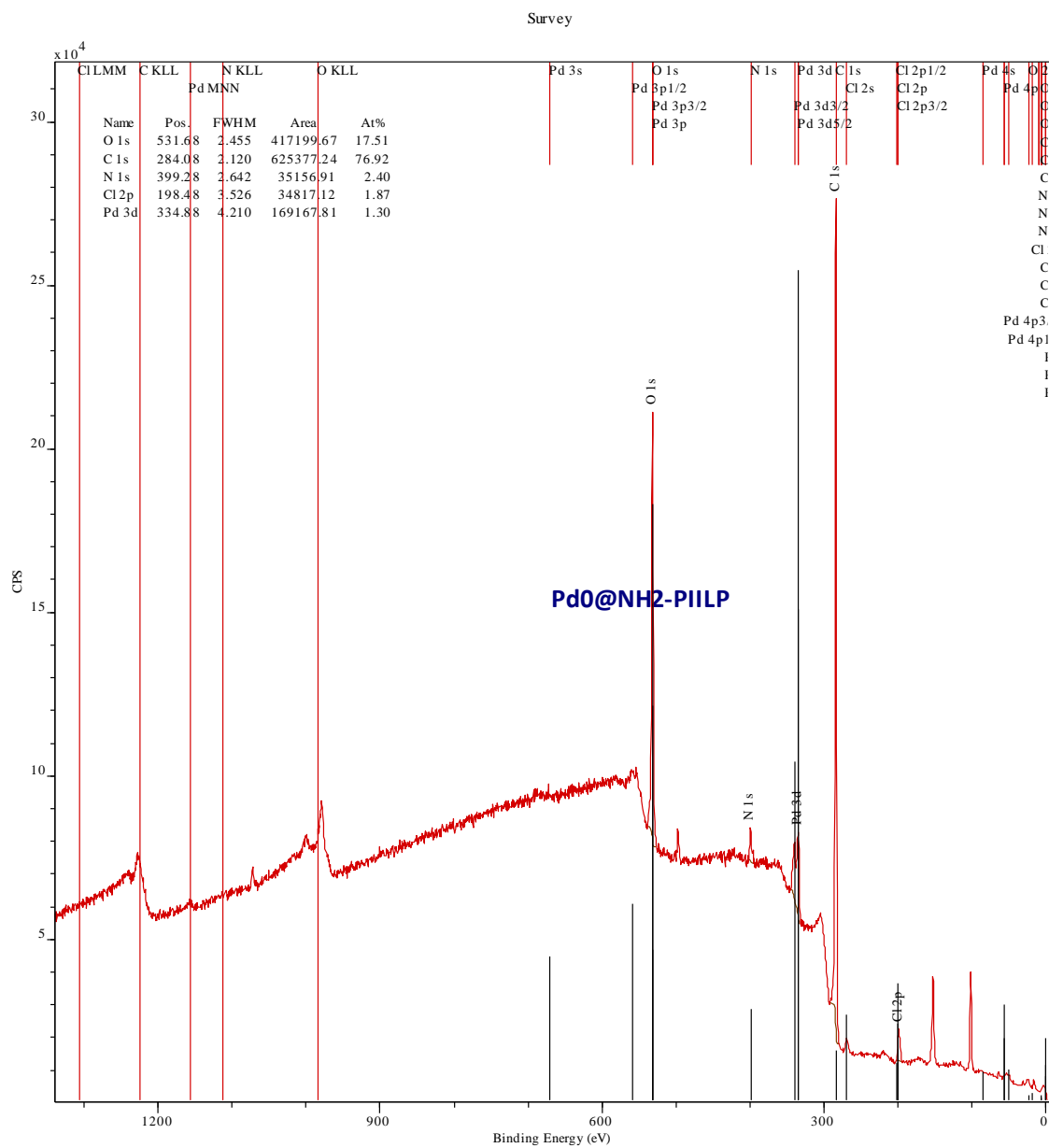
1. $\text{NH}_2\text{-PIILP}$



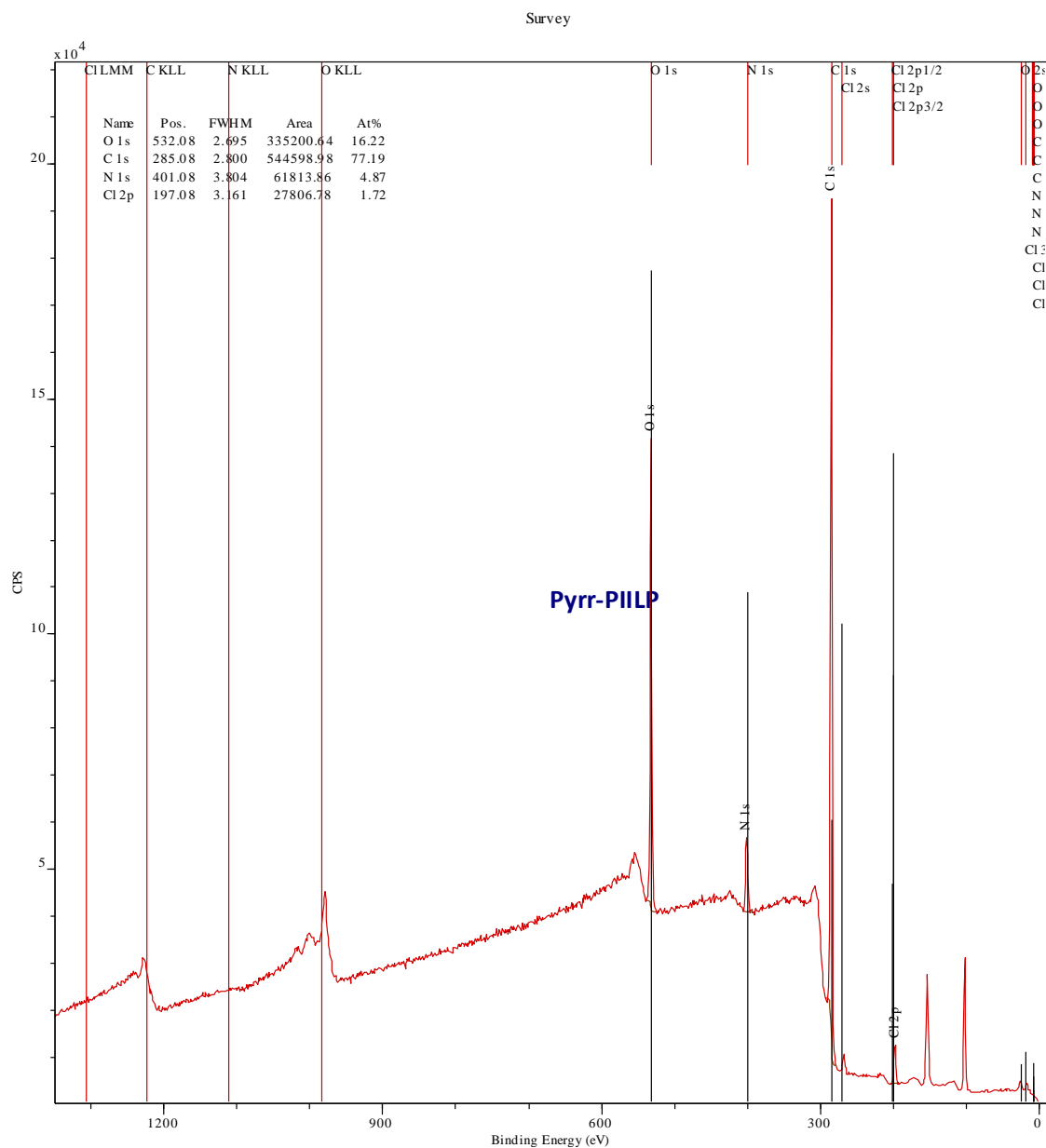
2. PdCl₄@NH₂-PIILP

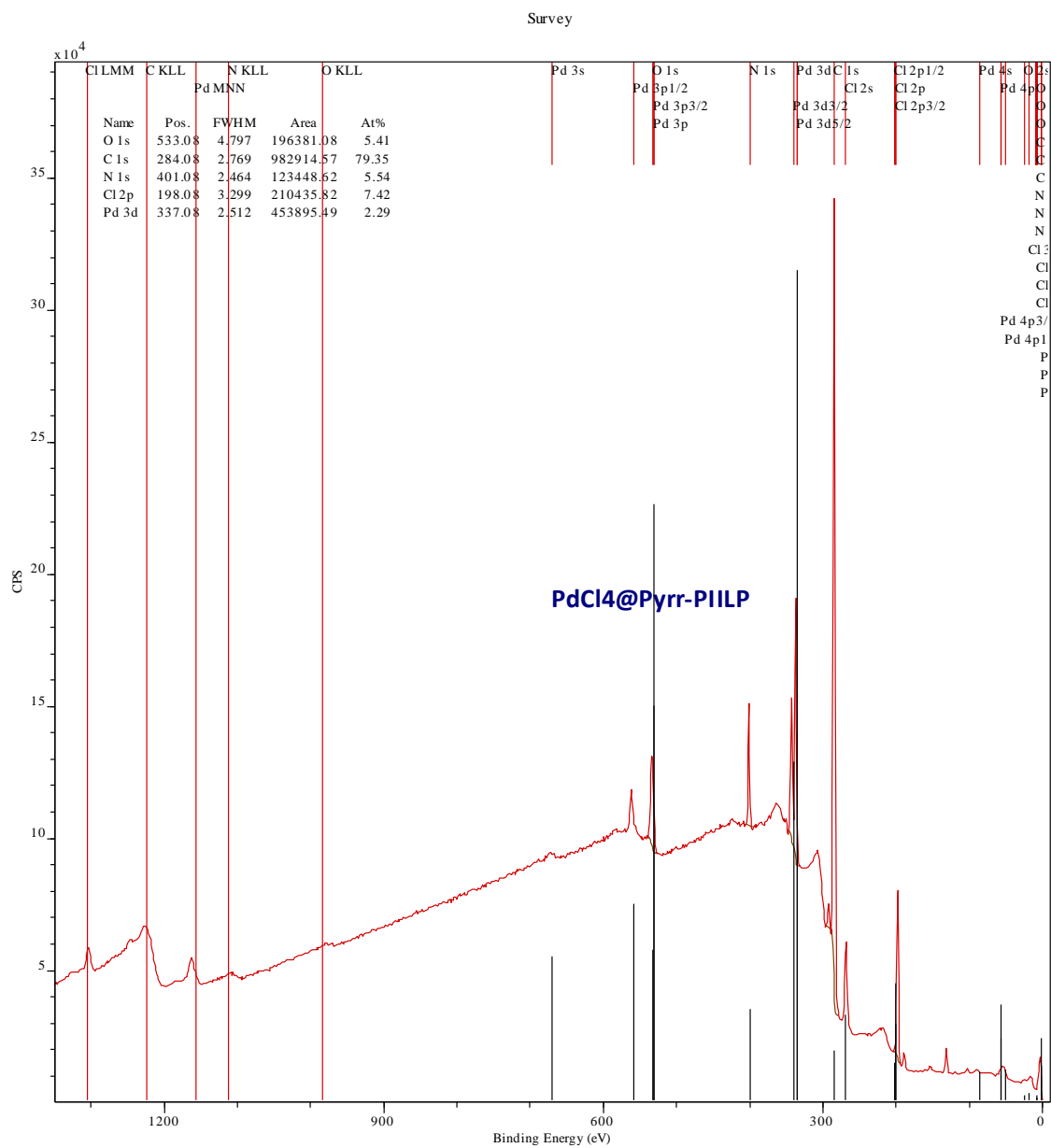


3. PdNP@NH₂-PIILP

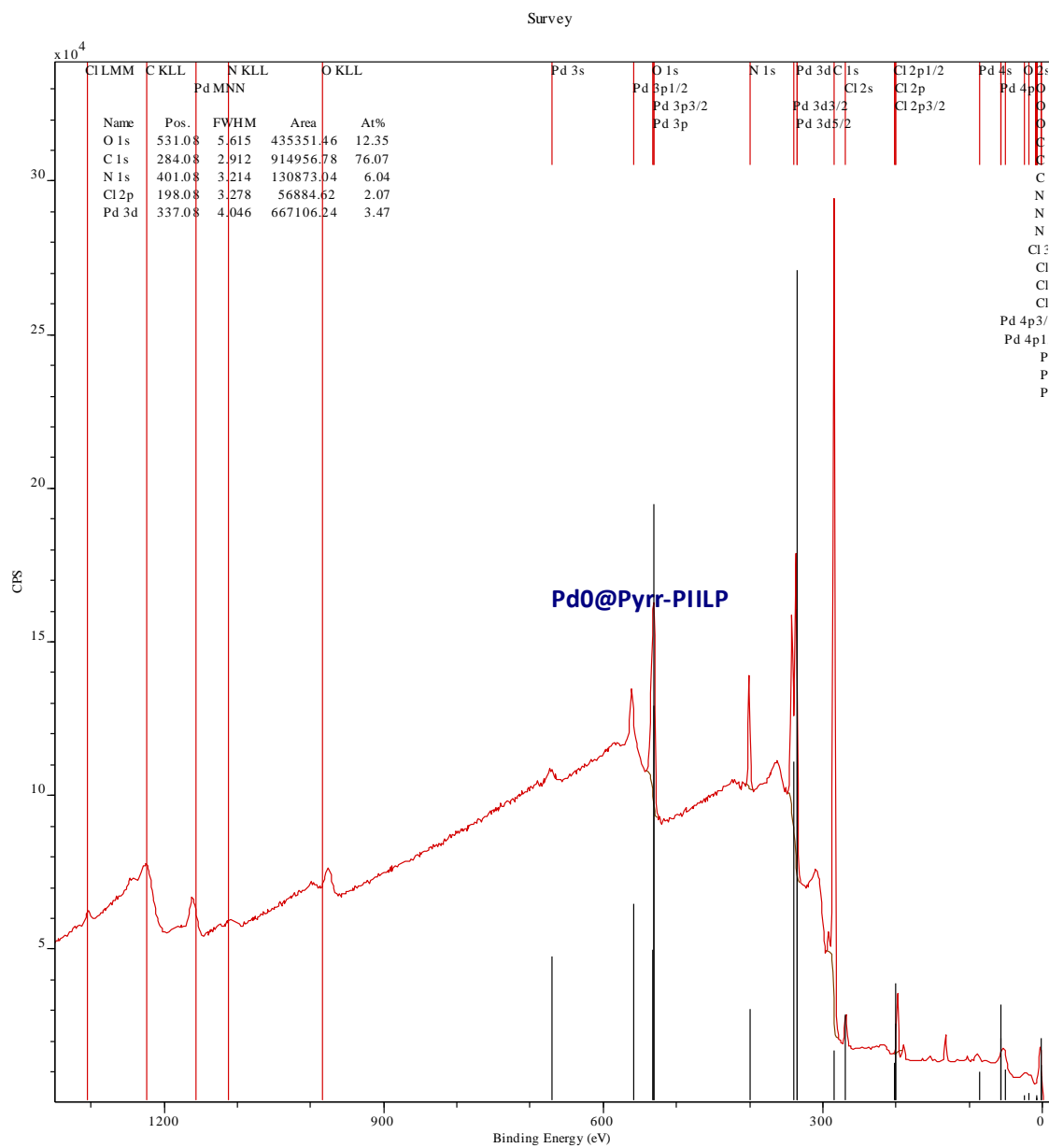


4. Pyrr-PIILP

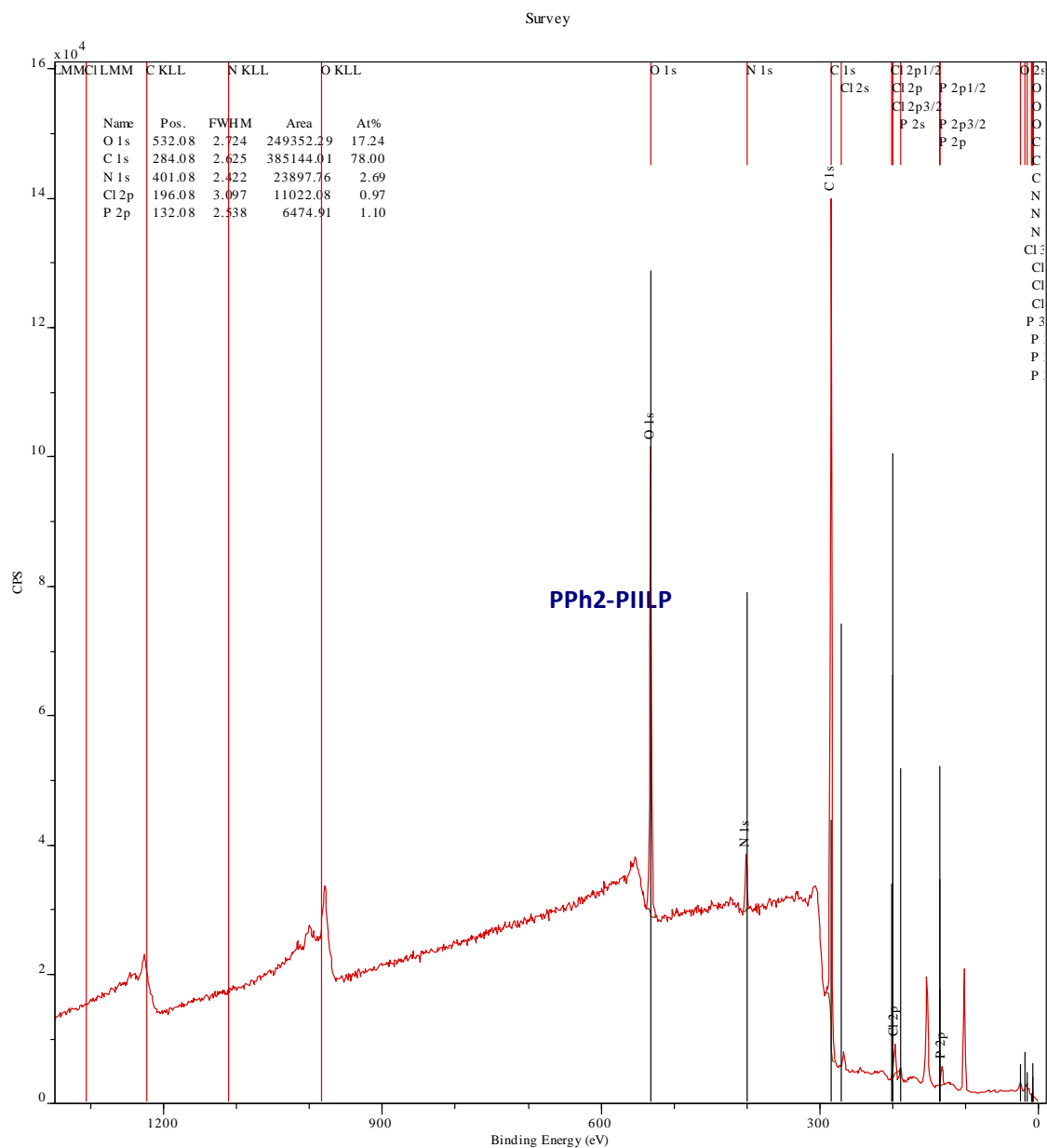


5. $\text{PdCl}_4\text{@Pyrr-PIILP}$ 

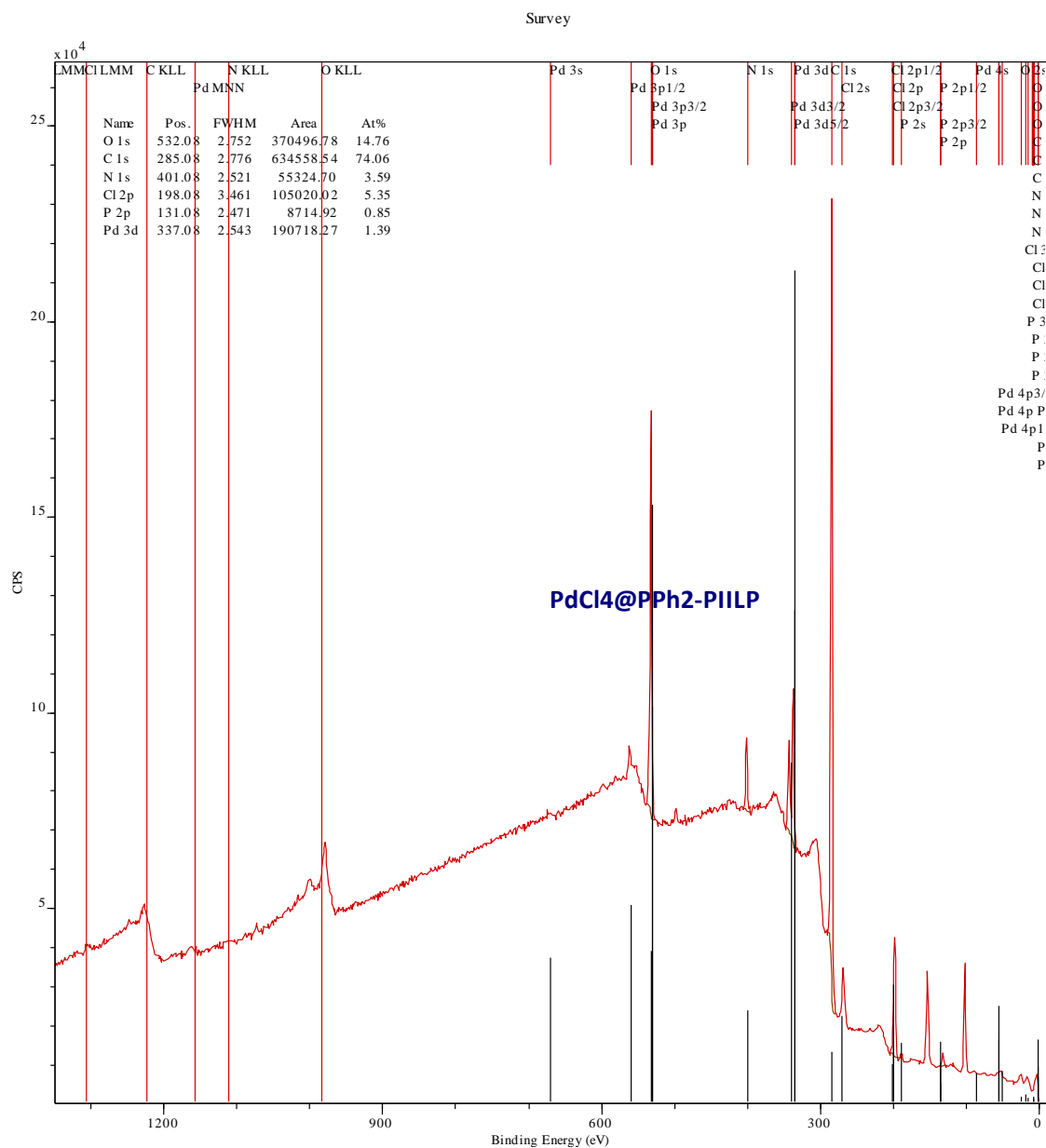
6. PdNP@Pyrr-PIILP

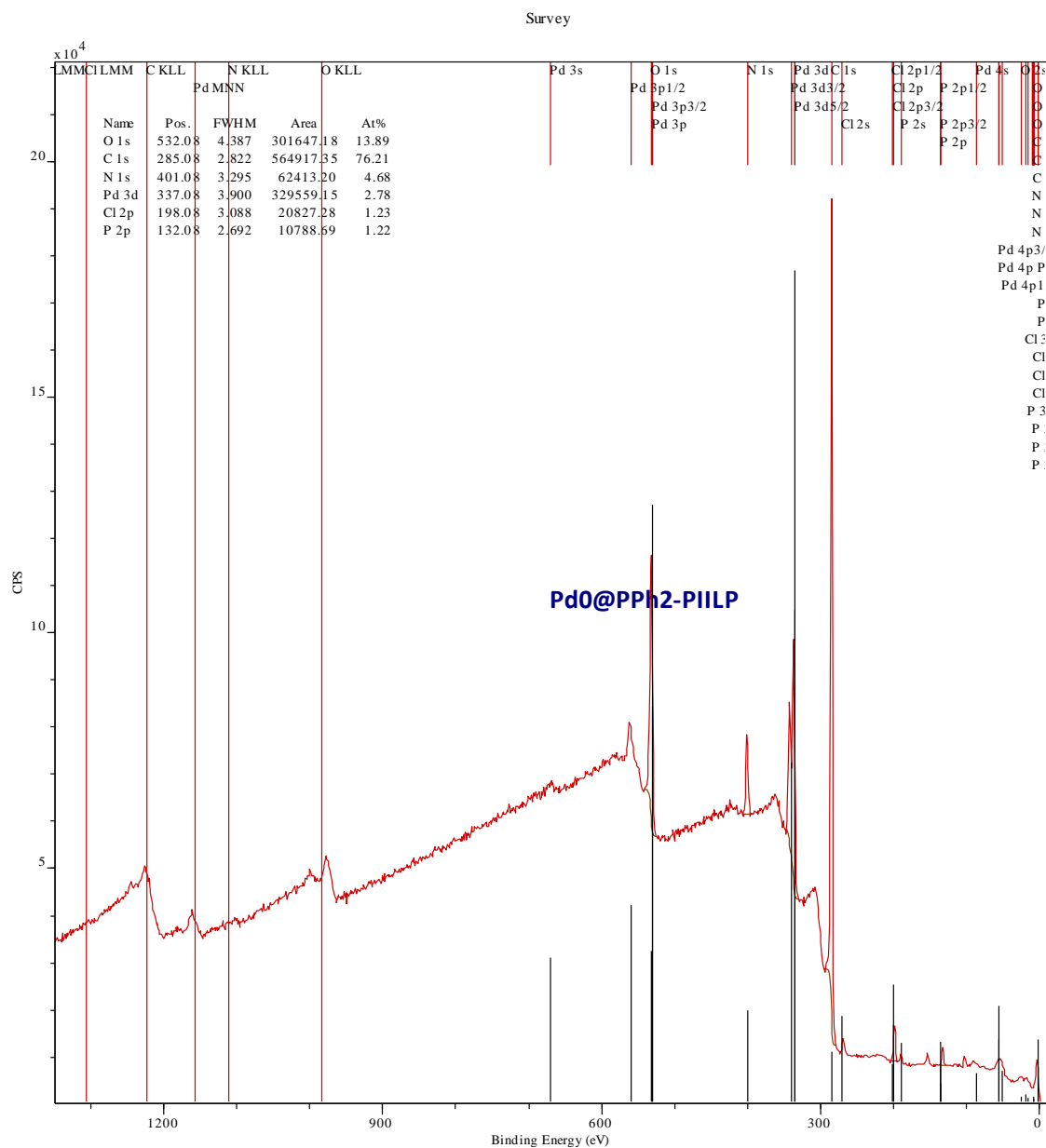


7. PPh_2 -PIILP

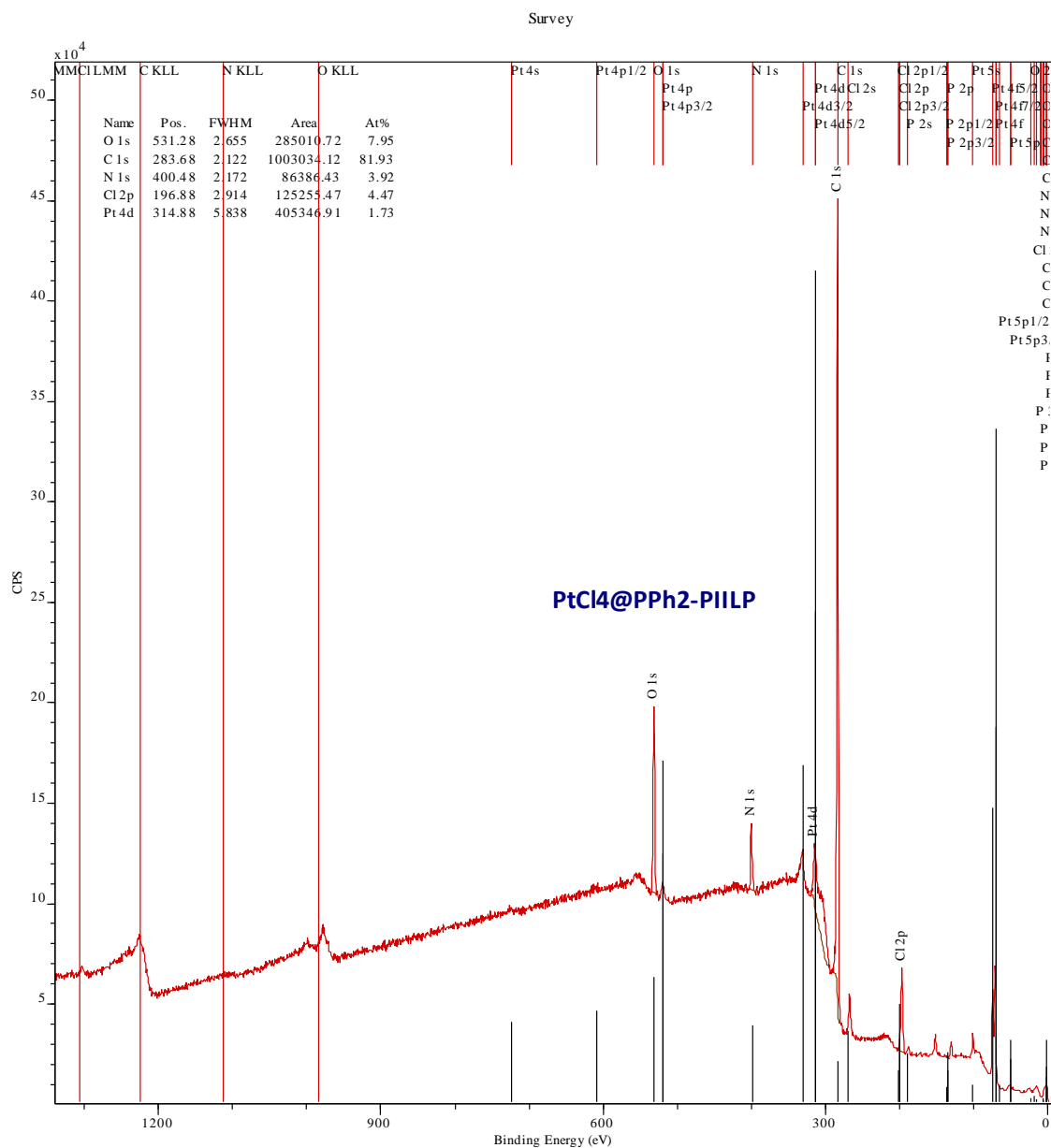


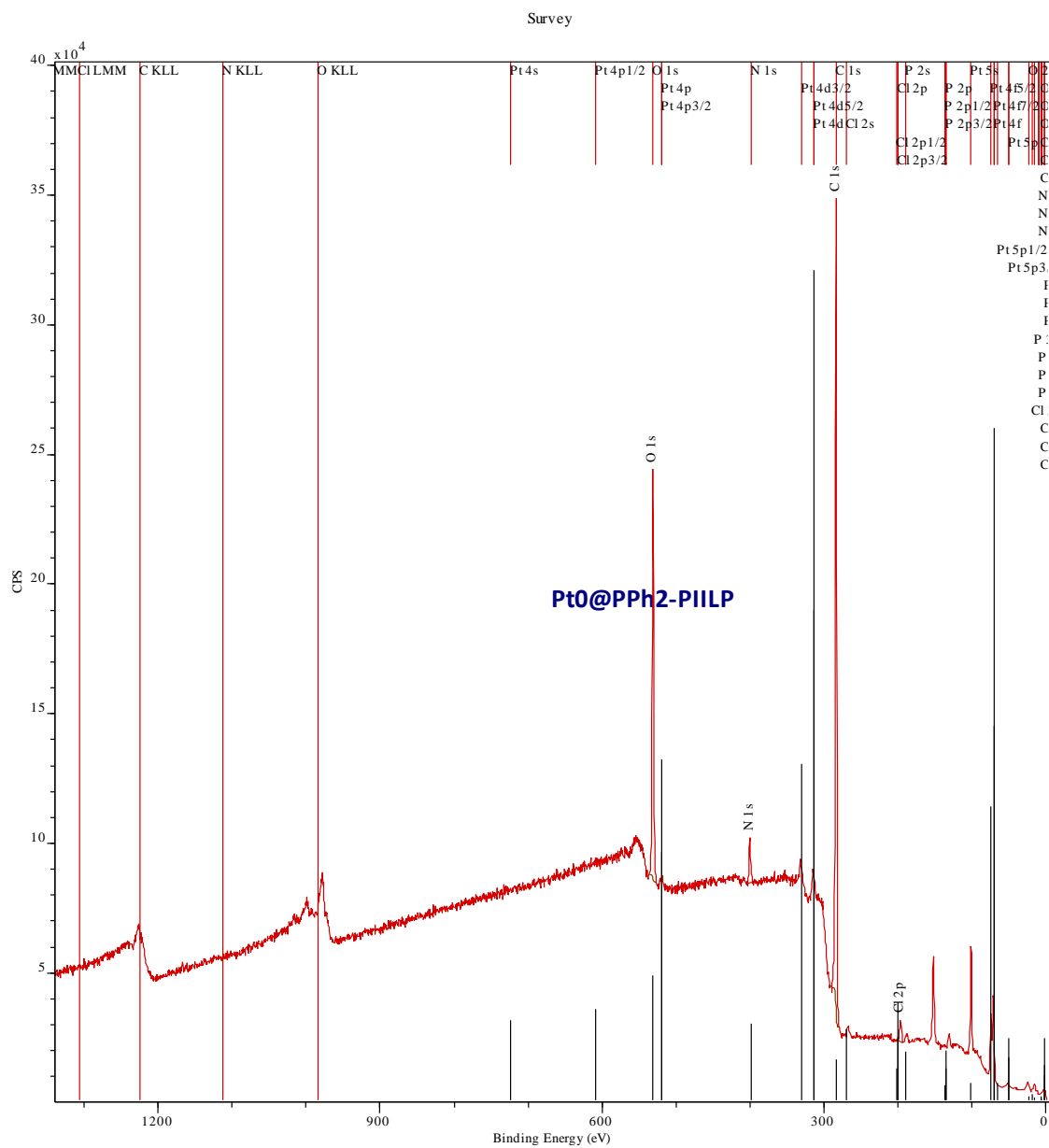
8. $PdCl_4@PPh_2$ -PIILP



9. PdNP@PPh₂-PIILP

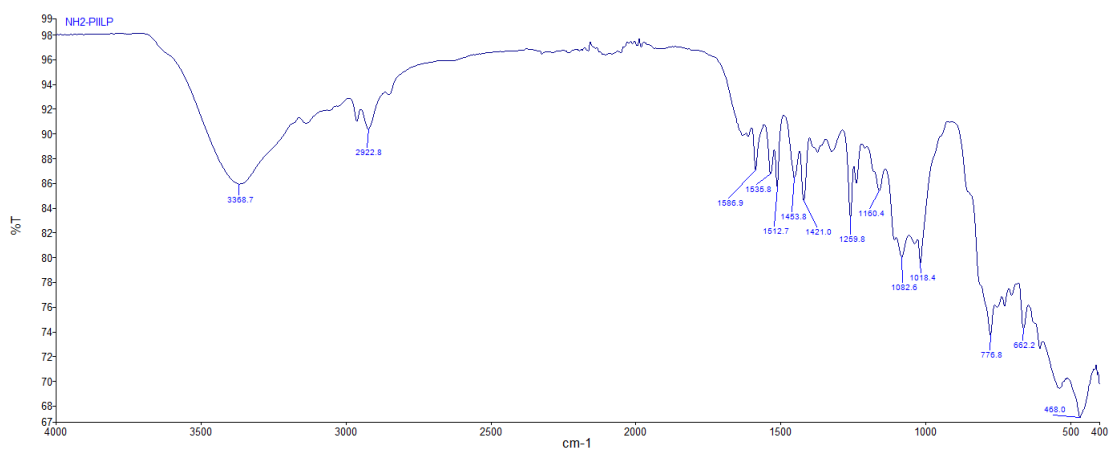
10. PtCl₄@PPh₂-PIILP



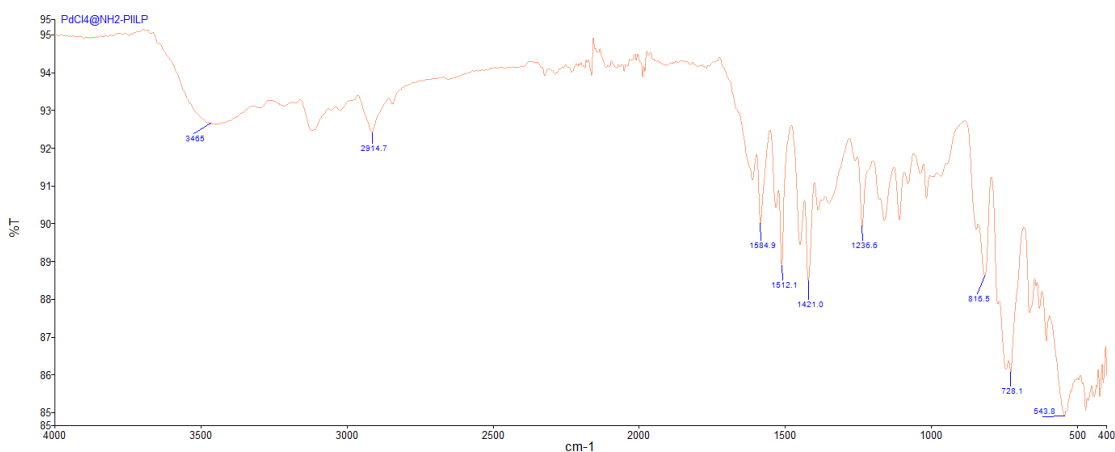
11. PtNP@PPh₂-PIILP

Appendix F. Infrared Radiation (FT-IR)

1. $\text{NH}_2\text{-PIILP}$



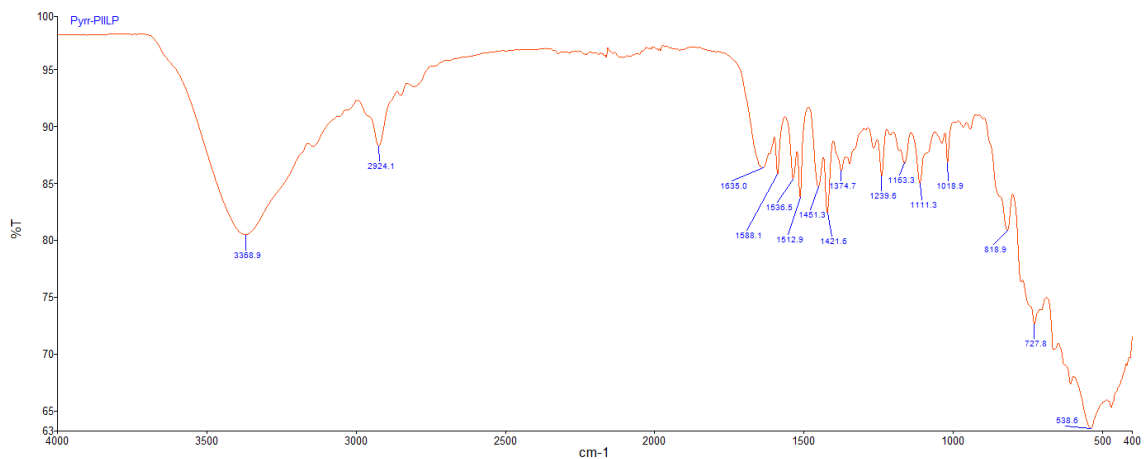
2. $\text{PdCl}_4@\text{NH}_2\text{-PIILP}$



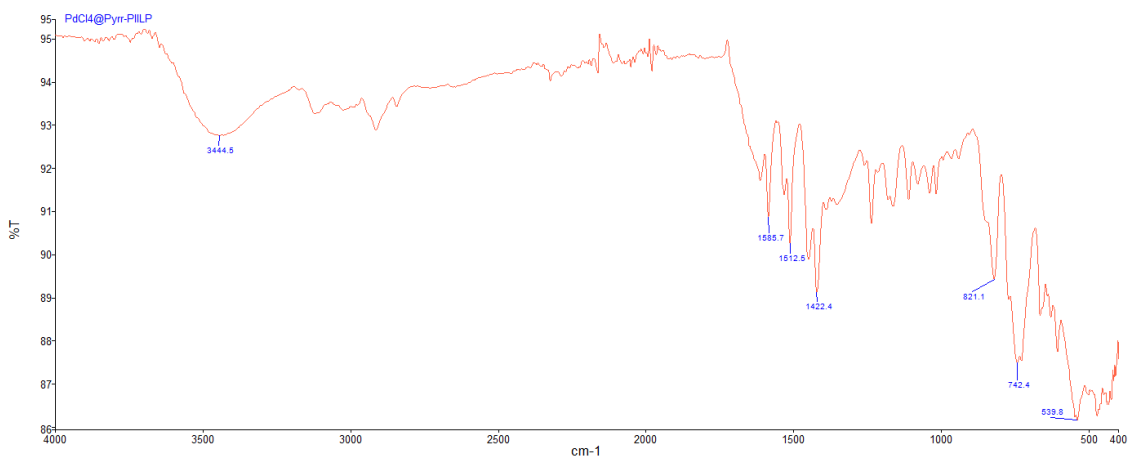
3. $\text{PdNP}@\text{NH}_2\text{-PIILP}$



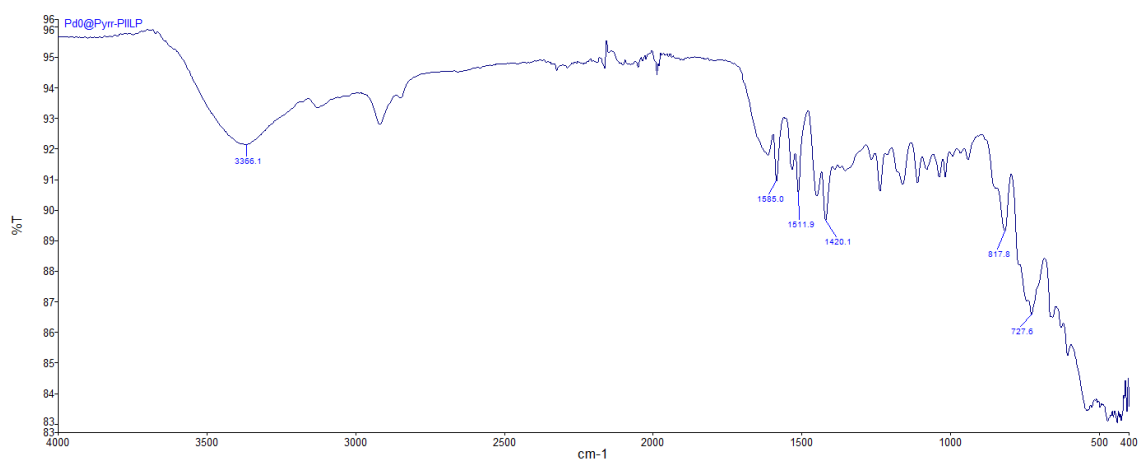
4. Pyrr-PIILP



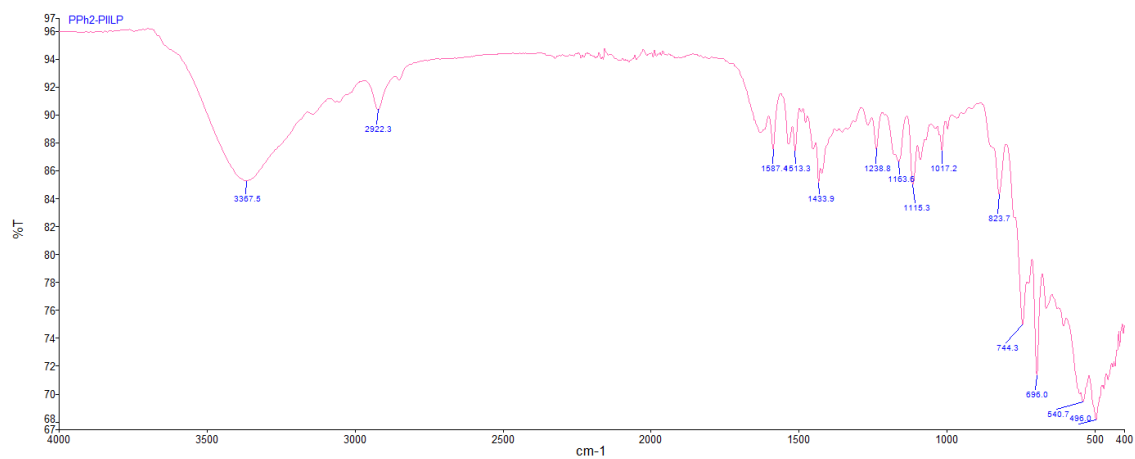
5. PdCl₄@Pyrr-PIILP



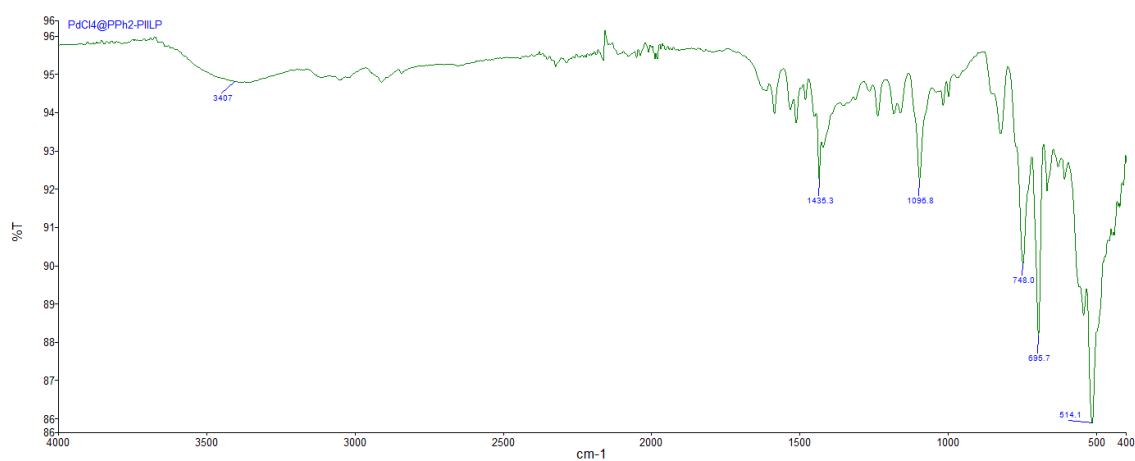
6. PdNP@Pyrr-PIILP



7. $PPh_2\text{-PIILP}$

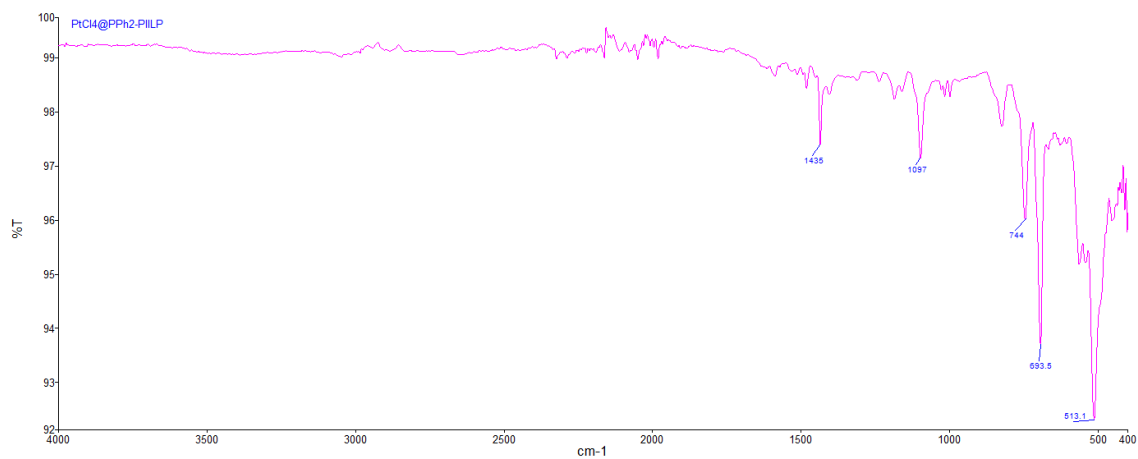
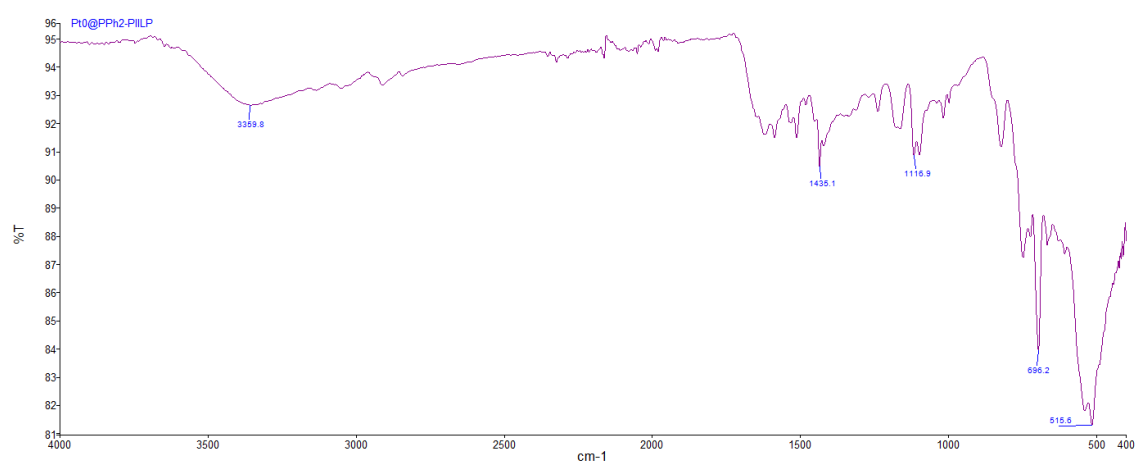


8. $PdCl_4@PPh_2\text{-PIILP}$



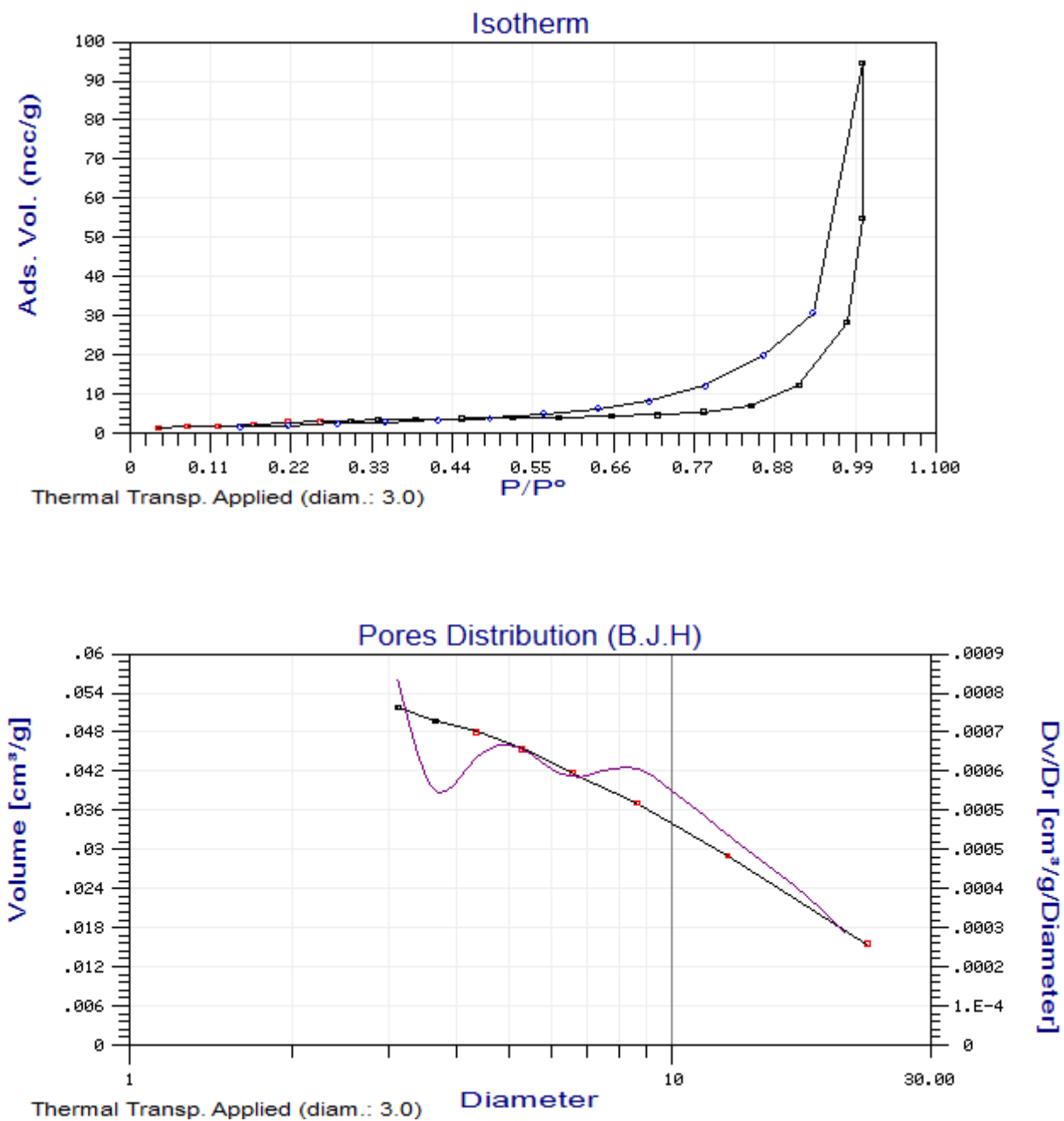
9. $PdNP@PPh_2\text{-PIILP}$

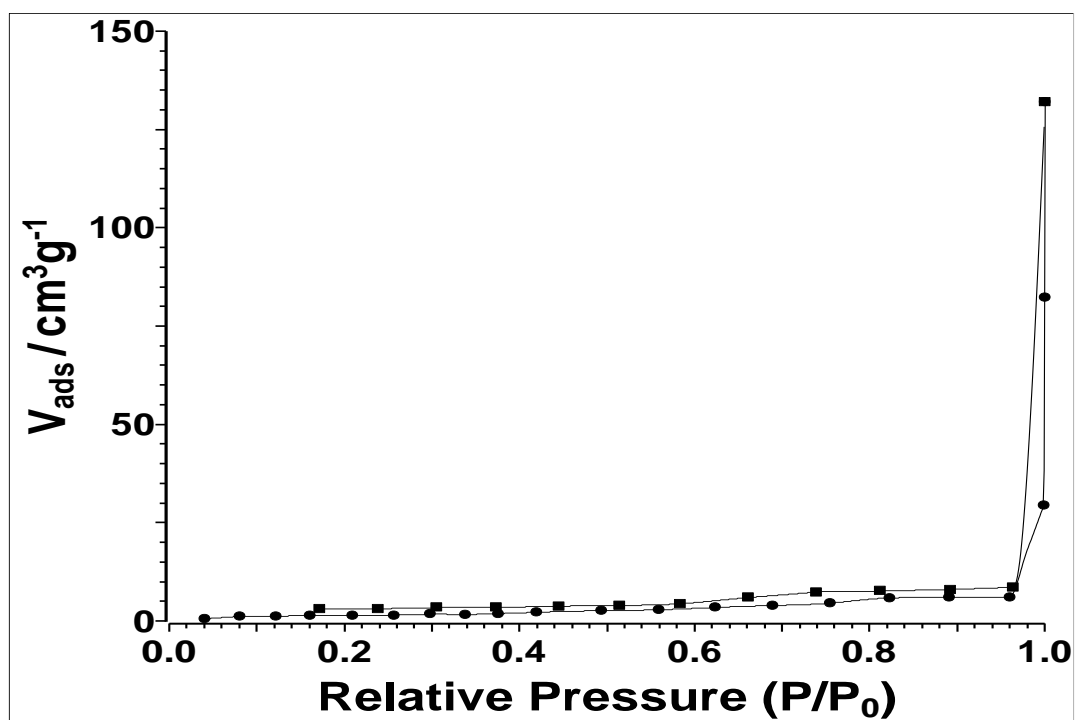


10. PtCl₄@PPh₂-PIILP**11. PtNP@PPh₂-PIILP**

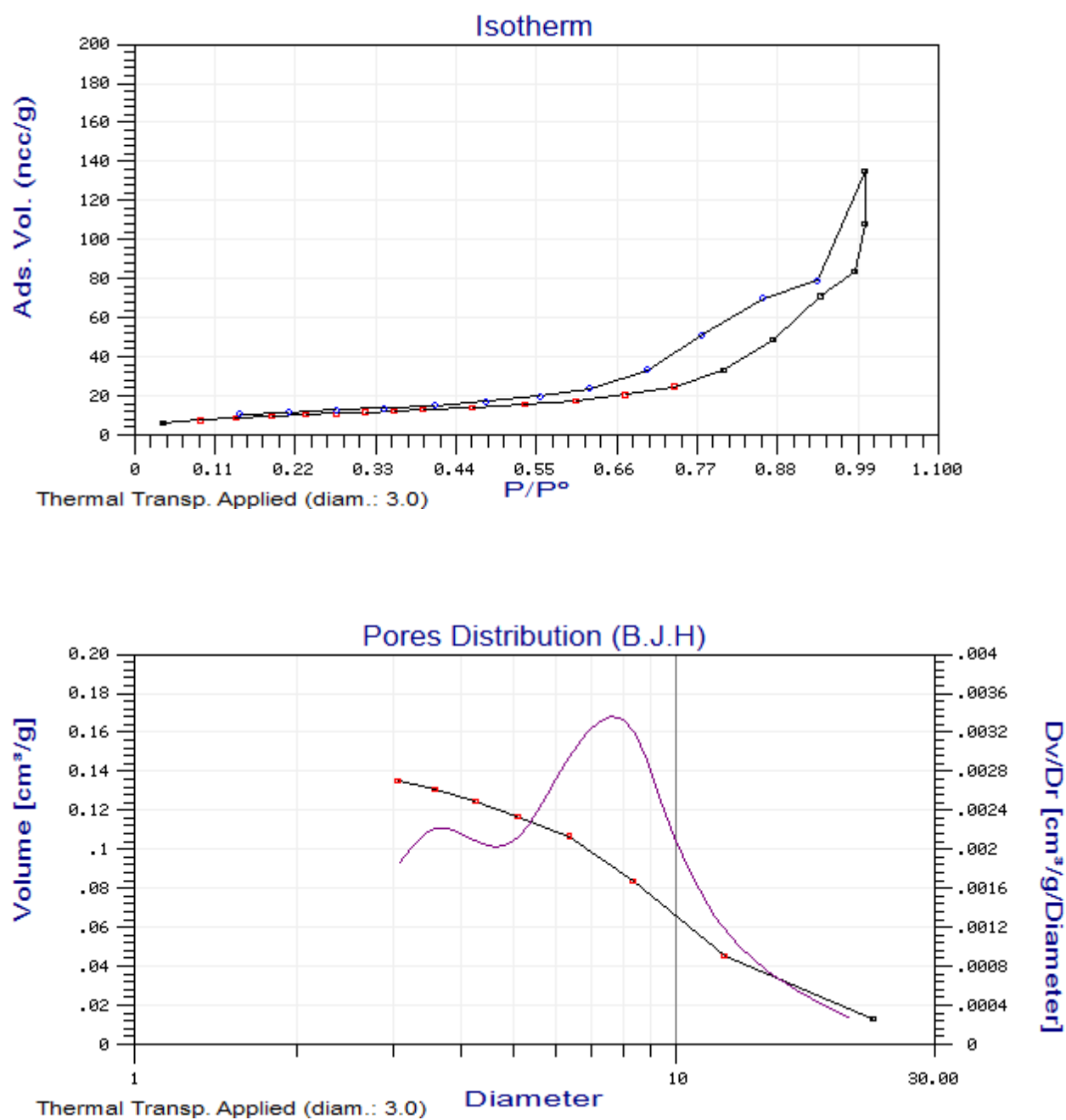
Appendix G. BET Surface Area Analysis

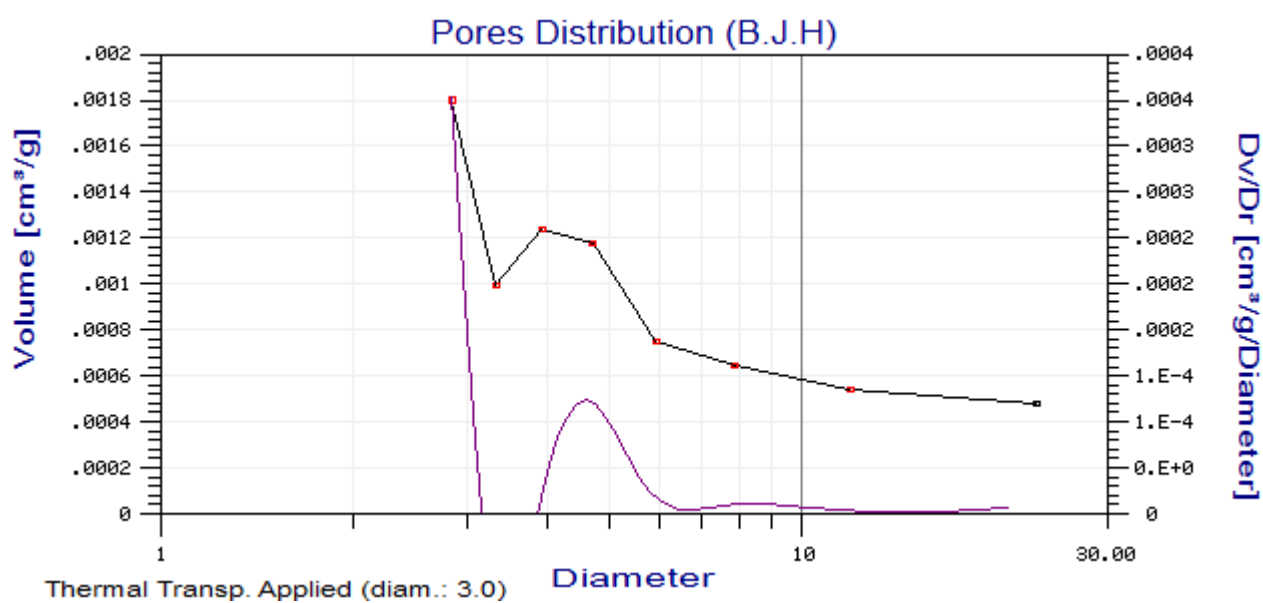
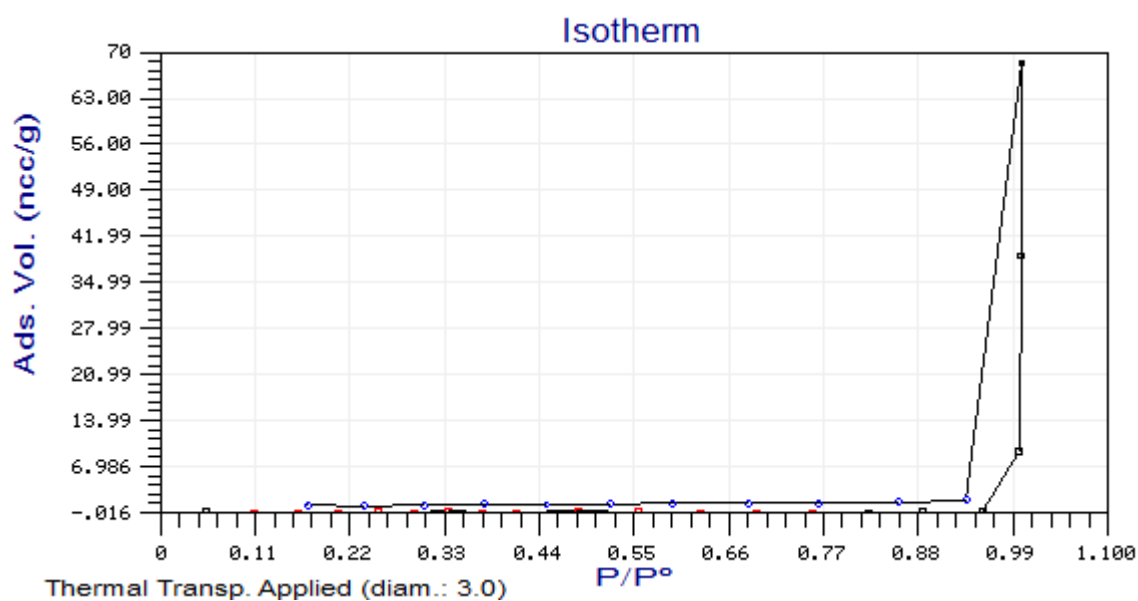
1. ROMP₁



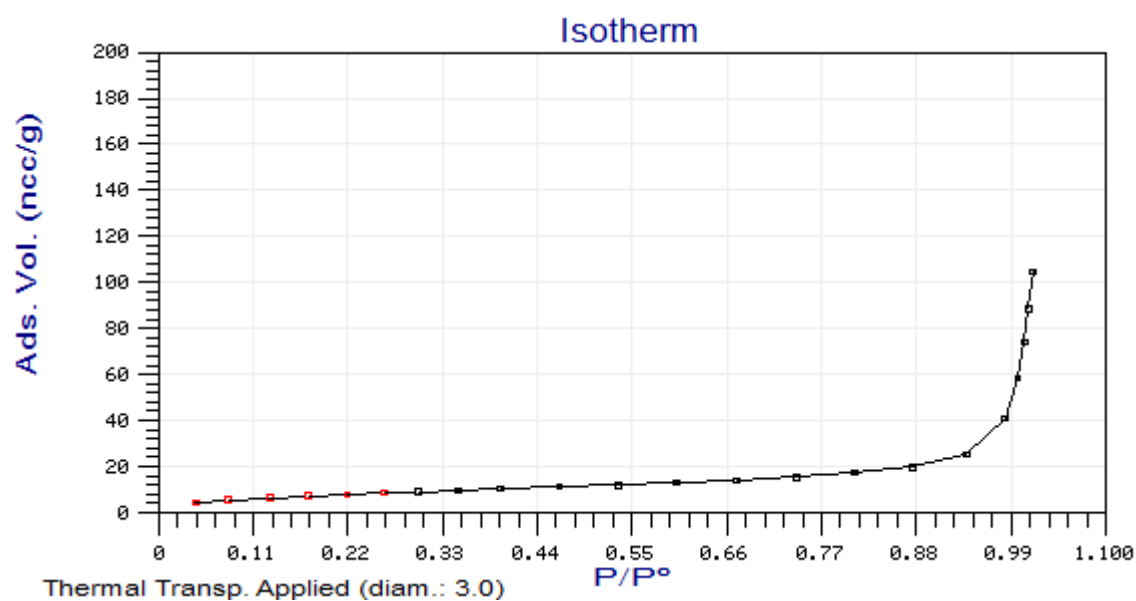
2. $\text{WO}_4@R\text{OMP}_1$ 

3. $PW_{12}O_{40}@ROMP_1$

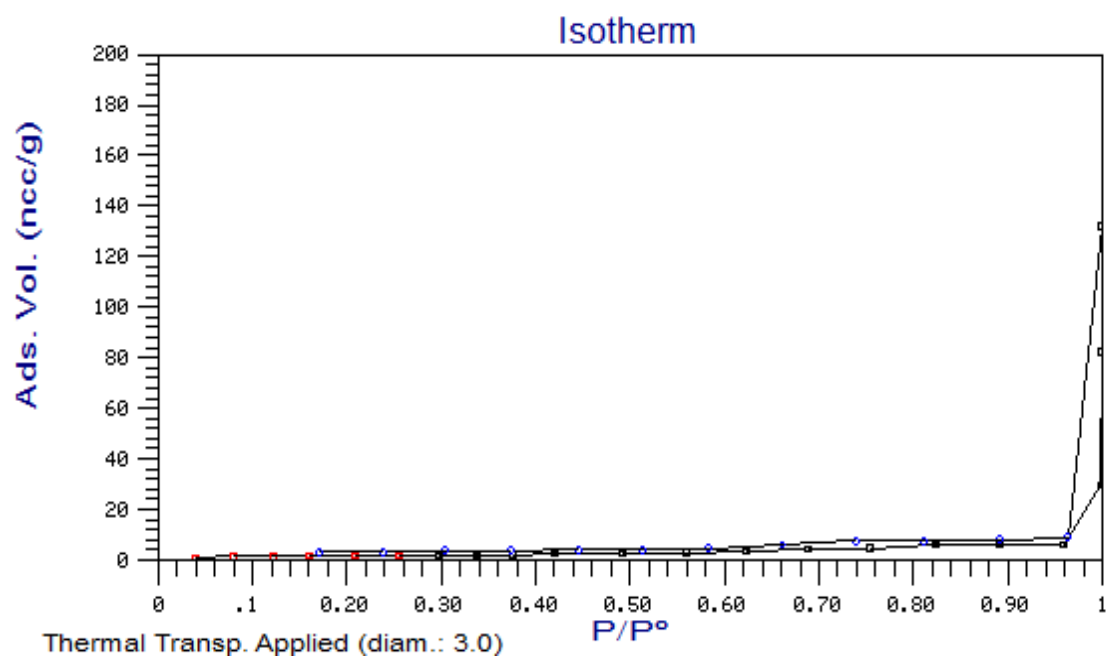


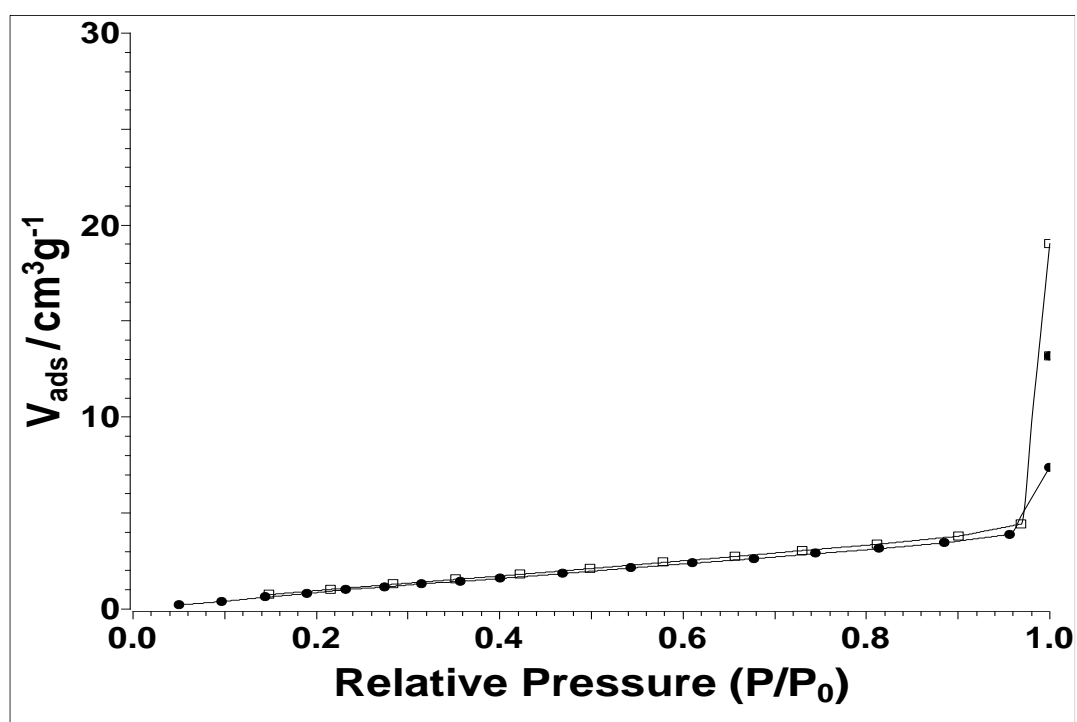
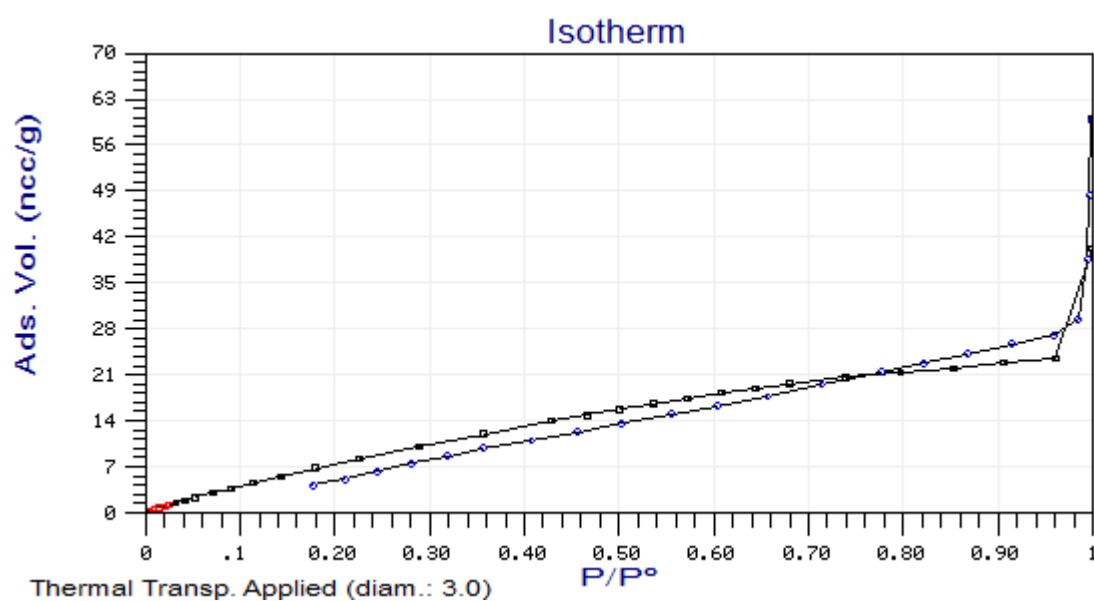
4. ROMP₂

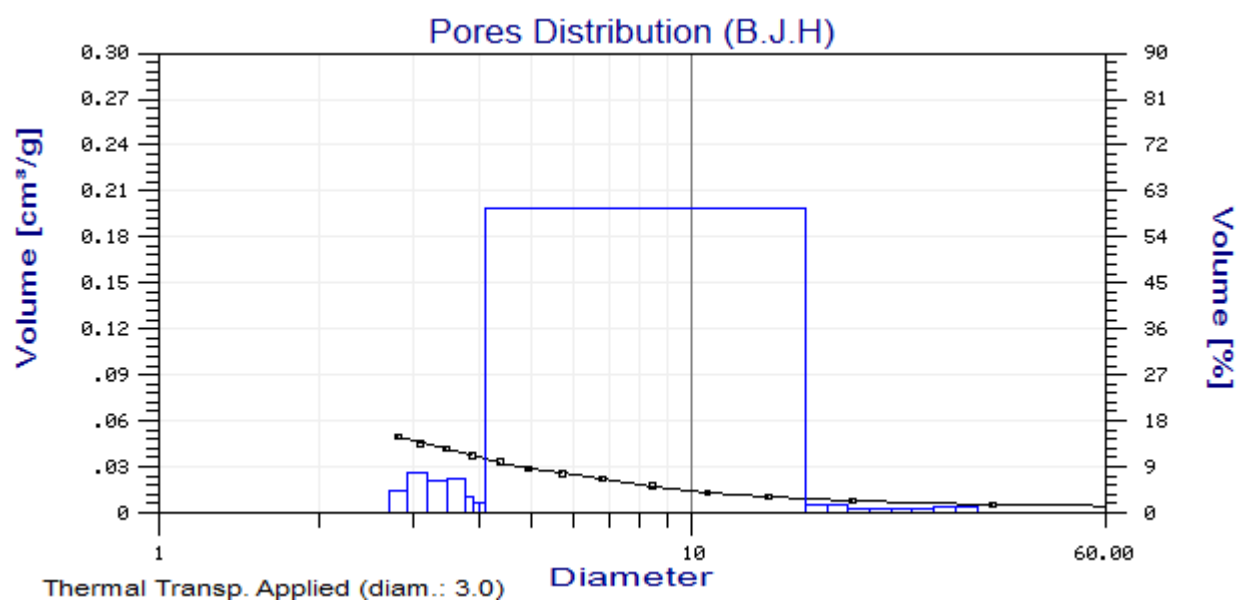
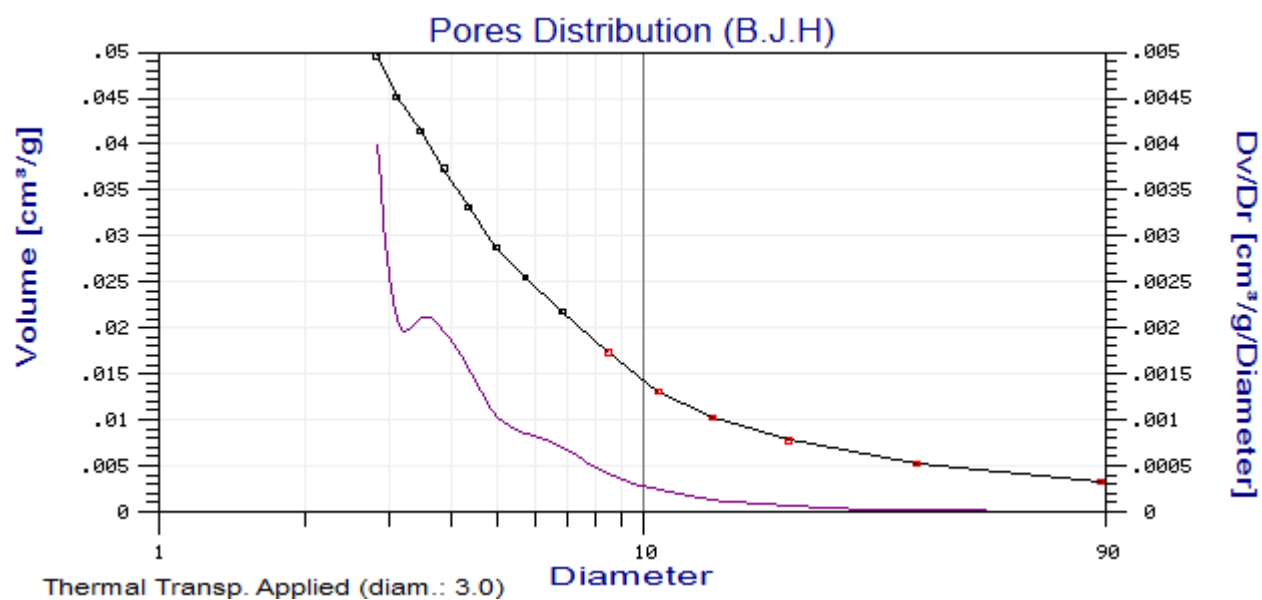
5. $WO_4@ROMP_2$



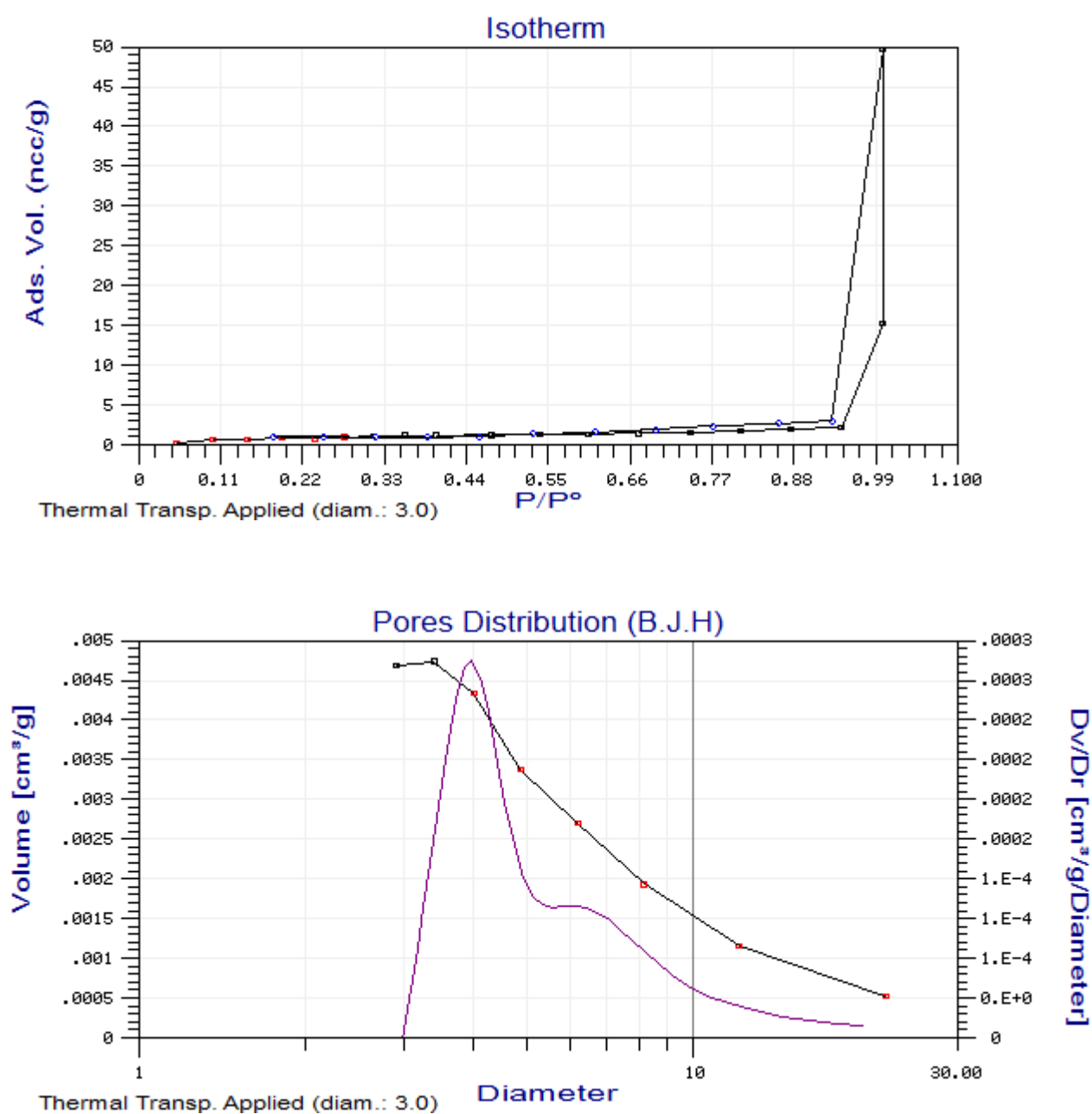
6. $NH_2-PIILP$

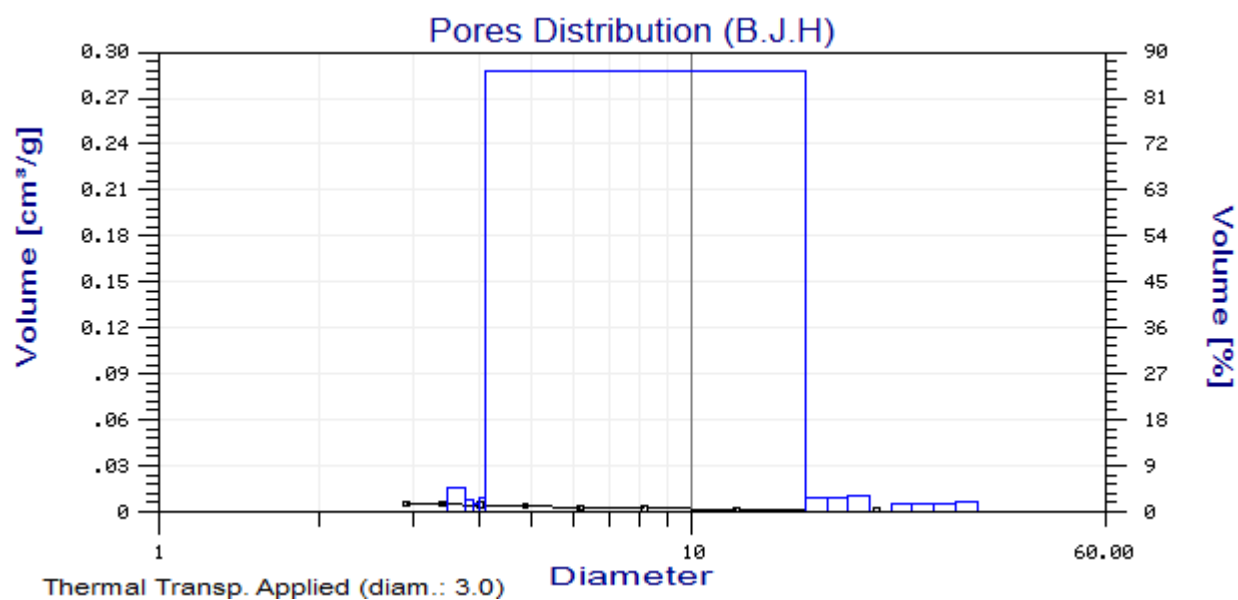


7. $\text{PdCl}_4\text{@NH}_2\text{-PIILP}$ 8. $\text{PdNP@NH}_2\text{-PIILP}$ 

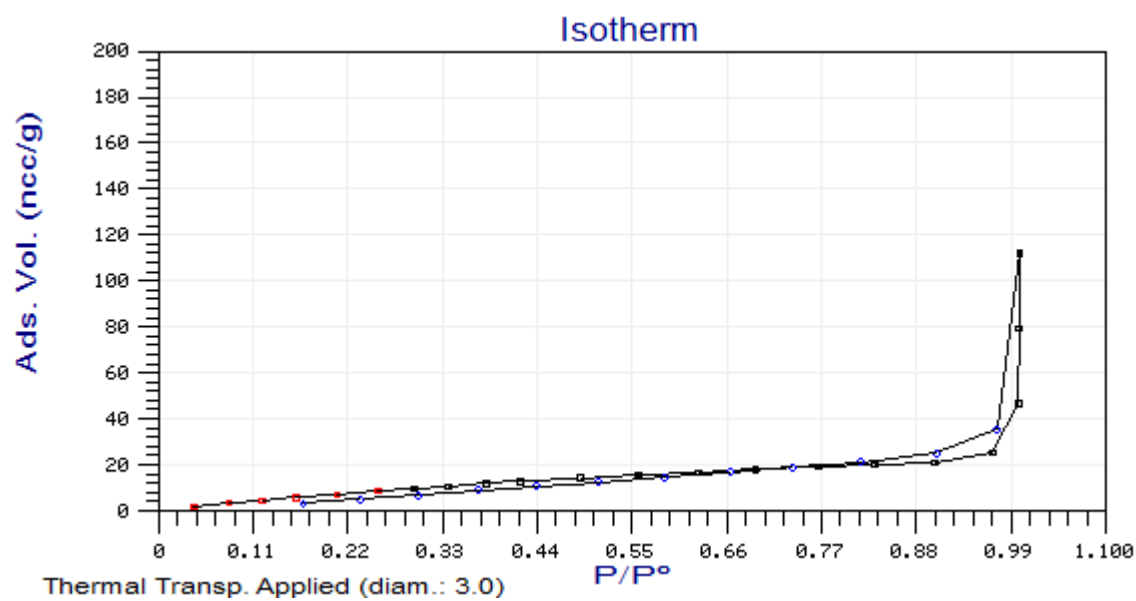


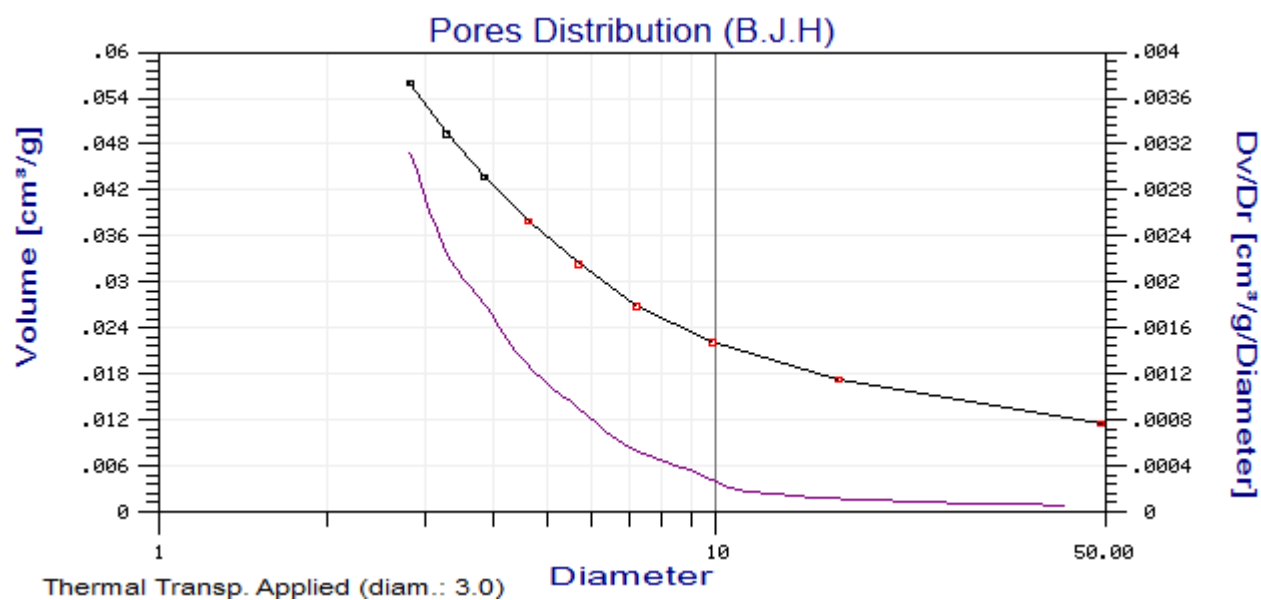
9. Pyrr-PIILP



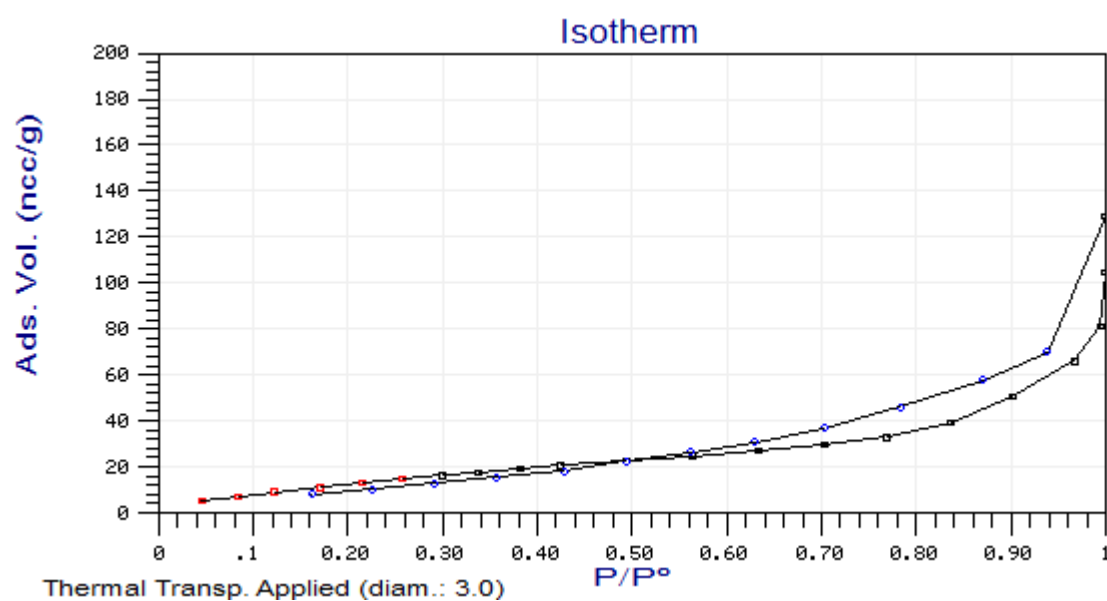


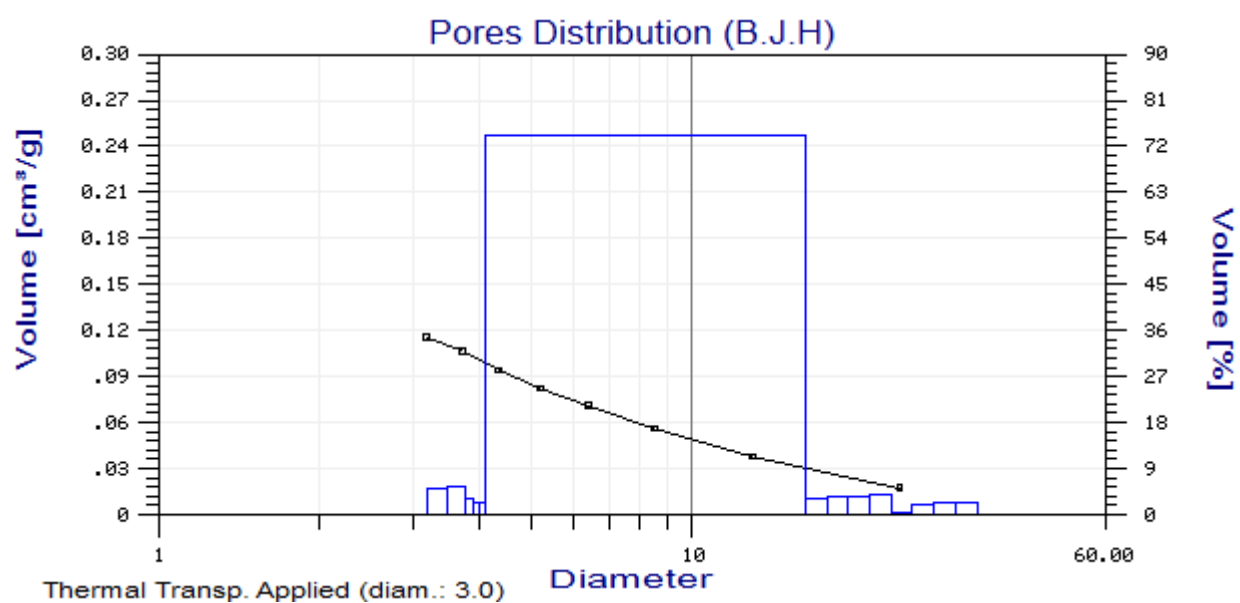
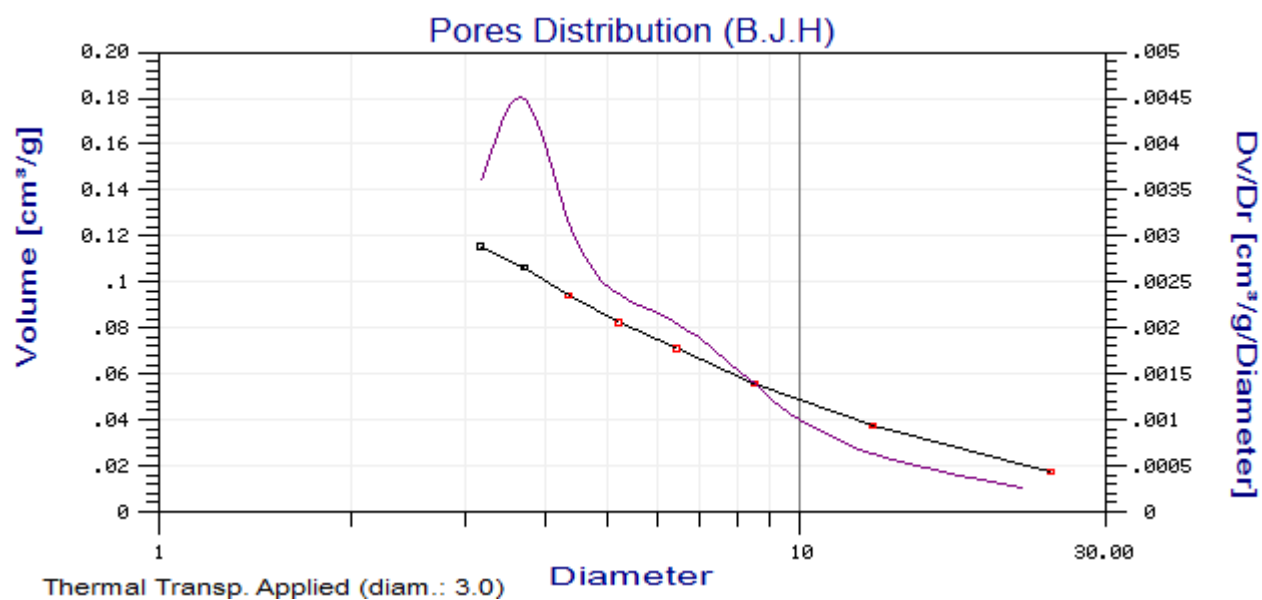
10. PdCl₄@Pyrr-PIILP

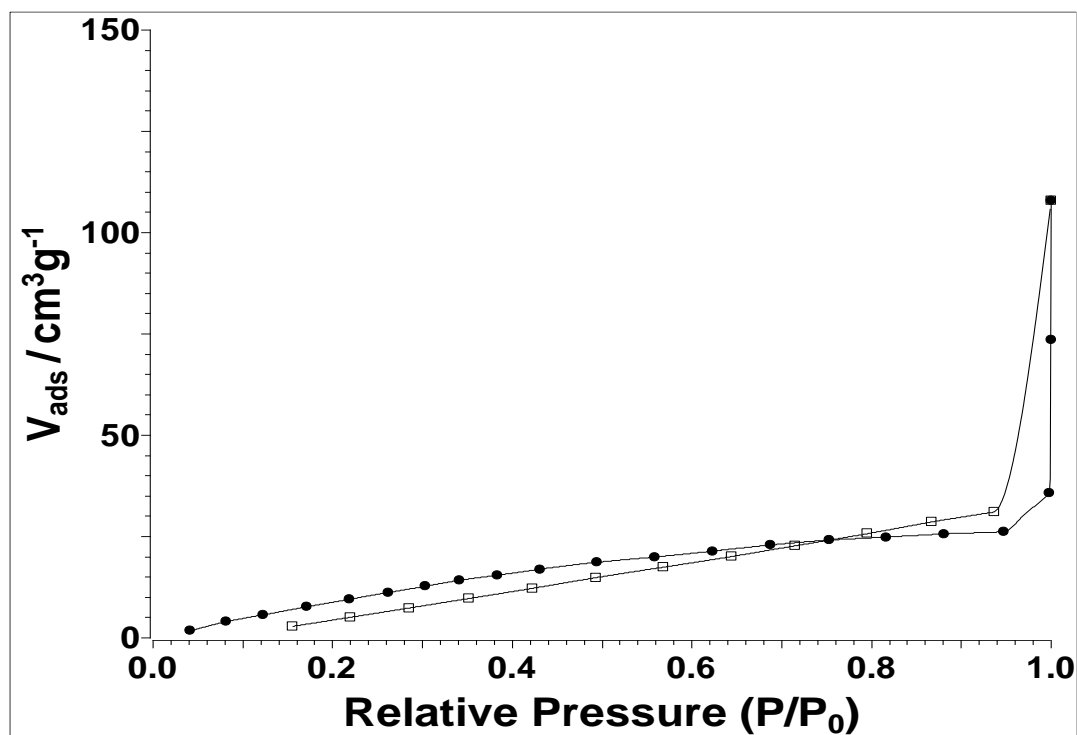
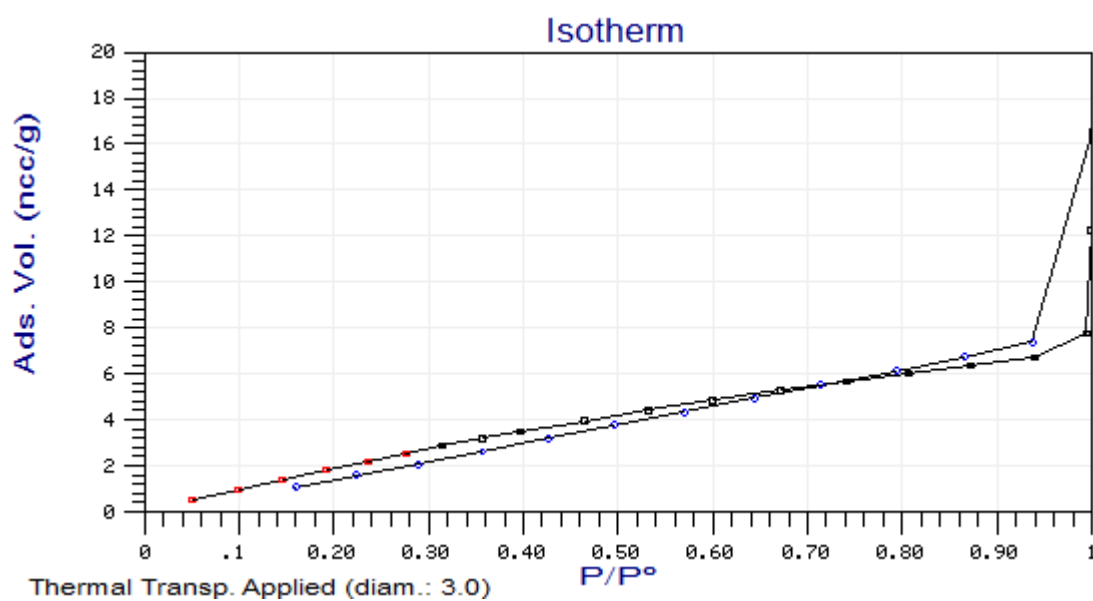


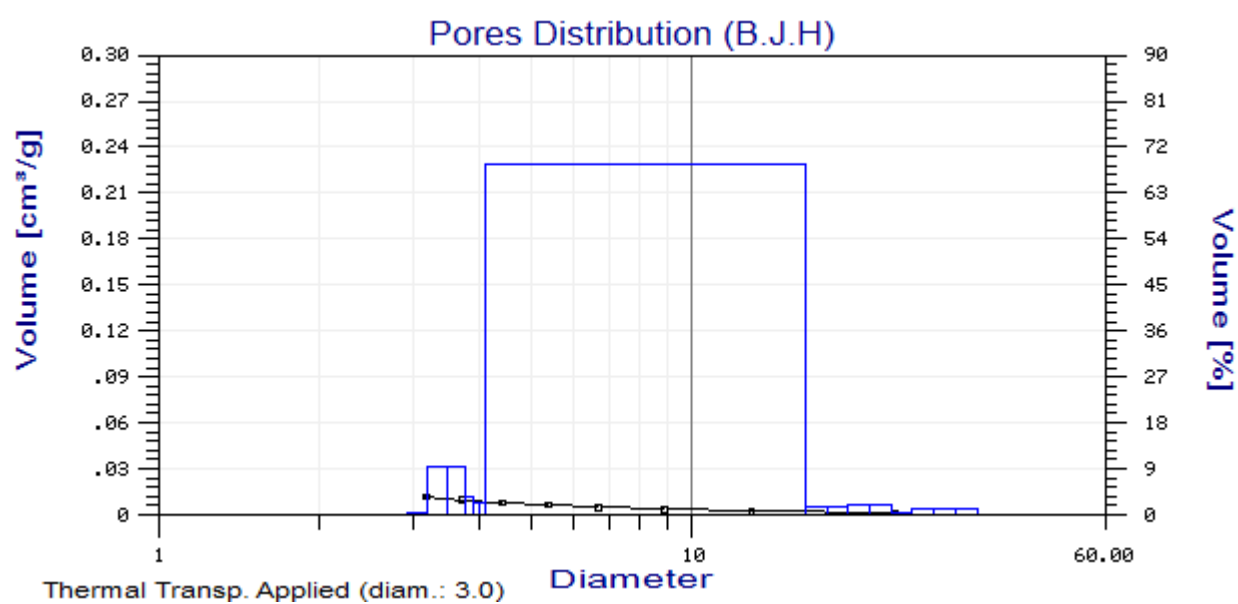
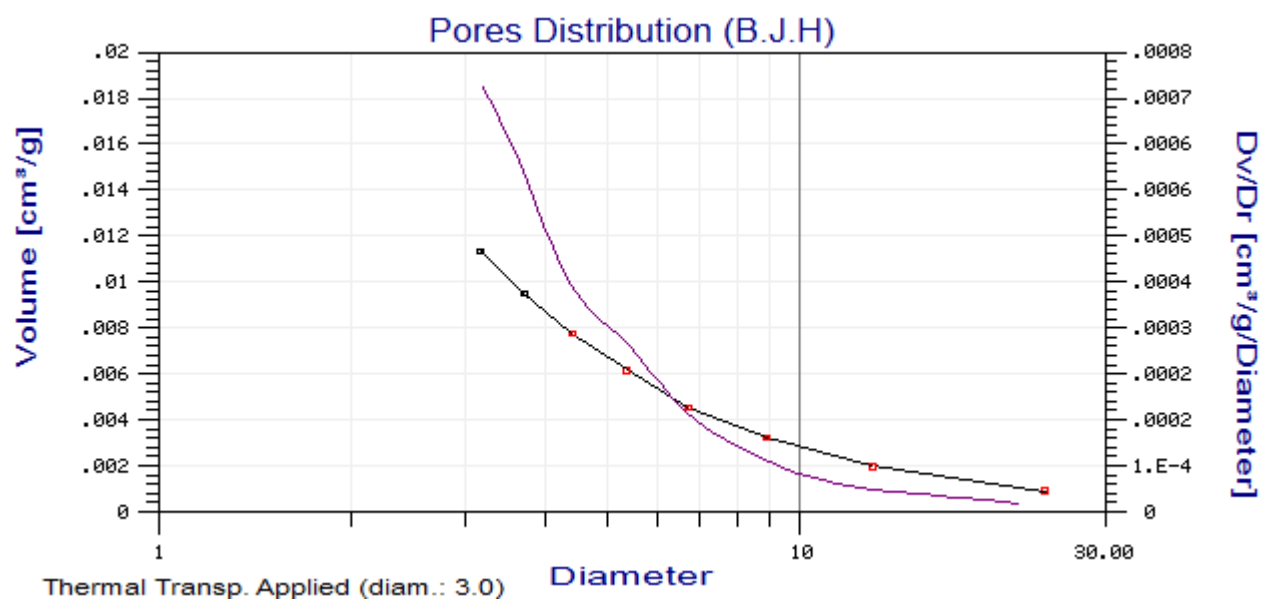


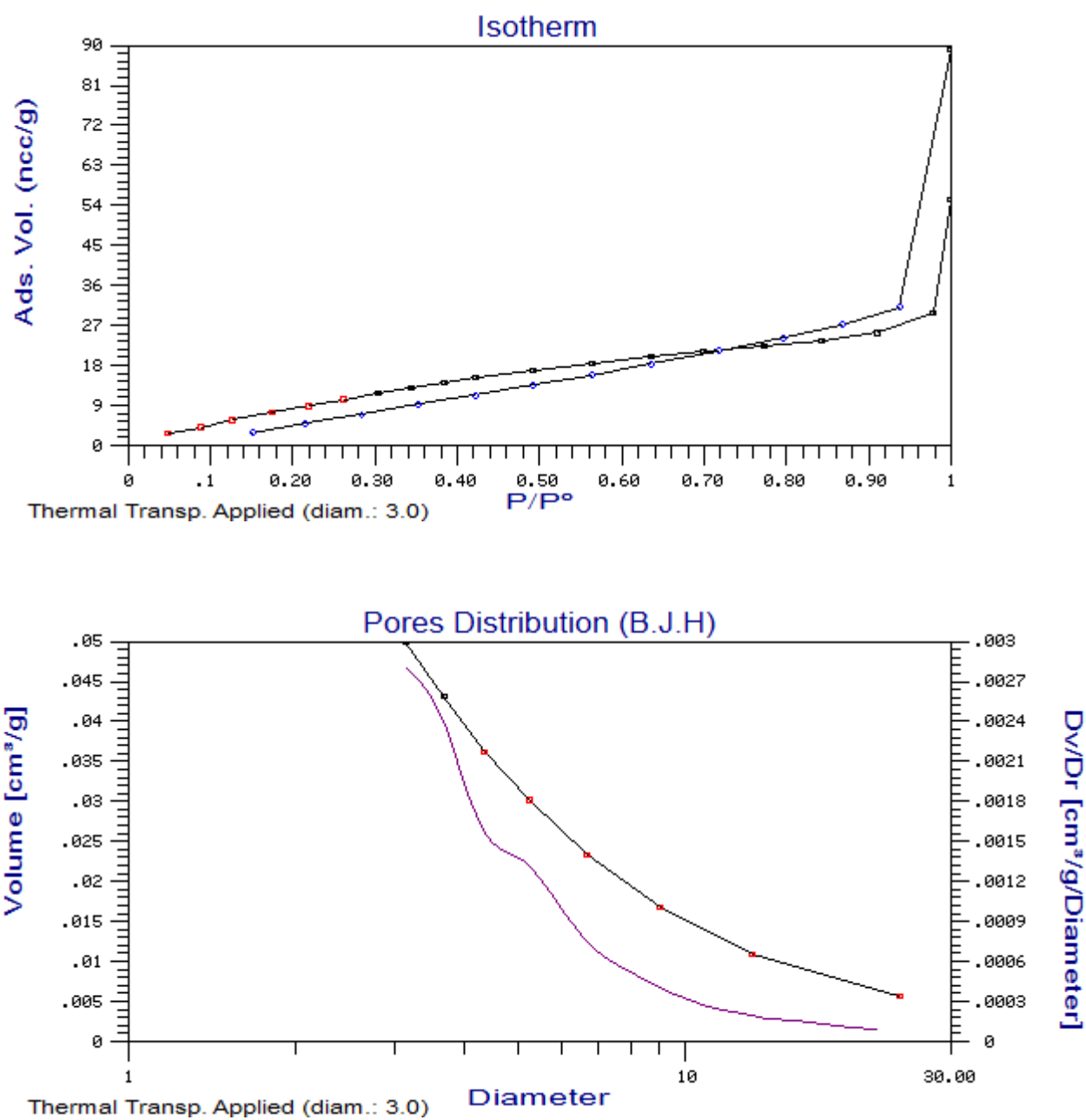
11. PdNP@Pyrr-PIILP

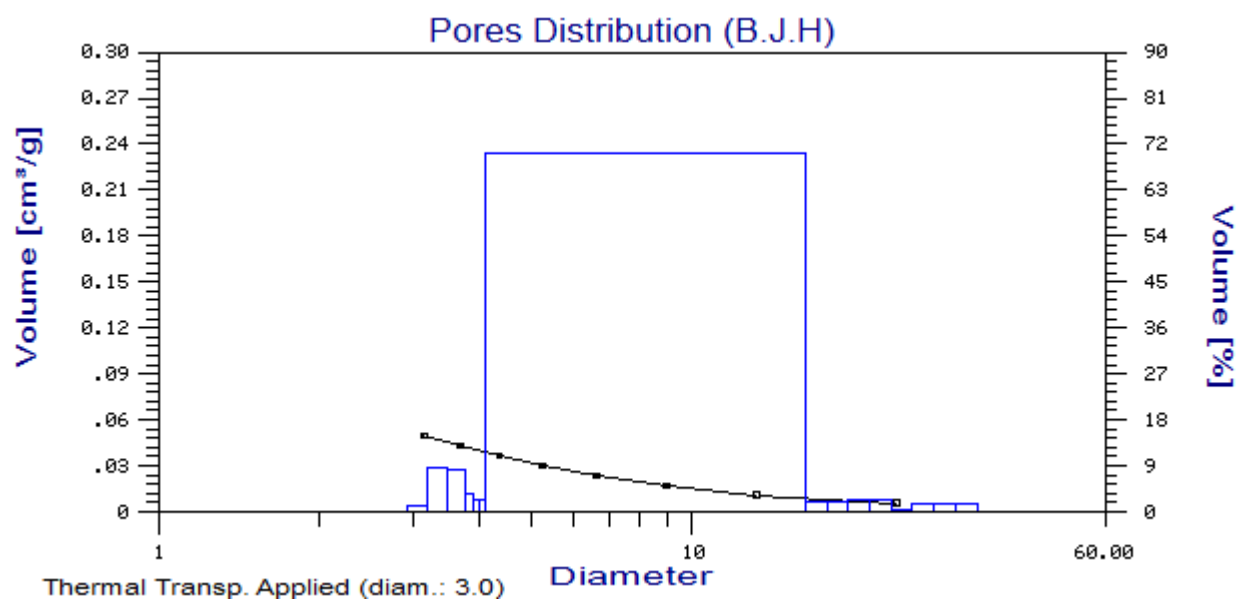




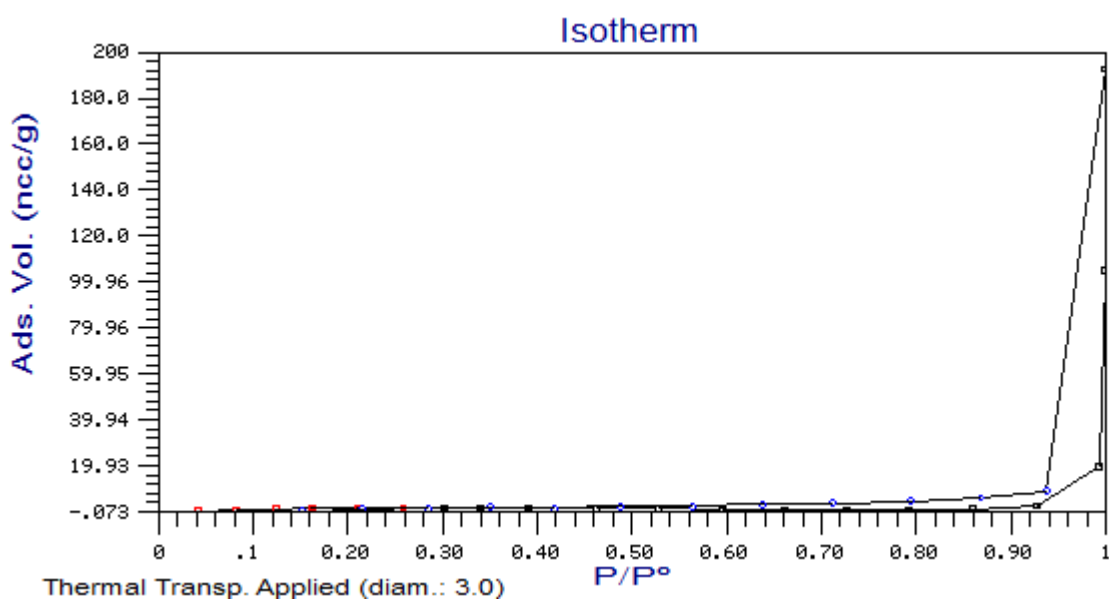
12. PPh_2 -PIILP13. $PdCl_4@PPh_2$ -PIILP

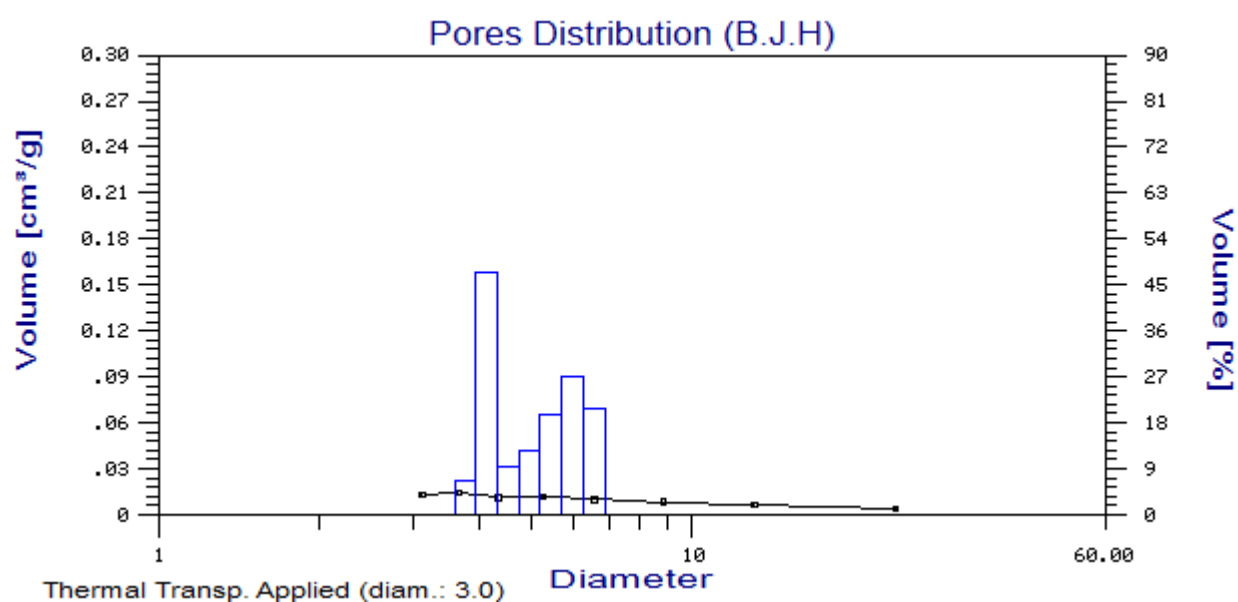
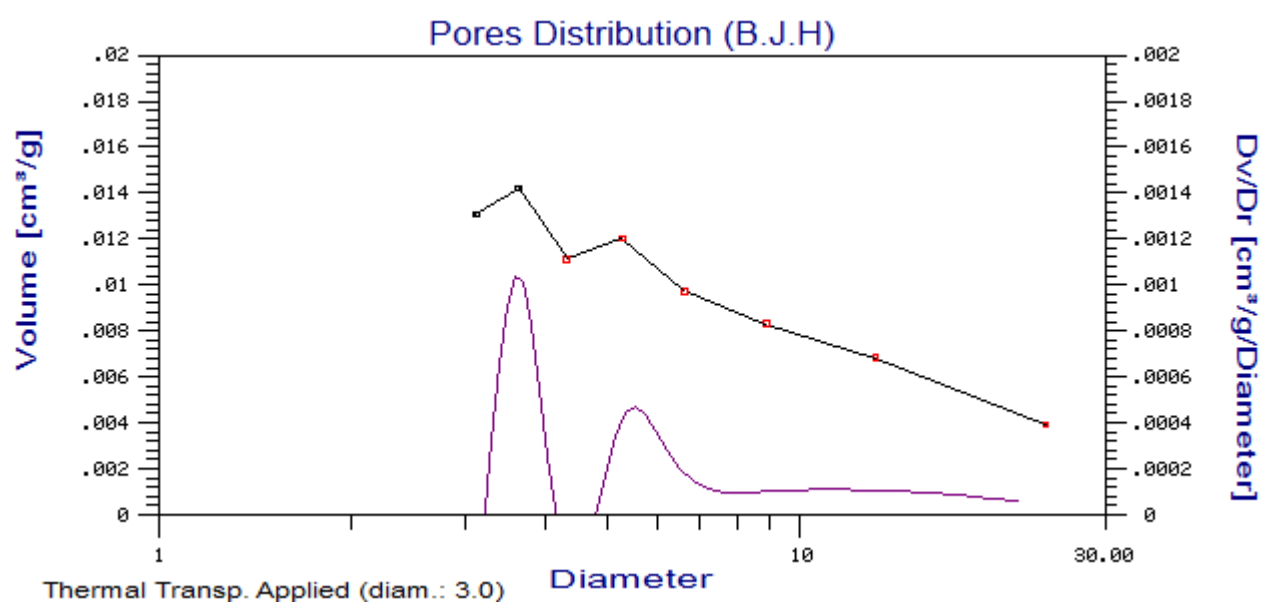


14. PdNP@PPh₂-PIILP

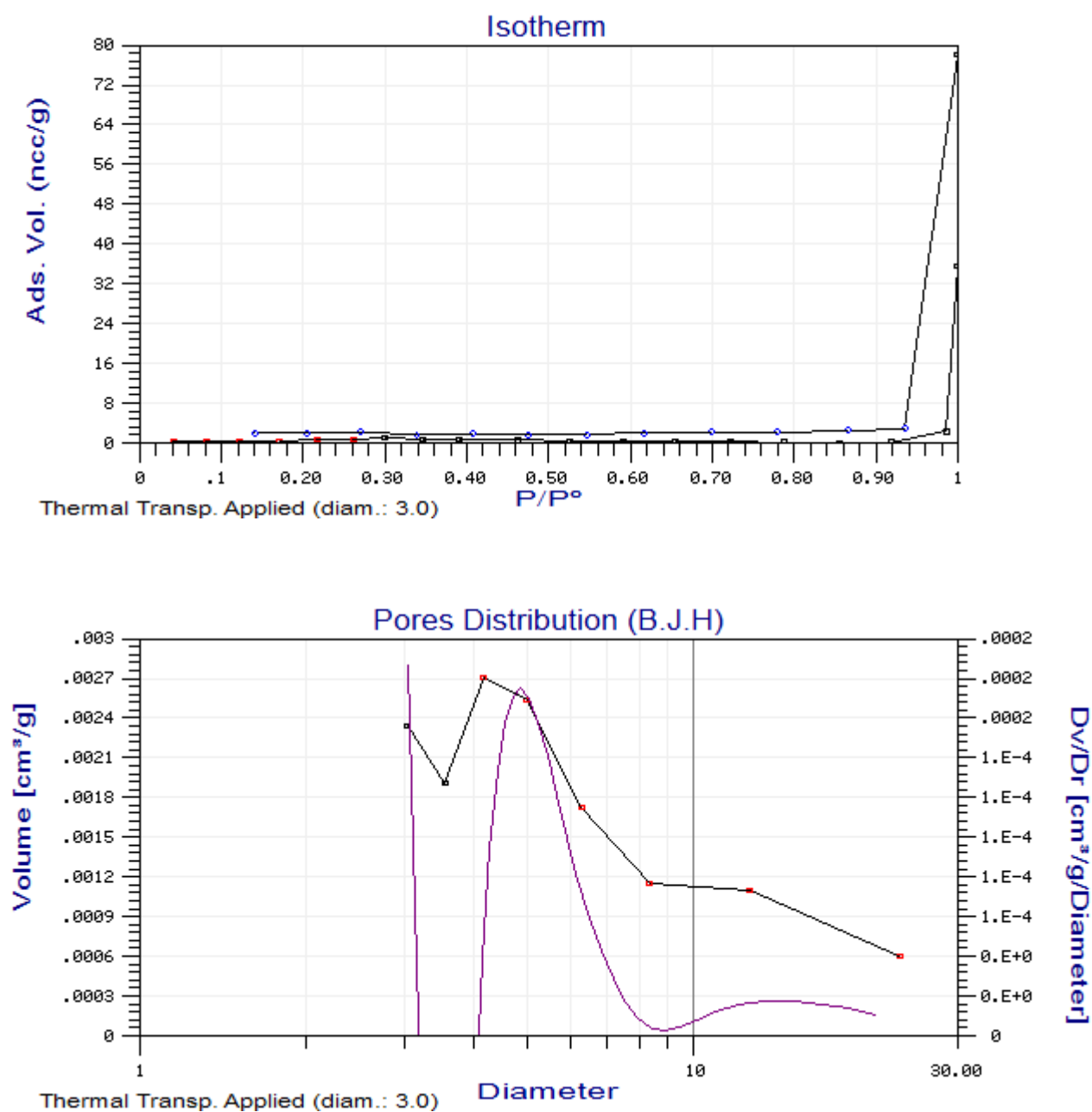


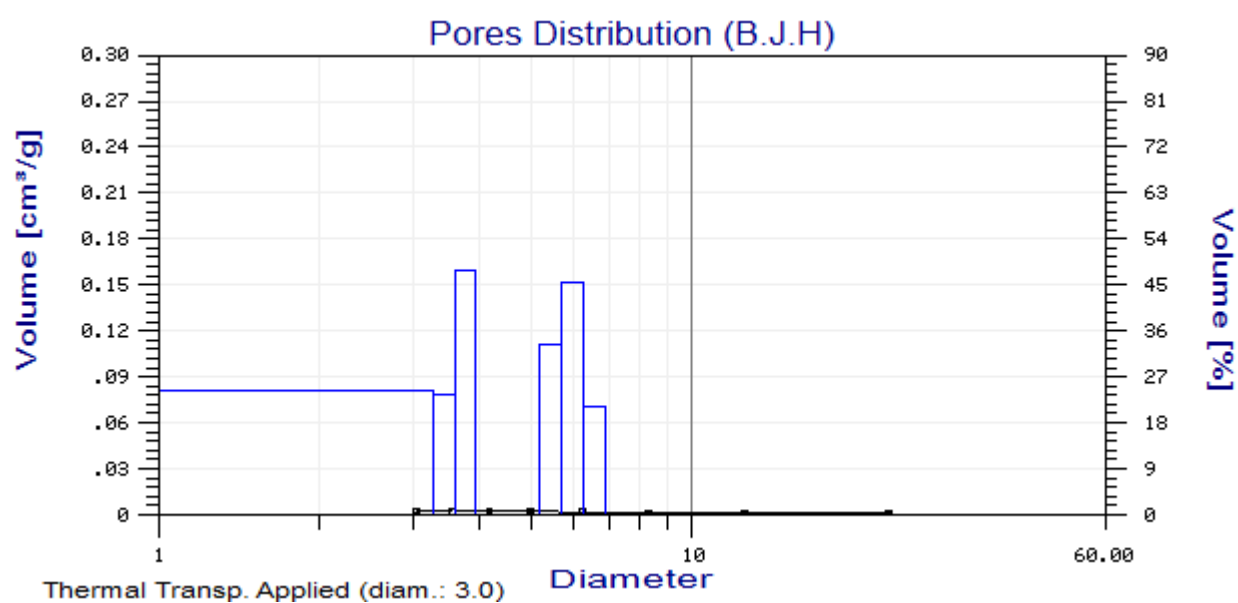
15. $PtCl_4@PPh_2-PIILP$





16. PtNP@PPh₂-PIILP





VITA

Einas Abdulaziz Abood

PhD Student at The School of Natural and Environmental Sciences: Chemistry,
Newcastle University, UK

Education

**School of The School of Natural and Environmental Sciences: Chemistry,
Newcastle University, UK**

Doctor of Philosophy (Ph.D.) Student,

Area of Research: Supported Molecular and Nanoparticles Catalysis Chemistry,

Research Skills: Inorganic and Organic Synthesis, Polymer Synthesis, Catalysis
Chemistry, Nanoparticles, 2014 – 2018.

**Chemistry Department, College of Education for Pure Science, University of
Basrah, Iraq**

Master's Degree, Organic & Catalysis Chemistry, 2005 – 2008.

**Chemistry Department, College of Education for Pure Science, University of
Basrah, Iraq**

Bachelor's Degree, General Chemistry, 2000 – 2004.

Honors and Awards

1. **The 27th International Conference on Organometallic Chemistry, (July 2016), The Royal Australian Chemical Institute (RACI), New Zealand Institute of Chemistry (NZIC).**

Melbourne, Australia.

- Student Award & Travel Bursary winner.

2. **UK-India Symposium on Functional Materials (January 2016)**

Royal Society of Chemistry Books.

- 1st Place poster prize.

3. **WYNNE-JONES POSTGRADUATE RESERCH DAY (May 2016)**

School of Chemistry/ Newcastle University.

- 3rd Place representation prize.

4. **Universities of Scotland Inorganic Chemistry Conference USIC 2015, (July 2015)**

Dalton Transactions.

- 1st Place poster prize.

5. **WYNNE-JONES POSTGRADUATE RESERCH DAY (May 2015)**

School of Chemistry/ Newcastle University.

- 3rd Place poster prize.

Publications

Highly efficient aqueous phase chemoselective hydrogenation of α,β -unsaturated aldehydes catalysed by phosphine-decorated polymer immobilized IL-stabilized PdNPs

Green Chem., 2017, **19**, 1635-1641.

Membership of Professional Organizations

Associate Member Royal Society of Chemistry (AMRSC) 2014

Location London, United Kingdom

Conferences, Symposia, and Workshops

- **Attendees at**

1. **Designing New Heterogeneous Catalysts Faraday Discussion (April 2016)**
Royal Society of Chemistry
Burlington House, Picadilly, London, UK.
2. **Organic Division North East Regional Meeting (April 2015)**
Royal Society of Chemistry
Norcroft Conference Centre, University of Bradford.
3. **Organic Division North East Regional Meeting (April 2014)**
Royal Society of Chemistry
University of Hull.
4. **Stereochemistry at Sheffield (January 2014)**
The 47th Annual Meeting on 'Modern Aspects of Stereochemistry'
Dainton Building, University of Sheffield.

- **Poster Presenter**

- 1. The 27th International Conference on Organometallic Chemistry (July 2016)**

The Royal Australian Chemical Institute (RACI), New Zealand Institute of Chemistry (NZIC).

Melbourne, Australia.

- Poster title: Polymer - Immobilized Ionic Liquid Phase (PIILP)
Stabilised Palladium Nanoparticles: Synthesis and Applications in Catalysis.

- 2. UK-India Symposium on Functional Materials (June 2016)**

University of Edinburgh, UK.

- Poster title: Polymer - Immobilized Ionic Liquid Phase (PIILP)
Stabilised Palladium Nanoparticles: Synthesis and Applications in Catalysis.

- 3. The 6th Chemical Nanoscience Symposium CNSN-6 (March 2016)**

Bedson Building, School of Chemistry, Newcastle University.

- Poster title: Polymer - Immobilized Ionic Liquid Phase (PIILP)
Stabilised Palladium Nanoparticles: Synthesis and Applications in Catalysis.

- 4. Sustainable Chemistry in Industry, Symposium and Workshop (November 2015)**

Department of Chemistry, Durham University, UK.

- Poster title: Polymer - Immobilized Ionic Liquid Phase (PIILP)
Stabilised Palladium Nanoparticles: Synthesis and Applications in Catalysis.

- 5. 5th NORSC PG Symposium (September 2015)**

King's Manor, York.

- Poster title: Polymer - Immobilized Ionic Liquid Phase (PIILP)
Stabilised Palladium Nanoparticles: Synthesis and Applications in Catalysis.

- 6. Applied Catalysis Group: Careers in Catalysis Symposium (September 2015)**

Newcastle University.

- Poster title: Polymer - Immobilized Ionic Liquid Phase (PIILP)
Stabilised Palladium Nanoparticles: Synthesis and Applications in Catalysis.

7. Universities of Scotland Inorganic Chemistry Conference USIC 2015 (July 2015)

Heriot-Watt University, Edinburgh, UK.

- Poster title: Polymer - Immobilized Ionic Liquid Phase (PIILP) Stabilised Palladium Nanoparticles: Synthesis and Applications in Catalysis.

8. The 5th Chemical Nanoscience Symposium CNSN-5 (March 2015)

Bedson Building, School of Chemistry, Newcastle University.

- Poster title: Polymer - Immobilized Ionic Liquid Phase (PIILP) Stabilised Palladium Nanoparticles: Synthesis and Applications in Catalysis.

• **Talk Presenter**

1. Universities of Scotland Inorganic Chemistry Conference 50th USIC (August 2016)

Thomas Graham Building, University of Strathclyde, Glasgow, UK.

- Presentation title: Polymer - Immobilized Ionic Liquid Phase (PIILP) Stabilised Palladium Nanoparticles: Synthesis and Applications in Catalysis.

2. Dalton 2016 (March 2016)

University of Warwick, UK

- Presentation title: Polymer - Immobilized Ionic Liquid Phase (PIILP) Stabilised Palladium Nanoparticles: Synthesis and Applications in Catalysis.

References

Dr Simon Doherty, Senior Lecturer, The School of Natural and Environmental Sciences: Chemistry, Bedson Building, Newcastle University, NE1 7RU.

Telephone: +44 (0) 191 208 6537

Email: simon.doherty@ncl.ac.uk

Dr Julian Knight, Senior Lecturer, The School of Natural and Environmental Sciences: Chemistry, Bedson Building, Newcastle University, NE1 7RU.

Telephone: +44 (0) 191 208 7068

Email: julian.knight@ncl.ac.uk